2018 International Theoretical and Practical Conference on Alternative and Smart Energy

TPCASE 2018

December 6-8, 2018
Voronezh State Technical University
Voronezh, Russia

DEStech Publications, Inc.

2018 International Theoretical and Practical Conference on Alternative and Smart Energy

DEStech Publications, Inc.
439 North Duke Street
Lancaster, Pennsylvania 17602 U.S.A.

Manufactured in the U.S.A.

Main entry under title:
2018 International Theoretical and Practical Conference on Alternative and Smart Energy (TPCASE 2018)

ISBN: 978-1-60595-617-6

Table of Contents

Preface

The first International Conference "Alternative and Intellectual Power Engineering" (AIE) was held on December 6–8, 2018 in Voronezh on the basis of the Voronezh State Technical University. The co-organizers of the scientific event were the Academy of Engineering Sciences named after A.M. Prokhorov and JSC "Corporation NPO" RIF ".

Scientists from Russia (Voronezh, Moscow, Nizhny Novgorod, Tambov, Belgorod, Saratov, Kazan, Tyumen, Novosibirsk, Tomsk, Astrakhan and other cities of Russia) and near and far abroad countries (Italy, France, Germany and Belarus) gathered to discuss new developments and achievements in the energy sector.

Energy is the most important driving force of world economic progress nowadays, and the well-being of billions of inhabitants of the planet directly depends on its condition. The steady growth of the world population leads to an increase in energy consumption. Every day more and more depleted reserves of natural resources (coal, gas, oil), necessary for the operation of traditional energy, so the problem of transition from traditional energy sources is becoming increasingly important. In addition, except depleting of traditional sources, there is also an environmental problem, since the burning of hydrocarbon fuels leads to harmful emissions into the atmosphere, worsening the human habitat, creating environmental problems. Therefore, it is important to find new sources of energy that are more environmentally friendly.

The world has already made significant progress in the use of alternative, renewable energy sources.

The conference discussed issues in the fields of hydrogen energy, solar energy, thermoelectric energy, wind energy, nuclear energy, ecology, functional materials for alternative energy, energy-saving technologies, systems and materials, intellectual energy, as well as new educational programs on energy efficiency and alternative energy.

All articles accepted at the conference are included in this Book.

The AIE Organizing Committee expresses its deepest gratitude to all participants and guests of the conference for their cooperation, their unusually hard work and high level of professionalism in their fields of knowledge.

Special thanks to the publishing house DEStech Publications, Inc. for publication of the best works.

Committees

ORGANIZING COMMITTEE

Chairman Sergey Alexandrovich Kolodyazhny, Rector of Voronezh State Technical University
Co-Chairman Yury Vasilyevich Gulyaev, Academician of the Russian Academy of Sciences, President of the Academy of Engineering Sciences named after A.M. Prokhorov
Vice-chairpersons
Dmitry Albertovich Konovalov, Associate Professor of the Department of Theoretical and Industrial Heat Power Engineering of Voronezh State Technical University;
Valery Yakovlevich Mishchenko, Director of the Research and Design Institute of Voronezh State Technical University

PROGRAM AND SCIENTIFIC COMMITTEE
Chairman Igor Genagievich Drozdov, Vice-Rector for scientific work of Voronezh State Technical University;
Vice-chairman Yury Egorovich Kalinin, Professor, Department of Solid State Physics, Voronezh State Technical University
Valentin Mikhailovich Ievlev, Academician of the Russian Academy of Sciences, Head of the Department of Interdisciplinary Materials Science, Moscow State University
Nikolay Vasilyevich Mozgovoy, Head of the Department of Industrial Ecology and Life Safety, Voronezh State Technical University
Viktor Ivanovich Tkach, Chief Researcher of the State University of Donetsk Physical and Technical Institute named after A.A. Galkin
Viktor Leonidovich Burkovsky, Head of the Department of electric drive, automation and control in technical systems, Voronezh State Technical University
Nail Farilovich Timerbaev, Director of the Advanced Energy Technologies Research Center, Kazan State Energy University
Stanislav Ivanovich Rembeza, Head of the Department of Semiconductor Electronics and Nanoelectronics, Voronezh State Technical University
Nathanael Riess, President of “HELLING”
Victor Narbenovich Melkumov, Head of the Department of Heat and Gas Supply and Oil and Gas Business, Voronezh State Technical University
Yuri Alfredovich Kuzma-Kichta, Professor of the Department of Engineering Thermophysics of the National Research University "MEI"
Vasily Igorevich Borzenko, Head of the Laboratory of Hydrogen Energy Technologies of the Federal State Budgetary Institution of Science Joint Institute for High Temperatures of the Russian Academy of Sciences

Alexey Alexandrovich Burkov, Head of production and technical department of PJSC "IDGC of CENTER "Voronezhenergo"
Viktor Ivanovich Ryazhskikh, Head of the Department of Applied Mathematics and Mechanics, Voronezh State Technical University
Alexander Leonidovich Gusev, Head of the “Hydrogen” Group of Companies
Alexander Sergeevich Ivanov, General Director of JSC “NPA Corporation“ RIF”
Anatoly Tikhonovich Ponomarenko, Chief Researcher of the Institute of Synthetic Polymeric Materials named after N.S. Enikolopov RAS
Vladimir Petrovich Povarov, Director of the branch of Rosenergoatom Concern JSC Novovoronezh Nuclear Power Plant
Sergey Viktorovich Fedosov, Head of the Department of Technosphere Safety, Ivanovo State Polytechnic University
Alexey Viktorovich Dedov, corresponding member of RAS, Director of the Institute of Thermal and Atomic Energy, National Research University "MEI"
Alexander Kirillovich Fedotov, Professor of the Department of Energy Physics, Belarusian State University
Vyacheslav Bukhmirov, Professor of the Department of Theoretical Foundations of Thermal Engineering, Ivanovo State Energy University
Andrei Vladimirovich Dmitriev, Head of the Department of Theoretical Foundations of Thermal Engineering, Kazan State Energy University
Semyon Leonidovich Podvalny, Head of the Department of Automated and Computing Systems, Voronezh State Technical University
Vladimir Vasilyevich Kuznetsov, Head of Thermophysics Laboratories of Multiphase Systems S. S. Kutateladze, Siberian Branch of the Russian Academy of Sciences
Sergey Anatolyevich Yaremenko, Head of the Department of Housing, Voronezh State Technical University
Viktor Ivanovich Terekhov, Chief Researcher of Institute of Thermophysics named after S. S. Kutateladze, Siberian Branch of the Russian Academy of Sciences
Dmitry Nikolaevich Korotkikh, Professor of the Department of Technology of Building Materials, Products and Structures, Voronezh State Technical University
Alla Vitalievna Zvyagintseva, Associate Professo of the Department of Chemistry and Chemical Technology of Materials, Voronezh State Technical University
Ernest Nikolaevich Muravev, Academy of Engineering Sciences named after A.M. Prokhorov
Sergey Viktorovich Dakhin, Associate Professor of the Department of Theoretical and Industrial Heat Power Engineering, Voronezh State Technical University
Marina Vyacheslavovna. Shitikova, Professor of the Department of Technology, Construction Management, Expertise and Real Estate Management, Voronezh State Technical University
Alexander Sergeevich Bagdasaryan, Researcher of the Institute of Radio Engineering and Electronics, Research Institute Radio
Ivan Ivanovich Popov, Director of the Center for Publication Activity, Voronezh State Technical University
Oleg Igorevich Shevaleevsky, Head of laboratory of solar photoconverters of the Institute of Biochemical Physics. N.M. Emanuel RAS
Gustavo Capannelli, TICASS Consortium (Italy)

Secretaries

Alexander Viktorovich Sergeev; Associate Professor of the Department of Solid State Physics, Voronezh State Technical University

Olga Vladimirovna Jilova Junior Researcher of the Department of Solid-State Physics, Voronezh State Technical University

Secretariat

Vadim Valeryevich Glotov; Leading Engineer of the Office for the Commercialization of Innovative Projects and Developments of the Voronezh State Technical University

Alevtina Sergeevna Samofalova, Engineer of the service of intellectual property, standardization and metrology of the Voronezh State Technical University

2018 International Theoretical and Practical Conference on Alternative and Smart Energy (TPCASE 2018)
ISBN: 978-1-60595-617-6

Rheological Behavior of Model Systems of Resource Matrix Efficient Self-Compacting Concrete

Dmitrii Korotkikh and Yulia Pogorelova

ABSTRACT

This paper considers the problem of resource-intensive production of self-compacting concrete. The possibility of using the by-product of the production of nitrogen phosphorus potash (NPK) in the OJSC "Mineral fertilizers" of the city of Rossosh as a component of self-compacting concrete is assessed. Thus, the article solves the problem associated with resource saving, namely, it proposes an alternative to natural filler in the form of technogenic calcium carbonate, dumps of which occupy a huge area and bring incontestable harm to the environment. The results of experimental studies of water systems "limestone flour + water", as well as "technogenic calcium carbonate + water" are given. The dependence of the water-solid ratio on the amount of the dosage of various additives at a constant viscosity of the systems is established.

INTRODUCTION

The problem of the widespread introduction of self-compacting concrete mixtures is their high cost due to the use of natural mineral fillers, the use of expensive superplasticizers and hyperplasticizers, fractionated aggregates [1-6]. The economic efficiency of widespread use in the construction of self-compacting concrete mixtures (especially concrete with ordinary strength) is largely leveled by an increase in the cost of concrete in comparison with traditional concrete [7-13]. These circumstances limit the widespread use of self-compacting concrete in construction.

In this regard, relevant research aimed at reducing their cost.

There are several ways to solve this problem:

Voronezh State Technical University (VSTU), 84, 20-Letiya Oktyabrya Street, Voronezh, 394006, Russia

- reduction of cement consumption, as an expensive component;- the choice of a rational chemical additive, based on the properties of the mixture;

- replacement of expensive filler for cheaper.

This question should be considered in context with the classification of self-compacting concretes [14-15]:

1) type 1: concrete mixes with a high content of dispersed materials, mainly mineral filler;

2) type 2: concretes with low filler content or without it at all, in this case, the necessary rheological characteristics of the concrete mixture are achieved through the use of special chemical additives—viscosity modifiers;

3) type 3: combined type: in fact, it is type 1 concrete with the use of viscosity modifiers.

Each of these types has its advantages and disadvantages. Type 1 in this sense has advantages since along with the improvement of the rheological properties of concrete mixes, they provide an increase in the physical, mechanical and operational characteristics of concrete. In addition, it has the greatest potential for resource saving, due to large dosages of mineral filler.

Therefore, one of the ways to save natural resources (resource saving), as well as reduce the cost of production of concrete mixes is to replace natural filler with industrial waste [15].

In connection with the above, the article discusses the possible replacement of natural raw materials - limestone flour with mineral filler (powder type) conversion chalk—waste production of chemical fertilizers of JSC “Mineral fertilizers”, Rossosh city (annual accumulation of waste is up to 300,000 tons).

Conversion of calcium carbonate is formed in the technology of nitrogen phosphorus potash (NPK) production in the form of fine powder containing mainly calcium carbonate (the total content of carbonates, in terms of calcium carbonate, is about 95%). And also up to ~ 3% ammonium compounds (in terms of ammonium nitrate), as well as compounds Sr (1.38%), P_2O_5 (0.58%) and SiO_2 (0.49%), SO_4 (<0.1%).

This article discusses a part of the problem of obtaining new compositions of the self-compacting concrete, which is associated with the rheology of water systems based on technogenic calcium carbonate and limestone flour.

MATERIALS AND METHODS

When conducting experiments for the preparation of pastes, technogenic calcium carbonate, waste from the production of chemical fertilizers by JSC Mineral Fertilizers, Rossosh, and limestone powder produced by <<VZMP>> LLC, Voronezh, were used as mineral fillers.

So, these two types of raw materials differ in the method of production, namely, the first is the result of exchange reactions, recrystallization processes in the

production of mineral fertilizers such as nitrogen phosphorus potash (NPK), the second is a product of mechanical transformations of natural raw materials (various kinds of limestone).

The main chemical components of limestone flour are carbonates, so the total mass fraction of CaCO3 + MgCO3 in terms of dry matter is equal to 95.17% (including the proportion of Ca - 37.27%).

As an alternative to limestone flour, technogenic calcium carbonate was considered, the chemical composition and properties of which are presented below. The product corresponds to technical conditions 2144-028-00206486-2008.

Obtaining self-compacting concrete mixtures is impossible without the use of modern additives, which are based on various kinds of polymeric compounds, such as polyaryls, polycarboxylates [16-18].

The work investigated the effect of various kinds of additives on the rheology of flooded systems.

Additives that have been reviewed cover the full range of these products on the market. The remaining uncovered names are just a combination of them.

Types of additives used:

Polyaryls (Polyheed 4030, manufactured by BASF);

Polycarboxylates (Glenium 430, manufactured by BASF);

Lignosulfonates (Centrament P 40, manufactured by MC Bauchemie);

Naphthalene sulfonates (Muraplast FK 48, manufactured by MC Bauchemie).

According to the above, it is advisable to make a study of the rheological characteristics of water systems of technogenic calcium carbonate and limestone flour, as well as the effect of various additives on the characteristics of this system.

To accomplish the tasks set in the work, it is necessary to carry out a dispersion analysis, which will allow a more thorough analysis of the particle size distribution of the used powder type fillers. And also you need to choose the optimal dosage and type of additives used.

Experimental studies were performed using standard and special methods.

The ANALZSETTE 22 Nano Tec laser analyzer was used to determine the dispersed parameters (particle size and particle size distribution functions), particle size distribution and analysis of the shape of technogenic calcium carbonate and limestone flour.

The study of the rheological characteristics of flooded systems (ultimate shear stress and the value of "effective" viscosity) was carried out using a rotational-type viscometer RV-8.

To obtain each of the systems 100 grams of conversion calcium carbonate (or limestone flour) were weighed and placed into a bowl, previously rubbed with a damp cloth. Then a recess was made in the powder, in which water was poured into one intake in an amount calculated on the basis of the specified water-hard ratio. Then 30 seconds after the addition of water, they were stirred until a homogeneous mass was obtained. The additive was introduced with the mixing water. The dosage of the additive was increased until the water-solid ratio ceased to depend on its

quantity, only after that the experiment was stopped. In the study, the fundamental point was to maintain a constant "effective" viscosity when changing the dosage of additives.

RESULTS OF EXPERIMENTAL STUDIES

Disperse analysis of technogenic calcium carbonate and limestone flour was carried out (the studies were carried out at the Center for Collective Use named after Professor YM Borisov of the VSTU (http://ckp-vrn.ru).

From the data of the histogram (Figure 1), it can be seen that the distribution of particles is normal. At the same time, the distribution region for technogenic calcium carbonate can be seen as the interval from 10 nm to 100 nm, while for limestone flour is from 0.5 nm to 50 nm.

Particles of technogenic calcium carbonate are presented in the form of compositions close to spherical shape, which is probably the result of the free growth of CaCO3 crystals during its synthesis during the technological process.

It was established that the conversion of calcium carbonate is represented by a fine powder with an average grain size of ~ 60 μm, for limestone flour this indicator is ~ 10 μm.

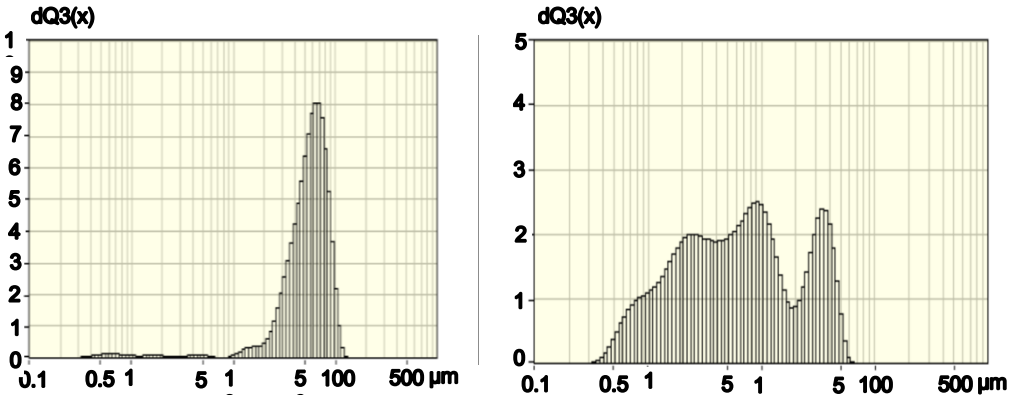

a) b)

Figure 1. Integral histograms of the particle size distribution of the studied powders
a) technogenic calcium carbonate; b) limestone flour.

Taking into account the specificity of the particle size of technogenic calcium carbonate, determined by dispersion analysis, as well as its close to monomineral composition, corresponding to natural raw materials, it was suggested that it can be used as a mineral filler in self-compacting concrete mixtures.

Due to the experiment, the following relationships were obtained for the two systems under study (Figure 2 and Figure 3).

Considering the distinctive relationships obtained for this system, we can conclude that all the considered additives can reduce the water-hard ratio while maintaining a constant value of the "effective viscosity".

It is established that for the system relationships are described by polynomials of the 4th order.

So the additive based on lignosulfonates (Centrament P 40), at a dosage of 1.2% by weight of solids, reduces W/S to a value of 0.316; the naphthalene formaldehyde sulfonic acid condensation product (Muraplast FK 48) reduces W/S to 0.292 in the same dosage; polycarboxylates (Glenium 430) reduce W/S to 0.28; polyaryls (Polyheed 4030) reduce W/S to 0.268.

Thus, a maximum reduction in W/S can be achieved using a polyaryl-based plasticizer. In this case, polycarboxylates are less effective.

Based on the relationships obtained, the optimal dosage is 0.4% by weight of the solid.

In the system of “limestone flour and water,” it is also possible to observe a decrease in the water-solid ratio with the introduction of various kinds of additives into the system.

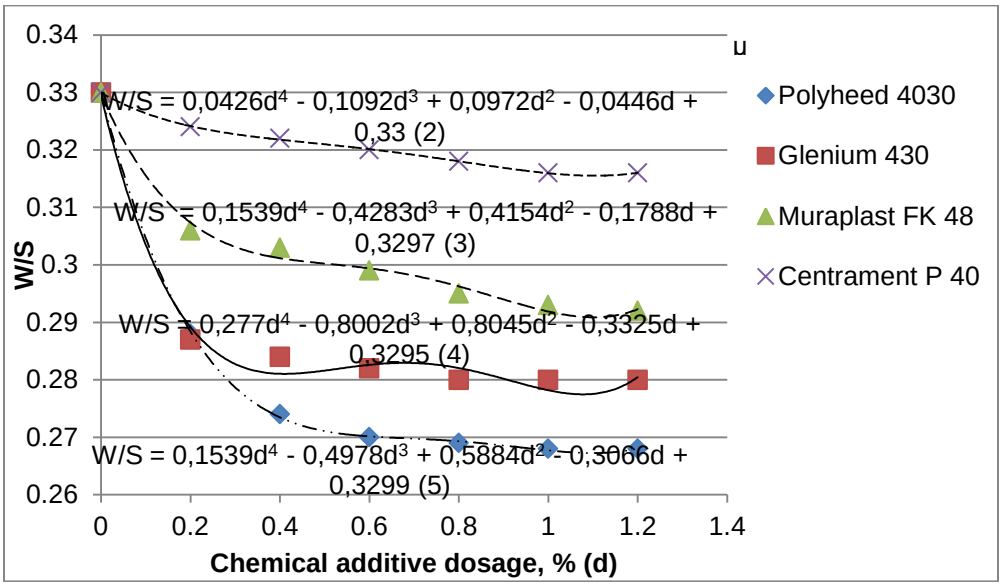

Figure 2. Dependencies of water-solid relationship in the system of calcium carbonate conversion + water.

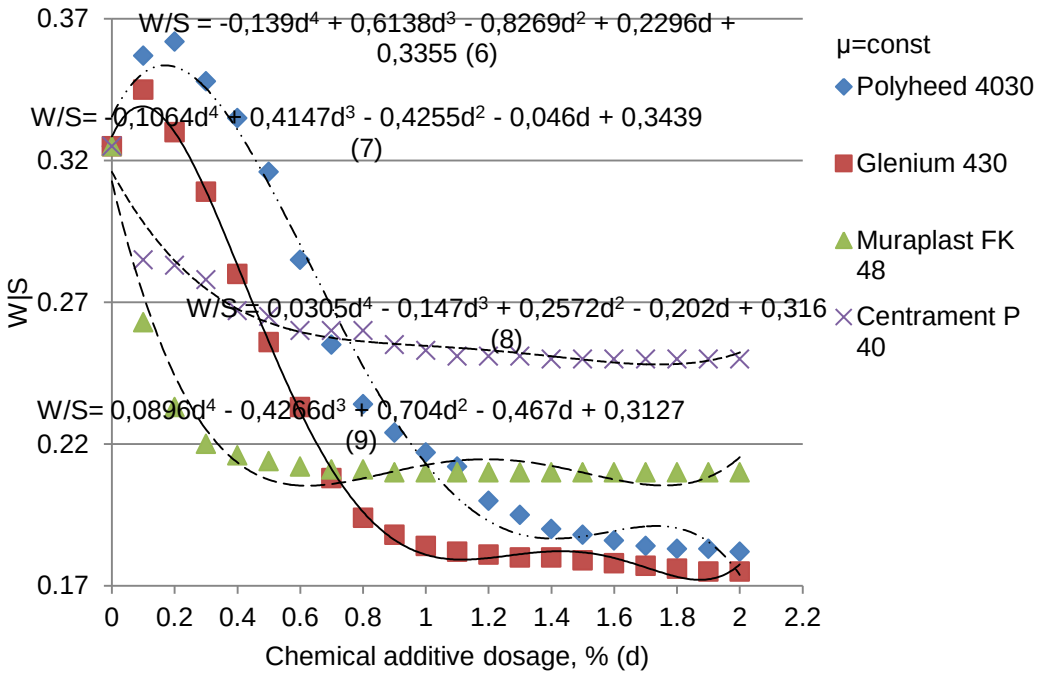

Figure 3. Dependencies of the water hard relation of the system limestone flour + water.

However, unlike the first system, with the introduction of small dosages of additives such as Polyheed 4030 (polyaryls) and Glenium 430 (polycarboxylates), an increase in the water-solid ratio occurs, perhaps due to the fact that limestone flour has a higher dispersion.

It was also found that relationships that can be described by fourth-order polynomials are characteristic of this system.

Additives based on polyaryls and polycarboxylates are more effective in the "limestone flour + water" system since their use allows a lower water-solid ratio to be obtained because the former reduce W/S to 0.182 and the latter to 0.175. The condensation product of naphthalene formaldehyde sulphonic acid (Muraplast FK 48) reduces W/S to 0.21. Additive based on lignosulfonates (Centrament P 40) - up to 0.25.

In this system, based on the obtained relationships, it is optimal to use an additive based on polycarboxylates at a dosage of 1% by weight of solid matter.

CONCLUSIONS

The obtained data on the dispersed composition of limestone flour and technogenic calcium carbonate in the future will allow the selection of the optimal composition of the concrete mix on the latter, which will make it possible to abandon the expensive natural filler.

Mathematical models describing the relationship of the water-solid ratio on the mass fraction of the additive, which can be described by fourth-order polynomials, have the following form:

$$W / S = a \times d4 + b \times d3 + c \times d2 + f \times d + k \quad (1)$$

This model allows one to choose the optimal dosage of the additive for various systems.

The optimal dosages of the studied additives were found, which will be used in the future for the selection of concrete mixtures.

REFERENCES

1. Okamura, H., and M. Ouchi. 1998. "Self-compacting high performance concrete," *Progress in Structural Engineering and Materials*, 1(4): 378-383.
2. "The European Guidelines for Self-Compacting Concrete: Specification, Production and Use" *SCC European Project Group*, May 2005.
3. Collepardi, M. 2003. "Innovative Concretes for Civil Engineering Structures: SCC, HPC and RPC," in *Proceedings of the Workshop on New Technologies*, pp. 1-8.
4. Collepardi, M. 2003. "Self-Compacting concrete: what is new?" in *Proceedings of Seventh CANMET / ACI Intern. Conf. on Superplasticizers and Other Chemical Admixtures In Concrete*, pp. 1-16.
5. Collepardi, M., Ogoumah Olagot, J.J., Skarp, U., and Troli R. 2002. "Influence of Amorphous Colloidal Silica on the Properties of Self-Compacting Concretes: Challenges in Concrete Construction," in *Proceedings of the Intern. Conf.*, pp. 473-483.
6. Vivek, S.S., and Dhinakaran G. 2015. "Condensation of silica fume," *International Journal of Chem. Tech. Research*, 8 (1): 1-5.
7. Madandoust, R., M.M. Ranjbar, R. Ghavidel, and S.S. Fatemeh. "Assessment of factors of steel fiber reinforced self-reinforced concrete," *Materials & Design*, 83: 284-294.
8. Jiang Yu. C., D. Huo, H.W. Teng, J. Xu. 2015. "A study of the coarse aggregate on the rheological properties of self-compacting," *Key Engineering Materials*, 633 (Testing and Evaluation of Inorganic Materials V):130-135.
9. Bazhenov, Yu. M., Demyanova, V.S., Kalashnikov, V.I. 2006. *Modified high quality concretes.* Scientific publication. Publishing house DIA, Inc., 368 p.

2018 International Theoretical and Practical Conference on Alternative and Smart Energy (TPCASE 2018)
ISBN: 978-1-60595-617-6

Simulation of the Energy Efficiency Dependence on Threshold Voltage in the CMOS Inverter

Aleksei Arsentev, Ekaterina Plotnikova and Maxim Harchenko

ABSTRACT

In this work, we show the CMOS inverter sensitivity of the threshold voltage on the channel doping in dynamic mode. Simulated transient response of the inverter determines the propagation delays for the high-low and low-high transitions. Current emissions at the time of switching were reduced by optimizing the channel impurities. According to the simulation results, it is possible to estimate the efficiency of energy saving depending on the threshold voltages of NMOS and PMOS transistors in the CMOS inverter.

Keywords: CMOS; Inverter; Channel Doping; Threshold Voltage; Leakage Current; Efficiency

INTRODUCTION

All electronic devices consume electrical energy, converting it into heat, but the turnaround efficiency is different. While less electricity is spent without conversion to useful work, then the device is more efficient. If we are talking about digital devices, they have electrical parameters such as performance per watt or number of operations per watt (FLOPS per watt). By increasing these parameters, we form a more efficient digital device [1].

Aleksei Arsentev, Ekaterina Plotnikova, VSTU, 14, Moskovsky Avenue., Voronezh, 394026, Russia
Maxim Harchenko, VZPP-S, 199a, Leninsky Avenue, Voronezh, 394033, Russia

In logic, “negation”, also called the logical complement, is an operation that takes a proposition P to another proposition "not P", written NOR P, which is interpreted intuitively as being true when P is false, and false when P is true (turning logical 0 into 1 and vice versa). So we can estimate the electrical efficiency at the cost of this operation [2]. Logical operation NOR corresponds to the “inverter” circuit element. The electric power is dissipated in two fundamentally different modes - static and dynamic (transient) in inverters.

TECHNOLOGICAL MODELING CMOS INVERTER

The conventional planar inverter consists of two complementary MOS transistors connected by drains and having common gates. The NMOS source is grounded (vdd); the PMOS source is connected to a power source (vss). The substrates of both transistors are connected to the respective sources.

The article simulates an inverter created using CMOS technology. It consists of n-channel and p-channel LDD (Lightly Doped Drain) field effect transistors (FETs). Technological norms of the device under study are 60 nm [3]. The standard technological operations and the specified geometric parameters allow the creation of the required inverter circuit. Additional data, such as the concentration of impurities and the boundaries of the p-n-junctions, are shown in Figure 1. This CMOS inverter design is a typical planar structure based on LDD field effect transistors.

THRESHOLD VOLTAGE VT MODELING

Classical field-effect transistors have 2 types of the threshold voltage. To measure unsaturated threshold voltage of the NMOS (PMOS) transistor, it is necessary to apply a positive (negative) offset to the drain (port vee) equal to - 0.05 V, then apply a positive (negative) voltage to the gate (port vgg) in the range from 0 to - 1.33 V, respectively.

To measure saturated threshold voltage of the NMOS (PMOS), it is necessary to apply a positive (negative) offset to the drain (port vee), equal to - 1.33 V (circuit supply voltage), then apply a positive (negative) voltage to the gate (vgg port) to range from 0 to - 1.33 V, respectively.

The results of the extraction of field-effect transistors Vt are shown in Table I.

TABLE I. VARIABLES HISTORY FOR PMOS AND NMOS MODELING.

Threshold voltage mode	NMOS	PMOS
Vt unsaturated, V	0.53	0.52
Vt saturated, V	0.46	0.42

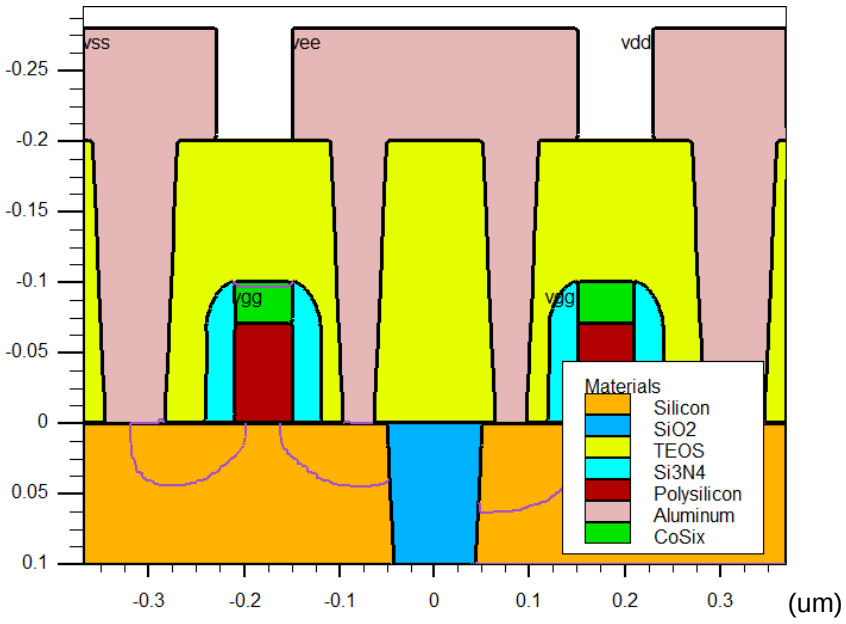

(a)

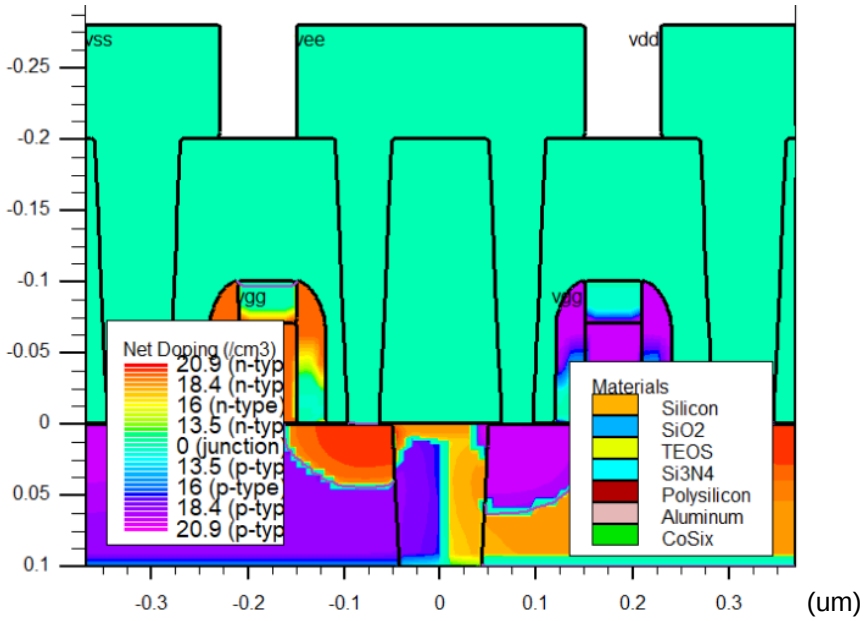

(b)

Figure 1. Cross section showing (a) the matherials and (b) the distribution of impurity concentrations by inverter structure with mapping of the border of p-n-junctions.

RANSIENT RESPONSE OF THE CMOS INVERTER

The assumption of the zero rise and fall times of the input waveforms is not correct. The finite slope of the input signal causes a direct current path between VDD and GND for a short period of time during switching, while the NMOS and the PMOS transistors are conducting simultaneously. The mechanism of power dissipation is due to the fact that at a certain time interval a channel with low resistance is formed between the power and ground terminals. A large current flows and heat are dissipated through this channel. This happens at the moment when the NMOS transistor is not completely closed, and the PMOS transistor is already opening and vice versa. Obviously, the faster one transistor opens and the other closes, the smaller the time interval in which a large current flows between the power supply and the ground. The less electricity is converted to heat. Reducing the switching time and, accordingly, minimizing current consumption peaks is a method of optimizing the inverter.

There are three methods for optimizing Vt in MOS.

The first is channel doping by ion implantation (i.e. P impurity). This method doesn`t work good on the submicron transistor sizes.

The second method is using high-k dielectrics.

The third is using a complex gate structure with Ti (n-type) or Mo (p-type) sublayers. Thus, the work function of the gate material is changed, which is equivalent to a change in the concentration of impurities in the channel.

In this research, we analyze the channel doping dependence of power dissipation in 60 nm inverter.

To obtain the transient response of the CMOS inverter, we perform a tran (time) analysis, changing the input voltage (vgg port), and measuring the output voltage (vee port) (Figure 2). The vdd port is powered with a supply voltage of 1.33 V, and the vss port is grounded.

Setting the threshold voltages of the FETs was carried out by the channel doping. Ion implantation of phosphorus with a dose of $0.65 / (1.6 \times 10^{-13})$ cm^{-2} and an energy of 2 keV was used. The dose of doping was chosen experimentally.

RESULTS AND DISCUSSION

Initially, both transistors have different threshold voltages, but after doping the threshold voltage of one of them decreases (NMOS), and the other increases (PMOS). At a certain point in time, the threshold voltages become equal. So the transistors in the CMOS inverter become balanced.

When switching a balanced inverter, the opening and closing of the transistors occur synchronously, and the flowing currents have the same values both at the time of switching from 1 to 0 and at the time of switching from 0 to 1. If the

threshold voltages are not optimized, the current in one of the operations will be higher than in a balanced state.

Since the power dissipation depends on I^2, the task of minimizing power consumption consists in reducing the flowing currents in the inverter (in this experiment all other conditions are being equal).

Figure 4 illustrates that the green curve of the flowing current has the same level both when switching along the signal front at the input of the inverter and at the cutoff. At the same time, the red and orange lines illustrating the unbalanced threshold voltages of the transistors, in one of the cases, have a higher level, and in the other, much lower than in a balanced state.

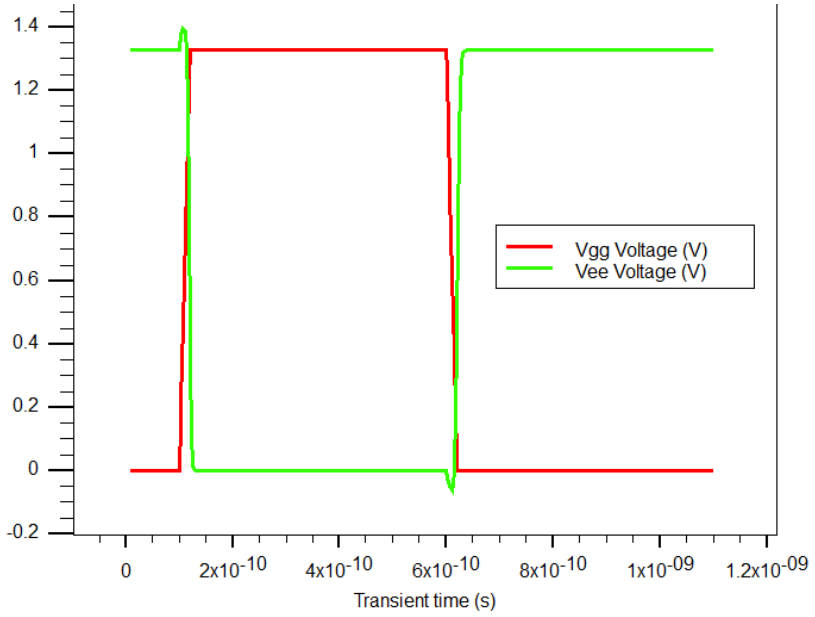

Figure 2. Transient simulation of CMOS inverter.

CONCLUSION

A CMOS inverter structure was formed according to 60nm design standards in technological CAD. Simulation of the CMOS inverter was performed, and the dynamics of transient output current and voltage characteristics were determined.

The simulation of the CMOS inverter operation in the technological CAD system was carried out. The currents and voltages time dependence at the moment of the switching were constructed. The relationship between power consumption and speed was shown. The doping value dependence became one of the most effective methods for “balancing” the threshold voltages for an inverter`s transistors couples.

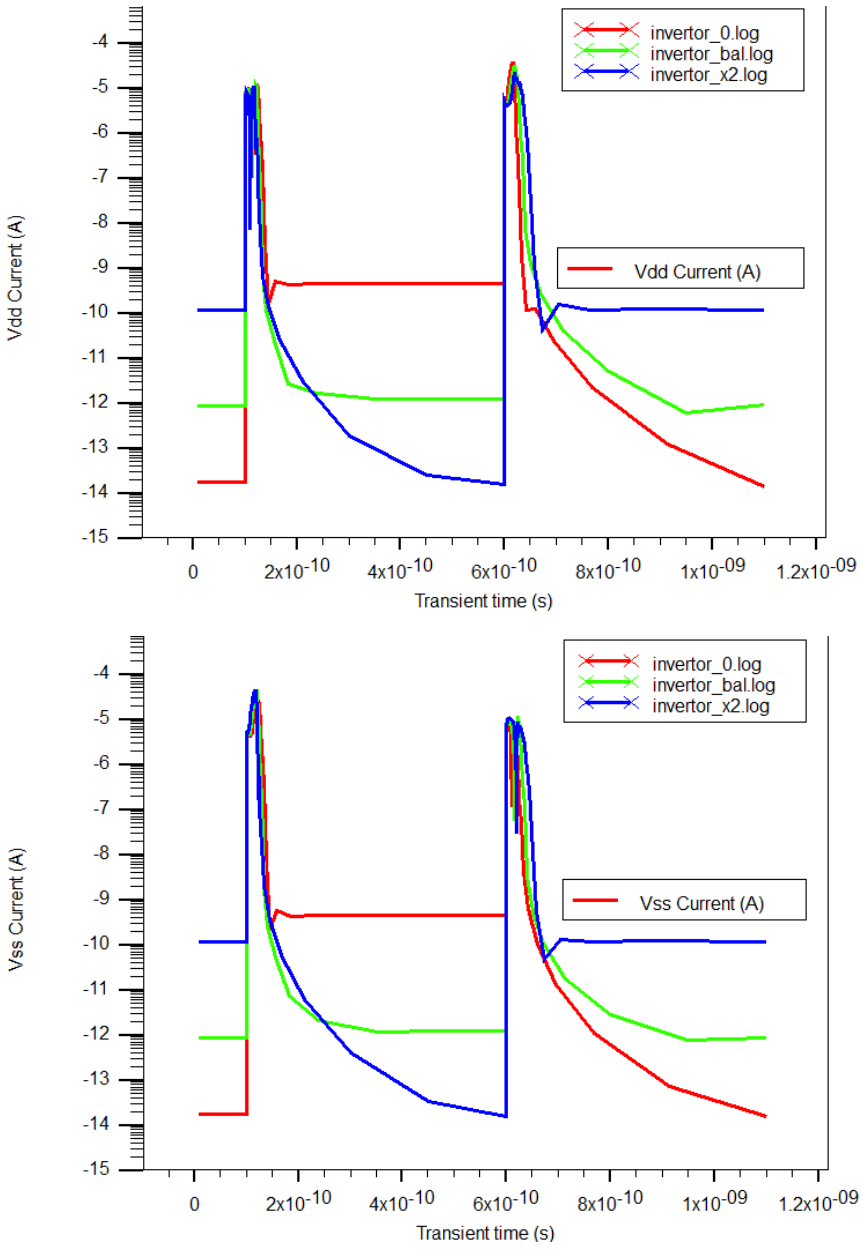

Figure 3. CMOS inverter short-circuit current at the time of swithing from 0 to 1 and from 1 to 0.

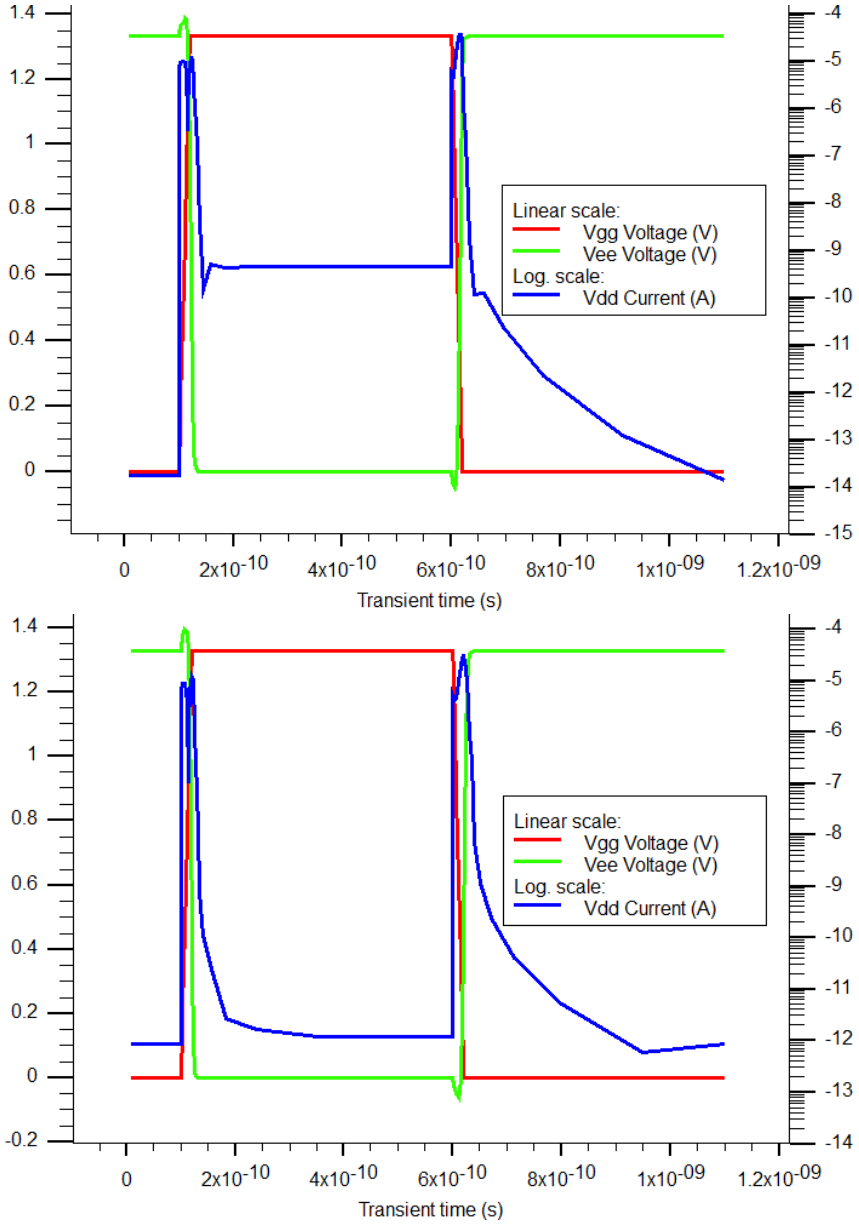

Figure 4. Current and voltage time dependence of CMOS.

REFERENCES

1. Uyemura, J. P. 2002. *CMOS design, layout and simulation.* Kluwer Academic Publishers.
2. Baker, R. J., Li, H. W., Boyce, D. E.1998. *CMOS design, layout and simulation.* IEEE Press, Chapters 3 and 4, www.ieee.org.
3. Razavi B. 2001. *Design of analog CMOS integrated circuits*. McGraw-Hill, www.mhhe.com.

2018 International Theoretical and Practical Conference on Alternative and Smart Energy (TPCASE 2018)
ISBN: 978-1-60595-617-6

Investigation and Development of a Thermoelectric Generator Heat Transferring System Based on a Ring Geometry Semiconductor Batteries

Igor Drozdov, Dmitry Shmatov, Alexander Afanasyev, Tatyana Timoshinova and Artem Chuiko

ABSTRACT

Key requirements for heat transfer systems design of thermoelectric generator modules with ring geometry semiconductor batteries are given in this article. It is established that a maximum value of extreme heat flux of the heat transfer system is determined by two factors: crisis phenomena and extreme volumetric steam content.

INTRODUCTION

Thermoelectric generator module (TEGM) is the main structural element of an autonomous thermoelectric current source (ATCS). TEGM is designed to provide direct conversion of thermal energy into electrical energy through burning natural gas [1].

Conceptually, the most rational heat transfer system of TEGM is a gravitational heat pipe—thermosyphon. On a basis of such system, both thermoelectric batteries (TB) heat supply system (heating system) to and a heat removal system (cooling system) [2] can be implemented.

The operation principle of a thermosyphon as part of a TEGM is schematically represented in Figure 1 on the example of a heating system (HS). A number of

Igor Drozdov, Dmitry Shmatov, Alexander Afanasyev, Tatyana Timoshinova, Department of Rocket Engine, Voronezh State Technical University, 14 Moskovsky Avenue, Voronezh, 394026, Russia
Artem Chuiko, AO RIF, 17/2 Dorozhnaya Street, Voronezh, 394062, Russia

key requirements are set to the main elements of the TEGM heat transfer system, described below.

The heat receiver of the evaporation zone of a thermosyphon is designed to warm the heat transfer fluid with combustion products coming from the burner. The heat receiver must:

- warm the heat transfer fluid in thermosyphon effectively, i.e. to provide a low temperature of the combustion products at an outlet of the heat receiver chamber;
- prevent local overheating of the heat transfer fluid;
- have a system that removes combustion products from the heat receiver chamber.

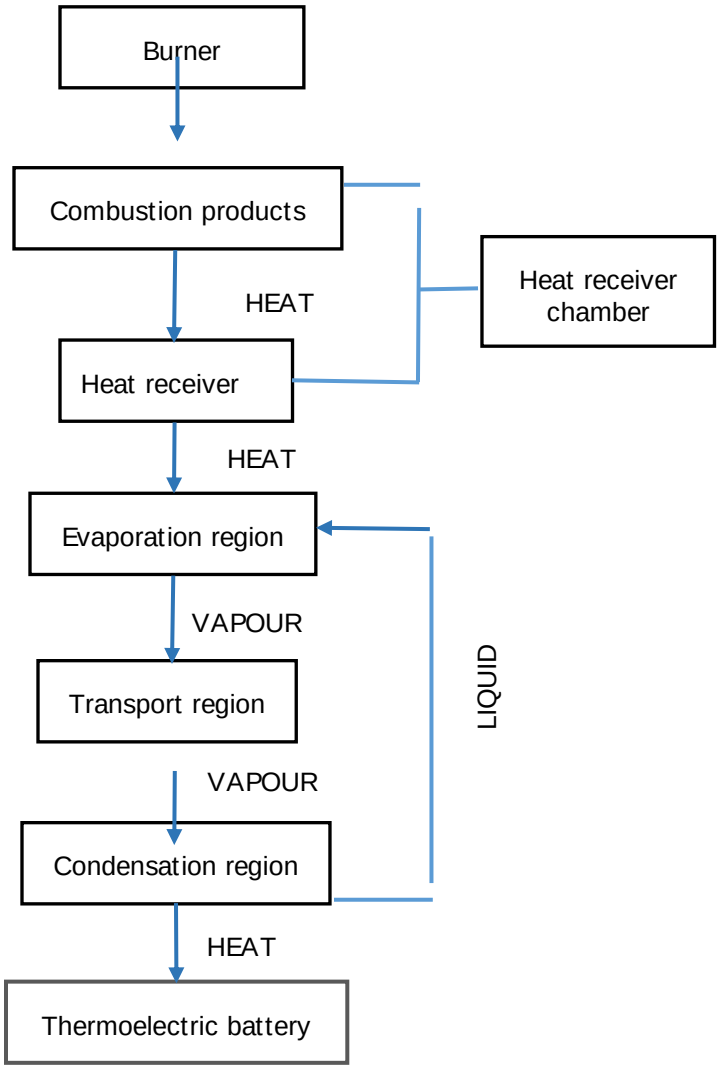

Figure 1. Scheme of the heat transfer HS elements of TEGM

The heat receiver together with the combustion products form a heat receiver chamber used to isolate the combustion products from the external environment. The heat receiver chamber should provide the most efficient heat exchange between the combustion products and the heat receiver.

A thermosyphon is a link that directly transfers heat to a block of TB. A region of heat transfer fluid flow in a thermosyphon can be divided into three subregions – an evaporation region, a transport region and a condensation region.

The evaporation region interacts with the heat receiver, which supplies heat from the burner. The heat transfer fluid boiling occurs in the evaporation region, and then vapors of fluid are transporting to the condensation region along the transport region. Due to the latent heat of vaporization, a small mass flow rate of heat transfer fluid vapor provides a significant amount of heat flow transfer.

Vapor changes its aggregation state to liquid in the condensation region and returns to the evaporation region under the action of capillary forces or gravity.

Basic requirements that must be set to a thermosyphon are:

- to provide a uniform temperature field along the length of the condensation region;
- to provide easy start-up of a TEGM;
- minimization of non-condensable gases production;
- to provide stable operation of the thermosyphon in a control range of the TEGM.

The stability of the thermosyphon itself will determine the compliance of the heat transfer system with the requirements stated above. Based on theoretical and experimental studies [3] of the stability of a liquid and vapor countercurrent flow, five types of crisis phenomena of this type heat transfer systems can be distinguished. The corresponding calculation equations are given in Table I. In these ratios, Bo – is the Bond number, y_0 – is the film thickness, δ – is the capillary constant, Y – is the film thickness criterion, K_p – is the pressure criterion allows the compressibility of a heat transfer fluid.

In addition to the crisis phenomena, another factor determining the performance of a thermosyphon is the extreme heat flux transmitted by thermosyphon [4, 5]. The basic equations that can be used for determination of extreme heat fluxes are considered below.

TABLE I. CALCULATION EQUATIONS FOR CRISIS PHENOMENA.

Type of crisis phenomenon	Calculation equation	Ranges of application
Achieving the maximum thickness of the liquid film	$K = \frac{\pi Bo^{0.5}}{\left(986\gamma^2\left(y_0/\delta\right)^2 + 0.962Bo\right)^{0.5}}$, где $\gamma = 3.6$ $\gamma = 5.71\cdot 10^3 Y^{1.8}$	$Y < 0.016$ $Y > 0.016$
Beginning of droplet breakaway	$K = \frac{\pi Bo^{0.5} f\left(K_p\right)}{\left(234\gamma^2\left(y_0/\delta\right)^2 + 0.962Bo\right)^{0.5}}$, где $\gamma = 3.6$ $\gamma = 0.5\left(Y/Ka^{1/12}\right)^{-0.5}$ $f\left(K_p\right) = \begin{matrix}4.06K_p^{-0.17}\\0.67\end{matrix}$	$Y/Ka^{1/12} < 0.019$ $Y/Ka^{1/12} > 0.019$ $K_p < 4\cdot 10^4$ $K_p > 4\cdot 10^4$
Liquid film hanging	$K = \begin{matrix}8.19K_p^{-0.17}\\1.35\end{matrix}$	$K_p < 4\cdot 10^4$ $K_p > 4\cdot 10^4$
Ejection of fluid from the flow core	$K = \begin{matrix}10.24K_p^{-0.17}\\1.7\end{matrix}$	$K_p < 4\cdot 10^4$ $K_p > 4\cdot 10^4$
Complete termination of downward fluid flow	$K = 3.2$	

To determine the surface density of the heat flow for thermosyphons with $d/l_н < 0{,}2$, the calculated-experimental relations are used:

$$q_F^{np} = 0.8r\rho_n^{0.5}\left(\sigma g\left(\rho-\rho_n\right)\right)^{0.25}\left(d/l_н\right)\left(th\left(\frac{Bo^{0.25}}{2}\right)\right)^2\left(1+\left(\rho_n/\rho\right)^{0.25}\right)^{-2} \quad (1)$$

$$q_F^{np} = 0.09r\rho_n^{0.5}\left(\sigma g\left(\rho-\rho_n\right)\right)^{0.25}\left(d/l_н\right)^{0.9} Bo^{0.5}\left(1+\left(\rho_n/\rho\right)^{0.25}\right)^{-2} \quad (2)$$

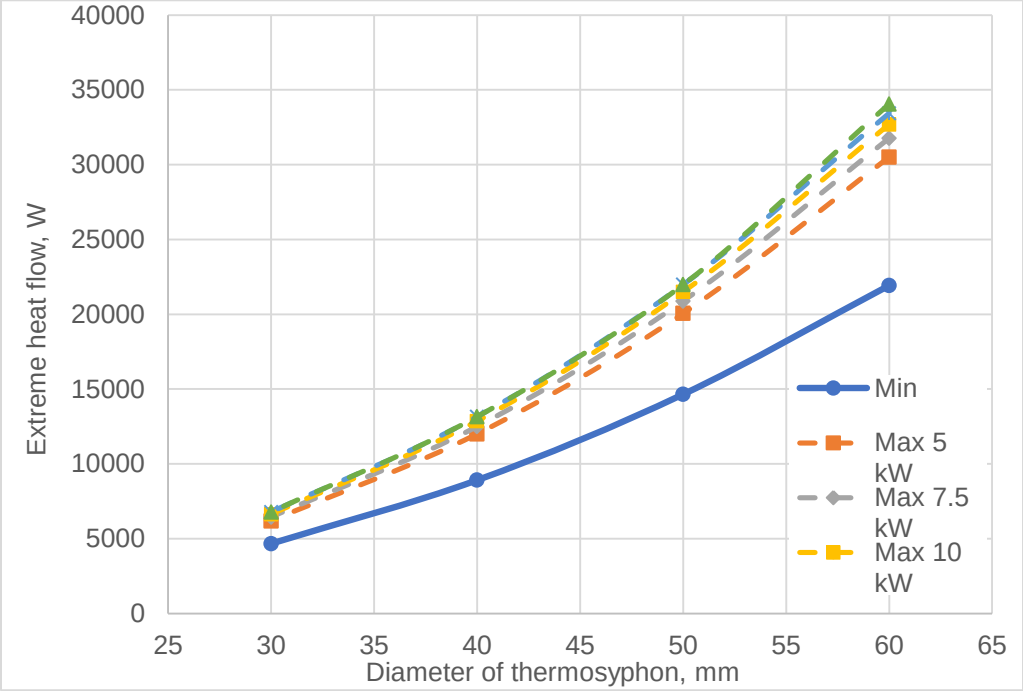

Figure 2. Extreme heat flow of TEGM HS.

During the analysis of optimization calculations of thermoelectric batteries of ring geometry, it was established that the area of TB maximum efficiency limits the maximum diameter of the thermosyphons HS at the range below 60 mm. Based on these geometric constraints, in accordance with relations (1) and (2), the region of extreme heat flow of the thermosyphons HS with water as heat transfer fluid was constructed. Relation (1) sets the lower limit of heat flows, and relation (2) sets the range of upper limits (Figure 2).

It is necessary to associate the operating mode of the thermosyphon with the type of extreme heat flow. Usually, the mode of operation is associated with the structure of a two-phase system in a device cavity, depending on the relative amount of the liquid heat transfer fluid phase. In this case, there are two main modes: the mode of a flowing liquid film and the bubbling mode.

The dependence of the stability criteria of the vapor-liquid system for different heat flows supplied to the heat receiver, depending on the diameter of the thermosyphon, is shown in Figure 3. Analysis of the obtained values showed that the extreme heat flux calculated by the formula (1) may be associated with the beginning of the first crisis of the heat transfer system in accordance with table 1. In the considered range of heat flows and diameters of thermosyphon other crises cannot be reached.

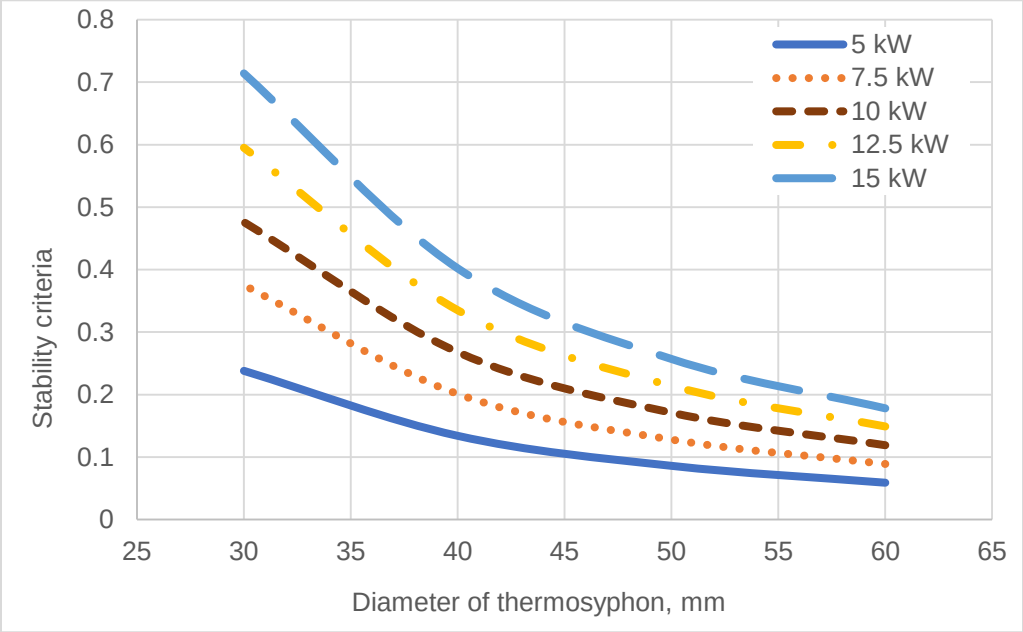

Figure 3. Stability criteria for different heat flows.

The upper limit of the extreme heat fluxes, calculated from the relation (2), thus cannot be correlated with the achievement of another systems crisis. It was assumed that extreme heat flux might be associated with the regime of flow of the heat transfer fluid in the evaporator, or rather with the integral value of an extreme volumetric steam content.

The equation for determination of the volumetric steam content $\bar{\varphi}$ should be sufficiently universal, taking into account the speed of ascent of bubbles in both large and small diameter pipes and use the critical speed of movement of bubbles and droplets in liquid and gas media as a speed scale. The first requirement can be satisfied due to the magnitude of the interaction factor ψ. Taking into account the possible influence on the process of bubbling of liquid viscosity, the interaction factor ψ in the general case should have the form of a function depending on the Bond and Archimedes numbers [6, 7].

On the basis of relation (3), the dependence of the volumetric steam content on the diameter of the thermosyphon was studied at different heat fluxes supplied to the system.

$$\bar{\varphi} = \frac{1}{1 + \dfrac{W^*}{W_O^{\Pi}\psi\left(Bo, Ar\right)}} \tag{3}$$

The results of the generalization of the study can be presented in the form of the dependence of the extreme volumetric steam content on the extreme heat flow, shown in Figure 4. Thus, the upper limit of the extreme heat flux correlates with the volumetric steam content as a linear relationship. The linear growth of $\bar{\varphi}$ may be associated with the fact that increasing of the thermosyphon diameter leads the bubbling process to boil a large volume.

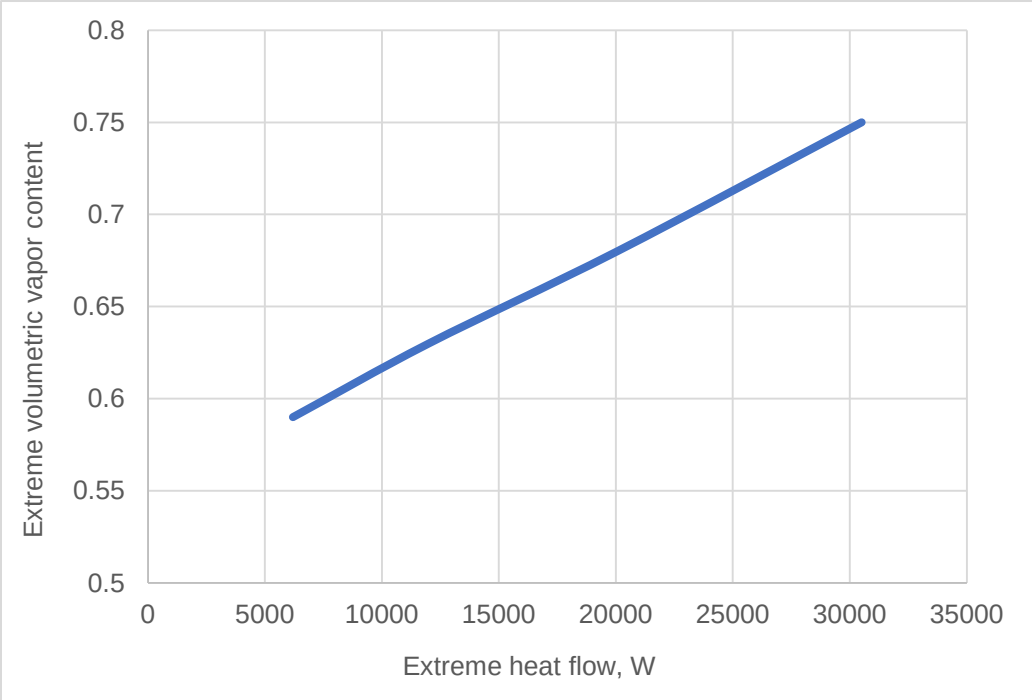

Figure 4 Extreme volumetric vapor content, depending on extreme heat flow

CONCLUSION

According to the results of the analysis of parameters of the heat transfer system of TEGM based on ring geometry TB, the limiting heat fluxes of HS were obtained. The lower limit of the extreme heat flux may be associated with the achievement of the maximum thickness of the liquid film, the upper limit with the achievement of the extreme volumetric steam content in the evaporator of a thermosiphon.

ACKNOWLEDGEMENTS

The work was done with the financial support of the Ministry of Education and Science of the Russian Federation under the Decree of the Government of the Russian Federation from April 9, 2010 № 218 (Contract № 03.G25.31.0246).

REFERENCES

1. Shmatov, D.P., I.E Sviridov., and T.S. Timoshinova. 2017. "Determination of optimization approaches in the design of a burner of an autonomous current source based on a thermoelectric generator module of ring geometry," *J. VSTU Bulletin*, 13(6): 52-57.
2. Kruzhaev, K.V., D.P. Shmatov, K.V. Zubarev, and I.G. Perevezentsev. 2018. "Determination of optimization approaches in designing a cooling system for a gas thermoelectric generator module," *J. VSTU Bulletin*, 14(3): 93-100.
3. Bezrodny, M.K., Pioro, I.L., and Kostyuk, T.O. 2005. *Transfer processes in two-phase thermosyphons. Theory and Practice*. Fact, Inc.,704 p.
4. Shiraishi, M. 1987. "Influence of the thermosyphons," *Prep. 6lh int. Heat Pipe Conf,*, Grenoble, France, pp. 609-613.
5. Tien, C.L., and K.S. Chung. 1979. "Entrainment limits in heat pipes," *J. AIAA*, 17: 643-646.
6. Labuntsov, D.A., I. P. Kornyukhin, and E. A. Zakharova. 1968. "Vapor content of a two-phase adiabatic flow in vertical channels," J. *Thermal Engineering*, 4: 62-67.
7. Kutateladze S.S., and Styrikovich M.A. 1976. *Hydrodynamics of gas-liquid systems*. Moscow, Inc., 296 p.

2018 International Theoretical and Practical Conference on Alternative and Smart Energy (TPCASE 2018)
ISBN: 978-1-60595-617-6

Computer Simulation of Systems of Axisymmetric Current-Carrying Superconducting Multi-Connected Bodies by the Method of Integral Equations

Igor Bataronov, Leonid Bataronov, Genadiy Shunin, Sergey Kostryukov and Vadim Peshkov

ABSTRACT

The system of integral equations for surface currents of superconductors is obtained on the basis of the condition of magnetic flux conservation in the superconductor circuit for the axisymmetric system of superconducting bodies. The equations of the system have weakly singular kernels. A numerical method for solving model equations is developed using the method of singularity location. The study of the numerical model showed its correctness and convergence. However, there is a poor conditionality of the numerical model. On the example of the three-body problem, it is shown that with the number of sampling points about 100 on the contour of each body the calculation accuracy is 0,1%. It is noted that in comparison with the finite element method the number of degrees of freedom decreases by an order of magnitude.

Keywords: current-carrying superconducting systems, integral equations, computer simulation.

INTRODUCTION

Modeling of superconducting current-carrying structural elements of superconducting energy devices [1,2] can be carried out by means of integral equations for surface current densities [3-7].

Voronezh State Technical University, 14 Moskovsky Avenue, Voronezh, 394026, Russia

The integral model can be theoretically constructed for an arbitrary system of superconducting bodies in the Meisner state on the basis of boundary conditions for the magnetic field at the body surface [8]:

$$\vec{n} \times \vec{H}_t = \vec{i}, H_n = 0,$$

where $\vec{i}$ – surface current density, $\vec{n}$ – unit vector of the external normal to the surface of the superconductor. The expression of the magnetic field here through the surface current density using the known integral relations [9] leads to a system of integral equations for the surface current densities. However, the kernel of the obtained integral equations is the double layer potential, which gives a discontinuous solution on the integration surface. Therefore, the numerical solution of such equations encounters significant difficulties, practically excluding the possibility of their real use.

FORMULATION OF THE GENERAL MATHEMATICAL MODEL

The situation is significantly simplified in the case where it is possible to put boundary conditions directly on the vector potential $\vec{A}$, since the core of the obtained integral equations will be the potential of a simple layer, and its solution will be a continuous function on the integration surface. This, in particular, is the case for a system of bodies obtained by rotating the system of their cross sections around one common axis Oz, that is, the axisymmetric system of bodies. From the symmetry of the problem, in this case, it follows that in the cylindrical coordinate system, only the components H_ρ and H_z of the magnetic field and, accordingly, only the component A_φ of the vector potential will be different from zero. The boundary condition for it on the surface of the *k*-body follows directly from the condition of preserving the magnetic flux in the superconductor circuit, that is, equal to zero of the magnetic field inside the superconductor [10]:

$$A_\varphi^{(k)} = \frac{\Phi_k}{2\pi\rho_k}. \qquad (1)$$

Here Φ_k is flux through *k*-body contour, ρ_k is the radial cylindrical coordinate on the surface of this body.

In turn, the full vector potential can be represented as a sum of vector potentials of surface currents of all bodies [10]

$$A_{\varphi}^{(\text{int})} = \frac{\mu_0}{2\pi} \oint_C J_{\varphi}(\rho', z') \sqrt{\frac{\rho'}{\rho}} f(m) dl', \tag{2}$$

and the vector potential of the external magnetic field, which, for example , for a uniform magnetic field parallel to the axis Oz, has the form

$$A_{\varphi}^{(\text{ext})} = \frac{\rho B_0}{2}, \tag{3}$$

where μ_0 is permeability of vacuum, $\vec{J}$ is surface current density, B_0 is induction of external homogeneous magnetic field,

$$f(m) = \frac{1}{\sqrt{m}} \left[(2-m)F(m) - 2E(m) \right], \tag{4}$$

Here F and E are full elliptic integrals of the first and second kind with the parameter

$$m = \frac{4\rho\rho'}{(\rho+\rho')^2 + (z-z')^2}, \tag{5}$$

and C is the contour of the cross section of superconductor.

As a result, the system of integral equations for surface currents of superconductors converted to symmetric kernel will have the form:

$$\sum_{n=1}^{K} \oint_{C_n} Q(l, l') J_n(l') dl' = \frac{\Phi_k}{\mu_0} - \frac{\pi \rho_k{}^2 B_0}{\mu_0}, \quad k = 1..K. \tag{6}$$

Here C_n is the contour of the cross section of the n-body, K is the number of connected bodies, and the kernel Q is determined by the formula

$$Q(l, l') = \sqrt{\rho\rho'} f(m). \tag{7}$$

The system (6) is a system of Fredholm integral equations of the first kind. However, the kernel (7) has a logarithmic singularity when $l = l'$, therefore, the usual methods of discretization to the system (6) are not applicable, and the development of a special algorithm for discretization of the system of integral equations is required.

SAMPLING AND STUDY OF THE MATHEMATICAL MODEL

On each contour C_n we choose a system of N_n equidistant points that divide the contour C_n into N_n segments. We denote the value of the surface current density in the middle of these segments as $J_i^{(n)}$.

To preserve the symmetry of the kernel when sampling we are to compute the kernel $Q(l,l')$ in the same points over two variables l and l'. However, the kernel is increasing to infinity at $l \to l'$, but it is integrable in the neighborhood of this point. Therefore, we use the singularity extraction method [11] to approximate the integral in (6). As a result, we obtain a system of linear algebraic equations

$$\sum_{n=1}^{K} \Delta l_n \sum_{i=0}^{N_n-1} Q_{j,i}^{(n,k)} J_i^{(k)} = \frac{\Phi_k}{\mu_0} - \frac{\pi\left(\rho_j^{(k)}\right)^2 B_0}{\mu_0}. \qquad (8)$$

Here the matrix elements of the interaction of the currents are determined by the expressions

$$Q_{i,j}^{(n,k)} = \begin{cases} \rho_j^{(k)}\left(\ln\dfrac{16\rho_j^{(k)}}{\Delta l_k} - 1\right), & i = j \wedge n = k \\ \sqrt{\rho_i^{(n)}\rho_j^{(k)}}\, f\left(\dfrac{4\rho_i^{(n)}\rho_j^{(k)}}{(\rho_i^{(n)}+\rho_j^{(k)})^2 + (z_i^{(n)} - z_j^{(k)})^2}\right), & i \neq j \vee n \neq k \end{cases}. \qquad (9)$$

The solution of the model (8.9) we perform on the example of a ring with a circular cross section with radius *a*, ring radius is *b*. The result of calculating the density distribution of the superconducting current along the perimeter of the ring section at the parameters b = 20 mm, a = 10 mm, $\Phi = -1\cdot10^{-7}$ Wb, $B_0 = 1{,}5\cdot10^{-4}$ T and N = 100 is shown in Figure 1 in polar coordinates.

The magnetic field induction was calculated using the formulas

$$B_\rho = -\frac{\partial A_\varphi}{\partial z}, \quad B_z = \frac{\partial A_\varphi}{\partial \rho} + \frac{A_\varphi}{\rho}, \qquad (10)$$

where the vector-potential component A_φ is expressed by formulas (2) and (3). The result of the induction calculation is also shown in Figure 1.

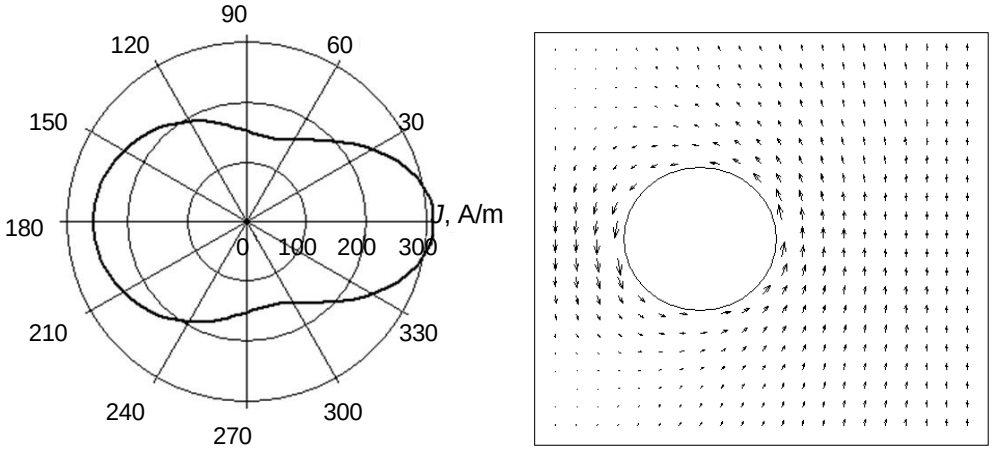

Figure 1. The estimated distribution of the surface current density on the surface of the ring and the distribution of the magnetic field for a circular ring shape.

On the base of the results of the surface current calculation we can found macro-characteristics of the system – the coefficient of inductance L and the force $\vec{F}$ acting on given superconducting body:

$$L = \left.\frac{\Phi}{I}\right|_{B_0=0}, \qquad F_z = \pi\mu_0 \oint_C \rho(l) J^2(l) n_z(l) dl \tag{11}$$

where I is total current in the ring, found by integrating the surface current density.

To check the stability of the calculation and the convergence of the model, calculations were carried out with a doubling number of steps to determine the condition number ν of the matrix (9) in the infinity and Euclidean norms, the inductance of the ring and the force acting on the ring in the external field. The latter must be zero for a uniform field, so the deviation of the calculated value of the force from zero indicates the asymmetry of the found distribution of the superconducting current density. The results of the study are presented in Table I.

TABLE I. TESTING THE MODEL FOR A RING WITH A CIRCULAR CROSS SECTION.

N	100	200	400	800	1600
ν infinity	281	568	1144	2295	4598
ν Euclidean	948	2688	7614	21550	60990
$L \cdot 10^9$/H	15.33187	15.35188	15.36189	15.36689	15.36939
$F \cdot 10^{15}$/dynes	9.21997	24.16275	-8.49803	-17.70065	10.07985

As can be seen from table 1, the model is characterized by poor conditionality, increasing in proportion to the number of sampling steps. The convergence of the numerical solution is rather slow, but the calculation is stable, and the asymmetry of the solution is practically absent.

As a second example, we consider the problem of several bodies in the form of a system of two rings in a cylindrical screen. The geometrical parameters of the system were: the radii of the rings 28 mm and 40 mm, the radii of cross-sections of rings 10 mm and 20 mm, the base radius of the cylindrical screen 65 mm, height 120 mm, the corner radius of 10 mm, clearance between the rings 10 mm, gap between the bottom ring and the bottom of the screen 20 mm. The magnetic fluxes in the rings were equal to $-1 \cdot 10^{-7}$ Wb on the upper ring and $1 \cdot 10^{-7}$ Wb on the lower ring, respectively. The 100 sampling points on each ring and 200 points on the screen are used. The calculation results are presented in Figures 2 and 3.

In the system of three bodies, there are three forces, the sum of which, according to Newton's third law, must be equal to zero. The results of the calculation show that with an accuracy of 0.1% this equality is performed, which indicates the correctness of the solution of the model.

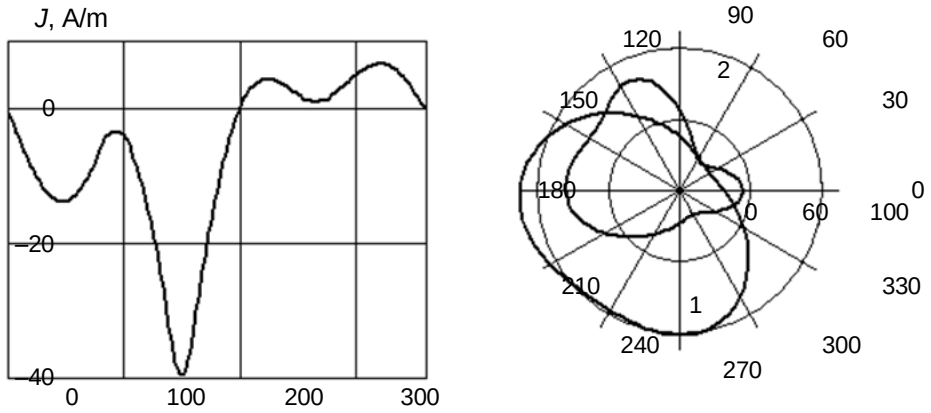

Figure 2. Distribution of the superconducting current density on the upper (1) and lower (2) rings and on the cylindrical screen.

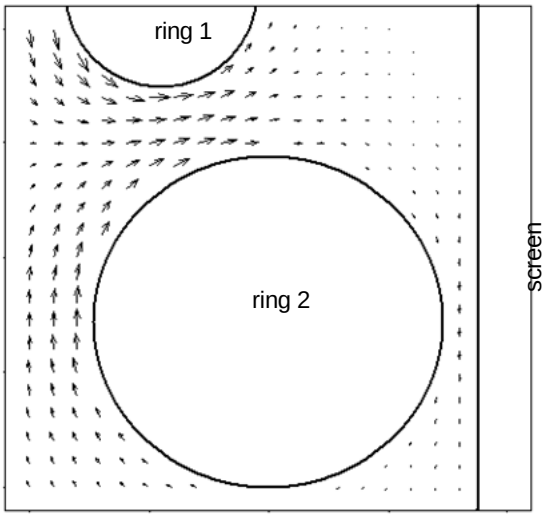

Figure 3. Distribution of the magnetic field in the gaps of two rings with a cylindrical screen.

DISCUSSION

The developed method allows, in principle, to build models for a complex axisymmetric system of multi-connected superconducting bodies. Superconducting screens in the form of surfaces of rotation or planes perpendicular to the axis of symmetry of the system can also be considered. However, the models are not applicable in violation of the axial symmetry of the system. Asymmetric systems should be analyzed in more General models, such as those based on the finite element method [12].

At the same time, the models are characterized by poor conditionality, sharply increasing with increasing number of bodies, slow convergence proportional to the number of discretization points, and sensitivity to the non-uniformity of the discretization step on the ring cross-section contour. This leads to the need to use a large number of sampling points, especially on non-circular sections, which leads to an increase in the calculation time and demands on computational resources. However, by reducing the dimension of the problem when using the method of integral equations, the number of degrees of freedom, with the same accuracy of the calculation, is an order of magnitude less than in the finite element method.

Numerical calculations were carried out using a universal system of computer mathematics Maple 14.

REFERENCES

1. Moon, F.C. 1994. *Superconducting levitation. Application to bearing and magnetic transportation*. Wiley-VCH Verlag Gmbh & Co. KGaA.
2. Kim, K.K. 2007. *Electric propulsion systems using magnetic suspension and superconductivity*. Mockow: FSBE APE "EICRT".
3. Bourke, R.D. 1964. *A theoretical and experimental study of a superconducting magnetically-supported spinning body*. NASA CR, 108.
4. Sass, A.R., and W. C. Stewart. 1968. "Self and mutual inductances of superconducting structures," *Journal of Applied Physics* 39(4): 1956–1963.
5. Chang, W.H. 1981. "Numerical calculation of the inductances of a multi-superconductor transmission line system," *IEEE Trans. Magn.* Mag.,17(1): 764–766.
6. Trencel, C., and C.C. Speake. 1996. "Geometrical optimization of superconducting levitation systems based on the complete Meissner effect," *Class. Quantum Grav,* 13(11A): 299–309.
7. Urman Yu.M. 1997. "Theory of calculation of power characteristics of electromagnetic suspension of superconducting body," *Technical Physics. The Russian Journal of Applied Physics* 67(1): 3–9.
8. Landau, L.D., and E. M. Lifshits. 2001. *Electrodynamics of continuous environments*. Moscow: Nauka.
9. Smyte, V. 1954. *Electrostatics and electrodynamics*. Moscow: Inostrannaya literatura.
10. Chernomorsky, A. I., and V. E. Plekhanov. 1981. "Calculation of the magnetic field near a two-connected axisymmetric superconducting body," *Russian Electromechanics*, (4): 360–362.
11. Kalitkin, N.N. 1978. *Numerical methods*. Moscow: Nauka.
12. Zienkiewicz, O. C., and R. L. Taylor. 2000. *The finite element method. V.1: The basis*. Oxford: Butterworth Heinemann.

2018 International Theoretical and Practical Conference on Alternative and Smart Energy (TPCASE 2018)
ISBN: 978-1-60595-617-6

A Model of Heat Transfer in Counter-Current Heat Exchanger with a Thermoelectric Cooling Element

Igor Bataronov, Alexander Kretinin, Vladimir Selivanov, Ekaterina Spytsina and Tatjana Nadeina

ABSTRACT

In disregard of conductive transfer in heat-transfer agents and using the Newton-Richman law, a model of heat transfer in a counter-current exchanger with a thermoelectric cooling element. The heat transfer coefficient of the thermoelement branch, the average temperature of the heat-transfer agents at the entrance to the heat exchanger, as well as the average length of heat transfer between the coolant and the thermoelement are chosen as the conversion scales to dimensionless variables. The model is converted to a form containing only coolant temperatures, and the General solution of the model is obtained. The study of the model found that the cooling capacity of the heat exchanger varies along the flow of the coolant and with an increase in the density of the electric current becomes negative at the initial heat exchange section.

Keywords: heat transfer, thermoelectric element, current heat exchanger.

INTRODUCTION

Thermoelectric coolers (TEC) are widely used in a variety of thermal converters [1-3]. The effective functioning of the TEC in the composition of the cooling

Igor Bataronov, Alexander Kretinin, Vladimir Selivanov, Ekaterina Spytsina, Tatjana Nadeina, Voronezh State Technical University, 14 Moskovsky Avenue, Voronezh, 394026, Russia
Igor Bataronov, Alexander Kretinin, Air Force Education and Research Center “The Zhukovsky and Gagarin Air Force Academy”, 54A Starikh Bolshevikov Street, Voronezh, 394064, Russia

device requires special techniques for improving its capacity: the enhancement of convective heat transfer from the surfaces TEC [4], design optimizations, such as the inclusion of additional conductive elements [5], optimization of thermal modes of TEC operation taking into account thermal resistances of the transition layers of the structure [6–12].Optimization of the TEC operation mode to the maximum cooling capacity has been widely considered in the literature [6, 9–12]. The influence of thermal characteristics of TEC and heat transfer media on the dynamic characteristics of the device is also studied [7]. However, typically it was considered the problem of heat transfer with the participation of TEC between the stationary media in the approximation of the law of Newton-Richman. For this case, analytical results are obtained and a complete numerical analysis is performed [6]. However, specific relationships may appear in moving heat-current media [8], therefore a separate model for heat transfer in a current heat exchanger with TEC is required. This model is considered in the present paper.

FORMULATION OF THE MATHEMATICAL MODEL OF HEAT TRANSFER

Heat transfer in a counter-current heat exchanger with TEC separating heat agents is considered (Figure 1). The heated fluid 1 moves at an average speed V_1 and has a temperature distribution $T_1(x)$ along the flow direction. This direction is taken as the axis *Ox* orientation. Cold fluid 2 moves at an average speed V_2 and has a temperature distribution $T_2(x)$. The direction of heat flow from fluid 1 to fluid 2 is considered positive. The intermediate layers A and B include the switching bus, ceramic insulators, radiators and other heat exchange elements and are described with the thermal resistance R_1 and R_2 between the surfaces of the thermocouple branches and heat transfer fluids [6]. The temperature of the cooling surface of the thermocouple is indicated as $T_a(x)$, and the heated surface as $T_b(x)$.

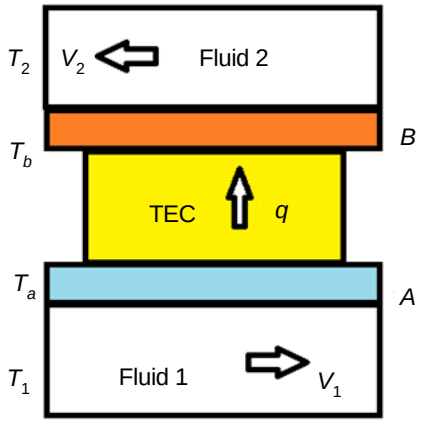

Figure 1. Scheme of heat transfer in counter-current heat exchanger with TEC.

When describing the heat transfer in heat agents, we will neglect the conductive component. Then, when using the Newton-Richman law, taking into account the selected flow direction (Figure 1) , we will have the equations:

$$H_i C_i V_i \frac{dT_i}{dx} = -q_i, \ i = \overline{1,2}. \tag{1}$$

Here H_i is the thickness of the streams of heat transfer fluids, C_i is their specific heat, and the heat flux density through the surface of the TEC is written in the form [2,6]

$$q_1 = \frac{T_1 - T_a}{R_1} = \alpha j T_a - \frac{\rho j^2 L}{2} - \frac{\lambda}{L}(T_b - T_a), \tag{2}$$

$$q_2 = \frac{T_b - T_2}{R_2} = \alpha j T_b + \frac{\rho j^2 L}{2} - \frac{\lambda}{L}(T_b - T_a), \tag{3}$$

where α is the Seebeck coefficient of the thermocouple branches, λ is thermal conductivity coefficient of branches, L is the height of the branches, j is the density of the electric current in the branch, and ρ is specific electrical resistivity of the branches. The correction factor for the ratio of the areas of all branches to the heat exchange area is considered to be related to the parameters α, λ, ρ.

We transform the model (1)–(3) to dimensionless variables:

$$j = j_0 \zeta, \quad T = T_0 \theta, \quad x = l_0 y, \quad q = q_0 \kappa, \tag{4}$$

To do this, we define the scale factors by the following relations:

$$j_0 = \frac{\lambda}{\alpha L}, \quad T_0 = \frac{T_1(0) + T_2(l)}{2}, \quad q_0 = \frac{\lambda T_0}{L}. \tag{5}$$

Here l is the length of the TEC in the direction of flow of the coolant.

To determine the length scale, we introduce the ratios for the thermal resistances of the transition layers A, B to the thermal resistance of the thermocouple branches:

$$r_i = \frac{R_i \lambda}{L}, . \tag{6}$$

with the use of which we define the parameters

$$\xi_1 = \frac{r_1}{1+\zeta r_1 + r_1}, \quad \xi_2 = \frac{r_2}{1-\zeta r_2 + r_2}. \tag{7}$$

Then, the characteristic thermal lengths in the heat current agents are given in the form

$$l_1 = \frac{H_1 C_1 V_1 L}{\lambda}\left(1-\xi_1\xi_2\right)\left(1+\zeta r_1 + r_1\right), \quad l_2 = \frac{H_2 C_2 V_2 L}{\lambda}\left(1-\xi_1\xi_2\right)\left(1-\zeta r_2 + r_2\right). \tag{8}$$

Finally, we define the length scale as the inverse mean of the lengths l_i:

$$\frac{1}{l_0} = \frac{1}{l_1} + \frac{1}{l_2}. \tag{9}$$

This definition allows the introduction of dimensionless normalized coefficients:

$$\nu_1 = \frac{l_0}{l_1}, \quad \nu_2 = \frac{l_0}{l_2}, \quad \nu_1 + \nu_2 = 1. \tag{10}$$

In the end, after the substitution of expressions (4) to (10) in equation (1) to (3) and eliminating variables θ_a, θ_b we obtain the system of equations of the model in the normal form

$$\begin{cases} \dfrac{d\theta_1}{dy} = -\nu_1\left[\left(\zeta+1-\xi_2\right)\theta_1 - \left(1-\xi_2+\zeta\xi_2\right)\theta_2 - \dfrac{\zeta^2}{2z}\left(1+\xi_2\right)\right] \\ \dfrac{d\theta_2}{dy} = -\nu_2\left[\left(1-\xi_1-\zeta\xi_2\right)\theta_1 - \left(\zeta-1+\xi_1\right)\theta_2 + \dfrac{\zeta^2}{2z}\left(1+\xi_1\right)\right] \end{cases}, \tag{11}$$

The solution of the system (11) is found under boundary conditions

$$\theta_1(0) = 1+\delta, \quad \theta_2(l) = 1-\delta. \tag{12}$$

Here δ is the value of the relative deviation of the initial coolant temperatures from the average value selected for the temperature scale, z – parameter ZT_0 thermocouple [2].

STUDY OF THE MODEL OF HEAT TRANSFER

The system of equations (11) differs from the classical model of heat transfer by the presence of heat sources in the heat transfer layer. These sources are constant along TEC, so the particular solution of the system (11) is directly:

$$\bar{\theta}_1 = -\frac{2-\zeta}{2z}, \quad \bar{\theta}_2 = -\frac{2+\zeta}{2z}. \tag{13}$$

To find the General solution of the corresponding (11) homogeneous system, we make a characteristic equation:

$$\mu^2 + \left[\zeta + \nu_1\left(1-\xi_2\right) - \nu_2\left(1-\xi_1\right)\right]\mu + \nu_1\nu_2\zeta^2\left(1-\xi_1\xi_2\right) = 0. \tag{14}$$

We denote the roots of the square equation (14) as μ_1, μ_2. In the classical model, one of the roots is zero, so the temperatures of both agents change by one exponential dependence. In this case, the temperature of the hot agent is always higher than the temperature of the cold one. This case is obtained from equation (14) when $\zeta = 0$. In the interval $0 < \zeta < \zeta_k$, both roots are real and negative, and when $\zeta > \zeta_k$ complex roots appear. In this case, the temperature of the hot agent somewhere becomes lower than the temperature of the cold one.

For real roots, the General solution is written as

$$\begin{pmatrix}\theta_1\\ \\ \theta_2\end{pmatrix} = \begin{pmatrix}-\frac{2-\zeta}{2z}\\ \\ -\frac{2+\zeta}{2z}\end{pmatrix} + D_1\begin{pmatrix}1-\xi_2+\zeta\xi_2\\ \\ \zeta+1-\xi_2+\frac{\mu_1}{\nu_1}\end{pmatrix}e^{\mu_1 y} + D_2\begin{pmatrix}1-\xi_2+\zeta\xi_2\\ \\ \zeta+1-\xi_2+\frac{\mu_2}{\nu_1}\end{pmatrix}e^{\mu_2 y}, \tag{15}$$

where the coefficients D_1, D_2 are determined from the boundary conditions (12) as a solution of a system of equations:

$$\begin{cases} D_1\left(1-\xi_2+\zeta\xi_2\right) + D_2\left(1-\xi_2+\zeta\xi_2\right) = 1+\delta+\frac{2-\zeta}{2z} \\ D_1\left(\zeta+1-\xi_2+\frac{\mu_1}{\nu_1}\right)e^{\mu_1 l} + D_2\left(\zeta+1-\xi_2+\frac{\mu_2}{\nu_1}\right)e^{\mu_2 l} = 1-\delta+\frac{2+\zeta}{2z} \end{cases}, \tag{16}$$

Equations (14) to (16) determine the General solution of the considered heat transfer model.

For calculations on model (14) to (16) we use typical values of parameters of thermoelectrics on the basis of Bi_2Te_3 [2]: $\alpha = 16$ mV/K, $\lambda = 1.4$ W/(m·K), $\rho = 6.7$ mkOhm·m, specific heat capacity of heat transfer fluids 4 MJ/(m^3K). The geometric dimensions take $L = 2$ mm, $H = 3$ mm, flow velocity $V_1 = 0.1$ m/s, $V_2 = 0.5$ m/s, thermal resistance $R_1 = 1$ m^2K/kW, $R_2 = 0.5$ m^2K/kW.

The results of the calculation of the temperature distribution, cold and heat capacity for the various electric current density are shown in Figure 2.

Note that the current density of the ideal maximum cooling capacity [2, 6] in the scale (5) used here is numerically equal to the parameter ZT and is 0.82. However, it follows from figure 2 that the maximum cooling of the hot coolant is achieved at a current density of 0.3, at which the relative cooling $\delta + 1 - \theta_1(l)$ at the outlet of the heat exchanger is 0.19. In addition, when the current density is greater than 0.4, a section of negative cooling capacity appears, on which instead of cooling the coolant is heated.

The study of the effect of thermal resistance on the degree of cooling showed that the reduction of thermal resistances can increase the relative cooling to 0.25 (Figure 2), while the main contribution is the cooling of the hot surface of the TEC. It is established that the level of thermal resistance does not affect the appearance of negative cooling capacity.

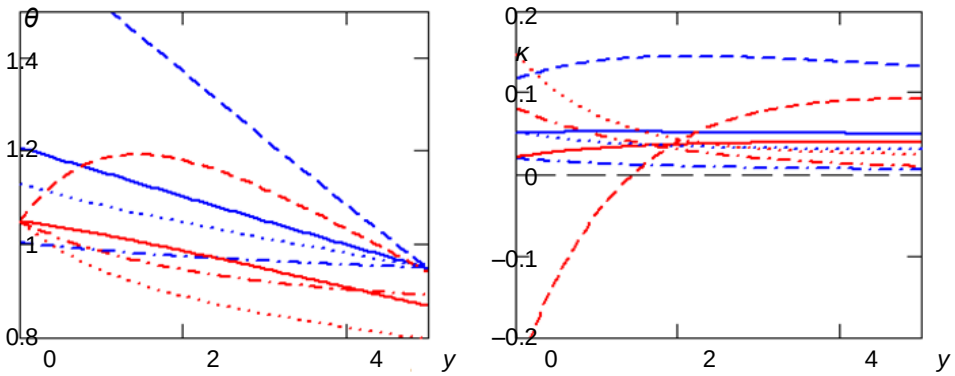

Figure 2. Temperature distribution of cold (blue lines) and hot (red lines) heat agents, cooling capacity (blue lines) and heating capacity (red lines) along the length of the heat exchanger at dimensionless current density 0.3 (solid lines), 0.1 (dashed-dotted lines) and 0.5 (dashed lines), dotted lines show the distributions for zero thermal resistance and current density of 0.3

DISCUSSION

The proposed model showed that the process of heat transfer in the current heat exchanger is significantly different from the stationary conditions, in particular, the appearance of areas of negative cooling capacity. The obtained

analytical solution of the model allows to optimize the operation mode of the TEC, as well as to design the values of the parameters that ensure the fulfillment of the required technical conditions for the heat exchanger. Note that the generalization of the model to the co-current scheme is carried out simply by replacing the sign in the right part of the second equation in (11).

At the same time, the model uses the integral value of thermal resistance and does not take into account the presence of the initial phase with an increased level of the heat transfer coefficient. The introduction of such a coefficient depending on the *x*-coordinate is possible in this model. In this case, the spatial coordinate transformation becomes nonlinear, and the possibility of an analytical solution of the system (11) is excluded. Research in such a model is possible only by numerical methods.

Numerical calculations were carried out using a universal system of computer mathematics Maple 14.

REFERENCES

1. Martinivsky, V.S. 1979. *Cycles, Schemes and Characteristics of Thermotransformers*. Moscow: Energiya.
2. Anatichuk, L.I. 1979. *Thermoelements and Thermoelectric Devices*. Kiev: Naukova Dumka.
3. Zebarjadi, M., K. Esfarjani, M. S. Dresselhaus, Z. F. Ren, and G. Chen. 2012. "Perspectives on thermoelectrics: from fundamentals to device applications," *Energy & Environmental Science*, 5(1): 5147–5162.
4. Ilyukhin, I.M., A.V. Kretinin, M.I. Kirpichev, and V.G. Stogney. 2014. "Analytical Assessment of Effects on Thermoelectric Heat Transfer Enhancement from the Cooling Finned Surfaces," *Bulletin of Voronezh State Technical University*, 10(4): 44–46.
5. Gorobez, N.V., and V.G. Okhrem. 2007. "Peltier Thermoelectric Cooler with Additional Conducting Element," *Plasma Physics Reports*, (4): 124-127.
6. Melnikov, A.A., A.M. Phiri, I.V. Tarasova, and N.V. Batrameev. 2017. "Modeling of Qmax mode of a thermoelectric cooler taking into account thermal resistances on cool and hot side," *Semiconductors*, 51(7): 896–899.
7. Zaykov, V., V. Mescheryakov, and Yu. Zhuravlov. 2018. "Analysis of Relationship Between the Dynamics of a Thermoelectric Cooler and Its Design and Modes of Operation," *Eastern-European Journal of Enterprise Technologies*, 1/8(91): 12–23.
8. Ryazhskikh, V.I., Yu. Yu. Gromov, A.V. Ryazhskikh, and A.A. Khvostov. 2017. "Analysis of Operating Modes of a Closed Circulation Cooling Circuit with an Intermediate Heat Carrier," *Applied Physics and Mathematics*, (4): 20-26.
9. Lee, H. 2013. "Optimal design of thermoelectric devices with dimensional analysis," *Applied Energy*, 106: 79-88.
10. Zhu, L., H. Tan, and J. Yu. 2013. "Analysis on optimal heat exchanger size of thermoelectric cooler for electronic cooling applications," *Energy Conversion and Management*, 76: 685–690.
11. Han, T., G. Gong, Z. Liu, and L. Zhang. 2014. "Optimum design and experimental study of a thermoelectric ventilator," *Applied Thermal Engineering* 67: 529-539.
12. Pearson, M.R., and C.E. Lents. 2016. "Dimensionless Optimization of Thermoelectric Cooler Performance When Integrated Within a Thermal Resistance Network," *Journal of Heat Transfer* 138(8): 081301–081301-11.

2018 International Theoretical and Practical Conference on Alternative and Smart Energy (TPCASE 2018)
ISBN: 978-1-60595-617-6

Metal Hydride Flow-through Biohydrogen Separation

Dmitry Blinov, Vasily Borzenko, Alexey Kazakov
and Aliya Glagoleva

ABSTRACT

The applicability of the novel metal hydride flow-throw hydrogen separation method is proved. New compositions of low temperature AB_5-type metal hydrides for biohydrogen purification are manufactured and tested. Thermal processes in the reactor during hydrogen separation from carbon dioxide are studied.

INTRODUCTION

The long-term strategic view of Russia on energy challenges includes the development of renewable energy technologies, where bioenergy technology plays a significant role. A biologically produced hydrogen is called "biohydrogen," which serves as a fuel in a wide range of applications including transportation and autonomous power plants. As a significant advantage of the technology, biohydrogen can be produced from various feedstocks, such as municipal, food, and livestock waste. One of the most promising biological hydrogen production technologies is dark fermentation that shows higher hydrogen production rates than other biological methods. The process is detached from the use of light and produces valuable by-products. Biohydrogen is a prospective energy source for the regions located outside of the grid with local biomass or waste available [1-3].

A significant disadvantage of biohydrogen technology includes the presence of high levels of gaseous impurities and, as a result, low partial pressure of hydrogen (less than 1 bar) in the mixture of gases, which limits the use of the technology in

Joint Institute for High Temperatures of the Russian Academy of Sciences, 13 Bd. 2, Izhorskaya Street, Moscow, 125412, Russia

fuel cell based power plants. One of the main impurities is carbon dioxide that can obtain up to 50-70% of the content [4]. Practical application of biohydrogen in PEM fuel cells is limited by low hydrogen content and low partial pressure of hydrogen. The fuel cell stack experiences the decrease in voltage due to the carbon dioxide appearance. This limitation is especially noticeable at the high current densities. Hence the necessary development of biological hydrogen systems demands concurrent improvement in both hydrogen purification and hydrogen storage systems.

The purification technology utilizing metal hydride concept can be an encouraging possibility to cover both purification and storage disadvantages. The intermetallic compounds (IMCs) present selective hydrogen sorption and reach a high recovery ratio of 75-90%, which enables the direct use of IMC for hydrogen purification from gas mixtures including high carbon dioxide content mixtures. IMCs hydrogen sorption is a reversible process. Desorption of hydrogen from IMC releases high-purity hydrogen (99.9999%) and the required pressure levels for power plants [5].

Primary criteria for the development of efficient hydrogen storage systems is the improved efficiency of heat and mass transfer for the heat supply and removal for the sorption and desorption processes of hydrogen. IMC in a hydrogen purification and storage system is present in the form of finely dispersed powder with 1-10 μm particles and low effective thermal conductivity of 0.1-1 W/m K. The latter is affected by the pressure of the filling gas and by hydrogen absorbed in the particles. Gas impurities cause changes in sorption kinetics and decrease the efficiency of the device [6]. Various systematic effects in power plants with solid state hydrogen storage materials need further research.

METALHYDRIDE FLOW-THROUGH PURIFICATION SYSTEM

This work presents the method of biohydrogen separation, which consists of continuous purging of impure hydrogen through a porous bed of hydrogen absorbing material [7]. During the separation process, hydrogen is absorbed by metal hydride, and gas impurity (CO_2) is continuously removed from the free space of the reactor.

Flow-through purification metal hydride reactors RSP (Reactors for Storage and Purification) are used to separation biohydrogen. The developed metal hydride reactors for hydrogen purification and storage RSP and RSP (I) are shown in Figure 1.

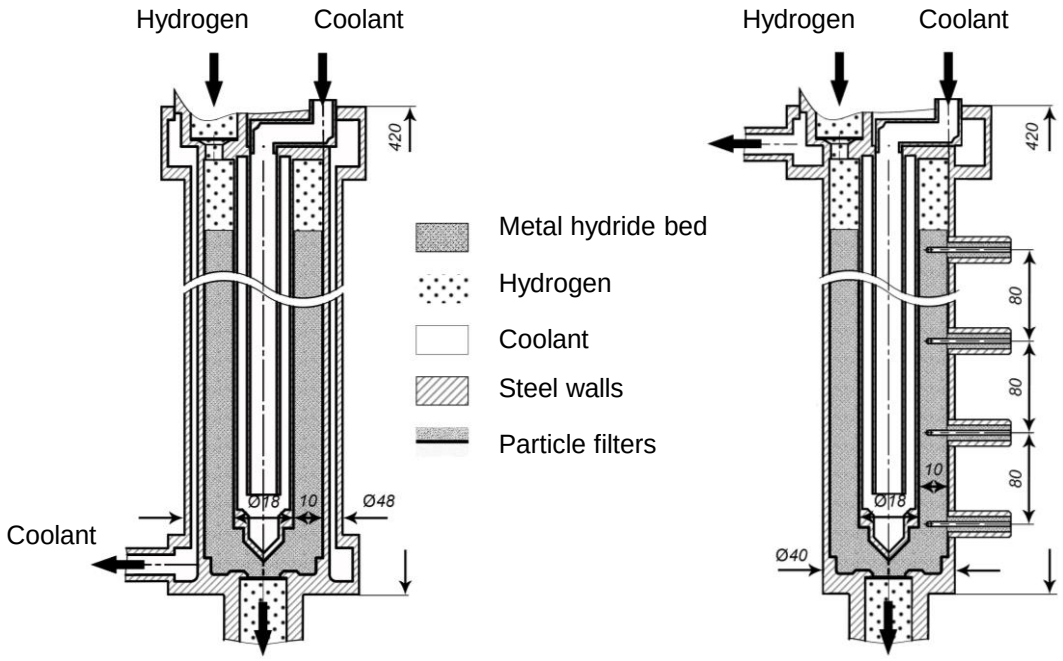

Figure 1. Storage and purification flow-through reactors RSP and RSP (I).

The RSP (I) reactor (Figure 1 right) has a tubular design; inner tube forms liquid internal heat exchanger (IHE) with an annular reaction chamber between IHE and an outer wall. Temperature sensors are installed on the outer wall of the reactor. The reaction chamber is filled with a metal hydride powder with an average particle size of 10 μm and has inlet and outlet tubes at both ends of the reactor so that gas can flow through the bed. RSP reactor (Figure 1 left) has a similar design, but it has an external heat exchanger (EHE) for more efficient heat transfer. Gas supply in both modifications is carried out in the upper part of the reactors.

Reactors are filled with $LaNi_{4.8}Mn_{0.3}Fe_{0.1}$ alloy mass of 1 kg.

LOW TEMPERATURE METAL HYDRIDES

Metal hydrides should meet requirements for effective biohydrogen separation. Biohydrogen produced from various organic substrates mostly consists of H_2 and CO_2, with hydrogen content about 30–50 vol% and for an overall gas pressure of 0.11–0.12 MPa hydrogen partial pressure does not exceed 0.04–0.06 MPa. Carbon dioxide does not affect AB_5-type alloys. In the presence of poisonous gases (CO, H_2S, etc.) surface modification of metal hydrides or removal of the impurities prior to hydrogen sorption are required. Thus, some La based AB_5 type metal hydrides are prospective materials for biohydrogen purification because their

equilibrium pressures are in the range of 0.02 – 0.06 MPa, which is suitable for direct sorption of hydrogen from the produced gas. On the other hand, Ce, Mm substituted alloys have higher equilibrium pressure to ensure required pressure levels for fuel cell supply.

Enthalpies and entropies of the reactions were calculated using Van't Hoff equation:

$$RlnP = \Delta H/T + \Delta S \quad (1)$$

where R is a universal gas constant, P is the equilibrium pressure, ΔH is the reaction enthalpy, T is the temperature and ΔS is the entropy change. Results of the thermodynamic measurements are listed in TABLE I.

TABLE I. EXPERIMENTAL AND CALCULATED DATA.

MH alloy	P_{des}, MPa	C_{rev}, wt%	C_{max}, wt%	ΔH_{des}, kJ/mol	ΔS_{des}, kJ/mol K
$LaNi_{4.6}Fe_{0.2}Al_{0.2}$	0.049	1.1	1.3	-36.8	120
$LaNi_{4.6}Mn_{0.2}Al_{0.2}$	0.029	0.9	1.1	-35.8	112
$LaNi_{4.4}Fe_{0.3}Sn_{0.3}$	0.06	1.0	1.2	-28.7	92
$La_{0.7}Ce_{0.3}Ni_5$	0.36	1.3	1.5	-33.1	123
$La_{0.5}Mm_{0.5}Ni_5$	0.55	1.3	1.5	-31.5	120
$MmNi_{4.15}Fe_{0.15}$	1.14	1.0	1.2	-28.3	116
$LaNi_{4.8}Mn_{0.3}Fe_{0.1}$	0.05	1.0	1.3	-34.0	108

EXPERIMENTAL PROCEDURE

The biohydrogen separation experiments are carried out in the following way: a prepared gas mixture modeling biohydrogen (H_2/CO_2 gas mixture) from the reservoir is fed to the inlet valve of the RSP(I) reactor at a constant flow rate (in). A gas mixture (Pin = 0.55 MPa) is filtered through the hydrogen-absorbing material bed ($LaFe_{0.1}Mn_{0.3}Ni_{4.8}$ alloy) and is ejected through the outlet valve with a limited flow rate (out <in). The metal hydride bed, cooled by the heat exchange liquid, absorbs hydrogen from the gas mixture. The internal and external heat exchangers of the reactor are filled by water: flow rate g = 0.1 l/s, temperature T = 20 ° C. The inlet and outlet gas flow rates are recorded by Bronkhorst EL-FLOW flow regulators. The gas analyzer controls the hydrogen passing through the outlet valve.

Hydrogen recovery during the purification process is determined by the following equation:

$$\eta = (V_{H2} - V_{lossH2})/V_{H2} \quad (2)$$

where V_{lossH2} is the volume of hydrogen in purged stream, st.l, V_{H2} is the volume of hydrogen in the feed stream, st.L.

RESULTS AND DISCUSSION

Results of H_2+CO_2 gas mixture separation through metal hydride bed with (a and b) and without (c and d) heat exchange liquid in the RSP reactor are presented in Figure 2.

In Figures 2a and 2c, the temperature change in the metal hydride bed shows evident maximum points that indicate a recovery ratio decrease throughout the purification process (Figures 2b and 2d). The heat transfer in the sorption process is challenging because of the low effective thermal conductivity of the intermetallic compound. Without cooling, the temperature in the reactor may reach 53-58 ºC at the beginning of the charging process and remains at these levels throughout the process of hydrogen sorption. A notable increase in temperature affects the absorption equilibrium pressure of the metallic alloy that becomes adjacent to the pressure in the reactor, which leads to the heat transfer crisis and terminates the process of sorption [6-8]. The phenomenon of crisis reduces the intensity of heat transfer and diminishes absorption process. The consequence of such a process causes hydrogen to break through an intermetallic compound, rising hydrogen concentration at the outlet of the reactor and an overall level of losses during the purification process, which lead to a significant reduction of the efficiency of the metal hydride flow-through purification concept (Figure 3). When the cooling is present, the temperature levels do not surpass 49 ºC and decrease at a faster pace. In the case where the intersection point of hydrogen concentration at the outlet and the recovery ratio is taken as the end point of the process for calculation, the hydrogen capacity utilization with and without cooling equals to 70% and 20% respectively.

The flow-through separation method for hydrogen purification enables the opportunity to reach up to 85% of recovery ratio at various inlet flow rates and to utilize over 80% of hydrogen capacity of the intermetallic compound in the metal hydride reactor. For the dark fermentation reactors with a low level of hydrogen production performance, usually up to 5 st.L/min only, the flow-through hydrogen purification reactors can raise the efficiency of hydrogen purification from the produced gas.

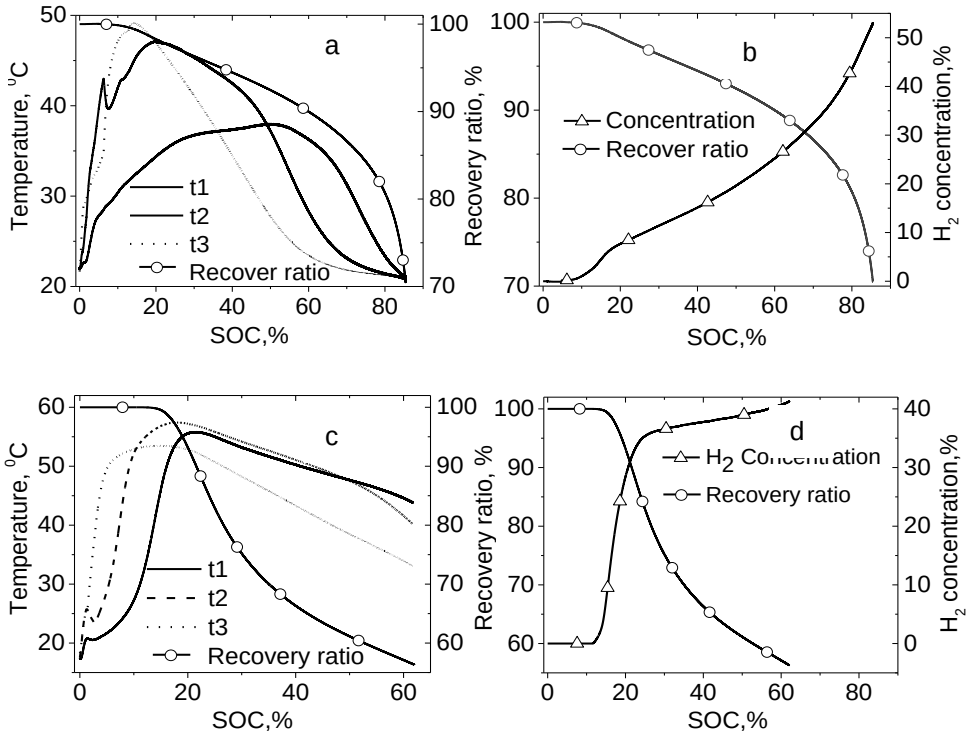

Figure 2. Temperature change in the metal hydride bed, recovery ratio and H_2 concentration at the reactor outlet during purification with cooling (a and b) and without cooling (c and d).

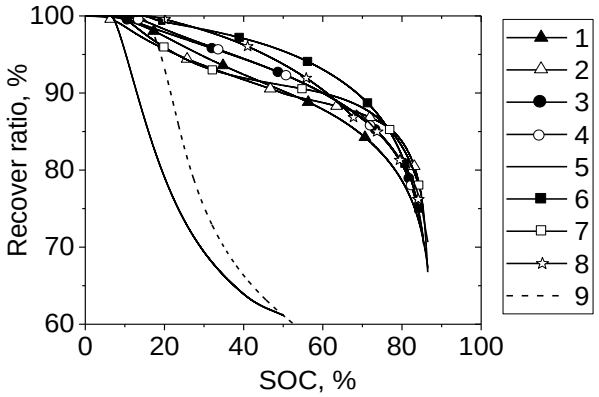

Figure 3. Recovery ratios for H2/CO2 mixture at different initial parameters. Setpoints of flow controllers are in brackets. Mixture: 60% H2+ 40% CO2: 1 - (in 20 / out 5), 2 - (in 2 / out 1); Mixture: 55% H2+ 45% CO2: 3 - (in 6 / out 3), 4 - (in 3 / out 1,5), 5 - (in 3 / out 1,5) No cooling; Mixture: 40% H2+ 60% CO2: 6 - (in 10 / out 5), 7 - (in 5 / out 3); Mixture: 27% H2+ 73% CO2: 8 - (in 2 / out 1), 9 - (in 3 / out 1,5) No cooling.

CONCLUSION

The H_2-CO_2 gas mixture with a structure resembling "biohydrogen" was separated using RSP-8(I) metal hydride reactor with AB_5 alloy. The process of purification through hydrogen extraction was investigated in varying initial conditions. It was concluded that the presence of cooling of the intermetallic compound is critical for efficient hydrogen sorption process and, as a result, the metal hydride reactor operation. The reactor using cooling system can utilize over 70% of the hydrogen capacity of the compound at the hydrogen recovery ratio close to 85%. The purification method using metal hydride reactors can be used for hydrogen extraction from gas mixtures containing a low level of hydrogen.

ACKNOWLEDGMENT

Authors acknowledges support from the Russian Science Foundation. The research was supported by Russian Science Foundation grant (project #17-79-20413).

REFERENCES

1. Wei, J., Z.T. Liu, and X. Zhang. 2010. "Biohydrogen production from starch wastewater and application in fuel cell," *Int. J. of Hydrogen Energy*, 35(7): 2949-2952.
2. Chu, C.Y., S.Y. Wu, P.C. Hsieh, and C.Y. Lin. 2011. "Biohydrogen production from immobilized cells and suspended sludge systems with condensed molasses fermentation solubles," *Int. J. of Hydrogen Energy*, 36(21): 14078-14085.
3. Balat, M. 2009. "Political, economic and environmental impacts of biomass-based hydrogen," *Int. J. of Hydrogen Energy*, 34(9): 3589-3603.
4. Debabrata, D., and T. N. Veziroglu. 2008. "Advances in biological hydrogen production processes," *Int. J. of Hydrogen Energy*, 33: 6046-57.
5. Verbetsky, V.N., S.P. Malyshenko, S.V. Mitrokhin, V.V. Solovei, and Y.F. Shmal'ko. 1998. "Metal hydrides: properties and practical applications. Review of the works in CIS-countries," *Int. J. of Hydrogen Energy*, 23(12): 1165-1177.
6. Borzenko, V., D. Dunikov, and S. Malyshenko. 2011. "Crisis phenomena in metal hydride hydrogen storage facilities," *High Temperature*, 49(2): 249.
7. Dunikov, D., V. Borzenko, D. Blinov, A. Kazakov, C.Y. Lin, S.Y. Wu, and C.Y. Chu. 2016. "Biohydrogen purification using metal hydride technologies," *Int. J. of Hydrogen Energy*, 41(46): 21787-21794.
8. Dunikov, D., V. Borzenko, and S. Malyshenko. 2012. "Influence of impurities on hydrogen absorption in a metal hydride reactor," *Int. J. of Hydrogen Energy*, 37(18):13843-13848.

2018 International Theoretical and Practical Conference on Alternative and Smart Energy (TPCASE 2018)
ISBN: 978-1-60595-617-6

Hydrogen KW-Scale Energy Storage Systems on the Base of Metal Hydrides and Fuel Cells

Vasily Borzenko, Dmitry Blinov and Aliya Glagoleva

ABSTRACT

The results of demonstration projects on development and testing of hydrogen fuel cell power units utilizing low-temperature metal hydrides of AB_5 type as hydrogen storage and purification tool are presented. In the effort to enable the technology for autonomous applications, the novel concept of using fuel cell exhaust air for hydrogen desorption process replacing an external heating agent was successfully proved. The technology of through-flow metal-hydride based hydrogen purification was also successfully utilized for biohydrogen. The results of two proof-of-concept projects show a good perspective for autonomous applications and open the opportunity for further research in the field of power system control.

INTRODUCTION

Wide implementation of hydrogen fuel cells (FC) of various types and the increase of efficiency of water electrolysis give a range of opportunities for development and creation of hydrogen based energy storage systems both for variable renewable energy as the fluctuations compensator and for back-up power applications. The key technical issue of hydrogen energy storage of kW-scale is the development of efficient and safe hydrogen accumulators and their integration into power units having *electrolyzer-storage-fuel cell* structure. One of the possible solutions is the use of low-temperature metal hydrides (MH) based on $LaNi_5$ and its modifications [1]. Besides, the interest to hydrogen produced by biological sources [2] and useful feature of MH to selectively absorb hydrogen from gas mixtures discover the possibilities to develop power production units having *bioreactor-purifier-storage-FC* structure, directly utilizing hydrogen within integrated autonomous power unit.

Joint Institute for High Temperatures, 13-2, Izhorskaya Street, Moscow, 125412, Russia

In [3] the possibility of successful thermal management of the system with 5 kW PEMFC and 13 st.m^3 MH hydrogen storage has been demonstrated. This result is based on the design of the heat exchanger of the reactor and operation regimes selection both optimized from the point of view of mass transfer crisis avoidance [4] the phenomenon, which is typical for the technology. The task of the demonstration of stability at power supply from MH hydrogen storage is simplified by the use of water (liquid) cooling loop and where PEMFC is the source of low potential heat (about 60^oC) and MH hydrogen storage is the heat absorber. However, water-cooled PEMFC stacks typically require complex water management subsystems that results in a larger system volume, weight and cost, while air-cooled PEMFCs that feature self-humidifying technologies developed to commercial level in recent years and are squeezing liquid–cooled PEMFCs out of the market at least in 1 – 10 kW range. The heat transfer coefficient at heat transfer from the metal hydride bed to the liquid accounts for more than 120 W/(m^2 K) and these values are hardly achievable if one tries to heat up MH hydrogen storage by hot air from PEMFC outlet. In [5] the qualitative possibility to supply reliably 1.1 kW FC with hydrogen from air heated low temperature MeH reactor was experimentally proved.

The present research describes two demonstration FC-based units with the features of stand-alone and logistics-free (H2Smart), and MH biohydrogen purification (H2Bio). The essential new process in H2Smart is the MH reactor discharge driven by hot air, while in H2Bio the main results are connected with the technology of through-flow hydrogen purification.

H2SMART

The structure of H2Smart, namely *electrolyzer—hydrogen storage—fuel cell* supposes the utilization of commercial equipment everywhere except the hydrogen storage reactor. The system (see Figure 1.) consists of electrolyzer with capacity100 l/h, up to 1 st. m^3 H_2 MH storage, 1 kW(e) PEM fuel cell and a battery. Electrolyzer produces hydrogen and dehumidifies it. Hydrogen then enters a sorption process in a hydrogen storage reactor, where together with metal alloy forms an MH. In order to perform this chemical reaction, heat is extracted by cold water in the water loop cooled in radiator due to natural convection. In order to produce electricity for the load demand, hydrogen is released from the storage system to PEM fuel cell. Desorption process requires heat that is supplied to the reactor in the form of hot water, which is heated by exhaust heat from PEM fuel cell using the radiator. In case the FC shuts down or experiences a low pressure of hydrogen from the MH back-up battery meets the demand of the load ensuring the reliability of the supply. MH system is the subsystem in H2Smart that is being studied with respect to heat and mass transfer processes thus an ability to measure temperature inside the reactor, input and output pressure, input and output heating agent parameters is needed.

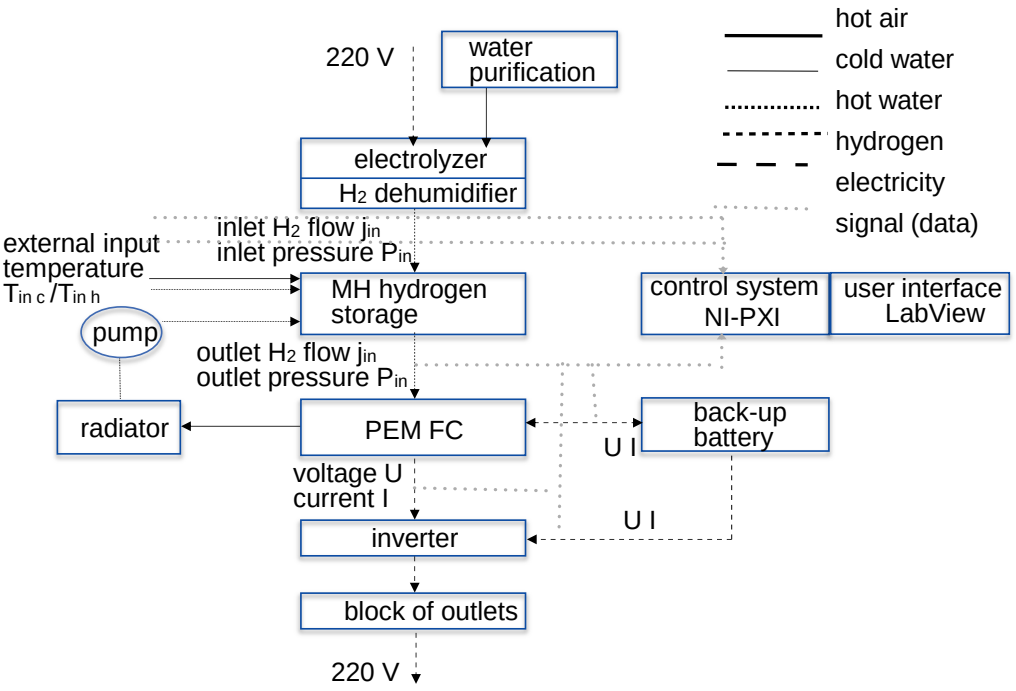

Figure 1. H2Smart scheme and rear view.

The reactor is filled with 5 kg of $La_{0.9}Ce_{0.1}Ni_5$, nominal H2 storage capacity is 750 st. l. The hydrogen-absorbing alloy $La_{0.9}Ce_{0.1}Ni_5$ was mechanically shredded to a particle size less than 5 mm and inserted into metal hydride hydrogen storage units. 100 g of the selected alloy were used to study the absorbing properties (see Figure 2). The heat of reaction determined by the Van't Hoff equation is ΔH = 30.7 ± 0.5 kJ/mol H_2, the entropy change ΔS = 110 ± 1 J/K mol H_2, the maximum hydrogen capacity of the alloy is 1.34 ± 0.005% of the mass. According to the 1 kW Hoppecke E-1100 PEM FC specification, operating pressures (excessive) of hydrogen should be in the range between 0.055 to 0.083 MPa. The lower average temperature level of output air of the FC is 30°C, and the $La_{0.9}Ce_{0.1}Ni_5$ alloy ensures required pressure levels with the heating agent temperatures around 20°C.

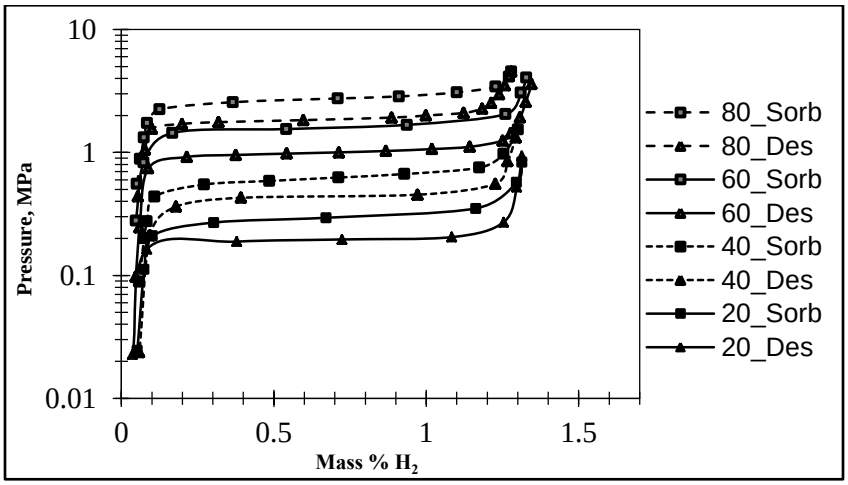

Figure 2. P-C-T (pressure, concentration, temperature) diagram of $La_{0.9}Ce_{0.1}Ni_{5.}$

H2SMART OPERATION TESTS

The findings of these tests are the following (see Figures 3,4):

- The FC heats up to 25-30^{o}C even in the absence of load
- Crisis shutdowns do not bring a rapid decrease in the FC, on the contrary, the temperature stays on the levels higher than the zero load temperature
- We can estimate 30^{o}C as a lower average FC internal temperature keeping in mind lower temperatures during the start-up procedures

The goal of the next stage of tests was to experimentally prove the possibility of integration of the proposed MH reactor with a commercial 1kW PEM FC, explore working regimes of the system, run the system coupled with a back-up power supply in the form of a battery. The experimental investigations were performed in two stages: zero demand load when all the energy from the FC charges the backup battery and increased demand load to 450W when the FC supplies both the battery and the demand (see Figure 4). Previously, the pressure level of an FC hydrogen inlet pressure was found experimentally to be around 0.13MPa [5]. In this experiment, the MH reactor was able to maintain needed pressure level for the entire duration of the experiment. Peaks on the graph are connected with the volatile rise of the heating agent temperature. Throughout the experiment, MH reactor produced enough hydrogen pressure to supply successful fuel cell performance.

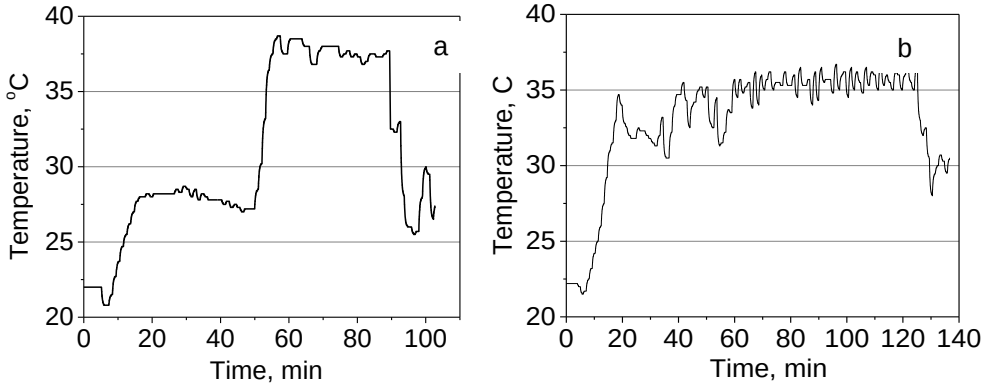

Figure 3. Temperature inside the 1 kW Hoppecke 1100 PEM FC during different working regimes: (a) – zero load, constant load (400W-500W); (b) – volatile load, maximum load (800W).

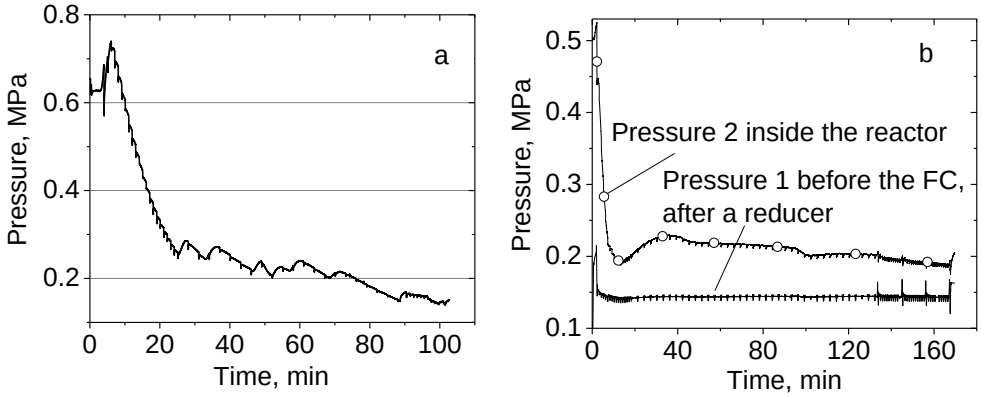

Figure 4. Pressure in the MH reactor (a), pressure levels in MH reactor and FC inlet (b).

H2BIO

2Bio has the variety of functions, including the process of storing hydrogen and cleaning biohydrogen that can be a mixture of gases with carbon dioxide and hydrogen or a model of the mixture of gases close to real biohydrogen. The cleaning and storing process uses the properties of intermetallic alloys that selectively absorb hydrogen from the mixture of gases forming metal hydrides. Purified hydrogen is stored in a solid-phase bound. The fuel cell energy system with hydrogen meets all required characteristics. The system includes the source of biohydrogen (see Figure 5), the MH block based on two reactors that clean and store hydrogen, PEM FC Hoppecke E-200 with 175W power, and an automatic control system for scientific research. In this set-up, MH storage is chosen to be lowpressure storage that can take hydrogen both from pure H2 and from the mixture of gases [6], providing additional practical implication. Hydrogen from the tank enters MH storage reactors or can be supplied to the FC directly. After the storage in MH reactor, hydrogen is supplied to PEM FC, which supplies the load.

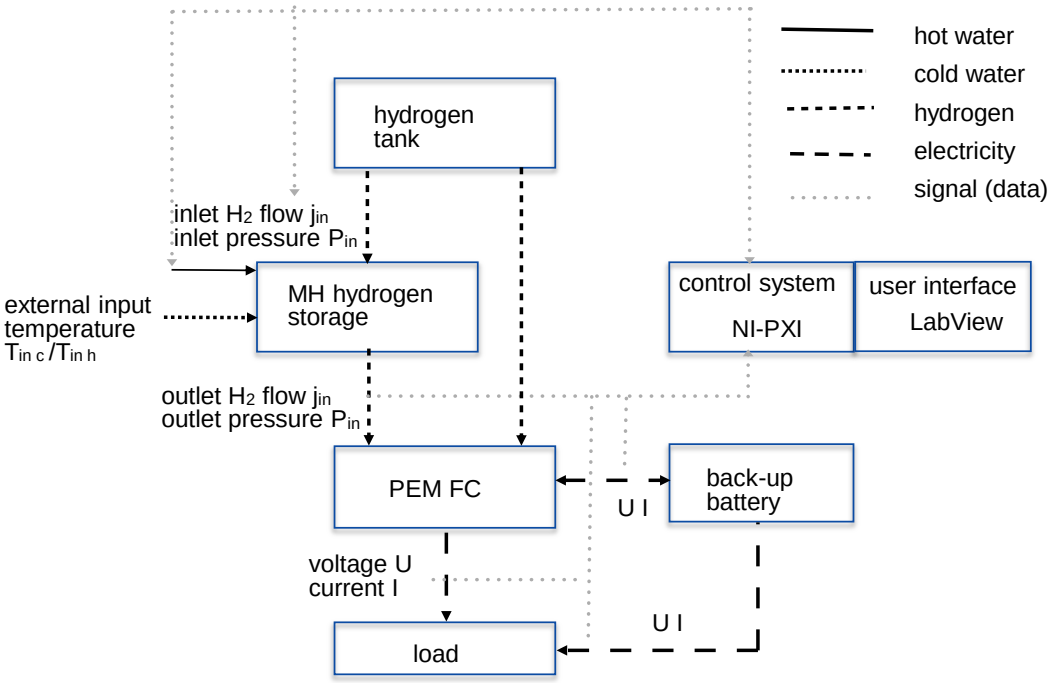

Figure 5. Scheme of H2Bio.

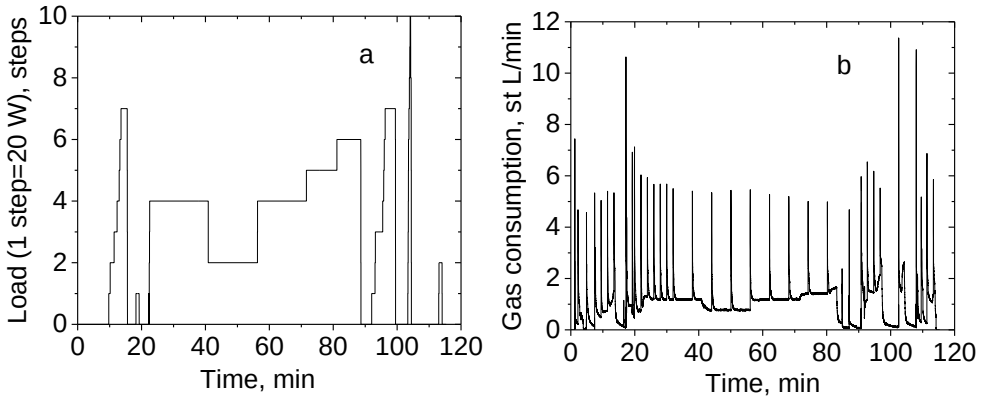

Figure 6. The electric load and gas consumption in H2Bio.

The results of the initial series of experimental investigations conducted with pure hydrogen are presented in Figure 6.

CONCLUSION

A novel type of hydrogen storage and purification systems with low-pressure MH hydrogen storage reactor, low-temperature PEM FC, electrolyzer, were designed and developed. The PCT diagram of an intermetallic compound with design requirements was obtained experimentally. Obtained results prove the technical feasibility of the proposed concepts. H2Smart experimental set-up utilizes MH reactor using exhaust heat inside the system and avoids external heat agents that previously eliminated the possibility of using MH hydrogen storage in an autonomous logistics free power supply. The biohydrogen based H2Bio system designed for the proof-of-concept for through flow hydrogen purification also passed initial tests successfully The proposed systems have significantly opened the possibility of creating a novel air-heated MH storage reactor and provided valuable kW scale experimental results for the further development of investigations of MH storage and purification in a bigger scale.

ACKNOWLEDGMENT

The research was performed with the support of Russian Science Foundation grant 17-19-01738.

REFERENCES

1. Sandrock, G. 1999. “A panoramic overview of hydrogen storage alloys from a gas reaction point of view,” *Journal of Alloys and Compounds*, 293-295: 877-888.
2. Dunikov, D, V. Borzenko, D. Blinov, A. Kazakov, C.Y. Lin, S.Y. Wu, and C.Y. Chu. 2016. “Biohydrogen purification using metal hydride technologies,” *Int. J. of Hydrogen Energy*, 41: 21787-21794.
3. Malyshenko, S.P., V.I. Borzenko, D.O. Dunikov, and O.V. Nazarova. 2012. “Metal hydride technologies of hydrogen energy storage for independent power supply systems constructed on the basis of renewable sources of energy,” *Thermal Engineering*, 59(6): 468-478.
4. Borzenko, V, D. Dunikov, and S. Malyshenko. 2011. “Crisis phenomena in metal hydride hydrogen storage facilities,” *High Temp*., 49(2): 249–256.
5. Borzenko, V., and A. Eronin. 2016. “The use of air as a heating agent in hydrogen metal hydride storage coupled with PEM fuel cell,” *Int. J. of Hydrogen Energy*, 41(48): 23120–23124.
6. Dunikov, D., V. Borzenko, and S. Malyshenko. 2012. “Influence of impurities on hydrogen absorption in a metal hydride reactor,” *International Journal of Hydrogen Energy*, 37: 13843-13848.

2018 International Theoretical and Practical Conference on Alternative and Smart Energy (TPCASE 2018)
ISBN: 978-1-60595-617-6

Synthesis of Metal-Based Nanoparticles by Acoustoplasma Discharge for Energy Storage Applications

Nikolay Bulychev

ABSTRACT

In this study, plasma discharge in a liquid at intensive ultrasonic field above the cavitation threshold has been proven to be of great interest for initiation of various physical and chemical processes. In such discharge, nanoparticles of tungsten and zinc oxides have been synthesized. Further exploration of synthesized nanoparticles has demonstrated that the factor of ultrasonic cavitation during the synthesis substantially affects physical and chemical characteristics of nanoparticles.

Keywords: nanoparticles, ultrasound, plasma, cavitation, metal oxide.

INTRODUCTION

The demand for energy is increasing day by day, which leads to the development of alternate energy sources like the non-conventional sources. This need also leads to the exploration of new energy storing and energy conversion devices with high energy density and power density. One such device is the supercapacitors. In comparison with batteries and electrolytic capacitors, supercapacitors catch much attention on account of their high power density. Their capacitances are in the order of higher magnitudes than those of the traditional ones. It can be used in many storage systems in combination with fuel cells or batteries. They differ from ordinary capacitors in two ways: (1) increased surface area of electrodes and (2) reduced distance between the electrodes.

P.N. Lebedev Physical Institute of RAS, 53, Leninsky Avenue, Moscow, 119991, Russia
Moscow Aviation Institute (National Research University), 4, Volokolamskoe shosse, Moscow, 125993, Russia

Supercapacitors are considered to be important for power devices especially in future generations. They find many applications in power systems and other devices. For realizing supercapacitors their energy and power densities must be enhanced. To achieve this and to meet the increasing demand for energy storing devices, new materials with high reliability and efficiency have to be explored. Recent studies are coming up with new nanomaterials that can store energy for a longer time, including graphene oxides; metal oxide-graphene nanocomposites, carbonbased nanoporous materials and ternary metal oxides are being widely used. Amongst all graphene oxide based nanomaterials show excellent electrochemical properties which make them suitable for supercapacitor applications. The nanocomposites of graphene exhibit even more enhanced supercapacitor performance on account of synergy effect.

Literature shows that nanomaterials can effectively be used in supercapacitor applications on account of its high surface area. Therefore, in the present work various nanomaterial systems will be prepared which include metal oxides (RuO_2, SnO_2, CuO, MnO_2, TiO_2, V_2O_5, Fe_3O_4 and α-$Co(OH)_2$), metal oxide-graphene nanocomposites, metal decorated-graphene nanostructures, nanoporous materials and ternary metal oxides ($MgCo_2O_4$, $ZnCo_2O_4$, $CuCo_2O_4$, $MnCo_2O_4$ and $NiCo_2O_4$) [1-4].

Various methods are available in literature for the preparation of above mentioned nanomaterials and their composites such as sol-gel, electrodeposition, solutionbased methods, co-precipitation, hydrothermal, solvothermal and microwave assisted methods etc. that enabled to obtain nanoparticles of titania, silica, mica, carbon black and other materials. Along with traditional chemical methods of synthesis, some physical methods, such as electric discharges and ultrasound cavitation became increasingly important in view of the creation of novel functional and composite materials.

SYNTHESIS OF NANOPARTICLES IN PLASMA DISCHARGE IN A CAVITATING LIQUID

One of the new promising ways to obtain nanoscale materials, including metal oxide powders is the combined effect of the elastic oscillations of high intensity ultrasound and pulsed or steady electric fields in a liquid medium. This type of plasma, being of great interest as a new object of physical study, has several advantages as a method for the synthesis of nanomaterials—a relatively narrow particle size distribution of the synthesized nanopowder, specific composition and the properties of nanomaterials [5,6].

More specifically, the traditional arc discharge in aqueous electrolytes, which is widely used in engineering, is the most well-known form of stationary plasma discharge in liquid media. For many years, such discharge is used in physicochemical studies and in the synthesis of various materials. The specific

feature of arc discharge in liquid media is the localization of plasma region near the electrode ends and "falling" form of volt-ampere characteristics.

However, when ultrasonic cavitation is applied to a liquid, phase composition and physical properties of the liquid change abruptly, and this effect can lead to some specific features of the formation of electric discharges in the liquid. In the region of intensive cavitation, the fraction of gas-vapor component in the liquid has a significant value, therefore it can be assumed that the conditions of electric breakdown in the cavitation region should become easier, which can result in the initiation of different forms of discharges. Varying the parameters of ultrasonic field, it is apparently possible to exert an influence on the processes of plasma glow in a cavitating liquid. Furthermore, in this configuration, ultrasonic cavitation will interact with micro- and nanoparticles obtained in plasma and affect their physical properties and surface characteristics. The objective of the present work is to check this hypothesis and, moreover, to analyze the features of such acoustoplasma discharge and possible chemical conversions that can occur under its excitation in water and water-hydrocarbon mixtures.

Acoustoplasma technique involves the initiating of an electric discharge in a liquid that goes along with ultrasonic power assisted cavitation. In general, the specially designed acoustoplasma reactor includes a reservoir with two immersed electrodes and ultrasonic cavitator. Cavitation bubbles in the liquid phase provide the outstanding characteristics of a discharge and these characteristics have been proven to be governed by the regimes of ultrasonification [5-8]. Furthermore, ultrasonic power prevents the secondary agglomeration of nanoparticles being synthesized from metal electrodes in electric discharge.

In previous studies, it was found that combined excitation of electric arc discharge and acoustic cavitation in water and organic liquids was an effective method to create free hydrogen and various kinds of solid nanoparticles. Chemical compositions, dimensions, morphologies, optical and other properties of these nanoparticles can be easily regulated by the plasma discharge parameters, materials of electrodes and liquids. In other works, it was demonstrated that ultrasonic cavitation itself is a promising way for modification of properties of solid nano- and microparticles [9-16].

Materials or nanostructures exhibiting superior electrochemical properties are advisable for supercapacitors. The main factors to be considered to develop a high performance electrode material are the activity of electro-active species, and the transport ease of electrolytes, electrodes and reactants. The structure of the active material plays a major role in the activity of the electrode material. From the technological and scientific point of view the fabrication of well-defined morphology with nano-architecture, macro/mesopores, and tunable size is to be considered. Literature shows a variety of materials being used for supercapacitor applications. Along with the above mentioned properties, the material must also be structurally and mechanically stable to retain a good life after repeated cycles of operation and should exhibit a good value of specific capacitance.

As a result of these experiments, acoustoplasma technique has been demonstrated to be a new interesting approach to get nanomaterials in two ways in the same reaction–solid powders precipitating in the reaction vessel and gaseous aerosol containing oxide nanoparticles exhibiting the density comparable with that of air. Two perspective avenues of the utilization of these nanopowders can be performed: nanoparticles could first be deposited on a flat substrate and so create a surface modifying coating and the second option is an entrainment of the nanoparticles into the monomer matrix which can be polymerized afterwards yielding a polymer with immobilized nanoparticles.

CONCLUSIONS

Acoustoplasma technique based on the combination of a discharge in liquid with acoustic cavitation treatment provides an effective route for the synthesis of solid nanoparticles of metals, metal oxides and semiconductors. Nanoparticles, synthesized by acoustoplasma technique demonstrate interesting physical properties and can be effectively applied for different applications, such as electrodes of energy storage devices.

ACKNOWLEDGEMENTS

This work has been partially supported by project RFBR No. 18-32-20150.

REFERENCES

1. Le, Yu, G. Zhang, C. Yuan and X.W. Lou. 2013. "Hierarchical $NiCo_2O_4$@MnO_2 core-shell heterostructured nanowire arrays on Ni foam as high performance Supercapacitor Electrodes," *Chem. Commun.*, 49:137-139.
2. Xu, K., W. Li, Q. Liu, B. Li, X. Liu, L. An, Z. Chen, R. Zou and J. Hu. 2014. "Hirarchical mesoporous $NiCo_2O_4$@MnO_2 core-shell nanowire arrays on Ni foam for aqueous asymmetric supercapacitors," *Journal of Material Chemistry*, 39(7):456-459.
3. Deng, F., J. Tie, B. Lan, M. Sun, S. Peng, S. Deng, B. Li, W. Sun and L. Yu. 2015. "$NiCo_2O_4$/MnO_2 heterosructured nanosheet, influence on preparation conditions on its electrochemical properties", *Electrochemica Acta*, 176:359-366.
4. Bao, F., Z. Zhang, W. Guo, and X. Liu. 2015. "Facile synthesis of three dimensional $NiCo_2O_4$@MnO_2 Core-shell nanosheet arrays and its Supercapacitive Performance," *Electrochimica Acta*, 157:31-40.
5. Klassen, N., O. Krivko, V. Kedrov, S. Shmurak, A. Kiselev, I. Shmyt'ko, E. Kudrenko, A. Shekhtman, A. Bazhenov, T. Fursova, V. Abramov, N. Bulychev and E. Kisterev. 2010. "Laser and Electric Arc Synthesis of Nanocrystalline Scintillators", *IEEE Transactions on Nuclear Science*, 57(3):1377-1381.
6. Bulychev, N.A., M.A., Kazaryan, E.S. Gridneva, E.N. Muravev, V.F. Solinov, K.K. Koshelev, O.K. Kosheleva, V.I. Sachkov and C.H. Chen. 2012. "Plasma discharge with bulk glow in the liquid phase exposed to ultrasound", *Bulletin of the Lebedev Physical Institute*, 39(7):214-220.

7. Bulychev, N.A., M.A. Kazaryan, L.L. Chaikov, I.S. Burkhanov and V.I. Krasovskii. 2014. "Nanoscale metal oxide particles produced in the plasma discharge in the liquid phase upon exposure to ultrasonic cavitation. 1. Method for producing particles," *Bulletin of the Lebedev Physical Institute*, 41(9):264-268.
8. Burkhanov, I.S., L.L. Chaikov, N.A. Bulychev, M.A. Kazaryan and V.I. Krasovskii. 2014. "Nanoscale metal oxide particles produced in the plasma discharge in the liquid phase upon exposure to ultrasonic cavitation. 2. Sizes and stability. Dynamic light scattering study," *Bulletin of the Lebedev Physical Institute*, 41(10):297-304.
9. Ganiev, R.F., N.A. Bulychev, V.N. Fomin, I.A. Arutyunov, C.D. Eisenbach, V.P. Zubov and E.B. Malyukova. 2006. "Effect of mechanical activation on surface modification in aqueous pigment disperse systems," *Chemical Reports*, 407:54-56.
10. Bulychev, N.A., E.V. Kisterev, I.A. Arutunov and V.P. Zubov. 2008. "Ultrasonic Treatment Assisted Surface Modification of Inorganic and Organic Pigments in Aqueous Dispersions," *Journal of the Balkan Tribological Association*, 1(14):30-39.
11. Ivanov, A.V., V.N. Nikiforov, S.V. Shevchenko, V.Yu. Timoshenko, V.V. Pryadun, N.A. Bulychev, A.B. Bychenko and M.A. Kazaryan. 2017. "Properties of Metal Oxide Nanoparticles Prepared by Plasma Discharge in Water with Ultrasonic Cavitation," *International Journal of Nanotechnology*, 14(7/8):618-626.
12. Bulychev, N., B. Dervaux, K. Dirnberger, V. Zubov, F.E. Du Prez and C.D. Eisenbach. 2010. "Structure of Adsorption Layers of Amphiphilic Copolymers on Inorganic or Organic Particle Surfaces," *Macromolecular Chemistry and Physics*, 9(211):971-977.
13. Zubov, V.P., N.V. Serebryakova, I.A. Arutyunov, I.F. Kuz'kina, N.A. Bulychev and Yu. A. Khrustalev. 2004. "The effect of mechanical activation of the surface of inorganic pigments on the stability of their aqueous dispersions in the presence of ethylhydroxyethyl cellulose," *Colloid Journal*, 66(3):302-310.
14. Ioni, Yu. V., S.V. Tkachev, N.A. Bulychev and S.P. Gubin. 2011. "Preparation of Finely Dispersed Nanographite," *Inorganic Materials*, 47(6):597-602.
15. Rudnev, A.V., N.G. Vanifatova, T.G. Dzherayan, E.V. Lazareva and N.A. Bulychev. 2013. "Study of stability and dispersion composition of calcium hydroxyapatite in aqueous suspensions by capillary zone electrophoresis," *Russian Journal of Analytical Chemistry*, 68(8):700-705.
16. Kirilina, Yu.O., I.V. Bakeeva, N.A. Bulychev and V.P. Zubov. 2009. "Organic-inorganic hybrid hydrogels based on linear poly(N-vinylpyrrolidone) and products of hydrolytic polycondensation of tetramethoxysilane,"*Polymer Science Series B*, 51(3-4):135-140.

2018 International Theoretical and Practical Conference on Alternative and Smart Energy (TPCASE 2018)
ISBN: 978-1-60595-617-6

Synthesis of Hydrogen by Pyrolysis of Liquid Media in Low-Temperature Plasma Under Ultrasonic Treatment

Nikolay Bulychev

ABSTRACT

The paper shows, that a low-temperature plasma initiated in liquid media in interelectrode discharge gap is able to decompose hydrogen containing organic molecules resulting in obtaining gaseous products with volume part of hydrogen higher than 90% (up to gas chromatography data). Tentative assessments of energy efficiency, calculated with regard for hydrogen and feedstock heating value and energy consumption, have shown efficiency factor of 60-70%, depending on the source mixture composition. Theoretical model calculations of discharge current and voltage have been performed; the values are in good accordance with experimental data.

Keywords: Plasma, hydrogen, liquid media, hydrocarbons.

INTRODUCTION

One of the issues in the modern alternative energy of the day is the development of methods and technologies of hydrogen production to be used as fuel.
The most commonly used technologies of hydrogen production today are steam reforming of methane and electrolysis. The advantage of methane steam conversion is a high value of energy efficiency (60-80%); however, it requires bulky and expensive equipment, and it also consumes methane, which is fuel and valuable feedstock for chemical industry itself. Water electrolysis is less expensive in terms

P.N. Lebedev Physical Institute of RAS, 53, Leninsky Avenue, Moscow, 119991, Russia, Moscow Aviation Institute (National Research University), 4, Volokolamskoe shosse, Moscow, 125993, Russia

of capital investments, but electrolysis process industrial efficiency has almost attained estimated performance nowadays and it ranks considerably below methane steam conversion in speed and energy efficiency; besides, electrolysis requires preliminary water treatment. Therefore, there is a necessity for developing alternative hydrogen production methods from varying available feedstock.

Pilot experiments have allowed finding out that new form of electrical discharge could be in existence in liquid in intensive ultrasonic field above cavitation threshold, characterized by volume glow throughout interelectrode gap and by increasing current-voltage characteristic peculiar to abnormal glow discharge in gas [1,2]. Such microbubbles with extended interface discharge could be of interest for generating new acousto-plasma-chemical processes, as extended gas-liquid interface leads to diffusion fluxes of reactive species augmentation from plasma into liquid. It is potentially possible to conduct a large number of new chemical reactions [2-4]. Pilot experiments have shown that solid-phase carbon-bearing products are derived as a result of liquid hydrocarbons decomposition reaction in acousto-plasma discharge, as well as chemical conversions in liquid phase take place and hydrogen-containing combustible gas is generated.

EXPERIMENTAL STUDIES

The setup consists of a reaction chamber, where discharge electrodes and an ultrasonic irradiator are introduced, a generator of high-voltage pulses for discharge initiation, a power supply of discharge in liquid, an ultrasonic generator and blocks of control of electric and acoustic characteristics. The chamber is provided with quartz windows for the observation of dynamic processes and registration of optical spectra of visible discharge glow. For a detailed description of the experiment, it is referred to the literature [2,3].

The ultrasonic generator with a piezoceramic transducer provides the output acoustic power up to 2 kW in the frequency range 27-44 kHz. The parameters of acoustic equipment allow one to implement the intensity of an ultrasonic field in the volume of liquid up to 10 W/cm^2 and to vary cavitation regime in a wide range.

Water, alcohols, hydrocarbons and their mixtures have been used as feedstock. Physicochemical fundamentals of the process consist in breaking down of complicated hydrogenous molecules and in their ionization succeeded by posterior recombination to form simple molecules: H_2, H_2O, C, CO_2, MOx, where M is plasma electrodes material. Plasma discharge, triggered in the reactor between metal and graphitized electrodes, is maintained by specially designed direct or alternating voltage supply, which allows investigating plasma characteristics effect on reaction and chemical composition of its products.

The investigation of reaction gaseous products during acoustoplasma discharge in fluid mediums has allowed finding out that the basic gaseous product is hydrogen [1,7]. Thus, the possibility of handed hydrogen production in the breakdown of

various liquids by acoustoplasma discharge has been investigated. In addition, discharge current and voltage, as well as evolved gas volume have been observed; besides, gas compositional analysis has been carried out by gas chromatography. Discharge current and voltage values are necessary for calculating the quantity of energy needed for resolution of source liquid mass identity, as well as for calculating the quantity of energy needed for hydrogen unit mass production.

Chromatographic analysis of gas mixture reveals that nearly pure hydrogen (98%) is produced in acoustoplasma water breakdown, carbon oxides are also constituents of evolved gas in organic liquid breakdown, but their concentration is no more than 5-6%, since main carbon in organic liquid breakdown is evolved as solid precipitation - colloidal carbon. Calculations of gas mixture quantity, formed in organic liquid breakdown, show that efficiency is heavily dependent on discharge current, as well as on discharge voltage, which could vary in relation to interelectrode gap size in the reaction chamber. In experiments discharge current is 4-8A, discharge voltage is 30-45V in relation to a type of liquid. It is found that the use of the lowest quality feedstock is assumed with the use of acoustoplasma method, i.e. there is no need for costly scavenging treatment.

A significant advantage is also the lack of toxic and hard recyclable waste by-products of the given synthesis, as well as the fact that gas mixture leaves reactor under slight pressure (0.2-0.3 atm), that simplifies its primary blowing-up. Hydrogen-bearing gas could be used as fuel immediately after synthesis, i.e. it doesn't require separation as it contains little more than CO_2 admixtures and water vapour in addition to hydrogen. The by-product of hydrogen production with the use of acoustoplasma method in organic liquid breakdown is carbon, formed in the shape of agglomerated nanoparticles of different structure and precipitated to the bottom of the reaction chamber during the reaction. Scanning and transmission electron microscopy analysis of these nanoparticles has shown that carbon fibers, nanotubes, plates etc. as well as metal oxide nanoparticles with peculiar physical properties could be obtained during the reaction [5-12]. Obtained nanoparticles and their agglomerates could be used also as filling material, colorants, components of composites etc.

CONCLUSIONS

Thus, it is shown that acoustoplasma method of hydrogen production has a number of advantages as compared with the most commonly used nowadays steam reforming of methane and electrolysis. At efficiency factor of 60-70%, comparable with steam reforming of methane, the suggested method doesn't require bulky and expensive equipment and it outperforms electrolysis for rate and energy efficiency. The essential advantage of the suggested method is the possibility to use a wide variety of source materials.

ACKNOWLEDGEMENTS

This work has been partially supported by project MD-3964.2018.8.

REFERENCES

1. Klassen, N., O. Krivko, V. Kedrov, S. Shmurak, A. Kiselev, I. Shmyt'ko, E. Kudrenko, A. Shekhtman, A. Bazhenov, T. Fursova, V. Abramov, N. Bulychev and E. Kisterev. 2010. "Laser and Electric Arc Synthesis of Nanocrystalline Scintillators," *IEEE Transactions on Nuclear Science*, 57(3):1377-1381.
2. Bulychev, N.A., M.A., Kazaryan, E.S. Gridneva, E.N. Muravev, V.F. Solinov, K.K. Koshelev, O.K. Kosheleva, V.I. Sachkov and C.H. Chen. 2012. "Plasma discharge with bulk glow in the liquid phase exposed to ultrasound," *Bulletin of the Lebedev Physical Institute*, 39(7):214-220.
3. Bulychev, N.A., M.A. Kazaryan, L.L. Chaikov, I.S. Burkhanov and V.I. Krasovskii. 2014. "Nanoscale metal oxide particles produced in the plasma discharge in the liquid phase upon exposure to ultrasonic cavitation. 1. Method for producing particles," *Bulletin of the Lebedev Physical Institute*, 41(9):264-268.
4. Burkhanov, I.S., L.L. Chaikov, N.A. Bulychev, M.A. Kazaryan and V.I. Krasovskii. 2014. "Nanoscale metal oxide particles produced in the plasma discharge in the liquid phase upon exposure to ultrasonic cavitation. 2. Sizes and stability. Dynamic light scattering study," *Bulletin of the Lebedev Physical Institute*, 41(10):297-304.
5. Ganiev, R.F., N.A. Bulychev, V.N. Fomin, I.A. Arutyunov, C.D. Eisenbach, V.P. Zubov and E.B. Malyukova. 2006. "Effect of mechanical activation on surface modification in aqueous pigment disperse systems," *Chemical Reports*, 407:54-56.
6. Bulychev, N.A., E.V. Kisterev, I.A. Arutunov and V.P. Zubov. 2008. "Ultrasonic Treatment Assisted Surface Modification of Inorganic and Organic Pigments in Aqueous Dispersions," *Journal of the Balkan Tribological Association*, 1(14):30-39.
7. Ivanov, A.V., V.N. Nikiforov, S.V. Shevchenko, V.Yu. Timoshenko, V.V. Pryadun, N.A. Bulychev, A.B. Bychenko and M.A. Kazaryan. 2017. "Properties of Metal Oxide Nanoparticles Prepared by Plasma Discharge in Water with Ultrasonic Cavitation," *International Journal of Nanotechnology*, 14(7/8):618-626.
8. Bulychev, N., B. Dervaux, K. Dirnberger, V. Zubov, F.E. Du Prez and C.D. Eisenbach. 2010. "Structure of Adsorption Layers of Amphiphilic Copolymers on Inorganic or Organic Particle Surfaces," *Macromolecular Chemistry and Physics*, 9(211):971-977.
9. Zubov, V.P., N.V. Serebryakova, I.A. Arutyunov, I.F. Kuz'kina, N.A. Bulychev and Yu.A. Khrustalev. 2004. "The effect of mechanical activation of the surface of inorganic pigments on the stability of their aqueous dispersions in the presence of ethylhydroxyethyl cellulose," *Colloid Journal*, 66(3):302-310.
10. Ioni, Yu. V., S.V. Tkachev, N.A. Bulychev and S.P. Gubin. 2011. "Preparation of Finely Dispersed Nanographite," *Inorganic Materials*, 47(6):597-602.
11. Rudnev, A.V., N.G. Vanifatova, T.G. Dzherayan, E.V. Lazareva and N.A. Bulychev. 2013. "Study of stability and dispersion composition of calcium hydroxyapatite in aqueous suspensions by capillary zone electrophoresis," *Russian Journal of Analytical Chemistry*, 68(8):700-705.
12. Kirilina, Yu. O., I.V. Bakeeva, N.A. Bulychev and V.P. Zubov. 2009. "Organic-inorganic hybrid hydrogels based on linear poly(N-vinylpyrrolidone) and products of hydrolytic polycondensation of tetramethoxysilane," *Polymer Science Series B*, 51(3-4):135-140.

2018 International Theoretical and Practical Conference on Alternative and Smart Energy (TPCASE 2018)
ISBN: 978-1-60595-617-6

Hydrogen Production from Polymer Waste in a Gas-Flow Reactor

Hunda Li, Svetlana Garelina, Nikolay Bulychev, Sergey Kolesnik and Mishik Kazaryan

ABSTRACT

We present a theoretical underpinning of technological and design requirements for a discharge device based on a high-voltage pulse-periodic discharge for the development of a reactor for plasma-chemical recycling of polymer waste into hydrogen and other valuable products. Geometrical parameters, gas flow velocity, power capacity of the discharge power supply, output, and the pulse repetition rate of the discharge device were determined. It was demonstrated that in order to reduce the energy needed for polymer waste recycling, the energy released at the mutual association of the dissociation products and their association with the reagent can be used for partial dissociation of the molecules of the processed materials.

Keywords: Hydrogen, polymer waste, recycling, discharge.

INTRODUCTION

The amount of polymer waste produced all over the world grows every year. This, naturally, adversely affects the environment [1, 2]. In most countries dumping

Hunda Li, Department equipment engineering, Shenyang Ligong University, 6, Nanping Central Road, Shenyang, 110159, China

Svetlana Garelina, Civil Defence Academy EMERCOM of Russia, Khimki, 141435, Russia

Nikolay Bulychev, P.N. Lebedev Physical Institute of the Russian Academy of Sciences, 53, Leninskiy Avenue, Moscow, 119991, Russia; Moscow Aviation Institute (National Research University), 4, Volokolamskoe shosse, Moscow, 125993, Russia

Sergey Kolesnik, Moscow Aviation Institute (National Research University), 4, Volokolamskoe shosse, Moscow, 125993, Russia

Mishik Kazaryan, P.N. Lebedev Physical Institute of the Russian Academy of Sciences, 53, Leninskiy Avenue, Moscow, 119991, Russia

and burning are still the most common ways for utilization of polymer waste [3, 4]. It is apparent, however, that dumping cannot be considered as a safe way for utilization of the polymer waste. In fact, only 9% of the polymer waste is recycled, 12% is burned, and 79% is sent to disposal sites or left in the natural environment [5]. The main factor that constrains the use of burning is the emission of toxic vapours and fly ash [6].

Plasma-chemical technologies can be considered as one of the promising methods. These technologies provide massive reactional opportunities as well as optimal parameters for technological processes, and consequently, they ensure ecological safety, cost-effectiveness, and versatility [7–10]. The technologies for plasma-chemical recycling of waste have appeared relatively recently. In spite of their obvious advantages, to date, polymer waste recycling involving the plasma-chemical technique has not been worked out at an industrial scale. This requires the development of reactors. In this respect, accumulation of experimental and theoretical data on the plasma-chemical processes that occur in such reactors is of vital importance for optimization of the reactor operation and prediction of its performance.

For plasma generation, a high-voltage source of pulse-periodic discharge was chosen. This discharge is widely employed in the lasers based on various chemical species [11], and the corresponding dissociation efficiency for different chemical compounds is comparable to that of the other types of discharge commonly employed in nonequilibrium plasma chemistry.

NUMERICAL EXPERIMENT

The goal of the present study is to consider the provability of technological characteristics of the device and the operating mode of the reactor for recycling of polymer waste with production of hydrogen and other valuable products. The discharge device suitable for the use in the proposed reactor was a cube with two dielectric walls and an electrode assembly with the working gas mixture pumped through the discharge gap. A similar device was previously used in the experimental constructions of different modules of copper vapour lasers [11]. The conditions for the numerical calculations were chosen based on the analysis of the operating mode of the high-voltage pulse-periodic discharge in copper vapour lasers [11]: the pumped inert gas (helium) involved a flow of polymer waste molecules and the reagent inside the discharge device, the gas temperature was taken to be equal to 1500 K, discharge efficiency was η = 30%, the reagent was calcium, the concentrations of the recycled materials were $n = 10^{14}$, 10^{15}, and 10^{16} cm^{-3}, the concentration of the inert gas was $n_g = 10^{17}$, 10^{18}, 10^{19} cm^{-3}.

The condition for efficient operation of the discharge device is minimization of the energy losses associated with excitation and dissociation of the association products. For clarity, it was suggested that the minimum times of volume

association τa min and diffusion $\tau_{D\,min}$ of atoms to the walls of the discharge device were 10 times higher than the time $t = c/u$ the molecules of the recycled materials stayed inside the discharge device: $\tau_{a\,min} = \tau_{D\,min} = 10t$.

The characteristic time of association was determined by relation (1) [12]:

$$\tau_a = \frac{1}{\alpha n_Y n_X}, \tag{1}$$

where n_X and n_Y are the concentrations of the dissociated polymer waste molecules, which associate mutually or associate with the atoms of the reagent added into the discharge device, α is the recombination coefficient.

The characteristic time of diffusion of atoms X to the walls and electrodes of the discharge device was found according to relation (2) [13]:

$$\tau_D = \frac{\Lambda^2}{D}, \tag{2}$$

where $D = \frac{3}{16 n_g (r_g + r)^2}\left(\frac{2kT}{\pi \frac{m_g m}{m_g + m}}\right)$ is the diffusion coefficient for atoms X in the inert gas, $\frac{1}{\Lambda^2} = \frac{2\pi^2}{D}$ is the characteristic diffusion length, m_g, r_g are the mass and the radius of the inert gas atoms, T is the temperature of the inert gas, m and r are the mass and the radius of atoms X.

The velocity v of the gas mixture flow through the volume was calculated as:

$$v = Su = \frac{cS}{0.1\tau_{a\,\min}}, \tag{3}$$

where $S = ab$ is the cross-section of the gas flow.

The power capacity of the power source and the rate of polymer waste recycling were determined using (4) and (5):

$$W = \frac{vnQ}{\eta}, \tag{4}$$

$$P = vnM, \tag{5}$$

where Q is the energy required for breaking all chemical bonds in the molecule, M is the mass of the molecule of the recycled material.

The repetition rate of the discharge pulses was calculated by (6):

$$f \geq f_{\min} = W\eta / VnQ, \tag{6}$$

where V is the volume of the discharge gap.

The concentration n_{Ca} of calcium atoms for the considered recycled material was found as (7):

$$n_{Ca} = \theta \cdot n, \tag{7}$$

where the value of θ specifies the maximum number of Ca atoms capable of reacting with the atoms appearing due to dissociation of the polymer molecule: for polyethylene θ is equal to 0.5, for polyvinylchloride – to 1.5, and for polyethyleneterephthalate it is 3 according to [14].

The value of $\tau_{a\ min}$ was calculated using (1) on the assumption that $n_X = n_{C2}$, and $n_Y = n_{Ca}$. The estimate value of the association coefficient α was taken as $\alpha = 2.98 \cdot 10^{-33}$ cm^6/s, which corresponds to the rate of recombination of Ca and C_2 at a temperature of 1500 K, according to [14]. The value of $\tau_{D\ min}$ for hydrogen atoms was calculated using (2).

The numerical results are given in TABLE I.

From the technological point of view, the velocities of several tens of m/s can hardly be suitable for a closed reaction chamber. Significant decrease in the gas flow velocity can be achieved by switching to pulse periodic discharges. In this case, the length of the discharge device can be increased greatly with respect to its lateral dimensions. In order to minimize the energy losses at dissociation and excitation of the molecules of the products, which are formed in the processes of mutual association of the dissociation products and association of the latter with the reagent, the duration t_{raz} of the discharge must satisfy the following requirements: $t_{raz} << \tau_a$, $t_{raz} << \tau_D$. Under these conditions, the time the molecules of the recycled materials stay inside the discharge device can be rather long: $t = k \cdot \tau_{a\ min}$, $k \geq 1$.

Using the data given in TABLE I it is simple to evaluate the output of the plasma-chemical reactor for a particular power source. For example, given that $n_g = 1 \cdot 10^{18}$ cm^{-3} and $n = 1 \cdot 10^{16}$ cm^{-3}, we obtain the power capacity of the power source to be 38377 J/s (TABLE I). For these conditions, let us find the output of the reactor using 1.31 kg of CaC_2, and 0.08 kg of H_2 will be obtained per hour, and 0.82 kg of Ca will be required for this. Thus, in the case of polyethylene recycling, the output will be 0.57 kg/h. Under the same conditions, the output of the plasma-chemical reactor will be 1.47 kg/h at polyvinylchloride recycling. For a 50 kW power source, the output of the reactor is 0.74 kg/h for polyethylene, 1.6 kg/h for polyvinylchloride, and 1.11 kg/h for polyethyleneterephthalate. It should be noted that the recycling products include hydrogen.

TABLE I. YIELDS OF RECYCLING PRODUCTS AND REAGENT CONSUMPTION (KG/H).

n_g (cm^{-3})	n (cm^{-3})	polyethylene			polyvinylchloride				polyethyleneterephthalate			
		CaC_2	H_2	Ca	CaC_2	H_2	$CaCl_2$	Ca	CaC_2	H_2	CO	Ca
$1\cdot10^{17}$	$1\cdot10^{14}$	13.08	0.82	8.17	15.1	0.71	13.08	14.17	32.03	1.33	18.66	20.03
$1\cdot10^{17}$	$1\cdot10^{15}$	41.35	2.58	25.83	47.75	2.24	41.35	44.8	101.3	4.22	59.01	63.35
$1\cdot10^{17}$	$1\cdot10^{16}$	130.8	8.16	81.68	151	7.07	130.8	141.7	320.3	13.33	186.6	200.3
$1\cdot10^{18}$	$1\cdot10^{14}$	0.13	0.008	0.08	0.15	0.007	0.13	0.14	0.32	0.01	0.19	0.200
$1\cdot10^{18}$	$1\cdot10^{15}$	0.41	0.03	0.26	0.48	0.02	0.41	0.45	1.013	0.04	0.59	0.634
$1\cdot10^{18}$	$1\cdot10^{16}$	1.31	0.08	0.82	1.51	0.07	1.31	1.42	3.20	0.13	1.87	2.000
$1\cdot10^{19}$	$1\cdot10^{14}$	0.001	$8\cdot10^{5}$	$8\cdot10^{4}$	0.002	$7\cdot10^{5}$	0.001	0.001	0.003	$1\cdot10^{4}$	0.002	0.002
$1\cdot10^{19}$	$1\cdot10^{15}$	0.004	$3\cdot10^{4}$	0.003	0.005	$2\cdot10^{4}$	0.004	0.004	0.01	$4\cdot10^{4}$	0.006	0.006
$1\cdot10^{19}$	$1\cdot10^{16}$	0.01	$8\cdot10^{4}$	0.008	0.015	$7\cdot10^{4}$	0.013	0.014	0.03	0.001	0.02	0.020

CONCLUSION

Thus, at present, there is the background for the development and construction of an experimental prototype of a reactor for plasma-chemical recycling of polymer waste with production of hydrogen. In order to reduce the energy required for recycling of the polymer waste, it is possible to partially use the energy, which is released at the mutual association of the dissociation products and their association with the reagent, for dissociation of the molecules of the recycled materials, thus reducing the energy needed for polymer waste recycling.

ACKNOWLEDGEMENTS

This work has been partially supported by project MD-3964.2018.8.

REFERENCES

1. Andrady, A.L. 1994. “Assessment of environmental biodegradation of synthetic polymers,” *J. Mol. Sci. C.*, 34(1):25-76.
2. Oehlmann, J., U. Schulte-Oehlmann, W. Kloas, O. Jagnytsch, I. Lutz, K.O. Kusk, L. Wollenberger, E.M. Santos, G.C. Paull, K.J.W. Van Look, and C.R. Tyler. 2009. “A critical analysis of the biological impacts of plasticizers on wildlife,” *Philos. Trans. Royal Soc. B*, 364(1526), 2047-2062.
3. Saleem, J., M.A. Riaz, and M. Gordon. 2018. “Oil sorbents from plastic wastes and polymers: a review,” *J. Hazard. Mater.*, 341:424-437
4. Zhou, C., W. Fang, W. Xu, A. Cao, and R. Wang. 2014. “Characteristics and the recovery potential of plastic wastes obtained from landfill mining,” *J. Clean. Prod.*, 80:80-86.
5. Geyer, R., J.R. Jambeck, and K.L. Law. 2017. “Production, use, and fate of all plastics ever made,” *Sci. Adv.*, 3(7):e1700782.

6. Siddique, R., J. Khatib, and I. Kaur. 2008. “Use of recycled plastic in concrete: A review,” *Waste Manag.*, 28(10):1835-1852.
7. Borodin, V.I. 2004. *Plasma technologies: A Guide*. Petrozavodsk: Federal Agency for Education. Petrozavodsk State University, 56 p. [in Russian]
8. Vlasov, V.A., S.A. Sosnovsky, and I.A. Tikhomirov. 2008. “Plasmachemical high-frequency plants for frade waste conversion,” *Bull. Tomsk Polytech. Univ.*, 305(3):352-358.
9. Petrov, S.V., S.G. Bondarenko, E.G. Didyk, and A.A. Didyk. 2010. “Plasma technologies for reproducible energy sources,” *Power and electrification*, (1):53-59. [in Russian]
10. Petrov, S.V., G.S. Marinsky, A.V. Chernets, V.N. Korzhyk, and V.M. Mazunin. 2006. “Employment of a vapour-plasma process for pyrolysis of organic waste, including medical and hazardous waste,” *Advances in Electrometallurgy*, (4):57-66.
11. Batenin, V.M., V.V. Buchanov, A.M. Boichenko, M.A. Kazaryan, I.I. Klimovskii, and E.I. Molodykh. 2017. *High-brightness Metal Vapour Lasers. Volume I: Physical Fundamentals and Mathematical Models*. Boca Raton: CRC Press, 542 p.
12. Panchenkov, G.M., and V.P. Lebedev. 1961. *Chemical kinetics and catalysis.* Moscow: Khimiya, 552 p. [in Russian]
13. McDaniel, E.W. 1964.*Collision phenomena in ionized gases*. New York: Wiley, 797 p.
14. Bulychev, N.A., M.A. Kazaryan, V.I. Sachkov, and I.N. Feofanov. 2014. “On the calculation of some kinetic constants for binary molecules in plasma,” in *Abstracts of all-Russian workshop Physical and technical aspects of volume neutron source for materials science, technological research, and nuclear power engineering purposes*, Zvenigorod, June 15-19, pp. 115-116, [in Russian].

2018 International Theoretical and Practical Conference on Alternative and Smart Energy (TPCASE 2018)
ISBN: 978-1-60595-617-6

Advanced Materials for Nickel—Metal Hydride Chemical Power Sources

Alexei Volodin, Boris Tarasov and Dmitry Blinov

ABSTRACT

A general survey on Ni-MH power sources is given, their advantages and disadvantages are shown, and the reported experimental data for improving their performance are summarized. The prospect of using carbon nanostructures to improve the performance of electrodes is considered and the effectiveness of their use is shown. The resulting materials can be used to produce electrodes for Ni-MH batteries and metal hydride fuel cells.

INTRODUCTION

Nickel-metal hydride (Ni-MH) alkaline power sources occupy one of the leading positions in the market due to their high energy density, cyclic stability, and good environmental compatibility [1, 2]. In terms of energy storage capacity and cyclic stability, Ni-MH sources are inferior only to lithium-ion (Li-Ion) batteries, and in terms of safety in operation, they significantly exceed the latter. The efficiency of a metal hydride power source is affected by the composition of cathode and anode materials, the method of preparing electrodes, the contact density between the active electrode material and the current collector, the diffusion of hydrogen in the volume of a metal hydride, the chemical and physical nature of the electrolyte, etc. In order to improve the performance of Ni-MH power sources a complex modification of the anode, cathode and electrolyte compositions can be used, as well as promising new materials able to increase electrical conductivity, to ensure good contact of the electrodes and high kinetics of charge-discharge processes.

Alexei Volodin, Boris Tarasov, Institute of Problems of Chemical Physics of the Russian Academy of Sciences, 1, Semenov Avenue, Chernogolovka, 142432, Russia
Dmitry Blinov, Joint Institute for High Temperatures of the Russian Academy of Sciences, 13 Bd.2, Izhorskaya Street, Moscow, 125412, Russia

ALKALINE POWER SOURCES

Alkaline power sources got their name from the electrolyte used in them. In most cases, it is an aqueous solution of potassium or sodium hydroxide. Among the alkaline power sources of the second kind (rechargeable batteries) and fuel cells, the most common elements are the ones with nickel as the cathode and a transition or rare-earth metal or polymetallic alloy as the anode (Ni-Fe, Ni-Zn, Ni-Cd, Ni-MH) [2, 3]. Here Ni-MH batteries are of particular interest since they have a high density of stored energy and good cyclic stability. Besides metal hydride fuel cells do not use platinum and are capable of operating at low temperatures. The capacity of different type batteries is shown in Figure 1.

In modern Ni-MH batteries, the anode consists of polymetallic alloys containing rare earth metals, and $Ni(OH)_2/NiOOH$ is used as a cathode [1–4]. During discharge hydrogen from the hydride interacts with the hydroxide ion of the electrolyte to form H_2O, and on the positive electrode, H_2O reacts with NiOOH to form $Ni(OH)_2$ and OH^-. During charging the reverse reactions take place. Thus, the reactions occurring in the battery represent the movement of hydrogen from one electrode to the other. Ni-MH batteries are more expensive than Ni-Cd, but they have 30% more capacity and do not have a memory effect.

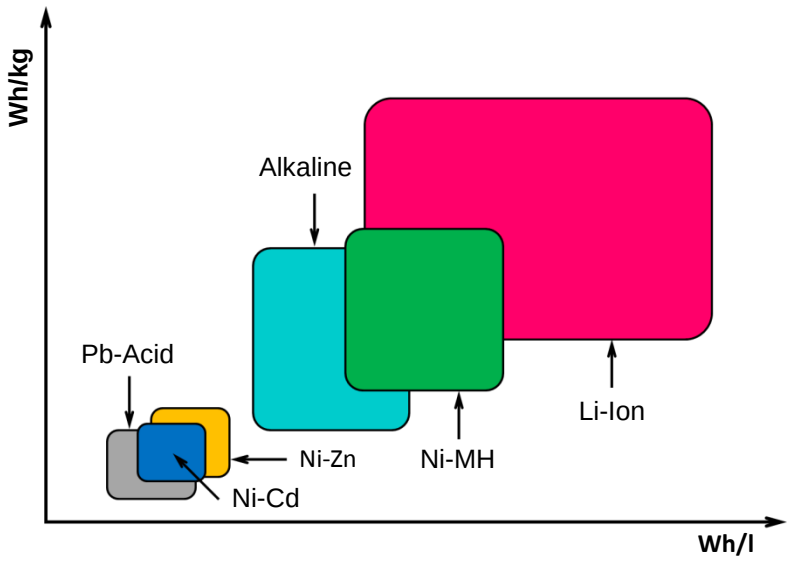

Figure 1. Energy storage capability of common rechargeable battery systems.

ANODE MATERIALS

At present, AB_5-type alloys are actively used as working materials for Ni-MH power sources. The hydrogen capacity of the $LaNi_5H_{6.6}$ hydride is ~ 1.4 wt.% [5], and the current sources based on Co-doped $LaNi_5$ reach ~ 350 mAh/g in capacity [6]. In order to increase the capacity, the alloys are usually alloyed with lighter elements, such as magnesium. It is impossible to directly introduce magnesium in the composition of $LaNi_5$, therefore, AB_3-, A_2B_7- and A_5B_{19}-type alloys are used [7]. It is also possible to improve the electrochemical parameters by combining two or more rare-earth metals (La, Ce, Nd, Pr). For example, the introduction of neodymium into the alloy can increase the resistance to oxidation, increase the exchange rate of the hydrogen reaction, as well as the rate of diffusion of hydrogen in the alloy [8]. One of the key problems in the work of anode materials is the delivery of electrons to the collector. Whereas a pure metal or intermetallic alloy has metallic conductivity, their hydrides are dielectrics. For example, the electrical conductivity of pure magnesium is 2.27×10^7 S/cm, and its hydride (MgH_2) is $10^{-18}\ldots10^{-12}$ S/cm.

CATHODE MATERIALS

$Ni(OH)_2$ is used as the cathode material in all alkaline nickel-based power sources due to its low cost, good performance and wide operating temperature range. The specific energy capacity of the cathode part (~ 290 mAh/g) is provided by the β-form of $Ni(OH)_2$. The performance of α-$Ni(OH)_2$ is somewhat better, but this phase is extremely unstable. To stabilize α-$Ni(OH)_2$, a partial substitution of nickel ions in the hydroxide lattice by cobalt ions [9] or aluminum [10] is used. In the latest work, it was shown that the addition of 7 mol.% Al to $Ni(OH)_2$ leads to an improvement in the reversibility of the reaction, a decrease in the electrochemical resistance, an increase in the specific capacity and cyclic stability. However, as in the case of anode materials, one of the key tasks remains the charge transfer process. β-$Ni(OH)_2$ has a very weak electronic conductivity ($10^{-14}\ldots10^{-8}$ S/cm) due to a large distance between neighboring Ni atoms ($d_{Ni–Ni}$ = 3.12 Å). Shorter Ni–Ni bonds (2.86 Å) of NiOOH favor a better overlap of the orbitals and higher electrical conductivity (0.01...0.05 S/cm), but this value also does not allow achieving the desired result.

COMPOSITE MATERIALS

Acetylene soot or graphite (G) is usually added to anodic and cathodic materials to improve electrical conductivity. However, as a result of side reactions (first of all, oxygen evolution at the cathode), soot oxidizes rather quickly, especially at high charge-discharge current densities. In addition, to achieve high conductivity, it is necessary to introduce these additives in large quantities, which reduces the specific capacity of the electrodes, and a small amount does not lead to the desired effect. When forming electrodes, powders of intermetallic compounds or $Ni(OH)_2$ are pressed with various additives on the collector. Such a preparation procedure can lead to a decrease in the efficiency of active materials due to poor contact between the active particles and the current collector. The inclusion of additional binding materials, such as polytetrafluoroethylene, which is a dielectric, also reduces the specific capacity of the electrodes.

The use of extended carbon nanostructures (CNS) such as Graphene-like material (GLM), carbon nanotubes (CNT) and carbon nanofibers (CNF), as alternatives to acetylene soot and graphite, is of particular interest. Composites of anodic and cathodic materials have been obtained earlier by mixing the active components with graphene-like materials [11]. In [12], multi-walled nanotubes were grown on the surface of electrode materials from nickel foam. The resulting electrode capacity was 360 mAh/g, which is 18% higher than the electrode capacitance without nanotubes. The authors of [13] grew $Ni(OH)_2$ crystals on the surface of a graphene-like material. Such composite materials not only improve charge transfer, but also reduce internal resistance. However, studies of this kind are sporadic and need to be developed systematically in order to achieve an optimal result.

In our studies [14, 15], it was noted that the addition of 3 wt.% of carbon nanotubes and nanofibers to titanium or lanthanum oxides leads to a significant increase in conductivity. Composites based on nickel hydroxide were also formed: $G/Ni(OH)_2$, $CNT/Ni(OH)_2$, $CNF/Ni(OH)_2$, and $GLM/Ni(OH)_2$ containing 3 wt.% of the carbon component. It is shown (Figure 2a) that the addition of graphite to $Ni(OH)_2$ increases the electrical conductivity from 3.7×10^{-9} to 1.33×10^{-7} S/cm; CNT – to 3.9×10^{-3} S/cm; CNF – to 6.8×10^{-3} S/cm; GLM – to 8.9×10^{-2} S/cm. The calculated volume fractions of carbon nanostructures in the composites were CNT – 6.2 vol.%; CNF – 7.1 vol.%; GLM – 6.7 vol.%. The obtained composites were used as materials for the electrodes of Ni-MH cells. Their electrochemical characteristics are studied. Preliminary results demonstrate the performance of composite electrodes in the composition of Ni-MH power sources. The addition of CNTs increases the capacity from 102 mAh/g (for pure hydroxide) to 265 mAh/g, the addition of nanofibers to 223 mAh/g, and graphene-like material to 195 mAh/g (Figure 2b).

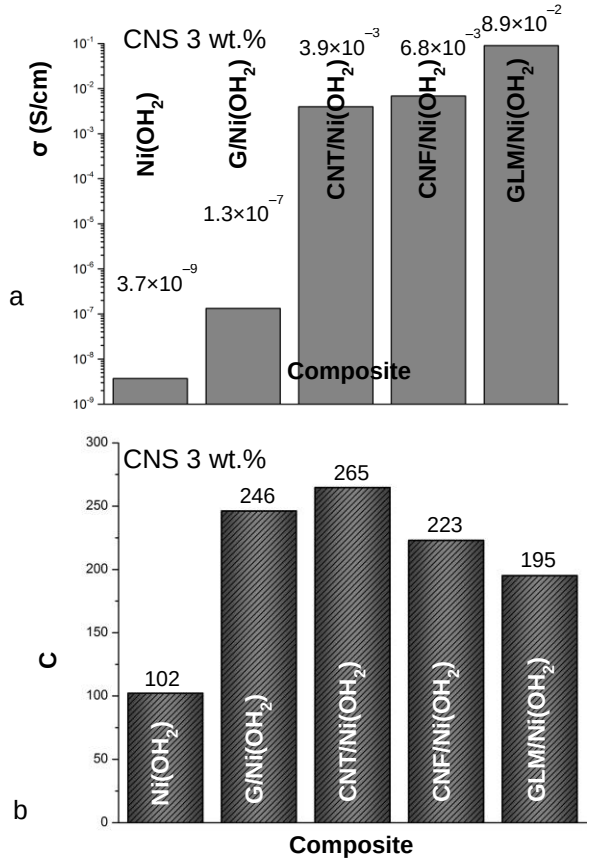

Figure 2. Electrochemical characteristics of electrode materials: a) Specific conductivity of composites; b) Specific capacity of the composite electrodes.

CONCLUSION

One of the key problems in the operation of anode and cathode materials is the delivery of electrons from active electrode materials to the collector. To achieve high conductivity, it is necessary to introduce acetylene soot or graphite additives in large quantities, which reduces the specific capacity of the electrodes, and a small amount does not lead to the desired effect. The addition of 3 wt.% carbon nanostructures (CNT, CNF, PMG) can increase the electrical conductivity of the electrode materials more than seven orders of magnitude. Composite electrodes exhibit high performance, oxidation resistance and good cyclic stability. The resulting materials can be used to produce electrodes for Ni-MH batteries and metal hydride fuel cells.

ACKNOWLEDGMENT

This research was supported by RSF (PRJ No. 17-79-20413). Boris P. Tarasov acknowledges support within the state assignment (PRJ No. 0089-2014-0030) at studies metal hydride materials microstructures.

REFERENCES

1. Winter, M., and R.J. Brodd. 2004. "What are batteries, fuel cells, and supercapacitors?" *Chem. Rev.*, 104(10):4245-4269.
2. Hannan, M.A., M.M. Hoque, A. Mohamed, and A. Ayob. 2017. "Review of energy storage systems for electric vehicle applications: Issues and challenges," *Renew. Sust. Energ. Rev*. 69:771-789.
3. Ovshinsky, S.R., M.A. Fetcenko, and J. Ross. 1993. "A nickel metal hydride battery for electric vehicles," *Science*. 260:176-181.
4. Yartys, V., D. Noreus, and M. Latroche. 2016. "Metal hydrides as negative electrode for Ni-MH batteries," *Appl. Phys. A.*, 122:43.
5. Liu, W., and K.F. Aguey-Zinsou. 2016. "Low temperature synthesis of $LaNi_5$ for hydrogen storage," *Int. J. Hydrogen Energy.*, 41:1679-1687.
6. Zhou, W., D. Zhu, Z. Tang, C. Wu, L. Huang, Z. Ma, and Y. Chen. 2017. "Improvement in low-temperature and instantaneous high-rate output performance of Al-free AB_5-type hydrogen storage alloy for negative electrode in Ni/MH battery: Effect of thermodynamic and kinetic regulation via partial Mn substituting," *J. Power Sources.*, 343:11-21.
7. Hu, W.K., R.V. Denys, C.C. Nwakwuo, T. Holm, J.P. Maehlen, J.K. Solberg, and V.A. Yartys. 2013. "Annealing effect on phase composition and electrochemical properties of the Co-free La_2MgNi_9 anode for Ni-metal hydride batteries," *Electrochim. Acta.*, 96:27-33.
8. Volodin, A.A., Ch. Wan, R.V. Denys, G.A. Tsirlina, B.P. Tarasov, M. Fichtner, U. Ulmer, C.C. Nwakwuo, and V.A. Yartys. 2016. "Phase-structural transformations in a metal hydride battery anode $La_{1.5}Nd_{0.5}MgNi_9$ alloy and its electrochemical performance," *Int. J. Hydrogen Energy*, 41:9954-9967.
9. Guo, D., E. Shangguan, J. Li, T. Zhao, Q. Li, X.Z. Yuan, and H. Wang. 2014. "Effects of γ-CoOOH coating on the high-temperature and high-rate performances of spherical nickel hydroxide electrodes," *Int. J. Hydrogen Energy.*, 39:3895-3903.
10. Huang, J., D. Cao, T. Lei, S. Yang, X. Zhou, P. Xu, and G. Wang. 2013. "Structural and electrochemical performance of Al-substituted β-$Ni(OH)_2$ nanosheets electrodes for nickel metal hydride battery," *Electrochim. Acta.*, 111:713-719.
11. Lin, J., C. Lu, Z. Cao, and L. Wang. 2016. "Ti−V−Ni with graphene-mixing icosahedral quasicrystalline composites: Preparation, structure and its application in Ni–MH rechargeable batteries," *Int. J. Hydrogen Energy.*, 41:1098-1103.
12. Xie, F., C. Dong, W. Qian, Y. Zhai, L. Li, and D. Li. 2015. "Electrochemical properties of nickel-metal hydride battery based on directly grown multiwalled carbon nanotubes," *Int. J. Hydrogen Energy*, 40:8935-8940.
13. Wang, H., H.S. Casalongue, Y. Liang, and H. Dai. 2010. "$Ni(OH)_2$ Nanoplates grown on graphene as advanced electrochemical pseudocapacitor materials," *J. Am. Chem. Soc.*, 132:7472-7477.

14. Volodin, A.A., A.A. Belmesov, V.B. Murzin, P.V. Fursikov, A.D. Zolotarenko, and B.P. Tarasov. 2013. “Electro-conductive composites based on titania and carbon nanotubes,” *Inorg. Mater.*, 49(7):656-662.
15. Volodin, A.A., P.V. Fursikov, A.A. Belmesov, Yu.M. Shulga, I.I. Khodos, M.N. Abdusalyamova, and B.P. Tarasov. 2014. “Electrical conductivity of lanthanum oxide based composites containing carbon nanofibers,” *Inorg. Mater.*, 50(7):673-681.

2018 International Theoretical and Practical Conference on Alternative and Smart Energy (TPCASE 2018)
ISBN: 978-1-60595-617-6

Simulating Thermoelectric Generator Using ANSYS Mechanical and ANSYS DesignXplorer Tools

Dmitriy Galdin, Igor Drozdov, Alexander Kretinin, Gennadiy Skomorokhov and Dmitriy Shmatov

ABSTRACT

This paper presents a description of the numerical model, and also the results of an element of a thermoelectric generating battery modeling using the ANSYS Mechanical package of the finite element analysis. To simplify the model, from the initial geometry consisting of 600 elements, only one segment was separated, containing a single junction of dissimilar semiconductor elements. The simulation was performed in a stationary formulation with the assignment of temperature dependences for the main physical properties of the used materials. Using the obtained numerical model, the dependence of the sampling efficiency on the resistance of the external load connected to the thermoelectric element was investigated. For the analysis of various variants of heat exchange systems, an analysis of the temperature gradient between the "cold" and "hot" junctions of semiconductor elements was performed. According to the obtained results, response surfaces were formed, allowing to specify the predicted efficiency at given temperature ranges. In addition, the analysis of changes in the characteristics of a thermoelectric element with different thermal conductivity properties of adhesive layers in contact with a ceramic battery cell was also described. When planning an experiment for each adhesive layer, its thermal conductivity was changed in the established range, and heat fluxes on the cooled and heated surface of the element were used as the main controlled parameters.

Keywords: thermoelectric generator, numerical simulation, Thermoelectric generator (TEG).

Voronezh State Technical University, 14, Moskovsky Avenue, Voronezh, 394026, Russia

INTRODUCTION

Modern approaches in materials science made it possible to produce thermoelectric generators (TEG). Such devices have their unique advantages over other types of mechanisms, which generate electricity. Their exclusive qualities include high reliability, durability, compact size, ecological efficiency, and the absence of vibrations, as well as operating in a wide range of temperatures. The principle of TEG operation is based on the 'Seebeck effect', which allows converting thermal energy into electrical energy. The significant amount of the research aimed at the development and improvement of the above generators have been conducted, however, thermoelectric technologies still have a long development path to a wide practical application [1-3]. The numerical method or the finite element analysis is one of the means that is widely used in the design and optimization of TEG in the early stages of the production process. They made it possible to quickly get the practical results in order to develop an optimized prototype of the product prior to conducting the full-scale tests. Several studies have described the experience of the successful appliance of finite element analysis for designing prototypes of thermoelectric devices [4, 5].

In their work, Chen et al. presented the numerical analysis of a solar thermoelectric generator. As a result, it was recognized that thermal resistance is one of the main factors in optimizing the performance of TEG. The results of Kossivakis et al. confirm the efficiency of using the finite element method for analyzing commercially available generator samples.

This paper presents the results of numerical modeling of a TEG battery cell using the commercial ANSYS software package, and, in particular, the Mechanical and DesignXplorer modules.

DESCRIPTION OF THE MATHEMATICAL MODEL

The governing equations [6-8] for describing the behavior of a thermoelectric material are determined by the pair of equations of heat conduction and the continuity equations of the current density:

$$\rho c \frac{\partial T}{\partial t} + \vec{\nabla} \cdot \vec{q} = Q \tag{1}$$

$$\vec{\nabla} \cdot \left(\varepsilon \frac{\partial \vec{E}}{\partial t} \right) + \vec{\nabla} \cdot \vec{j} = Q \tag{2}$$

Whereas: "ρ" is the density, "c" is the heat capacity, "T" is the temperature, "t" is the time, "q" is the heat flux, "Q" is the internal heat generation, "ε" is the

dielectric constant, "*E"* is the electric field, "*j"* is the density of the electric current.
The current density generated by the coupling of the reversible Seebeck effect and the irreversible Joule-Thomson effect can be formulated as:

$$\vec{J} = \sigma\vec{E} - \sigma S\vec{\nabla}T \tag{3}$$

Heat flow *q* is generated by the Peltier and Fourier pair effects and is defined as:

$$\vec{q} = \Pi\vec{j} - \kappa\vec{\nabla}T \tag{4}$$

Whereas: "Π" is the Peltier coefficient, "k" is the thermal conductivity, "σ" is the electrical conductivity, "S" is the Seebeck coefficient.
The electric field can be obtained from the electric scalar potential "ϕ" as:

$$\vec{E} = -\vec{\nabla}\phi \tag{5}$$

The related equations (1) and (2) are transformed into finite-element equations by approximation of primitive physical unknowns. Temperature "T" and electric potential "ϕ" into interpolation functions and values in a particular element node are defined as:

$$T = [N]\{T_e\} \tag{6}$$

$$\phi = [N]\{\phi_e\} \tag{7}$$

Whereas: T_e is the nodal temperature vector, "ϕ_e" is the nodal electric potential vector, "N" is the element shape function. After lengthy manipulations based on the Galerkin weighting scheme, differential equations become algebraic equations of finite elements:

$$\begin{bmatrix} C_T & 0 \\ 0 & C_E \end{bmatrix} \begin{Bmatrix} \dfrac{\partial T^2}{\partial t} \\ \dfrac{\partial \phi^2}{\partial t} \end{Bmatrix} + \begin{bmatrix} K_T & 0 \\ K_{ET} & K_E \end{bmatrix} \begin{Bmatrix} T^e \\ \phi^e \end{Bmatrix} = \begin{Bmatrix} Q \\ I \end{Bmatrix} \tag{8}$$

The global matrix equation is assembled based on individual finite element equations [9]. The solution gives the values of T_e temperature and electric φ_e potential at unlimited nodes, or reactions in the form of heat flux and, respectively electric current at nodes with superimposed temperature and electric potential.

DESCRIPTION OF NUMERICAL MODEL

Numerical simulation using the ANSYS Mechanical package of the finite element analysis can be divided into the following main stages: setting the physical properties of materials, building a geometric and grid model, and assigning the corresponding properties to different regions of the geometry, setting boundary conditions, numerical solution and analyzing the results [10-12].

As they are viewed from the 'physical properties' angle and within the framework of this particular paper, the applied semiconductor elements are of the greatest interest.

Their properties are shown in Table I.

The battery of a TEG (Figure 1) includes numerous separate elements. Semiconductor elements are connected in series. The composition of the geometry includes 600 separate three-dimensional bodies in total. They could be divided into groups based on their purpose – namely - "n-type" semiconductor element "p-type" semiconductor element, ceramic cylinders, nickel switching from the hot side, copper switching from the cold side, sub-coupling layers, adhesive thermal interfaces, and textolite gaskets.

TABLE I. PHYSICAL PROPERTIES OF SEMICONDUCTOR ELEMENTS.

Material	Temperature,(K)	Thermal conductivity, (J / (kg * K)	Seebeck coefficient, (V/ C)	Electrical resistivity (Ohm / m)
N-type	40	1,75	-0,00015	$8,47\times10^{-6}$
	80	1,63	-0,000165	$9,80\times10^{-6}$
	125	1,68	-0,000178	$1,136\times10^{-5}$
	175	1,51	-0,000161	$1,298\times10^{-5}$
	225	1,4	-0,000137	$1,449\times10^{-5}$
	275	1,06	-9×10^{-5}	$1,574\times10^{-5}$
	325	0,63	-4×10^{-5}	$1,680\times10^{-5}$
P-type	42,19	1,11	0,0001467	$8,389\times10^{-6}$
	84,77	0,93	0,0001613	$1,029\times10^{-5}$
	134,32	0,77	0,0001774	$1,322\times10^{-5}$
	185,05	0,68	0,000188	$1,670\times10^{-5}$
	234,16	0,57	0,0001762	$2,037\times10^{-5}$
	283,23	0,4	0,0001275	$2,381\times10^{-5}$
	330,13	0,24	$8,12\times10^{-5}$	$2,662\times10^{-5}$

Simulation of this kind of geometry - in its 'full formulation' and the finite element method applied - is an extremely resource-intensive task, requiring a significant amount of computational resources [13-17]. Considering this, we simulated only one pair of thermoelectric elements. From the initial geometry,

one segment was isolated, which is the junction of two dissimilar semiconductor elements. The obtained "layered" geometry consists of 14 different elements, for which the corresponding temperature dependences of the physical properties were specified.

The computational domain was formed using a grid model consisting of 633,624 catches and 1,49600 elements. SOLID226, a three-dimensional twenty-node hexagon-shaped element, was used as the main element in the construction. The binding of the grid models in this segment was performed by the direct connection of conformal nodes of the grid model (as opposed to the method, which presumes the use of contacts between its geometrical components) [18-21]. The geometric and grid model of the element is shown in Figure 2.

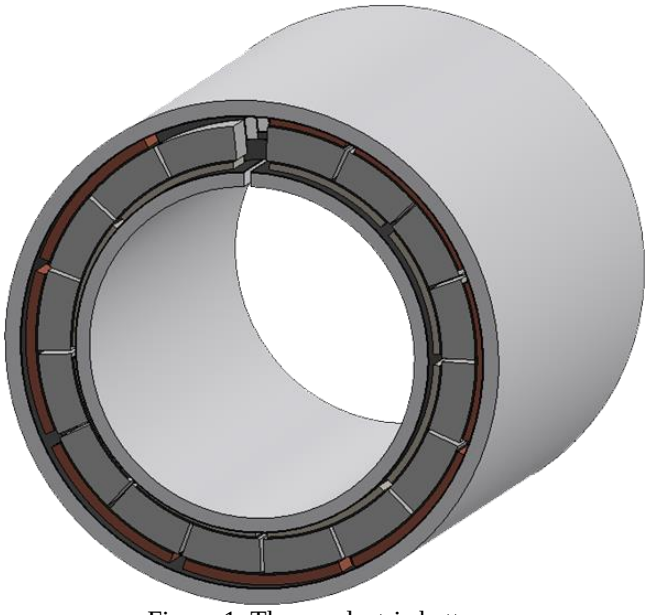

Figure 1. Thermoelectric battery.

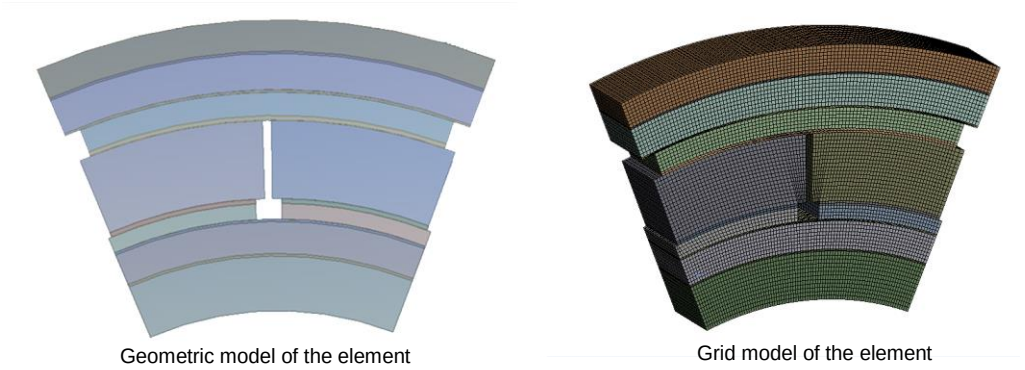

Figure 2. Geometric and grid model of the investigated TEG element.

The next step in our research was the modeling of the boundary conditions. During the initial simulation, the temperature of the surface of the steel pipe on the hot-contact side was set with a uniform distribution of a constant value equal to 300 ºC. With a similar condition, the temperature was assigned from the side of cold contact, but equal to 70 ºC. For the correct start of the thermoelectric analysis, due to the limitations of the software complex, it was necessary to set the electric potential, so on the outer contour of the steel pipe from the cold side, it was set to 0 V. The initial temperature in the calculated area was set to 22 ºC. The electrical circuit of the segment was closed by adding an external load to the system with different values of electrical resistance.

The load increased gradually, to achieve the established criteria for convergence in current strength and heat flux of 0.1 × 10–8 and 0.8861 × 10–3, respectively.

SIMULATION RESULTS

The purpose of the primary analysis was to study the element in order to determine the magnitude of the external load at which the efficiency would reach its maximum level. The results are presented in Table II.

The results obtained indicate that the efficiency of TEG significantly depends on the magnitude of the external load, therefore, when this parameter is being designed it should be treated with special care.

TABLE II. PRIMARY SIMULATION RESULTS.

External load resistance, (Ohm)	Load Power as recorded, (W)	tº on the surface of 'cold' switching, (°C)	tº of the 'hot' switching at "N", ° C	tº 'hot' switching at "P", °C	Efficiency, %
1	$3{,}7138\times10^{-3}$	80,484	276,43	284,93	0,07
0,1	$3{,}5478\times10^{-2}$	80,57	276,14	284,57	0,6833
0,01	0,23605	81,307	273,94	281,87	4,0611
0,001	0,2892758	83,85155	268,591	275,403	3,9575
0,002	0,35526	83,011	270,06	277,16	5,1491
0,003	0,35963	82,5	271,08	278,39	5,4372
0,0031	0,35868	82,46	271,17	278,5	5,4424
0,0032	0,35758	82,421	271,25	278,6	5,4448

The visualization of the fields of temperature and electrical voltage distribution for the maximum efficiency option is presented in Figure 3.

With a load resistance of 0.0032 Ohms, TEG analysis was performed at various temperatures of cold and hot junctions. The ANSYS DesignXplorer

module was used as a tool for analysis. Response Surface Optimization technology has the highest robust properties as the toolkit of this module.
The essence of this approach can be shortly formulated as follows:

- plan of a physical or numerical experiment is generated;
- the experiment is conducted to obtain the values of the response function at points in the plan;
- the multifactor response surface is constructed from the obtained points;

response surface can then be used to calculate the values of the objective function at an arbitrary point in the factor space and to optimize it in order to find the extreme value of the objective function.

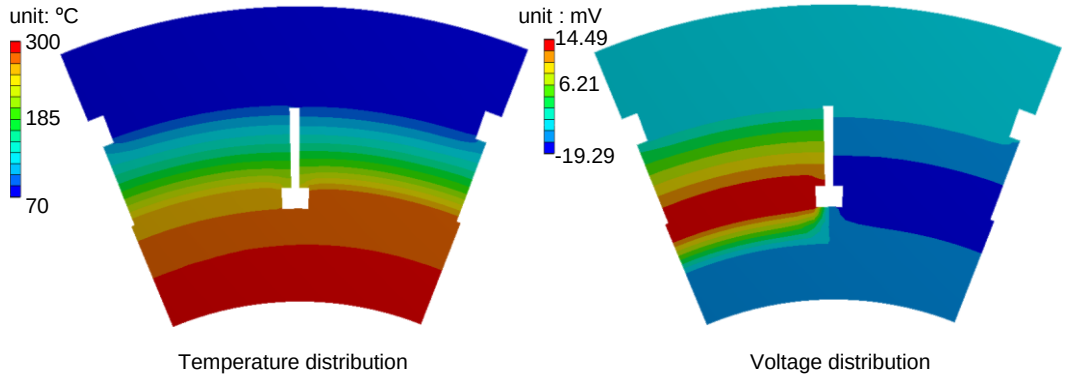

Figure 3. Visualization of temperature and voltage distribution fields.

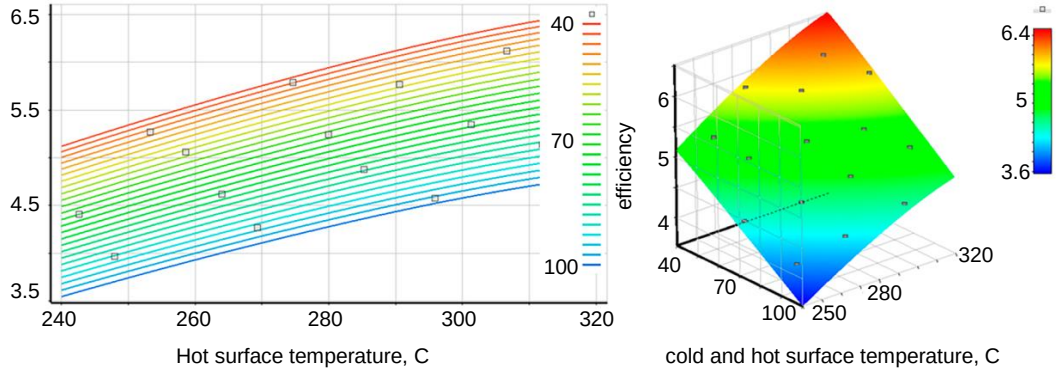

Figure 4. Dependence of the efficiency of the segment on the temperature on a hot and cold surface.

An experiment plan set the following temperature ranges: hot contact temperature from 240 to 320 ° C, cold contact temperature from 40 to 100 ° C. The experiment plan was designed using the algorithm of optimal filling of the search space. A full quadratic polynomial was used as an approximation model.

The obtained dependences of the efficiency of a TEG battery segment on temperatures on a hot and cold surface are presented in Figure 4.

An important condition for the optimal functioning of a TEG is to maintain a constant temperature at the cold and hot junction of semiconductor elements. However, due to changing environmental conditions, this task is much more complicated and requires the development of more productive thermal stabilization systems.

Nevertheless, there are temperature ranges at which the efficiency required in the technical specifications for the generator will be achieved, but from a technical point of view, heat exchange systems are more robust for these operating conditions. Using the response surface obtained for the thermoelectric element, we searched for 20 different possibilities to combine the boundary conditions under which the desired values of the efficiency of the thermoelectric generator segment are achieved. The results of our search are presented in Table III.

In addition to the temperature ranges study, we also carried out the analysis of changes in the characteristics of a thermoelectric element with different thermal conductivity properties of adhesive layers. They consist of four layers in the given sample. The previously considered version of the TEG battery segment was used as the base geometrical model.

TABLE III. SEARCH RESULTS FOR TEMPERATURE RANGES

No.	Efficiency = 4,5%		Efficiency = 5%		Efficiency = 5,5%	
	t^o of the hot surface ^oC	Δt^o, ^oC	t^o of the hot surface ^oC	Δt^o, ^oC	t^o of the hot surface, ^oC	Δt^o, ^oC
1	289,88	192,14	253	196,80	284,36	224,58
2	264,12	181,79	305,56	217,54	268,52	219,47
3	253,56	178,61	269,32	201,52	293	228,30
4	285,4	190,00	248,68	195,99	297,48	230,44
5	280,6	188,19	292,28	210,71	271,72	220,09
6	243,72	176,50	303	215,92	265	218,29
7	272,28	185,02	258,76	198,34	275,56	221,12
8	278,04	186,56	277,24	204,51	315	239,87
9	287,32	190,51	290,36	209,49	312,44	238,25
10	281,56	188,97	316,44	224,44	300,04	232,06
11	245	175,91	313,88	222,81	318,84	242,31
12	282,84	188,38	263,56	199,98	310,52	237,03
13	276,76	187,16	286,52	208,46	263,72	218,89
14	241,16	174,88	261	198,35	295,56	229,92
15	247,8	176,36	310,04	219,68	261,16	217,26
16	258,36	179,19	294,84	212,33	307,96	235,41
17	261,56	180,16	242,92	194,45	278,6	221,81
18	274,84	186,65	307,48	218,06	274,28	221,71
19	251	176,99	264,84	199,38	281,8	222,96
20	254,84	178,01	249,96	195,40	306,68	236,01

The following boundary conditions were used: hot surface temperature 300 ºC; cold surface temperature 70 ºC; zero potential on the edges of a metal pipe from a cold surface; external load resistance is 0.0032 Ohm. When planning an experiment for each adhesive layer, its thermal conductivity was set in the range from 0.1 to 2 W / (m • ° C).

The main controlled parameters were the heat fluxes on the cooled and heated surface of the element. Figures 5 and 6 show the dependences of the criteria on the input parameters constructed using response surfaces.

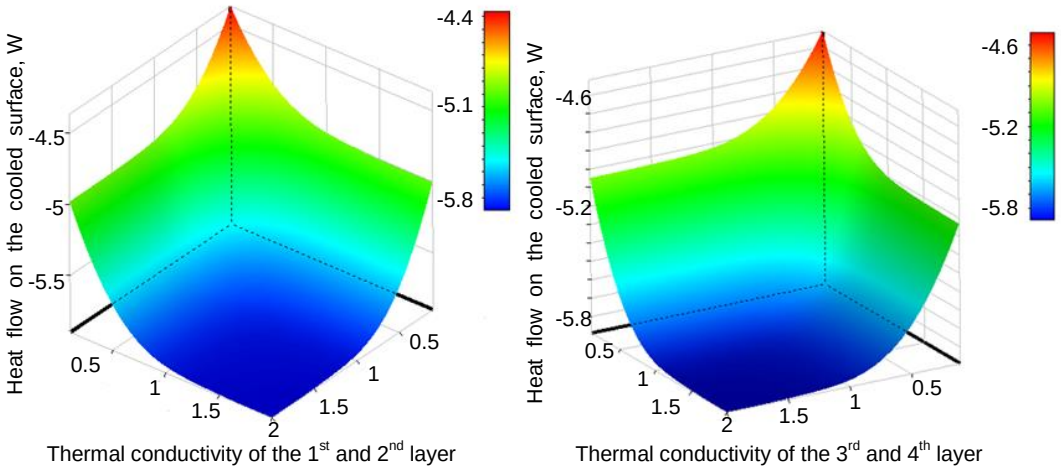

Figure 5. Dependence of the heat flux on the cooled surface from the thermal conductivity of adhesive layers.

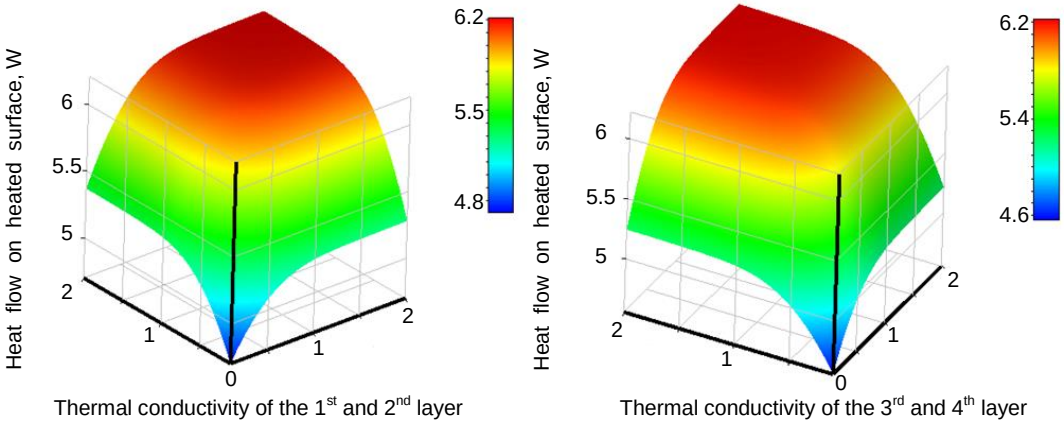

Figure 6. Dependence of the heat flux on the heated surface of the thermal conductivity of adhesive layers.

CONCLUSION

The article used ANSYS Mechanical and ANSYS DesignXplorer commercial product for the numerical study of the effectiveness of a thermoelectric generator battery. A certain value of external load resistance was selected for each simulation variant, at which the efficiency of the thermoelectric module is maximum. The obtained results indicate that the efficiency of TEG significantly depends on the magnitude of the external load, therefore, when designing this parameter should be treated with special care. The provided search for temperature ranges under which a given efficiency of a thermoelectric generator makes it possible to determine the conditions under which the efficiency required in the technical specification for the generator will be achieved, but from a technical point of view, for these operating conditions, heat exchange systems are more robust. A database of necessary parameters for the functioning of the product under various operating conditions has been formed. The analysis of changes in the characteristics of a thermoelectric element with different properties of thermal conductivity of adhesive layers was performed. The resulting dependences of the heat flux on the heated and cooled surfaces on the thermal conductivity of adhesive layers for a specific TEG sample will provide an opportunity to estimate the deviation of the battery efficiency due to the heterogeneity of the adhesive composition.

The research is performed with the financial support of the Ministry of Education and Science of the Russian Federation under the Decree of the Government of the Russian Federation of April 9, 2010 No. 218 (Contract No. 03.G25.31.0246).

REFERENCES

1. Tritt, T.M., and M.A. Subramanian. 2006. “Thermoelectric materials, phenomena, and applications: a bird’s eye view,” *MRS Bulletin*, 31(3):188-198.
2. Snyder, G. J. 2008. “Small thermoelectric generators,” *Electrochemical Society Interface*, 17(3):54-56.
3. Zhao, H. et al. 2014. “High thermoelectric performance of MgAgSb-based materials,” *Nano Energy*, 7: 97–103.
4. Chen, W.H., C.C. Wang, C.I. Hung, C.C. Yang, and R.C. Juang. 2014. “Modeling and simulation for the design of thermal-concentrated solar thermoelectric generator,” *Energy*, 64:287–297.
5. Kossyvakis, D.N., C.G. Vossou, C.G. Provatidis, and E.V. Hristoforou. 2015. “Computational and experimental analysis of a commercially available Seebeck module,” *Renew Energy*, 74:1–10.
6. Fraisse, G., J. Ramousse, D. Sgorlon, and C. Goupil. 2013. “Comparison of different modeling approaches for thermoelectric elements,” *Energy Convers Manag*., 65:351–356.
7. Anatychuk, L.I., O.J. Luste, and R.V. Kuz. 2011. “Theoretical and Experimental Study of Thermoelectric Generators for Vehicles,” *J Electron Mater*., 40:1326–1331.

8. Yu, C., and K.T. Chau. 2009. "Thermoelectric automotive waste heat energy recovery using maximum power point tracking," *Energy Convers Manag.*, 50:1506–1512.
9. Niu, Z., H. Diao, S.Yu, K. Jiao, Q. Du, and G. Shu. 2014. "Investigation and design optimization of exhaust-based thermoelectric generator system for internal combustion engine," *Energy Convers Manag*., 85:85–101.
10. Clin, T., S. Turenne, D. Vasilevskiy, and R.A. Masut. 2009. "Numerical simulation of the thermomechanical behavior of extruded bismuth telluride alloy module," *J. Electron Mater.*, 38:994–1001.
11. Erturun, U., K. Erermis, and K. Mossi. 2014. "Effect of various leg geometries on thermo-mechanical and power generation performance of thermoelectric devices," *Appl Therm Eng*., 73:128–141.
12. Li, W., M.C. Paul, A. R. Knox et al. 2015. "Multiphysics Simulations of a Thermoelectric Generator," *Energy Procedia*, 75:633 – 638.
13. Riffat, S.B., X. Ma, and R.Wilson. 2006. "Performance simulation and experimental testing of a novel thermoelectric heat pump system," *Applied Thermal Engineering*, 26:494-501.
14. Kossyvakis, D.N., C.G. Vossou, C.G. Provatidis, and E V. Hristoforou. 2015. "Computational analysis and performance optimization of a solar thermoelectric generator," *Renew Energy*, 81:150–161.
15. Li, W. et al. 2017. "Multiphysics simulations of thermoelectric generator modules with cold and hot blocks and effects of some factors," *Case Studies in Thermal Engineering*, 10:63-72.
16. Tsai, H.L., and J.M. Lin. 2010. "Model building and simulation of thermoelectric module using Matlab/Simulink," *J. Electron. Mater.*, 39(9):2105–2111.
17. Hogblom, O., and R. Andersson. 2014. "Analysis of thermoelectric generator performance by use simulations and experiments," *J. Electron. Mater.*, 43:2247–2254.
18. Li, W., M.C. Paul, A. Montecucco, et al. 2015. "Multiphysics simulations of a thermoelectric generator," *Energy Procedia*, 75:633–638.
19. Lineykin, A., and S. Ben-Yaakov. 2007. "Modeling and analysis of thermoelectric modules," *IEEE Trans. Ind. Appl.*, 43(2):505–512.
20. Chen, M., L.A. Rosendahl, T.J. Condra, and J.K. Pederson. 2009. "Numerical modelling of thermoelectric generators with varying material properties in a circuit simulator," *IEEE Trans. Energy Convers.*, 24(1):112–124.
21. Seetawan, T., U. Seetawan, A. Ratchasin et al. 2012. "Analysis of thermoelectric generator by finite element method," *Procedia Engineering*, 32:1006–1011.

2018 International Theoretical and Practical Conference on Alternative and Smart Energy (TPCASE 2018)
ISBN: 978-1-60595-617-6

Features of the Development and Implementation into the Educational Process of VSTU of the International Master's Program in Innovative Technologies in Energy-Efficient Buildings for Russian and Armenian Universities and Stakeholders in the Framework of the International Project + MARUEEB 2015–2018

Valeriy Mishchenko, Elena Gorbaneva and Elena Rodina

ABSTRACT

The article describes the phases of familiarization, development and implementation of the international master's program in innovative technologies in energy-efficient buildings for Russian and Armenian universities and stakeholders in the framework of the international project Erasmus+ MARUEEB 2015-2018 into the educational process of Voronezh State Technical University. The specific features and uniqueness of this program for the university and the city of Voronezh are revealed, and the concept of teaching methods developed according to the recommendations of the European partner universities on the Erasmus+ MARUEEB grant are also presented.

THE CONCEPT OF THE MASTER'S PROGRAM IN INNOVATIVE TECHNOLOGIES IN THE FIELD OF ENERGY-EFFICIENT BUILDINGS FOR RUSSIAN AND ARMENIAN UNIVERCITIES AND STAKEHOLDERS

In 2015, Voronezh State Technical University had the opportunity to participate

Department of Technology, Construction Organization, Expertise and Property Management, Federal State Budgetary Educational Institution of Higher Education "Voronezh State Technical University" (FSBEI HE "VSTU"), 84, 20-Letiya Oktyabrya Street, Voronezh, 394006, Russia

in the international grant of the Erasmus+ program, the project MARUEEB (Master Degree in Innovative Technologies in Energy-Efficient Buildings for Russian and Armenian Universities and Stakeholders). The goal of the program is the introduction of an environmental education program into Russian and Armenian universities, the exchange of experience and the training of young teaching staff of Russian universities basing on materials of existing energy-efficient construction programs in the European Union.

The Erasmus+ program covers fields of education, vocational and sports training for young people, offers a synergistic development way aimed primarily at international exchange and new forms of cooperation, tending to "become a more effective tool for addressing real needs in terms of human development and social capital in Europe and beyond" [1]. The program is led by a grantee - the University of Genoa (Genoa, Italy), along with such consortium members as the University of Naples, Technical University of Iasi (Iasi, Romania), Slovak University of Technology in Bratislava (Slovenia), Kaunas University of Technology (Lithuania). Armenian universities are represented by National Polytechnic University of Armenia, American University of Armenia and Armenian International Academy of Engineering. From Russian side, the program includes: Ural Federal University, Peter the Great St. Petersburg Polytechnic University, Tambov State Technical University, South Ural State University of Chelyabinsk, and Voronezh State Technical University (hereinafter referred to as VSTU).

Construction and architectural enterprises potentially interested in new personnel trained by European standards were indicated in order to develop international exchange between students and professors, to disseminate the results of the educational program during its life cycle (2015-2018), as well as to test the educational program for the specific features of the labor market in the Voronezh region.

Based on the statistical survey of potential employers of the Voronezh region, recommendations of the educational and methodical management of VSTU, as well as the directions of the Department of technology, construction organization, expertise and property management (TCOEPM), the Erasmus+ master's program was given the name "**Buildings of Energy-Efficient Life Cycle (ERASMUS+)"** in the direction 08.04.01 Construction. In accordance with the Federal State Educational Standard (FSES), the main professional educational program of higher education was developed - the master's program, which includes the general characteristics of the educational program, curriculum, calendar training schedule, work programs of subjects (modules), practice programs, evaluation and teaching materials.

The curriculum of the educational program includes the following mandatory disciplines/basic part: Philosophical problems of science and technology, Methodology of scientific research, Business foreign language, Mathematical modeling, Eco-conceptual architectural design (part I and part II), Design, construction and operation of low-energy buildings, Ecological architecture and

design of energy-efficient buildings, Bim-technology of energy-efficient buildings, Energy and environmental monitoring of the state of construction objects; elective disciplines: Economic features of life-cycle design of energy-efficient real estate objects, Decision theory, Design of engineering systems for energy-efficient buildings, Innovative building materials, Principles of ecological urban planning, Special issues of acoustics, lighting and heat engineering, Integrated biosphere compatibility of urbanized spaces, Energy management of the enterprise; practices: the practice of obtaining primary professional skills and abilities, research work, the practice of obtaining professional skills and professional experience, final state certification. The program is implemented in English with the assistance of a qualified bilingual faculty.

The methodological approach of the master's program tends to involve the students in an open pedagogical process in the most commonly used form that is free exchange of views. The goal of this approach is not only to establish pedagogical control over what students have learned, what they strive for, what they are looking for in the new disciplines. It is important to create conditions for self-education, the expansion of students' consciousness in the field of energy saving and solving environmental problems. The basis of this method of teaching students is to work in teams throughout the entire period of study. Thus, a synergistic interdisciplinary approach to solving energy saving problems is used in the process of work, at the same time students enrich each other with skills and knowledge in various fields.

In the market economy, this method of working in teams is also a strong prerequisite for the possible formation of small joint business firms by the members of these groups after graduation, and this is a direct contribution to the development of the Russian economy and private entrepreneurship. Moreover, after graduation, the MAs of this particular program will already have, according to our expectations, a different level of qualification and a different paradigm of consciousness in matters of ecology and the preservation of the Earth. Also, the concept of this program involves the participation of the student groups in international student eco-competitions, where the students can check the level of their creative abilities at the international level.

For teaching and methodological support of the master's program "Buildings of Energy-Efficient Life Cycle (ERASMUS+)" with the direct participation of VSTU three manuals were written:

- "Eco-conceptual Architectural Design" (under the general editorship of E.V. Rodina, I.N. Mal'tseva);
- "Biosphere Compatible Energy-Saving Technologies" (under the general editorship of E.V. Rodina, Dušan Petráš);
- "Design Features of the Life Cycle of Energy-Efficient Premises" (under the general editorship of E.P. Gorbaneva).

All the developed study guides within the framework of the Erasmus+ (MARUEEB) program are intended for undergraduates studying in the direction

08.04.01 Construction, as well as for bachelors, graduate students, professors and scientific and technical workers specializing in energy saving.

IMPLEMENTATION OF THE MASTER' PROGRAM "BUILDINGS OF ENERGY-EFFICIENT LIFE (ERASMUS+)" AT THE VORONEZH STATE TECHNICAL UNIVERSITY

Based on the admission tests and the Order of accepting the applicants in the number of first-year students of full-time education to the direction 08.04.01 Construction, the program "Buildings of Energy-Efficient Life Cycle (ERASMUS+)" 15 students were accepted at the beginning of the 2017-2018 school year, and 10 students - at the beginning of the 2018-2019 school year. Admission to study for the master's program was carried out according to personal applications of citizens with higher professional education, according to the results of entrance tests conducted by the University independently in accordance with the Regulations on admission to the magistracy.

During the 2nd semester of the 2017-2018 school year, professors from European universities of the consortium visited VSTU (Table 1, Figure 1), as well as young professors from our university went to Europe for an internship.

TABLE 1. INFORMATION ON THE CONDUCTED SEMINARS BY EUROPEAN PARTNERS AT VSTU.

Date	Information about the scientific and pedagogical worker, university, country	Seminar topic
16-17 February 2018	Ph.D., Associate Professor of Energy and Thermal Science Vincenzo Bianco The University of Genoa , Italy	«Evaluating Energy Efficiency in Buildings. A technical and economic analysis»
26-27 February 2018	Ph.D., Associate Professor Michal Krajcik (Slovakia)	«Energy Efficiency and Energy Saving in Urban Environment» «Energy Efficiency and Energy Saving for Sustainable Development»
9-10 April 2018	Ph.D., Associate Professor, Oronzio Manca (The University of Genoa , Italy)	«Thermal Insulation, Thermal Bridges, Moisture. Condensation and Thermo-Hygrometric Verification»
23-24 April 2018	Ph.D., Associate Professor Nicanor Cimpoesu («GHEORGHE ASACHI» Technical University of Iasi, Rumania)	«Renewable energy and sustainable solutions»
14-15 May 2018	Associated Prof. at Kaunas University of Technology (KTU) Institute of Environmental Engineering (APINI) Irina Kliopova	«Energy efficiency through Sustainable industrial development»
17-18 May 2018	Arthur Khalatyan American University of Armenia	«Use of mobile data for smart urban development and management»

As a result of the seminars and study of the disciplines of the curriculum of the master's program "Buildings of Energy-Efficient Life Cycle (ERASMUS+)" the necessary competencies are formed among the students. Students acquire theoretical knowledge about the life cycles of energy resources and real estate objects, stages of the life cycle of energy resources and real estate objects. They learn to choose the energy efficient resource supply option taking into account the service life and chronological age of the property, to apply methods for assessing the introduction of energy saving measures and their results to the environmental situation at all stages of the life cycle of objects, using skills to calculate the energy saving potential of the property taking into account its life cycle, to demonstrate the results of the analytical work with the help of a visual presentation.

Today, the students, divided into teams, devote their time and energy to solving the environmental and energy-efficient problems of Voronezh, having chosen the topics of the master's theses related to the reconstruction of individual residential buildings of public worship in Voronezh in order to improve their energy efficiency, environmental friendliness and viability, and also topics related to the design of new ecological neighborhoods in the vicinity of the city, as well as to solving the problem of water purification in the Voronezh reservoir, etc.

Figure 1. Training workshops by professors from European universities of the consortium.

REFERENCES

1. Official website of Erasmus+, available at: https://eacea.ec.europa.eu/erasmus-plus_en (date of access 27.10.2018).
2. Official website of VSTU (Erasmus+): [available at: http://cchgeu.ru/education/programms/zezc/(date of access 27.10.2018).
3. The film "Earthlings" (2005) (https://www.youtube.com/watch?v=EQ2rhZ-3ZTo).
4. Mishchenko, V. Ya, E.P. Gorbaneva, A. Yu. Manukovskiy, and A.O. Safonov. 2014. "Genetic algorithms in solving multicriteria problems of optimization of resource allocation when planning energy saving measures," *Scientific Herald of the Voronezh State University of Architecture and Civil Engineering. Construction and Architecture*, 3(35):77-82.
5. Mishchenko, V. Ya., E.P. Gorbaneva, and E.V. Ovchinnikova. 2018. "Improving production efficiency using the optimal distribution of repair and construction brigades using the Little / FES algorithm: Finance. Economy. Strategy," *A series of "Innovation Economics: the human dimension": scientific, practical and methodological journal*, 5:30-36.
6. Mishchenko, V. Ya., V.N. Barinov, E.P. Gorbaneva, and A.N. Nazarov. 2012. "Energy survey (energy audit) of social facilities," *Scientific Herald of Voronezh State Agrarian University Control Institute. Construction and architecture*, 1(25):77-84.
7. Mishchenko, V. Ya., E.P. Gorbaneva, Ye. A. Pogroblenaya, and K. Yu. Zubenko. 2007. "The role of ecological expertise in the real estate expertise system," *Proceedings of the 10th international scientific-practical conference "High technologies in ecology,"* Voronezh branch of the Russian Ecological Academy. Voronezh, pp.160-166.
8. Gorbaneva, E.P., O.K. Meshcheryakova, and L.P. Myshovskaya. 2017. "Features and prospects of resource supply by public utilities of industrial enterprises of the Russian economy / Higher education institutions," *Textile Industry Technology: Sat Sc. Art*., ISTA - Ivanovo, 1 (367):33-37.
9. Matreninsky, S.I., V. Ya. Mishchenko, I.E. Spivak, and K.Yu. Zubenko. 2008. "Methodological approach to the assessment of moral deterioration of the areas of mass residential development, "*Industrial and civil construction*, 11: 59-62.

2018 International Theoretical and Practical Conference on Alternative and Smart Energy (TPCASE 2018)
ISBN: 978-1-60595-617-6

Forecasting of Volumes of Power Consumption in the Electrical Distribution Networks Based on Hybrid Models

Valerii Krysanov, Viktor Burkovskii, Aleksander Danilov and Konstantin Gusev

ABSTRACT

The article deals with increasing the prediction accuracy for electricity consumption in electrical grids under conditions of the modern wholesale electricity and capacity market and actual performance of grid operators. It contains the analysis of currently applied electricity consumption forecast methods. The article shows the necessity of accounting unpredictable and hardly definable factors, such as technical and economic factors (production schedule, end-consumer's equipment load characteristics, electric power sector support and development costs), as well as climate factors (environment temperature, luminance, light day length, natural disasters). The most accurate accounting of these factors provides an opportunity to increase supervisory control quality and reduce electricity losses by reducing balancing market share, as well as output costs of generating company (end consumer). It is proposed to establish the use of Mamdani algorithm-based fuzzy neural networks as a core principle. The results show that electricity consumption forecast, based on using fuzzy neural networks is more accurate than the method currently specified in power supplier regulations. The article also contains an expert assessment of the economic viability of using said method for power supply to large regional industrial plants.

INTRODUCTION

Electricity distribution network is an essential part of any electric power system

Voronezh State Technical University, 14, Moskovsky Avenue, Voronezh, 394026, Russia

(EPS), as it links electric power (EP) generators with the consumers. Such network is a complex multi-level structure with many distributed objects with various technical and electrical specifications. Its complete and effective operation is only possible when a certain balance between consumption and generation capacity is ensured, which, in turn, is not possible without optimal control of electrical grid (EG) operation modes in criteria like energy efficiency and savings, EP quality, as well as power supply reliability.

Currently, optimal control of EP transition, distribution and consumption at all EG levels is complicated by a high rate of its deprecation, constant upsurge of consumption and unbalanced time-specific consumer's requirements for EP. Therefore, the electricity distribution network control system requires a major overhaul in engineering, supervision and business analysis areas.

In accordance with the worldwide trend of power generating industry, such overhaul involves the creation of active-adaptive networks (Smart Grid), equipped with a software solution capable of multi-parameter optimisation of existing EG using modern and efficient mathematical methods and algorithms. Despite the significance of this trend, the subject of full-scale accounting of hardly definable factors (such as economic and climate factors) still lacks a comprehensive study. This leads to an unreasonably high energy-output ratio of Russian power industry [1-3]. The conducted research shows that this issue can be resolved by applying a unified methodological approach using a modern mathematical tool, such as the ones based on artificial neural networks (ANN) and fuzzy neural networks (FNN), in particular – for forecasting EP consumption in EG [4-8]. It would be especially helpful for decreasing energy total loss, mainly – by countering technical losses (under load, no load, climate-related). These types of losses are difficult to determine, which hinders optimisation of thermal and electric power output efficiency. Today, in order to predict EP consumption, power generation companies use approximate linear extrapolation methods (growth/decline method), statistical models (regression models, based on time-series data) and judgment-based models.

Generally, grid operators refer to connected capacity and overload capacity. With that, consumed power must be between contracted and maximum values, which are calculated based on semi-annual performance readings, equipment checks and statistics analysis. However, in practice, consumers try to set contracted capacity higher than needed on the expectation of future EP consumption increase. This pushes power generation companies to increase not only connected, but also overload capacity for those consumers. In these conditions, technical losses and EP transportation costs escalate. These losses, in turn, are added to the tariff costs for next year to be imposed on consumers. A consumer's task in this situation is to adjust their forecasted consumption in order to scale back the EP transportation tariff costs. Grid operator would also benefit from that: forecast adjustment allows for better loss prediction and grid operating mode optimisation. The respective studies proved the viability of using fuzzy logic methods, ANN and FNN [9-13]. These hybrid methods not only provide fuzzy approximator with advanced facilities in the

presence of underformalized functions, but also increase neural network adaptability during power flow dynamics monitoring [14-16].

FORECASTING MODEL AND METHODS

The proposed method of forecasting EP consumption by industrial facilities is based on analysis of the correlation between consumption value and required gross proceeds (RGP, economic factor) and average air temperature (climate factor) [17].

For example, database receives information from an industrial plant's automated electricity commercial accounting system (monthly EP consumption value), average monthly air temperature and RGP values for a select period (month, the quarter of a year, year, three years). This data is then used to calculate correlation (see pictures 1–3). The result serves as a basis for an EP consumption forecasting model, which uses FNN method.

This is followed by the creation of a rule base, which is a selection of standardised climate and economic parameters, along with some indeterminate and nonlinear functional relationship between them and consumption value. The portion of RGP, which corresponds to the first month of the select time period, serves as a reference value. Monthly RGP portions are in direct ratio to EP consumption.

The described method of EP consumption is more than 5% more accurate than the method currently specified in power supplier regulations. This enables the decreasing amount of EP losses in energy grids up to 20% (with energy flow redirection and underutilisation taken into account).

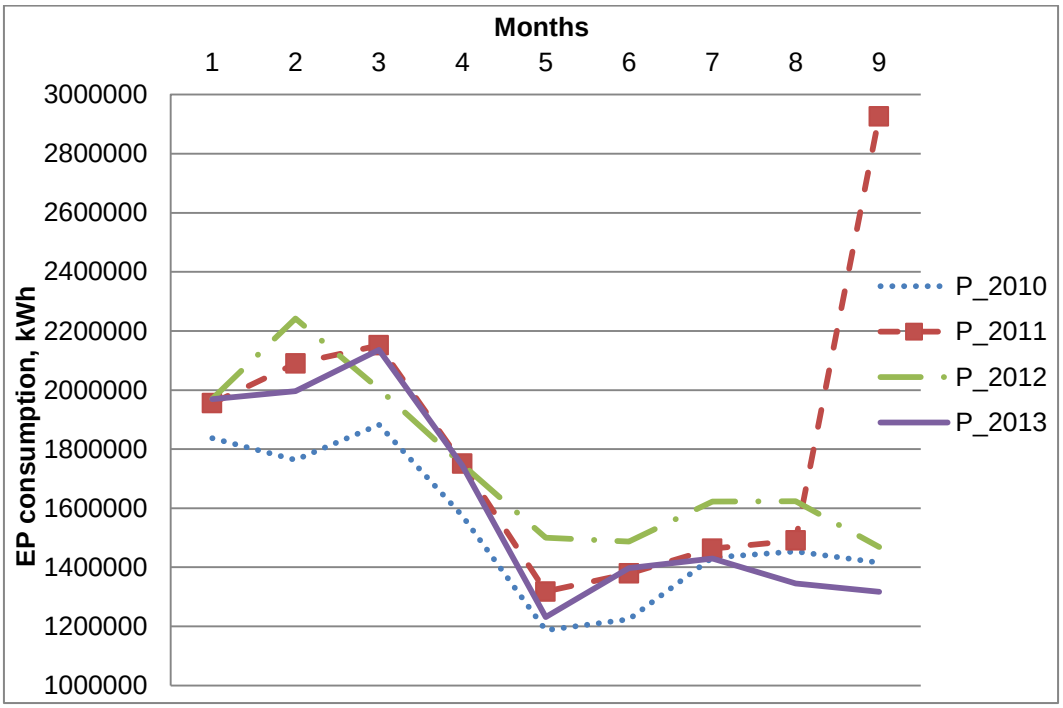

Figure 1. EP consumption by an industrial plant for a selected period.

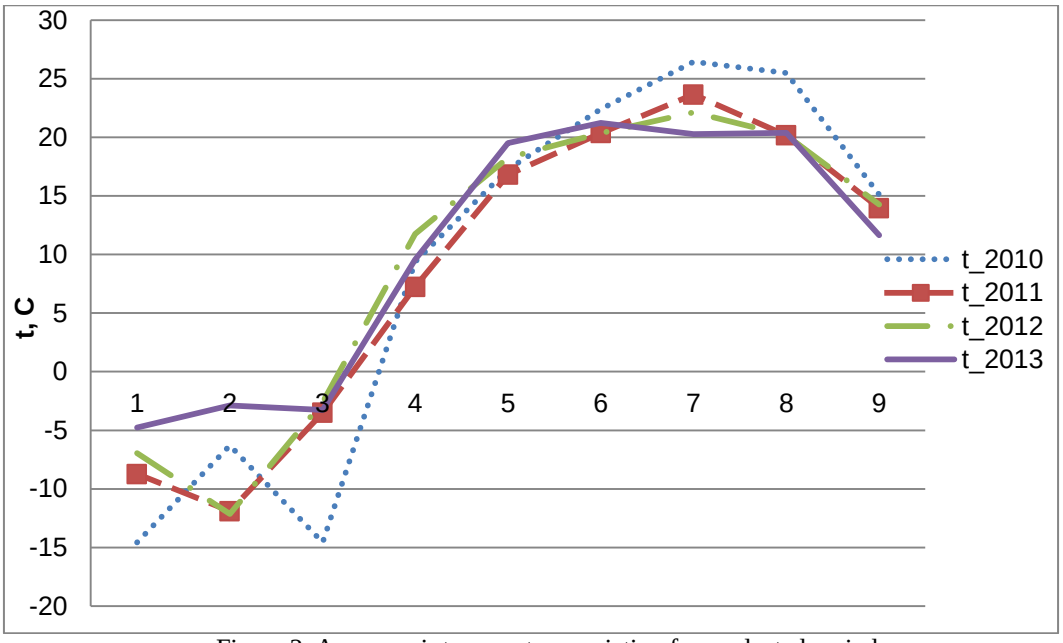

Figure 2. Average air temperature variation for a selected period.

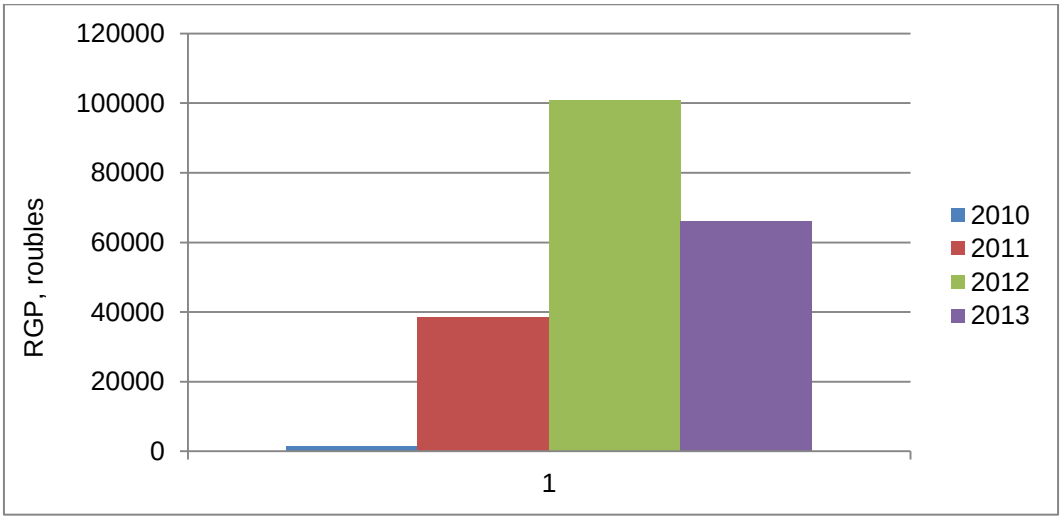

Figure 3. RGP of an industrial plant for a selected period.

The reference value for the climate factor is a difference between optimal temperature (which factors in minimal EP consumption, $\approx 18^0$C) and the average temperature of the first month of a selected period [18].

Modelling of the EP consumption forecasting was conducted with Matlab 2012b [19]. The proposed model uses Mamdani's fuzzy inference algorihm [20]. Neural network structure: 2 – 10 (5/5) – 25 – 1. Terms: gaussmf, linear. Learning periods: 100.

RESULTS

The results of FNN model's work show the functional relationship between EP consumption and economic and climate factors (see picture 4).

Predictive error for a year (the difference between last and reference selection values) varied between 3.5 to 5.3 %.

The effectiveness of the proposed model was checked by assessing predictive error with the fixed growth/decay factor method. Actual error for the selected period equaled 10,7 %.

Application of this method to predict EP consumption for a regional grid operator allows decreasing EP losses by reducing balancing market share. For example, Voronezh EPS grids can cut down expenses amounting to 9 624 219.27 roubles/year (with EP weighted average price on balancing market – 101 425.8 MW·h) [21]. The required additional investment for software procurement would not exceed 24 million roubles, which makes payback time about 5 years.

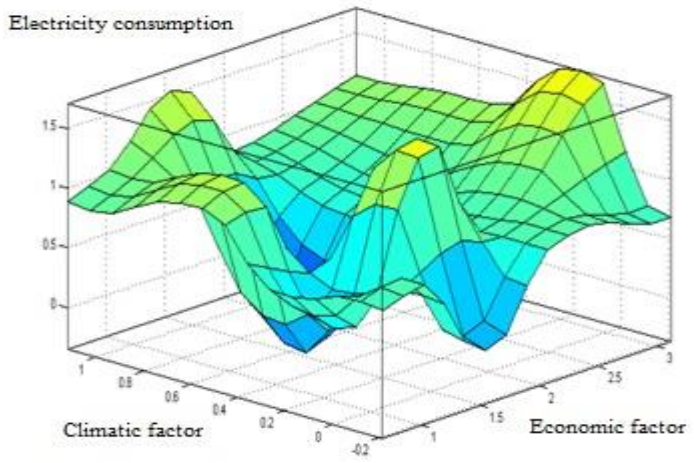

Figure 4. Functional relationship between EP consumption and economic and climate factors

CONCLUSIONS

With the results achieved, it is safe to conclude that increasing EP consumption forecast accuracy by 5 % using ANN- and FNN-based methods allows to decrease EP losses in grids by up to 20 %. Payback time after introducing said method is less than 5 years.

REFERENCES

1. Kamaev, V. A., M. V. Shcherbakov, D. P. Panchenko, N. L. Shcherbakova, and A. Brebels. 2010."Using connectionist systems to predict electricity consumption in shopping centers," *Managing large systems*, M. IPU RAS, 31:92-109.

2. Antoniadis, A., X. Brossat, J. Cugliari, and J. Poggi. 2013. "Clustering functional data using wavelets," *International Journal of Wavelets, Multiresolution and Information Processing*, 11(01).
3. Cho, H., Y. Goude, X. Brossat, and Q. Yao. 2013. "Modeling and forecasting daily electricity load curves: a hybrid approach," *Journal of the American Statistical Association*, 108:7-21.
4. Rosenblatt, R. 1961. *Principles of Neurodynamics: Perceptrons and the Theory of Brain Mechanisms.* Spartan Book, Washinghton D.C.
5. Hopfield, J.J. 1982. "Neural networks and physical systems with emergent computations abilities," *Proc. Of the National Academy of Sciences*, 79: 2544-2558.
6. Krysanov, V.N., and A.L. Rutskov. 2013. "Application of the principles of neuro-fuzzy networks (FNN) to predict electricity consumption in the production sector," *VSTU Bulletin*, 9(6-3): 62-66.
7. Solomkin, A.V. 2009. "The use of neural network methods for predicting electricity consumption," [Electronic resource] *Electronics and Information Technology*, 2 (7). Access mode: http://fetmag.mrsu.ru/ (free access).
8. Krysanov, V.N., K.S. Hamburg, and A.L. Rutskov. 2014. "Questions of conceptual development of Smart Gird in electric power industry using the principles of artificial neural (ANN) and neuro-fuzzy networks (FNN)," *Electrotechnical complexes and control systems*, (1):7-15.
9. AlRashidi, M.R., annd M.E. El-Hawary. 2009. "A survey of particle swarm optimization applications in electric power systems," *IEEE Transactions on Evolutionary Computation*, 13(4):913-918.
10. Panklib, K., C. Prakasvudhisarn, and D. Khummongko. 2015. "Electricity consumption forecasting in thailand using an artificial neural network and multiple linear regression," *Energy Sources, Part B: Economics, Planning, and Policy*, 10(4):427-434.
11. Shi, B., L.I. Yu-Xia., and Y.U. Xin-Hua. 2009. "Short-term load forecast based on modified particle swarm optimizer and back propagation neural network model," *Journal of Computer Applications*, 29(4):1036-1039.
12. Devaine, M., P. Gaillard, Y. Goude, and G. Stoltz. 2013. "Forecasting electricity consumption by aggregating specialized experts," *Machine Learning*, 90(2):231-260.
13. Eban, E., A. Birnbaum, S. Shalev-Shwartz, and A. Globerson. 2012. "Learning the experts for online sequence prediction," in *Proceedings of ICM*.
14. Burkovsky, V.L., and R.A. Kharchenko. 2006. *Models of optimal energy distribution in regional energy consumption systems.* Voronezh: VGU, 137p.
15. Vasiliev, D.A., M.V. Kolokolov, and V.A. Ivashchenko. 2011. "Models of automated prediction of electrical loads of industrial enterprises," *Management of large systems*, Moscow: IPU RAS, (34):254-266.
16. Krysanov, V.N., K.S. Hamburg, and A.L. Rutskov. 2014. "Prediction of electricity consumption by territorial grid organizations using the methods of neuro-fuzzy networks," *Electrotechnical complexes and control systems*, (2):40 - 46.
17. Monteleoni, C., G.A. Schmidt, S. Saroha, and E. Asplund, 2011. "Tracking climate models," *Statistical Analysis and Data Mining*, 4(4): 372-392.
18. //http://pogodaiklimat.ru/archive.php
19. Leonenkov A.L. 2005. *Fuzzy modeling in MATLAB and fuzzyTECH*. SPb.: BHV-Petersburg, 736p.
20. Mamdani, E.H. 1977. "Advances in the linguistic synthesis of fuzzy controllers," *IEEE Trans. on Computer*, 26:1182-1191.
21. Information reviews of JSC SO UES for June and December 2014 // http://so-ups.ru/index.php?id=tech_disc

2018 International Theoretical and Practical Conference on Alternative and Smart Energy (TPCASE 2018)
ISBN: 978-1-60595-617-6

Determination of the Parameters that Make the Greatest Contribution to the Change in the Quality of the Open Cell Foam Filters Based on Numerical Simulation and Experimental Studies

Andrey Dmitriev, Sergei Solovev, Olga Soloveva
and Rishat Khusainov

ABSTRACT

Numerical simulation and experimental studies of the air flow in open foam cell material, which is a model of an aerosol filter, have been carried out. The experimental sample duplicates the geometry of the computational model and is created from the inverse matrix using three-dimensional printing. The results of the experiments are in good agreement with the calculated data for air flow rates providing the laminar flow regime. Some difference in the data is manifested in the case of the turbulent regime, which can be explained by the additional quality requirements of the grid partition. The essentially nonlinear nature of the curve in all flow regimes for a medium with minimal porosity indicates a complex flow pattern with the formation of small vortices even at low flow rates.

Particle deposition efficiency has a maximum value for a material with a minimum porosity; however, the filter quality parameter at this value is the smallest and is determined by the pressure drop. Studies show that the use of open cell foam materials with a higher porosity of the medium is more preferable to improve the filter quality parameter, but there is a certain limiting value of the average porosity at which the filter quality parameter takes the maximum value. The search for the specified value is the goal of our further research.

Andrey Dmitriev, Sergei Solovev, Olga Soloveva, Rishat Khusainov, Kazan State Power Engineering University, 51, Krasnoselskaya Street, Kazan, 420066, Russia
Sergei Solovev, Kazan Federal University, 18, Kremlyovskaya Street, Kazan, 420008, Russia

INTRODUCTION

The growth of production capacity and industrial emissions poses a problem for the fuel and energy complex to improve ways to trap small particles. One of the effective filters with minimal aerodynamic resistance is the open cell foam material. The structure of this material is multifaceted cells that are located randomly in volume. Depending on the composition of the material, open cell foam materials can be used as filters to protect the environment from the harmful effects of hazardous substances released into the atmosphere during heating or production, as thermal insulation (due to its porous structure), since electromagnetic protection and energy absorption elements when car accidents [1], [2]. Nickel open cell foams are also used to increase battery capacity [3]. The use of open cell foam materials in burners provides high heat output and low levels of pollutants such as NO_x and CO. In addition, open cell foams can be used in power generation and transmission systems because they have low weight due to their porous structure. Al, Ti, Pd, Ni, Mg are commonly used as materials for such open cell foams. Various studies of metallic foams have shown that their use in heat exchangers contributes to an increase in the rate of heat transfer.

The study of processes occurring in porous bodies on the basis of experimental studies is difficult because the porous matrix limits visual and mechanical access inside the medium, therefore, to describe processes in porous bodies, they resort to the possibility of numerical modeling [4], [9-11], [14]. Open cell foam materials for industrial purposes, as a rule, have a small pore size and a complex internal structure. The values of the permeability coefficient and the pressure drop are the main characteristics of the study when working with these materials and are directly dependent on the porosity and average cell diameter [5], [6]. Studies on the effects of changes in pore size on pressure drop are incomplete. A detailed literature review on the relationship between the value of the pressure drop and the parameters of the structure of porous materials is given in [7].

When using open cell foam materials in filtration, the main characteristic is the efficiency of particle deposition. The study of deposition efficiency is devoted to the articles [8], [12], [13], [15]. The purpose of this work is to determine the parameters of open cell foam material that influence the efficiency of particle deposition by detailed numerical modeling to improve the filter quality parameter.

PROBLEM FORMULATION

Numerical simulation of gas flow in porous media is based on two approaches. The first approach is to use the averaged model of gas flow in a porous medium, the second approach is reduced to a detailed calculation of the flow in each cell using the method of direct numerical simulation (DNS). The use of the averaged model is based on the previously known permeability coefficient value of the porous

medium, which can only be obtained from experimental data. In this paper, the calculation of gas flow through an open cell foam material was carried out using the ANSYS Fluent software package, the calculation was based on direct numerical simulation. The grid partitioning was 20 million cells, which, with a tube radius of 2 cm and a total tube length of 12 cm, provides the necessary accuracy of the calculation. The size of the porous insert was 4 cm, the official size was sufficient to eliminate the transparency of the material. At the inlet to the pipe, the condition "mass flow inlet" was set (that means the value of the mass flow rate at the inlet), at the outlet "pressure outlet" (that mean the value of the atmospheric pressure at the outlet). Studies were carried out for media with a fixed pore diameter $d_c = 4$ mm for three values of porosity: $\varepsilon = 0.6$, $\varepsilon = 0,7$ and $\varepsilon = 0.8$.

THE RESULTS OF NUMERICAL AND EXPERIMENTAL RESEACH

To verify the accuracy of the results of the numerical simulation, experimental studies were carried out using pipes printed on a three-dimensional printer containing an insert of porous material (Figure 2). Air in the pipes with test specimens was injected with a compressor. The pressure drop value was measured using "testo 510 manometer" at a short distance from the porous material to directly evaluate the resistance of the medium. The average flow rate value was measured using "testo 450 hot-wire anemometer".

a b

Figure 1. The geometry of the calculation area in cross section (a) and part of the experimental sample, which is a pipe with an insert of the open cell foam material created using three-dimentional printing (b).

The complex internal structure of the material ensures the non-linearity of the change in pressure drop depending on the air flow. The values of pressure drop obtained as a result of numerical simulation are in good agreement with experimental data (Figure 2).

Analysis of the results shows that there is a complete agreement of experimental and calculated data at a lower flow rate. Some discrepancy of data is observed at increased rates when the average flow rate in the pipe approaches 10 m/s, a turbulent flow regime appears with the formation of many vortices, which places even greater demands on the quality of grid partitioning for direct numerical simulation of processes inside the porous medium.

For values $\varepsilon = 0.7$ and $\varepsilon = 0.8$ of the medium porosity and for flow rates less than $Q = 0.003$ m^3/s, the laminar flow regime is preserved and the dependence of the pressure drop on the gas flow rate is linear. As the flow rate increases, nonlinearity is manifested, and for porosity $\varepsilon = 0.6$ due to the complex geometry of the inner region, substantial nonlinearity appears even at low gas flow rates. Studies have shown that there is a certain "borderline" value of the porosity of the medium, at which there is a transition from a linear change in the curve to a non-linear character. The search for this range will be of interest to our further research and is of particular importance for designing filters with a reduced value of aerodynamic drag while maintaining the efficiency of their work.

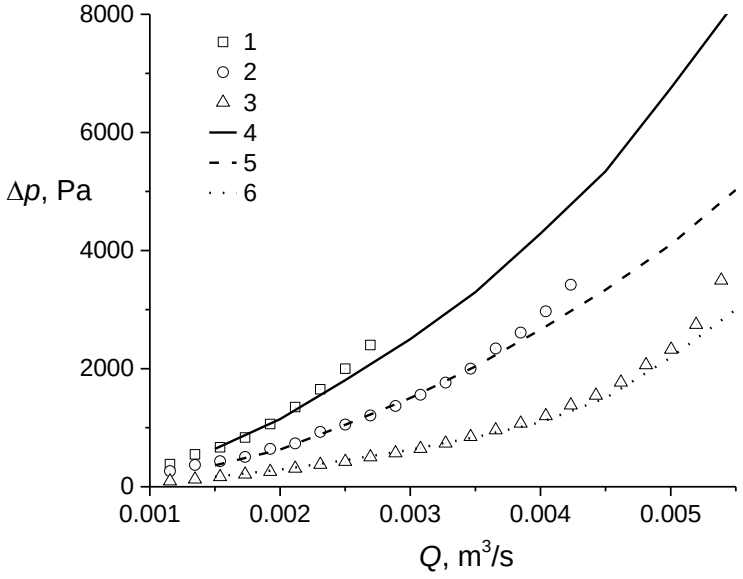

Figure 2. The dependence of the pressure drop on the air flow in the pipe; 1, 2 and 3 – are the results of experiments for ε=0.6, ε=0.7 and ε=0.8, respectively, 4, 5 and 6 – are the results of numerical simulation for ε=0.6, ε=0.7 and ε=0.8, respectively.

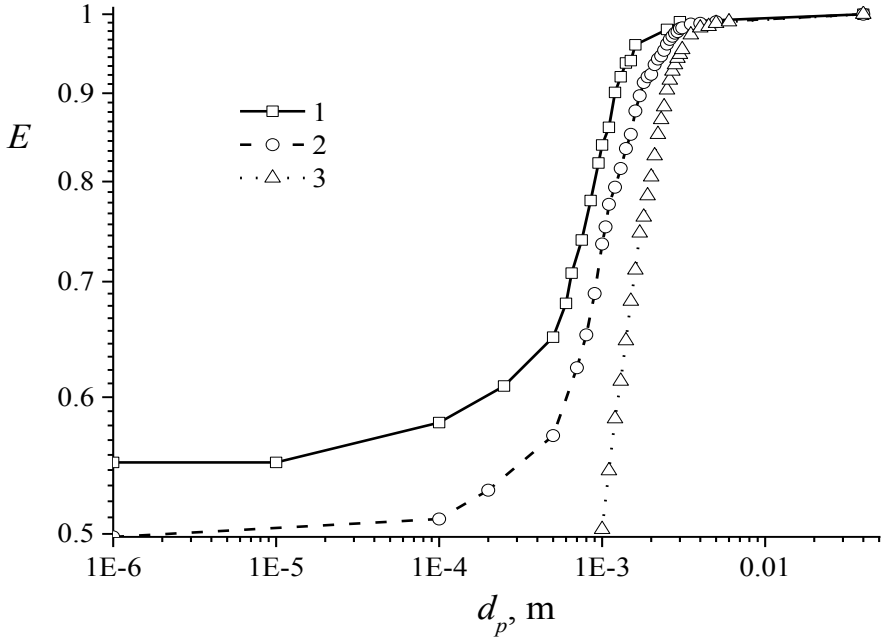

Figure 3. The change in deposition efficiency depending on the particle diameter at the average flow rate *u*=5 m/s; 1 – ε=0.6, 2 – ε=0.7 and 3 – ε=0.8.

For the same particle diameter, the value of the deposition efficiency is higher in the case with a lower porosity of the medium (Figure 3). Table I shows the values of pressure drop and particle deposition efficiency at the average flow rate $u = 5$ m/s and particle diameter $d_p = 1$ mm. The filter quality parameter is calculated from the ratio $QF = E/\Delta p$.

TABLE I. CALCULATED DATA.

ε	Δp, Pa	E	QF
0.6	708	0.84	0.0011864
0.7	356	0.753	0.0021152
0.8	170	0.503	0.0029588

From the values shown, it is seen that the filter quality parameter is mostly determined by the value of the pressure drop, and is minimum at maximum deposition efficiency.

CONCLUSION

Studies of the air flow in the open cell foam material, which is a model of filters used in production, have been carried out. Calculations and experiments were carried out for a fixed value of the diameter of the cells for three different porosities

of the medium and are in good agreement. It has been obtained that for the porosity of the material $\varepsilon = 0.7$ and $\varepsilon = 0.8$ the curves of change in pressure drop in the case of the laminar mode are linear, non-linearity is manifested in the turbulent flow regime. For a medium with porosity $\varepsilon = 0.6$, a nonlinear change in pressure drop occurs in all flow regimes.

The porosity of the medium $\varepsilon = 0.6$ provides the maximum efficiency of the particle deposition with the same parameters in comparison with media of porosity $\varepsilon = 0.7$ and $\varepsilon = 0.8$. However, the value of the pressure drop, in this case, is also the maximum, which reduces the value of the filter quality parameter. For industries where the increase of efficiency is a priority and the pressure drop does not lead to serious economic costs, the use of a filter with the lowest porosity ensures the greatest trapping of particles.

ACKNOWLEDGMENTS

The reported study was funded by RFBR according to the research project № 19-07-01188. Also, the reported research was funded by Russian Foundation for Basic Research and the government of the Republic of Tatarstan of the Russian Federation, grant № 18-41-160005.

REFERENCES

1. Liu, X., X. Yin, L. Kong, Q. Li, Y. Liu, W. Duan, and L. Cheng. 2014. "Fabrication and electromagnetic interference shielding effectiveness of carbon nanotube reinforced carbon fiber/pyrolytic carbon composites," *Carbon*, 68:501-510.
2. Walther, G., B. Klöden, T. Büttner, T. Weissgärber, B. Kieback, A. Böhm, and L. Timberg. 2008. "A New Class of High Temperature and Corrosion Resistant Nickel- Based Open-Cell Foams," *Advanced Engineering Materials*, 10(9): 803-811.
3. Badiche, X., S. Forest, T. Guibert, Y. Bienvenu, J. D. Bartout, P. Ienny, and H. Bernet. 2000. "Mechanical properties and non-homogeneous deformation of open-cell nickel foams: application of the mechanics of cellular solids and of porous materials," *Materials Science and Engineering: A*, 289(1-2): 276-288.
4. Howell, J. R., M. J. Hall, and J. L. Ellzey. 1996. "Combustion of hydrocarbon fuels within porous inert media," *Progress in Energy and Combustion Science*, 22(2): 121-145.
5. Mancin, S., C. Zilio, A. Cavallini, and L. Rossetto. 2010. "Pressure drop during air flow in aluminum foams," *International Journal of Heat and Mass Transfer*, 53(15-16): 3121-3130.
6. Dukhan, N. 2006. "Correlations for the pressure drop for flow through metal foam," *Experiments in Fluids*, 41(4): 665-672.
7. Regulski, W., J. Szumbarski, K. Gumowski, J. Skibiński, M. Wichrowski, and T. Wejrzanowski. 2015. "Pressure drop in flow across ceramic foams—A numerical and experimental study," *Chemical Engineering Science*, 137: 320-337.

8. Solovev, S. A., O. V. Soloveva, andO. S. Popkova. 2018. “Numerical Simulation of the Motion of Aerosol Particles in Open Cell Foam Materials,” *Russian Journal of Physical Chemistry A*, 92(3): 603-606.
9. Bhattacharya, A., V. V. Calmidi, and R. L. Mahajan. 2002. “Thermophysical properties of high porosity metal foams,” *International Journal of Heat and Mass Transfer*, 45(5): 1017-1031.
10. Wang, M., and N. Pan. 2008. “Predictions of effective physical properties of complex multiphase materials,” *Materials Science and Engineering: R: Reports*, 63(1): 1-30.
11. Mardanov, R. F., O. V. Soloveva, and S. K. Zaripov. 2016. “Flow past a porous cylinder in a rectangular periodic cell: Brinkman and Darcy models comparison,” in *IOP Conference Series: Materials Science and Engineering*, 158(1): p. 012065.
12. Hellmann, A., M. Pitz, K. Schmidt, F. Haller, and S. Ripperger. 2015. “Characterization of an open-pored nickel foam with respect to aerosol filtration efficiency by means of measurement and simulation,” *Aerosol Science and Technology*, 49(1): 16-23.
13. Dmitriev, A., I. Madyshev, and O. Dmitrieva. 2018. “Cleaning of Industrial Gases from Aerosol Particles in Apparatus with Jet-Film Interaction of Phases,” *Ecology and Industry of Russia*, 22(6): 10-14. (In Russian)
14. Soloveva, O. V., S. A. Solovev, R. R. Khusainov, O. S. Popkova, and D. O. Panenko. 2018. “Investigation of the influence of the open cell foam models geometry on hydrodynamic calculation,” in *Journal of Physics: Conference Series*, 944(1): p. 012113.
15. Dmitriev A.V., V. E. Zinurov, and O. S. Dmitrieva. 2018. “Influence of elements thickness of separation devices on the finely dispersed particles collection efficiency,” *MATEC Web of Conferences*, 224: 02073.

2018 International Theoretical and Practical Conference on Alternative and Smart Energy (TPCASE 2018)
ISBN: 978-1-60595-617-6

Storage of Renewable Energy in Hydrogen Using Power-to-Gas Technology

Dmitry Dunikov

ABSTRACT

In Kamchatka region up to 30% of electricity is produced from renewables, to avoid curtailment by the grid operator the excess power should be used for hydrogen production by water electrolysis. For each 1% of saved geothermal steam 92 t of H_2 can be annually produced. Blending the produced hydrogen with natural gas is a promising option due to the availability of existing infrastructure. The H_2/CH_4 mixture suits for commercial and domestic use, hydrogen as well can be separated from the mixture and used in fuel cells.

INTRODUCTION

The share of renewable energy sources (RES) in electricity generation increases rapidly. Variable nature of RES is one of their major drawbacks, capacity factors are quite low: 0.13-0.54 for wind and 0.10-0.35 for solar PV [1]. Integration of the renewables into grid raises several problems [2]:

- Matching supply and demand (market level—hourly perspective). In periods with high RES generation, supply may exceed demand, creating negative electricity prices in the spot market. On the other hand, for periods with low RES generation costly back-up capacity has to be available.
- Safe network operation (balance of supply and demand on a second to minute basis). To accommodate unpredicted fluctuations, grid operators need to provide increased reserve power on the balancing market, and energy production may need to be curtailed.

Joint Institute for High Temperatures RAS, 13 building 2, Izhorskaya Street, Moscow, 125412, Russia; National Research University "Moscow Power Engineering Institute", 14, Krasnokazarmennaya Street, Moscow, 111250, Russia

Current power storage capacity is just under 3% of global electricity generation capacity (or 150 GW) and is dominated by a single technology, pumped storage hydropower (PSH) [3]. Hydrogen for energy storage fits into a global sustainable energy strategy for the 21st century that confronts the three-pronged challenge of irreversible climate change, uncertain oil supply, and rising pollution. The role of hydrogen at national and international strategic levels relies entirely on renewable energy and energy efficiency. Hydrogen would play a crucial role in medium and long distance road and rail vehicles; in coastal and international shipping; in air transport; and for longer-term seasonal storage on electricity grids relying mainly on local renewable energy sources and feedstocks [4].

Hydrogen produced from renewable electricity by water electrolysis could facilitate the integration of high levels of variable renewable energy into the energy system [5]. Power-to-Gas is defined as the production of a high-energy density gas via electrolysis of water. Blending hydrogen with natural gas is a promising option due to the availability of existing infrastructure. The key challenge today is to identify concrete short-term investment opportunities, based on sound economics and robust business cases, initial business cases will likely be based on producing green hydrogen and supplying it to industry and mobility ("Power-to-Hydrogen" and "Hydrogen-to-X") [6].

RENEWABLE POWER GENERATION IN RUSSIA

RES share in Russia is very low due to cheap and abundant fossil fuels, data on wholesale electricity market show that renewables generated only 0.01% of the total electricity in 2016 and about 0.04% in 2017. On the other hand, about 2/3 of Russia's territory with the population about 20 million is not covered by unified grid system and these regions supplied by isolated grids, where renewables can play a greater role [7]. There are ca. 900 diesel power stations generating 2.54 billion kWh/year (2% of total generation in Russia) with generation cost in the range 0.25-2 Euro/kWh [8]. The power supply of isolated regions is heavily subsidized from the federal and regional budgets and causes significant environmental damage.

The only region in Russia with a high share of RES is isolated energy system of Kamchatka, where operate geothermal power plants including Mutnovsky GeoPP-1 (50MW), Verkhne-Mutnovsky GeoPP (12 MW), and Pauzhetsky GeoPP (11.0 MW) [9]. Today the Mutnovsky power plants produce 27-30% of electricity generation in the Central power district of Kamchatka, which covers 65% of the region and supplies power to 360,000 people (95% of the population). In 2016 the geothermal power was sold to the grid for 2.69 RUB/kWh (ca. 0.045 $/kWh), while generation from fossil fuels cost 5.01 RUB/kWh (ca. 0.08 $/kWh), thus further development of geothermal power stations in Kamchatka can be feasible. The most promising projects are expansion of the Mutnovsky and Verkhne-Mutnovsky GeoPPs, a use of waste brine in a combined power unit can give additional 8 MW

[10] - 10 MW [9] in a steam cycle and 5 MW [10] – 6.5 MW [9] in a binary cycle, and construction of a 50 MW second stage of the Mutnovsky GeoPP is also considered [9].

Although geothermal power production has a very high capacity factor, it has problems with integration to the grid. Annually 12.3% of geothermal steam is lost [11], and a significant part of the losses arises from a curtailment by the grid operator. At night, the load can be dropped by 60% in favor of combined production of electricity and heat from fossil fuels at thermal power plants.

POSSIBLE HYDROGEN PRODUCTION FROM GEOTHERMAL POWER

Various hybrid schemes have been proposed for the geothermal cycle improvement, including combination with another source of energy [12], co- or multi-generation including hydrogen production greatly increases the efficiency of geothermal systems [13, 14]. Electrolyzers of MW-class are available on the market, at 10 bar output pressure their efficiency is between 52 and 62% (LHV) for alkaline and 57–64% for PEM models [15].

Calculations by thermodynamic model, described in [11], show that there is a potential to increase power production on the Mutnovsky GeoPP-1 by the use of energy of separated liquid and by decreasing steam losses (see Figure 1).

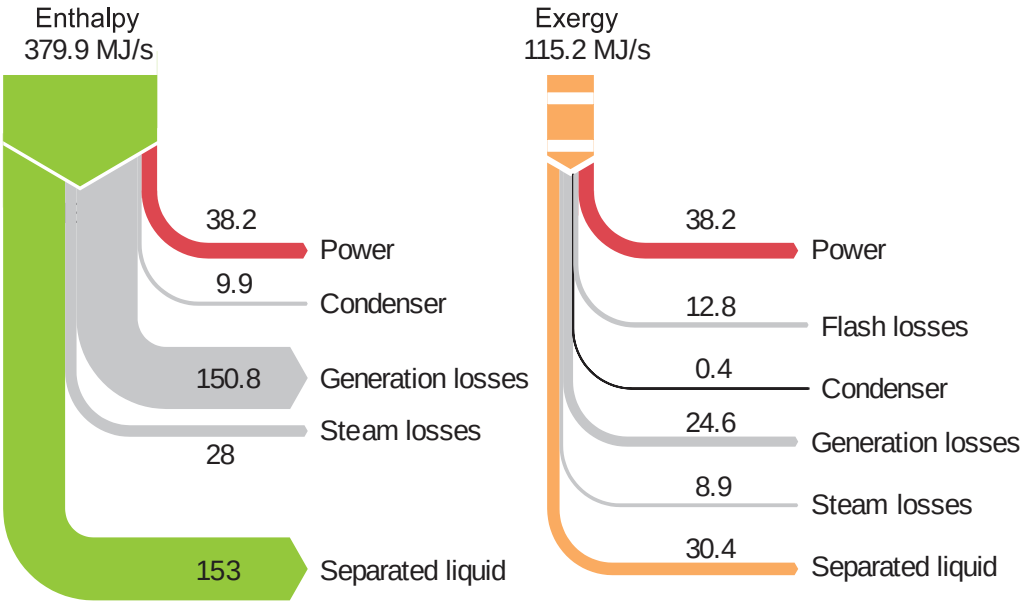

Figure 1. Enthalpy and exergy balances for the Mutnovsky GeoPP-1.

Both thermal and exergy efficiencies of the plant are linear functions of technological steam losses. The steam losses at Mutnovsky GeoPP-1 are in the range

from 3.1% - 18.8% (see Figure 2). Since a significant part of losses arises from curtailment to demand side management, there is a possibility to increase generation and use additional energy, e.g. for hydrogen production. If a full load of turbines is maintained, there will be excess energy for water electrolysis. It appears that for each 1% of saved steam 92 t of H_2 can be annually produced.

Standards permit to add around 10% of hydrogen into natural gas. According to the Russian standard, GOST 5542-2014 components of natural fuel gases are not normalized, and possible hydrogen content is only restricted by requirements for Wobbe index and low heating value.

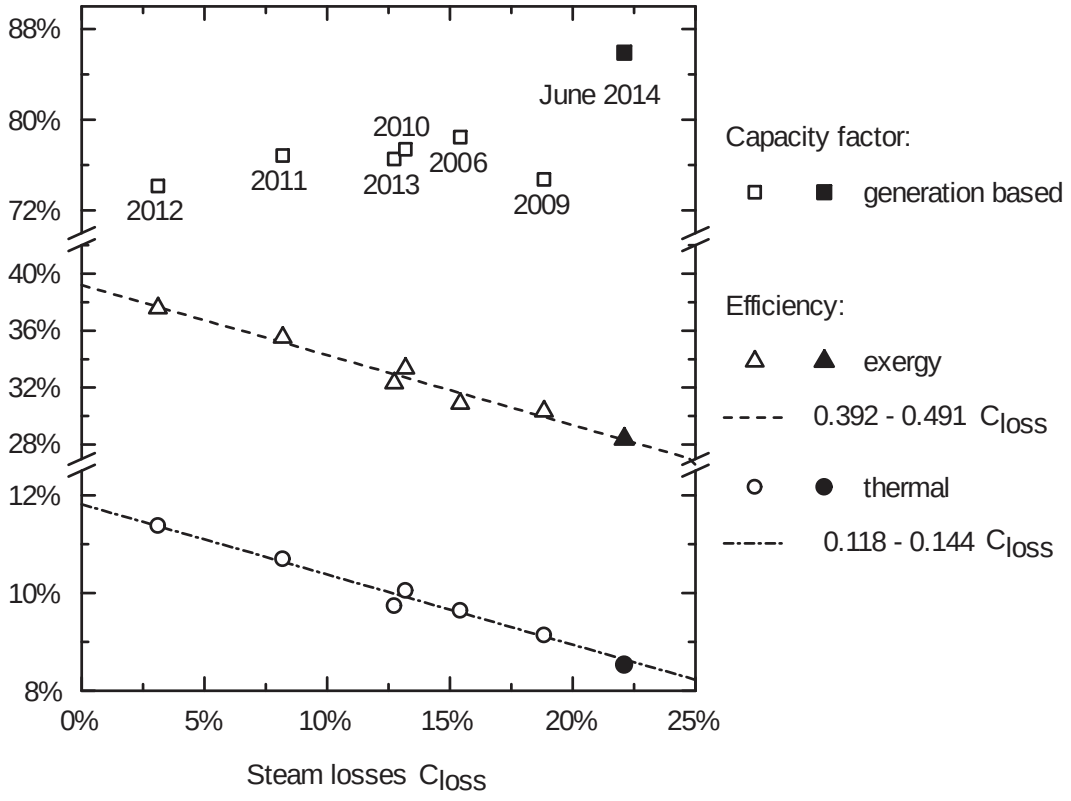

Figure 2. Capacity factor, thermal and exergy efficiencies for Mutnovsky GeoPP-1 for selected years.

CONCLUSIONS

In Kamchatka region up to 30% of electricity is produced from renewables, to avoid curtailment by the grid operator the excess power should be used for hydrogen production by water electrolysis. Blending the produced hydrogen with natural gas is a promising option due to the availability of existing infrastructure. The H_2/CH_4

mixture suits for commercial and domestic use, hydrogen as well can be separated from the mixture and used in fuel cells.

The work was supported by Russian Ministry for Science and Higher Education, subsidy #14.607.21.0188 RFMEFI60717X0188.

REFERENCES

1. REN21 2017 *Renewables 2017 Global Status Report*, Paris: REN21 Secretariat.
2. Lehmann, P., F. Creutzig, M.H. Ehlers, N. Friedrichse, C. Heuson, L. Hirth, and R. Pietzcker. 2012. "Carbon Lock-Out: Advancing Renewable Energy Policy in Europe," *Energies,* 5:323.
3. IEA 2016 *World Energy Outlook 2016*, Paris: IEA.
4. Andrews, J., and B. Shabani. 2012. "Re-envisioning the role of hydrogen in a sustainable energy economy," *International Journal of Hydrogen Energy,* 37:1184-203.
5. IRENA 2018 *Hydrogen from renewable power: Technology outlook for the energy transition*, Abu Dhabi: International Renewable Energy Agency.
6. HINICIO and Tractebel 2017 *Study on early business cases for H_2 in energy storage and more broadly power to H_2 applications*, FCH JU.
7. Dunikov, D.O. 2015. "Russia's view on development of novel and renewable energy sources, including hydrogen energy," *International Journal of Hydrogen Energy,* 40:2062-3.
8. Elistratov, V. 2016. "Autonomous energy supply in Russia by power generation complexes based on renewable energy sources," *Energy Bulletin,* 21:37-44.
9. Tomarov, G.V. and A.A. Shipkov. 2017. "Modern geothermal power: GeoPP with geothermal steam turbines," *Thermal Engineering,* 64:190-200.
10. Tomarov, G. V., A.A. Shipkov, A.I. Nikol'skii, and V.N. Semenov. 2016. "Combined cycle power unit with a binary system based on waste geothermal brine at Mutnovsk geothermal power plant," *Thermal Engineering,* 63:409-13.
11. Dunikov, D.O. 2018. "Cycle improvement and hydrogen steam superheating at Mutnovsky geothermal power plant," *Case Studies in Thermal Engineering,* 12:736-41.
12. DiPippo, R. 2016. *Geothermal Power Generation.* Woodhead Publishing, pp. 391-420.
13. Yuksel, Y.E. and M. Ozturk. 2017. "Thermodynamic and thermoeconomic analyses of a geothermal energy based integrated system for hydrogen production," *International Journal of Hydrogen Energy,* 42:2530-46.
14. Ghaebi, H., B. Farhang, T. Parikhani, and H. Rostamzadeh. 2018. "Energy, exergy and exergoeconomic analysis of a cogeneration system for power and hydrogen production purpose based on TRR method and using low grade geothermal source," *Geothermics,* 71:132-45.
15. Felgenhauer, M. and T. Hamacher. 2015. "State-of-the-art of commercial electrolyzers and on-site hydrogen generation for logistic vehicles in South Carolina," *International Journal of Hydrogen Energy,* 40:2084-90.

2018 International Theoretical and Practical Conference on Alternative and Smart Energy (TPCASE 2018)
ISBN: 978-1-60595-617-6

Energy Saving Electric Winding Machine

Aleksandr Litvinenko, Evgeniy Evtushenko and Denis Baranov

ABSTRACT

Modern electrical engineering is impossible to imagine without transformers, electromagnetic relays and solenoids. The base of this device is an electric coil. Quality of this component depends on the uniformity of winding and compliance with the limits of deformation of the wire. Winding machines use to create electrical coils on an industrial scale. Their improvement is a priority. Advanced precision devises require high-quality winding of thin wires.

INTRODUCTION

Modern electrical engineering is impossible to imagine without transformers, electromagnetic relays and solenoids. The base of this device is an electric coil. Quality of this component depends on the uniformity of winding and compliance with the limits of deformation of the wire. Winding machines are used to create electrical coils on an industrial scale. Their improvement is a priority. Advanced precision devises require high-quality winding of thin wires.

PROCESS DESCRIPTION

The operation of the machine for winding coils occurs by starting an electric motor that the intermediate shaft rotates. On the belt shaft, there is a friction clutch, which performs the clutch. The clutch begins its work after turning the lever into the plug. This method of starting gives you the opportunity to start work and turn off the machine, without jolts. Next, the gear pair begins to rotate the spindle with the frame.

Voronezh State Technical University, 14 Moskovsky Avenue, Voronezh, 394026, Russia

The winding machine starts to wind the wire onto the coil. The basis of any winding machine is a coil-wire-frame technological system. This system includes the following elements: 1) the margin of wires required for winding an electric coil; 2) tension control mechanism; 3) Wire motion devices 4) winding devices 5) receiving frame. Figure 1 shows the winding machine model [1].

MODEL DESCRIPTION

Model winding machine consists of: 1 - coil; 2 - cylinder limiter; 3 - the guide roller; 5, 6, 7 - guide rollers; 4, 8, 10 - asynchronous motors; 9 - wire feeder.
The electric winding machine works as follows, the wire winding from the coil 1, passes through the cylinder limiter 2, which protects the rotating loop of the wire. The guide roller 3 provides the movement of the wire at a right angle. The guide rollers 5, 8, 9 determine the trajectory of the wire. The tension of the wire is provided by rollers 4,8,10 mounted on the shaft of induction motors.

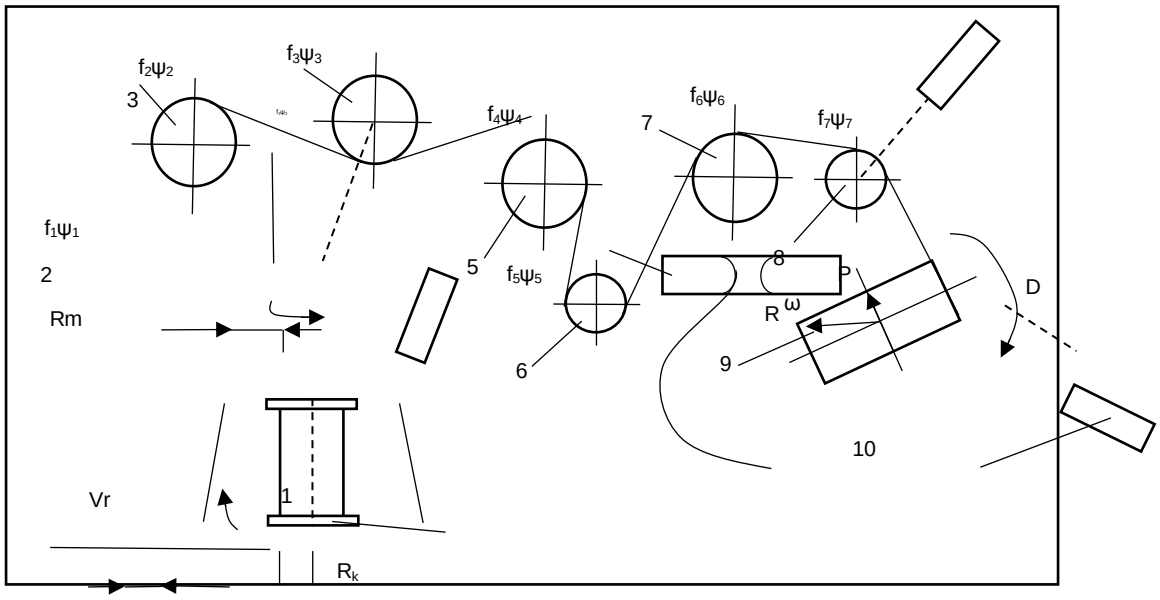

Figure 1. Model of the winding machine

ENGINE PARAMETERS

Tables I, II, III show Engine parameters.

TABLE I. CHARACTERISTICS OF THE ENGINE TENSION DEVICE DID-5TV.

engine's type	Maximum shaft power, Wt.	Starting torque, g • cm, not less	Starting currents, mA, not more		Idle speed, rpm, not less
			excitation	control	
DID-5TV	5,0	220	1200	530	6000
Power					
Power supply, V					frequency Hz
In the excitation circuit		In the control circuit			
36±2		30			400±8

TABLE II. CHARACTERISTICS OF THE MOTOR WINDING UNIT AIR-63-0.37 KW.

engine's type	Power kw	Synchronous frequency rotation, rpm	Nominal current, A	Nominal twisting moment kgm	Efficiency %	Cos φ	Slip %
AIR63B4	0,37	1500	1,37	0,26	68,0	0.70	8,7

TABLE III. CHARACTERISTICS OF THE ENGINE LAYOUT UNIT.

engine's type	Angle step, hail	Current phase SM, A	Torque, kg × cm	Inductance / phase, mH	Resistance / Phase, Ohm	The moment of inertia of the rotor, g x cm ^ 2
FL86STH80-5504	1,8	5,5	46	4	0,46	1400

WIRE TENSION STABILIZATION

One of the dominant problems is a high reject rate – 50%. This is due to inaccurate control of the stretching of the thin wire during winding. This leads to frequent wire breaks.

The article aims to reduce the percentage of reject and energy costs in the manufacture.

To this end, a mathematic model of the electric winding machine was built in the Mathcad program.

The system is set up for a given tension statically before the machine is started by breaking the wire with a roller 4 with a certain force, which in this case can be determined from the expression [2]

$$T_{\text{St}} = \text{T}_0 + 2pf_3 \tag{1}$$

With the static setting of the machine, we can approximately assume that the tension of the driven wire branch $T_0 = 0$; from here

$$p = \frac{T_{\text{St}}}{2 \cdot f_3} \tag{2}$$

Let us determine the change in the magnitude of the tension along the entire length of the moving wire and the actual tension with which the winding winds up. To do this, we determine successively the tension of the wire at each section of the schematized technological system. [3]

Section 1. It is known from theory that with the axial winding of wires with a fixed coil in the ballooning part of the passing values at the top of the balloon and can be calculated by the formula

$$T_1 = T_c + \frac{1}{2} \cdot m \cdot \omega^2 \cdot R_{\max} \cdot \sin^2(\omega_0 \cdot H_c) \tag{3}$$

The angular velocity of ballooning wire is

$$\omega = \frac{1000 \cdot \nu_r}{60 \cdot R_k} \tag{4}$$

The linear mass of the ballooning wire is equal to [3]

$$m = \frac{10 \cdot P}{g \cdot L_\delta} \tag{5}$$

Substituting the formula, we get

$$m = \frac{\pi \cdot d_M^2 \cdot \gamma}{400 \cdot g} \tag{6}$$

Determine the value of sine [4]

$$\sin(\omega_0 \cdot H_c) = \sin(\frac{\pi}{H} \cdot H_c) \quad (7)$$

Substituting the obtained values into the equation, we determine the tension at the top of the cylinder:

$$T_1 = T_c + \frac{1}{2} \cdot m \cdot \omega^2 \cdot R_{\max}^2 \cdot \sin^2(\omega_0 \cdot H_c) \quad (8)$$

Section 2. In this section, the wire passes the guide roller 2. By neglecting the rotational movement of the wire and considering only its longitudinal movement, the tension of the leading branch of this section can be determined from the equation

$$T_2 = T_1 e^{f_1 \psi_1} + f_1 \cdot m_1 \cdot \nu_r^2 \cdot \psi_1 \quad (9)$$

Section 3. In this area with sufficient accuracy can be considered (without taking into account the longitudinal and transverse oscillations of the wire) that the tension is kept constant until roller 3 [5].

Section 4. The tension of the leading branch of the wire is determined from the expression

$$T_3 = T_2 \cdot e^{f_2 \psi_2} \quad (10)$$

Section 5. Tension is kept constant until the wire contacts the tension roller 4Section 6. The tension of the leading branch will be determined from the expression

$$T_4 = T_3 + 2 \cdot f_3 \cdot p \quad (11)$$

Similarly, we will perform the calculation of the remaining sections.

EXPERIMENTAL RESULTS

As can be seen from figures 3, 4 - stabilization of the tension allows reducing the tension of the wire by three times. This reduces the power consumption of the machine and increases its productivity. These results were tested experimentally on a real electric drive of a model winding machine (SNP-0.1-150V “Pulsar”), which reduced the reject rate by two times.

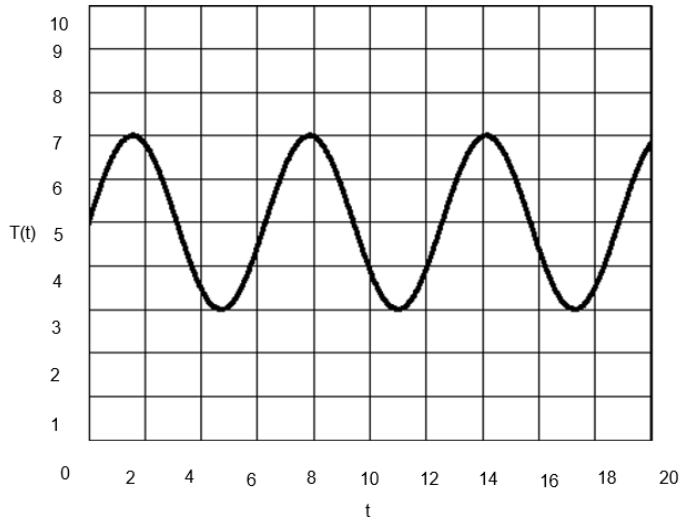

Figure 2. Thread tension using a rectangular frame.

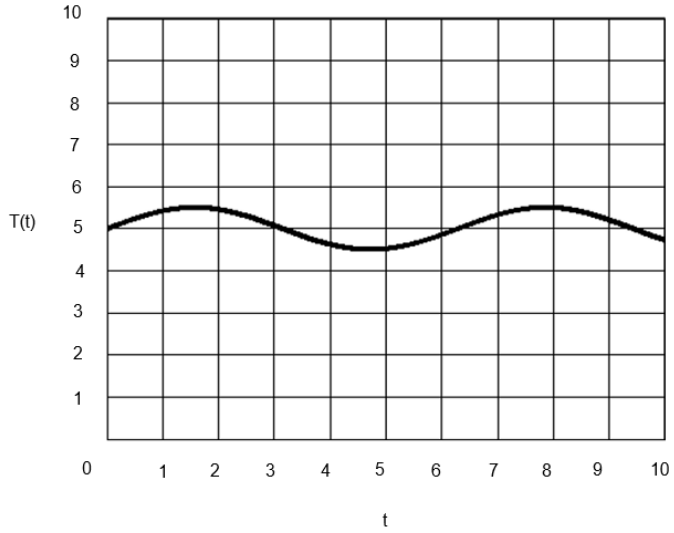

Figure 3. Thread tension using compensated frame.

CONCLUSION

As can be seen from figures 3, 4 - stabilization of the tension allows reducing the tension of the wire by three times. This reduces the power consumption of the machine and increases its productivity. These results were tested experimentally on a real electric drive of a model winding machine (SNP-0.1-150V “Pulsar”), which reduced the reject rate by two times.

REFERENCES

1. Shmelev, V., and S. Sbitnev. 2006. “Space-phase modeling of electromechanical Processary Motion Machines. 2D Model realization,” *Except from the proceedings of the COMSOL user conference*, Prague. pp. 8–13.
2. Kozlov, Ye.M. 1968. *Designing and calculation of winding devices of electrical machines*. Energy, pp 37–49.
3. Zhukov, V.A. 1969. *Technology of production of radio equipment*, Gosenergoproizdat, pp. 67-106.
4. Peshkov, I. B. 1968. *Enameled wires*. “Energy”, pp. 44–82.
5. Loktaev, V.S. 1969. *Ways to increase labor productivity in the manufacture of windings. In the book.: Reducing the complexity of products in the instrument*. Ed. A.N. Gavrilova. Energy, pp. 213-301.

2018 International Theoretical and Practical Conference on Alternative and Smart Energy (TPCASE 2018)
ISBN: 978-1-60595-617-6

Passive Solar Heating with Adjustable Heating Modes

Tatiana Shchukina, Mariya Zherlykina, Roman Sheps and Ekaterina Burak

ABSTRACT

This paper discusses different schemes of the performance of passive solar heating of buildings. Based on the solution for heat conduction equation for active building constructions taking into account the influence of convective heat transfer and heat flux, incoming solar radiation, the ways of energy-saving facilities' operation is analyzed. It is shown that to increase the efficiency of such systems, an individual design should be performed taking into account the climatic features of the construction area, and the choice of rational combinatorics for the outer shell, such as movable shielding heat-protective device, and creating an air gap between the accumulating and heat-insulating layers. Based on the calculations, the energy-active area of the bearing course of buildings, protected from the outer side with the translucent barrier is revealed. The suitable thickness of the accumulation layer for recycling process of solar radiation is determined. The presented innovative technical solutions could help to enhance the efficiency of solar energy utilization and contribute to more active implementation of passive solar heating, expanding the scope of their territorial application.

Keywords: energy saving, solar radiation, thermal energy, passive solar heating, thermal regime of outer shells.

INTRODUCTION

Switching from the traditional energy sources to the modern ones, such as solar power, is not only capable of significantly saving money, but also has a positive

Department of Housing and communal services, Voronezh State Technical University, 84, 20-Letiya Oktyabrya Street, Voronezh, 394006, Russia

impact on the environment. In contrast to the developed countries, such as the USA or Germany, in the developing countries, solar energy is not widely used. This is due to the lack of the necessary technological level [1]. However, the growth of energy demand leads to the search for new energy sources.

One of the options to soften the energy demands is the development of passive solar construction design. In passive solar construction design, windows, walls, and floors are made to collect, store, and distribute solar energy in the form of heat in the winter and reject solar heat in the summer. This is called passive solar design because, unlike active solar heating systems, it does not involve the use of mechanical and electrical devices. Therefore, the passive solar heating can be considered as a rather cheap alternative to the other energy technologies.

The key to designing a passive solar building is to best take advantage of the local climate performing an accurate site analysis. For example, highly optimized systems of the passive solar heating allowone to dramatically reduce the estimated 40% of energy consumed in the average Australian home [2] and more than 75% in the southwest United States [3] for space heating and cooling. Elements to be considered include window placement and size, and glazing type, thermal insulation, thermal mass, and shading [4]. Passive solar design techniques can be applied most easily to new buildings, but existing buildings can also be adapted or modified.

Despite the accessibility and simple execution of passive solar heating devices, their operation may be accompanied by unreasonably high losses of useful heat or excessive overheating in the summer months. The expected efficiency increase of such systems for solar radiation utilization will be possible if the design of the structural elements is based on mathematical modeling and the application of the shielding devices of various modifications. In this paper, the ways of energy-saving operation of facilities are examined based on the solution of heat conduction equation for active building constructions taking into account the influence of convective heat transfer and heat flux, coming from solar radiation. It is shown that to increase the efficiency of such systems, an individual design should be performed taking into account the climatic features of the construction area, and choice of rational combinatorics of external enclosure, such as movable shielding heat-protective device, creating an air gap between the accumulating and heat-insulating layers, etc.

PURPOSE OF THE STUDY

The aim of this study is to increase the efficiency of passive solar heating.

METHODS

For the rational construction of the face-integrated solar heating systems, the main issue is the distribution of the thermal regime generated in absorbing and

accumulating layer. To study the temperature field arising in energy-active building constructions, we use the heat conduction equation of the plate in the following form

$$\frac{\partial \theta}{\partial \tau} = a \frac{\partial^2 \theta}{\partial x^2}, \tag{1}$$

where θ – the environment temperature in a certain point of space and time (^{o}C); τ – time (s); a – temperature conductivity coefficient (m^2/s).

Under given conditions of heat transfer, the origin of coordinates is advisable to place on the surface (Figure 1) exposed to solar radiation. In this case, the boundary conditions can be written as

$$\text{when } x = 0, \quad -\lambda \left.\frac{\partial \theta}{\partial x}\right|_{x=0} = q_S - \alpha_1 \theta_{x=0}; \tag{2}$$

$$\text{when } x = \delta, \quad -\lambda \left.\frac{\partial \theta}{\partial x}\right|_{x=\delta} = \alpha_2 \theta_{x=\delta}; \tag{3}$$

where λ – coefficient of thermal conductivity of the wall material, W/(m·^{o}C); δ – thickness of wall (m); q_S is the capacity of solar radiation received per area unit of the construction through the glass shell, W/m^2; α_1, α_2 – heat transfer coefficients, W/(m^2·^{o}C).

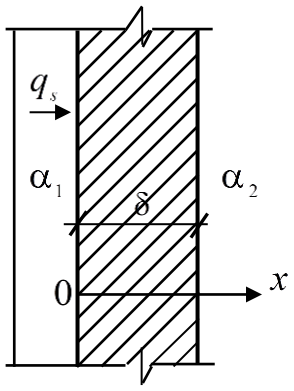

Figure 1. Scheme of heat transfer in passive solar heating.

The calculations are carried out for conditions of the middle latitudes (~50 °N), which is a large part of the territory of Europe, Russia and North America.

DATA, ANALYSIS, AND RESULTS

It should be noted that the most reliable results of the analytical solutions of the heat equation can be obtained for tasks of semibounded arrays of different homogeneous materials [5]. As it was shown in works [6], numerical simulation of temperature regimes of the absorbing accumulating layer requires a thorough analysis of design values database to identify parameters that have a major influence on the studied process. Therefore, we propose to represent the solution of equation (1) in the form of correspondence, which models periodic changes in the present thermal conditions the most adequately

$$\theta = e^{kx}\left[A_1 \cos(\omega\tau + kx) + A_2 \sin(\omega\tau + kx)\right] + e^{-kx}\left[A_3 \cos(\omega\tau - kx) + A_4 \sin(\omega\tau - kx)\right] \quad (4)$$

The first member on the right side of expression (4) is determined by energy radiation into the environment by the building construction as it is heated by solar radiation; the second one is recorded on the basis of absorption of the heat flux to the external surface of the construction and transmission of it into an array by conduction.

We define a constant k by differentiating the equation (4) in terms of the variables τ and x in accordance with (1),

$$k = \sqrt{\frac{\omega}{2a}}, \quad (5)$$

where $\omega = 2\pi/z$ – oscillation frequency; z is the period of oscillation.

To determine the constants in the correspondence (4), we use boundary conditions (2) and (3). As the equation (2) contains the heat flow transferred to the surface of the shell, which is used in passive solar heating, then we will use the function of the form (Ministry of Regional Development of Russia, 2012) for its approximation

$$q_S = C\cos\omega\tau + D\sin\omega\tau \quad (6)$$

For this reason, we consider passive heating carried out using the south outer wall made of sand-lime brick and having the translucent coating from the outer side (Figure 1). The fencing material has the following properties: coefficient of thermal conductivity 0.76 W/(m·°C), specific heat 0.88 kJ/(kg·°C) and a density of 1800 kg/m^3. Calculations are going to be performed for four design options for the wall, where its thickness corresponds to the following sizes: 120, 250, 380 and 510 mm.

The coefficients of heat transfer from the outside and the inside of the fence will be taken in accordance with equal to 12 and 8.73 W/(m^2·^{o}C).

Heat flow, transferred in March through the glazing to the surface of the vertical fence, can be used for areas of 50°N with sufficient accuracy of the correspondence

$$q_S = -84\cos\omega\tau - 56{,}84\sin\omega\tau \quad (7)$$

Then solving the system of equations for the given conditions using the Cramer formulas, we will get the correspondences:

when δ = 120 mm

$$\theta = e^{8{,}71x}\left[0{,}0656\cos(\omega\tau + 8{,}71x) + 0{,}2715\sin(\omega\tau + 8{,}71x)\right] + \\ + e^{-8{,}71x}\left[-2{,}9409\cos(\omega\tau - 8{,}71x) - 4{,}2032\sin(\omega\tau - 8{,}71x)\right]; \quad (8)$$

when δ = 250 mm

$$\theta = e^{8{,}71x}\left[-0{,}0049\cos(\omega\tau + 8{,}71x) - 0{,}027\sin(\omega\tau + 8{,}71x)\right] + \\ + e^{-8{,}71x}\left[-3{,}0532\cos(\omega\tau - 8{,}71x) - 4{,}1285\sin(\omega\tau - 8{,}71x)\right]; \quad (9)$$

when δ = 380 mm

$$\theta = e^{8{,}71x}\left[-0{,}0025\cos(\omega\tau + 8{,}71x) + 0{,}00068\sin(\omega\tau + 8{,}71x)\right] + \\ + e^{-8{,}71x}\left[-3{,}0421\cos(\omega\tau - 8{,}71x) - 4{,}1338\sin(\omega\tau - 8{,}71x)\right]; \quad (10)$$

when δ = 510 mm

$$\theta = e^{8{,}71x}\left[0{,}00014\cos(\omega\tau + 8{,}71x) - 0{,}00026\sin(\omega\tau + 8{,}71x)\right] + \\ + e^{-8{,}71x}\left[-3{,}0429\cos(\omega\tau - 8{,}71x) - 4{,}1347\sin(\omega\tau - 8{,}71x)\right]; \quad (11)$$

As it can be seen from equations (8-11), with increasing thickness of the material layer, its radiation to the environment greatly reduces, which is described by the first member of the equation, therefore, this component can then be neglected.

The graph of temperature change (Figure 2) at 3 PM, built according to the equation (11) for the wall of sand-lime brick for the building, located near 50 °N., shows that intense temperature damping takes place in the fences with thickness up to 250 mm. At the same time, at the thickness of 380 mm or more, the impact of these changes on the indoor microclimate is significantly reduced during the day. Therefore, if the air environment of the premises should be warmed in a short time, then it is expedient to use less massive building constructions for passive solar heating, using them mostly for buildings of public and industrial purposes, with a single-shift operation mode. In other cases, the thickness of the fence should not be significantly increased, but it is necessary to set the heat shielding devices, which

regulate the solar radiation flow between the glazing and supporting construction [7].

Taking into account the difficult weather conditions of winter seasons in most of the middle latitudes, particularly in Russia, construction of fencing and utilizing of the solar radiation should have not only the storage layer but also the high heat-protective properties. An appropriate technical solution is proposed in the patent [8], offering bearing accumulative layer, closed from external influence by translucent enclosure, and having effective thermal insulation with organized air gap (Figure 3).

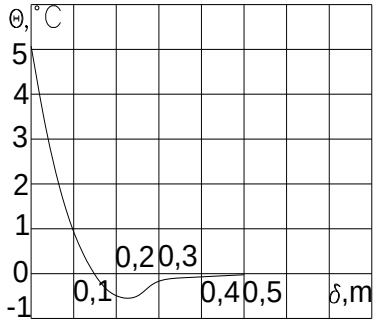

Figure 2. Change of relative temperature in the thickness of the fence

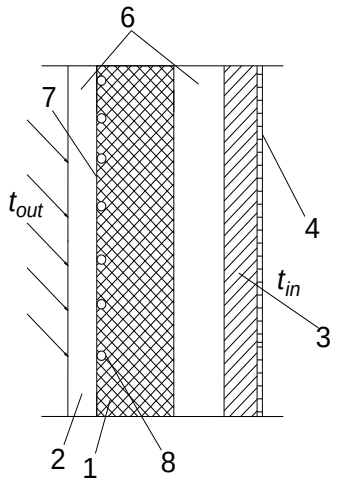

Figure 3. Top view of the energy-active outer fencing cut: 1 — heat storage bearing layer of the enclosing construction; 2 — translucent cover; 3 — heat insulating material; 4 — interior furnishing; 5 — valves; 6 — air gap; 7 — dark paint coating with a high coefficient of thermal conductivity; 8 — pipes with the heat conductor.

IMPLICATIONS AND RECOMMENDATIONS

On the basis of theoretical research, we developed recommendations for the creation of optimal regimes of passive solar heating operation. It is shown that the

optimal conditions are achieved as a result of the combination and structural performances of the storage material, shielding devices, and thermal protection, which prevents heat loss and excess heat input, respectively. A distinctive feature of the developed model from previously proposed models of thermal regimes is a more precise definition of the energy-active layer thickness in storage material for designing new generation constructions. In particular, on the basis of the obtained results, we can anticipate that in the outdoor design of energy-efficient buildings' walls for the southern regions, corresponding to 40 oN, the thickness of the accumulation layer should not exceed 200 mm. Moreover, for buildings located to the North, with each subsequent degree, you need to reduce the accumulation layer thickness for 6-7 mm. The thickness of thermal insulation is appropriate to calculate in accordance with the regulatory calculation from the energy conservation condition for the project area. The reliability of the obtained results is confirmed by good convergence in the harmonic oscillations description, which is specific for the periodic impact of solar radiation on the fence surface.

REFERENCES

1. Dimitriev, O. P. 2013. "Global Energy Consumption Rates: Where is the Limit?" *Sustainable Energy*, 1(1): 1–6. http://doi.org/10.12691/RSE-1-1-1
2. Department of the Environment, Water, H. and the A. (DEWHA). (2008). Energy use in the Australian residential sector 1986–2020. Canberra.
3. New Mexico Solar Association. (n.d.). Passive Solar Design. Retrieved November 11, 2015, from http://www.nmsea.org/Passive_Solar/Passive_Solar_Design.htm
4. Norton, B. 2014. *Harnessing Solar Heat*. Springer.
5. Rizzi, F., N.J. Van Eck, and M. Frey. 2014. "The production of scientific knowledge on renewable energies: Worldwide trends, dynamics and challenges and implications for management," *Renewable Energy*, 62:657–671. http://doi.org/10.1016/j.renene.2013.08.030
6. Tyagi, R. K., R. Ranjan, and K. Kishore. 2014. "Performance studies on flat plate solar air heater subjected to various flow patterns," *Applied Solar Energy*, *50*(2):98–102. http://doi.org/10.3103/S0003701X14020133
7. Shchukina, T. V., D.M. Chudinov, and L.V. Kuznetsova. 2006. Patent 2327847 IPC E06B 9/24. Solar-control window.
8. Shchukina, T. V., and R.A. Sheps. 2016. Patent 2604119 IPC F24J 2/24, F24J 2/34, F24J 2/14, F24J 2/16. Solar Thermal Collector.

2018 International Theoretical and Practical Conference on Alternative and Smart Energy (TPCASE 2018)
ISBN: 978-1-60595-617-6

The Implementation of Energy-Saving Technologies for Reactive Power Compensation in Grids of All Voltage Levels Based on Static Converters

Valery Krysanov, Konstantin Ivanov, Ilya Haychenko and Vladimir Babenko

ABSTRACT

In this paper, the technology of increasing the level of energy-saving due to the effective compensation of reactive power (RP) is considered in electric power grids of high and ultra-high voltage. For these grids, two variants of hardware implementation of static compensation devices of reactive power, based on capacitor batteries and power transformer equipment, have been developed. The conclusions are made about economic feasibility of the application of the developed devices in modern electric power systems (EPS) on the basis of the analysis of the obtained technical and economic characteristics of these devices.

INTRODUCTION

Modern EPS are a complex multi-level system that performs the functions of generation, transportation and distribution of electric energy. Its efficiency and reliability is largely determined by the degree of controllability including the one at the hardware level. In this context, the wide application of the principles of Smart Grids in EPS is of great importance.

The Smart Grid is a complex technology based on the use of devices in the EPS that allow to quickly change the parameters of grid in order to maintain the operating mode with maximum energy efficiency in the conditions of changing load parameters. This technology combines all elements of the EPS at the physical level and manages them.

Voronezh State Technical University, 84, 20- Letiya Oktyabrya Street, Voronezh, 394006, Russia

The relevance of implementation of modern hardware solutions for a wide class of grids (from 6 kV to the class of ultra-high voltages of 750, 1150 kV) which satisfy all technological requirements (including price—quality ratio) is determined by their ability to optimally control the modes of EPS.

These solutions completely comply with the technology of flexible alternating current transmission systems (FACTS) as one of components of the Smart Grid direction. At present, a large amount of research and development has been carried out in the field of creating devices for regulating the modes of grids of different EPS voltage classes[1-7]. The main devices used in the framework of FACTS technology in relation to reactive power (RP) compensation are:

- Controlled thyristor capacitor installations (CTCI);
- Controlled shunt reactors;
- Static reactive power compensators (SRPC).

At present, the above-mentioned devices are well developed in theoretical terms and widely used in grids of appropriate EPS voltage levels [8-10]. Nevertheless, there is an urgent need to create the unified hardware and cost—effective solutions that could be applied to grids of all EPS voltage levels. The authors see the solution of these issues, among other things, in implementation of the functions of static compensators on the basis of capacitor batteries and power transformers connected in a certain way. In this connection, two variants of static devices, RP regulators, are of particular scientific-practical interest and discussed below.

STATIC CAPACITOR COMPENSATION RP DEVICES

The developed controlled thyristor capacitor installation (CTCI) is a capacitor battery that is connected in parallel to the grid with the help of power switching devices [11]. The analysis of various methods of switching capacitor batteries showed the economic feasibility of using power thyristors and solid–state relays as switching devices [12]. This allows to completely get rid of moving mechanical parts that increases the life of product. On the other hand, the use of semiconductor devices increases the speed of the system and service life. The controlled thyristor capacitor installation can be easily integrated into the automated process control system (APCS) of industrial enterprises with the developed microcontroller control system and corresponding software [13]. This applies to distribution grids of 0.4 -10.0 kV where the low specific cost (compared with similar devices) of the compensating RP is predicted, that is, of the order of 115 r/kVAr. Thus, the energy-saving is estimated at 2.4 million rubles per year in the RP compensation of three asynchronous pump motors of the boiler house with the help of the controlled thyristor capacitor installation. The efficiency of the developed circuit design and software solutions of the controlled

thyristor capacitor installation was experimentally confirmed for low–voltage physical models [15].

But this hardware solution is universal for grids of all voltage levels. So, the connection of controlled thyristor capacitor installations in high-voltage networks (35-330 kV) is assumed with the help of power thyristor assemblies in conjunction with high-voltage electro–gas and vacuum circuit breakers. In addition to increasing the life of switches, this method allows to achieve greater saving when switches are already installed on substations. In this case, the specific cost of RP reaches, on average, 30 r/kVAr, for compensation of 50 MVAr. The conducted research of a typical substation 110/220 kV allows us to conclude that the use of controlled thyristor capacitor installations can reduce the average value of load losses by more than twice. It corresponds to saving of 30 thousand rubles per day when the substation is loaded at 2500 MW*h/day [14].

STATIC TRANSFORMER COMPENSATION DEVICES OF RP

The loading of high–voltage transmission lines is carried out in stages during their operation in the EPS. As a rule, in the early stages, the high – voltage transmission lines are not fully loaded and, to maintain the required voltage levels, the compensation is needed for the charging power of lines. For this purpose, reactors are used. This article shows the possibility and feasibility of using power auto-transformers, i.e. booster transformers, incorporated in their neutral, as to compensate for RP [16,17].

Hardware solutions are known when the power transformers with booster transformers are used to regulate the high–voltage transmission lines (220-1150 kV). The power transformers with booster transformers usually have a device for switching the release adjustment under load. The efficiency of such devices can be increased by replacing mechanical devices with thyristor voltage regulators. According to conducted research, various circuit variations of thyristor voltage regulators for power transformers with booster transformers provide high - quality regulation on high—voltage transmission lines both at lower voltage (at first stages of line operation) and increasing voltage (at the stages of full load of transmission lines) [8]. As noted above, the compensation is required for charging power of lines and the adjustment effect from using the thyristor voltage regulators is insufficient in order to maintain the required levels of voltage. However, there is a possibility of implementing such an algorithm for operation of power (thyristor) switches of thyristor voltage regulators in which power transformers and booster transformers are transferred to an operation mode, similar to conventional controlled shunt reactors with magnetization [18, 19]. In this case, power transformers and booster transformers function as controlled shunt reactors at the required time compensating for RP (by calculations, compensation of up to 30 % of the total capacity of power transformers and

booster transformers is possible). Such a hardware solution is very effective as it allows either to completely abandon the use of controlled shunt reactor or to use reactors with much lower installed capacity. The algorithm of power switches of thyristor voltage regulators does not provide RP regulation, but the regulation of transmission lines downwards with the following voltage increase (which gives the ability to provide the required levels of voltage, minimize power losses and increase the capacity of the line) [20].

CONCLUSION

The conducted technical and economic analysis of the proposed hardware solutions shows the efficiency of the specially connected capacitor batteries, power transformers and auto-transformers use as static compensations of reactive power.

The controlled thyristor capacitor installation discussed above can be effectively applied to ultra- high, high and low voltage grids.

By using the proposed method, the control of power transformers and autotransformers allows to significantly expand their functionality for voltage and reactive power regulation in ultra–high and high voltage grids.

REFERENCES

1. Galaev, A. N. and I.V. Shevchenko. 2010. "The Problems of Improving the Energy Efficiency in the Electric Power Industry," *Finance and Credit,* 11:8-13.
2. Podkovalnikov, S.V., S.M. Senderov, and V.A. Stennikov. 2004. *The Energy Systems and their Management*. Energy XXI., 364 p.
3. Padiyar, K.R. 2007. "Facts Controllers in Power Transmission and Distribution," New Age International, New Delhi.
4. Kobelts, B.B. and I.O. Volkova. 2010. *Innovative Development of Electric Power Industry on the Basis of the Concept SMART GRID*. PAC Energy., p. 121.
5. Narain, G. Hingorani. 2000. "Understanding FACTS: Concepts and Technology of Flexible AC Transmission Systems," Wiley-IEEE Press, New York.
6. Schweppe, F.C. 1970. "Power System Static-State Estimation. Part III: Implementation," IEEE Trans Power Apparatus and Systems, № 1.
7. Arrillage, J. 1980. "Thyristor-Controlled in Phase Boosting for h.v.d.c. Convertors," IEEE PROC.
8. Sharzaf, A. M. 1983. "Controller Designs for Power System Stability Enchancement using Static Phase Shifters," IFAC Control in PowerEelectronics and Electrical Drives, Switzerland.
9. Debs, A. S. and R. E. Larsob. 1970. "A Dynamic Estimator for Tracking the State of a Power System," IEEE Transactions on Power Apparatus and Systems, # 4.
10. Glanzmann, G. 2005. "Flexible Alternating Current Transmission Systems," Power Systems Laboratory ETH, Zurich.
11. Alieva, L.F., V.N. Krysanov, Y.S. Pubin, and V. N. Bykov. 1990. "Device for Connecting a Capacitor Battery in Electrical Grids," Patent of USSR # 4498481.

12. Krysanov, V.N., and K.V. Ivanov. 2017. “The Possibilities of using Thyristor Capacitor Installations for Reactive Power Compensation in the Automated Power Supply Control System of Industrial Enterprises,” *Bulletin of VSTU,* 13(1):40-45.
13. Krysanov, V.N. and K.V. Ivanov. 2017 "Control of Power Switching Elements of the Capacitor Installations”. The Certificate of State Registration of the Program for Electronic Computer №2017615137, Application № 2017611850, Date of Receipt 06.03.2017; Date of State Registration in the Register of Computer Programs 03.05.2017.
14. Krysanov, V.N. 2017 “Efficiency of Use of Thyristor Condenser Installations in Industrial Power Supply Systems” *Energy Security and Conservation*, 3:15-20.
15. Krysanov, V.N., V.L. Burkovskii, A.D. Danilov, A.M. Litvinenko and A.L. Rutskov 2018 “A Physical Model of Power Electronic Devices Based on Static Voltage Transducers Russian Electrical Engineering,” *Allerton Press, Inc*, 89(6):381–384.
16. Krysanov, V.N. and K.S. Hamburg. 2011 “Selection of Power Part of High-Voltage Thyristor Voltage Regulators” *Energy Security and Conservation*, 3:35-39
17. Krysanov, V.N. and U.V. Sharapov. 2017. “The AC Voltage Regulator,” Patent of Russian Federation #2612621
18. Choi, S.S. and T.X., Wang. 2005 “Vilathgamuwa D.M. Transmission Series Compensation with Short-Circuit Current Limiting.” *IEEE Trans.on Power Delivery*, 20(3):2248-2256.
19. Christl, N., R Hedin., K Sadek., P Lutzelburger., P.E. Krause, S.M. McKenna., A.H. Montoya, and D Torgerson. 1992 “Advanced Series Compensation(ASC) with Thyristor Controlled Impedance,” *CIGRE*, Paper 14/37/38-05.
20. Krysanov, V.N. 2008 “Reactive Power Compensation of High – Voltage Transmission Lines by a Voltage Regulator,” *Scientific-Technical Journal “Electro-Technical Complexes and Control Systems”*, 3(11):24–27.

2018 International Theoretical and Practical Conference on Alternative and Smart Energy (TPCASE 2018)
ISBN: 978-1-60595-617-6

Features of Computer Modelling of the Medical Waste Thermal Decomposition Process

Nikolay Zroychikov, Sergey Fadeev, Aleksandr Kaverin, Yaroslav Biryukov, Artem Pai and Georgiy Tarasov

ABSTRACT

This paper presents a computer model of a thermal decomposition reactor for medical waste in the ANSYS Fluent software package and results of a non-stationary calculation of a two-phase medium motion in a reactor with a nominal capacity, taking into account heat exchange, drying and pyrolysis of the material. The profiles of velocities and temperatures of the phases, the concentration of the reacting substances in the reactor were obtained.

INTRODUCTION

Medical waste (MW) account for a small part of the total amount of waste produced by the industrial and municipal sectors, but because of its hazard, the issue of its disposal is very important. This type of waste contains infected materials which consist of medical instruments, sharp objects, organic operating waste, chemical or pharmaceutical waste, as well as radioactive and cytotoxic waste or broken mercury thermometers [1]. In this regard, the sanitary regulations and standards set strict conditions for the treatment and special disposal regulations. Most categories should undergo decontamination and a change in physical configuration, precluding secondary use [2]. Their composition is very different and may not be uniform in time and depend on the operation mode of the medical institution (cleaning schedule, days of collection of medical samples for analysis,

Nikolay Zroychikov, Sergey Fadeev, Yaroslav Biryukov, Georgiy Tarasov, JSC "ENIN", 7, Kosinskaya Street, Moscow, 111538, Russia
Aleksandr Kaverin, Artem Pai, NRU "MPEI", 14, Krasnokazarmennaya Street, Moscow, 111250, Russia

time of routine preventive measures). The results of studies of the morphological composition of MW (class B and C) presented in [3, 4] show that the greatest part of the waste of treatment-and-prophylactic institutions consists of textiles, paper, polymeric materials, gypsum, metal, rubber, glass, disinfectants, food and biological waste (Figure 1). At present, the main morphological groups of infected waste are polymeric and composite materials, rubber and textile products.

Combustion of MW is a highly effective way of its disposal, but MW's composition includes chlorine compounds, so due to its incomplete oxidation with oxygen dioxins and furans are formed—substances with strong toxicity that accumulate in a human body and the biosphere. This fact makes pyrolysis an optimal solution for thermal neutralization of MW.

Pyrolysis of organic substances is their thermal decomposition, carried out in an absence of oxygen with the formation of non-condensing gas, tar and coke. The use of pyrolysis technologies to MW due to high temperature guarantees its complete neutralization and excludes secondary use which is required by sanitary regulations and standards [2]). Unlike combustion, the yield of dioxins and furans during pyrolysis is small due to the lack of oxygen. The heat of combustion of pyrolysis products - hydrocarbon vapors and gases is quite high due to the high content of polymers and plastics in MW. Gaseous products can be effectively burned and use the gained heat to maintain the pyrolysis process and supply heat consumers. The solid residue consists mainly of inorganic part of medical waste (glass, gypsum, metal) and a small amount of coke, which basis is carbon.

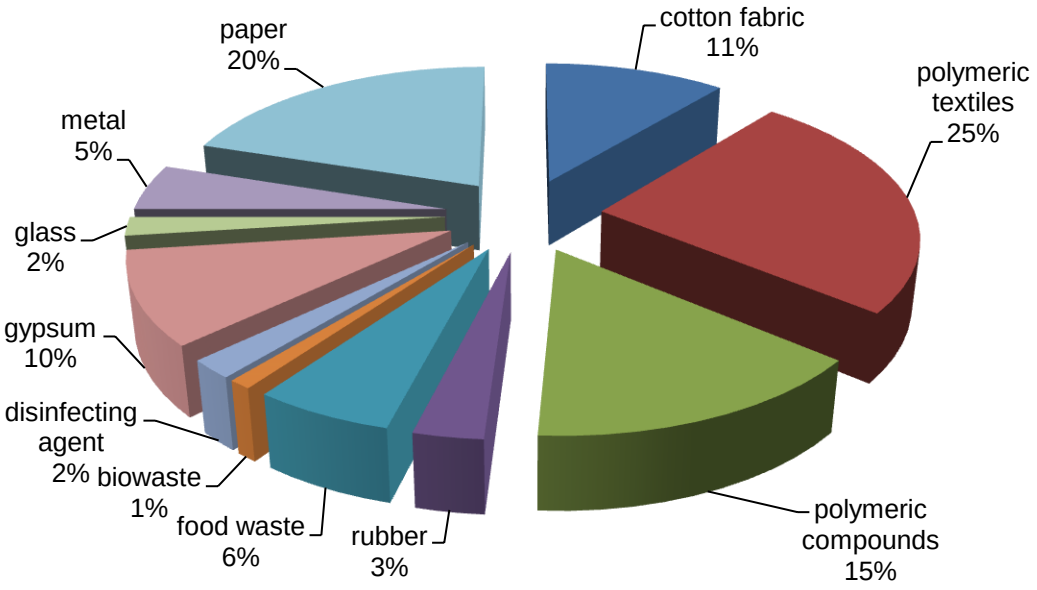

Figure 1. Morphological composition of medical waste.

One of the main problems in the design of MW pyrolysis installations is the heterogeneity of MW's morphological composition due to specific features of medical waste class B and C treatment. Depending on the content of certain components in the total mass heat and mass transfer processes, composition and calorific values of output products and the rate of thermal decomposition will vary. This fact complicates task and imposes additional requirements on the process of regulation and maintenance of continuous and trouble-free operation of the installation. Errors at the design stage may lead to the impossibility of stable operation of the object. Based on this, it is necessary to use modern means of numerical simulation to analyze the pyrolysis process.

RESEARCH OBJECTIVES

The object of the research is the thermal decomposition chamber of the continuous operation pyrolysis installation (Figure 2). The reactor is a cylinder with a diameter of 0.5 m and a length of 1.7 m. The source material is loaded through a pipe 1 that adjoins reactor on the top. MW are pre-shredded and placed to the reactor of 10-20 mm in size. The shredded particles are moved by a screw 2, ensuring an average residence time in the reactor of 20 minutes. The heat required for the process is generated in the combustion chamber 3 and through the wall 4 is transferred to the reactor 5. Gas is removed through the pipe 6. The solid residue of pyrolysis is removed through the lower pipe 7. Some of the gaseous products are taken by the ejection burner 8 into the combustion chamber to ensure the autothermic process, the other part goes to the consumer. The main characteristics of the pyrolysis studied reactor are presented in Table I.

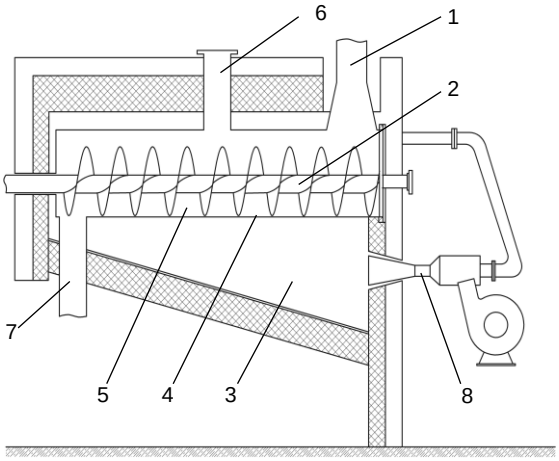

Figure 2. Scheme of MW pyrolysis installation.

TABLE I. CHARACTERISTICS OF PYROLISYS REACTOR.

Parameter	Value	Unit
Mass flow of MW	200	kg/h
Calorific value of MW	20	Mj/kg
Heat consumption of reactor	116	kW
Temperature of the process	400-600	°C
Composition of pyrolisys products (char/gases/tar)	21.6/49.3/29.1	%
MW residence time in the reactor	20	min

The above-described problems of design and operation of this device require a deep understanding of the processes taking place inside the pyrolysis reactor. Taking into account the complexity of the process, the means of computational fluid dynamics (CFD) are used as a research tool.

DESCRIPTION OF THE COMPUTER MODEL

The objective of modeling of the pyrolysis process was solved numerically with the finite element analysis method in the ANSYS Fluent software complex. The unsteady problem of particle motion in two matched zones – sliding and stationary - was solved. In the moving zone, there was set rotating with a constant speed of 0.3 rpm, equivalent to the translational motion of the particles at a speed of 1 mm/s. Example of numerical simulation of a similar object is presented in [5], where the problem of multistage pyrolysis of wood pellets was considered in the COMSOL Multiphysics software complex.

The authors have chosen Pressure Based Solver with a Phase Coupled SIMPLE algorithm (PC-SIMPLE). Flow medium was modeled as a two-phase: gaseous phase and the phase of the solid bulk material. Species Transport model was used for the gaseous phase which was modeled as a mixture. The solid material was modeled as the Eulerian phase with the inclusion of the Granular model. The friction between the phases was described by the Gidaspow model, the heat transfer between the phases was described by the Gunn model. MW particles were taken monofractional with a diameter of 15 mm, packing limit of the MW's bed is equal to 0.55.

The evaporation rate of the particle's moisture was set by an equivalent chemical reaction, which rate (kmol/(m^3·s)) is determined by the following relation:

$$R_{vap} = k_{vap} \cdot C_w^{\,n} \tag{1}$$

where k_{vap} - kinetic constant of the evaporation reaction, s^{-1}; C_w - molar concentration of MW's moisture, kmol /m^3; n - order of chemical reaction.

Kinetic constant of the reaction is determined by the Arrhenius equation:

$$k_{vap} = k_0 \cdot \exp(-E_a/(R \cdot T)) \tag{2}$$

where k_0 - pre-exponential factor, s^{-1}; E_a - activation energy, kJ/mol; R = 8.31 kJ/(mol·K) - universal gas constant; T - temperature of MW, K.

The kinetic constants of the process are taken from [6], where the drying constant of municipal solid waste with a moisture content of 30% has been obtained by the thermogravimetric method. The pre-exponential factor is taken equal to $k_0 = 14.5\ s^{-1}$, the activation energy E_a = 25.97 kJ/mol, the reaction order n = 1.531, the reaction initiation temperature (dew-point temperature) $t_{d.p.}$ = 80°C. The heat of the evaporation is set equal to Q_{evap} = 44 kJ/mol (2.44 MJ/kg).

Stages of solid material inert heating are determined by the heat capacity of the particles, assumed constant c_p = 1800 kJ/kg. In the calculations, as the first approximation assumed that 25% of the MW's mass is moisture and the remaining 75% is the organic mass. Impact of mineral impurities that make up 5% of the mass of waste in this study was not taken into account but will be included in future calculations. The pyrolysis stage of the MW's organic mass was modeled by a one-step heterogeneous chemical reaction:

$$mMW_{org} = n_1 char + n_2 CH_4 + n_3 tar + n_4 H_2O \quad (3)$$

where MW_{org} - organic mass of MW; *char* - semi-coke; *tar* - tarry matter (characterizes condensing gases); CH_4 - methane (characterizes non-condensing gases); H_2O - water vapor; m, n_1, n_2, n_3, n_4 - stoichiometric coefficients of the initial substance and reaction products.

Another approximation in the calculations consists of assuming that the whole organic mass corresponds plastic: polyethylene with a molecular mass of μ_{PE} = 200 kg/mol. The mass component composition of the plastic tarry matter obtained as a result of pyrolysis at a temperature of 600°C was taken from [6]. According to these data, 91.3% of the tar consists of carbon, 4.1% of hydrogen, 2.2% of nitrogen and other components that do not exceed 2.5% in total. Accepting the remainder of the other substances equal to nitrogen, the tarry matter can be represented by the equivalent molecule $C_{7.6}H_{4.1}N_{0.3}$ with a molecular weight μ_{tar} = 100 g/mol. In the non-condensable pyrolysis gases of plastic, the predominant substance is CH_4 (more than 80% by mass), the fraction of each of the remaining components does not exceed 0.5%; therefore, it was decided, to simulate the yield of non-condensible gases by one equivalent substance - methane.

The stoichiometric coefficients are chosen in such a way (taking into account the molecular weights of pyrolysis products) to ensure following products mass fractions: semi-coke 21.4%, methane 41%, tar 29.1%, water vapor 8.5%. The kinetic constants are taken from [7] for high-density polyethylene: $k_0 = 1.9 \cdot 10^{13}\ s^{-1}$, E_a = 220 kJ/mol, n = 1, reaction initiation temperature t_{in} = 380°C. The heat of pyrolysis reaction is set equal to Q_{pyr} = 460 MJ/mol (2.3 MJ/kg). The wall temperature of the shell of the reactor is assumed to be constant, equal to 1100 K (827°C), the wall of the screw is adiabatic, the temperature of the reactor's sidewall is assumed to equal to 600 K (327°C).

RESULTS ANALYSIS

The Figures 3-5 illustrate the results of numerical simulation of the pyrolysis process. Figure 3 shows the distribution of the solid phase in the reactor. The MW loading occupies a relatively small height of the reactor and its level is displaced in the direction of rotation of the screw. The portion of the MW pours from the rotor blades into the bottom of the reactor.

Figure 4 characterizes the mass fractions of the gas components in the reactor. Figure 4a shows that intense evaporation zone occupies half the length of the reactor, as can be noted from the distribution of H_2O concentration in the reactor volume. Further pyrolysis of dry MW begins, the most intensive stage of which occurs in the central part of the reactor.

The most intensive zones of evaporation and thermal decomposition of the MW (Figure 5) correspond to the layers of the bed adjoining the hot walls and the rotor. This fact can be explained by the absence of radiant heat transfer in the model.

Based on the results of calculations, it was found that the moisture of the MW evaporates completely, the organic mass of the waste is processed to 70-75%, what can also be explained by the lack of accounting for the radiation heat transfer in the reactor. The average temperature of the gases at the reactor outlet is 460°C.

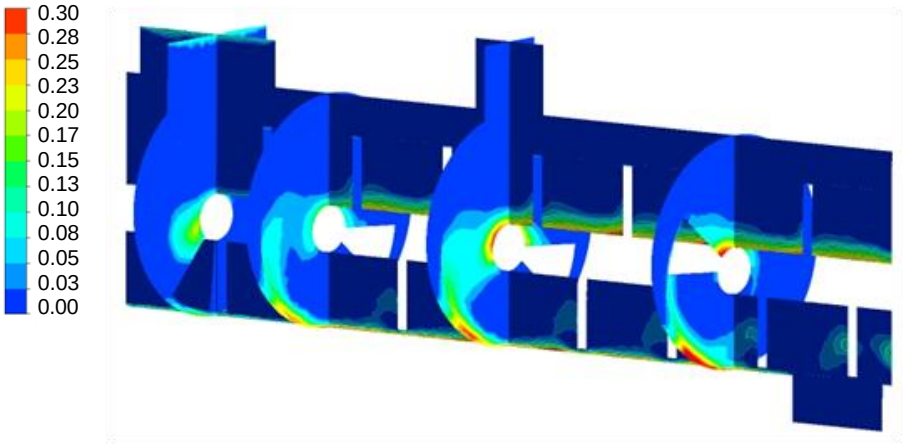

Figure 3. Volume fraction of a solid phase.

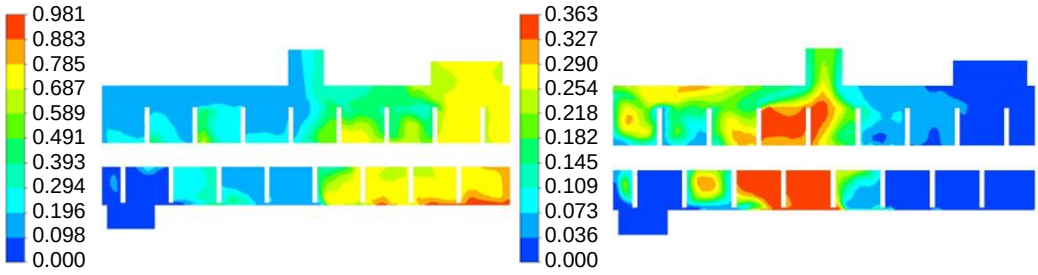

a) water vapour b) condensing gases

Figure 4. Mass fraction of gaseous products of thermal decomposition in the reactor.

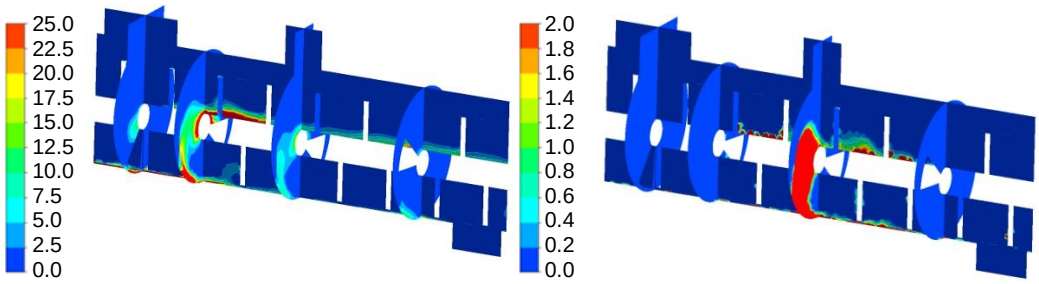

a) rate of moisture evaporation b) rate of pyrolisys

Figure 5. Rate of thermal decomposition of MW in the reactor, mol/(m^3·s).

CONCLUSIONS

The ANSYS Fluent software package was used to model pyrolysis reactor. Analysis of the results of numerical modeling of the thermal decomposition reactor showed the principal possibility of solving the specified problem by the means of computational fluid dynamics. The qualitative picture of the flow of phases and the distribution of components in the volume of the reactor have reasonable and realistic character.

Modeling without taking into account radiant heat transfer has shown that the moisture evaporation zone occupies about half the length of the reactor, and the organic mass of the MW decomposes incompletely (up to 70-75%). The results indicate that after the necessary modifications the model can be successfully used as a tool for the pre-design analysis of a pyrolysis reactor performance capability.

ACKNOWLEDGEMENTS

The work was carried out in JSC «ENIN» within the framework of the applied project "Development and research of the process of environmentally safe disposal of hazardous medical and biological waste based on pyrolysis" (RFMEFI57617X0101) with the financial support of the Ministry of Education and Science of the Russian Federation.

REFERENCES

1. Official website of the World Health Organization. 2018. WHO | World Health Organization. [ONLINE] Available at: http://www.who.int/home. [Accessed 26 June 2018]

2. Decree of the Chief State Sanitary Doctor of the Russian Federation of December 9, 2010 № 163 "*On approval SanPiN 2.1.7.2790-10*" *Sanitary and epidemiological requirements for the management of medical waste*".
3. Akimkin, V. G. 2004. *Treatment of waste in health facilities. Nursing allowance.* Moscow: MCFER.
4. Abramov, V. N. 1998. *Disposal waste in health facilities.* Moscow: MCFER.
5. Levin, A.A., A. N. Kozlov, D. A. Svishchev, and I. G. Donskoy. 2017. "CFD-Modeling of the Multistage Gasifier Capacity of 30 kW," *J. Phys.: Conf. Ser.*, 891 012229.
6. Cai, Junmeng, Yang Yang, Wenfei Cai, and Tony Bridgwater. 2016. "Drying Kinetic Analysis of Municipal Solid Waste Using Modified Page Model and Pattern Search Method," *Waste and Biomass Valorization*, 8(2), pp. 301-312.
7. Westerhout, R.W.J., J. Waanders, J. A. M. Kuipers, and W. P. M. van Swaaij. 1997. "Experimental Determination of the Yield of Pyrolysis Products of Polyethene and Polypropene. Influence of Reaction Conditions," *Ind. Eng. Chem. Res.*, 36:1955-1964.

2018 International Theoretical and Practical Conference on Alternative and Smart Energy (TPCASE 2018)
ISBN: 978-1-60595-617-6

Multicomponent Metal Hydride Materials for Hydrogen Energy Storage Systems

Alexey Kazakov and Vasily Borzenko

ABSTRACT

This paper presents the results of experimental studies of new hydrogen absorbing materials based on AB_5 type alloys used for solid-phase hydrogen storage. The crystal structures, morphology, and hydrogen absorption properties of the new prepared samples were investigated. The effect of different metal additives on the properties of intermetallic compounds was studied.

INTRODUCTION

Renewable energy is becoming increasingly widespread due to the need for CO_2 emission and environmental load reductions. However, most renewable energy sources cannot supply a steady source of electrical energy, thus electricity storage method is required [1]. Hydrogen is an attractive, pollution-free energy carrier, which is characterized in addition by a flexible and efficient energy conversion. But low density of hydrogen gas, low temperature of its liquefaction, as well as high explosive risk in combination with its negative influence on the properties of design materials bring to the forefront the problems of the development of effective and safe hydrogen storage systems [2].

A number of methods can be used to achieve practical densities for the purpose of storage: compressed H_2 storage, liquid H_2 storage, non-reversible chemical H_2 storage and solid-state H_2 storage [3]. Metal hydrides (AB_5, AB_2, AB, V-based bcc alloys, etc.) show favorable hydrogen sorption properties, in terms of the kinetics, operating pressures and temperatures, and gaseous impurity resistance. Metal hydride hydrogen storage is based on the process of the reversible hydrogen

Joint Institute for High Temperatures of the Russian Academy of Sciences, 13 Bd 2, Izhorskaya Street, Moscow, 125412, Russia.

absorption/desorption in hydride forming metals or intermetallic compounds with the formation of metal hydrides (MH).Hydrogen-absorbing intermetallics form a number of different groups, which can be distinguished by their stoichiometries, including AB_5, A_2B_7, AB_3, AB_2, AB and A_2B compounds [4-7]. The formation of metal hydrides is typically exothermic and hydrogen desorption from the hydrides can be achieved endothermally under appropriate thermodynamic conditions (Reaction 1).

$$M_s + \frac{x}{2} H_2 \leftrightarrow MH_{x(s)} + Q. \quad (1)$$

Applications of metal hydrides utilize a reversible heat-driven interaction of hydride-forming material with hydrogen gas. Common characteristic is PCT isotherm and related hydrogen capacity, plateau slope and hysteresis, which have significant influence in practical applications of metal hydrides. According to hydrogen production from renewables (wind, solar and biomass) most important properties for metal hydride storage system are low plateau pressure at near ambient conditions, cyclic stability and gas impurity resistance.

AB_5-based intermetallics show some remarkable cycling properties including excellent resistance to gaseous impurity contamination, good long term cycling stability and a high volumetric storage density, and are therefore a prime example of a practically effective reversible hydrogen storage material.

EXPERIMENTAL PROCEDURE

We have prepared AB_5 alloys by arc melting of pure La (99.9%), Ce (99.9%), Ni (99.95%), Fe (99.99%), Al (99.9%), Mn (99.9%) and Sn (99%) several times in a water cooled copper crucible under argon atmosphere. In each case, we added 2% to calculated weight of Mn, Sn, Al in order to compensate evaporation during the melting process. At first the furnace chamber was vacuumed to a final pressure of $4 \cdot 10^{-5}$ Pa and subsequently purged three times with argon at 41 kPa. Pure elements were joined together at a low voltage and were melt later 2 or 3 times at full power. Each melting step lasted about 1 min. After each step, alloy ingots were cooled and turned upside down. The resulting alloy ingots weighted 40 - 50 g each.

In order to determine structural parameters, powder samples were measured at room temperature by X-ray diffraction (XRD) using D8 Advance (Bruker) diffractometer with Cu Ka radiation. Samples for X-ray analysis were prepared by mechanical grinding to a powder. The step was 0.02 and the exposition time was 60.8 s by step. The 2θ angles scanned were ranged from 10 to 120. Processing of diffraction patterns was performed using Jana2006 and Search-Match software.

Experimental technique and setup for characterization of desorption isotherms are described elsewhere [8].

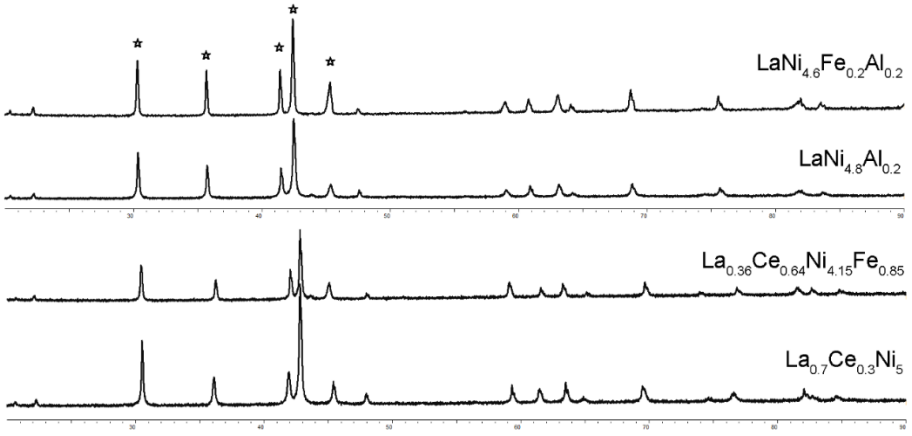

Figure 1. XRD patterns of AB_5 alloys (Symbol ☆ marks main peaks of $CaCu_5$ structure).

RESULTS AND DISCUSSION

The X-ray diffraction of AB_5 alloys have shown high homogeneity of the samples, XRD diagrams confirm that the structure of the samples belong to $CaCu_5$ type (Figure 1).

The lattice constants (*a* and *c*) of the hexagonal structure calculated from these XRD peaks are summarized in Table I. Replacement of Ni atoms by larger Al and Sn atoms leads to an increase in lattice size. On the other hand, La substitution by Ce leads to decrease crystal structure. The particular behavior of Ce-subsituted alloys has been attributed to the intermediate valence state of Ce (Ce^{3+}, Ce^{4+}) [9].

PCT curves are measured in 298 – 333 K temperature range for all samples. Enthalpies and entropies of reactions are calculated using Van't Hoff equation:

$$RlnP = \frac{\Delta H}{T} + \Delta S\,, \tag{2}$$

where, *R* is the universal gas constant, *P* is the equilibrium pressure, ΔH is the reaction enthalpy, *T* is the temperature and ΔS is the entropy change. Results of the thermodynamic measurements are listed in TABLE I.

PCT isotherms at temperature 298 K are shown in Figure 2. For low-pressure alloys equilibrium pressures are in small pressure range 0.05 – 0.075 MPa, which is preferable for hydrogen storage from renewable biological hydrogen production sources. Al substituted AB_5 alloys show larger hydrogen capacity and flat plateau slope.

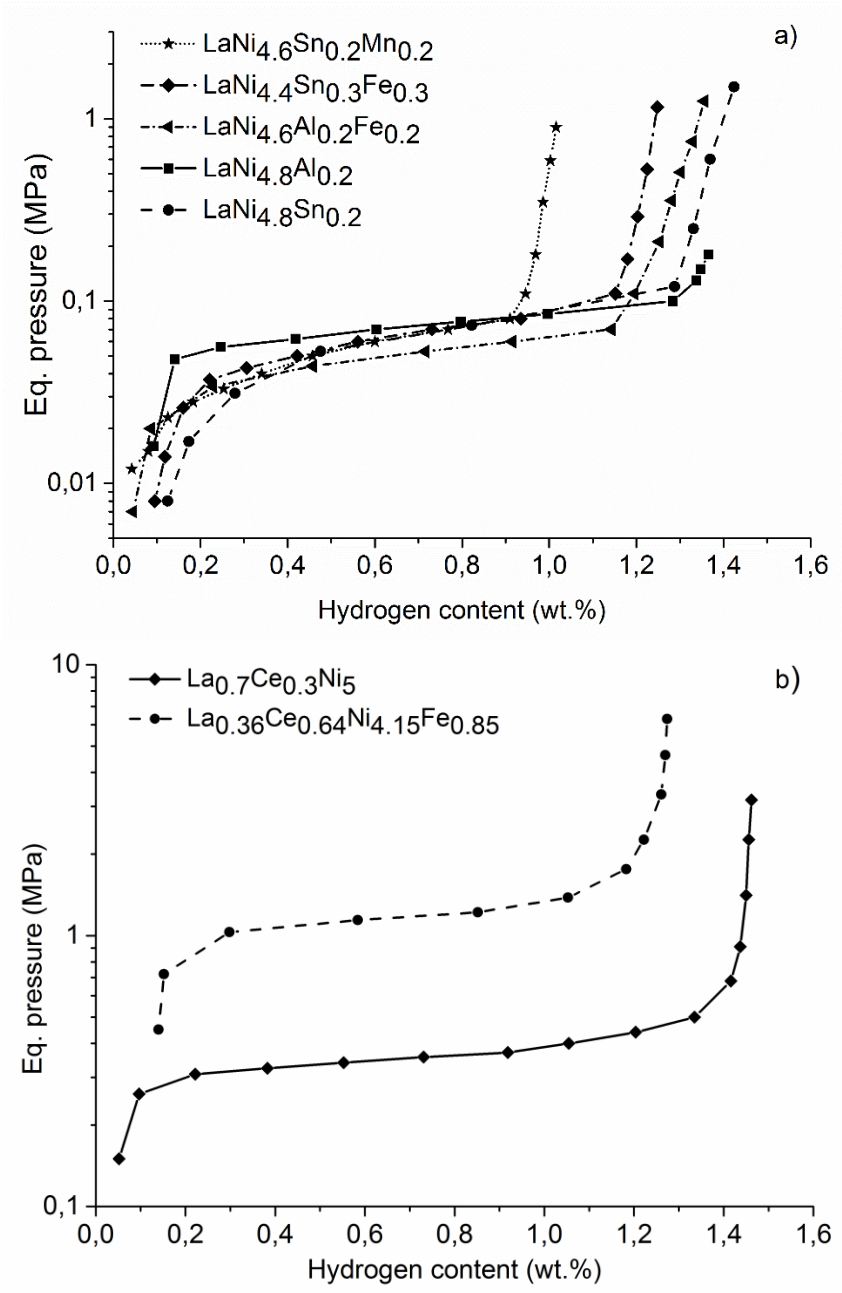

Figure 2. Hydrogen desorption PCT isotherms of AB_5 alloys at 298 K: a) low pressure alloys; b) high pressure alloys.

TABLE I. EXPERIMENTAL AND CALCULATED DATA.

MH alloy	P_{des} at 298K, MPa	P_{des} at 333K, MPa	C_{rev} at 298K, wt.%	Crystal structure parameters		ΔH_{des}, kJ/mol	ΔS_{des}, kJ/mol K
				a, nm	*c*, nm		
Low pressure alloys							
$LaNi_{4.6}Fe_{0.2}Al_{0.2}$	0.049	0.3	1.1	0.5031	0.4005	-36.8	119.7
$LaNi_{4.6}Mn_{0.2}Sn_{0.2}$	0.05	0.21	0.9	0.5039	0.4011	-29.8	94.7
$LaNi_{4.4}Fe_{0.3}Sn_{0.3}$	0.065	0.26	1.0	0.5043	0.4028	-28.7	92.4
$LaNi_{4.8}Al_{0.2}$	0.074	0.4	1.2	0.5022	0.3999	-35.5	116.9
$LaNi_{4.8}Sn_{0.2}$	0.063	0.4	1.1	0.5033	0.3998	-34.2	114.2
High pressure alloys							
$La_{0.7}Ce_{0.3}Ni_5$	0.36	1.74	1.3	0.4974	0.3992	-33.1	123.0
$La_{0.36}Ce_{0.64}Ni_{4.15}Fe_{0.15}$	1.18	3.98	1.1	0.4958	0.4024	-28.3	115.8

Also, desorption pressure at 333 K is as high as 0.3 – 0.4 MPa, what is enough to direct supply PEM fuel cells for energy generation. Sn-containing alloys also have suitable equilibrium pressures, but unfortunately low capacity and high plateau slope, which are disadvantages in practical use. Thus, low-pressure Al-substituted alloys are perspective materials for direct use as hydrogen purification and storage media for PEM fuel cell supply. For Ce-substituted alloys pressure increases with increase of Ce content, but reversible capacity decreases. These alloys are suitable for stationary storage of hydrogen, produced from solar and wind power plants by means of electrolysis.

CONCLUSION

The experimental investigations of AB_5 alloys suitable for hydrogen storage from renewable sources were conducted. Low-pressure Al-substituted alloys (P_{eq}=0.05-0.075 MPa, 1.1 – 1.2 H_2 wt.%) are perspective materials as hydrogen purification and storage media for PEM fuel cell supply. Ce-substituted alloys (P_{eq}=0.36-1.18 MPa, 1.1 – 1.3 H_2 wt.%) are suitable for stationary storage of hydrogen, produced from solar and wind power plants by means of electrolysis.

ACKNOWLEDGMENT

The research was supported by Russian Science Foundation grant (project #17-19-01738).

REFERENCES

1. Nowotny, J., and T.N. Veziroglu. 2011." Impact of Hydrogen on the Environment," *International Journal of Hydrogen Energy*, 36(20):13218-13224.
2. Yartys, V.A., and M.V. Lototsky.2005. "An Overview of Hydrogen Storage Methods," in *Hydrogen Materials Science and Chemistry of Carbon Nanomaterials*, T.N. Veziroglu, et al. Editors, Springer Netherlands: Dordrecht, pp. 75-104.
3. Eberle, U., M. Felderhoff, and F. Schüth. 2009. "Chemical and Physical Solutions for Hydrogen Storage," *Angewandte Chemie International Edition*, 48(36):6608-6630.
4. Gary, S. 1999. "A Panoramic Overview of Hydrogen Storage Alloys from a Gas Reaction Point of View*," Journal of Alloys and Compounds*, 293-295(0):877-888.
5. Lynch, F.E. 1991. "Metal Hydride Practical Applications," *Journal of the Less Common Metals*, 172–174, Part 3(0):943-958.
6. Tarasov, B.P. 2011. "Metal-Hydride Accumulators and Generators of Hydrogen for Feeding Fuel Cells*," International Journal of Hydrogen Energy*, 36(1):1196-1199.
7. Yartys, V.A., I.R. Harris, and V.V. Panasyuk. 2001. "New Metal Hydrides: A Survey*," Materials Science*, 37(2):219-240.
8. Kazakov, A.N., D.O. Dunikov, and S.V. Mitrokhin. 2016. "AB5-Type Intermetallic Compounds for Biohydrogen Purification and Storage*," International Journal of Hydrogen Energy*, 41(46):21774-21779.
9. Senoh, H., et al. 2004. "Systematic Investigation on Hydrogen Storage Properties of RNi5 (R: Rare Earth) Intermetallic Compounds with Multi-Plateau," *Materials Science and Engineering: B*, 108(1-2):96-99.

2018 International Theoretical and Practical Conference on Alternative and Smart Energy (TPCASE 2018)
ISBN: 978-1-60595-617-6

Silver Halide- and Quartz-Based Infrared Fiber Sensor for Measuring Moisture Content in Transformer Oil

Anastasiya Lashova, Victor Korsakov, Elena Korsakova, Alexander Korsakov and Liya Zhukova

ABSTRACT

The paper presents a fiber-optic sensor, which allows determining the moisture content using the method of attenuation total reflection (ATR) Fourier transform infrared spectroscopy in the wavelength range from 1.2 to 6.5 μm. The fiber sensor comprises of a transmitting fiber bundle, a receiving one, and an ATR element. The modeling results of the sensor are given. The geometric parameters of the ATR cone were estimated depending on the fiber bundle's size. The optical losses of each fiber element were calculated and the total output power of the receiving bundle was estimated.

INTRODUCTION

In high-capacity power transformers, hydrocarbon-based oils are used as an insulating material. During operation, the oils accumulate moisture, dissolved gases, and oxidation products, which causes aging insulation and increasing the risk of accidents. It is known that there is a high risk of insulation emulsification when the moisture concentration in the oil reaches 5% of the total insulation volume. This lead to a high failure probability of the transformer. To measure the moisture content in the transformer oil, one can use monitoring devices operating in continuous and periodic modes. The continuous sensors of moisture are the most effective for the early stage detection of oil impurification. These sensors implement electrical and spectral methods [1].
The moisture determination by means of the electric sensors is based on measuring the electrical capacitance or electromagnetic resonance. The relative error of the

Ural Federal University named after the first President of Russia B.N. Yeltsin, 19 Mira Street, Ekaterinburgh, 620002, Russia

measurement methods for electrical capacitance is 0.05-2 %. The second group of electric sensors measures moisture using electromagnetic resonance when the radiation directly interacts with a medium. Such devices have a low accuracy (the relative error of the method is about 10%), therefore they are rarely used for high-capacity power transformers.

The main disadvantage of the electric moisture sensors is the low interference resistance that limits their usage for the transformers of the voltage class from 1.5 to 2.5 kV. Sensors, which realize spectral methods, are widely used for measuring the composition of gases contained in oils. Such devices have high sensitivity, but they are not able to contact with test media, because they are installed above the oil level, and therefore cannot determine the moisture content in oils.

FUNDAMENTALS

To quantify the moisture content in transformer oils, the authors proposed the sensor with an immersion probe. This sensor is intended for ATR Fourier transform infrared spectroscopy in the range from 1.2 to 6.5 μm. The specified range of the spectrum is justified by the absorption peaks of water at the wavelengths of 1.45 μm, 1.95 μm, 2.94 μm, and 6.02 μm, which are associated with valent vibrations of OH groups and H–O–H deformation vibrations [2]. The main characteristic absorption bands of transformer oils are 2920 cm^{-1} and 2860 cm^{-1} (the wavelengths of 3.42 and 3.49 μm, respectively), which are determined by the stretching vibrations of the CH groups (namely, CH_2 and CH_3). In the near IR, there is also the corresponding absorption band at λ = 1.725 μm [3]. Most intensively, water absorbs at a wavelength of 2.94 μm, and this absorption is 15 times higher than the absorption of radiation at λ = 1.95 μm, while the intensity of absorption at a wavelength of 6.02 μm is rather low [2]. Thus, the use of the near- and mid-infrared ranges combination is the most relevant for the proposed sensor.

The sensor system consists of a broadband IR-source, a fiber probe, and an optical signal detector [4]. As a sensitive element for attenuation total reflection, we use a zinc selenide cone with the transmission range of 0.2–18 μm (see Fig. 1). Fiber bundle elements of the sensor comprise both quartz glass fibers (cover the wavelength range of 1.2–2.5 μm) and AgCl-AgBr crystal fibers (cover the wavelength range of 2.5–20.0 μm) [5-6].

The proposed fiber sensor allows setting the units of IR-source and optical signal detector outside the strong field of EM-interference. One more advantage of the sensor is that the immersible element does not react with test media. The total optical losses is one of the main functional parameters of sensor systems. It determines the requirements for electro-optical components of the sensor. In this paper, we theoretically estimated the total optical losses of the proposed fiber probe depending on the refractive indices, the geometric configuration, and the detected wavelengths.

OPTICAL LOSSES SIMULATION

Each fiber bundle of the sensor comprises seven hexagonally arranged fibers-channels: four channels operated in the NIR range for the detection of water absorption peaks, two channels operated in the MIR range for the detection of oil absorption peaks, and one channel operated at a wavelength of 1.6 μm for the reference signal. The power distribution P_0 from the used broadband radiation source is characterized by a Gaussian beam, thus the input power distribution across the transmitting channels was assumed as 100% for the central fiber and 85% for the peripheral fibers. Three radially arranged channels were made of single-layer AgCl-AgBr crystal fibers, four peripheral channels were made of single-layer quartz fibers. The ATR element was made of ZnSe glass in the shape of the cone with an angle between the generator and the base of 45°. This form provides the multiple total reflection of optical signals from the cone surface and their transmission from each channel of the transmitting bundle to the corresponding channel of the receiving bundle (Figure 1) [1]. The radius of the ATR cone base depends on the size of receiving and transmitting bundles and the value of the numerical aperture, and it is determined by the following relationship:

$$R_k \geq \frac{D_b}{1-2\sin(NA)} \quad (1)$$

where R_k is the radius of the cone base, D_b is the diameter of the fiber probe, NA is the numerical aperture of the fibers.

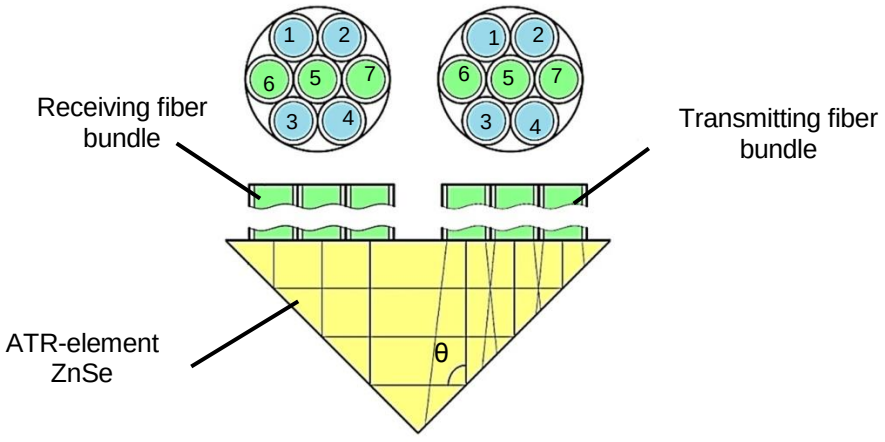

Figure 1. A model of the radiation propagation from the transmitting bundle to the receiving bundle through the conical ATR-element. The channels 1, 2, 3, 4 are made of quartz glass fibers; the channels 5, 6, 7 – are made of AgCl-AgBr crystal fibers

The parameter NA is calculated by the formula:

$$NA = \sqrt{n_{core}^2 - n_{clad}^2} \quad (2)$$

where n_{core} is the refractive index of the fiber core, n_{clad} is the refractive index of the fiber cladding. In this case, the numerical aperture should not exceed 0.1.

The calculation of optical losses depending on the refractive index dispersion is presented in Table I. The authors determined refractive indices and intrinsic optical losses of AgCl-AgBr fibers experimentally in [6]. The intrinsic losses values of quartz fibers were taken from [7]. The authors assumed that the optical losses of zinc selenide can be neglected due to the small optical path. Fresnel losses are defined as the radiation reflection coefficients r from the end surfaces between the sensor elements. They were calculated by the formula [8]:

$$r = \left(\frac{n_e - n_{core}}{n_e + n_{core}}\right)^2, \quad (3)$$

where n_e is the refractive index of the studied medium.

Total losses, as the sum of the Fresnel losses r on the number N of the end surfaces of the sensor elements and intrinsic losses a on the radiation attenuation, were calculated by the formula:

$$\Delta P = Nr + a\,. \quad (4)$$

TABLE I. CALCULATED OPTICAL LOSSES OF THE FIBER PROBE.

	Channel						
Material	**Quartz**				**AgCl-AgBr**		
λ, μm	1.45	1.60	1.73	1.95	2.94	3.42	6.02
n	1.445	1.443	1.442	1.439	1.907	1.850	1.542
P_i, %	85.0	85.0	85.0	85.0	100.0	85.0	85.0
a, dB/m	$14\cdot10^{-6}$	$14\cdot10^{-6}$	$14\cdot10^{-6}$	$14\cdot10^{-6}$	0.2	0.2	0.2
r, dB/m	0.0331	0.0329	0.0328	0.0324	0.0974	0.0890	0.0455
	Transmitting bundle						
P_{tr}, %	79.4	79.4	79.4	79.5	60.5	52.9	60.3
	ATR-element of the “cone” type						
n	2.460	2.452	2.450	2.446	2.437	2.436	2.425
r, dB/m	0.1781	0.1769	0.1766	0.1761	0.1748	0.1747	0.1731
P_{tr}, %	51.1	51.3	51.4	51.5	34.2	29.2	29.4
	Receiving bundle						
P_{tr}, %	47.7	47.9	48.0	48.2	23.8	21.4	27.9

The power of the transmitted radiation through the separate element *i* of the sensor system was defined as:

$$P_{tr} = P_i \cdot \Delta P \, . \tag{5}$$

The results of optical losses calculations showed that from 21.4 to 48.2% of the input power of the radiation, passed through the transmitting fiber bundle and ATR element, reaches the receiving fiber bundle. Our future goal is a simulation of more complex sensor system included electro-optical components, optical filters, radiation detectors, and signal amplifiers. This will allow taking into account the non-uniformity of the power distribution across the sensor channels.

CONCLUSION

Thus, in the frame of this study, a fiber optic sensor targeted to the detection of moisture content in transformer oil was designed. The modeled fiber optic probe has a length of 1 m, which makes it possible to deploy the electronic part of the sensor outside the transformer case, thereby providing the protection against electromagnetic interference. Moreover, the maximum possible length of AgCl-AgBr fiber probes is more than 10 m. Such lengths cover the most types of fiber probe applications. The use of fibers based on the AgCl-AgBr system is limited to a length of 10 m, therefore, with a fiber probe length of more than 10 m, they can be replaced by chalcogenide fibers [9].

ACKNOWLEDGMENT

This work was supported by the Russian Science Foundation under grant No. 18-73-10063.

REFERENCES

1. Rakhimov, N.R., et al. 2015. "Optoelectronic Methods for Measuring and Controlling Technological Parameters of Oil and Oil Products," *Automat. and Software Engine*, 2:85-108.
2. Zatsepina, G.N. 1974. *Physical Properties and Structure of Water*. MSU Publish. House, p. 168.
3. Lynch, P.F. and Ch. W. Brown. 1973. "Identifying Source of Petroleum by Infrared Spectroscopy," *Environ Sci. Technol.* 7(13):1123-1127.
4. Zhukova, L. 2013. "Fiber Probe for the Spectral Range of 2-45 μm for IR-Fourier Spectrometer," in *Imaging and Applied Optics Congress*, L. Zhukova [et. al.] eds.: OSA Technical Digest, Fourier Transform Spectroscopy (FTS), paper: FTu3D.5.
5. Korsakov, A.S., et al. 2014. "Investigating the Properties of Infrared PCFs Based on AgCl-AgBr, AgBr-TlI, AgCl-AgBr-AgI(TlI) Crystals Theoretically and Experimentally," *Optics and Spectroscopy*, 117:960-963.

6. Zhukova, L.V., et al. 2008. "$AgCl_xBr_{1-x}$ and $AgCl_xBryI_{1-x-y}$ Crystals for IR Engineering and Optical Fiber Cables," *Inorganic Materials*, 44:1372-1377.
7. Blistanov, A.A., et al. 1982. *Acoustic Crystals. Reference Book. Science*, p. 632.
8. Katsuyama, T. and H. Matsumura. 1992. *Infrared Optical Fibers*. World, p. 272.
9. Korsakova, S.V. 2018. "IR Analysis of Characteristics of the Sensing Elements for the Fiber-Based Evanescent Wave Spectroscopy in the Mid-IR," *Optics and Spectroscopy*. 125 (3):416-424.

2018 International Theoretical and Practical Conference on Alternative and Smart Energy (TPCASE 2018)
ISBN: 978-1-60595-617-6

Infrared Fiber Bundles Based on Silver Halide Crystals for Monitoring and Control Systems in Heat and Power Engineering

Elena Korsakova, Natalia Muftahitdinova, Victor Korsakov, Ivan Kashuba, Alexander Korsakov and Liya Zhukova

ABSTRACT

We develop and fabricate ordered fiber bundles based on silver halide crystals. They are thin, flexible, and non-hygroscopic. These bundles allow detecting temperatures in the interval of -130 – 900 ^{o}C with good spatial resolution and can be embedded in monitoring and control systems. To show their suitability for infrared thermography in the heat and power engineering, the temperature distribution over the height of a gas turbine blade was measured using an IR thermographic system contained a linear silver halide fiber bundle.

INTRODUCTION

Infrared (IR) thermography is widely used in the energy industry because the data on the temperature distribution is important for many heat-power processes. In most cases, thermograms are recorded directly by thermal imaging cameras. It leads to some restrictions of the method. IR fiber bundles can significantly expand the application area of IR thermographic systems. They can be used as multipoint probes in the systems of control, monitoring and research of various units and components for the heat and power engineering.

IR fiber bundles based on silver halide crystals have optimal functional parameters since they are flexible, thin, long, non-hygroscopic, highly transparent in the wavelength range from 2.5 to 20 μm without absorption windows, have a wide range of operating temperatures and are capable to transmit thermal images with

Ural Federal University named after the first President of Russia B.N. Yeltsin, 19, Mira Street, Yekaterinburg, 620002, Russia

good temperature and spatial resolution [1, 2]. They can deliver the IR radiation from restricted spaces and places where there is no direct visibility between the object and the thermal camera. We have already discussed the use of silver halide fiber bundlesfor the energy industry [3]. In this study, we report on the progress in the development of these bundles.

IR FIBER BUNDLES OF SILVER HALIDES

According to Wien's law of maximum radiation shift:

$$\lambda_m = \frac{b}{T} \tag{1}$$

where λ_m – the wavelength at which the maximum radiation intensity of the black-body is observed (at a given temperature), μm, b= 2900, μm·K – Wien's constant, T – temperature, K.

The spectral radiant emittance of the black-body at various temperatures and the spectrum of total optical losses of silver halide fibers are shown in Figure 1. It is seen in Figure 1 that the low loss region of single silver halide fibers covers most of the radiation wavelength range of the black-body from -130 to +900 °C.

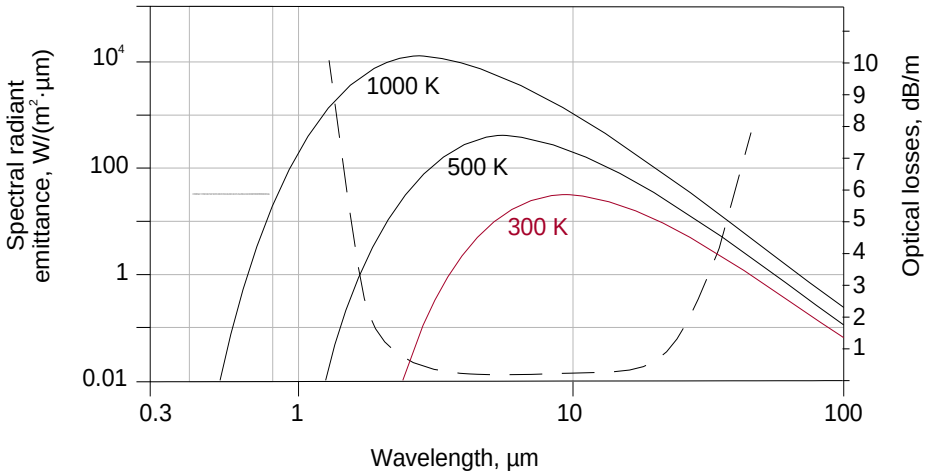

Figure 1. Transmission losses of silver halide fibers (dashed line) and black-body radiation spectrum of various temperatures (solid lines).

We realized the complete cycle of the fiber bundle fabrication. First, using the program package COMSOL Multiphysics, we simulated a regular IR fiber bundle comprised of 7x7 single-layer fibers in a common cladding (matrix). The fibers were arranged as a grid. Varying the diameters of the fibers and the distance between them, as well as the composition of the fibers and the matrix (hence, the refractive indices [4]), we chose optimal parameters of the bundle for operating in the

wavelength range of 8-14 μm. Figure 2 shows one of the modeled fiber bundle modes. The same modal distribution is observed for every single fiber. It is seen in the figure that the mode does not leak into adjacent fibers and has a rather high intensity.

Then, the raw materials were acquired by the thermal-zone crystallization-synthesis. Next, the silver halide single crystals were grown by the Bridgman method from these raw materials, the multi-element billet was obtained, and the bundle was fabricated by a high-temperature extrusion [5, 6]. The diameter of single fibers is about 30 μm, the distance between the boundaries of adjacent single fibers is about 60 μm, and the outer diameter of the bundle is 1.12 mm. The gained geometric parameters of the bundle are in good agreement with the modeled ones. The photo of the cross-section of this 7x7-fiber bundle, made by a microvisor LOMO vizo-MET-221, is shown in Figure 3. Such bundles allow investigating 2D temperature field distribution with good spatial resolution even in narrow gaps between the working parts of heat engineering equipment due to small diameters, large lengths, and flexibility.

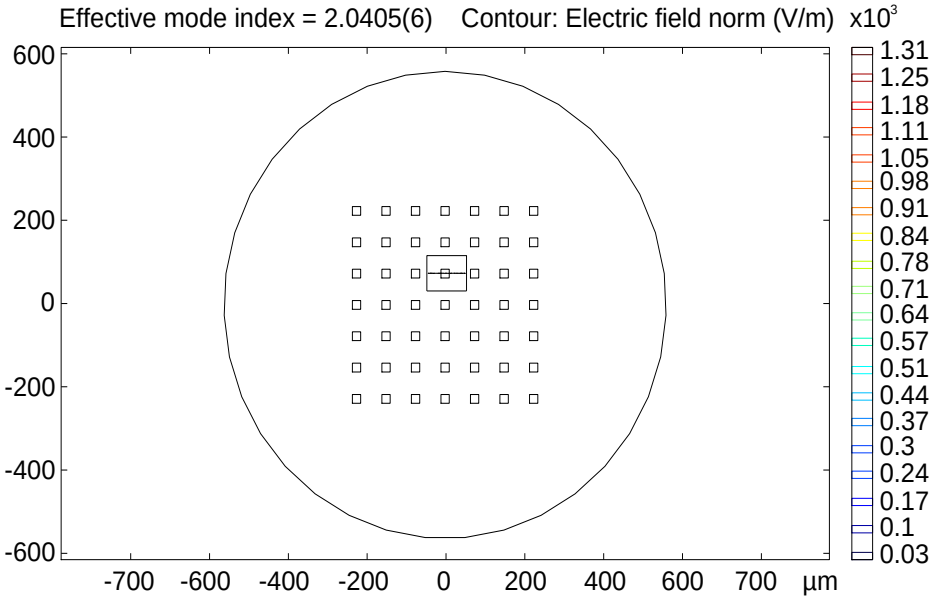

Figure 2. Model of the mode field distribution across the fiber bundle cross-section.

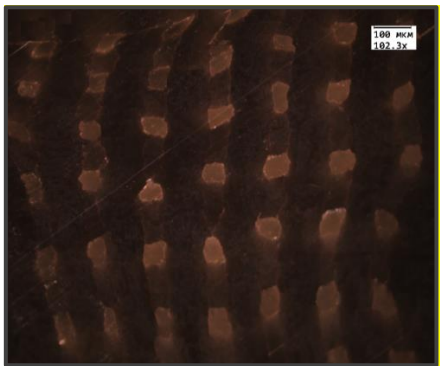

Figure 3. Photo of the cross-section of 7x7-fiber bundle based on silver halide crystals.

THERMOGRAM ACQUISITION

As an example of the use of silver halide fiber bundles, we present the study of the temperature distribution along the height of a gas turbine blade. To solve this problem, a pilot set-up contained a fiber bundle was produced (see Figure 4). The fiber bundle comprised of four single-layer fibers, derived from $AgCl_{0.25}Br_{0.75}$ crystals, with the diameter of 1.12 mm and the length of 25 cm. The fibers were arranged linearly.

The blade root of the gas-turbine unit was placed in the bath with the heated transformer oil for heating. The temperature distribution along the height of the blade feather was maintained uneven, due to constant cooling on account of the mechanisms of free convection and radiation. The thermal images of the gas turbine blade were obtained using IR fiber bundle and using thermal camera directly, which is shown in Figure 5 (a) and (b), respectively.

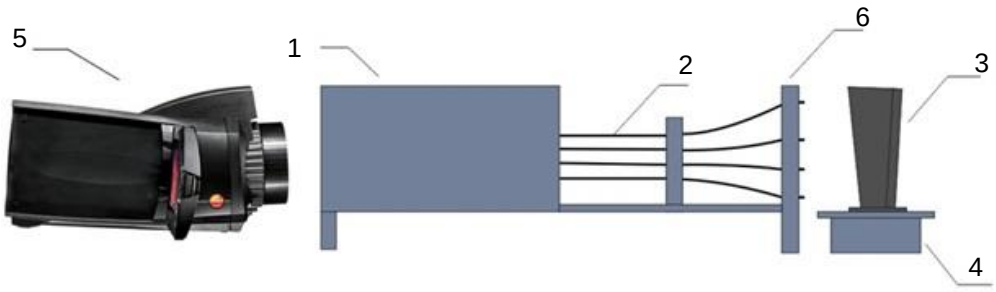

Figure 4. IR thermographic set-up with a linear fiber bundle: 1 – housing, 2 – linear IR fiber bundle, 3 – gas turbine blade, 4 – transformer oil bath,
5 – thermal camera NEC 7102WV, 6 – holder.

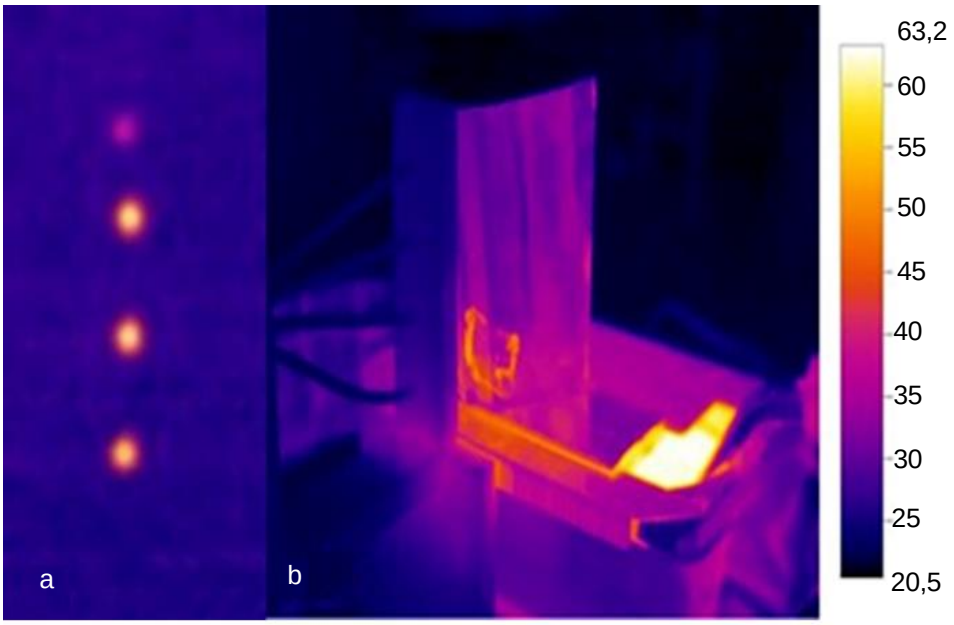

Figure 5. Temperature distribution over the height of the gas turbine blade obtained: (a) using IR fiber bundle, (b) using thermal camera directly.

^{0}C

As expected, the IR thermographic system showed the non-uniformity of the blade temperature distribution (see Figure 6). The measured difference between the temperatures of upper and lower parts of the blade was more than 10 ^{o}C.

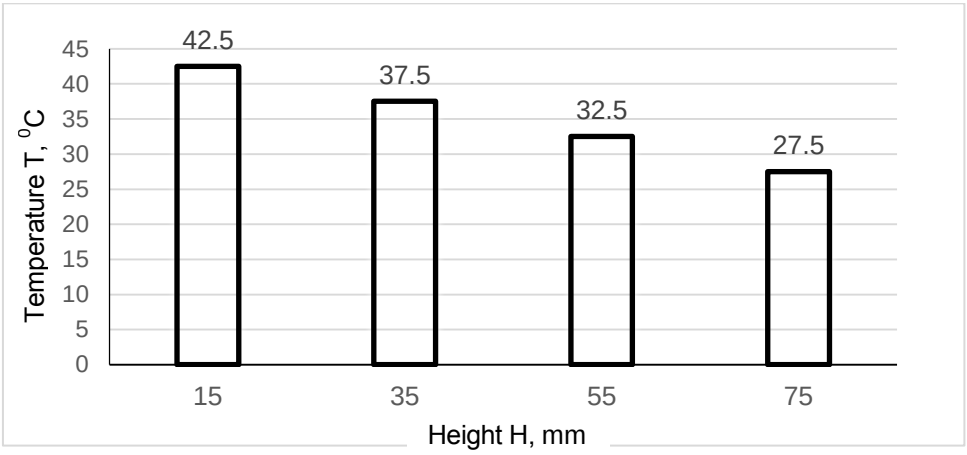

Figure 6. Graph of the temperature distribution along the gas turbine blade height.

Since we experimentally confirmed the suitability of our IR thermographic system for the application in heat and power engineering, we plan to develop IR thermographic system with more complex IR fiber bundle for carrying out advanced research.

FUTURE GOALS

In the future, we plan to use silver halide crystals doped with thallium (I) as a material for the fiber bundles, since these crystals possess the functional characteristics which allow expanding the scope of fiber bundles application [7, 8]. In particular, they are resistant to ultraviolet [9] and ionizing radiation [10, 11]. It is worth to mention, that they are resistant to γ rays at a dose of up to 500 kGy. In addition, they have a wider band of transmission, therefore they allow detecting temperatures in a wider range. It is also interesting to try crystals of AgBr-AgI and AgCl-AgBr-AgI systems as the materials for the fiber bundles since we expect that these crystals can improve functional characteristics of the bundles and, in some cases, may be more appropriate than crystals doped with thallium (I).

ACKNOWLEDGMENT

This work was supported by the Russian Science Foundation under grant No. 18-73-10063.

RFERENCES

1. Korsakova, E. A., L. V. Zhukova, A. S. Korsakov, A. S. Shmygalev, and M. S. Korsakov. 2018. "Thermal imaging by means of IR-fiber bundle for medical applications," in *International Conference Laser Optics 2018, ICLO 2018*, St. Petersburg, 529p.
2. Lavi Y., A. Millo, and A. Katzir. 2005. "Thin ordered bundles of infrared-transmitting silver halide fibers," *Applied Physics Letters*, 200587:241122.
3. Korsakova, E. A., A. S. Korsakov, V. S. Korsakov, and L. V. Zhukova. 2018. "IR thermographic system supplied with an ordered fibre bundle for investigation of power engineering equipment and units,", in *ASRTU Conference on Alternative Energy: Materials, Technologies, and Devices*, United Arab Emirates: KnowledgeE, pp. 223-230.
4. Korsakov, A. S., D. S. Vrublevsky, A. E. Lvov, and L. V. Zhukova. 2017. "Refractive index dispersion of $AgCl_{1-x}Br_x$ ($0 \le x \le 1$) and $Ag_{1-x}Tl_xBr_{1-x}I_x$ ($0 \le x \le 0.05$)," *Optical Materials*, 64:40-46.
5. Korsakov, A. S., L. V. Zhukova, D. S. Vrublevsky, and E. A. Korsakova. 2014. "Investigating the properties of infrared PCFs based on AgCl-AgBr, AgBr-TlI, AgCl-AgBr-AgI(TlI) crystals theoretically and experimentally," *Optics and Spectroscopy (English translation of Optika i Spektroskopiya)*, 117:960-963.
6. Zhukova, L. V., N. V. Primerov, A. S. Korsakov, and A. I. Chazov. 2008. "$AgCl_xBr_{1-x}$ and $AgCl_xBr_yI_{1-x-y}$ crystals for IR engineering and optical fiber cables," *Inorganic Materials*, 44:1372-1377.

7. Korsakov, A. S., L. V. Zhukova, V. S. Korsakov, D. S. Vrublevsky, and D. D. Salimgareev. 2014. "Research of phase equilibriums and modelling of structure of AgBr-$TlBr_{0.46}I_{0.54}$ system," *Non-ferrous metals*, 8:50-54.
8. Korsakov, A. S., L. V. Zhukova, E. A. Korsakova, V. V. Zhukov, and V. S. Korsakov. 2013. "Thermodynamic research of the crystals of AgBr-TlI system and obtaining of infra-red light conductors with nanocrystallic structure, based on these crystals," *Non-ferrous metals*, 4:62-66.
9. Korsakov, A. S., A. E. Lvov, D. S. Vrublevsky, and L. V. Zhukova. 2016. "Investigating the light stability of solid-solution-based AgCl-AgBr and AgBr-TlI crystals," *Chinese Optics Letters*, 14:020603.
10. Korsakova, E., A. Lvov, D. Salimgareev, A. Korsakov, S. Markham, A. Mani, S. Silien, T.A.M. Syed, and L. Zhukova. 2018. "Stability of MIR transmittance of silver and thallium halide optical fibres in ionizating β- and γ-radiation from nuclear reactors," *Infrared Physics and Technology*, 93:171-177.
11. Salimgareev, D. D., A. E. Lvov, E. A. Korsakova, A. S. Korsakov, and L. V. Zhukova. 2018. "Optical fibers based on modified silver halide crystals for nuclear power," in *ASRTU Conference on Alternative Energy: Materials, Technologies, and Devices.* United Arab Emirates: KnowledgeE, pp. 231-236.

2018 International Theoretical and Practical Conference on Alternative and Smart Energy (TPCASE 2018)
ISBN: 978-1-60595-617-6

Fuzzy Modeling of the Estimation of the Regional Energy System Functioning Efficiency

Vladimir Biryulin, Alexey Gorlov, Daria Kudelina, Oleg Larin, Alexandr Chernyshev and Alexey Gladyshkin

ABSTRACT

The article deals with the problems of the fuzzy logic mathematical apparatus applying to assess the effectiveness of the fuel and energy resources use. The main problems arising during the investigation of the regional energy systems by traditional mathematical methods are given. The reasons for the appearance of these problems, including the uncertainty of the initial information, are indicated. It is shown that in these cases the use of the fuzzy inference systems allows to obtain more reliable and complete picture of the energy consumption by the various industrial consumers. The process of the fuzzy inference systems developing for the fuel and energy resources efficiency estimation use is considered on the example of the energy enterprises.

Keywords: regional energy system, energy efficiency, fuel and energy resources, information uncertainty, fuzzy logic, mathematical model.

INTRODUCTION

Reasonable assessment finding of the regional fuel and energy complex effectiveness makes it possible to identify the problem sides of the region energy

Vladimir Biryulin, Southwest State University, 69b, Soyuznaya, Kursk, 30500, Russia
Alexey Gorlov, Southwest State University, 78A, Teatralnaya, Kursk, 305009, Russia
Daria Kudelina, Southwest State University, 11, Schepkina, Kursk, 305016, Russia
Oleg Larin, Southwest State University, 3, Profsoyuznaya, Kursk, 305009, Russia
Alexandr Chernyshev, Southwest State University, 6b, K. Zelenko, Kursk, 305000, Russia
Alexey Gladyshkin, Southwest State University, 94, 50 let Oktyabrya, Kursk, 305040, Russia

enterprises and engineering networks work and to make decisions on the further development of the regional energetics.

In the study of the energetics at the level of the country, region, district it is necessary to use a large amount of knowledge about the various quantitative and qualitative patterns inherent in the energy facilities under consideration. The regional fuel and energy complex is an elaborate geographically limited multifactor system consisting of several levels and complicated connections between levels and objects [1, 2].

The search and practical testing of various regularities which are different in the energy sector at different levels are very often not possible for a variety of reasons [3]. The given fuzzy model for regional power effectiveness assessing gives the possibility to get this estimate, taking into account heterogeneous input information (we use different characteristics of the heat and electricity distribution processes, as well as other parameters), both quantitative and qualitative taking into consideration incompleteness and uncertainty, which are inevitable for a part of the initial information.

This approach allows us to find more reliable results of the created model output parameter or the assessment of the effectiveness of the regional fuel and energy complex compared with the use of the similar models which are focused on processing only quantitative initial data.

RELEVANCE AND PROBLEM STATEMENT

Since the processes of production, transmission, distribution and consumption of fuel and energy resources are essentially independent of each other, it is advisable to divide the overall task of research and assessment of the effectiveness of the regional energetics into the following sub-tasks:

- sources of energy resources;
- thermal and electrical networks;
- industrial consumers of energy;
- consumers of energy in the housing sector;
- energy consumers in agriculture, transport, etc.

Additional difficulties in mathematical models creating for solving these subtasks arise when a part of the input information is uncertain [4].

Such problems can be successfully overcome with the use of fuzzy modeling apparatus or fuzzy logic [5]. Currently, the use of fuzzy models belongs to the most actively developing areas of the complex organizational and technical systems research.

THEORY AND PRACTICAL IMPLEMENTATION

The input variables for the developing models or factors represent the indicators of the regional energetics functioning. These factors are presented as the qualitative assessments of the characteristics of the investigation systems. For each factor is determined its own linguistic variable [6].

A characteristic feature of the created model is the simultaneous use of the heterogeneous data, for example, relating to the power industry, thermal energetics and other components of the energy industry of the region. So, for electric power, we use information about the production volumes, the supplies to the other regions, the amount of electricity received from the other regions, the losses in the electric networks, specific consumption per unit of the gross regional product, etc.

The output parameter of the developed model is a quantitative assessment of the regional fuel and energy complex work effectiveness. The creating model belongs to the class of MISO-systems with many (n) input variables and one output variable (many inputs – various input data, one output – the efficiency evaluation). Creating a fuzzy inference system, we accept the conditional boundaries for this estimate from 0 to 100.

Taking this aspect into account, the model of the regional energy sector efficiency will represent a functional view of the form:

$$X = (X_1,.., X_n) \rightarrow Z[0;100], \quad (1)$$

where X_1, .., X_n – the input data, Z – the output parameter or efficiency evaluation

To perform the operation of effectiveness evaluation finding, the developing fuzzy inference system includes the following components:

- rule base;
- fuzzy inference mechanism;
- the membership functions of the output value *y*.

The rule base is compiled using input variables. Each rule in this database has the form IF a condition is THEN a conclusion and is built on the basis of the concepts of a linguistic variable and a fuzzy statement. forming the base of fuzzy rules, the data obtained from experts and from various sources were used.

To prepare a training set, to each example from it is assigned a separate rule. Many such examples of training sets are defined in the following way:

$$(x_1^{(k)}, x_2^{(k)}, x_3^{(k)}, x_4^{(k)}, x_5^{(k)} ..... x_n^{(k)}, y), k = 1, \ldots, K, \quad (2)$$

where $x_1^{(k)}, x_2^{(k)}, x_3^{(k)}, x_4^{(k)}, x_5^{(k)} ..... x_n^{(k)}$ - the values of n input variables; y – the value of the output variable y in the k-th example; K – the total number of examples in the training set.

The compiled rule base was tested for such conditions as consistency, connectedness and redundancy [7]. Such verification is necessary, since the

originally established rule base may be redundant and contain contradictions or rules with the same prerequisites, but different final conclusions.

Let us consider the construction of mathematical models based on the fuzzy system on the example of modeling sources of energy resources (we consider combined heat and power plant). The limited length of the article does not allow a detailed description of the entire system, so we give the most important information.

We will combine the initial data into the following groups: annual expenditures, unit costs and efficiency, costs for consumed resources, personnel costs; equipment costs; cost indicators of energy resources produced.

For example, the composition of the group annual costs:

- annual consumption of equivalent fuel for the supply of the electricity,
- annual consumption of equivalent fuel for the thermal energy supply,
- annual consumption of equivalent fuel for heat supply, taking into account electricity for own needs, referred to heat supply,
- annual consumption of equivalent fuel for the supply of electricity, taking into account its own needs attributable to the production of electricity.

All these data are mostly clear or expressed by some quantitative indicators. But for the analysis of energy efficiency, such data do not provide the necessary information to analyze the initial information and make decisions, since these numerical indicators cannot show in most cases the achieved or real level of efficiency. It is due to the fact that analyzing such information it is not clear, for example, high or not is the level of fuel consumption for energy generation relative to other energy companies, especially considering the different conditions of their location, equipment composition.

With a large number of input data, it is convenient to present their influence on the final result obtained at the output of the system in the form of a hierarchical logical inference tree [6, 7]. This tree is presented in Figure 1.

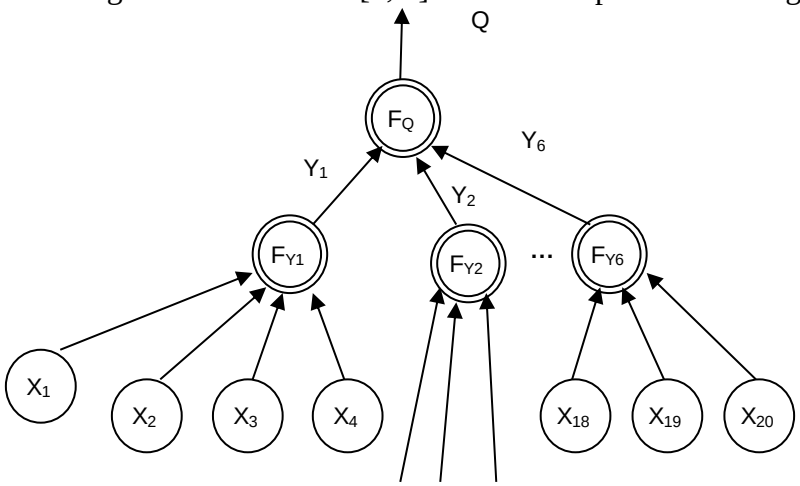

Figure 1. Hierarchical classification of the factors affecting the efficiency of the combined heat and power plant.

Elements of the tree are interpreted as:

• the root of the tree—the efficiency of the regional energetics considered enterprise *Q*;

• the terminal vertices—the initial data (X_1,.., X_{20});

• non-terminal vertices (double circles)—convolutions of the initial data or the results of intermediate conclusions;

• graph arcs emanating from non-terminal vertices—enlarged fuzzy indices (Y_1–Y_6).

Terminal tops represent the annual costs Y_1, unit costs and efficiency Y_2, the cost of consumed resources Y_3, the cost of personnel Y_4, the cost of equipment Y_5, cost indicators of produced energy sources Y_6.

CONCLUSIONS

The given fuzzy model for evaluating the effectiveness of regional energetics makes it possible to obtain this assessment taking into account heterogeneous input information (the characteristics of the processes of production, transmission, distribution of thermal and electrical energy, as well as other parameters are used), both quantitative and qualitative. Also, it takes into account the incompleteness and uncertainty which inevitably exist for a part of the initial information. This approach allows us to find more reliable results of the output parameter of the created model work or the assessment of the effectiveness of the regional fuel and energy complex compared with the use of similar models which are focused on only quantitative initial data processing.

REFERENCES

1. Mikhailov, S.N., and A.A. Balyabina. 2008. “Regional energy clusters: problems and prospects,” *Russian Journal of Entrepreneurship*, pp. 20–25.
2. Karimov, A.R. 2008. “The most important task of reforming the power industry of Russia is the formation of a regional electric power complex,” *Russian Journal of Entrepreneurship*, pp. 64–68.
3. Halper, V.I. 2014. “The application of a multi-agent approach for the development of software systems for estimating states of electric power system,” in *System Studies in Energy*. Irkutsk: ISEM SB RAS, 175 p.
4. Aliyev, R.A., A.E. Tserkovny, and G.A. Mamedova. 1991. *Production management with fuzzy initial information.* Moscow: Energoatomizdat, 240 p.
5. Belyaev, L.S. 1978. *The solution of complex optimization problems in conditions of uncertainty*. Novosibirsk: Science, 128 p.
6. Shtovba, S.D. 2007. *Design of fuzzy systems using MATLAB.* Moscow: Hotline-Telecom, 228p.
7. Pegat, A. 2013. *Fuzzy modeling and management*: Moscow: Knowledge Lab, 804 p.

2018 International Theoretical and Practical Conference on Alternative and Smart Energy (TPCASE 2018)
ISBN: 978-1-60595-617-6

Boiling Heat Transfer Enhancement on Micro- and Nanoscales

Yuriy Kuzma-Kichta and Alexander Lavrikov

ABSTRACT

Microchannel heat exchangers for future electronics, air conditioning systems and heat pipes must provide an extremely high heat flux. Conventional heat transfer enhancement methods may not be applicable due to the small size of these heat exchangers. The present investigation is directed to solve problems of an effective cooling at high heat flux in microchannels and CHF increasing with help of an artificial nanorelief of the surface. The relief is formed by alumina nanoparticles which are deposited on the heating surface of the channel.

INTRODUCTION

Many methods of heat transfer enhancement under boiling are well-known nowadays. Heat transfer surface modification methods are probably the most effective of them. In [1] it was shown that porous coating of the surface increases CHF and heat transfer coefficients both for nucleate, transition and film boiling . There are no difficulties to form this relief inside or outside a pipe but it is not so simple to use it in microchannels.

Actually the heat transfer enhancement in a microchannel is not a trivial [2]. Suzuki and others [3] investigated microbubble emission boiling (MEB) in mini- and microchannels as a heat transfer enhancement method. The MEB allows to increase the CHF in subcooled boiling, but occur of the boiling crisis depends on a flow velocity and liquid subcooling.

Moscow Power Engineering Institute, 14 Krasnokazarmennaya Street, Moscow, 111250, Russia

Microchannel surface can be covered with a layer of nanoparticles which deposit from a colloidal solution (also known as nanoliquid or nanofluid). This relief of nanoparticles can increase the CHF and the boiling heat transfer coefficient [4]. At first researchers used nanoliquid as a heat carrier and the relief of nanoparticles was formed all along the experiment.

The present study is aimed at studying of the heat transfer on the surface with artificial relief of alumina (Al_2O_3) nanoparticles.

PROPERTIES OF THE INVESTIGATED RELIEF

These nanoparticles are deposited on the inner surface of the microchannel before the experiment [5]. The thickness of the nanoparticles layer, its properties depend much from the deposition method, initial surface roughness and other factors. The relief of nanoparticles seems to be a perspective heat transfer enhancement method but poor theory is developed nowadays in spite of the fact that many investigations were provided.

As shown in [6-9] the mechanism of CHF increase is connected with a contact angle reduction. Analysis of pool boiling data for different surfaces (with different contact angles) allowed selecting relief of alumina nanoparticles as one of the most effective for the heat transfer enhancement.

The test setup is aimed for investigations of water-based fluids boiling in a single microchannel[7]. The heating surface of the channel (3mm width, 13.7mm length, 0.2mm height) is made of copper. The distribution of temperature in the test section and the heat flux are measured using the IR-camera, it allows to make 30 frames per second IR-recordings. The high-speed video recording is provided to monitor bubble formation and growth.

Calculation of heat flux is provided according to the Fourier law by the measured temperature distribution along the height of the test section. The heat conduction coefficient of the test section is supposed to be known. The heating surface temperature is approximated by values of temperature inside the test section. Thus the accuracy of heat flux and wall temperature depends much on the distance measurement accuracy and temperature measurement accuracy. The relative heat losses are small enough and can be neglected. The absolute error of temperature measurement is 1-3 ^{O}C, the relative error of the heat flux is assumed to be 10-15%.

During the experiment the flow rate is measured by a rotameter and it can be checked using mass-measuring method on a precision laboratory balances.

The Al_2O_3-water nanofluid is applied to obtain the artificial nano-scale relief of the test section. Nanoparticles deposit on the heating surface during boiling of nanofluid before the main experiment and form the artificial relief where the average size of nanoparticles is 50-100 nm. The relief will be discussed below.

Two properties of the nanoparticles layer are very important in its application but poor investigated: its thickness and durability. These two characteristics are interrelated and depend on many factors.

As it was already said before, the nanoparticles layer on the heating surface is obtained during boiling of nanoliquid. The layer thickness can be measured from SEM pictures of the heating surface (Figure 1). This coating thickness varies from 1 to 10 micrometers. In some parts of the surface one can see bald spots which look free from nanoparticles, but it is possible to find a very thin layer of nanoparticles in a greater magnification.

Thus we can assume the next way of nanoparticles deposition on the heating surface during boiling of nanoliquid based on deionized water. Nanoparticles aggregate (deposite on the surface) only in a three-phase line which exists on the border of a dry spot under the bubble. According to the theory of microlayer the liquid film exists under the bubble, vapor is above this layer and the heating surface is below.

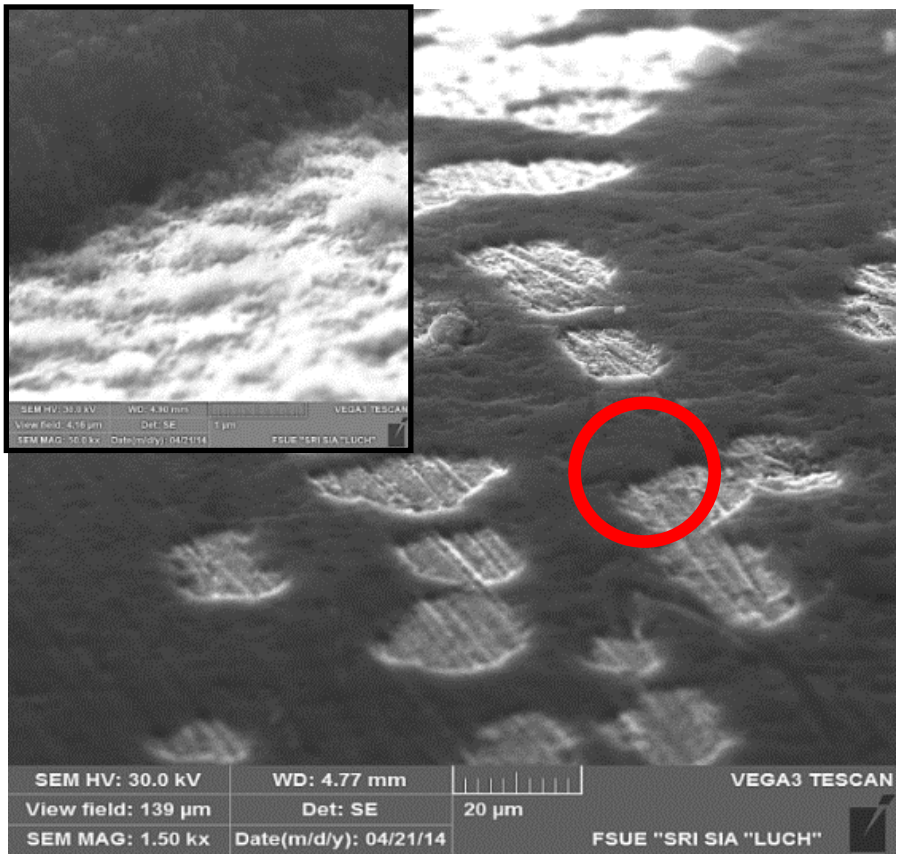

Figure 1. Nikel surface with coating from nanoparticles Al_2O_3.

RESEARCHES ON BOILING IN MICROCHANNEL

Researches on boiling in a single microchannel were conducted for different heating surfaces: clean copper and copper with an artificial nano-relief [10-17]. Experiments were provided in quasi-stationary conditions. Quasi-stationary conditions of the experiment allowed to provide measurements in different regimes of boiling: nucleate boiling, transition boiling and even film boiling.

Boiling curves for a clean microchannel and the microchannel with the coating of nanoparticles are shown on Figure 2. The critical heat flux is higher in the channel with nanoparticles rellief. Also the heat transfer coefficient in the transition boiling is higher in the channel with the nanorelief than in a clean channel. The CHF depends much on the contact angle (clear surface θ=81º, nano-relief θ=9º). The heat transfer coefficient in the transition boiling also depends on the contact angle. It can be explained by a better contact of fluid with the heating surface in the case of a small contact angle (better wettability).

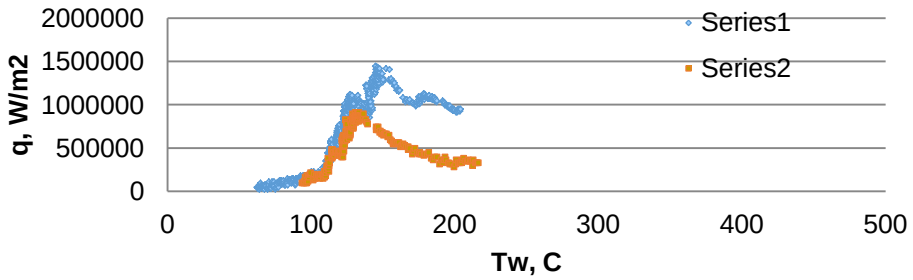

a) mass velocity 100 kg/m^{2}s

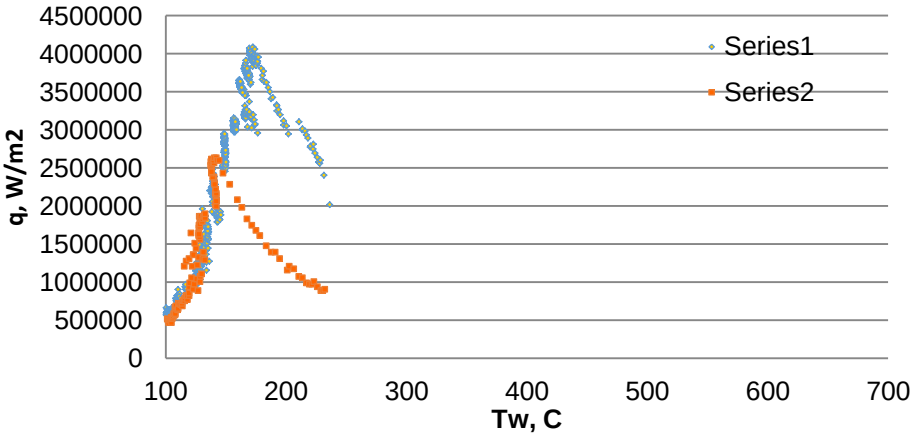

b) mass velocity 300 kg/m^{2}s

Figure 2. Boiling curves for the microchannel with nanorelief and for a clean channel. Series 1- boiling curve 1(microchannel with nanorelief), Series 2- boiling curve 2 (microchannel with clean surface). Water, Tsub=80K, atmospheric pressure.

CONCLUSIONS

Nanorelief in microchannel can be obtained by nanoparticles deposition from the nanoliquid. This relief changes the contact angle, the CHF and the heat transfer coefficient in transition boiling.

The contact angle decreases on the surface with alumina nanorelief in comparison with the contact angle on a clear surface. The CHF at water boiling is 30% higher on the surface with alumina nanorelief.

The transition boiling heat transfer coefficient is twice higher for the channel with alumina nanorelief than for the channel without coating.

ACKNOWLEDGMENT

This work was supported by RFBR, Grant # 18-08-00183

TABLE I. NOMENCLATURE

CHF	Critical heat flux	(W/m^2)	t	Time	(s)
F	Channel cross section	(m^2)	W	Velocity	(m/s)
G	Mass flux	(kg/s)	ΔP	Pressure drop	(Pa)
q	Heat flux	(W/m^2)	ΔT	Temperature difference	(^OC)
T	Temperature	(^OC)	Θ	Contact angle	(deg)
T_w	Wall temperature	(^OC)	ρ	Density	(kg/m^3)
T_{sub}	Subcooling temperature	(^OC)			

REFERENCES

1. Dzyubenko, B., et al. 2016. *Intensification of Heat and Mass Transfer on Macro-, Micro-, and Nanoscales*. Begell House, Inc., 564 p.
2. Bergles, A. and S. Kandlikar. 2005. "On the Nature of Critical Heat Flux in Microchannels," *Journal of heat transfer*, 127:101-107.
3. Nomura, T., et al. 2009. "*Subcooled Flow Boiling In Mini And Micro Channel. Contribution Towards High Heat Flux Cooling Technology for Electronics*," Proceedings of Inter PACK'09, San Francisco, CA/USA.
4. Vafaei, S. and D. Wen. 2011. "Flow boiling heat transfer of Alumina Nanofluids in Single Microchannels and the Roles of Nanoparticles," *Journal of Nanoparticle Research*, 13(3):1063-1073.
5. Kuzma-Kichta, Yu. A. and A.V. Lavrikov, Patent of Russian Federation #2433949 "*Method of Nanorelief Produced on the Heat-Transfer Surfaces*".
6. Kuzma-Kichta, Yu. A, et al. 2014 "Studying Heat Transfer Enhancement for Water Boiling on a Surface with Micro- and Nanorelief, Thermal Engineering," *Pleiades Publishing Inc*, 61(3):210-213.
7. Kuzma-Kichta, Yu. A., et al. 2014. "Boiling Investigation in the Microchannel with Nano-Particles Coating Proceedings of the 15th International Heat Transfer Conference (IHTC15)," *Kioto, Japan IHTC-Digital Library*, p. 12345.

8. Heitich, L.V., et al. 2012. "*Effect of Nanostructured Surfaces on the Nucleate Boiling of Water*", EPFL, Lausanne, Switzerland, p. 1512.
9. Masahiro, T., et al. 2012. "*Subcooled Boiling from a Surface with Spotted Patterns of Hydrophilic and Hydrophobic Coatings*", EPFL, Lausanne, Switzerland, p. 1520.
10. Lavrikov, A.V., J. Hammerschmidt, and Yu. A. Kuzma-Kichta, S. Scholl. 2015. "Thermosiphon Reboilers with Enhanced Tubes," *Chem. Eng. Tech*., 87(3):1-8.
11. Kuzma-Kichta, Yu.A., et al. 2015. "Measurement of the Dynamic Contact Angle on a Surface Coated with Nanoparticles for Improving the Boiling Crisis Model," *Intern Journal of Energy for a Clear Environment*, 16(1-4):171-182.
12. Kuzma-Kichta, Yu., et al. 2015. *Investigation of Heat Transfer in a Heat Pipe with Nanoparticles Coating*. *Report. 9th Minsk International Seminar "Heat Pipes, Heat Pumps, Refrigerators, Power Sources*. Minsk, Belarus.
13. Shustov, M.V., Yu.A. Kuzma-Kichta, and A.V. Lavrikov. 2017. "Nanoparticle Coating of a Microchannel Surface is an Effective Method for Increasing the Critical Heat Flux," *Thermal Engineering*, 64(4):301–306.
14. Alekseenko, S.V., et al. 2017. *Vortex Technologies for Energy*. Moscow Publishing House MEI., p. 350.
15. Lavrikov, A.V., et al. 2017. "Investigation of Heat Transfer Enhancement and Thermal Resistance of Weakly Inclined Thermostabilizer," *J. Phys. Conf. Ser*., p. 891.
16. Zhukov, V.M., et al. 2018. "Heat Transfer Under Transition and Film Boiling of Liquids at Dimpled Spheres and Cylinders," *J. Phys. Conf. Ser.*, p. 980.
17. Chugunkov, D.V., et al. 2018. "Protective Materials Thermal Conductivity Research for Heat Exchanger Tubes of a Networking Heater," *J. Phys. Conf. Ser*.

2018 International Theoretical and Practical Conference on Alternative and Smart Energy (TPCASE 2018)
ISBN: 978-1-60595-617-6

Generator System on the Basis of Segment Wind Generators of Synchronous-Inductor Type

Andrey Novikov, Kseniya Chebotok and Alexander Litvinenko

ABSTRACT

A new type of wind power generation systems with increased reliability due to the absence of a reducer while maintaining the main characteristics of the gear units is proposed. The main difficulties of realization of these installations are revealed, ways of their overcoming by use of new technical solutions are specified. Methods of construction and application of the offered devices are offered.

INTRODUCTION

As part of the implementation of National technological initiatives in the field of new energy, it seems appropriate to improve the generator systems of distributed energy. Among the generator systems that do not consume organic fuel, i.e. are the most environmentally friendly, traditionally, much attention is paid to photoelectronic converters and wind turbines (WEG). In any case, such systems are subject to the requirements of increased reliability [1].

SEGMENT WIND GENERATORS

As known, the composition of most of the VEG traditionally includes the actual generator and reducer, which converts a relatively low angular velocity of the wind wheel into an increased rotational speed of the generator.

Voronezh State Technical University, 84, 20- Letiya Oktyabrya Street, Voronezh, 394006, Russia.

An essential feature of the wind power generators of the segment type is the placement of their rotary elements at the ends of the blades of the wind wheels, while these elements can partially perform the function of the winglet, that is, aerodynamic surfaces that prevent the flow from descending along the ends of the blades. As for the stator elements, they are segments of the stator of electric machines of the usual type, but preferably with coil windings[1,2].

The purpose of the report is to determine the characteristics of these devices, and on this basis, the development of ways of synthesis of segment direct-drive wind generators.

It is possible to allocate following features of the segment generator sets:

The absence of a gearbox, which increases reliability.

The segment design of the stator makes it possible to implement within certain limits, the flow control of permanent magnets - exciting elements.

Unilateral generations rotary and stator elements in combination with the uneven rotation causes increased vibroactivity and requires the adoption of measures to weaken and compensation, for example, the use dvukhstadiinogo performance, improving the blade stiffness, increased bearing unit.

Specific requirements for the energy-power unit, in particular, difficult to direct impact energy to the grid, therefore requiring an initial DC voltage. For low-power stations, this is generally accepted, because it allows the use of automotive electrical equipment, including consumers, designed for 12 or 24 volts[3,5].

In this regard, the use of an intermediate storage device is very desirable, not only in terms of long-term energy reserve, but also the reserve during one revolution of the wind wheel.

Can distinguish 2 possible embodiment of segment generators:

- Purely inductor type, when only passive ferromagnetic elements are located on the blades;

- The classic synchronous version, when the ends of the blades are pole tips with sources of excitation, for example, permanent magnets for low-power generators.

The first option is characterized by a smaller mass of rotating parts, but also in less efficiency due to the presence of a constant component of the flow on the stator.

The second option is more productive, but has a large mass of moving parts.

Meanwhile, it is known that segmental WEG have a characteristic feature-a large length of the circumferential air gap compared to conventional machines, caused by an increased radius of the WEG blade[4,8].

This feature of the WEG can be used to increase energy efficiency. This is due to the fact that the most commonly used structural element as a pole magnetic circuit are the corners, one (parallel to the axis of the blade) side of which is oriented along the radius of the wind wheel blade, and the other—the tangential side is perpendicular to the parallel and directed along the circumferential air gap.

This makes it possible to increase the width of the tangential side of the tip to the width of the inter-pole distance on the stator. Thus, under the condition of the location of the excitation sources (for example, permanent magnets) on the stator and on the rotor (the case of the active rotor), it becomes possible with one passage of the blade along the stator element to realize the passage of three generating sets of pulses:

- From the first pole tip (inductor mode);
- From two tips with the inclusion of the active section of the rotor (classic synchronous mode);
- From the second pole tip (again inductor mode)

Consider the implementation of this feature in more detail [6].

A key feature of this design is that the pole tips are made in the form of corners with a radial part in contact with the excitation source and a tangential part facing the gap, the width of the tangential part 11 is set from the condition 11≥1, where l is the width of the interpolar space of the stator elements.

The basic design relations necessary for the synthesis of the considered generator systems are based on mechanical and electrical calculations. As you know, for segment machines, it is important to value the design coefficient KP, showing the overlap of the stator and rotor zones:

$$K_{п} = \frac{\alpha_r . \alpha_S}{4\pi^2}, \quad (1)$$

Where a_r and a_s are, respectively, the total (Central) angles of the rotor and stator segments.

For conventional machines:

$\alpha_r = \alpha_s = 2\pi$ и $K_п = 1$.

In the case under consideration, the a_r has an increased value and can be represented a_s:

$\alpha_r = \alpha_{r1} + 2\alpha_{r2}$,

where a_{r1}-characterizes the classical synchronous generator (within the module); a_{r2}-refers to the inductor mode [9].

It is obvious that the possible reduction of the Gearbox in comparison with the unit should be compensated by something to preserve the electromagnetic power. The natural way to achieve this is to increase the speed component in the mechanical power supplied to the wind wheel. Of course, this may be accompanied by an increase in the torque component.

In general, the generated voltage is pulsed, with failures in the absence of overlap.

Natural is the desire to compare the energy characteristics of conventional machines and segment, it is advisable to obtain a value of the radius of the blade (rotor), which will allow due to the higher circumferential speed of the rotor element, to compensate for the loss in energy production at the mismatch of the axis ar.

The intensification of power output of segment generators is possible in several directions: some parameters are conditionally independent.

1. The diameter and length of the shoots (axial length) is assumed to be specified;

2. The number of rotor and stator modules - also in the first approximation are given;

3. Initially, the pulse nature of electromagnetic processes implies a possible increase in electromagnetic loads, in particular, current density and magnetic induction.

4. An increase in magnetic induction is possible with a decrease in the air gap provided that the radial force is compensated, for example, by a two-stator design.

5. The transition from concentrated to distributed windings, including two-layer. On the one hand, this leads to a reduction in copper consumption due to the smaller departure of the frontal parts and creates conditions for obtaining higher quality energy, but on the other hand, it is less technological, more expensive.

6. Excitation control (up to minimization at minimum wind), which leads to a decrease in the starting torque.

7. Implementation of several rotors - wind wheel on one stator[1,12].

To study the segment generator module of this design scheme, a simulation of a specific module using the Matlab mathematical environment and a comparison of the results with a real physical expert was carried out[1].

The physical model consisted of a fragment (single module) segmented generator, the angle size of the magnetic circuit are 40x40x2 mm, the size of the magnets: rotary ∅18x5mm, stator - ∅25x7 mm, the parameters of the working coil of 4000 turns, a wire of PEL ∅0,25. The rotor module was driven in rotation from an external motor at a speed of 0÷75 R / s, the radius of departure of the rotor - 0.5 m[2,11].

However, it should be noted that the correct choice of material and dimensions of the cross section of the blades, for example, duralumin, will not lead to a dangerous situation. In this regard, the choice of the number of blades (i.e. the type of wind wheel) is also important. Preferred for the case under consideration is the choice of a low-speed wind wheel, which, although it has a large number of blades, which somewhat complicates the design, but has a natural speed limit associated with a large number of aerodynamic resistance and a significant braking (fan) moment. The increase in the number of blades automatically leads to an increase in the number of rotor elements, and of course, to an increase in productivity, in particular, to an increase in power. As for the dynamic forces, vibrations of the blades, they are effectively stopped by increasing the rigidity of the structure, the introduction of links forming force triangles [4,5,6].

CONCLUSION

The introduction of direct-drive wind turbines of the segment type is a logical step in the development of at least low-power VEG, at the expense of various design solutions, it is possible to overcome the shortcomings of this design scheme in its simplest form. Thus, it seems expedient the prospects of this direction and the need for further improvement of the existing images of the WEG.

REFERENCES

1 Litvinenko, A.M. and A.B. Kirilov. 2018. "Control of the Excitation of the Segment Generators of the Wind Power Plants by the Change of the Air Gap," *Electricity*, 1:28-32.
2. Litvinenko, A.M. and V.A. Tikunov. 2003. *Design of Wind Power Generators*. Proc. Benefit, Voronezh, Quart, p. 96.
3 Litvinenko, A.M. 2003. "Wind Turbine" Patent of Russian Federation #2204052.
4. Litvinenko, A.M. 2003. "Stator Vetroelectrogenerator*"* Patent of Russian Federation #2204734.
5. Litvinenko, A.M. 2003. "Wind" Patent of Russian Federation #2211366
6. Litvinenko, A.M. 2003. "Vetroelectrogenerator" Patent of Russian Federation #2211949.
7. Litvinenko, A.M. 2003. "Contrrotornyvetroelectrogenerator" Patent of Russian Federation #221948.
8. Litvinenko, A.M. 2003. "Vetroelectrogenerator" Patent of Russian Federation #2211951.
9. Gourieres, D.Le. 1982. *Energie'eolienne. Theorie, Concept et Calculpratiaue des Installation*, Paris: EYROLLES, p. 279.
10. Franklin, J. Debry. 1980. *Energieeolionne. Traduction*. *Preface de Bonin*. Edition, Paris: SCM, p. 203.
11. "General Electric," Available at: http://www.ge.com.
12. "Siemens," Available at: www.siemens.com.

2018 International Theoretical and Practical Conference on Alternative and Smart Energy (TPCASE 2018)
ISBN: 978-1-60595-617-6

Assessment of the Climatic Factors Influence on the Reliability of Power Lines in the Moscow Region

Olga Kondrateva, Oleg Loktinov, Dmitriy Burdyukov and Ekaterina Myasnikova

ABSTRACT

This article deals with the problems of the climatic factors influence on the reliability of power lines in the Moscow region. Using the method of hierarchical clustering, the most significant meteorological factors leading to technological disturbances are determined and the values of Spearman correlation coefficients between the causes of accidents and climatic factors are calculated.

INTRODUCTION

The electric power complex of Russia is a set of generating capacities and transportation infrastructure, providing continuous power supply to industrial facilities and the population of the country. Power facilities, which are elements of a strategically important industry, must be resistant to both internal and external influences, as well as meet the requirements of reliability, characterized by the ability to perform specified functions with a certain degree of probability.

In accordance with the energy development strategy of Russia for the period up to 2030 the goal of the energy complex is to ensure reliable, high-quality and safe energy supply, taking into account the continuity and energy security.

National Research University, MPEI, 14, Krasnokazarmennaya Street, Moscow, 111250, Russia.

REASON DISCONNECTION OF POWER LINES IN RUSSIA

According to the annual reports of PSC rosseti, which is a backbone electric grid company, more than 150 thousand technological violations (accidents) are recorded in the country for more than 2.3 million km of power lines and 500 thousand substations with an average duration of power supply interruptions of about 2.5 hours [2]. The following reasons were recorded as the main violations of the normal functioning of the power facilities of PSC Rossetti in 2017:

1. Natural impact - 47%
2. Resource exhaustion - 23%
3. External impact - 19%
4. Other reasons - 11%

Based on the above classification of accidents, one of the key factors to improve the stability and reliability of the power system is currently a reduction in the number of emergency shutdowns as a result of the observed natural impacts.

The climate sensitivity of the electric power industry is determined by a significant number of infrastructure facilities exposed to weather and climatic factors, and the most vulnerable and damaged element of the electric power complex are air power lines due to their territorial dispersion and greater exposure to climatic factors compared to the failure parameters of switches and transformers that are part of the substation.

The issues of improving the reliability of power lines under the influence of climatic factors over the past decade are actively discussed not only in Russia but also at the international level. Already in 2012, the intergovernmental panel on climate change (IPCC) prepared the report "Managing the risks of extreme events and disasters to advance climate change adaptation" dedicated to the problems of managing the risks of extreme climatic conditions for successful adaptation to climate change.

This study emphasizes the need to investigate each case of disconnection and establish reliable reasons for disconnection of power lines for the formation of the administrative and administrative apparatus of energy companies array of data to minimize operational risks associated with the impact of climatic factors. At the same time, it should be noted that the application of the analysis of the trip risk for power lines as a result of the influence of climatic factors is a time-consuming multifactorial task due to the probability that several climatic factors can have a cumulative effect on the object under study.

Climate impact analysis on power lines

Retrospective analysis of the causality of emergency shutdowns at power facilities revealed a constant increase in the number of cases related to the manifestation of climate, both directly and indirectly, which include:

1. The impact of recurrent natural phenomena - 19.8%
2. The fall of trees on the power line wires - 16.3%.
3. The atmospheric surge - 13.5%
4. Excessive exposure to natural disasters - 2.4%

The frequency and power of meteorological impacts directly affects the smooth operation of the power supply and transmission system via overhead power lines. Thus, the combination of meteorological factors and climate change contribute to the emergence of more than 50% of all possible violations and failures in the energy supply of consumers.

As part of the analysis of regulatory documents [3-5] and studies on the negative impact of climate on power lines [6], the main causes of technological violations, as well as the possible consequences of such emergencies were identified and shown in Table I.

ANALYSIS OF ACCIDENTS IN THE MOSCOW REGION

The paper assesses the efficiency of the power grid economy of the Moscow region in a changing climate. The initial data on a technical condition of networks was used the attention of the Western electric networks, JSC "MOESK" about outages on the limits of territorial areas of the organization's activities for the period from 2013 to 2017, To determine the values of meteorological parameters were used data of 8 meteorological stations are relatively equally distributed over the area of the Western electric networks, JSC "MOESK".

During the analysis, it was hypothesized that such a phenomenon as, for example, "falling trees on power lines", may be an indirect effect of other phenomena (for this example, such a phenomenon was increased wind load). On the basis of this hypothesis, it was determined the need to isolate from the initial array of climatic factors that lead to technological disturbances, groups (clusters), including various causes related to the same type of aggregate properties.

The key difference between clustering and classification is the lack of well-defined groups, which are determined in the process of clustering algorithm. Cluster analysis allowed taking into account and combining in the form of a hierarchical dendrogram both the most frequent manifestations of natural phenomena and rather rare climatic anomalies. The resulting hierarchical dendrogram, presented in Figure 1, clearly shows the relationship between objects (meteorological phenomena, external influences) and the groups in which they are combined.

TABLE I. MAIN CAUSES OF TECHNOLOGICAL FAILURES.

Meteorological phenomenon	Consequences for power lines
Wind	Additional mechanical loads on the nodes of the transmission line (appearance clashes and wire breaks)
Precipitation (rain, snow, hail)	Wire vibration (vibrations with low frequency from 0.2 to 0.4 Hz and high frequency from 5 to 50 Hz)
Extreme temperatures (heat, cold)	Decrease in margin of safety wires, supports, elements, transmission lines (appearance clashes and wire breaks)

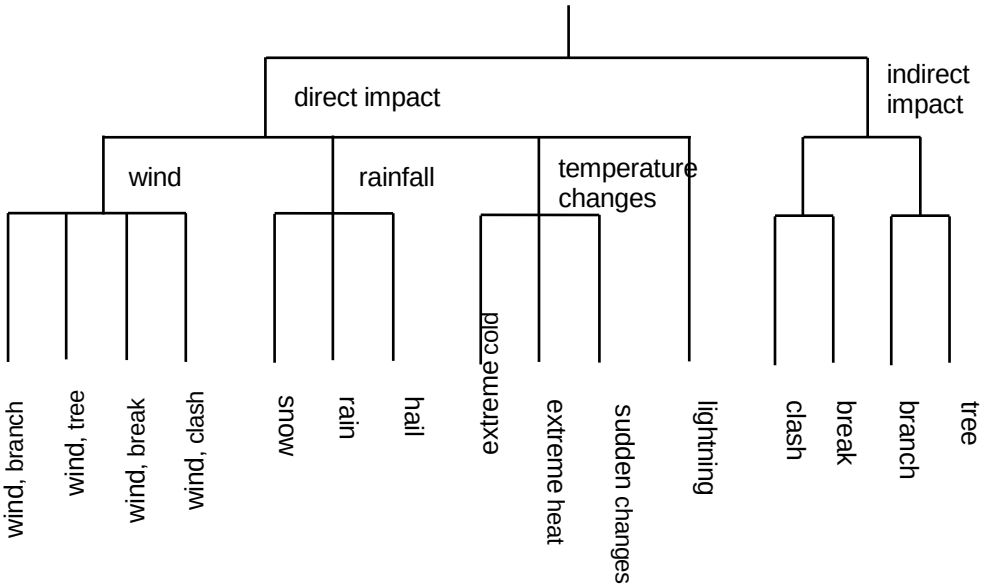

Figure 1. Hierarchical clustering of the technological failure causes.

To assess the impact of natural phenomena and climatic anomalies on the reliability of the operation of overhead power lines, a correlation analysis was used as a method of assessing the relationship between the components, which allows to characterize the dependence of the effective sign (power line disconnection) on the variation of the sign-factor (natural phenomena).

The matrix with Spearman correlation coefficients for external causes given at the second and third levels of the hierarchical clustering tree (wind, rainfall, temperature changes and indirect impact) for the period from 2013 to 2017 for Western electric networks of JSC MOESK is given in table II.

The obtained values of Spearman correlation coefficients indicate the presence of a stable medium and high relationship between the technological disturbances occurring in the Western electric networks of PJSC MOESK and such external influences as: wind, rainfall and indirect climate impact with the level of significance $p<0.1$

TABLE II. THE COEFFICIENTS OF CORRELATION COEFFICIENT FOR EXTERNAL CAUSES OF TECHNOLOGICAL ACCIDENTS IN THE WESTERN ELECTRIC NETWORKS, JSC “MOESK”.

External influence	**Name of the electrical networks area**			
	Volokolamskaya	**Lotoshinskaya**	**Mozhayskaya**	**Odintsovskaya**
Wind	0.63	0.59	0.83	0.9
Rainfall	0.43	0.36	0.7	0.28
Temperature changes	0.2	0.15	0.08	0.04
Indirect impact	0.55	0.48	0.35	0.38

CONCLUSION

Thus, it was found that there is a correlation between the power line outages in the Western electric networks of JSC "MOESK" and such climatic factors as: wind, rainfall and indirect climate impact. The results of this work will allow to develop methods for assessing the vulnerability of power supply systems in changing climatic conditions and to minimize the risk of possible emergency shutdowns on the basis of models of the General circulation of the atmosphere, which are recommended for the assessment of climate change and the forecast of the studied meteorological parameters.

ACKNOWLEDGEMENT

Work is performed with the support of RSCF grant #18-79-10255.

REFERENCES

1. "About Energy Strategy of Russia for the Period till 2030," Order of the Government of the Russian Federation of 13.11.2009 N 1715-p.
2. Annual Reports of JSC "ROSSETI" for 2010-2017.
3. "Rules for Electrical Installations (PUE-7)" Section 2. Electricity Transmission
4. "Construction Climatology," Set of Rules SP 131.13330. 2012.
5. "Loads and Impacts," Set of Rules SP 20.13330. 2016.
6. “Assessment of the Economic Consequences of the Impact of Adverse Weather Conditions (Weather Sensitivity) on the Power Facilities of RIHMI-WDC”.

2018 International Theoretical and Practical Conference on Alternative and Smart Energy (TPCASE 2018)
ISBN: 978-1-60595-617-6

Optical Properties of Quaterthiophenes and Their Dimers End-Capped with Electron-Withdrawing Hexyl-Dicyanovinyl Groups

Yuriy Luponosov, Nikolay Surin and Sergey Ponomarenko

ABSTRACT

In this work the optical properties of novel quaterthiophene-based materials, D1 and D2, having both flexible alkylsiloxane core and electron-withdrawing hexyl-dicyanovinyl (DCV) groups, as well as their model DCV-containing quaterthiophene oligomers 1 and 2 were studied and compared. The results revealed that the number of both DCV and quaterthiophene units influences significantly on absorption and luminescence spectra of the molecules as well as their molar extinction coefficients. As compared to the model α,α′-dihexylquaterthiophene without DCV groups the electronic spectra of the novel molecules are red-shifted up to 100-160 nm.

INTRODUCTION

Macromolecules consisting of thiophene repeating units are of significant interest to researchers from the point of view of their applications as functional materials in organic electronics and photonics.[1] Thiophene-containing oligomers are promising classes of small molecule semiconductors due to their high thermal and thermo-oxidative stability in additional to high charge carrier mobility.[2] However, oligothiophenes poorly absorb sunlight and have emission usually in

Yuriy Luponosov, Nikolay Surin, Enikolopov Institute of Synthetic Polymeric Materials of the Russian Academy of Sciences, 70 Profsoyuznaya Street, Moscow, 117393, Russia
Sergei Ponomarenko, Moscow State University, Faculty of Fundamental, Physical and Chemical Engineering, GSP-1, 1-51 Leninskie Gory Street, Moscow, 119991, Russia

short-wave region of the visual spectrum, which limits their application in organic solar cells and organic light emitting devices. In order to shift absorption and luminescent spectra of oligothiophenes to the long-wave region the modification with strong acceptor (A) groups can be used.[3,4] Dicyanovinyl groups are widely used to design various donor-acceptor molecules for organic electronics.[5-8] In this work, we study optical properties of a series of molecules containing quaterthiophene and dicyanovinyl units (Figure 1).

DISCUSSION

The optical properties were studied by means of absorption and luminescence spectroscopy and the data are summarized in Figure 2 and Table 1). The spectra were recorded over a range of 250-800 nm in dilute solutions in tetrahydrofurane (THF) (UV-grade) with a concentration of 10^{-5}-10^{-6} M in order to avoid self-absorption. The luminescence measurements were performed on an ALS01M multifunctional absorption-luminescence spectrometer. The absorption spectra were recorded on a Shimadzu UV-2501PC spectrophotometer (Japan). The synthesis of the molecules will be published elsewhere.

The shape of absorption spectra for all molecules under discussion is quite similar. The low intensive absorption peaks at 330–370 nm usually are ascribed to the π-π* transition of the conjugated backbone, whereas the intense absorption band with absorption maximum (λ_{abs}) close to 500 nm, respectively, are ascribed to the intramolecular charge transfer transition. However, both electronic bands are also suggested to have a mixed character and the intensity of the absorption feature in the short-wave part of the spectrum is a direct measure of the degree of conformational disorder in the molecule.

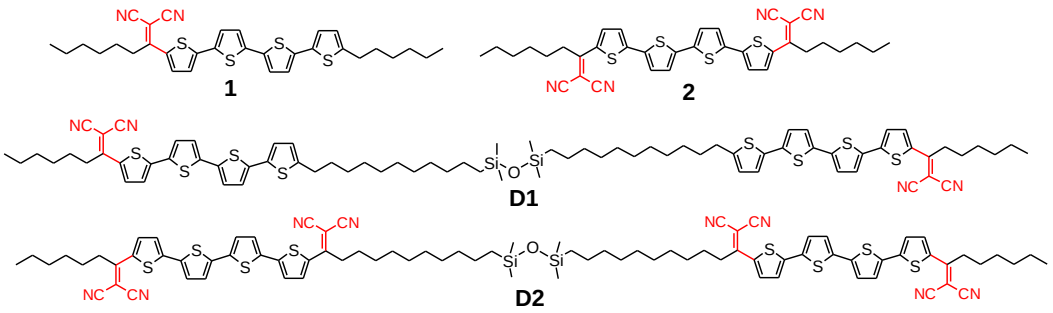

Figure 1. Structural formulas of compounds **1, 2, D1** and **D2**.

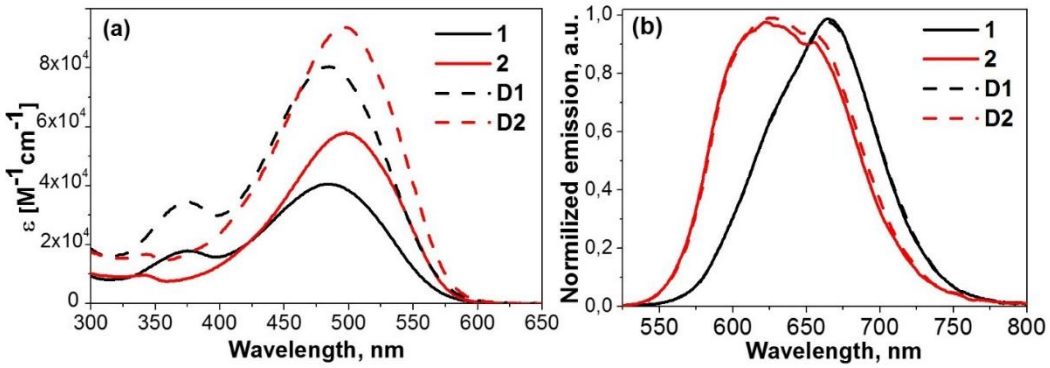

Figure 2. Absorption (a) and normalized luminescence spectra (b) of quaterthiophene-based molecules in THF.

The molar extinction coefficient (ε) tends to increase with increasing number of DCV groups and quaterthiophene units in the structure of molecules. The number of quaterthiophene units has no influence on the shape of luminescent spectra and their maximums (λ_{lum}). In contrast, the number of DCV groups has a pronounced effect on the luminescent spectra. Thus, the molecules with two DCV groups have more broadened and blue-shifted spectra as compared to the direct analogs with one DCV group. The quantum yield of luminescence (Q_{lum}) was found to be a bit higher for molecules 1 and 2 as compared to the dimers D1 and D2. The most interesting thing is a comparison of the optical properties of the molecules 1 and 2 to those of the direct analog without DCV groups – Hex-4T-Hex. One can see that addition of DCV blocks to the quaterthiophene fragment leads to a large enhancement in molar extinction coefficient and shifts the maxima of luminescence and absorption to a long-wave region up to 100 nm and 160 nm, respectively.

TABLE I. OPTICAL DATA.

Molecule	λ_{abs} (nm)	ε ($M^{-1}cm^{-1}$)	λ_{lum} (nm)	Q_{lum} (%)
1	483	43600	663	15
2	498	58000	625	19
D1	485	80400	663	13
D2	497	93800	630	15
Hex-4T-Hex	393	39000	492	24

CONCLUSIONS

DCV derivatives of oligothiophenes have much larger molar extinction coefficients and significantly red-shifted absorption and luminescent spectra as compared to the model α,α′-dihexylquaterthiophene. Thus, the combination of number of DCV groups and quaterthiophene blocks can be an efficient tool to

change and finely tune the optical properties of oligothiophenes for various applications in organic electronic devices.

ACKNOWLEDGEMENTS

The work was supported by the Russian Foundation for Basic Research (grant 18-33-20224). The work was performed in the framework of leading science school NSh-5698.2018.3

REFERENCES

1. Mishra, A., C.Q. Ma and Bauerle. 2009. "Functional Oligothiophenes: Molecular Design for Multidimensional Nanoarchitectures and Their Applications," *Chem. Rev.,* 109:1141-1276.
2. Takimiya, K., S. Shinamura , I. Osaka and Miyazaki. 2011. "Fundamental Aspects of Property Tuning in Push–Pull Molecules," *Adv. Mater.,* 23:4347-4370.
3. Bures, F. 2014. "Fundamental Aspects of Property Tuning in Push–Pull Molecules," *RSC. Adv.,* 4:58826-58851.
4. Ni, W., et al. 2015. "A-D-A Small Molecules for Solution-Processed Organic Photovoltaic Cells," *Chem. Commun.,* 51:4936-4950.
5. Kim, M.J., et al. 2018. "Solvent-Vapor-Annealed A–D–A-type Semicrystalline Conjugated Small Molecules for Flexible Ambipolar Field-Effect Transistors," *J. Mater. Chem. C,* 6:5698-5706.
6. Liu, Y., et al. 2009. "Synthesis and Properties of Acceptor–Donor–Acceptor Molecules Based on Oligothiophenes with Tunable and Low Band Gap," *Tetrahedron,* 65:5209-5215.
7. Paek, S., et al. 2017. "Dopant-Free Hole-Transporting Materials for Stable and Efficient Perovskite Solar Cells," *Adv Mater.,* 29:1606555.
8. Min, J., et al. 2018. "Effects of Bridging Atom in Donor Units and Nature of Acceptor Groups on Physical and Photovoltaic Properties of A-π-D-π-A Oligomers," *Org. Electron.,* 53:185-190.

2018 International Theoretical and Practical Conference on Alternative and Smart Energy (TPCASE 2018)
ISBN: 978-1-60595-617-6

Energy Management—Organizational Technological Innovation of Energy Efficiency

Aleksandr Lyakhomskii, Evgeniya Perfil'eva and Stepan Petukhov

ABSTRACT

The essay substantiates innovative aspect of energy efficiency based on the implementation in real-time mode the provisions and requirements of energy management. The implementation is supported by the automated software and analytical complex for energy resources management. There are listed methods and ways of realization of energy management systems using digital, infocomm technologies providing unification of all participants of the energy consumption process on the basis of a single organizational and technological platform.

INTRODUCTION

Improving energy efficiency provides competitiveness, sustainable economic development, reducing the negative impact on the environment.

According to the expert community's assessments the solution of the problems of energy efficiency improvement, stated in the state legislative and program documents [1-3], follows an inertial scenario.

Energy resources (ER) expense is a significant part of the production cost of industrial enterprises. So at the enterprises of the mineral complex the share of spending comes up to the level of 20-25% in the production cost. It could be even above for some enterprises.

In this regard, sustainable energy efficiency requires an innovative scenario that can be achieved using methods of energy management, digital infocomm technologies [4].

Aleksandr Lyakhomskii, Evgeniya Perfil'eva, National University of Science and Technology (MISIS), 6 Leninsky Prospect Street, Moscow, 119991, Russia
Stepan Petukhov, JSC (SUEK), 53 Building 7 Dubininskaya Street, Moscow, 115054, Russia

THE PROCESS OF ENERGY CONSUMPTION AS A SUBJECT OF MANAGEMENT

The sustainable energy efficiency improvement is based on the system control of ER, realized by means of the representation of the energy consumption process as "human-machine"- ergatic process.

The ergatic process of energy consumption is characterized by both techno-technological component and the administrative component. The techno-technological component is conditioned by the consumption of ER in machines, equipment, buildings, etc. The administrative component is conditioned by the actions of the personnel involved in the process of energy consumption (from the staff operating energy-consuming objects to the company management).

The techno-technological part is described by the following components: the efficiency of energy resources conversion - useful effect; the ratio of active and total energy consumption—electrical power factor; specific consumption per unit of production, unit of work; online accounting of energy resources consumption; certification of the process of energy resources consumption (electricity), etc.

The administrative part includes the following components:

- energy policy of the enterprise (organization)—a formal document that includes the declaration of interest of enterprises in the energy-efficient use of energy, goals, objectives, liability in activities to improve energy efficiency, resources, controlling, the upgrade procedures;
- scheduling of energy management, which is characterized by organizational and functional structure, located at all levels of the production and management chain and in all departments of the enterprise (company), which sets the functional, management, personnel components of the energy management process;
- motivation of personnel in the field of effective management of energy resources, which is provided by a system of methods and activities aimed at achieving high motivation of personnel in the field of energy efficiency;
- software providing energy resources management, which includes a system for obtaining, processing, analysis and provision of information that is important for participants of the energy consumption process and helps them to make decisions to maintain and improve energy efficiency;
- marketing support of energy resources management, which includes a system of methods and activities aimed at identifying, studying, providing, expanding and promoting services in the field of energy efficiency for personnel involved in the consumption of energy resources;
- investment support of energy resources management, which includes a system of methods aimed at feasibility evaluation of projects and activities to improve energy efficiency; preparation of investment plans, and actual return of investment which have been made in energy efficiency.

The inertial scenario of increasing energy efficiency in many companies is largely due to the lack of development of all-important tools in the administrative component which have been mentioned above.

IMPLEMENTATION OF THE ENERGY MANAGEMENT SYSTEM (ИЛИ IMPLEMENTATION OF MANAGEMENT SYSTEM OF EMERGY)

Integration of the techno-technological component and the administrative component into a unified system of energy resources management – energy management system - is required to be carried out with the use of automated software and analytical systems (ASAS) [5].

ASAS is implemented as information and analytical communication system integrated into the existing IP of the enterprise and uniting all participants of the energy consumption process based on a single organizational and technological platform for the controlling and management of ER in order to improve energy efficiency. The figure 1 shows one of the functional schemes of ASAS, which provides implementation the aforementioned main components of the administrative part of power management in real-time and in regular mode.

According to the scheme, the following operations are performed.

Issue of the daily task on specific power consumption to the personnel who is responsible to manage and control the certain power consuming object (PCO) (positions 1 and 4). The task is issued using energy technology profile of this PCO which has been automatically installed by ASAS. The energy technology profile represents the correlation dependence of the specific energy consumption on the volume of work performed $w = f(Q)$. Planned shift specific power consumption for *i*-th PCO for *j*-th shift ($w_{pl\ sh\ ij}$) is automatically calculated after the shift foreman inputs planned volume of work for the current shift according to the mathematical expression.

$$w_{pl\ sh\ ij}=f\left(Q_{pl\ sh\ ij}\right) \quad (1)$$

On the basis of received data from information system of the enterprise about factual shift volume of work and volume of energy consumption, shift specific power consumption *i*-th PCO for *j*-th shift (positions 2, 3, 5) is calculated according to the mathematical expression

$$w_{f\ sh\ ij}=\frac{W_{f\ sh\ ij}}{Q_{f\ sh\ ij}}. \quad (2)$$

Deviation of factual shift specific power consumption from planned task for *i*-th PCO for *j*-th shift (position 6) is calculated according to the mathematical expression

$$\Delta_{sh\ ij}=\left(w_{pl\ sh\ ij}-w_{f\ sh\ ij}\right). \quad (3)$$

The average shift deviation of the specific PCO for the *i*-th PCO (position 7) for the reporting month is determined by the mathematical expression

$$\Delta_{av\ sh\ i}=\frac{1}{n}\sum_{j=1}^{n}\left(w_{pl\ sh\ ij}-w_{f\ sh\ ij}\right). \quad (4)$$

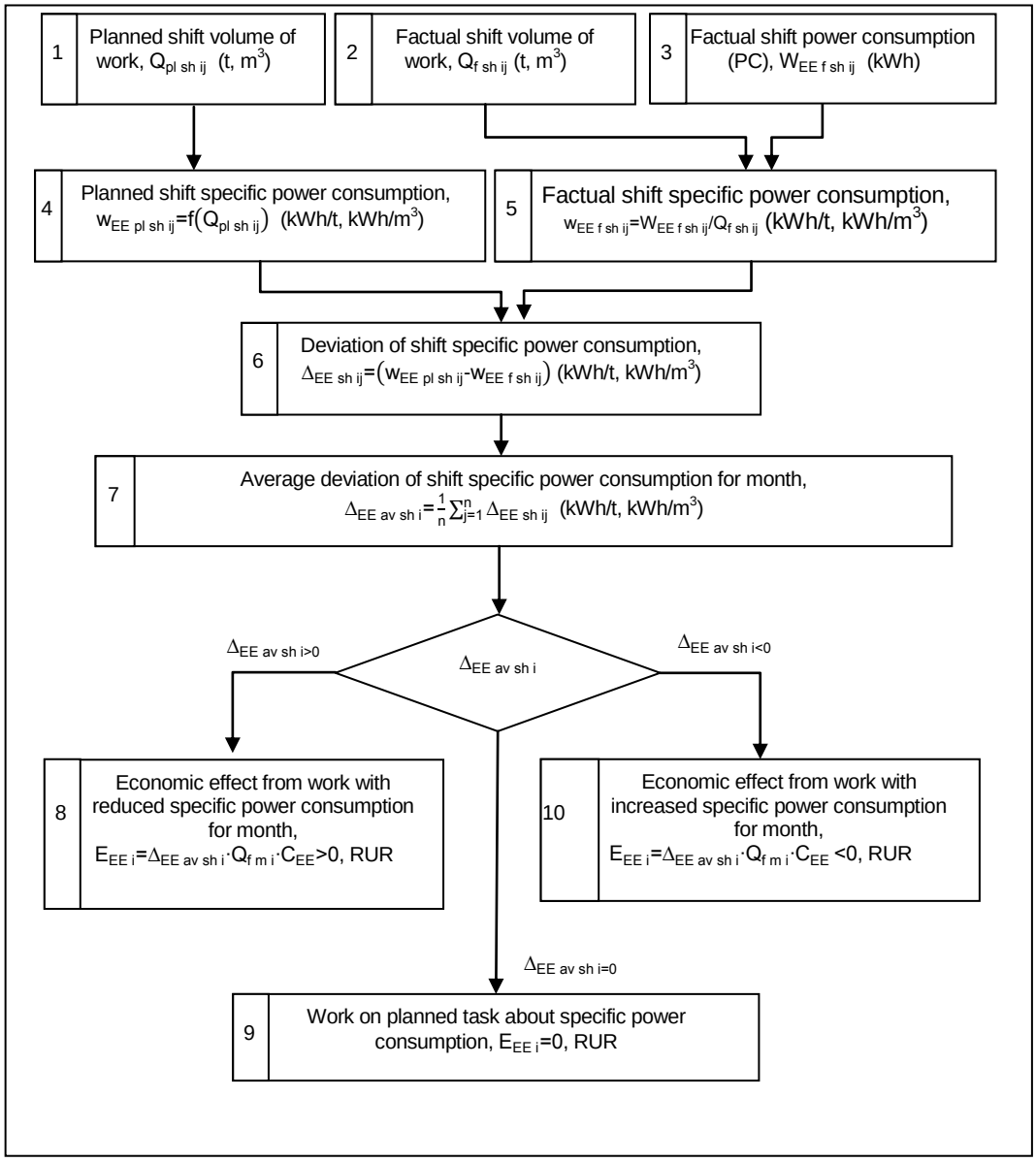

Figure 1. The scheme of implementation for components of administrative part of power management system.

Economic effects are determined by the results of energy efficiency of the *i*-th PCO under the conditions $\Delta_{sv\ sh\ i} > 0$, $\Delta_{av\ sh} = 0$, $\Delta_{av\ sh} < 0$ (positions 8-10) according to the expression

$$E_i = \Delta_{av\ sh\ i} \cdot Q_{f\ m\ i} \cdot C_{EE}, \quad (5)$$

where $Q_{f\ m\ i}$ – volume of work for *i*-th PCO for month; C_{EE} – the price of 1 kWh of electricity.

The abovementioned operations create the conditions for continuous energy efficiency in the main energy-consuming production processes such as:

– goal-setting and targeted responsibility of personnel in the work to improve energy efficiency, which are one of the main provisions of the energy policy of the enterprise;

– calculating planned shift specific power consumption, targeted monitoring and the report for its implementation, which is important to ensure energy efficiency;

– establish key indicators of work performed to motivate staff according to the results of increasing energy efficiency;

– providing staff with the above-mentioned organizational, information and communication, motivational conditions (services) that relates to marketing component of energy efficiency;

– calculating of the economic effect that is included in the investment provision of energy efficiency.

RESULTS

On the basis of the above provisions the energy management system developed and implemented in a number of branches of the Siberian coal energy company.

CONCLUSION

The energy management system, implemented on the basis of developed energy management systems, provides a significant improvement in the existing process of energy resources consumption through its digitalization, development of infocomm environment for economic growth, reducing the negative impact on the environment. It is considered as a combined organizational and technological innovation.

REFERENCES

1. State Program of the Russian Federation "Energy Saving and Energy Efficiency for the Period up to 2020", Moscow: Ministry of Energy of the Russian Federation, 2010.
2. State program "Energy Efficiency and Energy Development," 2014.
3. Long-Term Program of Development of the Russian Coal Industry for the Period up to 2030, 2014.
4. Lyakhomskii, Aleksandr; et al. 2015. "Conceptual Design and Engineering Strategies Energy Efficiency at Enterprises: Research, Technologies and Personnel," *IV Forum Strategies Partnership of Universities and Enterprises of Hi-Tech Branches (Science. Educations. Innovations)*, pp. 45-48.
5. Lyakhomskii, A.V., et al. 2015. "A Software-Hardware System of Remote Monitoring and Analysis of the Energy Data," *Russian Electrical Engineering*, 86(6):314-319.

2018 International Theoretical and Practical Conference on Alternative and Smart Energy (TPCASE 2018)
ISBN: 978-1-60595-617-6

Effect of Carbon on the Thermoelectrical Properties of Copper Oxide-Based Composites

Yuriy Kalinin, Maxim Kashirin and Vladimir Makagonov

ABSTRACT

The effect of carbon filler on the electrical resistance, thermopower and thermoelectric power factor of copper oxide-based composites has been studied. It is established, that thermoelectrical properties of investigated composites are determinated by interaction between filler and matrix materials at phase boundaries. This interraction leads to changes in the energy spectrum of charge carriers. It is found that in composites CuO – CNF (carbon nanofibers) the dependences of the electrical resistivity and the thermopower on the filler concentration are characteristic by s - like curves that are typical for percolation systems. While using fullerene as filler material the dependences of the electrical resistivity and the thermopower on the filler concentration cannot be explain within percolation theory.

INTRODUCTION

Thermoelectric materials have attractive applications in electric power generation and solid-state cooling. The conversion efficiency of thermoelectric materials is related to a value called the figure of merit (Z) or its dimensionless combination with the absolute temperature (ZT) which is defined by equation [1]:

$$ZT = \frac{\sigma S^2 T}{k}, \quad (1)$$

where S is the Seebeck coefficient, σ and κ are the electrical and thermal conductivity, respectively, T is the absolute temperature. To maximize the ZT of a

Voronezh State Technical University, 84, 20-Letiya Oktyabrya Street, Voronezh, 394006, Russia

material, a large S, high σ, and low κ are required [2]. Copper oxides are promising thermoelectric materials with a high Seebeck coefficient (S ~ 1000 μV/K), but low electrical conductivity, which negatively influences the thermoelectric Z of a material. The increase in the conductivity by introducing conducting fillers to copper oxides enables an increase in Z of such systems. The aim of this work is to study the influence of carbon filler on the thermopower and the conductivity of bulk copper oxide-based composites.

EXPERIMENTAL TECHNIQUE AND SAMPLES STRUCTURE

The copper oxide-based composites were fabricated by ceramic technology using hot one-side pressing in air at a pressure of 500 MPa and a temperature of 375°C within 15 minutes. As the matrix material the analytically pure copper oxide CuO nanopowder with average particle size of 50 – 100 nm produced by electrical explosion of a copper conductor in an oxygen atmosphere was used. The active filler was powders of carbonnanofibers "TAUNIT" (CNF) and fullerenes C_{60}. Mixing of the initial components was carried out in an energy-intensive planetary AGO-3 mill by a "wet" method in commercially pure ethyl alcohol.

To analyze the phase composition of the composites, we performed X-ray diffraction studies using a Bruker D2 Phaser diffractometer. The results were processed using the Bruker DIFFRAC EVA 3.0 software and the PDF2012 data base. From the results of XRD analysis, the phase composition of the obtained samples was determined, according to which the oxide matrix of all composites contains: 23.8 wt. % of the Cu_2O, 75.3 wt. % of CuO and 0.9 wt. % of Cu. It is attributed to reduction effect of ethyl alcohol on CuO during treatment in an energy-intensive planetary mill.

The electrical resistance was measured on a direct current by the amperemeter–voltmeter method. The dependences of the thermopower of the composites on the carbon concentration were obtained using differential methodic.

RESULTS AND DISCUSSION

To determine the influence of a carbon filler on the electrical properties in the obtained composites the dependences of the specific electrical resistance (ρ on Figure 1) and thermopower (S on Figure 1) on the concentration of the conductive phase X were measured at room temperature. To evaluate the perspectives of practical application the investigated materials as thermoelectrics the thermoelectric power factor that is defined as $P=S^2/\rho$ was also calculated (Figure 2).

The relationships between the resistivity and copper oxide-based composites had a s - like shape that is characteristic of percolation systems: ρ decrease as the content of the carbon filler increases. The percolation threshold, defined as middle of the

segment of the most significant decrease in ρ and S with the increase in the carbon filler content, was ~3.5 wt. % for CuO - CNF composites and 2.4 wt. % for CuO - C_{60} composites. It is important to note that the difference in the dependences of the specific electrical resistance between CuO - C_{60} and CuO - CNF systems is a slight increasing in ρ for CuO - C_{60} composites at low filler concentrations, what is not observed in the CuO - CNF system. The reason for this difference can be established from the analysis of the dependences of the thermopower, which is significantly more sensitive to changes in the energy spectrum of charge carriers.

The thermopower is positive for all the composites, which indicates the hole type of conduction in these composites. For the CuO - CNF composites the dependence of thermopower on carbon filler content correlate with the dependence of resistivity. So, the introduction of 5 wt. % CNF decreases S of the CuO - CNF composites from 350 μV/K (pure CuO in our investigation) to 10 μV/K characteristic of carbon structures [3]. For the CuO - C_{60} composites the dependence of thermopower on carbon filler content not typical for percollation systems, consisting of electrically conductive filler particles distributed in a non-conductive matrix. As well as for CuO – CNF composites, the addition of small content of fullerenes (less than 1,5 wt. %) leads to a decrease in thermopower from 350 μV/K to 250 мкВ/К. However, a further increase in the content of fullerenes from 1.5 to 5 wt. % leads to dramatically increasing in thermopower values is almost two times relatively to pure CuO. It is important to note that the dependence of the thermopower on the content of fullerenes also tends to saturation at concentration above X ~ 5 wt. %. The described dependence cannot be explained within the framework of percolation theory [4] or the effective medium theory [5] and requires taking into account the more complex interaction between the filler particles and a matrix material.

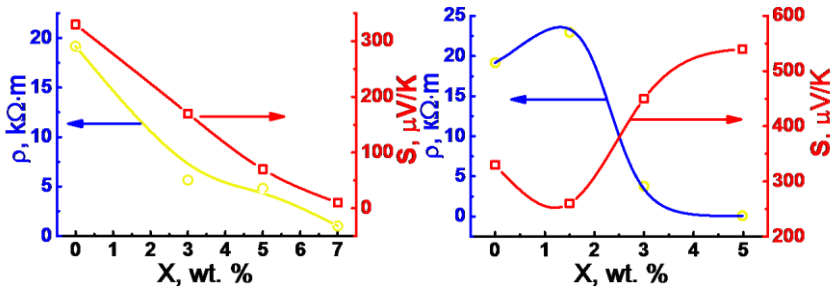

Figure 1. Relationships between resistivity (ρ) and thermopower (S) and the carbon filler content (X) of copper oxide-based composites: a) CuO – CNF, b) CuO - C_{60}.

According to the described in [6] literature data the C_{60} molecules act as acceptor impurity in Bi_2Te_3–C_{60} nanocomposites. The explanation of the acceptor effect of fullerene molecules remains due to an increase in the electron affinity of C_{60} molecules due to their interaction with semiconductor crystallites. Such

interaction can significantly change the density distribution of electrons trapped by C_{60} molecules in comparison with this density distribution in fullerides.

It is known, that the thermopower is determined by the energy derivative on electronic density of states g(E) and the relaxation time of charge carriers τ through the Mott relationship written in the form [7]:

$$S = \frac{\pi^2 k_B^2 T}{3e}\left(\frac{d\ln g(E)}{dE} + \frac{d\ln \tau(E)}{dE} + \frac{d\ln \nu(E)^2}{dE}\right)_{E=E_F}, \qquad (2)$$

where k_B is the Boltzmann constant, T is the absolute temperature, g(E) is the density of charge carriers states, τ(E) and ν(E) are the relaxation time and the charge carriers velocity respectively. The increasing of thermopower at content 1,5 – 5 wt. % of fullerene becomes possible, if at least one item in parentheses of eq. (2) is increased too. Then, it should be recognized that the addition of fullerenes C_{60} in composites CuO - C_{60} leads not only to an increase in carrier concentration (holes in our case), as can be seen from the decreasing in the values of electrical resistivity at concentrations C_{60} more than 1.5 wt. % (Fig. 1b), but also to a change in the distribution of density of electronic states at the Fermi level.

On the other hand, the thermopower of nanocomposite is determined by the charge carrier's relaxation time τ, which in the case of free electron scattering on nanoinclusions determined according to the Matthiessen rule:

$$\tau^{-1} = \tau_{bulk}^{-1} + \tau_i^{-1}, \qquad (3)$$

where τ_{bulk} is the charge carrier's relaxation time, determined by scattering on the deformation potential of acoustic and optical phonons, and polar scattering by optical phonons in matrix material without nanoinclusions, τ_i – relaxation time due to scattering by scattering potential of randomly distributed inclusions:

$$\tau_i^{-1} = n_i \nu \sigma_t . \qquad (4)$$

Here $n_i = 3x/4\pi R^3$ is the concentration of inclusions, σ_t is the electronic transport scattering cross section, R and x is the dimension of inclusions and its content, and $\nu = d_p E_p$ - is the electronic velocity with p the momentum.

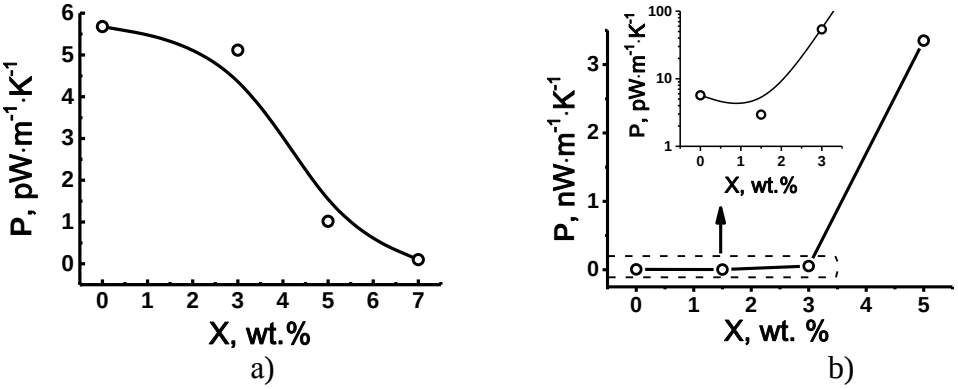

Figure 2. Relationships between the thermoelectric power factor and the carbon filler content of copper oxide-based composites: a) CuO – CNF, b) CuO - C_{60}.

It is probably, that the described above contributions to the thermopower take a place both in CuO - CNF and CuO - C_{60} composites, however the magnitude of these contributions extremely depends on the type of carbon filler. So, the introduction of 3 wt. % CNF decreases ρ of the CuO - CNF composites (from 19 kOhm·m to 5.6 kOhm·m) more substantially with the increase in the carbon content as compared to the value of the thermopower (from 330 μV/K to 170 μV/K). Such regularities was observed earlier and as a rule results in the fact that the thermoelectric power factor has a clear maximum at the carbon filler concentration corresponding to the percolation threshold [9]. In our case, the thermoelectric power factor at percolation threshold characterized by a plateau (X < 3.5 wt. %), which is probably due to an additional contribution of charge carriers scattering on CNF nanoinclusions.

The dependence of the thermoelectric power factor P on the carbon filler content for the CuO - C_{60} significantly different from the dependence of the CuO – CNF composites (Fig. 2) and CuO-based composites, described in [8].

As well as for CuO - CNF composites, the thermoelectric power factor of CuO - C_{60} composites decreases slightly at low C_{60} content, reaching a minimum at X = 1,5 wt. % (inset in Figure. 2b). However, the subsequently increasing of thermopower and decreasing of specific electrical resistance values at X > 1,5 wt. % lead to significant, almost three orders of magnitude, increasing in P for sample with 5 wt. % C_{60} relatively to pure CuO (Figure. 2b).

Unfortunately, the obtained values of thermoelectric power factor of all composites, even maximal achieved for CuO - C_{60} composite, contained 5 wt. % C_{60}, are very low to be used in practice application [9], however, this approach to modify the thermoelectric properties of a material with conducting carbon nanoparticles seems very promising.

CONCLUSIONS

1. The influence of carbon filler on the resistivity and the thermopower of copper oxide has been investigated. It is found that the concentration dependence of the resistivity of bulk CuO - C_{60} and CuO − CNF composites are characterized by the s - like curves typical for percolation systems. The percolation threshold of the CuO - CNF system is defined as 5 and 7 wt. % of CNF. For CuO - C_{60} composites the percolation threshold is defined as the middle of the segment of the most significant decrease in $\rho(X)$ and S with the increase in the carbon filler content, and was ~2.5 wt. % C_{60}.

2. For the CuO - CNF composites the thermopower monotonically decreases and the electrical resistivity decreases too while the carbon content increasing. It leads to lower values of the thermoelectric power factor compared with CuO without the addition of nanoparticles.

3. For the $CuO - C_{60}$ composites nonmonotonic dependencies of the thermopower on the carbon filler content have been found and a minimal value S at 1,5 wt. % C_{60} is observed. The addition of fullerene from 1.5 to 5 wt. % of C_{60} leads to increasing of the thermopower are almost doubled relative to pure CuO and simultaneously decreasing of the electrical resistivity of more than order of magnitude. As the result the thermoelectric power factor of carbon filled nanocomposites was improved by more than 300 times in comparison with pure CuO. The increasing of the thermopower with fullerene addition can be explained by the acceptor action of C_{60} molecules at the interaction with CuO crystallites, which leads to a change in the distribution of density of electronic states near the Fermi level.

ACKNOWLEDGMENT

This work was supported by the Ministry of Education and Science of the Russian Federation in the framework of the state task (project no. 3.1867.2017/4.6).

REFERENCES

1. Minnich, A.J., et al. 2009. “Bulk Nanostructured Thermoelectric Materials: Current Research and Future Prospects,” *Energy & Environmental Science*, 2:466–479.
2. Lan, Y.C., et al. 2010. “Enhancement of Thermoelectric Figure-of-Merit by a Bulk Nanostructuring Approach,” *Advanced Functional Materials*, 20:357–376.
3. Bhattacharyya, S. 2009. “Anomalous Thermoelectric Power in Conducting Amorphous Carbon Thin Films Incorporating a High Concentration of Nitrogen,” *J. Phys. D. Appl. Phys.*, 42:085407.
4. Tarasevich, Yu. Yu. 2002. *Percolation: The Theory, Applications, Algorithms.* URSS, p. 112 (in Russian).
5. Bergmann, D.J. and O. Levy. 1991. “Thermoelectric Properties of a Composite Medium,” *J. Appl. Phys.*, 70(11):6821-6833.

6. Kulbachinskii, V.A., et al. 2011. "Thermoelectric Properties of Bismuth Telluride Nanocomposites with Fullerene," *Semiconductors,* 45:1194-1198.
7. Faleev, S.V. and F. Léonard. 2008. "Theory of Enhancement of Thermoelectric Properties of Materials with Nanoinclusions," *Phys. Rev.,* 77:214304.
8. Kalinin, Y.E., et al. 2018. "Effect of Carbon on the Electrical Properties of Copper Oxide-Based Bulk Composites," *Phys. Solid State,* 60:681-690.
9. Pozdnyakov, B.S. and E.A. Koptelov. 1974. *Thermoelectric Power Engineering.* Atomizdat, p. 264 [in Russian].

2018 International Theoretical and Practical Conference on Alternative and Smart Energy (TPCASE 2018)
ISBN: 978-1-60595-617-6

Technical and Economic Analysis of the Gas Reduction Schemes

Oksana Medvedeva and Aleksander Chilikin

ABSTRACT

In the course of the work, an analysis of existing gas reduction schemes at the gas distribution stations was carried out. For development of an optimal reduction scheme, there was made a selection of equipment operating in the pressure range from 1,2 to 6,4 MPa with single-stage gas reduction. According to the results of the technical and economic calculation of each scheme, it was concluded that they should be used from the point of view of technological efficiency and economy. Gas reduction schemes are proposed for the study and use. They contain a regulator-monitor that performs the role of a redundant regulator and its use solves two problems at the same time—increasing the reliability of the gas reduction line and automating the throttling process.

INTRODUCTION

The relevance of the chosen subject is caused by the increasing pace of the natural gas use both in the field of household consumption (by expanding gas supply zone) and in the field of industrial consumption (introduction of the more complex technological processes), which significantly increases the requirements for failure-free and safe operation of the gas supply systems. Reliability issues and sustainability of the gas distribution systems directly influence the efficiency of transportation of the natural gas to the final consumer. Also, the fundamental factors should include the creation and maintenance of an optimal technological

Oksana Medvedeva, Yuri Gagarin State Technical University of Saratov, 77 Politekhnicheskaya Street, Saratov, 410054, Russia
Aleksander Chilikin, Gazprom Gazoraspredelenie Kirov, 4 Pugacheva Street, Kirov, 610035, Russia

state of the operational parameters of the gas distribution networks and gas-using equipment. The purpose of the study is assessment economic efficiency of the gas reduction schemes at the gas distribution stations on the basis of the amount of investment in the process of installation schemes, the cost of purchasing equipment and devices involved in the setup of the reduction lines.

Due to the geographical features of the territory of Russia, a single technological chain of the gas pipelines can run for many kilometers and pass through several climatic zones. The main costs are accounted for the transportation of the natural gas, so development of a new equipment, optimization of the schemes and methodical approach, as well as the issues of technical re-equipment still remain relevant. Technological reduction of the gas pressure at the gas distribution stations and the gas reduction points is implemented with the help of reducing valves and equipment, the main principle of which is the process of the gas throttling when an adjustable hydraulic resistance is generated on the way of moving the gas medium [1, 2].

SUBJECT AND RESEARCH METHODS

The regulator-monitor is configured for a specific range of input pressure values at which the automation operates [3]. In a steadily operating reduction line, regulator-monitor controls the level of inlet pressure and controls the main pressure regulator, while it is in a fully open state to skip the working medium. In a case of an emergency, regulator-monitor takes over the regulation function, or, otherwise, stops the gas flow through the reduction line. Regulator-monitor schemes use for a long time, but the absence of a shut-off valve was legislatively forbidden earlier.

Uninterrupted gas supply and, as a result, reducing the accident rate of the gas distribution systems, can mainly be achieved through various variations of the setup of the gas reduction points reduction unit, for clarity, the following variations can be demonstrated:

- Scheme 1—lock valves (LV), regulator-monitor, pressure regulator, LV, safety valves (SV).
- Scheme 2—LV, shut-off valves, regulator-monitor, pressure regulator, LV, SV.
- Scheme 3—LV, shut-off valves, regulator-monitor, pressure regulator, LV.
- Scheme 4—LV, regulator, controlled lock valves, LV, SV.

Consider in detail the basic setup schemes. Scheme 1 shows the simplest example of the regulator-monitor use. The main point of this scheme is a replacement the shut-off valve in the conventional setup of the reduction point with a regulator-monitor, which is enter into operation in a case of failure of the main pressure regulator. Operational principle is sequential installation of two

regulators on the reduction line. The main regulator operates in the normal mode, the regulator-monitor located in front of it and operates in the tracking and monitoring mode in the fully open position. Regulator-monitor has the same capacity and adjusted to a slightly higher output pressure than the main regulator. In the presented setup, it is necessary to choose a normally open type for the main regulator, and normally closed type for the regulator-monitor. When the main regulator fails, the pressure in the outlet collector rapidly grows, while the pressure of the regulator-monitor is set, it starts working, thus uninterrupted gas supply becomes possible. In this scheme, a two-stage consumer protection is implemented only against an emergency pressure increase. The disadvantage of this scheme is the lack of consumer protection from pressure drop in the networks, therefore it can be applied only if there is another step down behind the gas reduction points, equipped with a shut-off valves.

Scheme 2 can be used to provide three-stage consumer protection from both increasing and decreasing pressure. The main difference from Scheme 1 is the inclusion of a shut-off valve in its composition. Here there are measures of protection from both the pressure increase and its decrease, which is its main advantage. The main disadvantages of this scheme are the increased demands on the accuracy of monitoring the pressure regulator and the ability to switch the gas supply from the main line to the backup manually only.

In cases where a three-stage protection is not required, but it is necessary to provide pressure drop protection, Scheme 3 is used, which does not have a safety valve in its composition. This option is less demanding on the pressure regulators, in particular, on the regulation accuracy, since the setting range is not limited by the operation threshold of the safety valve. The scheme has the same advantages and disadvantages as Scheme 2. Currently updated documentation prescribes use of at least two reduction lines (at least one main and one backup) at the reduction points, and the submitted schemes represent variations of only one reduction line. Thus, if you follow the regulations of the standard literature, the scheme of the reduction point should have the form shown in Scheme 4. The scheme itself is one of the many variants of the functional scheme of the reduction point with the use of the regulator-monitor.

The schemes, using regulator-monitor, have different requirements for themselves, one of the main ones is the increased regulation accuracy. Consider this fact, in scheme 4 (without a safety valve) it is possible to implement the requirements of standard documents in terms of setting up the main regulator and the redundant line regulator to automatically switch the reduction point from the main line to the backup one. Thus, for Scheme 4, fourfold protection against pressure increase and decrease is carried out, while the pressure increase protection is carried out without stopping the supply of the gas to the consumer.

Scheme 5 (Figure 1) is one of the mostly promising setup variations of the reduction points with controlled shut-off valves, which are quick-acting valve. The main difference from the conventional scheme is that the shut-off valve is not

compulsory at all, since its function is performed by a quick-acting valve. In addition, in a case of an emergency, the quick-acting valve also automatically switches (without service personnel) from the main reduction line to the backup one. Compared to the shut-off valve, it has a different principle of operation: instead of mechanical (pneumatic) control, electric (more precisely, electronic) control is used. In this variation, the presence of a telemetry system as part of the equipment of the reduction point is imperative [4].

The basic principle of operation of this scheme is as follows: the telemetry system controller (equipped with pressure sensors) controls the quick-acting valves, automatical switch from the main to the backup reduction line is provided. In the normal mode, the lock valves on the main and backup lines operate in the open position, the quick-acting valves on the main reduction line is open, and on the backup one is closed; pressure control is performed by the main line regulator. In a case of pressure regulator failure, it either closes completely, and the pressure drops at the outlet, or ceases to reduce, and an abrupt increase in pressure occurs at the outlet.

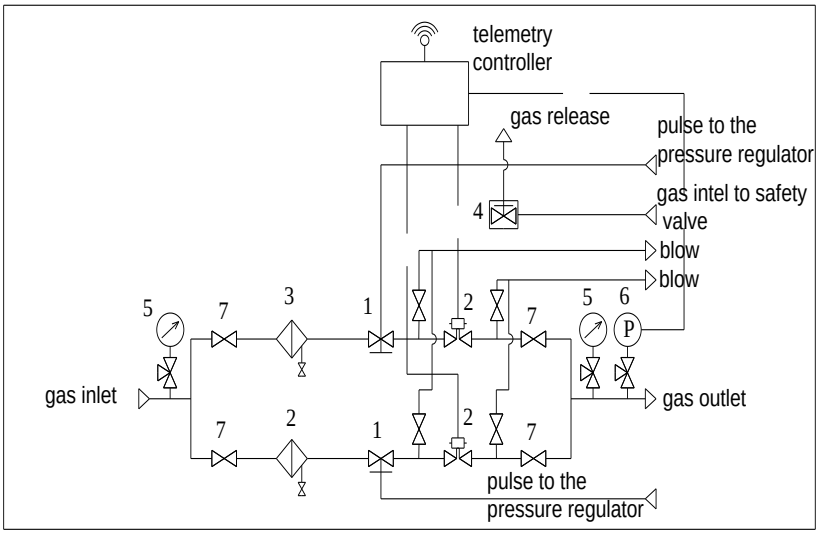

Figure 1. The gas reduction scheme 5: 1 – pressure regulator; 2 – redundant line regulator; 3 – regulator-monitor; 4 – shut-off valves; 5 – manometer; 6 – pressure meter; 7 – lock valves

The sensor records data on pressure changes, and subsequently transmits all information to the telemetry system. Then it gives commands to close the valve of the main line of reduction and open the valve of the backup line, thereby ensuring uninterrupted gas supply to the consumer. Advantages of this scheme: there are

no specific requirements for the type and characteristics of the regulators, the possibility of using reduction lines in parallel, the possibility of automatic transition from one line to another. The main disadvantage is the obligatory presence of a managing controller and dependence on an external power supply source. However, since there is a steady tendency to equip telemetry systems with almost all reduction points at facilities, that need uninterrupted gas supply, this disadvantage does not affect the reliability of the system, since it exists regardless of the product setup.

We will conduct comparative analysis of the five developed gas reduction schemes and one conventional schematic diagram consisting of a different combination of equipment.

The main comparative economic effect will be calculated on the basis of the formula below:

$$E=M_1-M_2=$$
$$=\left[\sum_{p=1}^{P} C_{b_1}\sum_{m=0}^{n}\alpha_{t-mt_0}+\sum_{p=1}^{P} C_{b_2}\sum_{m=0}^{n}\alpha_{t-mt_0}+\ldots+O_{b_1}\sum_{t=1}^{T}(1+E)^{-t}+O_{b_2}\sum_{t=1}^{T}(1+E)^{-t}\ldots\right]- \quad (1)$$
$$-\left[\sum_{p=1}^{P} C_{p_1}\sum_{m=0}^{n}\alpha_{t-mt_0}+\sum_{p=1}^{P} C_{p_2}\sum_{m=0}^{n}\alpha_{t\text{-}mt_0}+\ldots+O_{p_1}\sum_{t=1}^{T}(1+E)^{-t}+O_{p_2}\sum_{t=1}^{T}(1+E)^{-t}\ldots\right]$$

where M_1 and M_2 are the integral costs of the basic and proposed options; C_{b1}, C_{p1} are the capital investments in the element according to the basic and proposed options, m is the number of the next capital investment; n is the number of the regular capital investments (the number of replacements of a piece of equipment during the service life of the system); t is the year of the next capital investment; t_0 is the element service life, years; α - capital investment efficiency ratio, 1/year; Ob_1, Op_1 are the operational costs for the maintenance, energy resources according to the basic and proposed options, respectively, ₽ per year; t is the year of operation; T is valve service life, years; E is discount rate, 1/year, is taken to be equal to the average credit rate of a bank in a market economy.

The service life of the elements in the compared variations is taken according to the data received from the equipment supplier.

RESULTS AND CONCLUSIONS

Calculations were carried out for all considered reduction schemes, the results are summarized in Table I. As follows from the economic effect indicators presented in Table I, proposed gas pressure reduction schemes have advantages over the conventional scheme. The most effective are the schemes 1÷3, but it

should be noted that these schemes have a narrow applicability to the gas distribution stations, since they have only one line of reduction.

Schemes 4 and 5 have a lower economic effect, but, compared to the others, provide a much greater level of reliability and failure-free reduction lines. From the point of view of the safety of the maximum economic output of the system, it is advisable to use scheme 1, to ensure maximum safety of operation of the gas reduction unit, scheme 4 is proposed for usage.

During calculation process the investment in the installation of the reduction line, the main costs accounted for the regulator-monitor. The increased cost of this equipment is caused by its wide functionality, and the lack of analogues in the domestic market. Calculations showed the effectiveness of the use of this regulator by reducing investment in automation, as well as measures to improve the safety of the gas reduction system.

Based on calculation results, it is possible to draw conclusion about the economic and practical effectiveness of the proposed options for the reduction lines compared to the conventional reduction scheme in operation.

TABLE I. ECONOMIC EFFECT OF THE PROPOSED SOLUTIONS ON THE CONVENTIONAL SCHEMATIC DIAGRAM.

Comparison with a conventional scheme	***E*, ₽ Economic effect**	**Δ%, in a relative term**
Scheme 1	325800	18
Scheme 2	300600	17
Scheme 3	285900	16
Scheme 4	-	-
Scheme 5	120560	12

The first three schemes are single-stage lines of reduction, with no backup line of reduction. It significantly reduces the cost of installation and operation of the system, but the main level of system security is achieved mainly through the use of the regulator-monitor. During operation, the monitor periodically traces the pressure level after the main regulator, and, if necessary, automatically adjusts or stops the gas supply. The fourth scheme is the most costly gas reduction line. It caused by the presence of the backup devices, as well as a backup line of reduction, designed for 100% power from the main line. In a case of an emergency, cleaning or replacement equipment, the flow of the transported medium can be directed through a backup line, without a loss of efficiency and performance of the reduction line, for a long time. The safety of the proposed scheme is caused by existence of several regulator-monitors, which allows several lines to have the same automation level, and, in fact, makes them independent of each other.

The fifth scheme is a compromise between capital costs and the operational safety of the gas reduction line at the gas distribution stations. Profitability and efficiency of the scheme is achieved due to the difference of the equipment used

in the main and backup lines, without losing the level of system efficiency. In the main line of reduction, the input pressure adjustment in the automatic mode is performed by the regulator- monitor. The pressure regulator, previously set to the calculated inlet pressure values, is installed in the backup reduction line. The backup line of reduction is designed for 100% efficiency from the value of the main line, but the process of manual regulation of the main reducing device reduces the safety of this line in comparison with the main one.

According to obtained comparisons of the economic effects, it can be concluded that, from the investment point of view, scheme 1 is the most profitable, however, scheme 5, which has a difference of 6%, shows the best result in assessing uninterrupted gas supply. Scheme number 5 suits the required automation level of the process of reduction. The main perspective task is development of more compact equipment, and the domestic analogue of the regulator-monitor. Domestic development will reduce the cost of transporting and manufacturing the product, as well as reduce the time and resources required to supply the product to the place of installation of the gas reduction scheme. Such developments, in the future, can significantly improve technical and economic indicators and, consequently, the effectiveness of the proposed schemes.

REFERENCES

1. Lapshin, V.I., A.N. Volkov, and I.M. Shafiev. 2013. "Analytical and Experimental Assessment of the Moisture Capacity of Natural Gases and the Effect of Condensation Water on the Phase Characteristics," *Vesti gazovoy nauki*, 1:79-85.
2. Medvedeva, O.N., A.S. Polyakov and A.V. Kochetkov. 2017. "Technical Solutions for the Reduction of Natural Gas at Gas Distribution Stations" *Chemical and Oil and Gas Engineering*, 7:33-37.
3. Karyakin, E.A., et al. 2013. *Industrial Gas Equipment:a Guide*. Saratov: Gazovik, p. 1280.
4. Medvedeva, O.N., A.V. Zhmurov, and A.S. Polyakov. 2014. "Justification of Gas Reduction Schemes for Gas Distribution Stations," *Scientific Bulletin of the Voronezh State University of Architecture and Civil Engineering. Construction and Architecture*, 4(36):39-44.

2018 International Theoretical and Practical Conference on Alternative and Smart Energy (TPCASE 2018)
ISBN: 978-1-60595-617-6

Large Eddy Simulations of Turbulent Flows at Supercritical Pressure in a Vertical Heated Pipe Using Unstructured Cartesian Grids with Local Refinement

Valery Artemov, Maksim Makarov, Konstantin Minko and Georgy Yankov

ABSTRACT

This paper presents the results of numerical simulation of turbulent flow of CO_2 at supercritical pressure (SCP) in a uniform heated vertical tube using the large eddy simulation (LES) with the Smagorinsky subgrid scale (SGS) model. Unstructured Cartesian grids with local anisotropic refinement were used for modeling hydrodynamics and heat transfer in a circular pipe. Such grids unlike structured grids in cylindrical coordinates allow one to construct more optimal meshes for the LES method. In addition, such meshes allow one to simulate flows in channels of arbitrary cross-section. To verify the proposed methodology the results of the direct numerical simulation were used. Numerical simulations have been performed using the "in-house" CFD code ANES.

INTRODUCTION

During the last decades, the problem of development of the nuclear power plants with supercritical pressure (SCP) water is intensely discussed [1]. Single-circuit plant layout with a nuclear reactor cooled by SCP water, delivery to a turbine of slightly activated steam of 25 MPa/540°C parameters, and steam reheating make it possible to reach a thermal efficiency that is close to that of the thermal power plants burning fossil fuels. Due to using pseudo phase transition heat (~1400 kJ/kg) and reducing the water flow rate through the reactor, the dimensions of the equipment and the plant as a whole can be substantially decreased and a considerable gain in capital cost can be obtained.

National Research University "Moscow Power Engineering Institute", 14, Krasnokazarmennaya Street, Moscow, 111250, Russia

Therefore it is very important to use the computer simulation of hydrodynamics and heat transfer to SCP water in the channels of the nuclear reactor in different operation conditions for safety substantiation at the stage of pre-design studies of new generation nuclear power plants. At present computer simulations of turbulent heat transfer in channels are used different approaches which based on: the Reynolds averaged Navier-Stokes equations (RANS), large-eddy simulation (LES), direct numerical simulation (DNS) of turbulence, and various hybrid methods (RANS+LES).

In most cases, results obtained using RANS models are quite satisfactory for practical purposes. However, for liquids with highly variable properties (typical representatives of which are the SCP coolants), RANS models do not allow to obtain reliable data for the regimes with a strong deterioration of heat transfer. In this sense very revealing the work S.H. Kim et al. [2], in which 14 popular models for the turbulent viscosity was used for heat transfer simulations of water upward flow in the heated pipe with performance parameters corresponding to the experiments of K. Yamagata et al. [3]. Although there were no regimes with a strong deterioration of the heat transfer, 10 models have shown quite unsatisfactory results, other models have led only to qualitative agreements.

There are several works [4,5,6] in which the DNS methods were used for predicting turbulent heat transfer to SCP CO_2 in a vertical tube for the inlet conditions Re_0=5400, P_0=8MPa, T_0=301.15 K and the length of the tube L/d=30 (d – the diameter of the tube). In these works, structural meshes were used with numbers of cells about $7\cdot10^6$ in [4], $62\cdot10^6$ in [5] and $6.3\cdot10^6$ in [6]. As follows from the comparison of the results of J. Bae et al. [4], H. Nemati et al. [5] and J. Yan et al. [6] for two regimes (marked «B» and «C» in [4]) noticeable differences in wall temperature were observed.

In the present paper, the results of simulation of the «B» and «C» cases from [4] using the LES method for unstructured Cartesian grids with local refinement [7], implemented in the "in-house" CFD code ANES [8] are compared with DNS date [4–6].

COMPUTATIONAL DETAILS

Three-dimensional non-steady equations of the LES [9], written in the dimensionless form in the Cartesian coordinate system were used. For low-speed internal flows, the compressibility effects and viscous dissipation in the energy equation may not be considered (low Mach-number assumption).

The Smagorinski subgrid scale (SGS) model [10] with the damping function of U. Piomelli et al. [11] was used:

$$\nu_{sgs} = \left(C_s \Delta V^{1/3}\right)^2 \left\{1 - \exp\left[-\left(y^+/25\right)^3\right]\right\} \sqrt{2 S_{i,k} S_{i,k}}\,,$$
$$y^+ = u_\tau\, y/\nu\,,\ u_\tau = \sqrt{\bar{\tau}_w/\rho}, \qquad (1)$$

$$S_{i,k} = 0.5\left(\partial u_i/\partial x_k + \partial u_k/\partial x_i\right),\ \bar{\tau}_w(z,\tau) = \int_P \tau_w dP\,,$$
$$C_s = 0.1,\ \mathrm{Pr}_{sgs} = 0.85\,, \qquad (2)$$

where ν, ν_{sgs} – the molecular and subgrid turbulent viscosities, u_i – the velocity components, ρ – the density, y – the distance from the wall, P – the perimeter of the tube, ΔV – the cell volume, τ_w – the shear stress in the wall.

The unstructured Cartesian grid is shown in Figure 1.
The number of cells in cross-section (x,y) was N_{xy}=8970. A uniform grid with the number of cells N_z=300 was used along z-axis. The total number of cells was equal to N_{cv}=2.69 million. The dimensionless sizes of the cells were: $\Delta x^+ = \Delta y^+ < 1.5$ near the wall, $\Delta x^+ = \Delta y^+ = 12.2$ near the center of the tube and $\Delta z^+ = 36$ along z-axis. Note that near the pipe wall, there was a layer of fractional cells with the coordinates of the nodal points y^+<0.7.

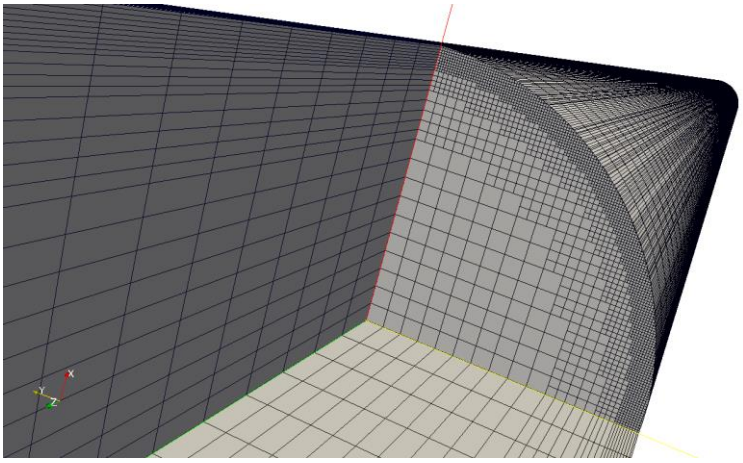

Figure 1. Unstructured Cartesian grid.

Time derivatives were calculated using the second order three-layer scheme. Spatial derivatives were approximated using the modified second order central-difference scheme which was protected from divergence by special algorithms. To solve the equations of hydrodynamics, a combination of SIMPLE and PISO algorithms was used, which made it possible to carry out the calculations without low relaxation and with a relatively small number of iterations at a time step. The dimensionless time step ($\Delta\tau$ = 0.01...0.02) was chosen from the condition that the Courant criterion is equal to 0.5. To set the turbulent content at the entrance to the pipe, the PIG (Periodic Inlet Generator) of the ANES code was used. The algorithms of PIG and input turbulence generators in [4-6] are similar. The quality of the generated turbulent content is shown in Figure 2.

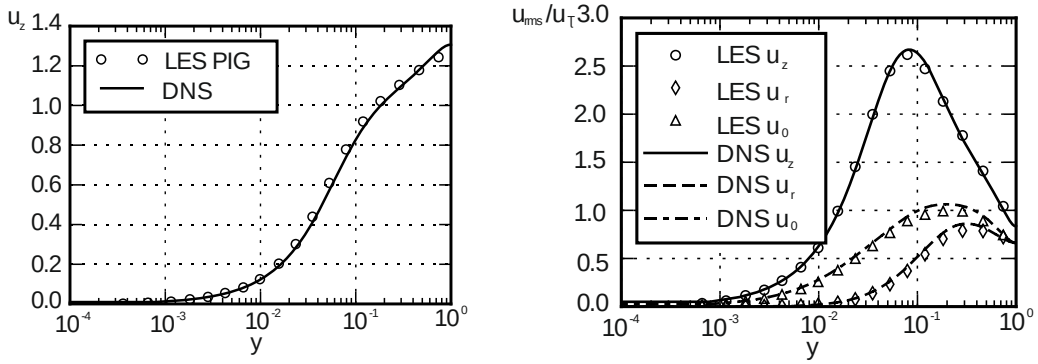

Figure 2. Comparison of the time-averaged axial velocity and the velocity components fluctuations with DNS data [12] for a fully developed flow in a circular pipe with $Re_\tau = u_\tau R/\nu = 180$ (R is the radius of the tube). Lines: DNS data; symbols: present work.

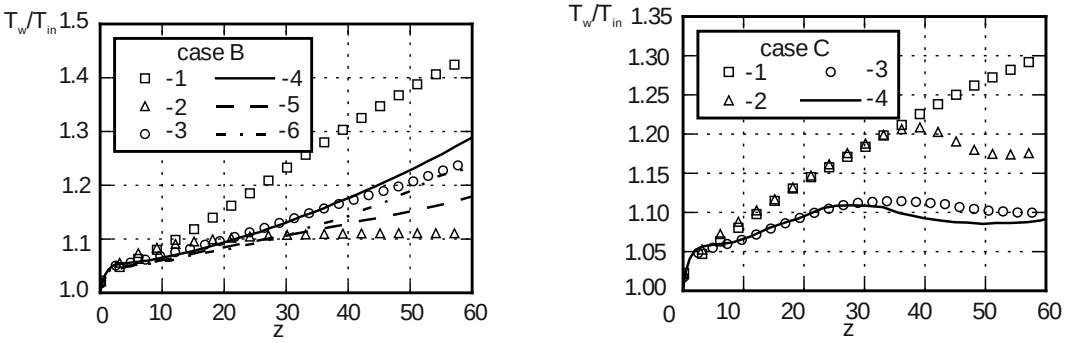

Figure 3. Comparison of streamwise mean dimensionless temperature of the wall along the pipe for cases B and C with DNS data [4-6]. Present work: 1–LS, 2-SST, 3–LES; DNS data: 4– [4], 5–[5], 6-[6].

RESULTS

Two cases from [4] were chosen for numerical simulation: case B with mass flux – 333.24 kg/(m^2s); heat flux – 61.74 kW/m^2; diameter of the tube – 1.0 mm and case **C** with mass flux – 166.62 kg/(m^2s); heat flux – 30.87 kW/m^2; diameter of the tube – 2.0 mm. The NIST REFPROP database was used for properties [13].

Figure 3 shows a comparison of the dimensionless mean wall temperature with the DNS data [4-6]. Figure 3 also shows the results of the present work performed by using RANS method with two popular models for turbulent viscosity: Launder-Scharma (LS) and SST.

As noted in the work [5] the main discrepancies between the results of work [5] and that of work [4] are different mesh resolution, fluid property databases, and numerical schemes. Note that the authors of [6] used the same database for properties, as in [5], but obtained noticeable differences in the results from the data of [6]. At the same time, as noted in [6], an increase in mesh resolution does not change the results. The data of the present paper are in good agreement with the results of [4, 6]. LS and SST turbulence models did not allow to obtain realistic results for considered cases. The authors [14] came to a similar conclusion regarding the LS model.

CONCLUSION

The above simulation results show that the LES with the Smagorinsky SGS model and Piomelli damping function can be used for prediction the turbulence flow of a supercritical coolant and deterioration due to buoyancy effect.

ACKNOWLEDGEMENT

The work was supported by the Russian Foundation for Basic Research (project #16-08-00981-a, #17-08-01007-a).

REFERENCES

1. Oka, Y. 2003. “Research and Development of the Supercritical—Pressure Light Water Cooled Reactors,” presented at the 10-th Intern. Topical Meeting on Nuclear Thermal Hydraulics, NURETH-10, Seoul, Korea, 2003.
2. Kim, S.H., Y.I. Kim, Y.Y. Bae, and B.H. Cho. 2004. “Numerical Simulation of the Vertical Upward Flow of Water in a Heated Tube at Supercritical Pressure,” *Proc. of ICAPP’04*, presented at Pittsburg, USA, June 13 – 17, 2004, paper 4047.
3. Yamagata, K., K. Nishikawa, S. Hasegawa, T. Fujii, and S. Yoshida. 1972. "Forced Convective Heat Transfer to Supercritical Water Flowing in Tubes, "*International Journal of Heat and Mass Transfer*, 15(12): 2575-2593.

4. Bae, J.H., J.Y. Yoo, and H. Cho. 2005. “Direct Numerical Simulation of Turbulent Supercritical Flows with Heat Transfer,” *Physics of Fluid*, 17:105104-1-105104-24.
5. Nemati, Hassan, Ashish Patel, Bendiks Jan Boersma, and Rene Pecnik. 2015. "Mean Statistics of a Heated Turbulent Pipe Flow at Supercritical Pressure, "*International Journal of Heat and Mass Transfer*, 83:741-752.
6. Yan, J., W. Wang, P. Jiang, and S. He. 2018. “Direct Numerical Simulation of Convective Heat Transfer in a Vertical Pipe for Supercritical Pressure CO2”, presented at the 16th International Heat Transfer Conference, Beijing, China, August 10-15, 2018.
7. Artemov, V.I., M.V. Makarov, K.B. Minko, and G.G. Yankov. 2017. "Large Eddy Simulations of Air Flow in a Vertical Heated Pipe Using Unstructured Cartesian Grids with Local Refinement," *Journal of Physics: Conference Series*, 891(1):012087.
8. “CFD code ANES.” Available at: http://anes.ch12655.tmweb.ru.
9. Sagaut, P., 2002. *Large Eddy Simulation for Incompressible Flows*. Berlin: Springer Heidelberg.
10. Smagorinsky, J. 1963. "General Circulation Experiments with the Primitive Equations: I. The Basic Experiment," *Monthly Weather Review*, 91(3):99-164.
11. Piomelli, U., T.A. Zang, C.G. Speziale, and M.Y. Hussaini. 1990. "On the Large Eddy Simulation of Transitional Wall Bounded Flows, "*Physics of Fluids A: Fluid Dynamics*, 2(2):257-265.
12. Khoury, E., K. George, P. Schlatter, A. Noorani, P.F. Fischer, G. Brethouwer, and A.V. Johansson. 2013. "Direct Numerical Simulation of Turbulent Pipe Flow at Moderately High Reynolds Numbers," *Flow, Turbulence and Combustion*, 91(3):475-495.
13. Lemmon, E.W., M. L. Huber, and M.O. McLinden. 2013. "NIST Standard Reference Database 23: Reference Fluid Thermodynamic and Transport Properties-REFPROP, Version 9.1, National Institute of Standards and Technology, Standard Reference Data Program, Gaithersburg." Available at: http://www.nist.gov/srd/nist23.cfm.
14. He, S., W.S. Kim, and J.H. Bae. 2008. "Assessment of Performance of Turbulence Models in Predicting Supercritical Pressure Heat Transfer in a Vertical Tube," *International Journal of Heat and Mass Transfer*, 51(19-20):4659-4675.

2018 International Theoretical and Practical Conference on Alternative and Smart Energy (TPCASE 2018)
ISBN: 978-1-60595-617-6

Simulation of Generator Transients with Asymmetry of Stator Phase Circuits

Igor Alferov, Nikolay Mitrofanov and Gleb Glazyrin

ABSTRACT

Transient processes of a synchronous machine operating on a load with a delta connection circuit are considered. A method is proposed for numerical simulation of transient processes of a synchronous machine with the possibility of taking into account the asymmetry of the stator winding. The model was verified by comparing the results of the calculation of generator transients with an asymmetrical stator winding, obtained using the developed model and using the MATLAB Simulink tools.

INTRODUCTION

Existing software packages for modeling transient processes in electric power systems, such as MATLAB Simulink [1], PSCAD, Mustang, are used to describe electromagnetic processes in a synchronous machine of the Park—Gorev equation [2] and, accordingly, cannot be used to calculate processes in a damaged synchronous machine. a machine with different parameters of phase windings. VF Sivokobilenko [3] (calculation of a synchronous machine with the rotor of the machine taking into account multi-circuit circuits) and S. A. Kharitonov [4] (description of electromagnetic transients in systems for generating electric energy for autonomous objects) are actively involved in practical methods for calculating transients of a synchronous machine.

As a result of the study, a system of differential equations describing transients of a three-phase synchronous machine with regard to individual active resistances and windings inductances is derived. Also, a comparison was made of

Novosibirsk State Technical University, 20, Prospekt Karla Marksa, Novosibirsk, 630073, Russia

the simulation results of the transient processes of a synchronous machine made using the library SimPowerSystems, which is part of the MATLAB Simulink environment, with the results obtained using the proposed method.

INITIAL EQUATIONS THAT CHARACTERIZE THE OPERATION OF A SYNCHRONOUS MACHINE

Consider a synchronous machine with three-phase windings, an excitation circuit, as well as one longitudinal and one transverse damping windings.

Denote by u_η $(\eta = a, b, c)$ and u_f – instantaneous voltages on the phase windings and the excitation winding, respectively; i_η and i_f – instantaneous currents; ψ_η and ψ_f – resulting winding flux couplings; R_η and R_f – active resistance of the phase windings and the excitation winding. Then the differential equilibrium equations and voltage drops in the contours of a synchronous machine will have the form [1]:

$$\begin{cases} u_\eta = -\dfrac{d\psi_\eta}{dt} - R_\eta i_\eta \quad (\eta = a, b, c); \\ u_f = \dfrac{d\psi_f}{dt} + R_f i_f . \end{cases} \tag{1}$$

In addition, the system of differential equations (1) should be supplemented with equilibrium equations of electromotive force (EMF) and voltage drops in the damper circuits:

$$\begin{cases} 0 = -\dfrac{d\psi_{yd}}{dt} - R_{yd} i_{yd}; \\ 0 = -\dfrac{d\psi_{yq}}{dt} - R_{yq} i_{yq}, \end{cases} \tag{2}$$

where ψ_{yd} and ψ_{yq} – the resulting flux linkage of the longitudinal and transverse damping windings, respectively, R_{yd} and R_{yq} – their active resistance, i_{yd} and i_{yq} – instantaneous values of currents in the damper circuits.

The proposed method for calculating transients is based on the joint solution of equations (1) and (2), supplemented by expressions of voltage drops on the load resistance. This approach makes it possible to simulate a synchronous machine with different parameters of phase windings by describing electromagnetic processes in each phase by a separate differential equation.

The simplest resulting differential system of equations is obtained in the case of connecting a star-shaped load with a neutral wire without resistance [6]: it suffices to replace u_η on $L_{\text{ng.}\eta}\left(di_\eta / dt\right) + R_{\text{ng.}\eta} i_\eta$ in equation (1).

DERIVATION OF A SYSTEM OF DIFFERENTIAL EQUATIONS FOR A GENERATOR OPERATING ON AN AUTONOMOUS LOAD WITH A DELTA CONNECTION SCHEME

As a matter of fact, the power distribution schemes of power plants provide for the operation of generators with insulated neutral (without neutral wire). As a rule, the generator is connected to the winding of a step-up transformer connected in a "delta". For accurate calculation of transients in such schemes, it is necessary to simulate both the generator and the transformer, which greatly complicates the mathematical calculations. The paper considers the case of generator operation for an autonomous load, connected according to the "triangle" scheme, figure 1. The calculation is based on the algorithm proposed by [5].

When calculating the operating modes of a generator operating on an autonomous active-inductive load connected in a "triangle" scheme, the following transformations should be taken into account, in which u_k $(k = ab, bc, ca)$ – instantaneous values of linear voltages at the terminals of the synchronous machine; i_k – instantaneous linear current values:

$$\begin{cases} u_{ab} = u_a - u_b; \\ u_{bc} = u_b - u_c; \\ u_{ca} = u_c - u_a; \end{cases} \tag{3}$$

$$\begin{cases} i_a = i_{ab} - i_{ca}; \\ i_b = i_{bc} - i_{ab}; \\ i_c = i_{ca} - i_{bc}. \end{cases} \tag{4}$$

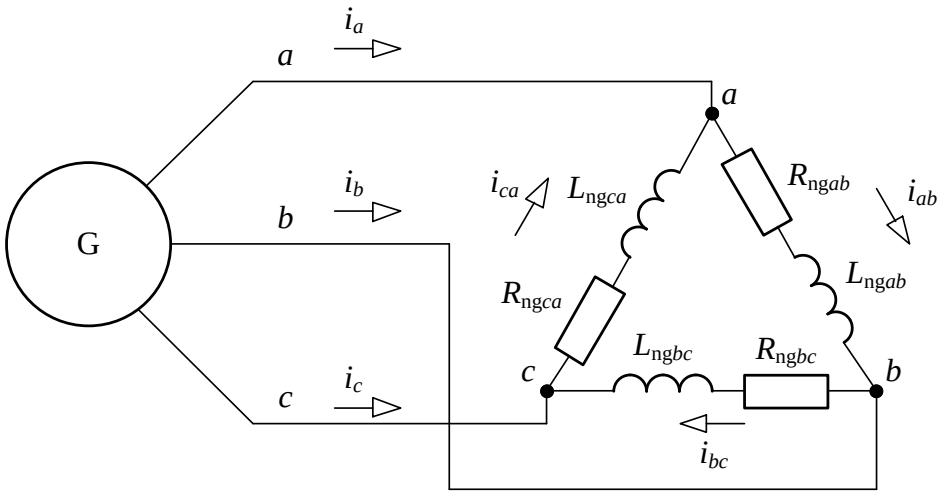

Figure 1. Load connection diagram.

Then the equilibrium EMF and voltage drops in the contours of a synchronous machine (1) will be defined as:

$$\begin{cases} u_{ab} = -\dfrac{d\psi_{ab}}{dt} - \left(R_{g.a} i_a - R_{g.b} i_b \right); \\ u_{bc} = -\dfrac{d\psi_{bc}}{dt} - \left(R_{g.b} i_b - R_{g.c} i_c \right); \\ u_{ca} = -\dfrac{d\psi_{ca}}{dt} - \left(R_{g.c} i_c - R_{g.a} i_a \right), \end{cases} \qquad (5)$$

where $R_{g.\eta}$ $(\eta = a, b, c)$ – active resistance of the phase winding circuit, u_k $(k = ab, bc, ca)$ – instantaneous values of linear voltages at the terminals of the synchronous machine, $\psi_{ij} = \psi_i - \psi_j$.

When calculating the operating modes of a generator operating on an autonomous active-inductive load connected in a "triangle" scheme, the system of differential equations takes the form:

$$\begin{cases} \dfrac{d\psi_{ab}}{dt} = -L_{n.ab}\dfrac{di_{ab}}{dt} - \left[\left(R_{g.a} + R_{g.b} + R_{n.ab}\right)i_{ab} - R_{g.a}i_{ca} - R_{g.b}i_{bc}\right]; \\ \dfrac{d\psi_{bc}}{dt} = -L_{n.bc}\dfrac{di_{bc}}{dt} - \left[\left(R_{g.b} + R_{g.c} + R_{n.bc}\right)i_{bc} - R_{g.b}i_{ab} - R_{g.c}i_{ca}\right]; \\ \dfrac{d\psi_{ca}}{dt} = -L_{n.ca}\dfrac{di_{ca}}{dt} - \left[\left(R_{g.c} + R_{g.a} + R_{n.ca}\right)i_{ca} - R_{g.c}i_{bc} - R_{g.a}i_{ab}\right]; \\ \dfrac{d\psi_{f}}{dt} = u_{f} - R_{f}i_{f}; \\ \dfrac{d\psi_{\mathrm{yd}}}{dt} = -R_{\mathrm{yd}}i_{\mathrm{yd}}; \\ \dfrac{d\psi_{\mathrm{yq}}}{dt} = -R_{\mathrm{yq}}i_{\mathrm{yq}}, \end{cases} \tag{6}$$

where $R_{n.k}$ – load resistance $(k = ab, bc, ca)$, $L_{n.k}$ – load inductance.

Entering the assumption of linearity of the relationship between the windings flux couplings and the currents flowing in them, as well as performing some transformations of the system (6), we obtain the following system of equations in a matrix form:

$$\begin{bmatrix} L_{ab\Sigma} & M_{.ab.e} & M_{ca.e} & M_{abf} & M_{abyd} & M_{abyq} \\ M_{.ab.e} & L_{bc\Sigma} & M_{bc.e} & M_{bcf} & M_{bcyd} & M_{bcyq} \\ M_{ca.e} & M_{bc.e} & L_{ca\Sigma} & M_{caf} & M_{cayd} & M_{cayq} \\ M_{abf} & M_{bcf} & M_{caf} & L_{f} & M_{fyd} & 0 \\ M_{abyd} & M_{bcyd} & M_{cayd} & M_{fyd} & L_{\mathrm{yd}} & 0 \\ M_{abyq} & M_{bcyq} & M_{cayq} & 0 & 0 & L_{\mathrm{yq}} \end{bmatrix} \times$$

$$\times \begin{bmatrix} di_{ab}/dt \\ di_{bc}/dt \\ di_{ca}/dt \\ di_{f}/dt \\ di_{\mathrm{yd}}/dt \\ di_{\mathrm{yq}}/dt \end{bmatrix} = \begin{bmatrix} -(\partial\psi_{ab}/\partial\gamma)\omega - u_{\Sigma ab} \\ -(\partial\psi_{bc}/\partial\gamma)\omega - u_{\Sigma bc} \\ -(\partial\psi_{ca}/\partial\gamma)\omega - u_{\Sigma ca} \\ -(\partial\psi_{f}/\partial\gamma)\omega - R_{f}i_{f} + u_{f} \\ -(\partial\psi_{\mathrm{yd}}/\partial\gamma)\omega - R_{\mathrm{yd}}i_{\mathrm{yd}} \\ -(\partial\psi_{\mathrm{yq}}/\partial\gamma)\omega - R_{\mathrm{yq}}i_{\mathrm{yq}} \end{bmatrix}, \tag{7}$$

where $L_{k\Sigma}$ $(k = ab, bc, ca)$ – own total inductances of the circuits, $M_{k.e}$ – equivalent mutual inductances of the circuits, $u_{\Sigma k}$ – instantaneous values of

voltage drops on active resistances of circuits, M_{kf}, M_{kyd}, M_{kyq} $(k = ab, bc, ca)$ – mutual inductance values of the excitation winding, longitudinal and transverse damping windings.

VERIFICATION OF THE IMPLEMENTED MODEL

As an example, for the comparison of models, calculations of transient processes of the TVV-200-2 generator with the full symmetry of the phase windings are performed.

The generator operation is considered in several modes: in a normal steady state under load, in idle mode and a three-phase short circuit on the generator terminals.

The results of calculations of a three-phase short circuit at the generator outputs during a three-phase short circuit at the generator terminals and its operation in the load mode using simulation by a numerical method and in the Simulink environment are shown in Figures 2 and 3.

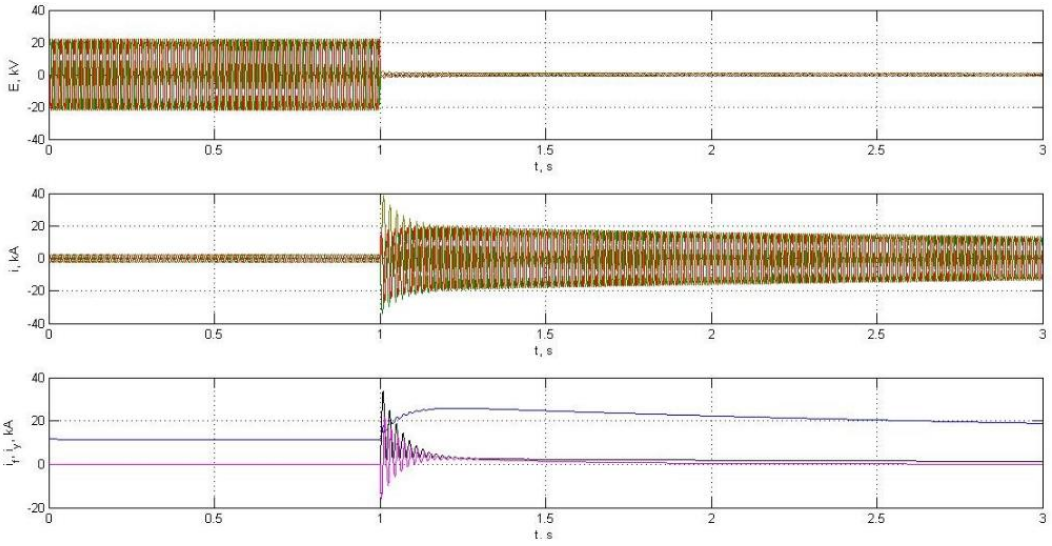

Figure 2. The results of calculations by a numerical simulation with a three-phase short circuit at the outputs of the generator and its operation in the load mode.

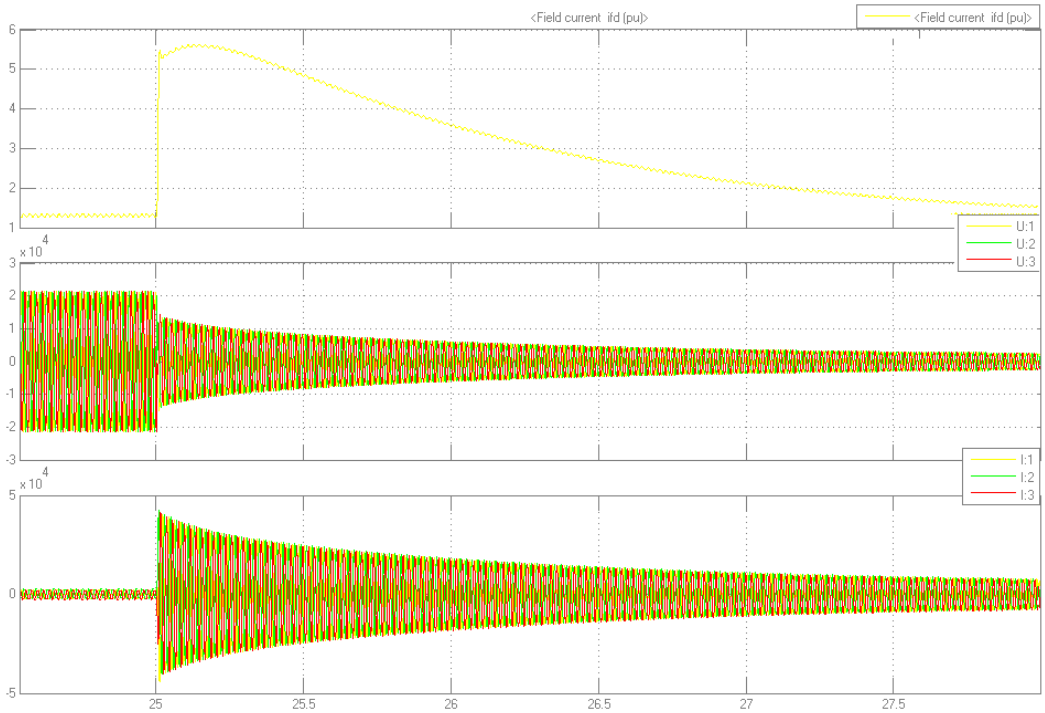

Figure 3. The results of calculations in the Simulink environment with a three-phase short circuit at the outputs of the generator and its operation in the load mode.

From a comparison of the results obtained with a three-phase short circuit at the generator terminals, it can be seen that in the numerical simulation method, the amplitude value of the shock short-circuit current $i_y = 38{,}4$ kA. When simulating a generator in MATLAB Simulink $i_y = 40{,}9$ kA.

The results of the comparison of the computational method and the model in the MATLAB Simulink environment obtained during the study with the symmetric phase circuits of the stator and without taking into account the saturation of the magnetic system showed the reliability of the proposed numerical simulation method. The implemented mathematical model makes it possible to consider the effect of the unbalance of the phase circuits of the stator and the saturation of the magnetic system in the simulation of a synchronous machine. In the future, the method will allow using the results of calculations of transient processes of a synchronous machine for analyzing the work and creating new algorithms for relay protection of generators of power plants.

REFERENCES

1. Chernykh, I.V. 2008. *Simulation of electrical devices in MATLAB. SimPowerSystems and Simulink*. M.DMK Press, 288 p.
2. Ulyanov, S.A. 1970. *Electromagnetic transients in electrical systems.* M.Energy, 518 p.

3. Sivokobyilenko, V.F. 2015. “Synchronous machine with a multi-loop rotor in phase coordinates,” *Technical electrodynamics*, (1):51–58.
4. Haritonov, S.A. 2011. *Processes in Power Generating Systems for Stand-Alone Units*. N.: NSTU. pp. 536.
5. Glazyirin, G.V. 2017. “Simulation of transient processes of a wind stator winding,” *Newsletter MEI*, (5):34–39.
6. Gorev, A.A. 1985. *Transient processes of a synchronous machine.* L: Science, pp. 502.

2018 International Theoretical and Practical Conference on Alternative and Smart Energy (TPCASE 2018)
ISBN: 978-1-60595-617-6

Energy-Saving Technologies in the Use of Heat Exchange Apparatuses with Turbulators

Anatoly Muravev, Igor Drozdov, Aleksandr Naumov, Aleksandr Nadeev and Yulia Vorobeva

ABSTRACT

In this paper, we consider measures to reduce the amount of deposits in heat exchange tubes and increase the intensity of heat exchange through the use of annular notches-turbulators in tubes of shell-and-tube heat exchangers.

INTRODUCTION

At present, at the enterprises of the energy complex and in the housing and communal services (HCS) there is an acute problem of the formation of deposits in heat exchange apparatuses (HEA). Deposits negatively affect the intensity of heat transfer and hydrodynamics, which leads to an increase in operating costs, as well as reduction in the efficiency of the device.

Recently, there has been an increasing interest in the method of reducing the amount of deposits on heat exchange surfaces due to the use of artificial turbulence of the coolant flow. The essence of this method boils down to the fact that the knurling of ring turbulators is performed along the entire length of the tube on its outer surface at certain intervals. Due to the use of additional grooves along the length of the tube, flow swirls are formed, which destroy the near-wall laminar sublayer. This helps to reduce the formation of deposits by preventing the sediment from attaching to the heat exchange surface and improving their entrainment by the coolant flow. In addition, the complication of the surface geometry of the tubes leads to an increase in heat transfer surface.

Voronezh State Technical University, 14, Moskovsky Avenue, Voronezh, 394026, Russia

DESCRIPTION OF THE DESIGN OF THE HEAT EXCHANGE APPARATUS

To conduct an experiment on the application of the above described method of reducing the number of deposits and intensifying heat exchange, two identical "shell-and-tube" heat exchangers were designed, the schematic diagram of which is shown in Figure 1. As heat exchange surfaces, tubes with annular turbulators applied to them were used, shown in Figure 2. The heating medium was saturated steam with a pressure of $P = 6$ atm. and temperature $t = 158\,°C$, located in the annular space. The heated medium was water located in a tube space with an inlet temperature of $t = 20$ °C. Technical indicators of water: hardness total. - 2.5 ml / eq / dm3, hardness Ca - 2.4 ml / eq / dm^3.

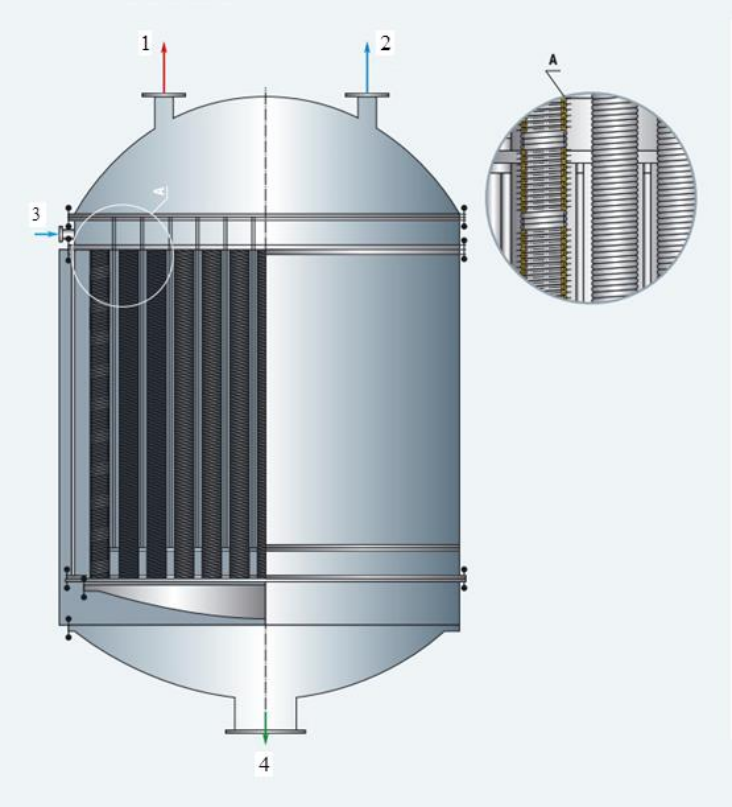

Figure 1. Heat exchanging apparatus design: 1 – hot water; 2 – cold water; 3 – vapour; 4 – condensate.

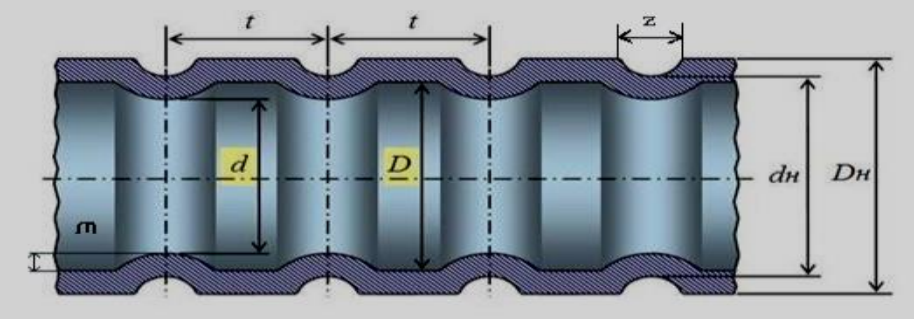

Figure 2. Longitudinal section of the tube.

Characteristics of the experimental tubes are presented in Table I.
External diameter of tubes $D = 19$ mm;
Internal diameter of tubes $d = 16$ mm;
Tube wall thickness $S = 1,5$ mm.

TABLE I. CHARACTERISTICS OF THE EXPERIMENTAL TUBES.

Test tube, No.	Tube material $D_н$, mm	Turbulator Step t, mm	Inner diameter of diaphragms d, mm	Groove depth of turbulator m, mm	d/D	t/D
1	1x18h10	-	-	-	-	-
2	Lo-70	-	-	-	-	-
3	Lo-70	2	14	1	0,875	0,125
4	1x18h10	4	15	0,5	0,937	0,25
5	Lo-70	4	14	1	0,875	0,25
6	1x18h10	4	12	2	0,75	0,25
7	Lo-70	8	14	1	0,875	0,5

EXPERIMENTAL RESEARCH ON A HEAT EXCHANGE APPARATUS

In the experiment, two heat exchangers were used. The first was operated in laminar, and the second - in the turbulent flow of the heated coolant. The total duration of all experiments was 2000 hours; 5 operating modes for each HEA were investigated. The purpose of the experiments was to determine the hydraulic resistance in the tubes, the flow rate of the heated coolant, the intensity of heat transfer and the influence of turbulators on the formation of deposits. After the experiment, the heat exchangers were disassembled, and the tubes were removed for detailed study using special means. The results of studies of the local distribution of sediments are presented in Figure 3 and in Table II.

TABLE II. THE RESULTS OF STUDIES OF THE LOCAL DISTRIBUTION OF SEDIMENTS.

Sample tubes, No.	Laminar mode Sediment thickness $\delta_н$, mm			Turbulent mode Sediment thickness $\delta_н$, mm		
	zone 1	zone 2	zone 3	zone 1	zone 2	zone 3
1	0,56			0,89		
2	0,59			0, 91		
3	0,78	0,86	0,82	0,49	0,57	0,56
4	0,82	0,87	0,84	0,49	0,55	0,52
5	0,83	0,86	0,84	0,48	0,54	0,51
6	0,81	0,85	0,83	0,48	0,53	0,5
7	0,83	0,81	0,86	0,53	0,49	0,56

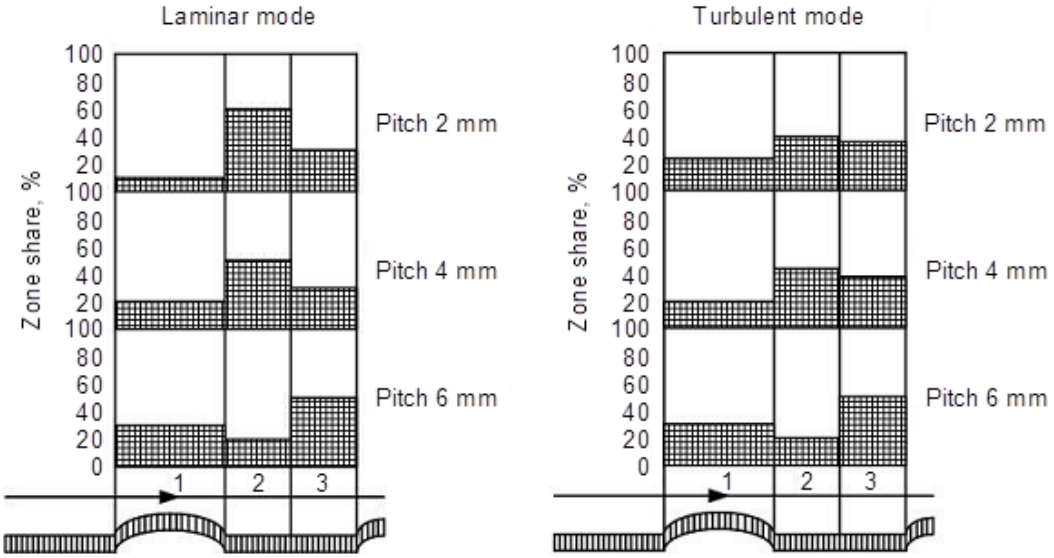

Figure 3. Percent sediment.

CONCLUSIONS

The results of the experiment showed that the use of tubes with turbulators in a heat exchange apparatus operating in a laminar mode is not effective, since tubes were subjected to greater fouling of deposits on the inner surface of heat transfer. Tubes with turbulators during turbulent operation of the heat exchanger, showed the opposite effect - there was a decrease in the amount of sediment. So the minimum value of sediment formation in the form of sediments was observed for pipes with turbulators in the ratio $m/d = 4 \cdot 10^3$ - $14 \cdot 10^3$. In sample No. 6, the amount of sediment was the lowest with a ratio of $d/D = 0,75$ и $t/D = 0,25$. Thus, the experiment confirmed theoretical studies in the field of heat and mass transfer, which is much less in tubes with turbulators than in smooth pipes, but

only under the condition of turbulent motion of the coolant. Again, almost all heat exchangers operate in the turbulent motion of the coolant, which confirms the relevance of their application. The use of rolled tubes in heat exchangers increases the service life of the plant, increases heat transfer, heat transfer and leads to an increase in heat transfer intensification. At the same time, the cost of rolling a single tube is 2-4% of its cost.

REFERENCES

1. Kopylov, A. S. 2003. *Water treatment in the energy sector*. Moscow: MAI Publishing House.
2. Dreitser, G. A. 1996. "Research on salt deposits in the flow of water with increased carbonate hardness in channels with discrete turbulators," *Thermal engineering*, 3: 30-35.
3. Klyuchkov, E. R. 1996. "Research on the formation of deposits on the fuel rods of water cooled reactors," *Thermal engineering*, 12: 52-54.
4. Drozdov, I. G., S. V. Dahin, E. R. Ogurtsova, A. B. Kuvaldin, and A. V. Muraviev. 2008."Electric heater of liquid type," License RU 77528, MPK H05B 6/40, published 10.20.2008.
5. Muraviev, A.V., I. L. Bataronov, and I. G. Drozdov. 2007. "Mathematical model of the formation process of deposits in the channels of heat exchangers," *Bulletin of the Voronezh State Technical University*, 3(8): 16-22.

2018 International Theoretical and Practical Conference on Alternative and Smart Energy (TPCASE 2018)
ISBN: 978-1-60595-617-6

Improving the Properties of Filled Gypsum Composites by Carbonization

Victoria Petropavlovskaya, Maria Zavadko, Kirill Petropavlovskii, Tatiana Novichenkova and Aleksandr Buryanov

ABSTRACT

Carbonization of modified composites based on gypsum binder has been proposed as a promising method for producing gypsum materials with high technical properties. To reduce costs and improve manufacturability, mineral modifiers are used in gypsum composites. Together with gypsum and lime the waste of basalt production is used. In contrast to other methods, the proposed carbonization during the formation of gypsum forms a gypsum stone, which has a reduced porosity. Of particular interest is the clogging of external pores, which communicate with the external environment. It is these pores that reduce the water resistance of gypsum composites. The formation of carbonate phases in the structure of gypsum stone will help improve the performance of the material. At the same time, the problem of preserving the natural environment for future generations is being solved. It also increases the economic and environmental attractiveness of the project.

INTRODUCTION

Gypsum binder finds increasing application in the construction industry. Materials based on them are safe and that their production does not require high temperatures [1], i.e. energy efficient. However, gypsum materials do not always meet the requirements of strength, and therefore research in this area remain relevant.

Victoria Petropavlovskaya, Maria Zavadko, Tatiana Novichenkova, Tver State Technical University, 22, Af. Nikitin, Tver, 170026, Russia
Kirill Petropavlovskii, Aleksandr Buryanov, Moscow State University of Civil Engineering (MGSU), 26, Yaroslavskoe shosse, Moscow, 129337, Russia

Explore the possibility of increasing the strength of gypsum materials through carbonation the work was dedicated.

Materials subjected to carbonation, not only safe, but also positively affect human health. Their positive impact on the environment describe the authors of work [1]. They talk about the need to create technologies that promote recycling of carbon dioxide from the atmosphere, and the benefits of such materials. Authors [2] describes the technology of manufacturing of paving stones, hardening in carbon dioxide environment. Such paving stones has increased strength characteristics. Other author discusses carbonization, as one of the factors for increase of compressive strength of concrete products and structures [3]. Also, the author draws attention to the considerable improvement in earthquake resistance of structures. The author of the work [4] says about improving seismic resistance too, but already porous concrete exposed to carbonation. A. A. Vahrushev [5] describes the process of making wall materials using forced carbonation. Carbonization promotes increase of compressive strength of finished products, with minimum energy consumption. I. Elkina [6] considers the influence of carbonation on strength properties of extruded waste rocks with cement and cement-limy binder. The author of the work notes the increasing speed of curing. Natural carbonation, as revealed by the authors of the works [7-8] to a lesser extent, affects the strength characteristics. Strength of such products, in view of time is stretched less CO_2. However, the use of such kind of carbonation for producing building materials also has a positive effect on the environment, promotes recycling gas from the atmosphere [9]. The author of the work [9] says about carbon dioxide, as a kind of additive-boosters. This supplement helps to accelerate curing. In addition, the author draws attention to the fact that the material past carbonation are biopozitive. These materials continue to absorb carbon dioxide indoors is already in operation. In article [10], the author focuses on describing the scientific principles of recycling carbon dioxide into building materials, gives recommendations.

METHODS

As the main component in the compositions of the raw mixes was used hemihydrate gypsum α-modification of the brand mark G-16, Samara gypsum plant (Samara, Russia). The gypsum binder of the brand mark G-16 was characterized by water demand of 36 %, start of setting – 5 minutes, end of setting –19 minutes, compressive strength - 16 MPa and bending – 7 MPa.

As source materials for research used waste production of basalt fibers in Tver region. Lime is used in the form of a saturated solution for mixing gypsum binder.

To obtain a saturated solution of lime required for molding the samples, ground lime was used according to GOST 9179. Water used for mixing lime was heated to 60 ° C in a 1: 3 ratio by weight. Within two hours, the mixture was

regularly stirred. Then the solution was allowed to settle until a solid precipitated and was filtered through a filter paper, after which it was ready for use.

To form cubic samples with a size of $0.02 \cdot 0.02 \cdot 0.02$ m, the gypsum binder in the dry state was mixed with a basalt additive for 30 seconds, after which it was shut with a saturated solution of lime and stirred for 60 seconds with a hand mixer until homogeneous mixes. Water-gypsum ratio was taken to correspond to the normal density, which was determined on the instrument-viscometer. The amount of basalt component in the composition of the mixtures was taken constant and amounted to 10% of the mass of the gypsum binder.

Hardening of the obtained samples was carried out in air-dry conditions for 20 minutes, after which the samples were unpacked and placed in an air-dry hardening chamber. In order to carry out forced carbonization, gypsum samples were kept in a chamber in carbon dioxide for 6 days. The average density and strength of gypsum samples-cubes were determined on the 7th, 14th, 28th day of hardening by standard methods. Water gypsum ratio was taken to correspond to normal density. The amount of basalt component in the composition of the mixtures was taken constant and amounted to 10% of the mass of the gypsum binder.

RESULTS AND DISCUSSION

In this work, we investigated the dependences of the density and ultimate compressive strength of gypsum on the composition of the raw mix and hardening conditions. The effect of exposure to carbon dioxide on the structure of gypsum composites based on pure gypsum, a mixture of gypsum and lime, as well as mixtures of gypsum, lime and industrial dust of basalt production has been studied.

The results of studies of the dependence of the physic-mechanical properties of modified gypsum composites on the composition and hardening conditions are shown in Figures 1, 2, 3. The obtained results showed that keeping in a chamber with carbon dioxide affects the compressive strength and density of the material. The studies found that the compressive strength of the samples exposed to carbonation, exceeds the compressive strength of the control samples more than 32 %. In the first case, the compressive strength was 36 MPa, in the case of a specimen – 24 MPa (Figure 1).

The increase in strength after carbonization is noted for a composition based on gypsum with the addition of lime and for a composition based on gypsum, lime and basalt waste.

Plaster-based compositions with waste additive, which did not undergo carbonization, showed the lowest strength. Their strength is reduced compared with gypsum-based specimens by 25%. This is due to the mineral composition of the waste, the presence of chlorides, which affect the processes of structure

formation, the nature of the crystallization of gypsum, its water demand. Thus, the use of waste did not show positive results.

However, when added to a composition based on gypsum with the addition of lime waste, an increase in strength over the strength of a control composition based on gypsum is noted. After aging such a composition in an environment of carbon dioxide, an increase in strength occurs, but small. Therefore, forced carbonation is effective for gypsum formulations with lime. As a result of the interaction of the components of the mixture and carbon dioxide, carbonate compounds are additionally formed. They contribute to the hardening of the structure. The presence of aluminum compounds in the waste contributes to the formation of hydroaluminates [11]. Compaction of the structure of gypsum composites with the introduction of additives and carrying out carbonization is confirmed by density studies.

The dependence of the density on the composition of the raw mix and hardening conditions is similar to the dependence on compressive strength. The density of the samples subjected to carbonization was the highest and amounted to 1561.1 kg / m3. The density of the control samples - 1497.2 kg / m3.

It should also be noted that in the first 7 days the most intensive hardening of the modified composite occurs, the compressive strength reaches 23.97 MPa, in the following periods - up to 14 days - the compressive strength increases by another 7 MPa, then the compressive strength gain is negligible. This is caused by the attenuation of hydration processes in the gypsum composite. The combined effect of carbonization and hydration on the compressive compressive strength is shown in Figure 3. The contacts of the intergrowth of crystalline tumors of dihydrate and carbonate are compressive strengthened, and there are prerequisites for compaction and hardening of the crystal structure. The structure of a gypsum stone is characterized by the presence of a prismatic, partially elongated form of gypsum crystals.

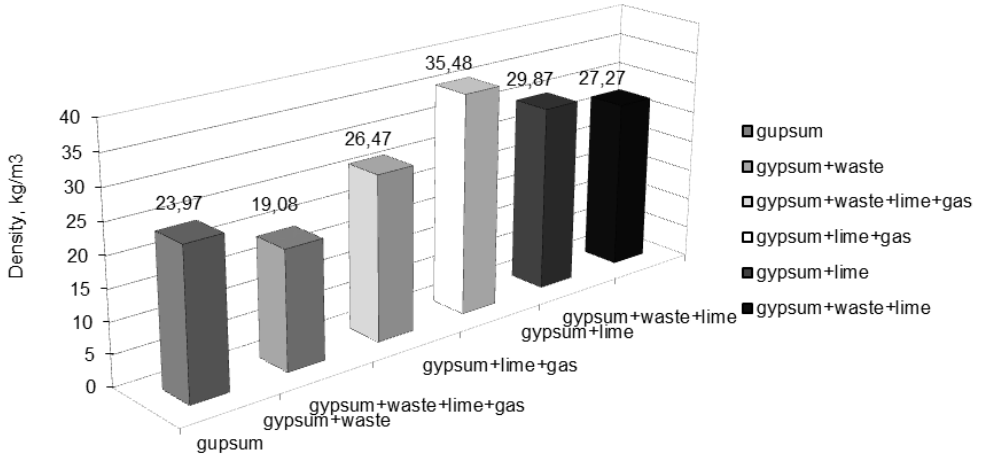

Figure 1. Compressive strength of gypsum composites of various mineral composition.

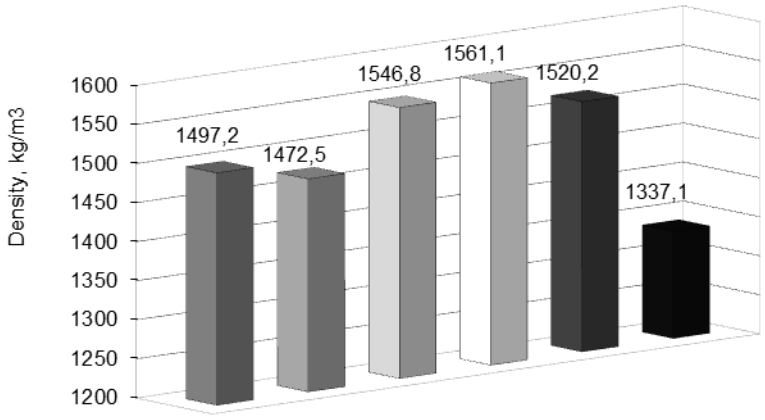

Figure 2. The density of samples of gypsum composite of different composition.

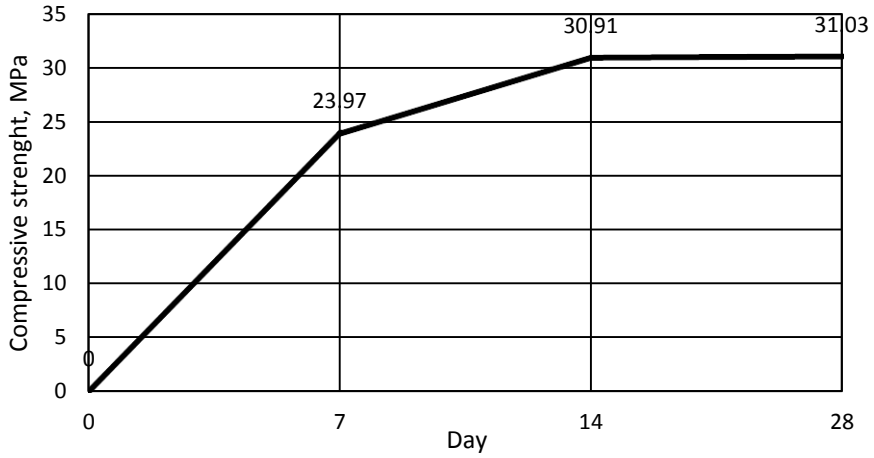

Figure 3. The rate of hardening gypsum subjected to carbonization.

At high concentrations of basalt waste and lime, gypsum crystals are formed in a shape close to needle-like.

Thus, in the course of the research, the possibility of using carbonization as an energy-efficient way to increase the strength of hemihydrate gypsum composites was established. Compaction of the structure makes it possible to improve the performance properties of gypsum composites. The introduction of basalt waste and carbonization can reduce the consumption of binder without loss of strength of materials and reduce the cost of production.

CONCLUSIONS

Carbonization can quite effectively accelerate the rate of curing of finished products based on gypsum, lime and basalt waste, without introducing expensive chemical modifiers. In addition, the resulting composites create the most comfortable conditions for living, meet the requirements of environmental standards to absorb carbon dioxide. Gypsum materials with high technical characteristics will be able to compete successfully in the market with other building materials as the basis for the production of wall and finishing products of high quality and safety.

REFERENCES

1. *IPCC Climate Change 2014: Impacts, adaptation, and vulnerability. Part A: Global and Sectoral Aspects*. Contribution of working group II to the fifth assessment report of the intergovernmental panel on climate change. Cambridge University Press, Cambridge, United Kingdom and New York, NY, USA. pp. 619-657.
2. Wang, L., T. L. K. Yeung, A. Y. T. Lau, D. C.W. Tsang, and C. S. Poon. 2017. "Recycling contaminated sediment into eco-friendly paving blocks by a combination of binary cement and carbon dioxide curing," *Journal of Cleaner Production*, 164:1279-1288.
1. Morozov, A. V., I. A. Bogomolov, D. D. Sokolov, R. I. Temirkanov, and L. K. Grigor'eva. 2017. "Carbonization as a factor in improving the strength of reinforced concrete," Science *and business: ways of development*, 3: 22-24.
2. Bataev, D. K., K. H. Mazhiev, M. A. Gaziev, R. R. Salgiriev, H. N. Mazhiev, and A. H. Mazhieva. 2014. "Change of seismic resistance of fine-grained cellular concrete during carbonization", presented at the International Science and Technology Conference Leonardo da Vinci, May 19-25, 2014.
3. Vahrushev, A. A. 2016. "Development of building wall products based on lime by the method of forced carbonization," in XIX *International intercollegiate scientific and practical conference of students, undergraduates, postgraduates and young scientists Construction - the formation of the living environment*, pp. 789-792.
4. El'kina, I. I. and S. I. Fedorkin. 2012. "The effect of carbonization on the strength of extruded samples from waste rock on cement and lime cement binder," *Construction and technological safety*, 44:41-45.
5. Murakami, T., G. Hodgins, and W. Simon Arleyn. 2013. "Characterization of lime carbonates in gypsums from Teotihuacan, Mexico: preliminary results of cathodoluminescence and carbon isotope analyses," *Journal of Archaeological Science*, 40: 960-970.
6. Levestam, A. Y. U. 2017. "Lime and carbonate hardening - the next step in the evolution of the production of building materials," *Construction Materials*, 8: 13-18.
7. Monkman, S. and M. Makdonal'd. 2017. "Using carbon dioxide as an additive accelerator," *Cement and its application*, 1: 82-89.
8. Lyubomirsky, N.V., and S.I. Fedorkin. "Scientific and technological principles of carbon dioxide utilization in biopositive building products," *Biosphere compatibility: man, region, technology*, 4:39-49.
9. Petropavlovskaya, V., A. Buryanov, T. Novichenkova, and K. Petropavlovskii. 2017. "Self-Hardening of a Gypsum," *Key Engineering Materials*, 737: 517-521.

2018 International Theoretical and Practical Conference on Alternative and Smart Energy (TPCASE 2018)
ISBN: 978-1-60595-617-6

Electrolyte for Hydronic Chemical Current Source Used as Hydrogen Generator with Aluminum Anode

Ariadna Farmakovskaya, Nadezhda Okorokova,
Konstantin Pushkin, Stanislav Sevruk and Elena Suvorova

ABSTRACT

This paper presents the results of experimental studies of the electrochemical characteristics for various anodic and cathodic materials used in a hydronic chemical current source with an aluminum anode in various electrolytes. And it was shown that it is advisable to add only organic inhibitors into an alkaline electrolyte instead stannate-ion to suppress corrosion of an aluminum anode.

INTRODUCTION

Due to the ecological and energy crises nowadays the priority direction of the world economy is the development of hydrogen energy. Hydrogen is already quite a long time been considered and used as an environmentally friendly fuel. The advantages of hydrogen as an energy carrier are in its almost unlimited reserves within the water resources of the planet, in the highest specific energy (119.0 MJ/kg) among the known fuels and in ecologically clean product (water) in reaction with oxygen. The most energy-efficient power plants among autonomous, that use hydrogen as fuel, are oxygen-hydrogen (O_2/H_2) fuel cells (FC). They are able to achieve the highest efficiency among all known power plants (up to 94%). Oxidizer – oxygen – for O_2/H_2 FC is used from air, when operating in ground conditions. For the fuel – hydrogen – the main difficulty is the problem of its storage and transportation. There are several ways to store hydrogen: gas balloon, cryogenic, and "associated". Gas balloon hydrogen storage

Moscow Aviation Institute (National Research University), 4 Volokolamskoe Shosse, Moscow, 125993, Russia

significantly reduces the specific energy-mass characteristics of the entire power plant (PP) [1]. Cryogenic storage, despite the fact that it is the most efficient from the point of view of the energy-mass characteristics of the PP, is not applicable during long pauses in operation or during a delayed launch, since the cryo-liquid evaporates quite actively. The "associated" storage of hydrogen in the composition of some molecules, for example, in water molecules, makes it possible to obtain it as needed, reduce it by active metals during the reaction of their interaction with water. According to the efficiency of hydrogen generation per mass unit of the working components, when hydrogen is reduced from water, only the "lithium-water" system is more efficient than the "aluminum-water" system.

It is given much attention worldwide to the study and development of autonomous hydrogen generators based on the aluminum-water system due to the high safety of the associated hydrogen storage method [2-5]. However, most often hydrogen is supposed to be obtained by chemical dissolution of aluminum in aqueous solutions. One of the main disadvantages of the method of aluminum's chemical dissolution in water (aqueous solutions) is that the energy released during dissolution is not useful and is completely converted into heat (ΔH_{298}=-1830.04 kJ).

EXPERIMENTS AND RESULTS

This problem is solved by us by creating a hydronic chemical current source (CCS). This is an electrochemical cell consisting of an aluminum anode, a cathode made of an inert material such as nickel or molybdenum and an electrolyte between them. Consumable substances in the hydronic CCS are aluminum anode and water. The reaction products are hydrogen, aluminum hydroxide $Al(OH)_3$, and electricity [1].

During the operation of the hydronic CCS with an aluminum anode in an aqueous alkaline electrolyte, an anode current-forming reaction is as follow:

$$Al - 3e + 4OH^- \rightarrow [Al(OH)_4]^- . \quad (1)$$

At the cathode hydrogen is reduced from water according to the reaction:

$$2H_2O + 2e \rightarrow 2H_2 \uparrow + 2OH^- . \quad (2)$$

The total current-forming reaction in a hydronic CCS with an alkaline electrolyte can be represented by the following equation:

$$2Al + 6H_2O + 2OH^- \rightarrow 2[Al(OH)_4]^- + 3H_2 \uparrow . \quad (3)$$

Since aluminum is thermodynamically unstable in water, the anode is consumed at the same time in current-forming and corrosion reactions described by exactly the same summary equation (3). The only difference that hydrogen is released in the cathode sections of corrosive aluminum.

The aluminate solution formed during the dissolution of aluminum in alkali is extremely prone to supersaturation. But after reaching a certain degree of supersaturation it decomposes with the release of solid aluminum hydroxide, which crystallizes in the form of gibbsite:

$$Na[Al(OH)_4] \rightarrow NaOH + Al(OH)_3 \downarrow . \quad (4)$$

In a neutral salt electrolyte, the current-forming reaction and the corrosion reaction are expressed by the summary equation:

$$2Al + 6H_2O \rightarrow 2Al(OH)_3 \downarrow + 3H_2 \uparrow . \quad (5)$$

As follows from equations (4) and (5), the processes in alkaline and neutral electrolytes lead to the same reaction products: $Al(OH)_3$ и H_2. But in a neutral electrolyte aluminum hydroxide precipitates as a gel. Thus, as mentioned earlier, aluminum and water are consumable substances in a hydronic CCS with an aluminum anode.

We made experimental investigations of the electrochemical parameters for the hydronic CCS: current-voltage characteristics (CVC) of the anodes from various aluminum alloys (A99 aluminum, protector alloys AP4N, AP2, AP3 (АП4Н, АП2, АП3), and A995 alloy + 0.6 wt.% In) and inert metal cathodes (Ni, Mo, Ti, steels Kh18N10T (Х18Н10Т) and St.3 (Ст.3)) in a pure alkaline electrolyte (4M NaOH), alkali-stannate (4M NaOH +, 06 mol/l Na_2SnO_3) and salt (4M NaCl) and the corrosion rates of the aluminum anode in these electrolytes. According to the results of the joint assessment of the obtained polarization and corrosion characteristics for the anodic and cathodic materials, it was found that the best composition of working components for the hydronic CCS is 4M NaOH + 0.06M Na_2SnO_3 electrolyte, molybdenum cathode and Al-In alloy anode. The AP4N protector alloy has a close complex of properties. For this composition, the range of current densities at which the hydronic CCS can work as a source of current increases to 2500-3000 A/m^2. Hydronic CCS with salt electrolyte due to high polarization losses at the cathodes can operate as a current source only at low current densities (short circuit mode 300-500 A/m^2), what leads to large dimensions of the hydrogen generator. For the salt electrolyte, the best composition of working components for the hydronic CCS is the cathode of steel St.3 and the anode of the protector alloy AP4N [1].

However, our further studies have shown that the addition of stannate-ion SnO_3^{2-}, significantly affects the CVC of any cathode materials for the hydronic

CCS. CVC for all electrodes of the above-mentioned metals in alkali-stannate electrolyte significantly deteriorated compared to CVC obtained in pure alkali (Fig. 1 and 2).

To explain this phenomenon, experiments were made to study the film on the cathodes formed in the process of CCS operation. The same nickel cathode was repeatedly investigated in the alkaline-stannate electrolyte and it was found that its CVC deteriorated significantly with each new experiment (Fig. 3).

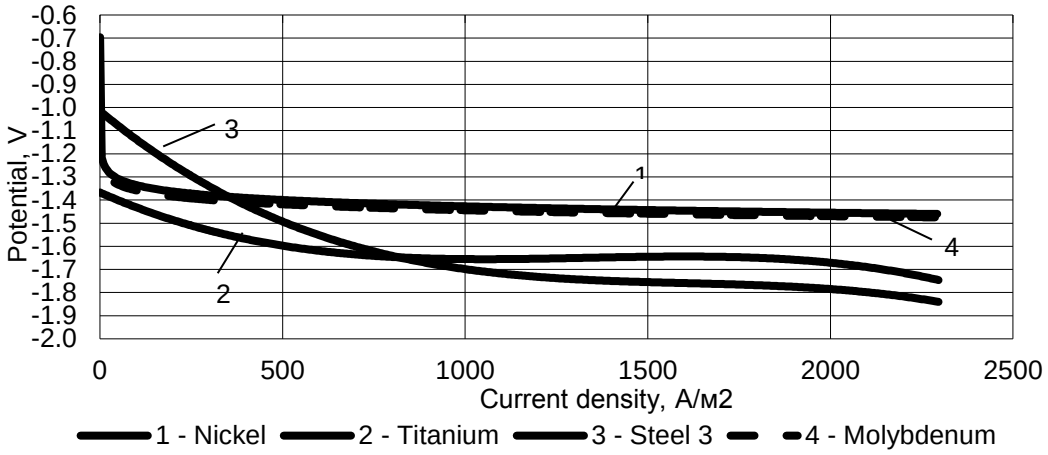

Figure 1. Current-voltage characteristics of various metal cathodes in 4M NaOH at 333K.

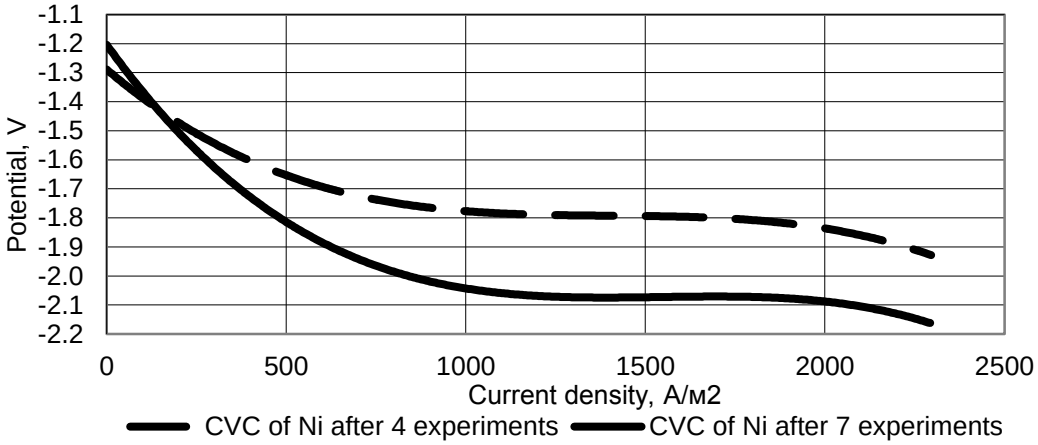

Figure 2. Current-voltage characteristics of a nickel cathode in the electrolyte 4M NaOH + 0,06M Na_2SnO_3, at T=333K.

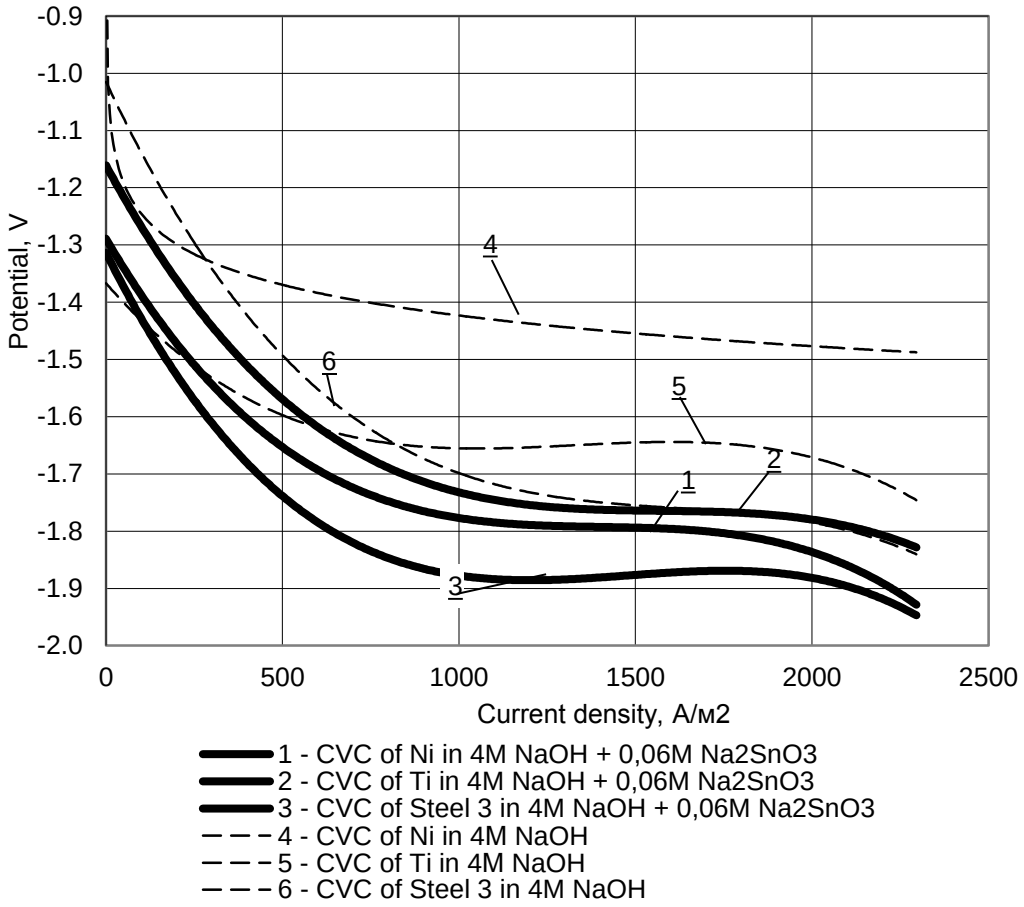

Figure 3. Current-voltage characteristics of various metal cathodes in the electrolyte 4M NaOH and 4M NaOH + 0,06M Na_2SnO_3, at T=333K.

Seems the reason for the varying degrees of potential decrease in cathodes made of different materials, when operating in an alkaline-stannate electrolyte, is the nature of the film formed on the cathode during the discharge of a CCS. The structure of this film (coating) was studied by us by X-ray structural analysis and scanning electron microscopy (SEM). The results of X-ray structural analysis of the coating on the nickel electrode are shown in a diffractogram (figure 4).

The diffractogram clearly shows the peaks of tin and tin compounds with indium $In_{0,2}Sn_{0,8}$. But the peaks of the nickel substrate are rather weak, which characterizes a rather large coating thickness (more than 15-20 microns). Indium is also presents in the coating in a rather large percentage, which is an activating element of the anodic Al-In alloy and formed a crystalline compound with tin in the ratio indicated above.

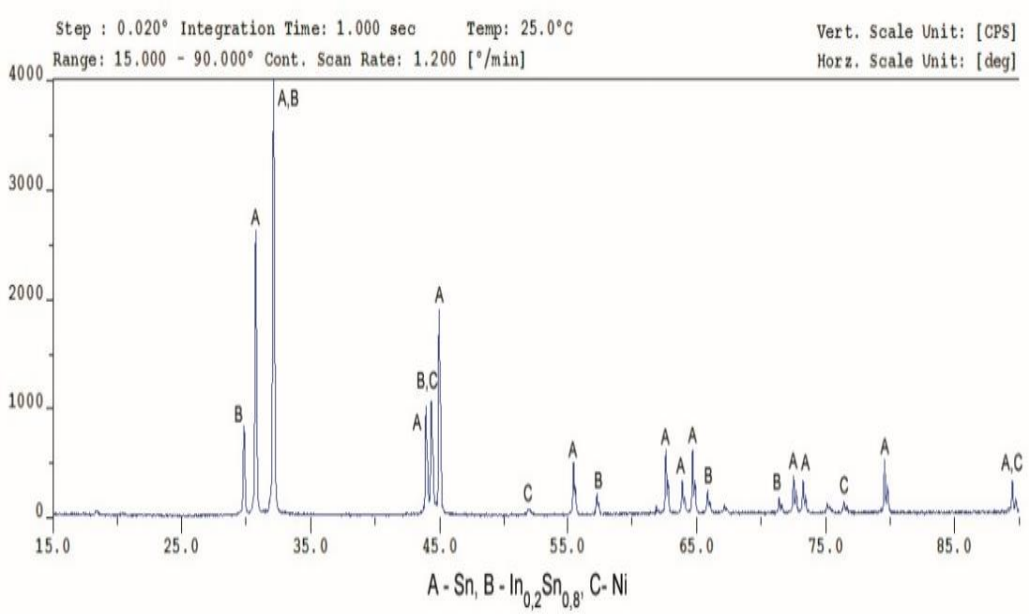

Figure 4. Diffractogram of the investigated coating.

Photographs of the surface obtained with an electron microscope with different degrees of magnification showed that the surface structure is volume-porous with a high visual porosity, which is estimated to be about 50%, especially with prolonged and/or repeated cathode use. This confirms the assumption put forward earlier by us that the coating is porous due to the release of gaseous hydrogen on it.

The formation of a porous tin coating on the cathode, firstly, worsens the CVC, and, secondly, explains the difference in the CVC of cathodes from different metals due to the release of hydrogen both on the substrate surface (base material) and on the surface of the coating.

CONCLUSION

Thus, we have shown that the use of stannate-ion additives to the alkaline electrolyte of the hydronic CCS is undesirable, since this leads to a deterioration in the characteristics of the cathodes. Therefore, in order to inhibit the corrosion process of the aluminum anode and, thereby, increase its useful life, it is necessary to use additives of organic inhibitors in the alkaline electrolyte for a hydronic CCS.

Preliminary experiments with a number of organic inhibitors showed that, with the addition of tartrate ion (tartaric acid anion) in 4M NaOH, the working range of the hydronic CCS current density reaches 2000 A/m^2. This is

approximately in 4 times higher than using the previously proposed electrolyte 4M NaOH + 0.06M Na_2SnO_3 [6].

REFERENCES

1. Pushkin, K.V. 2014. "Controlled Hydrogen Generator and Additional Source of Electrical Current for Independent Oxygen-Hydrogen Power Plants," 29th Congress of the International Council of the Aeronautical Sciences (ICAS), St. Petersburg; Russian Federation.
2. Lluis, S., et al. 2007. "Aluminum and Aluminum Alloys as Sources of Hydrogen for Fuel Cell Applications," *Journal of Power Sources*, 169:144-149.
3. Lluis, S., et al. 2007. "Synergistic Hydrogen Generation from Aluminum, Aluminum Alloys and Sodium Borohydride in Aqueous Solutions," *International Journal of Hydrogen Energy*, 32:4702-4710.
4. Jung, C.R., et al. 2008. "Hydrogen from Aluminium in a Flow Reactor for Fuel Cell Applications," *Journal of Power Sources*, 175:490-494.
5. Amendola, S.C., et al. 2000. "An Ultrasafe Hydrogen Generator: Aqueous, Alkaline Borohydride Solutions and Ru Catalyst," *Journal of Power Sources*, 85:186-189.
6. Pushkin, K.V., et al. 2018. "The most efficient corrosion inhibitors for aluminum anode of electrochemical cell used as a controlled hydrogen generator," *Periodico Tche Quimica*, 15(Special Issue 1):414-425.

2018 International Theoretical and Practical Conference on Alternative and Smart Energy (TPCASE 2018)
ISBN: 978-1-60595-617-6

Energy Characteristics of a Combined Power Plant Based on a Hydronic Chemical Current Source

Ariadna Farmakovskaya, Nadezhda Okorokova,
Konstantin Pushkin, Stanislav Sevruk and Elena Suvorova

ABSTRACT

This paper presents the results of energy characteristics calculations of a combined power plant (PP) based on a hydronic chemical current source (CCS) with an aluminum anode, as a hydrogen generator for an oxygen-hydrogen electrochemical generator (O_2/H_2 ECG). Calculations based on current-voltage characteristics (CVC) of sources. It has been shown that the hydronic CCS over the entire operating time of the O_2/H_2 ECG increases its CVC and power characteristic by 30% at the beginning of work and by 20% at the end of the 24-hour resource when using pure nickel cathodes in the hydronic CCS. Using cathodes with a MoS_2 catalytic coating in a hydronic CCS increases CVC of the ECG by 50% at the beginning of work and by 40% at the end of a 24-hour resource. At the same time, the hydronic CCS provides the O_2/H_2 ECG with hydrogen in full volume during the whole period of operation.

INTRODUCTION

The active consumption of oil and gas by mankind during the 20th century led to significant negative consequences for the environment, such as smog in large cities, the greenhouse effect, environmental disasters resulting from oil spills due to tanker accidents during transportation of fuel and much more. Therefore, the use of hydrogen as an energy carrier is considered as an alternative due to the practically unlimited reserves in the composition of the planet's water resources, the highest specific energy (119.0 MJ/kg) among the known fuel and ecologically clean product (water) in reaction with oxygen.

Moscow Aviation Institute (National Research University), 4 Volokolamskoe Shosse, Moscow, 125993, Russia

Among autonomous power plants (PP) that use hydrogen as fuel, the most energy efficient are oxygen-hydrogen fuel cells (O_2/H_2 FC), which are able to achieve the highest efficiency among all known power plants (up to 94%). In [1-5], it was shown that the combined use of hydronic CCS together with O_2/H_2 FC can form a combined PP consisting of two current sources – hydronic CCS and O_2/H_2 FC (O_2/H_2 electrochemical generator – ECG). Here the hydronic CCS is a source of hydrogen for O_2/H_2 ECG and an additional current source at the same time. Obviously, this should increase the energy characteristics of the PP compared to the PP, consisting only of the source of hydrogen and O_2/H_2 ECG.

EXPERIMENTS AND RESULTS

In this work, we calculated the energy characteristics of the combined power plant "Hydronic CCS + O_2/H_2 ECG" taking into account the functioning of the sources with a serial connection scheme (Figure 1).

An estimate calculation was made for O_2/H_2 ECG of power 3 kW (current 70A, voltage 43V, 72 cells in the battery) for 24 hours. Data on the characteristics of O_2/H_2 ECG are taken from its technical documentation. Its current-voltage characteristic and power characteristic are presented in Figure 2.

The CVC equation of the ECG is approximated by the equation:

$$U = -56 \cdot 10^{-4} \cdot I_{ECG}^3 + 18{,}79 \cdot 10^{-2} \cdot I_{ECG}^2 + 56{,}39 \cdot I_{ECG} + 12{,}53, \quad (1)$$

where I_{ECG} is the discharge current of ECG.

The CVC of the hydronic CCS was calculated for the source with the anode A995, electrolyte 4M KOH + 0.08M tartrate ion. Two electrodes were considered as cathodes: from nickel of mark N-0 and nickel cathode with experimental catalytic coating of molybdenum disulfide – Ni + MoS_2.

The interelectrode gap of the cell is assumed to be equal to $\delta = 3$mm The calculations took into account the change in the interelectrode gap during the operation time and was defined as the algebraic sum of the CVC of the cathode, anode and voltage loss in the interelectrode gap by the equation:

$$U = \phi_c - \phi_a - \frac{\delta}{\sigma} \cdot j \ , \quad (2)$$

where, φ_c, φ_a – electrodes potentials, σ – electrolyte conductivity; δ – interelectrode gap width.

CVC characteristics of electrodes are presented in Figure 3.

Taking into account the CVC of the working components of the hydronic CCS, the allowable current density of the hydronic CCS is assumed to be j_{hydr} = 1200 A/m^2 at the rated discharge current of the O_2/H_2 ECG (70 A). When choosing the current density of the hydronic CCS, the condition was taken into

account that it should operate in the mode of the current source, at the rated power of the O_2/H_2 ECG (3kW).

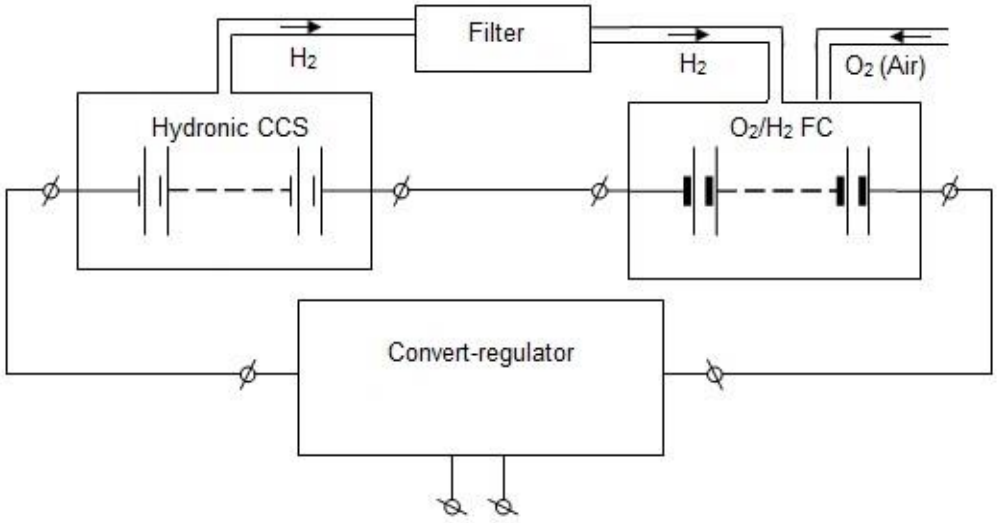

Figure 1. Schematic diagram of the combined power plant "hydronic CCS – O_2/H_2 ECG " with a series connection of sources.

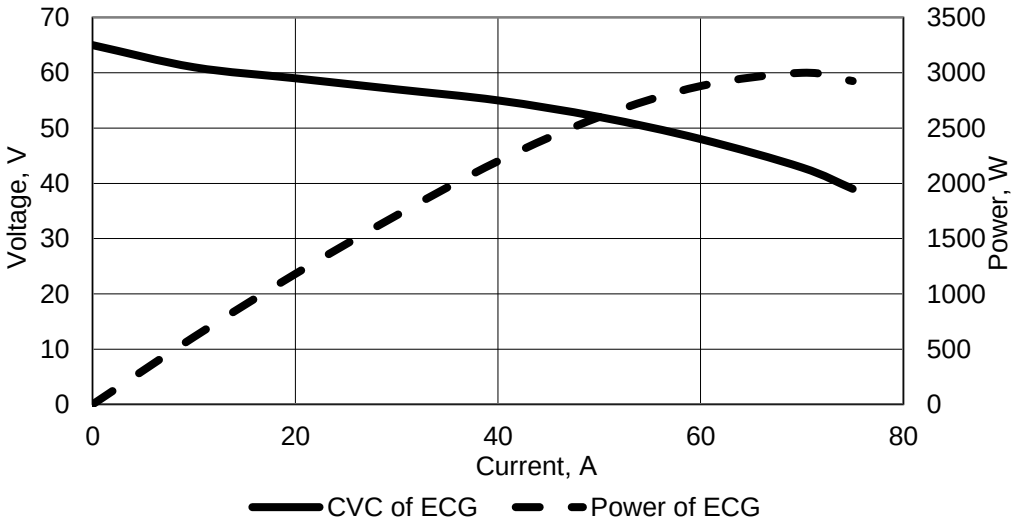

Figure 2. The current-voltage and power characteristics O_2/H_2 ECG power 3kW.

The calculated assessment results of the energy characteristics for the combined power plant "Hydronic CCS + O_2/H_2 ECG" (and each of the sources separately) are shown in Figures 4 and 5.

From the obtained data it follows that the hydronic CCS throughout the entire operating time of the O_2/H_2 ECG increases its current-voltage and power characteristics by 30% at the start of work and by 20% at the end of the 24-hour resource when using pure nickel cathodes in the hydronic CCS.

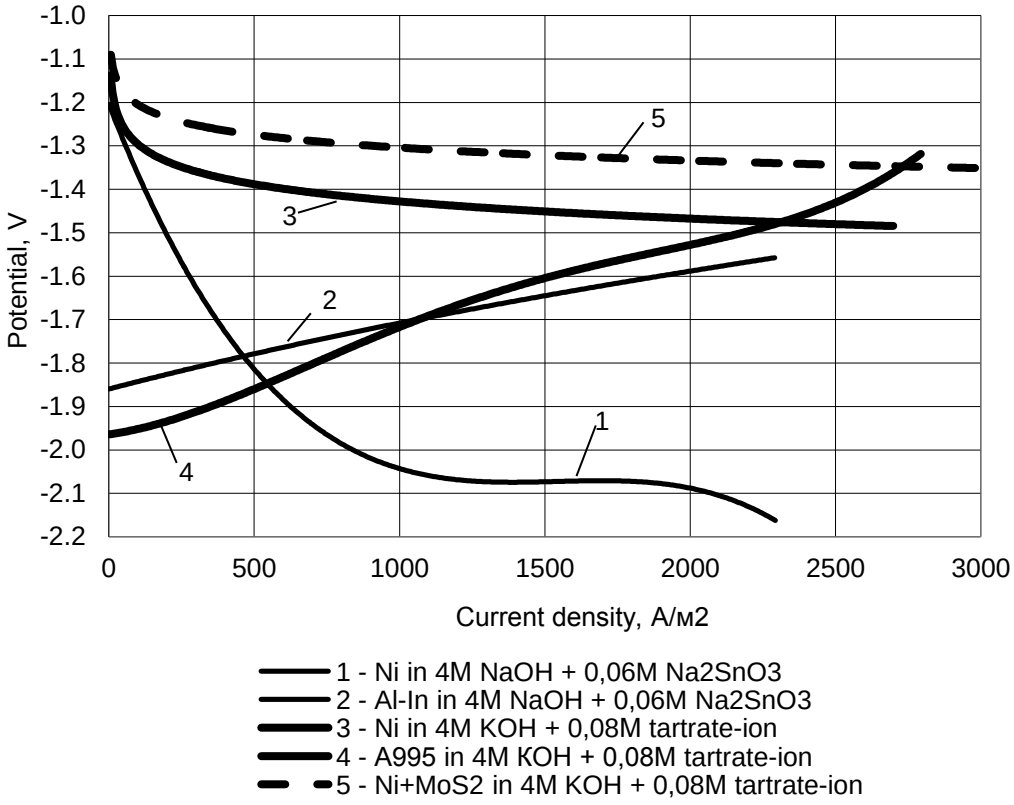

Figure 3. Current-voltage characteristics of anodes A995, Al-In and Ni and Ni + MoS_2 cathodes at 333 K.

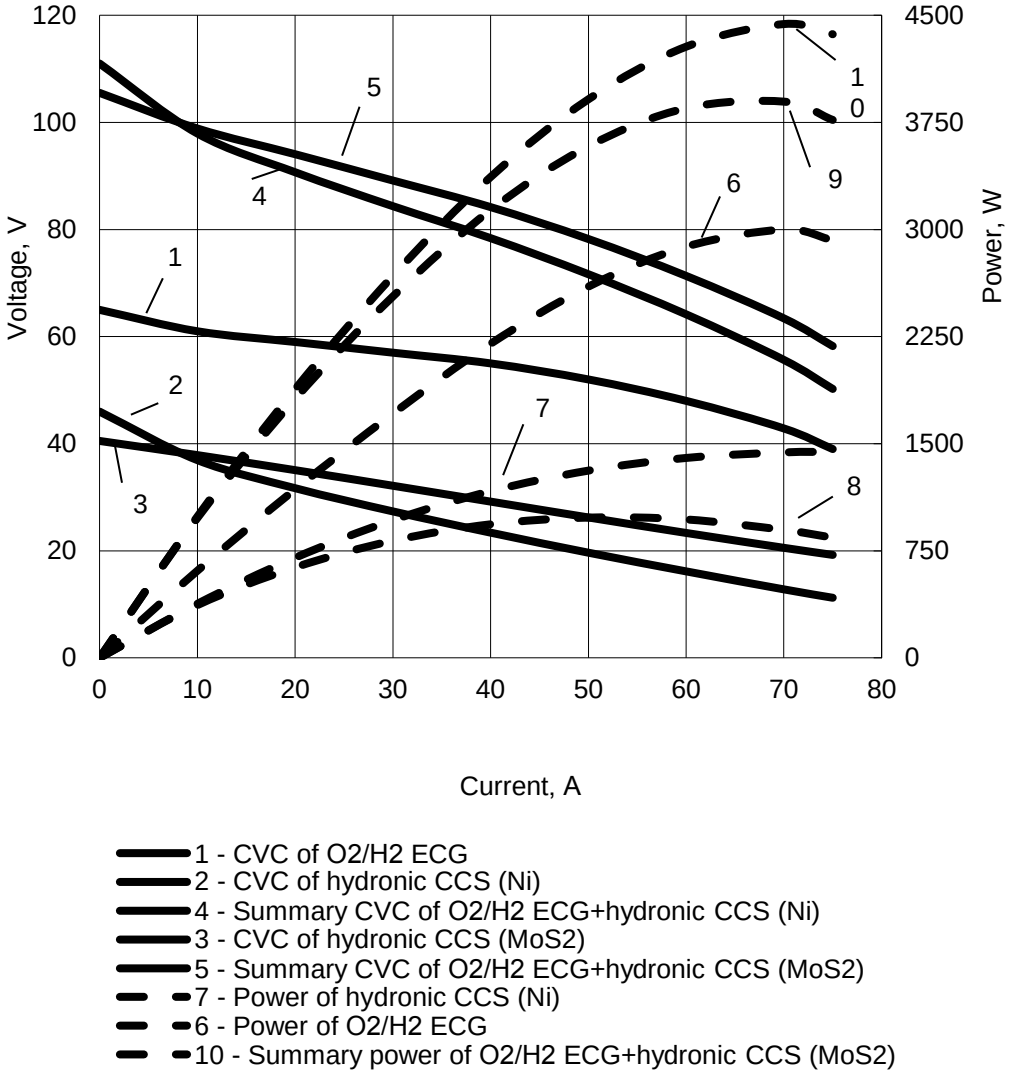

Figure 4. Initial current-voltage and power characteristics of a hydronic chemical current source, O_2/H_2 electrochemical generator and a combined power plant.

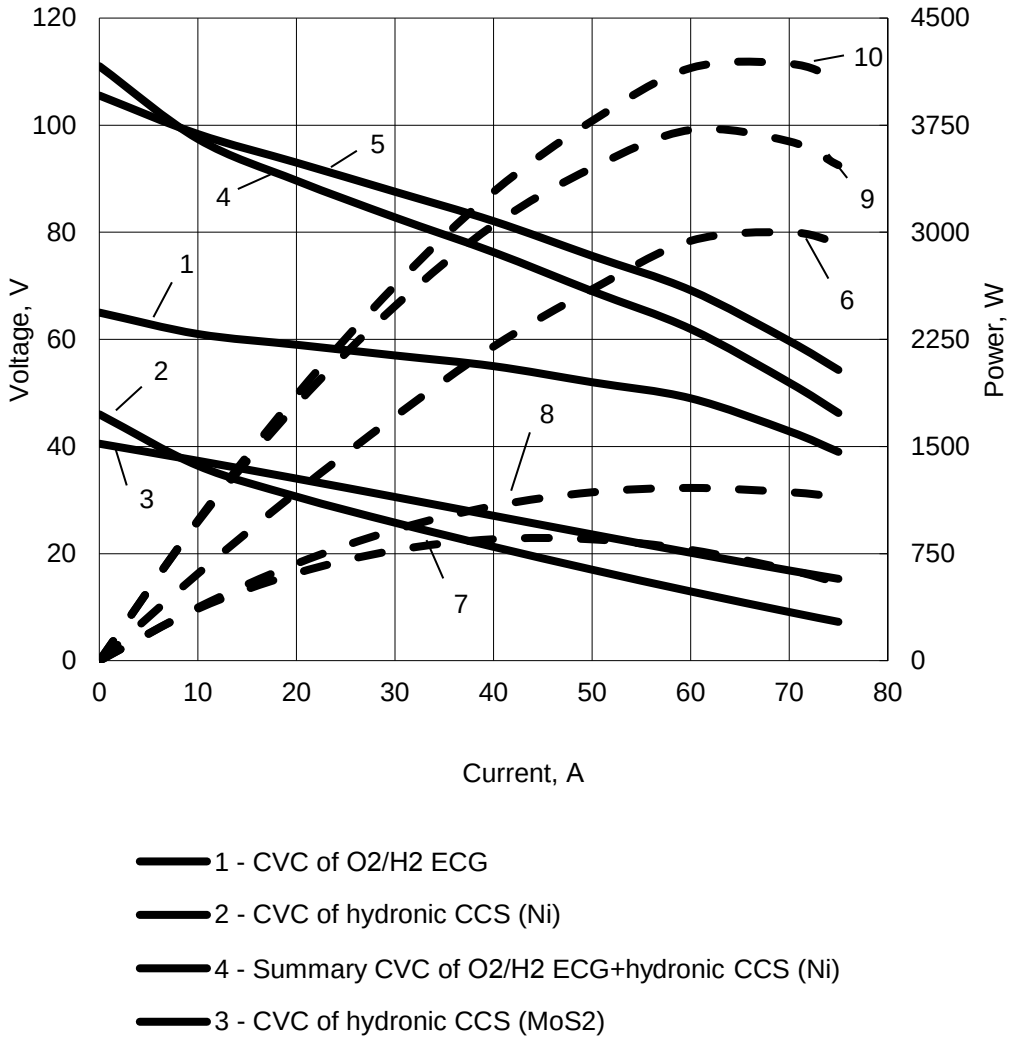

Figure 5. Current-voltage and power characteristics of a hydronic chemical current source, O_2/H_2 electrochemical generator and a combined power plant after 24 hours of operation.

Using cathodes with a MoS_2 catalytic coating in a hydronic CCS increases its current-voltage and power characteristics of the O_2/H_2 ECG by 50% at the beginning of work and 40% at the end of the 24-hour resource. The results of the energy characteristics calculations of the hydrogen generator based on the hydronic CCS as part of a combined power plant are given in Table I.

TABLE I. ENERGY CHARACTERISTICS OF A HYDROGEN GENERATOR BASED ON A HYDRONIC CCS AS PART OF A COMBINED POWER PLANT.

Characteristic	**Combination of the working components**	
	A995 – 4M KOH + 0,08M tartrate-ion – Ni	**A995 – 4M KOH + 0,08M tartrate-ion – Ni+MoS_2**
The voltage of the hydronic CCS at I_{ECG}=70A, V	0,208	0,335
The power of hydronic CCS at I_{ECG}=70A , W at the beginning of work after 24 hours of operation	 896 637	 1439 1180
The average specific energy for 24 hours of discharge, kJ/kg (W·h/kg)	334 (93)	571 (159)

CONCLUSION

Thus, the results of calculations show that to increase the characteristics of a combined power plant, it is preferable to use a cathode with a MoS_2 catalytic coating in a hydronic CCS. This allows to increase the CVC and power characteristic up to 50%. At the same time, the hydronic CCS provides the O_2/H_2 ECG with hydrogen in full volume during the whole period of operation.

REFERENCES

1. Pushkin, K.V. 2014. “Controlled Hydrogen Generator and Additional Source of Electrical Current for Independent Oxygen-Hydrogen Power Plants,” 29th Congress of the International Council of the Aeronautical Sciences, (ICAS), St. Petersburg, Russian Federation.
2. Lluis, S., et al. 2007. “Aluminum and Aluminum Alloys as Sources of Hydrogen for Fuel Cell Applications,” *Journal of Power Sources*, 169:144-149.
3. Pushkin, K.V., et al. 2018. “The most efficient corrosion inhibitors for aluminum anode of electrochemical cell used as a controlled hydrogen generator,” *Periodico Tche Quimica*, 15(Special Issue 1):414-425.
4. Okorokova N.S., et al. “Combined current source,” *Utility Model Patent* No 105528, utility model priority as of 24 Dec. 2010.
5. Okorokova N.S., et al. “Combined current source with a parallel connection of batteries,” *Utility Model Patent* No 116257, utility model priority as of 7 Dec. 2011.

2018 International Theoretical and Practical Conference on Alternative and Smart Energy (TPCASE 2018)
ISBN: 978-1-60595-617-6

Algorithms and Techniques of Effective and Safe Processing of Radioactive Waste on Nuclear Power Plant

Maksim Parinov and Sergey Rosnovskiy

ABSTRACT

The article offer techniques and algorithms for effective and safe processing of radioactive waste on nuclear power plant. The main idea of automation based on special algorithms for location of containers relative to each other. Optimal container location provide minimization of dose rate. Proposed techniques and algorithms allow to find this optimal location.

INTRODUCTION

Safety, reliability and efficiency of radioactive waste storages is important problem of modern nuclear power plants. There are a lot waste storages types. They have different indexes of safety, reliability economic efficiency, usability and others. Hangar type storages show excellent main indexes. It has proved during exploitation on Novovoronezh nuclear power plant (Figure 1).

The main feature of these storages is radiation shielding that provided by containers with radioactive waste. External lines containers shield ones from internal lines. We can ignore internal containers radiation because it is weak. Therefore we can store quite active waste in internal lines.

It provides high radiation safety and few other benefits. Design of hangar type storages provides very good economic efficiency because it is simple and cheap. It increases storages usability because containers is located above ground level and they are accessible by ordinary forklift truck. Design solves problem with drain water.

Voronezh State Technical University, 14, Moskovskiy Avenue, Voronezh, 394026, Russia

PROBLEM

The main problem during filling these storages is maintaining of safe dose rate on storage walls and storage borders. It can provide by special scheme of containers placing. It would be quite simple task if we have all containers for this storage simultaneously. But we receive containers in random batches of several ones. We don't know which containers will be gotten at this moment. Any containers can come in any time. The fact that external line can be absent complicates the task.

Today this task solved by engineers. They use their experience to determine places for received containers. Correctness of these actions verifies by dose rate measurement. They can use special mathematical approach that was designed on Novovoronezh nuclear power plant [1].

Used method has some important disadvantages. For example, at a certain point we can find that dose rate exceed norm and we can do nothing without moving previously installed containers. Existing mathematical approach is weak and difficult to practical use.

Figure 1. Hangar type storage.

SOLUTION (OFFERED TECHNIQUE)

We offer technique which can correct these deficiencies. The base of the technique is algorithm. It will be used for developing new mathematical approach and software. The algorithm considers the fact that storages must be disassembled after maximal allowed storage time.

Disassembling of storages will be for long time. Containers will be removed batches. Vacancies can be used for new containers. Thereby storage can contain radioactive waste from different time periods. If we are planning exploit storages in dynamic mode when we change only part of containers any time we should provide transport corridors in storages for forklift truck.

If storage will be exploited in static mode with full disassembling in one time then we do not need transport corridors and can place containers closely. In this case the mathematical approach is simplified. We can remove from the algorithm transport corridors and disassembling modules.

Consider the base algorithm (Figure 2).

Unit of calculating load parameters uses for definition of minimal and maximal loading (containers amount) and priority of loading density or accessibility. If we are planning good accessibility we should leave a plenty of space for transport machines.

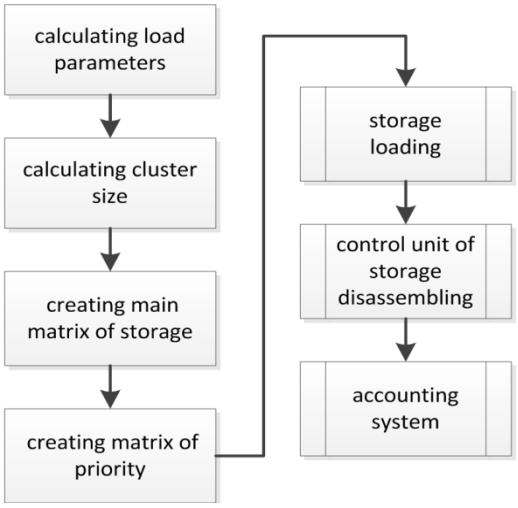

Figure 2. Base algorithm.

Cluster size defines accessibility, load density and geometric parameters. It can be calculated automatically or set by an operator. The automatic calculation can use formula 1:

$$S = n \times k, \quad (1)$$

S - cluster size;
n - typical cluster size (table value);
k - density priority coefficient.

The main matrix of storage contains all parameters. Geometrical data are most important. The matrix part that contains geometrical parameters describes whole storage space. The space divided by typical cells. Each cell contain it status code. For example:

1-4 - cells with container (4 positions);
5-9 - cells with container in corridor (4 positions);
10 - corridor, not allowed for loading;
11 - temporary (allowed for loading) corridor;
12 - place, not allowed for any access.

Container position is fundamental parameter of this technique. Waste in containers are placed irregularly. Figure 3 shows typical container with waste. Barrels are placed in the container corner. It is corner close-in to faces 2,3. Such location provides directional pattern of radiation (Figure 4). Therefore we can minimize dose rate storage outside if we will use the scheme like Figure 5.

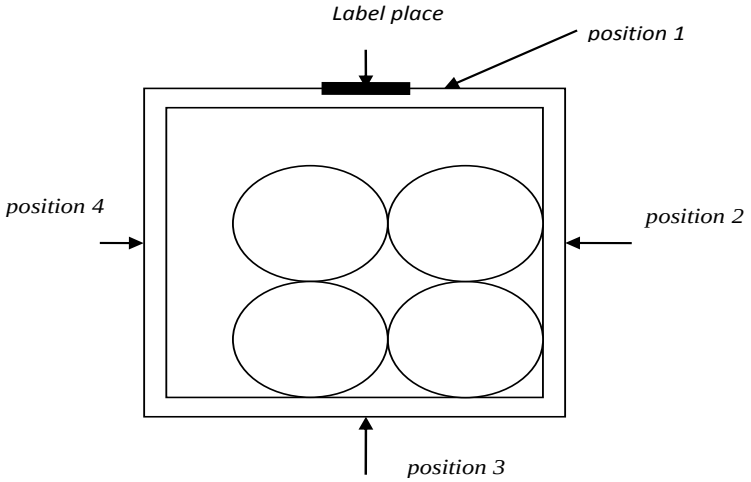

Figure 3. Container position.

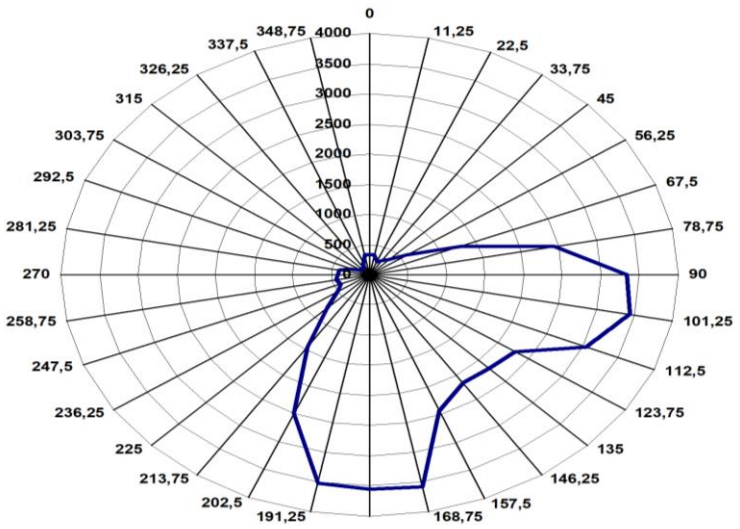

Figure 4. Pattern of radiation.

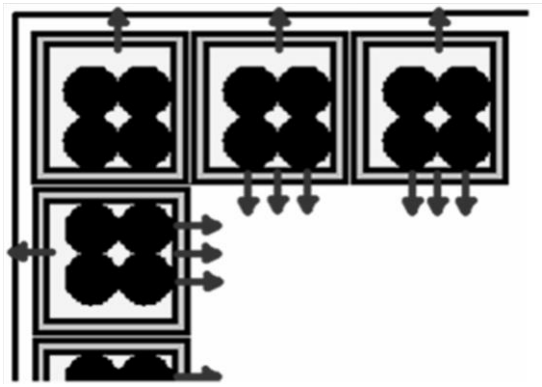

Figure 5. Containers location.

Next step is addition of the priority parameter to the main matrix. It define places that must be used first. The priority parameter provides creation of optimal geometric scheme of storage. The optimal scheme provides lowest dose rate the storage outside and, good transport accessible to any point of the storage and no empty inaccessible places inside clusters.

Storage loading is the main step of the algorithm. It will be described later.

Control unit of storage disassembling is under construction now. Its main function is definition the optimal containers for replacement and extraction. Extracted containers will be moved to special place for permanent storage.

The algorithm contains the accounting system. It stores data about any operation with radioactive waste that were in this storage. This system will be included in unified system of digital production.

Figure 6 shows storage loading algorithm. It is simplified variant that not include number of steps. For example it doesn't show sub algorithm that demand new containers if we can't place current ones. All steps of the algorithm are presented simplified. Despite this the algorithm is quite clear.

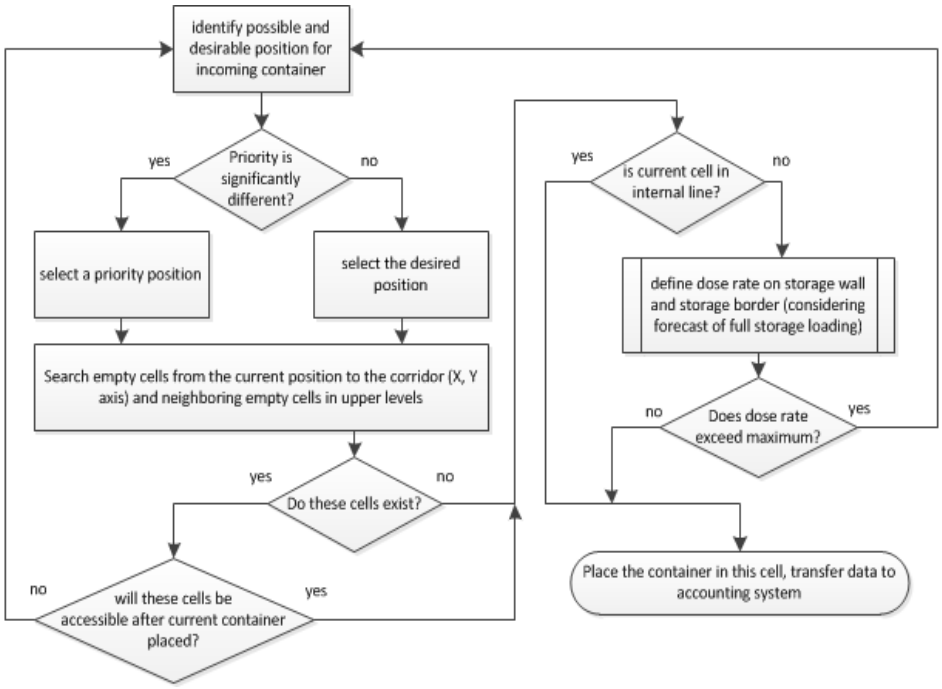

Figure 6. Storage loading algorithm.

CONCLUSION

Using this algorithms and techniques we developed special software that shows their correctness. Current version of software is alpha and can't be used on real nuclear power plant. Today our team is working with advanced techniques and new software.

The software is planned for unified digital production system of nuclear power plant. It will be integrated in common information space and work with other software unit of the enterprise together.

REFERENCES

1. Bulka, S.K. and S.V. Rosnovskii. 2014. "Experience Gained at the Novovoronezh Nuclear Power Plant with Development and Introduction of a Unified Automated System for Accounting and Control of Radioactive Substances and Radioactive Wastes," *Thermal Engineering*, 61(2):144-152.

2. Duro, L., et al. 2014. “Redox Processes in the Safety Case of Deep Geological Repositories of Radioactive Wastes. Contribution of the European RECOSY Collaborative Project,” *Appl. Geochem*., 49:206-217.
3. Ojovan, M.I. and W.E. Lee. 2014. “Transport and Storage of Radioactive Waste,” *in an Introduction to Nuclear Waste Immobilisation (Second Edition)*, M.I. Ojovan, W.E. Lee, eds. Oxford: Elsevier, pp. 307-319.
4. Ojovan, M.I. and W.E. Lee. 2014. “Treatment of Radioactive Wastes,” *in an Introduction to Nuclear Waste Immobilisation (Second Edition)*, M.I. Ojovan, W.E. Lee, eds. Oxford: Elsevier, pp. 171-203.
5. Ojovan, M.I. and W.E. Lee. 2014. “Immobilisation of Radioactive Waste in Cement,” *in an Introduction to Nuclear Waste Immobilisation (Second Edition)*, M.I. Ojovan, W.E. Lee, eds. Oxford: Elsevier, pp. 205-232.

2018 International Theoretical and Practical Conference on Alternative and Smart Energy (TPCASE 2018)
ISBN: 978-1-60595-617-6

Halide Perovskite Solar Cell Efficiency Improvements: New Device Type Simulation

Danila Saranin, Marina Orlova, Sergey Yurchuk,
Oleg Rabinovich, Alexander Panichkin, Mikhail Konovalov,
Yuriy Osipov, Sergey Didenko and Pavel Gostischev

ABSTRACT

Trihalide perovskite photovoltaic (P-PV) solar cells have a promise to be connected into tandems with inorganic PV systems. In this paper, we present p-i-n GaAs & P-PV cells in either in a series way or parallel connection. Comparisons made for two types of tandems by a non-monolithic connection of two experimental sub-cells and results are being discussed based on simulation analysis. It is shown that the parallel connection is always preferable when the sub-cells photocurrent is not balanced while V_{oc} (open circuit voltage) is close to each other. Total efficiency over 20% is demonstrated for GaAs shading effect by $MAPbI_3$ (methylammonium lead halide) film, with achieved J_{sc} - 41 mA/cm^2 (short circuit current density) and high $V_{oc.}$

INTRODUCTION

Perovskite-based photovoltaics, that recently has created a fastest growing solar cell efficiency curve in the photovoltaics history, need improving [1]. Recently the new route has been suggested via the lead acetate precursor [2] which allows one to obtain the organic transport layer based planar PERO-PV with very high J_{sc} and the record efficiency ~18% for stable devices. Among the new perspective which developing of P-PV have opened, the most exact (including flexible, semitransparent design) is probably the promise to create high-efficiency tandems with the conventional inorganic solar cell are Si, CIGS, CdTe devices [3-5]. Although the sizable efficiencies achieved the photocurrent are quite modest (up to 26 mA/cm^2) [6] and the fundamental achievement for lower J_{sc} is the limiter thesis that in-series connection has - since it requires the balanced currents in two sub-cells. In-series tandem generates the minimal current of the sub-cell with lowest I_{sc} (short circuit current). In this paper, the motivation is to demonstrate that high-quality perovskite based-photovoltaics can be used to create high current tandems even with inorganic PV. For such

National University of Science and Technology “MISiS”, 4, Leninskiy Avenue, Moscow, 119049, Russia

inorganic sub-cell, we have chosen p-i-n GaAs diodes, which are usually used as sensitive photodetectors due to their high charge carrier's mobility and sample design. It is known that the high-efficiency PV device requires the GaAs/AlGaAs heterojunction that has large $\eta \sim 25\%$, due to the better charge separation at the heterojunction. But our goal is to demonstrate that even using simple p-i-n GaAs diodes the parallel tandem can be created with high photocurrents ~ 40 mA/cm^2. It has been created for these two sub-cells: perovskite sub-cell that shows $J_{sc} \sim 22$-23 mA/cm^2, $V_{oc} \sim 0.75$ V, power conversion efficiency (PCE) 13.7 % and GaAs cell with $J_{sc} \sim 20$mA/cm^2, and $V_{oc} \sim 0.75$ V. The two non-monolithic connections are tested by traditional in-series connection, when GaAs is shadowed by the perovskite sub-cell film placed on it, and the parallel one.

EXPERIMENTAL PART

Figure 1 shows the tandem device front view, where perovskite sub-cell is installed directly on the top of GaAs sub-cell. The sub-cell positioning was made in shading configuration without taking into account the back perovskite electrode. The tandem connection was done with a combining of cathodes for negative charge accumulation in parallel mode as it presented in Figure 2 (in short circuit regime) in band diagram schematics. The in-series connection was done with combining of positive GaAs electrode and negative perovskite cathode (bias was applied to GaAs cathode and perovskite anode respectively).

The structure was grown by chloride vapor phase epitaxy (system Ga-$AsCl_3$-H_2) on the two-inch GaAs substrates with 400 micron-thickness and Si-doped to $2 \cdot 10^{18}$ cm^{-3} level. Transitional buffer layer with 4 microns thickness was grown on the substrate and doped with sulfur to a concentration of $7 \cdot 10^{17}$ cm^{-3} to reduce the influence of defects. Over the buffer, GaAs working layer was grown by chloride epitaxy high-purity film with resulting 5-micron thickness with background concentration on the level at $3 \cdot 10^{11}$ cm^{-3}. Perovskite sub-cell was created on ITO (In_2O_3:Sn) coated glass worked as a transparent electrode in the next order: hole transporting layer (30 nm thickness) PEDOT:PSS (poly(3,4-ethylenedioxythiophene) polystyrene sulfonate), absorbing film (450 nm) - $MAPbI_3$; electron transport layer (30 nm) -C_{60} all films were deposited with spin coating method. Finally, a silver cathode with 100 nm thickness was deposited by thermal evaporation at 2 10^{-6} Torr pressure.

I-V performance measurements were done at standard 1.5 AM G spectrum of incident light (100 mW/cm^2) with aperture mask usage (1 mm^2) to balance current densities of sub-cells. The tandem device in-parallel and in-series connection was investigated for I-V with Keithley 2400 SMU using Thermo Oriel ABA solar simulator and QE X6 system for external quantum efficiency measuring.

We used single diode model equations for tandem operation simulation. Output parameters, such as Rseries (series resistance), R_{shunt} (shunting resistance), n (non-ideality factor), J_o (dark saturation current density) were used for fitting of experimental and simulated curves and then a calculation and simulation for tandem I-V characteristics. For tandem operation regimes GaAs and perovskite sub-cells were connected in parallel and in-series, respectively (see Figures 3 a, b). GaAs sub-cell is showed as an equivalent circuit of diode (representing p-i-n structure); Iph1 (representing GaAs sub-cell photocurrent); Rsh1

(representing shunt resistance of GaAs diode) and Rs1 (representing series resistance of GaAs sub-cell contacts with electrodes), while perovskite sub-cell is showed as equivalent circuit of diode (representing PEDOT:PSS–$MAPbI_3$– C_{60} heterostructure); Iph2(representing perovskite sub-cell photocurrent); Rsh2 (representing shunt resistance of perovskite cell heterostucture) and Rs1 (representing series resistance of perovskite sub-cell contacts with electrodes).

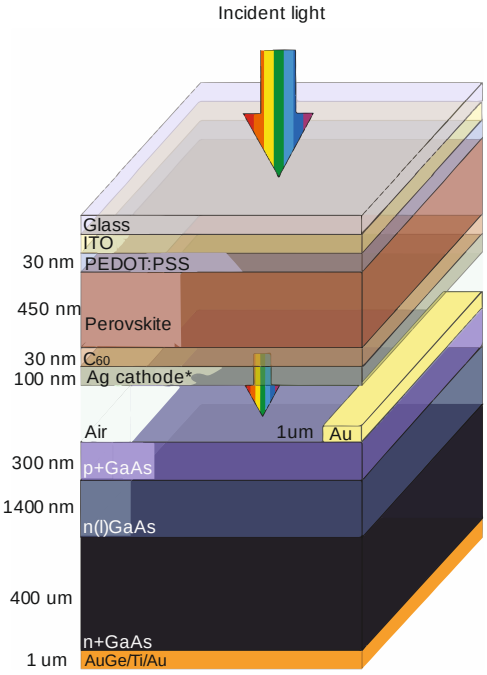

Figure 1. Tandem device schematics.

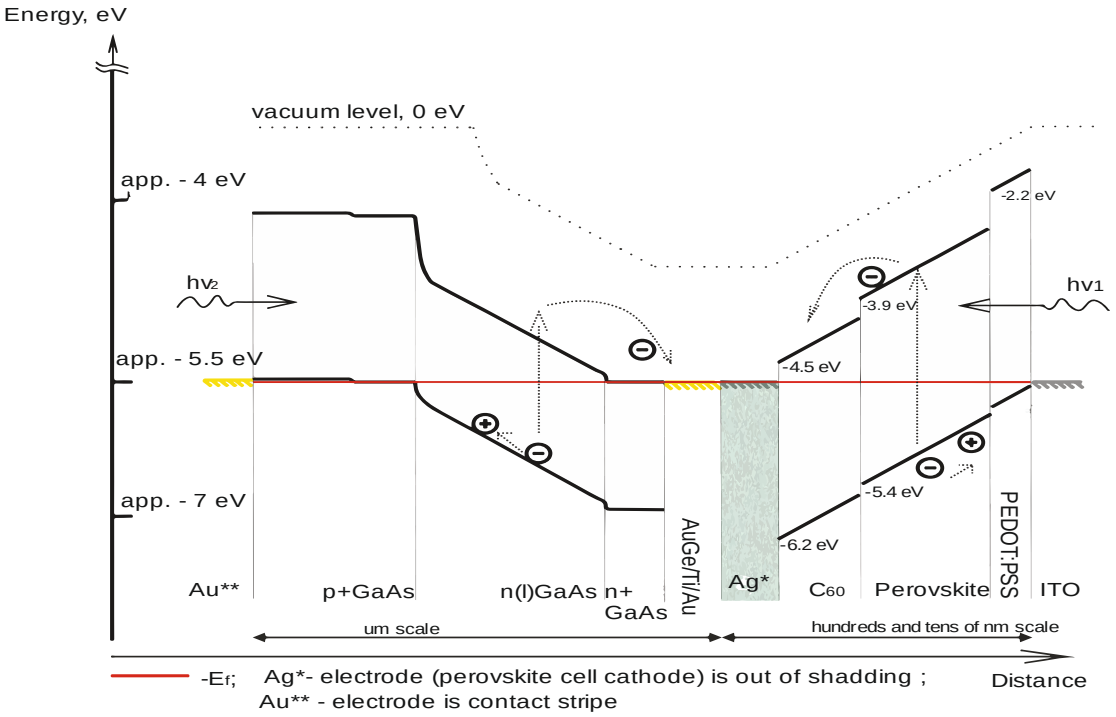

Figure 2. Tandem device sketch band diagram.

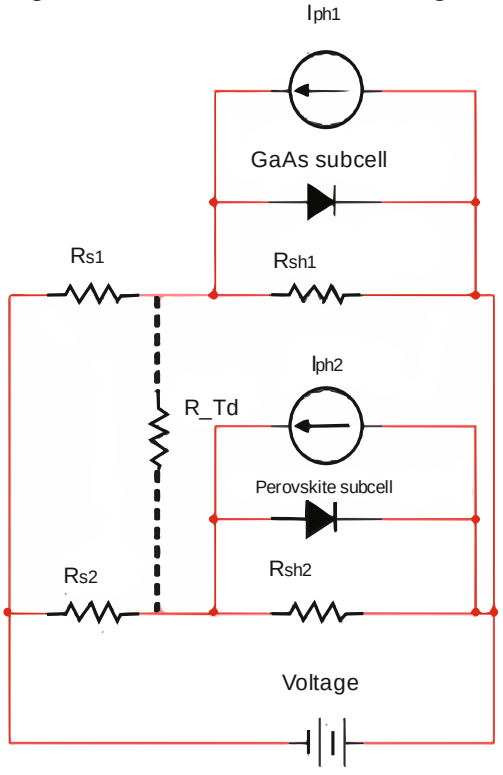

a)

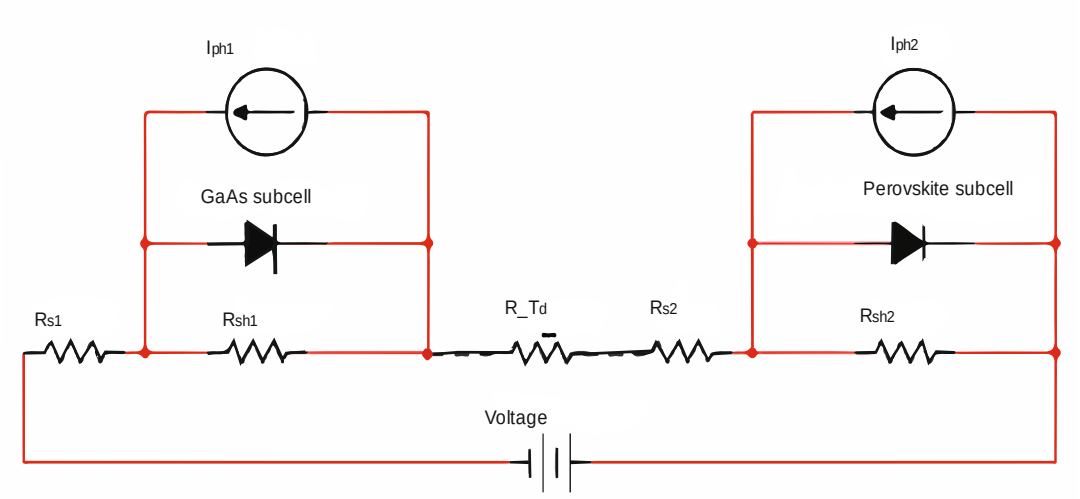

b)

Figure 3. Equivalent circuits of parallel (a) and series (b) tandems for simulation.

RESULTS

The cells connection can be either in-parallel or in-series. It is important to understand how the parameters and characteristics of individual structures influence the characteristics and efficiency of the tandem. Basic equation (1) for parameters calculation with later their comparing with experimental data was used:

$$J = J_0 \left\{ \exp\left[\frac{q(U - J \cdot R_{in\ ser.})}{n \cdot k \cdot T} \right] - 1 \right\} + \frac{U - J \cdot R_{in\ ser}}{R_{shunt.}} - J_{Ph}, \quad (1)$$

where J - the current through the photostructure, A;
U - the voltage applied to the structure, V;
J_{Ph} – the photocurrent, A;
n - the nonideality coefficient;
k - the Boltzmann constant, J / K;
T – the temperature, K;
$R_{in\ ser}$ – the series resistance, Ohm;
R_{shunt} – the shunt resistance, Ohm.

Formula (1) describes the electrical model of the photodiode structure for a single diode. In the work, both structures for photovoltaic cells and structures with in-parallel and in-serious connection were considered. The total current-voltage characteristic for a tandem structure can be described using the same expression. In this case, one of the aims in this work was to determine dependence between the characteristics (parameters) of the structure included in the tandem in-parallel or in-series, and of the individual structures included in the tandem.

In this work, the aim is to find trends for different tandem configurations using high – current sub-cells, based on GaAs p-i-n detector structure and $CH_3NH_3PbI_3$ perovskite. So for

output parameters extraction, we simplified the calculation route to single diode model (see Figure 4).

In-parallel connection with unbalanced sub-cells, we have no such current loss because shunt and series resistances can be leveled in parallel circuit with the current sum, that's why tandem operation tends to be closer for better sub-cell . Of course, this way has advantages only when V_{oc} of sub-cells has similar value, in the opposite situation they can cut the power of tandem with the mismatch of current generation direction [6].

Analyzing the results of this work, it should be noted that GaAs and perovskite technologies are the most effective and promising at the moment for applications in their areas – substrate and solid-state technology, thin-film technology of organometallic semiconductors. The main advantage of this device is the high photocurrent production, which allows us to obtain high power. Therefore, in this paper, we have developed a tandem in a parallel, non-monolithic connection showing a high short-circuit current from a square centimeter 39 mA and obtained an efficiency of about 19 %. The approach presented in this paper clearly shows the advantages of parallel tandems over in-serious ones with appropriate balancing the output characteristics: the filling factor and the idling voltage.

Band gaps for the sub-cells are 1.42 eV for GaAs and 1.58 eV for perovskite. Such difference - 0.16 eV gave a spectral window for GaAs sub-cell. It means that GaAs sub-cell will absorb light remained from perovskite in 420-760 nm region, mostly after 600 nm. Moreover, the near infra-red spectral window is fully absorbed by GaAs sub-cell, mostly contributing to sub-cells tandem operation.

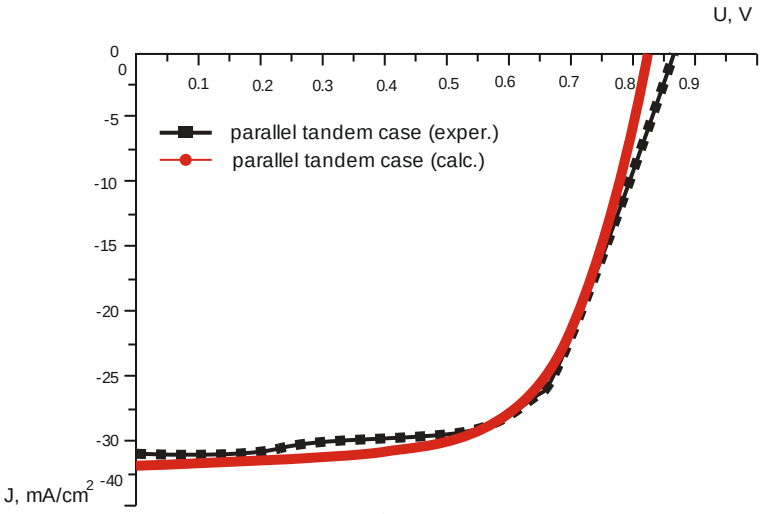

a)

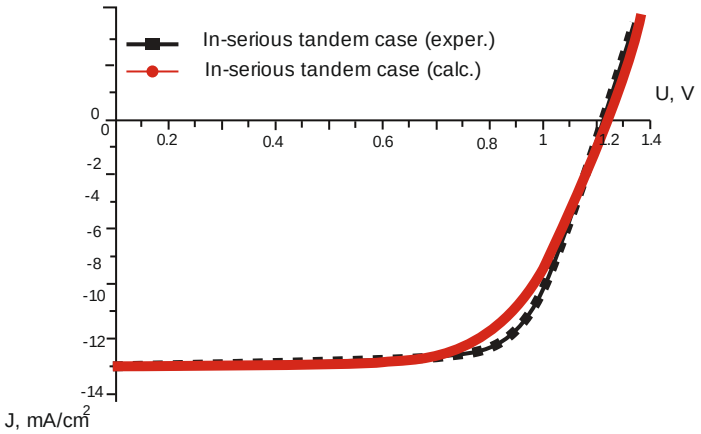

b)

Figure 4. Simulated and experimental dependences with in-parallel (a) and in-series connection (b).

CONCLUSIONS

In this work, we developed a tandem in-parallel, non-monolithic connection showing a high short-circuit current ~ 39 mA/cm^2 and obtained an efficiency ~19 %. Typical tandem devices today are mainly represented by various modifications of silicon-based solar cells with in-series connected elements for other types that need current balancing, which significantly reduces efficiency since each current of the sub-cells is usually much lower than in devices for this type in a single performance. The approach presented in this paper clearly shows the advantages of parallel tandems over successive ones with appropriate balancing of the output characteristics of the filling factor and the open circuit voltage. As shown by the experimental results, the parallel connection of GaAs and perovskite solar cells has an advantage over more than 5-7 % in-series connection even with a small perovskite spectral window for GaAs (about 100 nm in the long wavelength region). At the same time, the calculation using a simplified single diode model allows us to assume that it not only has an advantage in the sum of sub-cell currents but also eliminates shunt leaks and possible imbalance of the tandem in the filling factor. We see that the offered 4 electrode tandem concept development in the gradual integration of a monolithic connection and spectral separation opens wide possibilities for optoelectronic modifications of the perovskite bandgap to achieve record efficiency more than 25 %. Besides the quantitatively high output performance, the main result of this work is that the efficiency of more than 17-19 % in various configurations is a demonstration of the parallel architectures potential, which has obvious advantages in the operation of the device over in-serious tandems.

ACKNOWLEDGEMENT

The work was carried out with the financial support of the Ministry of Education and Science of the Russian Federation within the framework of the state task to the university #3.2794.2017/4.6

REFERENCES

1. Park, N.G. 2015. "Perovskite Solar Cells: an Emerging Photovoltaic Technology," *Materials Today*, 18(2):65-72.
2. Zhang, W. et al. 2015. "Ultrasmooth Organic-Inorganic Perovskite Thin-Film Formation and Crystallization for Efficient Planar Heterojunction Solar Cells," *Nat Commun*, 6:6142
3. Fedorchenko, I.V. et.al. 2018. "Growth Method for $A^{III}B^{V}$ and $A^{IV}B^{VI}$ Heterostructures," *Journal of Crystal Growth*, 483:245-250.
4. Albrecht, S. et al. 2016. "Monolithic Perovskite/Silicon-Heterojunction Tandem Solar Cells Processed at Low Temperature," *Energy Environ. Sci.*, 9(1):81-88.
5. Bailie, C.D. et al. 2015. "Semi-Transparent Perovskite Solar Cells for Tandems with Silicon and CIGS," *Energy Environ. Sci.*, 8(3):956–963.
6. Sun, W. et al. 2016. "High-Performance Inverted Planar Heterojunction Perovskite Solar Cells Based on Solution-Processed CuOx Hole Transport Layer," *Nanoscale*, 10806-10813

2018 International Theoretical and Practical Conference on Alternative and Smart Energy (TPCASE 2018)
ISBN: 978-1-60595-617-6

Capacitive Power Taking Off From High Voltage Transmission Lines

Marina Rozhina, Nadezhda Buryanina, Yury Korolyuk
and Anna-Mariia Timofeeva

ABSTRACT

A complex infrastructure and transport scheme of fuel supply, long and busy power lines, extreme continental climate with temperature changes from -50 to +45 ºC - all these factors have a negative impact on the quality of electricity. There is high probability of accidents due to the unreliability of electrical networks. This paper describes a method of power supply to remote consumers of "low" power without the construction of high-power transformer substations and the use of diesel generators.

INTRODUCTION

The Russian Federation is the largest country in the world by area. It occupies a huge area of 17.1 million square kilometers. Most of its territory is concentrated in the North. The energy problems of the Republic of Sakha (Yakutia) are due to its territory and non-settlement. Occupying the sixth part of Russian territory, the population of Yakutia is only about one million. Yakutia is divided into 4 energy areas—Central, Western, South Yakutian and Northern. More than 900 thousand people live in these four energy areas.

The research considers the Northern energy area, which occupies 2/3 of the territory of the whole Yakutia (2.2 million square kilometers). The total installed capacity is 184.9 MW (electricity) and 92.4 Gcal/h (heat). The main sources of heat and electricity are diesel power plants, but in addition, 19 solar power plants

Marina Rozhina, North-Eastern Federal University, 808 Office, 50 Kulakovskogo Street, Yakutsk, Russia
Nadezhda Buryanina, Yury Korolyuk, Anna-Mariia Timofeeva, Chukotka branch of North-Eastern Federal University, 4-106 Office, 3 Studencheskaya Street, Anadyr, Russia

with a total capacity of 1.6 MW operatein the Northern part of Yakutia, which are the largest in the Arctic, and 2 wind power plants (290 kW). Because ofthe large number of diesel power plants (120), the problem of fuel delivery is acute, and the cost of electricity is accordingly high. Fuel is delivered to 23 Northern regions of Yakutia on the rivers and the Northern sea route. Every year supply of fuel and energy resources for the needs of the Northern and Arctic regions becomes more difficult. A technological consumption of electricity for its transport is about 13% of the electricity released into a network [1].

All power districts are not connected by electric networks by now. Now the construction of large inter-system power lines is going on: VL-220 kV "Chernyshevsky-Mirny-Lensk-Peleduy" and VL-220 kV "Nizhny Kuranakh–Tommot–Maya", which will connect the disparate energy areas into a single power system.

In the future, we should also take into account the connection of Yakutian electric networks to Magadan ones.

PRACTICAL PART

Electricity supply to the Northern territories is a serious problem due to remoteness of facilities, mainly small settlements, often limited to several houses.

The territory of the Russian Federation is huge, which explains the presence of a large number of long overhead power lines. Power transmission lines of 110 – 220 kV are laid along roads, on which there are settlements of a few houses, geological party, agricultural lands, and wood processing plants. It is not economically feasible to build substations with transformers taking into account their operation. Therefore, such settlements are supplied with electricity from small diesel generators. As a rule, there is no qualified service. That's why blackouts are frequent.

At Physics and Technology Institute of North-Eastern Federal University at the Department of Power Supply and its Chukotka branch, research is being conducted that will improve the reliability of electrical networks of existing power lines.

An alternative solution to the problem of the power supply without the construction of high-power transformer substations and using of diesel generators is capacitive power taking off from the power transmission line. There are several options for capacitive power taking off. The classical scheme of capacitive power taking off [2] is shown in Figure 1.

The design schemes of substitution of capacitive power taking off are shown in Figure 2.

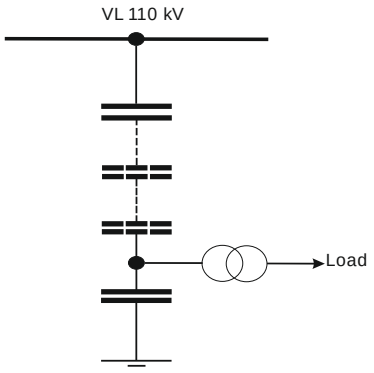

Figure 1. Classical scheme of capacitive power taking off.

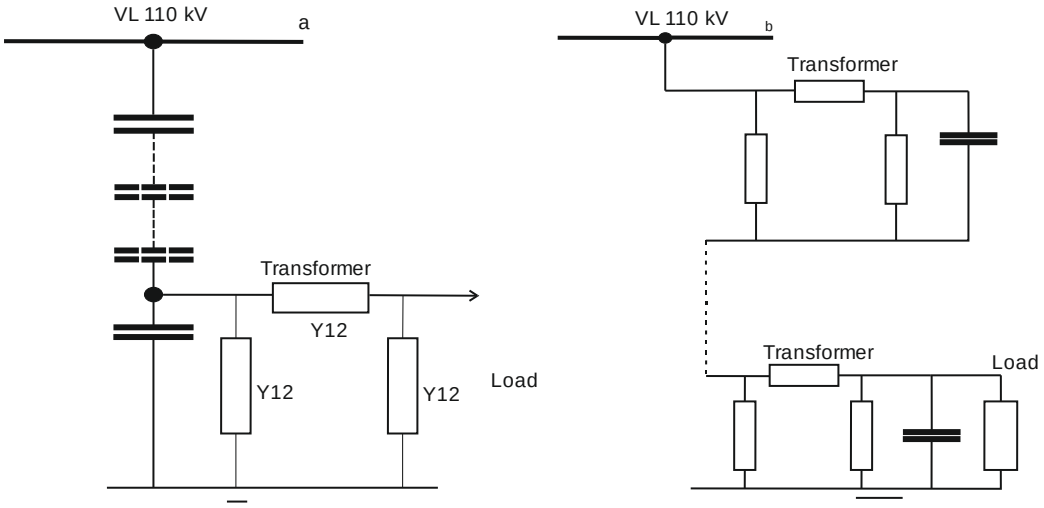

Figure 2. Design scheme of the capacitive power taking -off: a) taking -off from the latest transformer; b) with inclusion of capacitors across transformers.

The conductivity of the U-shaped equivalent circuit of the transformer is calculated as:

$$Y_1 = \frac{1-k_t}{Z_t} + Y_{xx}\,; \qquad Y_2 = \frac{k_t^2-1}{Z_t}; \qquad Y_{12} = \frac{k_t}{Z_t}, \tag{1}$$

where k_t- the transformer transformation ratio as the ratio of high voltage to a low voltage; Z_t – the resistance of the transformer, converted to a high voltage; Y_{xx}- the conductivity due to no-load current (generally accepted designations), which is described as:

$$Y_{xx} = \frac{\Delta P_{xx}}{U_v^2} - j\sqrt{\left(\frac{I_{xx}\%}{100} \cdot \frac{S_{nom}}{U_v^2}\right)^2 - \left(\frac{\Delta P_{xx}}{U_v^2}\right)^2}. \quad (2)$$

The nominal low voltage U_{nom} on the conductivity Y_2 is 0.38 kV. Figure 3a shows two dependences of a voltage on a load S (in relative units) with a power ratio of 0.8. Curve 1 (Figure 3a) shows the dependence of a voltage on a load with a linear change in the power of additional capacitors to maintain voltage levels within the specified limits (from 0.95 to 1.05 U_{nom}). The required power is 1.3 times more than the reactive power (dependence 1 in Figure 3b). For linear changes in a power of additional capacitors is characterized by an increase in voltage in the range of minimum loads, and the more power capacitors relative to reactive power, a voltage level is higher. In this example, the voltage at low loads reaches 1.07 U_{nom}, and the voltage at the full load is reduced to 0.95 U_{nom}. At higher power capacitors both voltages increase, and if the full load voltage is equal to the nominal, at low loads it will exceed 1.1 U_{nom}. Therefore, this method of voltage regulation should be considered inappropriate.

Therefore, it is necessary to pay attention to voltage regulation by a non-linear change of capacitors power depending on a load change. Figure 3a shows the dependence of voltage on the load (curve 2) of the non-linearly variable capacitor power (Figure 3b, curve 2). From idle to max load the voltage varies from 1.05U_{nom} up to the nominal. The given dependence of voltage leads to the conclusion that it is enough to control the voltage level and maintain it within the specified limits by changing a power of capacitors without adhering to any specific law or regulation.

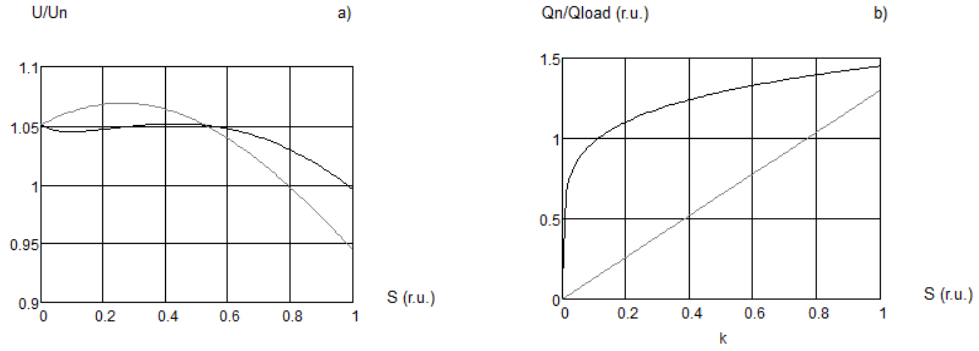

Figure 3. a) dependence of voltages at the load from capacitors power, which are included to maintain the voltage levels; b) the corresponding capacity of capacitors.

CONCLUSION

A serious problem that needs to be solved is the disconnection of capacitive power taking off from the line. A switch setting is expensive. Therefore, the

disconnection of capacitive power taking off from disconnector is considered. At the voltage of 110 kV when the distance between the poles of 3.5 m in accordance with the Rules of Electrical device installations charging currents of a line can be disabled. Charging currents of a line, as currents of capacitive power taking off, are capacitive, so the above rule also applies for deactivation of a current of capacitive power taking off in idle mode. It is guaranteed that the idle current can be switched off at a power of three-phase taking off of 150 kVA. The shutdown current will be 3 A. The load has to be disabled first, which can be done by load switch.

ACKNOWLEDGMENTS

The research was carried out with the financial support of RFFI and constituent entity of the Russian Federation-the Republic of Sakha (Yakutia) #18-48-140 010

REFERENCES

1. "About a Strategic Planning in the Russian Federation" in *Federal law of June 28, 2014 № 172-FZ The energy strategy of Russia for the period up to 2035*.
2. Korolyuk, Y.F., N.S. Buryanina, E.V. Lesnykh, and M.A. Rozhina. 2016. "Device of Capacitive Power Taking off from Power Transmission Line," patent of the Russian Federation #2594890.

2018 International Theoretical and Practical Conference on Alternative and Smart Energy (TPCASE 2018)
ISBN: 978-1-60595-617-6

Analysis of the Effect of Variation Air Temperature on Injection Gas Burner of the Thermoelectric Generator

Ilia Sviridov, Aleksey Ignatov, Konstantin Kryzhaev,
Igor Perevezencev and Dmitriy Shmatov

ABSTRACT

In this work, simulation of a premixing injection gas burner with various air temperatures with ANSYS Fluent software was performed. A natural gas fired injection gas burner was used as a heat source as a part of a thermoelectric generator. Assuming that the gas-air mixture flow is one-dimensional and axisymmetric, the issues were solved in axisymmetric setting, taking into account the gas compressibility. In the performance of a task, a set of assumptions was made: k-epsilon realizable model was picked as turbulence model with scalable wall functions; the flow in the ejector, mixing chamber and diffuser is subsonic; the pressure of the injected air was set to atmospheric pressure; pressure at the inlet to the gas burner is subcritical (≤ 86 kPa for methane). Based on the calculations, the dependence of the equivalence ratio on the air temperature was determined. Experimental researches helped develop a gas burner.

INTRODUCTION

Thermoelectric energy technologies are currently being actively developed by leading power-engineering manufactures [1]. Thermoelectric generators (TEGs)

Ilia Sviridov, Aleksey Ignatov, Konstantin Kryzhaev, Dmitriy Shmatov, Voronezh State Technical University, 14, Moskovskiy Avenue, Voronezh, 394026, Russia
Igor Perevezencev, The Scientific and Production Enterprise InterPolyris Ltd, 6, Parkovyi Passage, Novovoronezh, 396073, Voronezh Region, Russia

found wide application in many industries, such as space, automotive industry, aviation, oil and gas industry, etc. [2, 3]. The following factors have a great influence on the efficiency of a TEG: constructive scheme of a thermoelectric installation, features of heat supply and removal, heat source selection, losses in auxiliary devices, etc. The heat source determines the design and application of TEGs. The most developed TEGs is a TEGs operating on gas fuel [4]. They are a part of autonomous power supply system (APSS). APSS are used for power supply remote and hard-to-reach places, including technological communication and telemetry facilities, natural gas storage and transport systems, systems for cathodic protection of gas pipelines and oil pipelines from electrochemical corrosion. In such areas, the operation of generating devices is often accompanied by abrupt changes in temperature, pressure, humidity. Therefore, high reliability and durability indicators are of particular importance. Gas usage simplifies the control of input heat due to a gas burner. A gas burner provides complete combustion at different temperatures. A gas burner is used without stockpiling combustion products. Fuel combustion processes play a special role here. Controlling of the combustion processes, the correctness of the selected gas burner and operating modes require great attention. It was reported in work [5]. The author shows information about analysis of the effect of variation equivalence ratio on the heat losses with combustion products and energy conversion efficiency. In a present-day usage of thermoelectricity for natural gas combustion, gas ejectors became widely used. Partially premixed gas burners and complete premixed gas burner are being developed on the basis of gas ejectors. Gas ejectors provide a homogeneous constitution of the gas-air mixture, have the self-regulate ability (the maintaining coefficient of ejection) in a certain range of stress changes, which can be reduced with heating the gas or air, establishing of the backpressure or rarefaction in the combustion chamber and other conditions.

MODEL AND METHODS

The target of the research in this work was an ejector whose geometrical dimensions were obtained using the method described in [6]. The k-epsilon realizable model with scalable wall functions was chosen as a turbulence model, which is most suitable for these issues. The gravity forces influence was not taken into account. The perfect gas equation, taking compressibility into account, was used. It was assumed that the air-gas mixture flow is stationary, axisymmetric; air is fed to the ejector with constant discharge. The wall surfaces roughness was set equal to zero. The input parameter for the Design of Experiments tool is the air

gap width specified in Figure 1. The output parameter is the equivalence ratio, calculated as the average over the output boundary of the diffuser.

The software ANSYS Fluent [7] performs a numerical solution of the systems of equations using the finite volume method. The basic equations of the mathematical model (continuity equations, the balance of momentum equations, energy equations) describing the behavior of the primary and ejected gas flow (1) – (8) have the form:

$$\frac{\partial}{\partial x_i}\left(\rho u_i\right)=0\,, \tag{1}$$

$$\frac{\partial}{\partial x_i}\left(\rho u_i u_j\right)=\frac{\partial P}{\partial x_i}+\frac{\partial \tau_{ij}}{\partial x_j}\,, \tag{2}$$

$$\frac{\partial}{\partial x_i}\left(u_i\left(\rho E+P\right)\right)=\vec{\nabla}\left(\alpha_{eff}\frac{\partial T}{\partial x_i}\right)+\vec{\nabla}\left(u_j\left(\tau_{ij}\right)\right), \tag{3}$$

$$\tau_{ij}=\mu_{eff}\left(\frac{\partial u_i}{\partial x_j}+\frac{\partial u_j}{\partial x_i}\right)-\frac{2}{3}\mu_{eff}\frac{\partial u_k}{\partial x_k}\delta_{ij}\,, \tag{4}$$

where τ_{ij} – the viscous stress tensor. Transport equations for the k-epsilon realizable turbulence model are represented as

$$\frac{\partial}{\partial x_j}\left(\rho k u_j\right)=\frac{\partial}{\partial x_j}\left[\left(\mu+\frac{\mu_t}{\sigma_k}\right)\frac{\partial k}{\partial x_j}\right]+G_k-\rho\varepsilon\,, \tag{5}$$

$$\frac{\partial}{\partial x_j}\left(\rho\varepsilon u_j\right)=\frac{\partial}{\partial x_j}\left[\left(\mu+\frac{\mu_t}{\sigma_k}\right)\frac{\partial \varepsilon}{\partial x_j}\right]+\rho C_1 S\varepsilon-C_2\frac{\varepsilon^2}{k+\sqrt{\nu\varepsilon}}\,, \tag{6}$$

where $G_k=\mu_t S^2$ – the turbulent kinetic energy, which is formed from average gradients, according to the Boussinesq hypothesis.

$$C_1=\max\left[0.43,\frac{\eta}{\eta+5}\right],\eta=S\frac{k}{\varepsilon}\,, \tag{7}$$

$$S=\sqrt{2S_{ij}S_{ij}}\,, \tag{8}$$

where $S_{ij}=\frac{1}{2}\left(\frac{\partial u_j}{\partial x_i}+\frac{\partial u_i}{\partial x_j}\right)$ – the deformation tensor.

The constants of the turbulence model are set by default $C_2 = 1.9, \sigma_k = 1$ $\sigma_\varepsilon = 1.2$. Turbulent viscosity $\mu_t = \rho C_\mu \frac{k^2}{\varepsilon}$. A mass-flow inlet boundary condition was added. Boundary conditions were set at the gas nozzle input. Gas temperature is set $300\ K$.

RESULTS AND DISCUSSIONS

As a result of the numerical simulation, the dependence of the equivalence ratio on the air temperature was obtained (Figure 1). The complete premixing gas ejection burner normally works with the equivalence ratio close to one ($\alpha = 1.05$).

Proceeding from the obtained dependence, the optimal ambient temperature for this ejector operating mode will be $306.52\ K$. Equivalence ratio nonlinearly increases with decreasing ambient temperature. In addition, it is necessary to take into account the operation features of a gas burner based on a gas ejector, such as backpressure or rarefaction in the combustion chamber, which affect the equivalence ratio.

Subsonic flow, the maximum Mach number in the gas nozzle is 0.67. In Figure 1 concentration distributions of methane and oxygen along the symmetry axis are constructed.

For experimental research, a gas burner was developed. The size of the air gap of the gas burner was 1.25 mm; this value was determined at the stage of previous studies and is optimal for this burner. The experiment was conducted on one mode for $\alpha = 1.05$. The parameters of the supplied components to the burner are given in Table I.

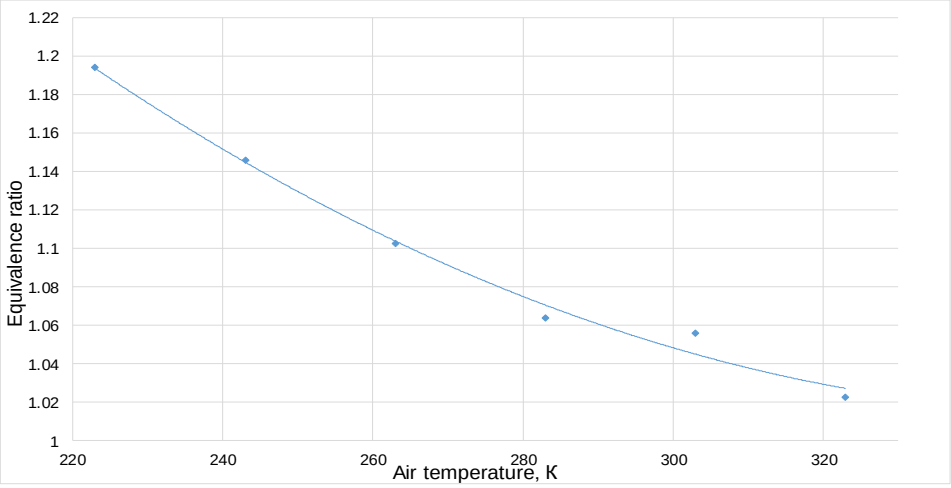

Figure 1. Dependence of the equivalence ratio on the air temperature.

TABLE I. TEMPERATURE OF THE SUPPLIED COMPONENTS.

Supplied component to the gas burner	**The average temperature of the gas burner during experiment °K**
Methane	301.4
Air	306.9

The quality control of gas combustion was controlled by the color of the flame. Poor gas flaring is characterized by a yellow smoke flame. When gas is fully burned, the flame is a short blue-violet torch with a high temperature. Typical examples of the flame are shown in Figure 3. In the course of experimental studies, the flame (Figure 4) is a short torch of bluish-purple color, which makes it possible to conclude that the theoretical studies carried out are correct. Experimental researches are planned to be continued and carried out for the range of air temperatures from - 50 to + 50 ° C.

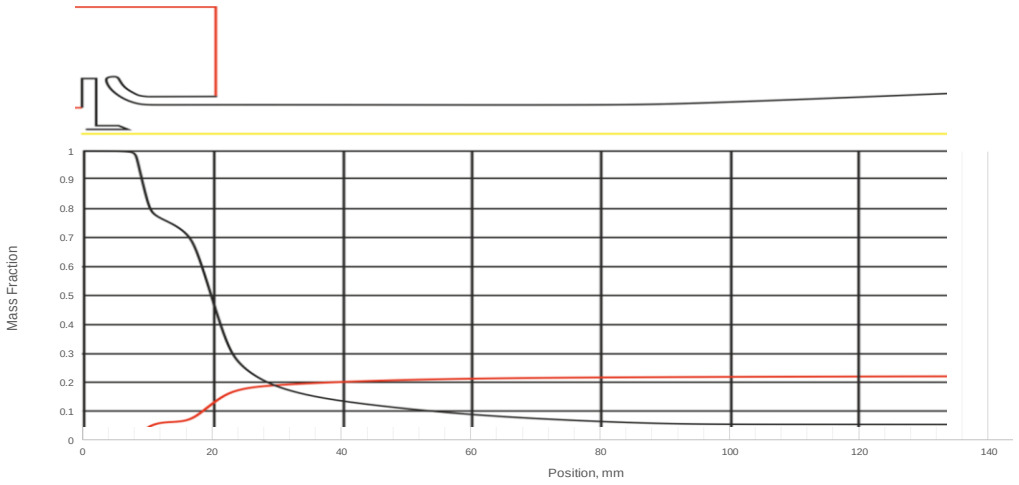

Figure 2. Oxygen and methane mass fraction distribution on the symmetry axis (red line –O_2, black line – CH_4).

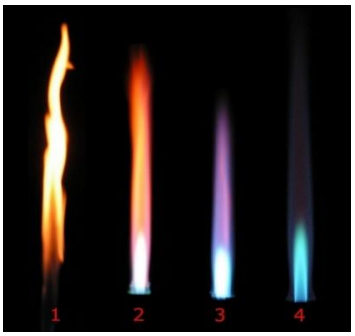

Figure 3. Different flame types of burner depend on oxygen supply. On the left - a rich fuel with no premixed oxygen produces a yellow sooty diffusion flame; on the right - a lean fully oxygen premixed flame.

Figure 4. Experimental research of the developed gas burner.

CONCLUSION

Based on the results of studies, the dependence of the equivalence ratio on the temperature of the ejected air was determined. Based on the obtained dependence, for this mode of operation of the ejector, the ambient temperature will be $306.52\ K$. Based on the simulation, a gas burner was developed. Experimental studies of the developed gas burner with the obtained values $306.52\ K$ of the temperature of air and the air gap are performed. The obtained data confirm the numerical simulation.

ACKNOWLEDGMENT

The research was carried out with the financial support of the Ministry of Education and Science of the Russian Federation in the framework of the Resolution of the Government of the Russian Federation No. 218 of April 9, 2010 (Agreement #03.G25.31.0246).

REFERENCES

1. Hvesuk, V.I., D.A. Ostanko, A.S. Skryabin, P.A. Tsyganov, R.I. Chelmodeev, and A.U. Tsirkov. 2016. "Marginal Efficiency of Thermoelectric Heat Conversion in High-Temperature Energy Facility," J. *Science and Education Bauman Moscow State Technical University*, 3:81-105.
2. Allen, D.T., J.C. Bass, N.B. Elsner, S. Ghamaty and C.C. Morris. 2000. "Milliwatt Thermoelectric Generator for Space Applications," in *Space Technology and Applications International Forum–2000*, American Institute of Physics, pp. 1476-1481.
3. Dubourdieu, P., and G. Tribou. 1997. "Thermoelectric Generator for Underwater Wellhead," in *16th International Conference on Thermoelectrics*, Cherbourg Naval, France, pp. 603-606.
4. Qiu, K., and A.C.S. Hayden. 2009. "A Natural-Gas-Fired Thermoelectric Power Generation System," J. *Journal of Electronic Materials*, 38(7):1315-1319.
5. Gluxov, A.P. 2013. "The Effect of Equivalence Ratio on Heat Losses with Combustion Products," J. *Enegry Saving Power Engineering Energy Audit*, 9:12-15.
6. Ionin, A. A. 1989. *Gas supply.* Moskow: Stroiizdat, 439 p.
7. "ANSYS FLUENT Theory Guide." 2011. Available at: https://ansyshelp.ansys.com

2018 International Theoretical and Practical Conference on Alternative and Smart Energy (TPCASE 2018)
ISBN: 978-1-60595-617-6

Environmental Improvement Based on the Use of Thermal Water from Nuclear Power Plants

Antonina Suzdaleva, Svetlana Goryunova, Natalya Ozerova, Elena Fedorova, Anastasiia Borovkova and Matvey Anufrikov

ABSTRACT

A common effect of nuclear power plants' operation is the discharge of heated water, for which the term "technogenic thermal water" is proposed, into water bodies. Despite the declared intentions to phase out nuclear power, the number of nuclear power plants in the world and their aggregate capacity keep increasing. This inevitably leads to bigger heat output. There are two alternative solutions to problems arising from the discharge of technogenic thermal water by nuclear power plants. The first, traditional, solution is in line with the currently prevailing "restrictive paradigm" of environmental activity and lies in stricter control over the thermal pollution of water bodies. The second solution implies creating conditions under which the energy of technogenic thermal water could be used to improve the state of water bodies for the purposes of fish farming, crops production, and seawater desalination. This will require active human participation in the development of environmental situation, as well as design and installation of special technical devices. Such methodological approach should, therefore, be referred to as the "creative paradigm" of environmental activity.

PROBLEM STATEMENT

Nuclear power plants' operation results in the generation of big amounts of heat that need to be constantly removed from power units. A common solution is

Antonina Suzdaleva, Natalya Ozerova, Elena Fedorova, Anastasiia Borovkova, Matvey Anufrikov, National Research University Moscow Power Engineering Institute, MPEI 14 Krasnokazarmennaya Street, Moscow, 111250, Russian Federation
Svetlana Goryunova, Moscow City Teachers' Training University, MCTTU, 4 2nd Sel'skokhozyaystvenny Passage, Moscow, 129226, Russian Federation

to use a water flow created by a specially designed water supply system. Water volume required to remove heat is quite significant. It is compared to the flow of medium-sized rivers. For the purposes of water conservation and nuclear safety, special water bodies—cooling ponds—are created. The bulk of the heated water discharged from nuclear power plants into these ponds is cooled and can be reused.

Various water bodies, such as reservoirs, modified lakes, and gulfs, can be used as the basis for cooling ponds [1]. The flow of heated water that can be referred to as technogenic thermal water significantly impacts the environment. The rise in water temperature to 40^{o} C kills the majority of aquatic organisms' species. However, technogenic thermal water with lower temperature promotes plants' and animals' growth and development, with the biodiversity of aquatic ecosystems preserved. In certain cases, discharging technogenic thermal water results in improved water quality in water bodies. A special term is proposed to denote this positive thermal effect—"calefaction" [2]. It is fundamentally different from the more common notion of "thermal pollution" used to describe the negative implications of the rising temperature of the environment.

IMPACT OF TECHNOGENIC THERMAL WATER

The environmental problem associated with discharging technogenic thermal water from nuclear power plants into the environment can be solved in two ways. The first, traditional, way corresponds to the currently prevailing "restrictive paradigm" of environmental activity and lies in stricter control over thermal pollution of water bodies. The second way implies creating conditions under which technogenic thermal water will produce a controlled positive effect. Measures aimed at accomplishing this task can be referred to as "environmental optimization" [3]. This notion implies active human participation in the environmental situation, as well as design and installation of special engineering devices for the purposes of environmental improvement. That is why such a methodological approach can be called the "creative paradigm" of environmental activity [4].

The search for solutions within the "creative paradigm" becomes an increasingly pressing problem. Despite the declared intentions of phasing out nuclear power, the number of nuclear power plants is steadily growing [5]. Some of them discharge thermal water into fresh and sea water bodies, and this trend is likely to stay in the near future. Thermal pollution control requires more spending, but positive effects from environment-friendly thermal water use can increase as well. In addition, some of them already bring economic benefits. The demand for new approaches to the environmental problem of technogenic thermal water will grow significantly if thermonuclear power plants are put into operation as their capacity will be considerably bigger (therefore, resulting in larger

amounts of water necessary for heat removal) [6]. The technological basis for creating such power facilities is already there, and the demand for cheap electricity at a certain point may overcome the resistance of environmental interest groups.

WAYS (FOCUS AREAS) OF ENVIRONMENTAL OPTIMIZATION

At present, there are two categories of problems that can be solved through environmental optimization of water supply systems at nuclear power plants. The first one is technical amelioration or the use of water supply systems' side-effects for improving the aquatic environment quality. Moderate water heating, aeration, and mixing in catch drains intensify self-purification processes [7]. Constant water circulation hinders the development of environmentally hazardous zones in water bodies near external sources of pollution. Incoming pollutants are floated away by the water stream, and their concentration quickly drops to permissible levels. Besides, appropriately organized transportation of technogenic thermal water prevents stagnation zones. For these reasons, water quality in cooling ponds is often significantly higher, as compared to the sources of their replenishment.

Another aspect of technogenic amelioration should also be emphasized. The number of bacteria on sites where heated water is discharged is usually hundreds and thousands of times higher than at nuclear power plants' water intake units [8]. During certain periods, the difference can reach 10^6. This phenomenon is caused by the development of the so-called "biofilm", consisting of bacteria and their slime, on the inner surface of water supply systems' technical units. In higher temperatures, bacteria begin to reproduce aggressively. Some of them constantly detach themselves from the substrate and float away into the cooling pond, where they are quickly spread in a considerable water area by the stream of technogenic thermal water. To describe this phenomenon, the term "biotechnological pulverization" is suggested [9]. These microorganisms are mostly comprised of heterotrophic bacteria (saprophytes) that are the main agents of natural self-purification processes. Thus, a process takes place in cooling ponds that is similar to the use of bacteria products for waste water treatment. Moreover, water purification as a result of heterotrophic bacteria biotechnological pulverization is to a certain degree a self-regulating process. Bacteria developing in water supply systems' technical units feed on organic substances carried by the water flow. It has been experimentally proved that biofilm grows faster with higher pollution levels at water intake units. In such conditions, the intensity of bacteria biotechnological pulverization inevitably increases, which leads to a more intense water purification process.

The efficiency of technical amelioration processes can be increased through environmental optimization of nuclear power plants' water supply systems by means of:

- integrating technogenic thermal water aeration devices in water supply systems;
- building hydraulic works that facilitate technogenic thermal water transportation and circulation and contribute to bringing about positive environmental effects;
- creating special facilities to manage the processes of biofilm growth and biotechnological pulverization (for example, chambers next to heat-exchange devices for heterotrophic bacteria propagation).

In every specific case, applying one of the above-listed methods may result in improved environmental conditions on a relatively small site. But taking into account the steadily growing volumes of technogenic thermal water discharged into the environment, as well as the ubiquitous increase in water body pollution, the implementation of this methodology can have a significant impact on the state of water resources.

The second category of problems is the prevention of socio-ecological crises. The main reason for such crises is the disbalance between the growing population and the number of environmental resources required for the normal life. These crisis occurrences gradually turn into full-scale global crises. Presently, the biggest threat is posed by the global food crisis (shortage of food resources), the global water crisis (shortage of drinking water), and the global overpopulation, or demographic, crisis (shortage of living space and normal living conditions). Today a significant portion of the planet's population lives under conditions of social discomfort, struggles with hunger and has to drink water that does not meet sanitary requirements. The progression of all socio-ecological crises is interrelated, and when it gets out of control, it is accompanied by a large-scale degradation of the environment and, eventually, by a global environmental and socio-economic catastrophe. A hungry man deprived of normal living conditions starts mindlessly depleting natural resources in order to survive, ignoring pollution issues.

Environmentally friendly use of technogenic thermal water can play an important role in solving these problems. Its bioproduction potential can bring a significant amount of new food products. Raising water temperature to a certain level (to 25-28^{O}C in most cases) contributes to faster growth and development of aquatic organisms. If not heated to extreme temperatures, technogenic thermal water leads to a large increase in organisms' productivity [3]. There is a considerable experience of this effect's practical application accumulated by now. For instance, the so-called "energy and biological systems" were routinely included in nuclear power plant construction in Russia in the 1970s-90s. These multi-purpose facilities comprised fish farming, greenhouses, microbiological waste management, as well as open ground plots heated by technogenic thermal water. Products' quality, including possible radionuclide concentration, was closely watched before the products could be marketed. Similar facilities were built in other countries as well. These activities should be considered not only as

taking advantage of thermal water's bioproduction potential but also as a form of energy conservation. Production at energy and biological facilities was mainly based on the utilization of randomly dispersed heat but not on traditional sources of energy.

The creative approach to utilizing the energy of technogenic thermal water will help accomplish some of the tasks in the prevention of water consumption crisis. Heat removed from nuclear power plant units can be used for seawater conversion. Industrial desalination systems of this kind have already been developed and are currently in demand in many regions [10]. With their capacity increasing, nuclear and, possibly, thermonuclear power industry will be able to not only meet the domestic demand for energy in regions where the power plants are located but also to facilitate crops cultivation, including desert areas where such activities and favorable conditions for human habitation were previously impossible. In addition, this contributes to alleviating demographic problems. In this case, the use of thermal water from power facilities can be viewed as a comprehensive solution to all major socio-ecological crises.

CONCLUSION

Thus, the solution to the technogenic thermal water problem can be represented as the following alternative. In terms of the restrictive paradigm of environment protection, the heat removed from power facilities should be dispersed in the environment. The main task is to avoid potential environmental damage. The creative paradigm alternative is the creation of hydraulic works and engineering systems that allow to use the energy of technogenic thermal water to improve the environmental situation in water bodies, as well as to prevent socio-ecological crises.

REFERENCES

1. Suzdaleva, A.L., and V.N. Beznosov. 2000. "Changes in the Hydrological Structure of Water Bodies and the Succession of Aquatic Biocenoses when they are Converted into Cooling Reservoirs of an Atomic (Thermal) Power Station," *Inzhenernaya Ekologiya,* 2:47-55. Available at: http://www.ntsyst.ru/pages/biointerference.html (in Russian).
2. Merriman, D. 1970. "The Calefaction of a River," *Sci. Amer.*, 222(5):42-52.
3. Suzdaleva, A., and S. Goryunova. 2014. *Technogenesis and Degradation of Surface Water Objects.* Moscow: ID ENERGIYA Publ. 456 p. (in Russian).
4. Suzdaleva, A.L., and S.V. Goryunova. 2017. *Biotechnosphere: Ecology and Life Safety.* Moscow: MGPU Publ. 240 p. (in Russian).
5. 2017. *Nuclear Technology Review*. *Vienna: IAEA.* 45 p.
6. Strelkov, V.S. 2016. "Thermonuclear Power Engineering: 60 Years of Investigations. What Next?" *Problems of Atomic Science and Engineering" (PASE), Ser. "Thermonuclear Fusion",* 39(1): 5-14.

7. Kuchkina, M.A. and V.N. Beznosov. 2012. “The Study of Pollution and Self-Cleaning Processes in the Natural-Technogenic System of NPP Cooling-Pond,” *Vestnik Rossiiskogo Universiteta Druzhby Narodov. Ser.”Ekologiya i bezopasnost' zhiznedeyatel'nosti”,* 3:48-52 (in Russian).
8. Suzdaleva, A.L. 2001. “The Effect of Circulating Water Masses of Nuclear Power Plants on the Distribution of Bacterial Plankton in Cooling Ponds,” *Water Resources*, 28(3):349-355.
9. Suzdaleva, A.L. 2001. “Effect of a Waters Discharge from Industrial Cooling Systems on the Plankton of the Reservoirs,” *Inzhenernaya Ekologiya*, 4:51-57 (in Russian).
10. Barak, A., L.A. Kochetkov, M.Dzh. Krins, and M. Khalid. 1990. “Seawater Desalination Using Nuclear Energy: Experience, Needs and Perspectives. Overview of Demonstration Facilities and Recent Research,” *IAEA Bulletin,* 3:48-54 (in Russian).

2018 International Theoretical and Practical Conference on Alternative and Smart Energy (TPCASE 2018)
ISBN: 978-1-60595-617-6

An Approximate Analytical Solution to the Problem of Natural Convection of a Newtonian Liquid in a Rectangular Area

Victor Ryazhskih, Victor Sumin, Andrey Boger
and Oleg Semenikhin

ABSTRACT

The problem of thermoconcentration convection of a viscous incompressible liquid in a rectangular area is solved analytically for a given heat flux through the boundary based on the physical linearization of the hydrodynamic subtask in the Stokes approximation. The solution is presented in form of convergent two-fold series. The computational experiment has confirmed the correctness of the accepted assumptions application.

PROBLEM FORMULATION

The problem of thermoconcentration convection of a viscous incompressible liquid in a rectangular area with a given heat flux through the boundary is considered. At the initial moment of time, the temperature and concentration of the impurity in the volume of the liquid are homogeneous and constitute t_0 and c_0, respectively. The mode of flow is assumed to be laminar. The Novier-Stokes equations are written in the Stokes form [1] under the assumption that $|V_X| << 1$, $|V_Y| << 1$ [2]:

Victor Ryazhskih, Oleg Semenikhin, Voronezh State Technical University, 14, Moskovsky Avenue, Voronezh, 394026, Russia
Victor Sumin, Andrey Boger, Air Force Education and Research Center “The Zhukovsky and Gagarin Air Force Academy”, 54A Starikh Bolshevikov Street, Voronezh, 394064, Russia

$$\rho \frac{\partial \bar{v}}{\partial \tau} = -\nabla p + \mu \Delta \bar{v} - \rho\beta(t - t_0)\bar{g} + \gamma\rho(c - c_0)\bar{g}; \quad (1)$$

$$\mathrm{div}\, \bar{v} = 0; \quad (2)$$

$$\frac{\partial t}{\partial \tau} = a\Delta t; \quad (3)$$

$$\frac{\partial c}{\partial \tau} = D\Delta c, \quad (4)$$

where ∇ is the Hamilton operator, Δ is the Laplace operator, $\bar{v}$, p, t, c, are the velocity vector, pressure, temperature, concentration; ρ, β - density and coefficient of volumetric medium expansion; τ - current time; $\bar{g}$ - gravitational vector.

In the component listing form, the system (1)-(4) is presented in the following dimensionless form for the current function, temperature and concentration:

$$\frac{\partial}{\partial \theta}\left(\frac{\partial^2 \Psi}{\partial X^2} + \frac{\partial^2 \Psi}{\partial Y^2}\right) = \frac{\partial^4 \Psi}{\partial X^4} + 2\frac{\partial^4 \Psi}{\partial X^2 \partial Y^2} + \frac{\partial^4 \Psi}{\partial Y^4} - \mathrm{Gr}_T \frac{\partial T}{\partial X} + \mathrm{Gr}_C \frac{\partial C}{\partial X}; \quad (5)$$

$$\frac{\partial T}{\partial \theta} = \frac{1}{\mathrm{Pr}}\left(\frac{\partial^2 T}{\partial X^2} + \frac{\partial^2 T}{\partial Y^2}\right); \quad (6)$$

$$\frac{\partial C}{\partial \theta} = \frac{1}{\mathrm{Sc}}\left(\frac{\partial^2 C}{\partial X^2} + \frac{\partial^2 C}{\partial Y^2}\right) - A^* \exp(A\theta); \quad (7)$$

$$\Psi(X, Y, 0) = 0; \quad (8)$$

$$\Psi(0, Y, \theta) = \Psi(d, Y, \theta) = \Psi(X, 0, \theta) = \Psi(X, b, \theta) = 0; \quad (9)$$

$$\frac{\partial \Psi(0, Y, \theta)}{\partial X} = \frac{\partial \Psi(d, Y, \theta)}{\partial X} = \frac{\partial \Psi(X, 0, \theta)}{\partial Y} = \frac{\partial^2 \Psi(X, b, \theta)}{\partial Y^2} = 0; \quad (10)$$

$$T(X, Y, 0) = 0; \quad (11)$$

$$-\frac{\partial T(0,Y,\theta)}{\partial X}=\frac{\partial T(d,Y,\theta)}{\partial X}=-\frac{\partial T(X,0,\theta)}{\partial Y}=1; \quad (12)$$

$$\frac{\partial T(X,b,\theta)}{\partial Y}=0; \quad (13)$$

$$C(X,Y,0)=0; \quad (14)$$

$$C(0,Y,\theta)=C(d,Y,\theta)=C(X,0,\theta)=0; \quad (15)$$

$$\frac{\partial C(X,b,\theta)}{\partial Y}=0, \quad (16)$$

where $X=\frac{x}{l}$, $Y=\frac{y}{l}$, $\theta=\frac{\tau\nu}{l^2}$, $\varsigma=\frac{h_1}{h_2}$, $T=\frac{t\lambda}{ql}$, $\mathrm{Gr}_T=\frac{\beta gql^4}{\nu^2\lambda}$, $\mathrm{Gr}_C=\frac{\gamma gql^3}{\nu^2\lambda}$, $l=\frac{2h_1h_2}{h_1+h_2}$, $\mathrm{Pr}=\frac{\nu}{a}$ - Prandtl number; $\mathrm{Sc}=\frac{\nu}{D}$ - Schmidt number; ν, a, D are the kinematic coefficients of viscosity, thermal conductivity and diffusions; Ψ - is the dimensionless current function $V_X=\frac{\partial\Psi}{\partial Y}$, $V_Y=-\frac{\partial\Psi}{\partial X}$; x, y - Cartesian coordinates; h_1, h_2 - width and height of the area; λ, γ are the coefficients of thermal conductivity and kinematic viscosity of the medium, respectively; V_X, V_Y are the projections of the velocity vector on the axes X and Y, q is the heat flux density through the wetted area boundary; A^*, A are the constants characterizing the kinetics of sediment dissolution, $d=\frac{\varsigma+1}{2}$, $b=\frac{\varsigma+1}{2\varsigma}$.

RESULTS

The disconjugate nature of system (5)-(16) allows one to use the solutions of the thermal and concentration problems when finding the dimensionless current function Ψ independently.

Thus, the task can be divided into three subtasks: 1) thermal; 2) concentration; 3) thermoconcentration.

To solve the thermal subtask to equations (6), (11)-(13), we apply the Fourier sine transformation successively according to X [3]:

$$T(X,Y,\theta)=\Lambda(X,Y,\theta)+\frac{2}{\varsigma+1}X^2-X+\frac{1}{2}(Y-1)^2-\frac{\varsigma-1}{\varsigma+1}(1-Y)\exp(Y-b), \qquad (17)$$

where the function $\Lambda(X,Y,\theta)$ is structurally double Fourier series.

The concentration subtask is represented by equations (7), (14)-(16).

Applying the Fourier sine transform according to *X*, we obtain the solution in the following form:

$$C(X,Y,\theta)=2A^*\,\mathrm{Sc}\sum_{k=1}^{\infty}\frac{\cos(\alpha_k d)-1}{\alpha_k}\left\{\frac{1}{\mathrm{A}\cdot\mathrm{Sc}+\alpha_k^2}\exp(\mathrm{A}\theta)-\right.$$

$$-\frac{\mathrm{ch}\left[\sqrt{A\cdot\mathrm{Sc}+\alpha_k^2}\,(b-Y)\right]}{(A\cdot\mathrm{Sc}+\alpha_k^2)\,\mathrm{ch}\sqrt{A\cdot\mathrm{Sc}+\alpha_k^2}}\exp(\mathrm{A}\theta)-$$

$$\left.-2\sum_{g=1}^{\infty}\frac{\cos\left[\frac{\beta_g}{b}(b-Y)\right]}{(\beta_g^2+\alpha_k^2+A\mathrm{Sc}\cdot b^2)\beta_g\sin\beta_g}\exp\left(-\frac{\frac{\beta_g^2}{b^2}+\alpha_k^2}{\mathrm{Sc}}\theta\right)\right\}\sin(\alpha_k X). \qquad (18)$$

Let's consider the third subtask—thermoconcentration.

Applying the final integral sine transform again with respect to *X* and *Y* to equations (5), (8)-(10), we obtain the solution:

$$\Psi(X,Y,\theta)=4\sum_{i=1}^{\infty}\sum_{j=1}^{\infty}\frac{1}{p_i^2+\eta_j^2}\left[p_i\left(\cos(p_i d)\cdot L_j-Q_j\right)\cdot M(p_i,\eta_j,\theta)-\eta_j\cdot F_i\cdot N(p_i,\eta_j,\theta)+\right.$$

$$\left.+\exp\left[-(p_i^2+\eta_j^2)\right]\cdot\int_0^{\theta}\Phi(\theta)\cdot\exp(p_i^2+\eta_j^2)\mathrm{d}\theta\right]\sin(p_i\,\mathrm{X})\sin(\eta_j\,\mathrm{Y}), \qquad (19)$$

where

$$M(p_i,\eta_j,\theta)=\frac{1-\exp\left[-(p_i^2+\eta_j^2)\theta\right]}{p_i^2+\eta_j^2}-\frac{\exp(-\eta_j^2\theta)-\exp\left[-(p_i^2+\eta_j^2)\theta\right]}{p_i^2};$$

$$N\left(p_i,\eta_j,\theta\right)=\frac{1-\exp\left[-\left(p_i^2+\eta_j^2\right)\theta\right]}{p_i^2+\eta_j^2}-\frac{\exp\left(-p_i^2\,\theta\right)-\exp\left[-\left(p_i^2+\eta_j^2\right)\theta\right]}{\eta_j^2};$$

$$\sin\left(p_i d\right)=0;\ \sin\left(\eta_j b\right)=0.$$

The coefficients L_j, Q_j and F_i in expression (19) are found from the system of equations (20), which is obtained after satisfying (19) the boundary conditions (9)-(10):

$$\sum_{i=1}^{\infty}\frac{p_i}{p_i^2+\eta_j^2}\left\{\left[p_l\cos\left(p_i d\right)\cdot L_j-Q_j\right]\cdot M\left(\xi_l,\eta_j,\theta\right)-\eta_j\cdot F_i\cdot N\left(p_l,\eta_j,\theta\right)+\right.$$

$$\left.+\exp\left[-\left(p_i^2+\eta_j^2\right)\theta\right]\cdot\int_0^{\theta}\Phi(\theta)\cdot\exp\left[\left(p_i^2+\eta_j^2\right)\theta\right]\mathrm{d}\theta\right\}=0;$$

$$\sum_{i=1}^{\infty}\frac{p_i\cos\left(p_i d\right)}{p_i^2+\eta_j^2}\left\{\left[p_l\cos\left(p_i d\right)\cdot L_j-Q_j\right]\cdot M\left(\xi_l,\eta_j,\theta\right)-\eta_j\cdot F_i\cdot N\left(p_l,\eta_j,\theta\right)+\right.$$

$$\left.+\exp\left[-\left(p_i^2+\eta_j^2\right)\theta\right]\cdot\int_0^{\theta}\Phi(\theta)\cdot\exp\left[\left(p_i^2+\eta_j^2\right)\theta\right]\mathrm{d}\theta\right\}=0; \qquad (20)$$

$$\sum_{i=1}^{\infty}\frac{\eta_j}{p_i^2+\eta_j^2}\left\{\left[p_l\cos\left(p_i d\right)\cdot L_j-Q_j\right]\cdot M\left(\xi_l,\eta_j,\theta\right)-\eta_j\cdot F_i\cdot N\left(p_l,\eta_j,\theta\right)+\right.$$

$$\left.+\exp\left[-\left(p_i^2+\eta_j^2\right)\theta\right]\cdot\int_0^{\theta}\Phi(\theta)\cdot\exp\left[\left(p_i^2+\eta_j^2\right)\theta\right]\mathrm{d}\theta\right\}=0. \qquad (21)$$

CONCLUSIONS

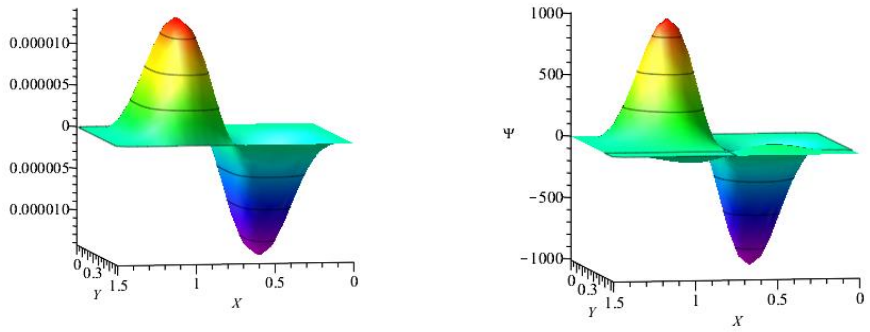

a b

Figure 1. Dynamics of the free-convective flow development in a rectangular area: at $\mathrm{Pr} = 1{,}01$, $\mathrm{Sc} = 2{,}1$, $\mathrm{Gr}_T = 1$, $\mathrm{Gr}_C = 4{,}84 \cdot 10^{-5}$ for different θ: a) – 0,002; b) – 0,05.

The result of the computational experiment is presented in Figure 1, which shows the dynamics corresponding to the well-known ideas about the free-convective flow [4].

REFERENCES

1. Khappel, Dzh., G. Brenner. 1976. *Hydrodynamics at small Reynolds scales*. M.: Mir, 630p. (in Russian)
2. Boger, A.A., S.V. Ryabov, V.I. Ryazhskikh, and M.I. Slyusarev. 2010. " Calculation of the conductive—laminar regime of thermo—convection of the Newtonian medium in a rectangularcavity with vertical isothermal walls," *RAN. Fluid and gas mechanics*, 3:17-21. (in Russian)
3. Sneddon, I. 1955. *Fourier Transforms*. M.: Izd-vo In. lit-ry, 655p. (in Russian)
4. Gebkhart, B., Y. Dzhaluriya, R. Makhadzhan, and B. Sammakiya. 1991. *Free convective flow, heat and mass transfer*. Book 1, M.:Mir, 678p. (in Russian)

2018 International Theoretical and Practical Conference on Alternative and Smart Energy (TPCASE 2018)
ISBN: 978-1-60595-617-6

Energy and Environmental Performance of the Steam Generator on the Basis of Pulsating Combustion

Nikolay Mozgovoy, Mikhail Tereshchenko and Lilia Zvyagina

ABSTRACT

An experimental study of a steam generator based on a pulsating combustion apparatus with a vortex-type combustion chamber, an aerodynamic valve and a Helmholtz resonator is described. A quantitative assessment of the process of formation and emissions of nitrogen oxides is given. A significant decrease in nitrogen oxides is due to the disequilibrium of the combustion processes due to the extremely insignificant residence time of the fuel components in the high temperature zone.

INTRODUCTION

The aim of this work is an experimental evaluation of the energy characteristics and environmental performance of steam generators based on pulsating combustion devices (PCD).

The steam generator is a PCD with a vortex-type combustion chamber with an aerodynamic valve and a Helmholtz resonator. Steam generation and overheating of steam occurs when water passes sequentially through the cooling jackets: of the aerodynamic valve, of the combustion chamber of the vortex type and the Helmholtz resonator. Combustion chambers of this type are well established in practical use [1].

The schematic diagram of the steam generator based on PCD with a cooling jacket is shown in Figure 1.

Voronezh State Technical University, 14, Moskovsky Avenue, Voronezh, 394000, Russia

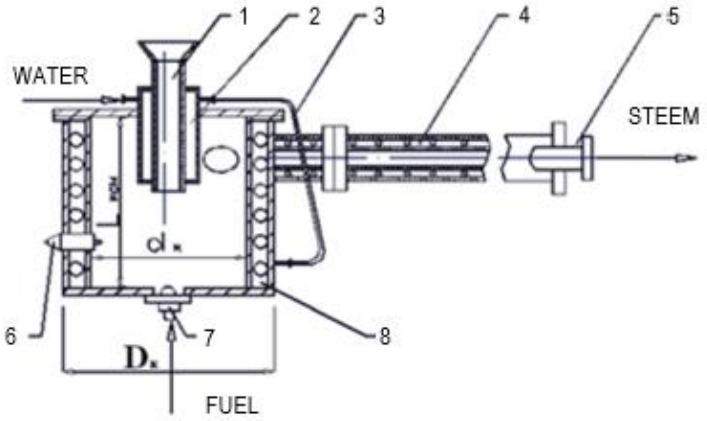

Figure 1. Steam generator on the basis of the PCD with a jacket
1 - aerodynamic valve; 2 - cooling jacket of the valve; 3 - connecting tube; 4 - cooling jacket of the resonant tube; 5 - outlet pipe for steam; 6 - electric light; 7 - centrifugal injector; 8 - cooling jacket of the combustion chamber.

TASK SETTING AND RESEARCH DESCRIPTION

In the course of research, the task was to determine the operating parameters of a stable pulsing combustion mode and the energy characteristics of the steam generator. The measurements were carried out at different hydrocarbon fuel consumption from 7.68×10^{-3} to 13.32×10^{-3} kg/s, which corresponded to the developed power from 310 to 410 kW [2]. Water consumption varied little and ranged from 0.312 kg/ s to 0.357 kg/s.

The pressure in the cooling jacket was changed due to the installation of orifice plates with a diameter of 6.5; 5.5; 4.5 and 3.5 mm. The most stable mode of operation was reached with of the orifice plates of 6.5 mm diameter. For this mode in Table I, the results of experimental measurements of steam generator energy parameters are presented. In column 13, the part of the energy of combustion of fuel which is transformed in thermal processes of the steam generator at reception of steam and the gaseous heat carrier is given.

In the physical sense, this value is exergy efficiency of heat flow. In the processes under consideration, losses are associated with irreversibility and, on average, constitute 18.4%. In similar processes with stationary combustion, they make up 57.5 percent [3]. Simultaneously PCD creates a flow of gaseous coolant of high temperature and an average speed of 50-60 m/s. This flow creates a pressure pulse of the carrier flow at the exit of the resonance tube, is equal to 1000-1300 Pa. In addition, pressure pulses occur as a result of acoustic disturbances and at the output of the resonant tube, their amplitude can be 2300-2500 Pa. It should be noted that the values given correspond to the pressure, which in gas dynamics is called the braking pressure. This circumstance makes it

possible to abandon the blast fan, which is usually supplied with stationary combustion heat generators. The final values of the efficiency of the steam generator will depend on the organization of the processes of use of thermal energy and flow energy.

The environmental performance of this steam generator can be judged by the results of the study of the yield of nitrogen oxides (NOs). Currently, the mechanism of formation of nitrogen oxides during combustion is structured into the following main groups: "fast", "thermal" and "fuel" nitrogen oxides [4].

The rate of formation of" fast "nitrogen oxides is an order of magnitude higher than "thermal", with a weak dependence on the temperature in the combustion chamber and a significant dependence on the fuel-air ratio. Their number can be estimated by the approximation formula obtained as a result of experimental data processing and given in [5]

$$C_{NO}=0.0745\times T-106, \quad (1)$$

where T is the temperature of combustion products, C_{NO} - the NO concentration.

In [6], it is noted that the main contribution to the pollution of the environment by the emissions of nitrogen oxides during combustion of fuels is made by the "thermal" pathway of NO formation by the mechanism of Y.B. Zeldovich. The expression for equilibrium concentration of nitric oxide in combustion products:

$$C_{NO}=\sqrt{2e^{-\frac{180}{RT}}\cdot C_{N_2}C_{O_2}}, \quad (2)$$

where C_{NO}, C_{N2}, C_{O2} - respectively, the concentration of nitric oxide, molar nitrogen and oxygen, kg/m^3; R - universal gas constant, kJ/mol·K.

TABLE I. PARAMETERS OF THE EXPERIMENTAL STUDY OF THE STEAM GENERATOR.

No	**Δp_{ing} MPa**	**$G_f\times 10^3$ kg/s**	**$Q_т$ kW**	**T_{ch} °C**	**$T_{c.p.}$ °C**	**G_w kg/s**	**$t_н$ °C**	**$W_{c.p}$ m/s**	**Q_w kW**	**$Q_{c.p.}$ kW**	**SQ kW**	**dQ %**
1	2	3	4	5	6	7	8	9	10	11	12	13
1	0.2	7.680	326.8	1040	670	0.357	115	42.9	156.7	153.5	310.2	95
2	0.3	9.844	418.9	1060	700	0.357	124	50.3	170.3	183.0	353.0	84
3	0.4	11.00	468.1	1125	700	0.312	132	60.3	160.0	223.0	383.0	79
4	0.5	11.98	509.8	1170	610	0.333	142	61.6	184.6	214.5	399.1	78
5	0.6	13.32	566.8	1250	500	0.357	147	62.4	205.4	203.4	408.8	72

Taking into account the dependence of the corresponding component concentrations on the excess oxidizer ratio, the expression for the equilibrium concentration of nitrogen oxide in combustion products will be as follows:

$$C_{NO} = \sqrt{2e^{-\frac{180}{RT}} \cdot \frac{0.768 \cdot \alpha \cdot \chi_0}{\frac{1}{\rho_F^{atm}} + \frac{\alpha \cdot \chi_0}{\rho_{air}^{atm}}} \cdot \frac{0.232 \cdot \alpha \cdot \chi_0}{\frac{1}{\rho_F^{atm}} + \frac{\alpha \cdot \chi_0}{\rho_{air}^{atm}}}}, \quad (3)$$

where α – the excess oxidizer ratio; χ_0 - the mass stoichiometric ratio of fuel components; $\rho_F^{atm}, \rho_{air}^{atm}$ - the densities of fuel and air at atmospheric pressure.

The resulting expression for determining the equilibrium concentration of "thermal" nitrogen oxides depends mainly on the temperature in the combustion chamber, as well as on the molecular concentrations of nitrogen and oxygen.

It should be noted that the actual yield of "thermal" nitrogen oxides is several orders of magnitude lower than the equilibrium ones calculated by the expression (3) (Table II). This is due to the short residence time of the fuel components at high temperatures [7], since the period of oscillation in the resonator does not exceed 0.02 s (Figure 2), and the residence time in the zone of maximum temperatures is even less (the time to reach the equilibrium state is about $1 \cdot 10^1$s).

"Fuel" nitrogen oxides are formed by burning a fuel that contains chemically bound nitrogen. Given that the proportion of conversion of such nitrogen into oxides does not exceed 0.2-0.3, as well as the fact that hydrocarbon fuels contain no more than 0.007% nitrogen as impurities, this mechanism can be neglected.

TABLE II. THE RESULTS OF THE COMPARISON OF EXPERIMENTAL AND CALCULATED DATA OF THE STEAM GENERATOR.

Parameter	**Symbol and unit**	**Calculational**	**Experimental**
Temperature in combustion chamber	T, K	1614	1313
The excess oxidizer ratio	α	1.74	1.67
Concentration of "thermal" of nitrogen oxides (in equilibrium),	C_{NO}, g/m^3	3.7	-
Concentration of "thermal" nitrogen oxides in conditions of pulsating combustion	C_{NO}, g/m^3	0.00013	-
The concentration of "fast" oxides of nitrogen calculated by the approximation formula (1)	$C_{NO(fast)}$, g/m^3	0.02138	-
Sum of NO	NO, g/m^3	0.02151	0±0.033

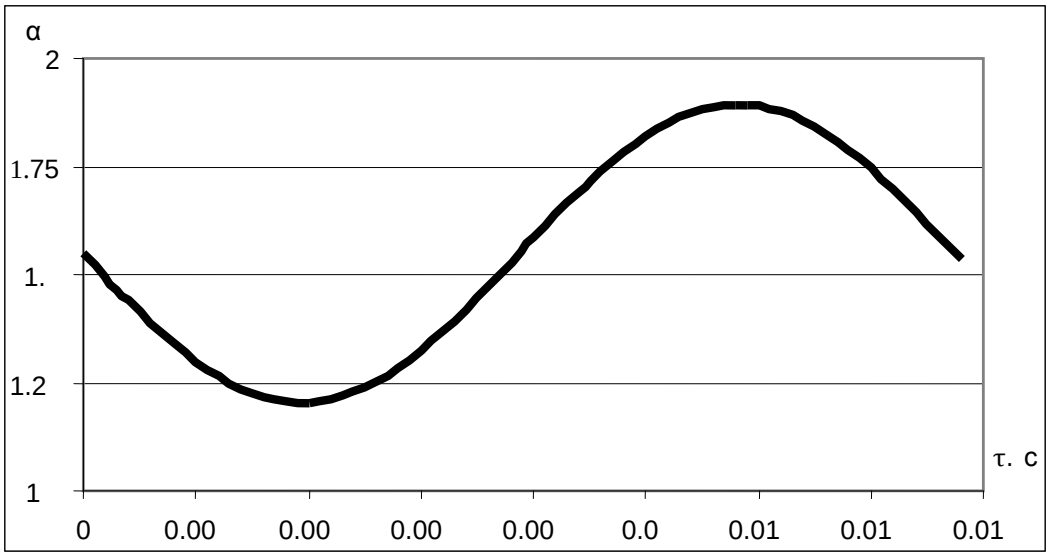

Figure 2. Graph of the excess oxidizer ratio in the combustion of hydrocarbon fuel in the air.

The mechanism of NO formation from nitrous oxide N_2O is considered separately in some sources. This mechanism was observed in poor and moderately rich hydrogen-air flames at high temperatures (about 2000K) and pressures typical for diesel internal combustion engines. In [8] it is stated that the contribution of nitrogen oxides through the formation of N_2O depends significantly on the pressure, and at operating pressures about 1 atm. can be estimated at a few percent. Given this fact, in the circumstances under consideration, this mechanism can be neglected.

MAIN CONCLUSIONS

Thus, the main contribution to the total output of nitrogen oxides is NO, formed by the "fast" mechanism.

A comparative analysis of the calculated and experimental data allows us to evaluate the advantages of this steam generator based on the pulsating combustion apparatus with a cooling jacket in terms of its performance and environmental friendliness over other types of steam generators.

Practically the only disadvantage of pulsating combustion devices is its acoustic characteristics. High noise level imposes some restrictions on the scope of these devices or requires special sound insulation protection.

REFERENCES

1. Tereshchenko, M.A., and N.V. Mozgovoy. 2009. "Experimental Investigation of the Steam Generator on the Basis of Pulsating Combustion and the Assessment of its Sustainability," *Teploenergetika*, 6:69-72.
2. Bychenok, V.I., and N.V. Mozgovoy. 2004. "Termoidraulica Stability of Self-Oscillation Processes in the Apparatus of the Pulsating Combustion with an Aerodynamic Valve," *Vestnik TGTU*, 10(4):887-895.
3. Delyagin, G.N., V.I. Lebedev, and B.A. Permyakov. 1986. *Heat-Generating Plants. Handbook for Universities.* Moscow: Stroyizdat.
4. Sigal, I.Ya. 1988. *Protection of the Air Basin During Fuel Combustion*. Leningrad: Nedra, 312 p.
5. Hodakov, Yu.S. 2003. *Nitrogen Oxides and Heat Power Engineering. Problems and Solutions*. Moscow: LLC "EST-M", 432 p.
6. Kovalev, S.D., I.P. Nazarov, and V.N. Prostov.1981. "Study of the Formation of Nitrogen Oxides in Turbulent Flames" in *Nitrogen Oxides in the Combustion Products of Fuels*, Kyiv: Nauchnaya Dumka., pp. 60-63.
7. Tereshchenko, M.A., and N.V. Mozgovoy. 2008. "The Influence of the Processes of Pulsation in the Combustion Chamber of a Pulsating Combustion Apparatus to the Output of Nitrogen Oxides," *The Bulletin of Voronezh State Technical University*, 4(7):73-76.
8. Warnatz, J., U. Maas, and R. Dibble. 2006. *Combustion. Physical and Chemical Aspects, Modeling, Experiments, Formation of Pollutants*. Moscow: FIZMATLIT, 352 p.

2018 International Theoretical and Practical Conference on Alternative and Smart Energy (TPCASE 2018)
ISBN: 978-1-60595-617-6

High-Voltage Power Lines Capacity and Methods of Its Improvement

Nadezhda Buryanina, Yury Korolyuk and Anna-Mariia Timofeeva

ABSTRACT

Increasing of high voltage lines capacity is one of the most important tasks of Russian Energy department. There are a lot of ways to increase. This paper describes a new method, which allows high voltage lines capacity increasing more than 2 times comparing with traditional methods. There is an electrical parameters calculation of a new design of high voltage overhead lines. Also the new design has less negative effect to environment.

INTRODUCTION

The territory of the Russian Federation is huge, which explains the presence of a large number of long overhead power lines. With a significant development of transport and housing and communal services, the share of electricity consumption in total energy consumption is projected to grow faster. The technological consumption of electricity for its transport is about 13% of the electricity released into a network [1]. Therefore, increasing of an existing and newly constructed transmission lines capacity is one of the main tasks of Russian Energy strategy, as well as losses reducing.

A capacity of power transmission lines is a maximum power transmitted along a line, which can be transmitted while respecting operating requirements and without duration of a power transmission mode subject limiting [2]. A maximum transmitted power is limited by the stability criteria for long-distance lines, and for relatively short lines - by the allowable voltage or current [3].

Chukotka branch of North-Eastern Federal University, 4-106 Office, 3, Studencheskaya Street, Anadyr, Russia

One of the ways to increase a capacity of power lines is a compact overhead line [4].

Electrical circuits of compact three-phase overhead lines are not fundamentally different from circuits of three-phase power lines of traditional design. Regulation of transmission operating parameters is through traditional or new control devices such as the FACTS that are installed in nodes of transmission [5].

Such lines for their normal operation require special equipment. This leads to certain difficulties in operation due to the need to use complex cybernetic devices.

DEVELOPMENT OF IMPROVED DESIGN OF HIGH-VOLTAGE LINES

An increase in a capacity at the limit of transmitted power is achieved in two main ways: by reducing a longitudinal inductive resistance of a line phases and increasing a transverse capacitive conductivity [6].

A radical increase in a natural power, and, consequently, a transmission capacity of a power line, can be achieved by using a different height suspension of wires [7]. With regard to 110 – 220 kV overhead transmission lines with modern fittings, such lines can have the structure shown in Figure 1.

The peculiarity of this scheme is that the lower wire is stretched without sag. This means that its horizontal and vertical deviations are excluded. When connecting the upper and lower wires with couplers of conductive material, the entire phase is deprived of a possibility of horizontal movement. Consequently, the phases can be brought closer together at a distance slightly exceeding the possible breakdown voltage.

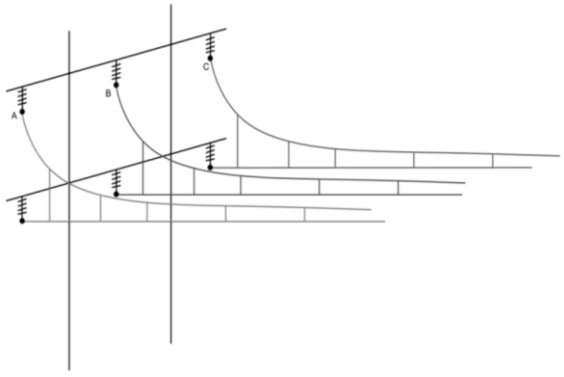

Figure 1. The scheme of a power line wire suspension with vertical splitting of the phases.

At one meter between a wire and a tower on the 110 kV overhead transmission line and two meters on the 220 kV line, the breakdown voltage of an air gap between a wire and a tower is more than six times than the nominal voltage, which is enough to fulfill a condition of not overlapping the air insulation between wires of a line and towers.

Carson [8] proposed equations that determine a resistance of lines taking into account a flow of currents in the earth. For a two-wire phase, an inductive resistance is defined as:

$$x_{ekv} = 0.1451g\frac{D_3}{r_{ekv}} \text{ , Ohm/km ,} \quad (1)$$

where r_{ekv} is the equivalent radius of a wire, the values of which for aluminum and steel wires is $r_{ekv} = 0.95r$, where r is the true radius of a wire; D_3 is a depth of a conditional reverse wire, defined as:

$$D_3 = \frac{0.085}{\sqrt{f\lambda 10^{-9}}}10^{-3} \text{ , m,} \quad (2)$$

where f is a frequency of a network (Hz); λ is a specific conductivity of the earth, 1/Ohm*cm.

When f = 50 Hz and the average value $\lambda = 10^{-4}$ 1/Ohm*cm the value D_3 = 935 m. In an absence of data on the conductivity of the earth D_3 is usually taken as 1000 m.

An inductive resistance due to a mutual induction between two parallel wires with a distance d between the axes of their wires can be determined from the expression:

$$x_{Msr} = 0{,}145\lg\frac{D_3}{d} \text{, Ohm/km.} \quad (3)$$

For a three-phase single-circuit line with a full cycle of wire transposition, a mutual induction resistance between the phases when a current returns through the ground should be determined by replacing the average geometric distance between wires of the phases a, b, c, and d:

$$x_{Msr} = 0{,}145 \lg \frac{D_3}{D_{\text{sr}}} \text{ , Ohm / km.} \quad (4)$$

Taking into account (1) and (3) direct sequence resistance, which determines, along with capacitive conductivity, a line capacity is defined as [7]:

$$x_1 = 0.145 \lg \frac{D_{sr}}{r_{sr}} \text{ , Ohm / km.} \quad (5)$$

Capacitive conductivity is defined as:

$$b_1 = \frac{7.58}{\log(\frac{2D_{sr}}{d})} 10^{-6} \text{ , Sm / km,} \quad (6)$$

where d is a wire diameter. A capacitance conductivity of a split phase line can be calculated according to (6) if a wire diameter d is replaced by the equivalent according.

Dependences of the given linear longitudinal resistance and transverse capacity on the place in the span of 200 m 220 kV overhead line (Figures 2a, 2b). (the Figures indicate the lower wire suspension options: 1-the wire touches the upper one in the middle of the span; 2 - between the upper and lower wires in the middle of the span 0.2 m; 3 - 1 m; 4 - 2 m.). If the wires in the phase concerned along the entire span, then the inductive resistance would be equal to 0.37 – 0.38 Ohm/km and the capacitive transverse conductivity is approximately 2.6 $*10^{-6}$ Sm/km, These figures are quite close to the parameters of real overhead lines, which confirms the correctness of calculations.

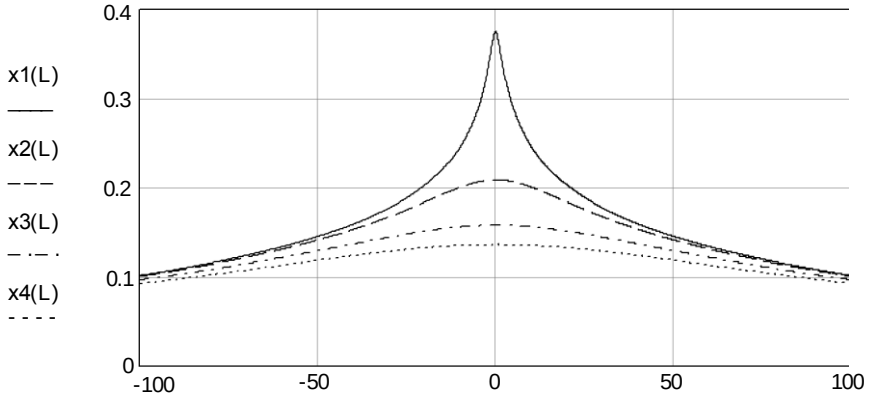

Figure 2a. Change in the longitudinal inductive resistance along the span length of 200 m 220 kV overhead line (the sag is 6 m.).

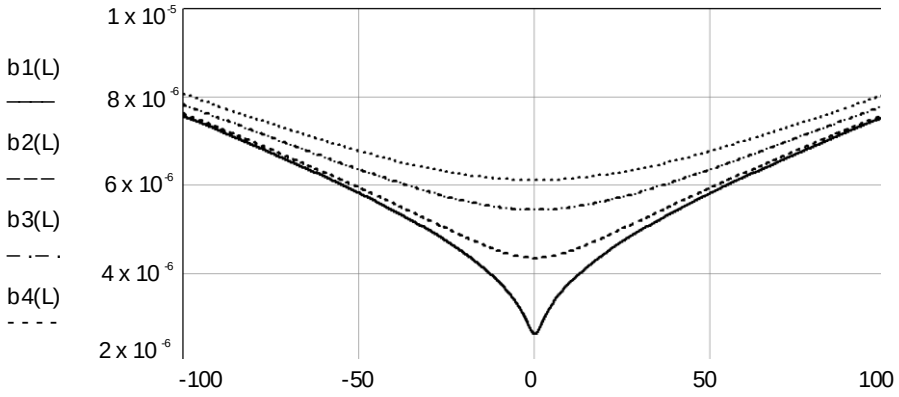

Figure 2b. The capacitive variation of the transverse conduction along the span length 200 m 220 kV overhead line (the sag is 6 m.).

Changes in natural powers for lines 110 and 220 kV, depending on a distance between wires in a phase in the middle of the span are shown in Figure 3, where the lines under consideration have a natural power of about 2-3 times more than that of traditional overhead lines.

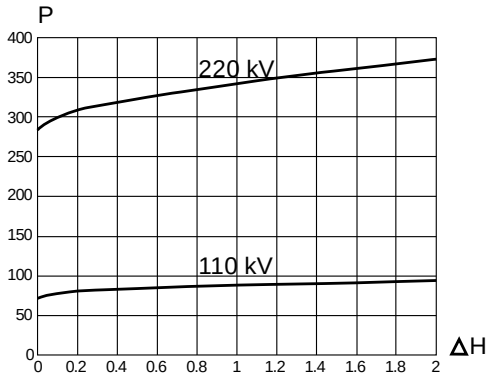

Figure 3. Natural power of lines 110 and 220 kV depending on a distance between phase wires in the middle of the span.

CONCLUSION

The proposed design of a power line can significantly increase a capacity of high-voltage lines. Although an experimental verification of a line capacity has not yet been carried out, it can be expected that the obtained values are close to optimal due to the assumptions made in the calculation of a line capacity.

ACKNOWLEDGMENTS

The research was carried out with the financial support of RFFI and constituent entity of the Russian Federation-the Republic of Sakha (Yakutia) #18-48-140 010.

REFERENCES

1. "About a Strategic Planning in the Russian Federation" in *Federal Law of June 28, 2014 № 172-FZ The Energy Strategy of Russia for the Period up to 2035*.
2. Alexandrov, G.N. 2009. *Transmission of Electric Power*. St. Petersburg: Publishing house of Polytechnical University, 412 p.
3. Chao-Ming Huang, and Yann-Chang Huang. 2014. "Hybrid Optimization Method for Optimal Power Flow Using Flexible AC Transmission System Devices," *IET Generation, Transmission & Distribution*, 8:2036-2045.
4. Hong, Liu, Jun Han, Shaoyun Ge, and Chengshan Wang. 2014. "Improved Analytical Method of Power Supply Capacity on Distribution Systems," *International Journal of Electrical Power & Energy Systems*, 63:97-104.
5. Postolaty, V.M., E.V. Bykova, V.M. Suslov, Y.G. Shakaryan, L.V. Timashova, and S.N. Kareva. 2012. "Managed Compact Power Line AC," presented at the International Conference "Energy of Moldova - Regional aspects of Development," October 4-6, 2012, Chisinau, the Republic of Moldova.
6. Korolyuk, Y.F., and A.V. Timofeeva. 2017. "Development of High-Voltage Line Construction with High Power Capacity," in *Proceedings of the All-Russian Scientific and Practical Conference. Sections 1-3*, Neryungri: Publishing house of Technical Institute, 387 p.
7. Korolyuk, Y.F., N.S. Buryanina, E.V. Lesnykh, and A.V. Timofeeva. 2016. "Overhead Transmission Line with Different Height Suspension Wires," patent of the Russian Federation #2656365.
8. Ulyanov S.S. 1970. *Electromagnetic Transition Processes in Electrical Systems*. Moscow: Energy, 520 p.

2018 International Theoretical and Practical Conference on Alternative and Smart Energy (TPCASE 2018)
ISBN: 978-1-60595-617-6

The Frequency Impact of Diagnostic Measurements on the Operational Condition of High-Voltage Transformers

Valery Tikhonov

ABSTRACT

This paper presents the substantiation of the phenomenon of the frequency of diagnostic measurements on the operational state of high-voltage transformers. The article gives examples of defects of switching devices of rectifier transformers and methods of their detection. The substantiation of the importance of a defect recognition is given in an early stage of their occurrence.

THE FREQUENCY OF DIAGNOSTIC MEASUREMENTS

The technique of diagnostic measurements of high-voltage transformers and switches in the operating mode has been widely introduced. In this case, diagnostics is carried out under a running voltage and operating load, that is without disconnection of converting transformers and switches from a network. Diagrams of the number of diagnostic asurements and emergency situations are submitted in Figure 1.

The analysis of the presented dependences shows that with the increase of diagnostic measurements [1], the accident rate of electrical equipment and transformers is reduced due to small and medium repairs. This reduces the probability of major accidents and consequently increases the reliability of the power supply system.

Bratsk State University, 7, Kosmonavtov Blvd, Bratsk, 665729, Russia

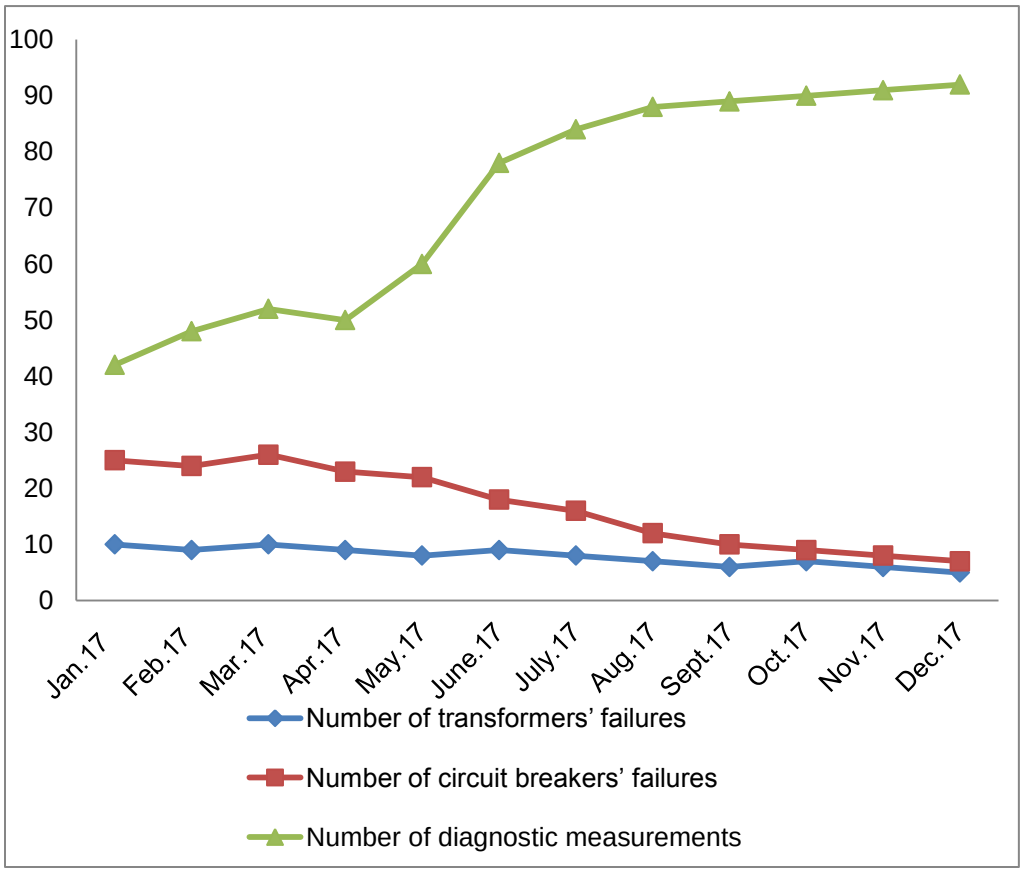

Figure 1. Monthly distribution of transformer and switch failures depending on the number of diagnostic measurements.

CHROMATOGRAPHY

The most famous example of diagnostics is chromatographic analysis of dissolved gases in transformer oil. With the help of measured concentrations of gases in the oil and comparing them with the boundary permissible values, the types of defects in the transformer are determined. The table presents the gas chromatogram of the rectifier transformer TDNL-40000/10.

It follows from Table I that during the planned diagnostic measurements on March 27, 2017, the excess of the boundary concentrations of gases: hydrogen, methane, acetylene, ethylene and ethane was detected. The quickened gases monitoring of the rectifier transformer had been carried out and over the next three days a positive dynamics of gas growth had been observed. It was decided on March 30, 2017 to switch off the rectifier transformer, to conduct medium urgent repairs with drainage of oil and opening of the switching device hatches, during which burnt plug-in contacts of the switching device PHTA-35/1000 were found.

TABLE I. THE CHROMATOGRAM RECTIFIER TRANSFORMER TDNL-40000/10 WITH A SWITCHING DEVICE OF RNTA-35/1000.

Date of analysis	Boundary concentrations of the transformer gases, formation rate %						
	Hydrogen	Methane	Acetylene	Ethylene	Ethane	CO	CO2
	0,01	**0,01**	**0,001**	**0,01**	**0,005**	**0,06**	**0,8**
14.11.16	0	0,001	0	0,0068	0,0002	0,037	0,505
21.12.16	0,004	0,0048	0	**0,0158**	0,0009	0,035	0,471
06.02.17	0,0028	0,0034	0	**0,0159**	0,0012	0,028	0,452
27.03.17	**0,0322**	**0,0645**	**0,00149**	**0,1445**	**0,0213**	0,045	0,512
27.03.17	**0,034**	**0,0641**	**0,0013**	**0,1398**	**0,0203**	0,044	0,492
28.03.17	**0,0271**	**0,0605**	**0,0014**	**0,1322**	**0,0199**	0,034	0,432
29.03.17	**0,0292**	**0,0626**	**0,0015**	**0,1359**	**0,0205**	0,034	0,419
30.03.17	**0,0293**	**0,0667**	**0,0016**	**0,1445**	**0,0218**	0,036	0,442
30.03.17	0	0,0004	0	0,0007	0,00002	0,0032	0,031
03.04.17	0,0011	0,0004	0	0,0006	0,0001	0,0036	0,038

REPAIRS BY THE CHROMATOGRAM

After the repair and replacement of the contacts, the rectifier transformer was put into operation and further put on gas control [2]. As can be seen from Table I, on 03/30/2017, after the rectifier transformer was put into operation, there was no growth of gases, and further the rectifier transformer continues to operate normally. The dependence of the results which confirmed the correctness of defect determination on the number of measurements was constructed [3]. Figure 2 shows that the repeatability of the correct result is high and accounts for 90% with the number of diagnostic measurements increase from 50 units [4].

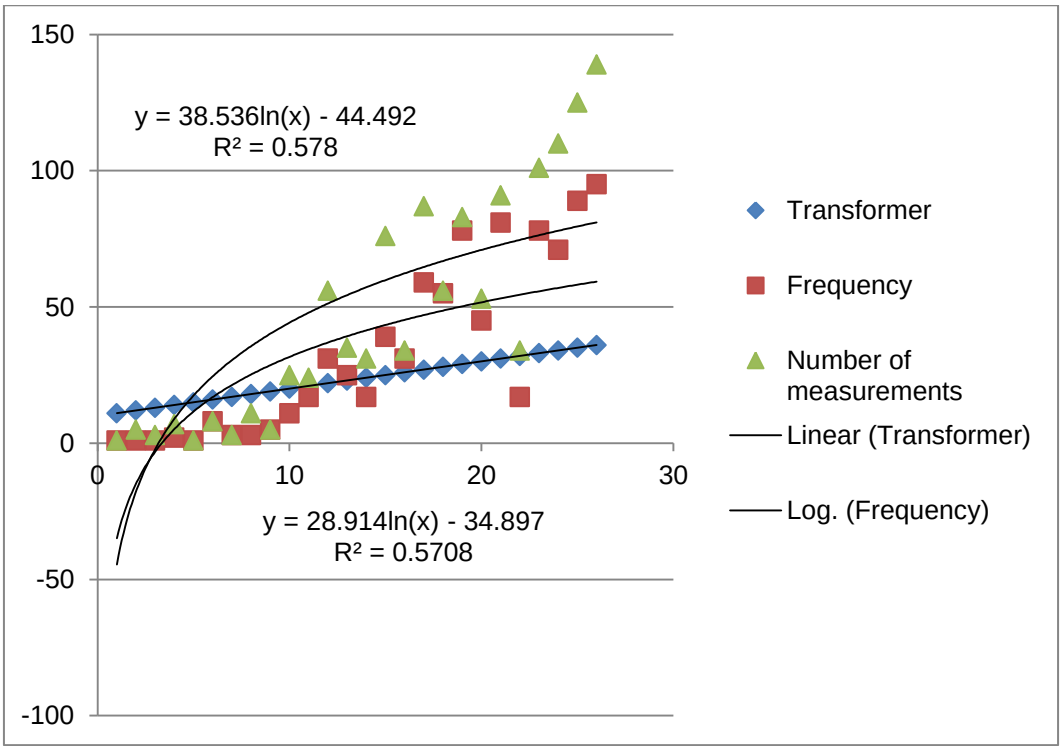

Figure 2. The dependence functions of the number of measurements and the repeatability of the results of the correct defects determination.

While switching the stages of the switching device, transition processes which cause switching over-voltages [5] proceed. Due to the pulse flowing at switching AC overvoltage, there is a vibration that destroys the paper insulation of the transformer.

The multiplicity of over-voltages leads to the partial destruction of the insulation due to the impact of the intensity of the pulsed electromagnetic field on the bond sites of the cellulose molecule, which leads to their rupture (Figure 3).

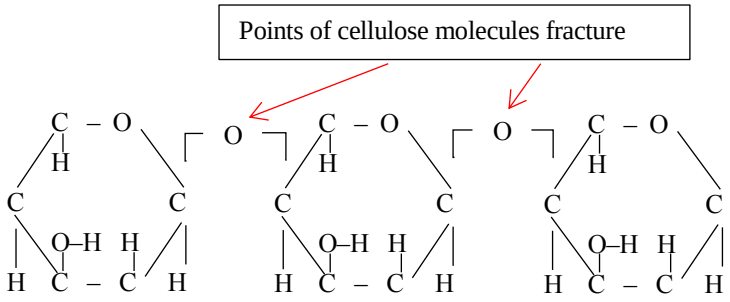

Figure 3. Cellulose molecule structure.

PAPER INSULATION

The breaking of bonds reduces the dielectric strength of paper insulation, which leads to an increase in leakage currents through the places of insulation damage, accompanied by intense heating of these areas and, subsequently, this area leads to insulation breakdown.

Paper insulation loses its physical properties during the operation. The reasons for the physical deterioration of paper insulation rectifier transformers are mechanical vibration, switching overvoltage, thunderstorm overvoltage, thermal heating of conductors and cooling systems, oxidation.

The main causes of cellulose molecules destruction, as can be seen from Figure 3, are the breaks in the molecules at the sites of oxygen bonds. The acceleration of this process is directly affected by the presence of moisture (H2O), oxidation (O2), and an elevated temperature, which leads to both intense oxidation and the process initiation—pyrolysis. Thus, the presence of influencing factors that are harmful to cellulose has a detrimental and irrevocable effect on the destruction of paper insulation and, in general, on the reliable operation of a transformer.

Therefore, it is very important to carry out rapid diagnostics of rectifier transformers during the overhaul period and under operating voltage and workload, at least 50 times during the controlled period, as mentioned above and illustrated in Figure 2.

CONCLUSIONS

As it is stated above, an increase in the frequency of diagnostic measurements leads to effective monitoring of the state of high-voltage transformers and allows the detection of defects at an early stage of their occurrence. In this case, the approximation of the reliability and repeatability of the results, according to Figure 3, is within acceptable limits, exceeding 1% [6]. Since transformers provide power supply to consumers of aluminum electrolysis production, which is characterized by continuity of the technological process, during the repair work associated with the disconnection of the power transformer, its load is redistributed to other transformers. With such a power supply repair scheme, the current in the line increases and the voltage in it decreases. Therefore, the current strength and, accordingly, the active power decrease. During the power system peak times, the consumed active power of the electrolysis plant is calculated. In this case, if the power is lower during the peak times, then the payment of electricity will be less. Therefore, in case of timely detection of defects and maintaining high-level operational readiness of high-voltage transformers, using parallelism of processes and the KANBAN operational control system during repair work, the work is carried out during the peak times of the power system [7]. Thus, there is a

simultaneous reduction of power and payment for it, and repair work is carried out, entering self-sufficiency mode.

REFERENCES

1. Mikheev, M. Yu., O.V. Prokofyev, J.I. Semochkina. 2014. *Methods of data analysis and their implementation in decision-making support systems*. Study guide, Penza, 118p.
2. Ostroukh, A.V. 2015. *Intellectual Systems*. Krasnoyarsk, Research and Innovation Center, 110p.
3. Dobaev, A.Z. 2014. "Using the methods of mathematical statistics for analyzing the data of electricity metering systems", *Proceedings of the VI International Conference*, Vladikavkaz: pp. 37-41.
4. Power, D. J., R. Sharda, and F. Burstein. 2015. *Decision Support Systems*. John Wiley & Sons, Ltd.
5. Medvedeva, M.L., S.V., Kuzmin, I.S., Kuzmin, and V.D., Shmanev. 2017. "Analyzing and predicting the distribution networks and electrical receivers 6-10kV in the mining industry," *Reliability and safety of energy*, 10(2):120-125.
6. Silakova, V.V. "Analysis of general economic factors of technological risk of enterprises of continuous type of production in Russia," *Economics and Management Systems Management*, 20(2): 54-62.
7. Pestereva, E. 2008. "KANBAN and "just in time" at Toyota", Management begins at the workplace, Moscow, Alpina Business Books: 218p.

2018 International Theoretical and Practical Conference on Alternative and Smart Energy (TPCASE 2018)
ISBN: 978-1-60595-617-6

Combined Additive Technology in the Restoration of Aircraft Parts

Gregory Trifonov, Nikita Penkov, Andrey Krasnov and Vassiliy Gritsyuk

ABSTRACT

This work proposes a method of combined additive technology, which includes plasma spraying and laser hardening. Also a system of equations for predicting the thickness of the deposited layer after plasma spraying on complex surfaces of parts was developed.

INTRODUCTION

To date, one of the main challenges facing the aircraft industry is to improve the performance the properties of the contact surfaces of aircraft components and assemblies. This issue is particularly relevant in Russia, in connection with the intensive development of aviation technology, the introduction of new generations of aircraft, reconstruction and construction of airfields, as well as the extensive use of ground-based aircraft special equipment [1-3].

The article proposes a method of combined additive technology, which includes plasma spraying and laser hardening. The purpose of the proposed method is to maintain the achieved wear resistance and ensure the high quality of the workpiece surface. A system of equations for predicting the thickness of the deposited layer after plasma spraying on complex profile surfaces of parts was also developed.

Gregory Trifonov, Nikita Penkov, Military Scientific Educational Center of Military-Air Forces "N.E.Zhukovsky and JU.A. Gagarin Military-Air academy", 54 A, Starykh bolshevikov Street, Voronezh, 394064, Russia
Andrey Krasnov, Vassiliy Gritsyuk, Voronezh State Technical University, 14, Moskovsky Avenue, Voronezh, 394026, Russia

THEORETICAL BACKGROUND

In the case of plasma spraying, further mechanical treatment is required to eliminate the defects of spraying, which means that part of the sprayed layer in the form of an allowance is removed [4]. However, the elimination of allowance entails a reduction in the thickness of a sufficiently small sprayed layer and also leads to an increase in surface stresses.

After analyzing various additive technologies using highly concentrated energy flows, a combination of two promising technologies was chosen:

- plasma spraying;
- laser finish hardening.

In the sprayed layers, as the coating thickness increases, the residual stresses, which, at a certain thickness, lead to the destruction of the sprayed part, increase [5]. This occurs when the residual stresses exceed the cohesive strength value. After the application of composite materials on the surface of the part is proposed to produce a finishing laser hardening, which theoretically should replace the heat treatment. This will reduce the level of residual stresses to the permissible value, increase the bond between the substrate and the sprayed layer and smooth the surface.

The theoretical basis of the proposed method is the ability to predict the melting depth of the deposited plasma layer during subsequent laser irradiation.

Based on a number of works [6,7] an equation for calculating the thickness of the plasma layer of the part was obtained:

$$H_{(x,y)} = H_{(x)} = H_{\max} \times \exp(-\frac{x^2}{\rho_1^2}), \quad (1)$$

where H_{max} – the height of the sputtered coating (mm); x – the coordinate of motion of the plasma torch nozzle relative to the plane of spraying details (mm); ρ_1 – the radius of the spot spray (mm).

As practice shows, the details of the aviation industry, requiring additive recovery and hardening, have significant dimensions. As a result, when the contact surface is sprayed, the number of rows of the applied plasma coating will certainly be more than three. Therefore, for three or more deposition series, the height of the deposited layer can be calculated by the formula [8]:

$$H = \frac{\delta \times \sqrt{\pi \rho_1}}{v} \times \left\{ \exp(-\frac{x^2}{\rho_1^2}) + \exp\left[-\frac{1}{\rho_1^2}(x-A)^2 \right] + \exp\left[-\frac{(x+A)^2}{\rho_1^2} \right] \right\}, \quad (2)$$

where δ – the coefficient characterizing the rate of increase in the thickness of the coating in the center of the spray spot; A – the offset step (mm); v – the travel speed of torch (mm/s).

RESULTS AND DISCUSSIONS

As can be seen from the formula (2), one of the important factors affecting the thickness of the applied layer during plasma spraying is the speed of movement of the plasma torch *v* relative to the treated surface.

Based on the obtained results of the work of A. Ilyushchenko [9], where the equations for determining the velocity of the plasma layer for different surfaces of the parts were developed, the system of equations for determining the thickness of the plasma layer for complex surfaces of the part was modeled:

$$H_D = \frac{\delta \times \sqrt{\pi \rho_1}}{\sqrt{\left(\frac{d\rho}{dt}\right)^2 + \beta\varphi^2\left(\frac{d\varphi}{dt}\right)^2}} \times \left\{ \exp(-\frac{x^2}{\rho_1^2}) + \exp\left[-\frac{1}{\rho_1^2}(x-A)^2\right] + \exp\left[-\frac{(x+A)^2}{\rho_1^2}\right]\right\}$$

$$H_C = \frac{\delta \times \sqrt{\pi \rho_1}}{\sqrt{\left(\frac{d\rho}{dt}\right)^2 + \left(tg\psi\beta_z\varphi\right)^2\left(\frac{d\varphi}{dt}\right)^2 + \left(\frac{dz}{dt}\right)^2}} \times \left\{ \exp(-\frac{x^2}{\rho_1^2}) + \exp\left[-\frac{1}{\rho_1^2}(x-A)^2\right] + \exp\left[-\frac{(x+A)^2}{\rho_1^2}\right]\right\}$$

$$H_{Cy} = \frac{\delta \times \sqrt{\pi \rho_1}}{\sqrt{R^2\left(\frac{d\varphi}{dt}\right)^2 + \left(\frac{dz}{dt}\right)^2}} \times \left\{ \exp(-\frac{x^2}{\rho_1^2}) + \exp\left[-\frac{1}{\rho_1^2}(x-A)^2\right] + \exp\left[-\frac{(x+A)^2}{\rho_1^2}\right]\right\}$$

$$H_H = \frac{\delta \times \sqrt{\pi \rho_1}}{\sqrt{\left(\frac{\pi\left(\sqrt{D^2\left(1+tg\varphi_1\right) - D_1^2\left(1+tg\varphi_1\right)}\right)}{\alpha}\right)^2\left(\frac{d\varphi}{dt}\right)^2 + \left(\frac{dz}{dt}\right)^2}} \times$$

$$\times \left\{ \exp(-\frac{x^2}{\rho_1^2}) + \exp\left[-\frac{1}{\rho_1^2}(x-A)^2\right] + \exp\left[-\frac{(x+A)^2}{\rho_1^2}\right]\right\},$$

where H_D – the thickness for disc type parts (mm); H_C – the thickness for cone type parts (mm); H_{Cy} –the thickness for cylinder type parts (mm); H_H – the thickness for parts with screw surface (mm); ρ, φ, z – cylindrical coordinates; β – the pitch of the helix of the trajectory of the center of the spot deposition on the surface; β_z – the step of the projection of the trajectory of the center of the spraying spot on the axis z; $tg\psi$ – the opening angle of the cone; R – the radius of the cylinder (mm); D – the outer diameter of the helix (mm); φ_1 – the angle of steepness of the rise; α – the angle of the opening; $\frac{d\varphi}{dt}$ – the speed of rotation of the workpiece (m/s); $\frac{dz}{dt}$ – longitudinal tool travel speed (m/s); $\frac{d\rho}{dt}$ – the radial speed of movement of the tool (m/s).

A promising additive technology for the restoration of aircraft parts, including plasma spraying and subsequent laser hardening, is proposed [10].

A system of equations for predicting and subsequent control of the thickness of the deposited plasma layer on the complex profile surfaces of parts is developed. This system of equations will more accurately assign the depth of the laser hardening effect on the plasma layer of the parts, which in the future will significantly increase the adhesive strength of the substrate and coating.

REFERENCES

1. Trifonov, G.I., and S. Yu. Zhackin. 2017. "Influence of Plasma Spraying of Composite Powder Materials on the Wear Resistance of Machine Parts," *Master's Journal*, Perm National Research Polytechnic University, 30-36.
2. Kutaladze, S.S. 1979. *Fundamentals of Heat Transfer Theory*. Moscow: Atomizdat, 416 p.
3. Kudinov, V.V., P. Yu. Pekshev, and V.E. Belashchenko. 1990. *Plasma Coating*, Moscow: Nauka, 408 p.
4. Sosnin, N.A., N.E. Sosnin, S.A. Yermakov, and P.A. Topolyansky. 2013. *Plasma Technology. Manual for Engineers.* St. Petersburg, 406 p.
5. Smirnova, N.A. 2012. "Features of Structure Formation during Laser Treatment," *Herald of Bauman Moscow state. Series Mechanical engineering*, 115–129.
6. Puzriakov, A.F. 2008. *Theoretical Bases of Technology of Plasma Spraying.* Moscow, 360 p.
7. Balanovsky, A.E. 2006. *Plasma Surface Hardening of Metals*. Irkutsk. Publishing house of ISTU, 180 p.
8. Trifonov, G.I., S. Yu. Zhackin, M.N. Krasnova, and N.A. Penkov. 2018. "Influence of Kinematics of Movement of the Tool on the Formation of a Wear-Resistant Coating," 14(4):142-147.
9. Ilyushchenko, A.F. 2011. *The Processes of Forming Thermal Spray Coating and Modeling.* Minsk: Belarus. Nauka, 357 p.
10. Trifonov, G.I., S. Yu. Zhackin, M.N. Krasnova, and N.A. Penkov. 2017. "Modeling the Kinematics of the Plasma Deposition on Complex Surfaces," in *Proceedings of GOSNITI*, pp. 133-139.

2018 International Theoretical and Practical Conference on Alternative and Smart Energy (TPCASE 2018)
ISBN: 978-1-60595-617-6

Estimation of a Heat Distribution in a Part Plasma Coating Process

Gregory Trifonov, Sergey Zhachkin, Nikita Penkov and Marina Krasnova

ABSTRACT

This work presents theoretical derivations for a plasma gun motion speed estimation which can be applied to part surfaces of different types. The heat distribution model of plasma coating process for complex parts has also been developed.

INTRODUCTION

Currently, plasma deposition technology is considered to be one of the most robust, inexpensive and efficient durable film high power density coating processes.

Various physical and chemical processes take place upon plasma flow contacts a part surface.The temperature of a restorable part is one of the major parameters that define a plasma deposition process and a quality of the obtained coating. Multiple layer coating with a tight geometrical parameter control is achievable when a precise mathematical estimation is applied. Therefore, a functional coating of a particular part can be modeled using numerical simulations of plasma processes [1-3].

This work covers an actual problem of heat distribution estimation in complex surface profile parts processed with plasma coating.

Gregory Trifonov, Sergey Zhachkin, Marina Krasnova, Voronezh State Technical University, 14, Moskovsky Avenue, Voronezh, 394026, Russia
Nikita Penkov, The Zhukovsky and Gagarin Air Force Academy, 54A, Starikh Bolshevikov Street, Voronezh, 394064, Russia

THEORETICAL BACKGROUND

An equation describing heat distribution in a part treated with a plasma flow can be expressed as follows [4]:

$$T - T_0 = \frac{Q}{2\pi\lambda v} \times \frac{\exp\left(\frac{z_1}{4at}\right)}{\sqrt{t\left(t_0 + t\right)}} \tag{1}$$

where T is a heated part temperature (K); To is an initial part temperature (K); y, z_1 are width and depth of a heated spot, respectively (μm); t is time (s); t_0 is an imaginary source spread time (s); Q is an effective plasma arc power (W); υ is a heat source motion speed (m/s); λ is a thermal conductivity (W/mK); a is a temperature conductivity coefficient.

According to equation (1) plasma gun motion speed v related to a processed part is one of the most crucial parameters affecting heat distribution on a treated surface. Consequently, a table describing plasma gun displacement speed for different part surface types was developed based on previous works [5-7], where ρ, φ, z are cylindrical coordinates; β is a helical displacement step of a deposition spot on a treated surface; β_z is a deposition spot projection on z axis; $tg\psi$ is a cone angle; R is a cylinder radius (mm); D is a helix outer diameter (mm); φ_1 is a helix slope angle; α is a helix cut angle; $\frac{d\varphi}{dt}$ is a processed part rotation speed (m/s); $\frac{dz}{dt}$ is a plasma gun longitudinal displacement speed (m/s); $\frac{d\rho}{dt}$ is a plasma gun radial displacement speed (m/s).

TABLE I. PLASMA GUN DISPLACEMENT SPEED ESTIMATION.

No.		Surface type	Plasma gun displacement speed equation
1.		Disc	$v_D = \sqrt{\left(\frac{d\rho}{dt}\right)^2 + \beta\varphi^2\left(\frac{d\varphi}{dt}\right)^2}$
2.		Cone	$v_C = \sqrt{\left(\frac{d\rho}{dt}\right)^2 + \left(tg\psi\beta_z\varphi\right)^2\left(\frac{d\varphi}{dt}\right)^2 + \left(\frac{dz}{dt}\right)^2}$
3.		Cylinder	$v_{Cy} = \sqrt{R^2\left(\frac{d\varphi}{dt}\right)^2 + \left(\frac{dz}{dt}\right)^2}$
4.		Helix	$v_H = \sqrt{\left(\frac{\pi\left(\sqrt{D^2\left(1+tg\varphi_1\right) - D_1^2\left(1+tg\varphi_1\right)}\right)}{\alpha}\right)^2\left(\frac{d\varphi}{dt}\right)^2 + \left(\frac{dz}{dt}\right)^2}$

RESULTS AND DISCUSSIONS

Equation (1) allows to estimate a processed part heat temperature, but further mathematical corrections are needed for more precise temperature estimation.

Based on calculations by A. F. Ilyushenko [5] we introduce an equation expressing temperature conductivity coefficient:

$$a = \lambda / c\rho_{nn} \tag{2}$$

where c is a thermal conductivity; ρ_{pc} is a plasma coating density (kg/m^3).

We also plug in an equation defining thermal conductivity coefficient dependent on porosity by A. F. Puzryakov [7]

$$\lambda = \lambda_M (1 - P) \times \lambda_B P \tag{3}$$

where λ_M is a coating material thermal conductivity coefficient ; λ_A is a thermal conductivity coefficient of air; P is a coating porosity.

However, given expression is used when alternating plasma coating and gas layers are parallel to a heat flow. So, in our case we use the Lichtnecker equation [8]:

$$\lambda = \lambda_M^{1-P} \times \lambda_B^P \tag{4}$$

As a result, considering introduced mathematical corrections (2,4) and modelled plasma gun motion speed equations [9,10], we derive a set of equations for temperature estimation in complex surface parts during plasma coating process:

$$T_D = \frac{Q}{2\pi\lambda_M^{1-P}\lambda_B^P\sqrt{\left(\frac{d\rho}{dt}\right)^2+\beta\varphi^2\left(\frac{d\varphi}{dt}\right)^2}}\times\frac{\exp\left(\frac{z_1 c\rho_{nn}}{4t\lambda_M^{1-P}\lambda_B^P}\right)}{\sqrt{t\left(t_0+t\right)}}+T_0$$

$$T_C = \frac{Q}{2\pi\lambda_M^{1-P}\lambda_B^P\sqrt{R^2\left(\frac{d\varphi}{dt}\right)^2+\left(\frac{dz}{dt}\right)^2}}\times\frac{\exp\left(\frac{z_1 c\rho_{nn}}{4t\lambda_M^{1-P}\lambda_B^P}\right)}{\sqrt{t\left(t_0+t\right)}}+T_0$$

$$T_{Cy} = \frac{Q}{2\pi\lambda_M^{1-P}\lambda_B^P\sqrt{\left(\frac{d\rho}{dt}\right)^2+\left(tg\psi\beta_z\varphi\right)^2\left(\frac{d\varphi}{dt}\right)^2+\left(\frac{dz}{dt}\right)^2}}\times\frac{\exp\left(\frac{z_1 c\rho_{nn}}{4t\lambda_M^{1-P}\lambda_B^P}\right)}{\sqrt{t\left(t_0+t\right)}}+T_0$$

$$T_H = \frac{Q}{2\pi\lambda_M^{1-P}\lambda_B^P\sqrt{\left(\frac{\pi\left(\sqrt{D^2\left(1+tg\varphi_1\right)-D_1^2\left(1+tg\varphi_1\right)}\right)}{\alpha}\right)^2\left(\frac{d\varphi}{dt}\right)^2+\left(\frac{dz}{dt}\right)^2}}\times\frac{\exp\left(\frac{z_1 c\rho_{nn}}{4t\lambda_M^{1-P}\lambda_B^P}\right)}{\sqrt{t\left(t_0+t\right)}}+T_0$$

REFERENCES

1. Trifonov, G. I., and S. Yu. Zhackin. 2017. "Influence of plasma spraying of composite powder materials on the wear resistance of machine parts," *Master's Journal*, Perm national research Polytechnic University, pp. 30-36.
2. Leonov, S. L., A. A. Sitnikov, M. E. Tatarkin. 2012. "Simulation of the wear of the deposited surfaces," *Polzunovski almanac.* (1): 228-229.
3. Balanovsky, A. E. 2006. *Plasma surface hardening of metals*. Irkutsk. Publishing house of ISTU, 180 p.
4. Sosnin, N. A., N. E. Sosnin, S. A. Yermakov, and P. A. Topolyansky. 2013. *Plasma technology. Manual for engineers*. St. Petersburg, Russia, publ., 406 p.
5. Ilyushchenko, A. F. 2011. *The processes of forming thermal spray coating and modeling*. Minsk: Belarus. Nauka, 357 p.
6. Trifonov, G. I., and S. Yu. Zhackin. 2018. "Calculation methods for assessing the abrasive wear of the plasma coating of the screw surface of the part," *Appendix to the journal. Bulletin of Tambov University. A series of Natural and technical Sciences,* 23(122): 294-298.
7. Puzriakov, A. F. 2008. *Theoretical bases of technology of plasma spraying.* M.: MGTU name of N. E. Bauman, 360 p.
8. Trifonov, G. I., and S.Yu. Zhackin. 2018. "Modeling of thermal processes in the composition "coating-base" in plasma spraying," *Appendix to the journal. Bulletin of Tambov University. A series of Natural and technical Sciences,* 23(123): 531-534.
9. Vasiliev, L. L. 1971. *Thermophysical properties of porous materials*. Minsk: Science and technology, 265 p.
10. Trifonov, G. I., S. Yu. Zhackin, M. N. Krasnova, N. A. Penkov. 2017. "Modeling the kinematics of the plasma deposition on complex surfaces," *Proceedings of GOSNITI,* 128: 133-139.

2018 International Theoretical and Practical Conference on Alternative and Smart Energy (TPCASE 2018)
ISBN: 978-1-60595-617-6

Research of the Remote Fault Location Algorithm Based on Sampled Values for Measured Primary Electrical Quantities

Andrey Yablokov, Alexander Timofeev and Galina Filatova

ABSTRACT

Digital current and voltage transformers are designed to large-scale transformation of voltage, alternating and/or direct current. Then they transmit the results of transformation to electricity metering systems, devices for measuring, relay protection, automatics, alarm, and control.

There was developed the remote fault location method using data (instantaneous values of primary quantities) from innovative current and voltage sensors, which are included in the digital transformer structure. The results of the research of algorithm performance in cases of the influence of different distorting factors are presented.

INTRODUCTION

Remote fault location on overhead power lines with the voltage of 110 kV and higher using recording devices (indicators), disturbance recorders, microprocessor-based devices for relay protection and automatics became an integral part of maintenance electrical grid service.

[1] requires fault location devices to be installed on overhead power lines with the voltage of 110 kV and higher; the maximum value of examination zone on overhead power lines and fault location using topographical methods after output receiving from fault location devices are also regulated.

Ivanovo State Power University, 34, Rabfakovkaya Street, Ivanovo, 153003, Russia

Nowadays these values of examination zone on overhead power lines cannot be considered as satisfactory, especially for overhead power lines with the length over 100 km.

The most important issue in remote fault location is the cases of self-removing short-circuit when it is impossible to find a fault visually during the examination. The effectiveness of fault location on overhead power lines in cases of unsustainable short-circuits was about 40% of examined power lines with such type of fault [1]. Thus, the development of the remote fault location algorithms with higher accuracy is considered a pressing challenge.

There was developed the remote fault location method using emergency-mode parameters and based on one-sided measurement [2, 3]. The advantages of this method are the absence of special generating equipment (in contrast to, for example, locating methods [4]), the absence of necessity in measurement synchronization, the simplicity of usage [5]. Also, the remote fault location methods based on measuring emergency-mode parameters have large (about 10-20%) error caused by errors of current and voltage sensors [6].

Usage of the data from digital current and voltage transformers can potentially increase the remote fault location accuracy. But the application of these converters for meeting the challenge of remote fault location requires additional research.

REMOTE FAULT LOCATION ALGORITHM BASED ON SAMPLED VALUES

Ivanovo State Power Engineering University (Russia) conjointly with scientific and production enterprise “Digital Measuring Transformer” developed digital current and voltage transformers and also combined transformers applied for the voltage classes of 6(10), 35, 110 and 220 kV. The developed transformers were included in the register of measuring instruments.

The usage of transformers as primary converters for connecting with remote fault location devices helps to improve the accuracy of fault location thanks to their advantages [7]. Presence of several current sensors (including the Rogowski coils) allows one to determine the values of alternating and direct currents and also, physically, the derivative of the input current.

Figure 1 represents the block diagram of the developed remote fault location method.

The developed remote fault location method using data from digital current and voltage transformers consists of such basic operations: calculation of module and argument of phase currents and voltages complex vectors, calculation of symmetrical components for primary quantities, determination of faulty phase (or phases) and short-circuit type, determination of the beginning and the end of the transient process in emergency mode (in case of short-circuit), calculation of inductance to the fault, and determination of the distance to the fault.

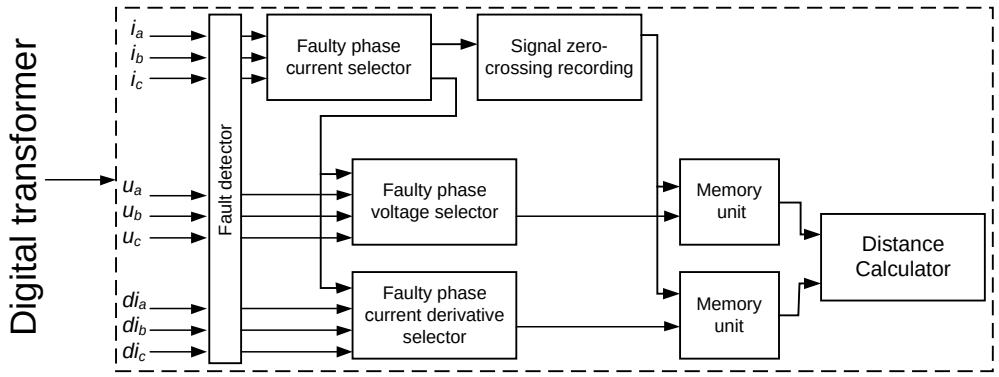

Figure 1. Block diagram of the remote fault location method.

Design equation (in Distance Calculator) corresponds to the expression of the transient process for instantaneous values in cases of different types of short-circuit. The calculation is made in the moments of short-circuit current zero-crossing.

Expression (1) represents the calculation of the distance to the fault in the case of phase-to-phase short-circuit (A-B) using instantaneous values of electrical quantities.

$$l_f(t_{0i}) = \frac{u_{AB}(t_{0i})}{L_1^{(1km)} \frac{d(i_A - i_B)}{dt}(t_{0i})}, \quad (1)$$

where t_{0i} – the moment of current ($i_A(t)$- $i_B(t)$) zero-crossing, sec; $u_{AB}(t_{0i})$ – the phase-to-phase voltage in the moment t_{0i}, kV; $\frac{d(i_A - i_B)}{dt}(t_{0i})$ – the current ($i_A(t)$-$i_B(t)$) derivative value in the moment t_{0i}, kA/sec, $L_1^{(1km)}$ – the specific positive (negative) sequence inductance of overhead power line.

Design equation (and design inductance) was determined in accordance with the boundary conditions for a certain type of short-circuit.

METHODOLOGY OF ALGORITHM RESEARCH

The research and refinement of the algorithm and the related computer simulation models (including data processing models) were made in two steps. During the first step, the design expressions were tested in Simulink, where the models of electrical grids and the algorithm itself were implemented. [7]. Then there were researched various options of algorithm realization (using different

sensors like Rogowski coil or traditional electromagnetic current transformer with further digitization) and algorithm performance in cases of various distorting factors (e.g. transient fault resistance) [7].

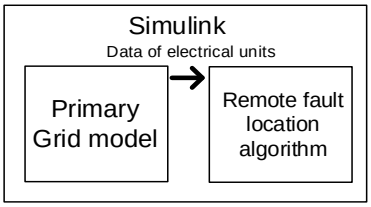

a)

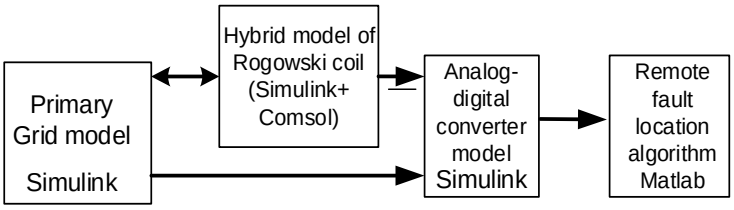

b)

Figure 2. Refinement of computer simulation models for the implementation of the remote fault location algorithm:
a – step 1; b – step 2.

During the second step, refinement of the computer simulation models consisted of taking into account the influence of analog-digital converter and frequency filters. Errors of developed primary converters in case of usage of the hybrid (field-based and chained) Rogowski coil model were also taken into account. The calculation of the distance to the fault using computer simulation models demonstrated the virtual absence of the influence of the developed current sensors on the method accuracy.

Taking into account conducted research and refinement of the software realization of the algorithm there was developed the code written on programming language MATLAB. This code includes all of the basic operations given above and provides the performance of the remote fault location algorithm with the error lower than 5%.

DEMONSTRATION OF ALGORITHM PERFORMANCE

As an example, there is given the demonstration of the algorithm performance in the case of phase-to-phase short-circuit (A-B) located 100 km from the head of the power line (measuring point).

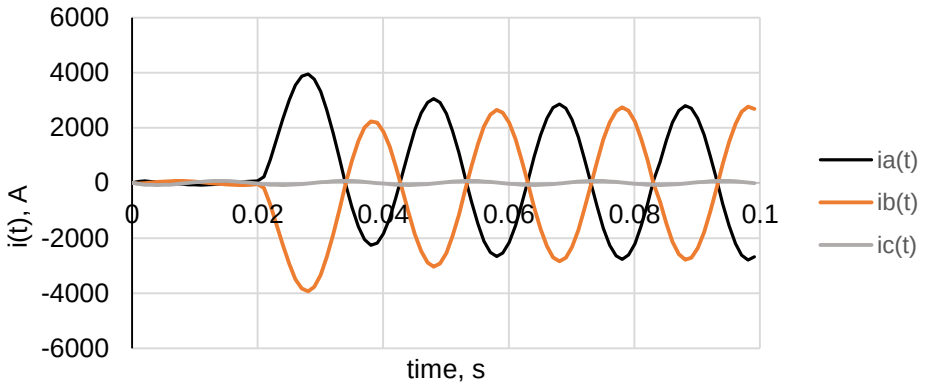

a)

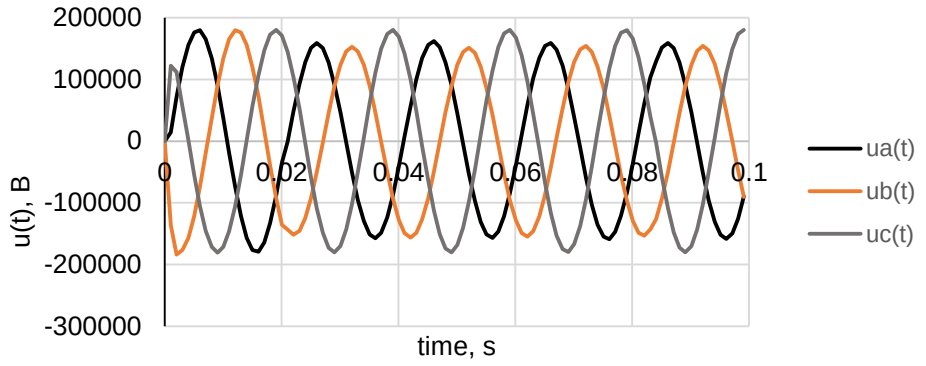

b)

Figure 3. Primary currents (a) and voltages (b) oscillograms (in short-circuit mode).

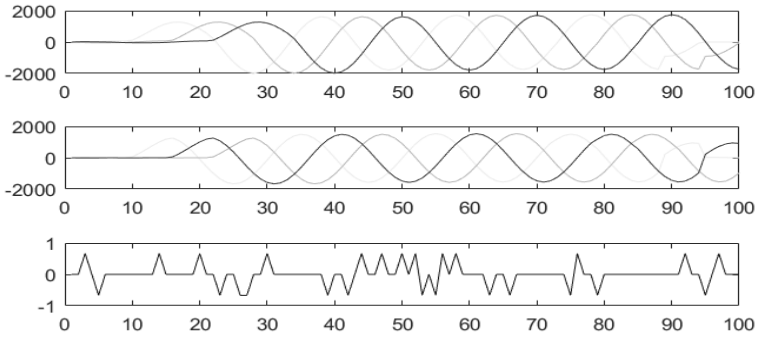

Figure 4. Symmetrical currents components (1 – positive sequence, 2 – negative sequence, 3 – zero sequence).

1. Figure 3 represents phase currents and voltages oscillograms, which illustrate initial data sets from the analog-digital converter model in Simulink
2. Figure 4 represents the results of the calculation of symmetrical currents components.
3. Determination of the faulty phase – phase-to-phase short-circuit (A-B).
4. Calculation of the distance to the fault in the moments of current $(i_a - i_b)$ zero-crossing using equation (1) – determination of the inductance in phase-to-phase short-circuit mode.

The arithmetic mean of the calculated distances to the fault is 101.53 km. The remote fault location algorithm error – 1.53%.

CONCLUSION

The developed remote fault location algorithm was researched in cases of the influence of different distorting factors: methods of current derivative calculation, the presence of fault transient resistance, the distance to the fault, the electrical load, the presence of fault voltaic arc, the phase-to-phase capacitance in power lines, the parameters of analog-digital converter.

Primary algorithm debugging was made with the usage of computer simulation models of electrical grids, which included the primary converters models. Algorithm performance in the case of phase-to-phase short-circuit is demonstrated.

ACKNOWLEDGMENTS

The research was carried out with the financial support of the Russian Science Foundation (project No. 17-7910455) at the Ivanovo State Power Engineering University.

REFERENCES

1. "Studies of Fault Location Determination on Overhead Power Lines Voltage 110 kV and More," *Standard 56947007-29.240.55.224-2016*.
2. Saha, M.M. 2010. *Fault Location on Power Networks*. London: SpringerVerlag London Limited, UK.
3. Kalamand, A., and B. Stojcevski. 2010. "Fault Location in Overhead Power Lines Using the IEC61850 International Protocol," *International Review on Modelling and Simulations*, 3(5):888–899
4. Kachesov, V.E., V.Y. Lavrov, and A.B. Cherepanov. 2003. "Parametric Method of Fault Location in Distribution Networks," *Power Technology and Engineering*, 37(4):262–268

5. Andersson, G., M. Bockarjova, and A. Sauhats. 2005. “Statistical Algorithms for Fault Location on Power Transmission Lines,” in *Proceedings of the 2005 IEEE Power Tech Conference*, St. Petersburg, Russia, June 2005.
6. Lebedev, V.D., and A.A. Yablokov. 2017. “Studies in Electromagnetic Compatibility of Optical and Digital Current and Voltage Transformers,” in *IOP Conference Series: Materials Science and Engineering*, 177:012099
7. Yablokov, A., G. Filatova, and A. Timofeev. 2017. “Using of Non-Traditional Current and Voltage Sensors for the Fault Location,” in *Proc. of MATEC Web Conf*., 141:1-5.

2018 International Theoretical and Practical Conference on Alternative and Smart Energy (TPCASE 2018)
ISBN: 978-1-60595-617-6

The Estimation of Wind Power Station on the Basis of Fuzzy Regression Model to Forecast the Speed and Direction of the Wind

Vadim Manusov, Nasrullo Khasanzoda and Gennady Ivanov

ABSTRACT

To forecast the wind speed and the angle of its direction, it is suggested to use autoregression based on the concept of fuzzy system, which is recognized as a fairly convenient modeling tool. The main goal of fuzzy regression analysis is to find a regression model that satisfies all the observed fuzzy data within specified optimality criterion. According to this method, the regression coefficient is fuzzy numbers, which can't be expressed as a number of the interval with membership values. In this work, the wind speed and direction are predicted for the Far Eastern coast. It is shown that on this basis the power and generation of a wind power plant with the possibility of covering its load schedule, and the function of energy storage can be determined. High introduction of wind power plants into system leads to some inconveniences in the operation of operator systems, primarily due to unpredictable and volatile nature of wind speed, and wind power generated, respectively. Despite fact that the power generated at the wind form is not regulated by the system operator, accurate prediction of wind speed and the angle of its direction could solve this problem, thereby making a significant contribution to improving the reliability of power supply systems.

INTRODUCTION

Rising fossil fuel prices accelerate the transition to renewable energy. Among the diversity of such sources, at present time, wind energy as one of the most

Vadim Manusov, Nasrullo Khasanzoda, NSTU, 20, K. Marx Avenue, Novosibirsk, 630073, Russia
Gennady Ivanov, TIU, 38, Volodarskogo Street, Tyumen, 625000, Russia

effective and clean energy sources is in rather great demand. From 1999 to 2017, the total installed capacity of wind turbines (wind turbines) in the world increased from 14 to 540 GW, with an increase in recent years of over 10% per year. The wind power engineering has received the greatest development in China, USA, Germany, Spain, India, and United Kingdom. In individual countries and regions, the share of installed capacity of wind turbines exceeds 20% and even 40% (Denmark). The maximum unit capacity of operating wind turbines is 8 MW, in the process of developing wind turbines with a capacity of up to 12 MW. Based on the level and rate of development of global wind energy achieved in 2017, it is assumed that by 2030 the installed capacity of wind turbines reaches 977 MW.

However, the integration of such energy sources into the electric power system causes various kinds of problems that today find their solution [1]. Along with this, it should be noted that the power generated by wind power plants strongly depends on meteorological factors, in particular, wind speed [2]. Accordingly, an unexpected change in WPP power may lead to such production costs as the need to increase the main backup power and increase the risks in the reliability of power supply [3].

System operators need to predict changes in power generated by wind power plants and to know exactly the volume of generation in order to plan the necessary amount of reserve and manage the processes in the network, taking into account the forecast data. To reduce the volume of reserve power and increase the level of WPP penetration into the power grid, accurate prediction of wind speed is necessary [4].

FUZZY LOGIC REGRESSION MODEL

Due to the complexity of building a wind speeds model, as well as the influence of unrecorded meteorological factors, such as air temperature, pressure, humidity and others, it is not always possible to unambiguously determine the type of statistically stable dependence $y = f(x)$. In this case, you can try to get a single adequate model on the original sample, making it much more complicated. Another way may be to build a piecewise regression. The disadvantage of the first (re-complicated) model is a significant risk of its use for prediction. Piece models require a fairly accurate definition of the definition of its individual parts. An alternative option is to build a model in the form of a system of vague rules. The advantage of such models is that the resulting solution is a fairly smooth function. The boundaries of the individual parts of the model are blurred, which reduces the requirements for their precise definition. The accuracy of the approximation can be varied by increasing or decreasing the number of blurry rules used. Fuzzy MISO type models (multiple input, single output) are a set of rules of the form [5]:

$$IF \;\; x_1 \subset A_{1i} \,\&\, \ldots \,\&\, x_n \subset A_{ni} \;\; THEN \;\; y = \eta^i\left(x_j\right), \; i = \overline{1..m}, \; j = \overline{1..n} \qquad (1)$$

where A_{ji} – fuzzy subset for variable x_j with accessory function $\mu_{A_{ji}}(x_j)$; m – the number of rules, n – number of factors, $\eta^i(x_j)$ – functions, determining the local dependence of the response on the regression set $x=(x_1,\ldots,x_n)^T$.

Clear variable value y, obtained using the defuzzification method of the center of gravity, is calculated by the formula:

$$y=\frac{\sum_{i=1}^{m}\mu_i\eta^i}{\sum_{i=1}^{m}\mu_i};\quad \mu_i=\prod_{j=1}^{n}\mu_{A_{ji}}(x_j) \tag{2}$$

The model in the form (1), (2) will be called the FLR (Fuzzy Logic Regression) regression model. Consider the FLR regression construction technique for the case of one-dimensional dependence construction.

With one variable, the rule system (1) takes the form:

$$IF\ \ x\subset A_i\ \ THEN\ \ y=\eta^i(x_j), i=\overline{1,m},\ j=\overline{1,n} \tag{3}$$

where A_i have a membership function $\mu_{A_i}(x)$.

The following are used as repressors:

$$\mu_{A_1}(x),\ldots,\ \mu_{A_m}(x),\ \ x\mu_{A_1}(x),\ldots,\ x\mu_{A_m}(x) \tag{4}$$

FUZZY WIND MODEL

It is known that wind speed can be represented by the Beaufort scale [6]. In it, wind speeds are divided into 9 intervals, among which intervals for the weakest and strongest winds can be eliminated, since at the minimum wind speed there is not enough impact on the wind power installation, and at the strongest installation they are turned off to avoid destruction. The Beaufort scale must be described by the membership functions of linguistic variables, that is, it must be indicated which wind speed u relates to which degree of belonging to which linguistic variable. In this case, the so-called LR-functions [7] are used, which can be easily represented graphically. Example, a wind speed of 11 m / s can be equally attributed to both fresh wind and strong wind, a wind speed of 18 m / s most likely refers to very strong wind, but to some extent can be attributed to strong.

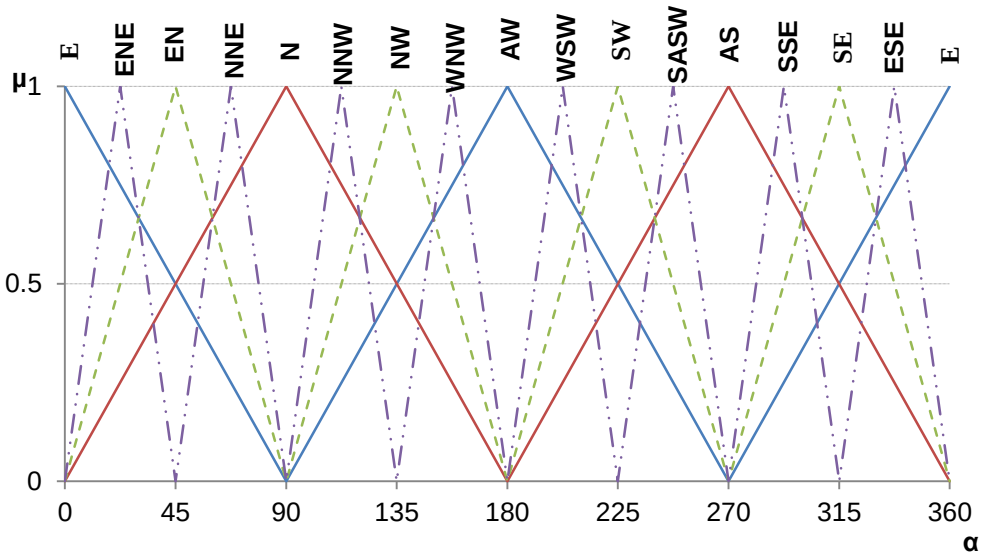

Figure 1. Membership functions of wind direction.

Along with this, the authors considered the prediction of the wind direction and proposed membership functions for individual wind directions. The basic directions of the world are taken as the basic directions: East - zero reading from the positive direction of the abscissa wasps; North is the positive direction of the ordinate wasp, shifted by 90 degrees counterclockwise; West - the negative direction of the abscissa of the wasp shifted by 180 degrees counterclockwise; South - negative direction of ordinate wasp shifted by 180 degrees counterclockwise (Figure 1).

Such a set of membership functions is approximate, therefore intermediate membership functions are introduced: the Northeast, the Northwest, the Southwest and the Southeast. However, to control wind turbines based on fuzzy logic and this gradation of the membership function may not be enough. In this regard, the authors propose new gradations of wind direction, namely: East-North-East (ENE), North-North-East (NNE), North-North-West (NNW), West-North-West (WNW), West-South-West (WSW), South-South-West (SSW), South-South-East (SSE) and East-South-East (ESE).

CONVERSION OF PREDICTED WIND SPEED TO POWER

It is known that the power at the output of wind turbines is directly dependent on the speed of the wind flow, which varies greatly in time, on local weather and the surface of the area. The relationship between the wind speed passing through the swept area of installation A (m^2) and power is expressed through the formula.

$$P = C_p \cdot \rho \cdot A \cdot \frac{V^3}{2} \quad (5)$$

where ρ – is the airflow density (kg / m3) depending on the temperature and air pressure, A is the area swept by the blades, V is the wind speed, C_p. – efficiency ratio of wind turbines, λ –coefficient of speed.

One of the simplest ways to convert wind speed into power is to use the power characteristic from the manufacturer of a particular installation. A similar method and the results of the study are described in detail in [8–10].

FORECAST RESULTS

For the day-ahead forecasting, it is necessary to obtain a separate forecast for each of the time series coefficients: wind speed and direction. The obtained results of wind speed prediction are presented in Table I, while the probabilistic characteristics of the wind flow are determined: mathematical expectation (m_x), standard deviation (σ_x) and variance (D_x). On this basis, using the formula (5), we determined the electric power of a wind turbine (P).

TABLE I. GENERATION OF ACTIVE POWER OF WIND TURBINES WITH ACTUAL AND PREDICTED WIND SPEED VALUES.

Times of day	m_x			D_x		σ_x		P, MW	
	A	F	σ, %	A	F	A	F	A	F
0	14	12,2	12,9	13,68	7,88	3,70	2,81	3,23	2,13
3	10	13,1	31,0	11,47	12,32	3,39	3,51	1,18	2,64
6	11	13,4	21,8	7,69	11,11	2,77	3,33	1,56	2,83
9	11	12,6	14,5	11,12	13,73	3,33	3,70	1,56	2,35
12	15	11,9	20,7	31,00	12,51	5,57	3,54	3,97	1,98
15	13	10,3	20,8	17,49	11,18	4,18	3,34	2,58	1,28
18	15	14,7	2,0	28,71	26,24	5,36	5,12	3,97	3,73
21	14	10,7	23,6	17,49	8,65	4,18	2,94	3,23	1,44
24	14	12,2	12,9	13,68	7,88	3,70	2,81	3,23	2,13

TABLE II. ANGLE FORECAST WIND DIRECTION.

Times of day	0	3	6	9	12	15	18	21	24
Actual value	112,5	112,5	112,5	112,5	112,5	90	90	157,5	112,5
Forecast value	96	102	89	78	215	127	106	158	96
Error	14,6	9,3	20,8	30,6	47	41	17,7	3	14,6

From table I it follows that the error in predicting the mathematical expectation of wind speed for three hours in a period is from 2 to 31%.

Along with this, the forecast of the direction of the wind, measured in the corners (Table II). The counting of the angle begins with the country east from the positive direction of the abscissa of wasp.

From table 2 it follows that the error in predicting angle of wind direction for three hours in the period ranges from 3 to 47%.

Thus, the initial information for controlling wind turbines can be used: expectation (m_x) and standard deviation (σ_x) of wind speed, as well as wind direction, which determines the turning angle of the gondola. This allows you to go to the predictor control of the wind energy installation according to the rules, taking into account the membership functions.

CONCLUSIONS

1. Calculations show that predicting wind speed and its angle based on fuzzy regression can be performed with acceptable accuracy three hours ahead. This allows you to plan the production of electricity using wind turbines.

2. For the first time, wind speed forecast is supplemented with wind direction predicting. This allows, at the second stage of power generation of the wind turbine, to carry out the predictor control of the nacelle, while the attack coal of the blade can be a secondary control element of the wind turbine.

3. In general, wind turbines should be controlled on the basis of fuzzy rules with choice of their priority impact, which allows for the highest energy efficiency of both individual plants and whole wind power plant.

REFERENCES

1. Grogg, K. 2005. *Harvesting the Wind: The Physics of Wind Turbines*. Carleton College. USA: Northfield, 42 p.
2. Chang, W.Y. 2013. “Comparison of Three Short Term Wind Power Forecasting Systems,” *Advanced Materials Research*, (684): 671-675.
3. Sideratos, G., and N.D. Hatziargyriou. 2007. “An Advanced Statistical Method for Wind Power Forecasting,” *IEEE Transactions on Power Systems*, pp. 258-265.
4. Ma L., S.Y. Luan, C.W. Jiang, H L. Liu and Y. Zhang. 2009. “A Review on the Forecasting of Wind Speed and Generated Power,” *Renewable and Sustainable Energy Review*, (13): 915-920.
5. Takagi, T., and M. Sugeno. 1985. “Fuzzy Identification of Systems and Its Applications to Modeling and Control,” *IEEE Trans. on Systems, Man and Cybernetics*, pp. 116-132.
6. Udalov, S.N., and V.Z. Manusov. 2013. *Modeling of wind-driven power plant and their control based on fuzzy logic*. Novosibirsk, NSTU Publ., 200 p. (In Russian).

7. Manusov, V.Z., N. Khasanzoda, and P.V. Matrenin. “Improving the energy efficiency of wind power plants on based swarm intelligence,” *New in Russian electric power-engineering*, 2018(10):36-43.
8. Manusov, V.Z., and N. Khasanzoda. 2018.“Optimization of the Far East wind resources energy efficiency on the basis of the swarm intelligence algorithm,” *Alternative Energy and Ecology (ISJAEE),* (19-21):12-22. (In Russian).
9. Manusov, V.Z., N. Khasanzoda, and Sh. A. Boboev. 2018.“Optimal modes research of intelligent networks with a two-way energy flow,” *Scientific Bulletin of NSTU,* (3):175-190. (In Russian).
10. Manusov, V. Z. 2018. “Using wind resources of far east in smart grid technology with the optimum two-way energy flow,” *13 International forum on strategic technology,* N. Khasanzoda and B.V. Palagushkin, eds. China, Harbin: IFOST, pp. 713-718.

2018 International Theoretical and Practical Conference on Alternative and Smart Energy (TPCASE 2018)
ISBN: 978-1-60595-617-6

Mathematical Model of Low-Temperature Air Rectification Process Factored in Non-stationary of Thermal and Physical Characteristics

Victor Ryazhskih, Anatoly Khvostov, Alexey Zhuravlev, Anatoly Nikitchenko and Andrey Boger

ABSTRACT

This paper considers a mathematical model of the low-temperature air rectification process. The model is based on balance equations for a low-boiling component on contact devices and on the laws of the phase transition for a binary mixture of nitrogen and oxygen. This model allows us to estimate the target product concentration in real time, taking into account the non-stationarity of the main thermophysical characteristics of the processing medium. The results of the computational experiment in form of the nitrogen concentration dynamics on mass transfer devices are presented.

MATHEMATICAL MODEL

During the operation of air separation plants (Oxygen producing mobile station type), dynamic modes arise associated with the presence of uncontrolled disturbances. This leads to a deviation from the typical operation of the installation. In this regard, the urgent task is to develop a dynamic model of the air separation process, taking into account the nonstationarity of the main thermal air characteristics and its components, which would allow us to calculate the optimal control actions.

Victor Ryazhskih, Anatoly Khvostov, Voronezh State Technical University, 14, Moskovsky Avenue, Voronezh 394026, Russia
Alexey Zhuravlev, Anatoly Nikitchenko, Andrey Boger, Military Scientific Educational Center of Military-Air forces “N.E. Zhukovsky and Ju. A. Gagarin Military-Air Academy”, 54A, Starykh Bolshevikov Street, Voronezh 394064, Russia

The proposed model of air rectification in real time includes the equations of general material balance, component-wise balance (balance on the concentration of low-boiling component on each sieve tray, phase equilibrium, equations for calculating the vapor phase composition leaving each tray. The model of the evaporator assembly is considered in [1].

The concentration of the low-boiling component in the liquid phase on each tray is described by a system of N differential equations [2]:
for exhausting section trays ($1 \le i \le f-1$),

$$M_{Li}\frac{dx_i}{dt} = (L+F)(x_{i+1}-x_i) + G(y_{i-1}-y_i), \quad (1)$$

for feeding trays

$$M_{Li}\frac{dx_f}{dt} = Lx_{f+1} - (L+F)x_f + G(y_{f-1}-y_f) + Fx_F, \quad (2)$$

for rectifying section trays ($f+1 \le i \le N$),

$$M_{Li}\frac{dx_i}{dt} = L(x_{i+1}-x_i) + G(y_{i-1}-y_i), \quad (3)$$

where M_{Li} - the mass of the liquid phase on the tray, kg; F - the mass flow rate of feed fluid, kg/f; L - the mass flow rate of the liquid phase flowing down from the above plate, kg/s; G - the steam mass flow coming from the lower tray, kg/f; x_i - the concentration of low-boiling component in the liquid phase, weight percentage; x_F - the concentration of low-boiling component in the feed fluid, weight percentage; y_i - concentration of low-boiling component in the vapor phase, weight percentage. Initial conditions: $x_i\big|_{t=0} = x_{i0}, \quad 1 \le i \le N$.

The concentration of the low-boiling component in the vapor phase, leaving the *i*-th tray:

$$y_i = y_{i-1} + \eta_i\left(y_i^* - y_{i-1}\right), \quad (4)$$

where η_i is the tray efficiency; y_i^* is the concentration of the low-boiling component in the vapor phase in equilibrium with the liquid phase (equilibrium concentration) the weight percentages.

Equilibrium concentration y_i^* is determined by the combined Raul-Dalton law:

$$y_i^* = \frac{\alpha x_i}{1+(\alpha-1)x_i}, \quad (5)$$

where α is the coefficient of relative volatility associated with the pressure P in the column by the ratio [2]

$$\alpha = 4.09(10.197 \cdot P)^{-0.2719}, \quad (6)$$

tray efficiency (according to Murfri):

$$\eta_i = 1 - \exp\left(-\frac{K_y S}{G}\right), \quad (7)$$

where K_y is the mass transfer coefficient in the vapor phase, kg/(m^2·s); S is the tray area, m^2. The mass transfer coefficient in the vapor phase [2] is

$$K_y = \frac{1}{\frac{1}{\beta_y} + \frac{m}{\beta_x}}, \quad (8)$$

where β_y is the mass transfer coefficient in the vapor phase, kg/(m^2·s); β_x - is mass transfer coefficient in the liquid phase, kg/(m^2·s); m is the distribution constant of low-boiling component concentrations in the mass transfer section phases, it is defined as the first-order derivative of the equilibrium curve function (5).

The mass transfer coefficients in the vapor and liquid phases were calculated by the well-known criterion relations, which take into account the thermophysical properties of the phase flows at the boiling point and their hydrodynamics on contact devices [3].

The boiling point of the nitrogen-oxygen mixture on each tray depends on the pressure in the column, the composition of the mixture and is determined by the numerical solution of the equation:

$$P_{01}x_1 + P_{02}x_2 = P, \quad (9)$$

where P_{01}, P_{02} are respectively the saturation pressure of low-boiling component and high-boiling component, mPa; x_1, x_2 are, respectively, the mole fraction of low-boiling component and high-boiling component in the mixture (Figure 1).

For low-boiling and high-boiling components, the relationship between the saturation pressure and their saturation temperature has the form of the Antoine equation, whose constants were determined from the experimental studies results [4, 5]:

$$\ln P_{01} = 6.7358 - \frac{698.22}{T}, \tag{10}$$

$$\ln P_{02} = 7.0771 - \frac{846.26}{T}, \tag{11}$$

where T is the saturation temperature, K.

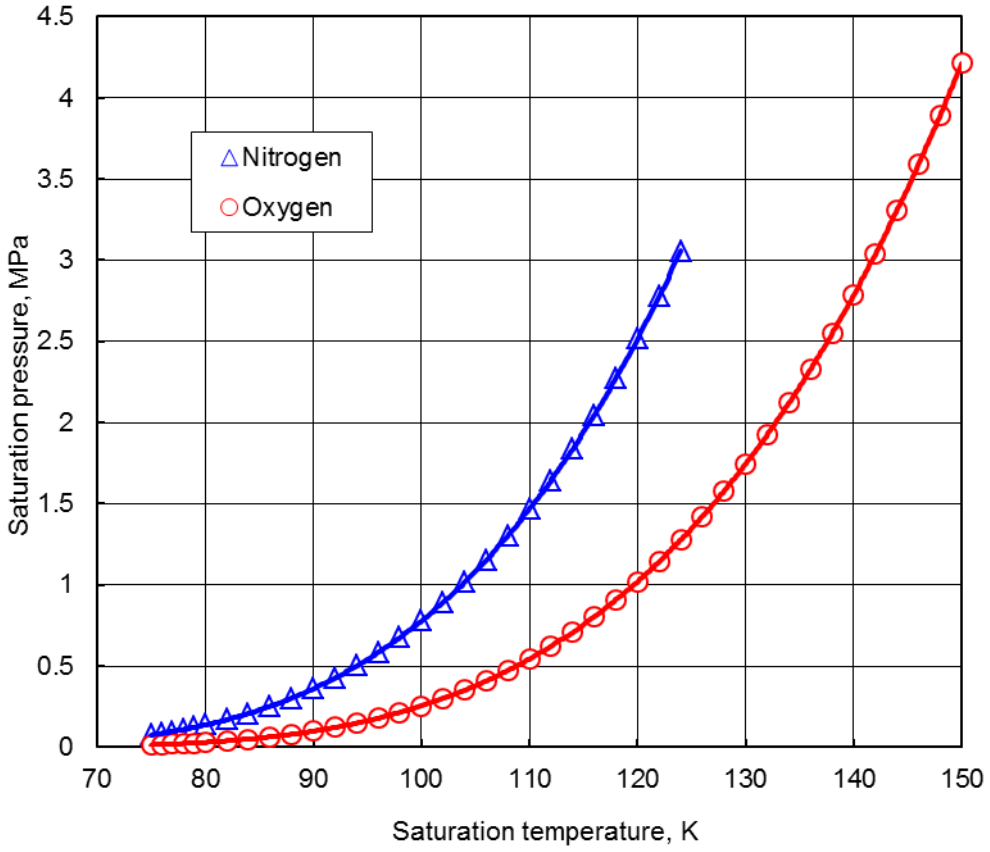

Figure 1. Isobaric condensation curves of steam nitrogen-oxygen mixtures.

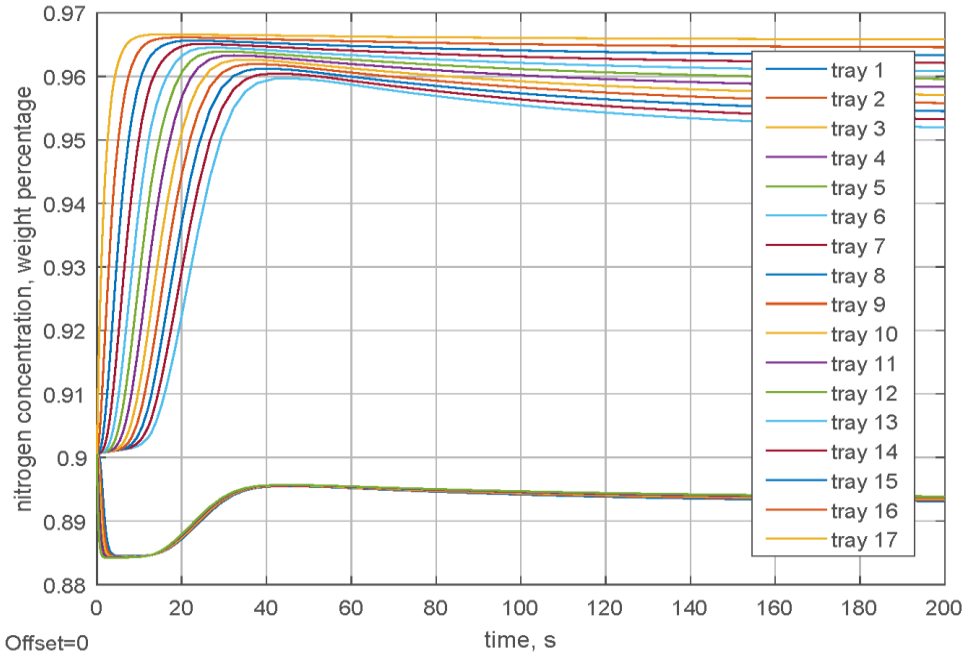

Figure 2. Nitrogen concentration dynamics on mass-transfer devices.

To calculate the thermophysical parameters of liquid and vapor mixtures of nitrogen and oxygen, the additivity property of parameters of pure components at a given pressure in the column *P* should be used.

The resulting mathematical model was implemented in the Matlab Simulink environment and allowed us to evaluate the target product concentration (Figure 2), which makes it possible to integrate this model as a subsystem into higher-level systems, simulate start-up modes, system response to disturbances, analyze the influence of constructive geometry elements of the evaporator, contact devices, etc. Accounting for the nonstationarity of thermophysical properties on the basis of experimental data allowed us to improve the calculations accuracy in transient conditions.

REFERENCES

1. Ryazhskih, V.I., A.A. Khvostov, A.A. Zhuravlev, A.V. Ryazhskih, and O.A. Semenikhin. 2018. "Model of the Evaporator of The Bottom Liquid of the Distillation Column of an Air Separation Unit with Variable Thermal Characteristics," in *Proc. of the International Scientific Conf.: Mathematical Methods in Engineering and Technology*, 12(1):92-95.
2. Khvostov, A.A., V.I. Ryazhskih, A.A. Zhuravlev, I.A. Kazmin, and A.A. Nikitchenko. "Mathematical Model of Mass Transfer on the Contact Devices of the Air Separation Unit," in *Proc. of the International Scientific Conf.: Mathematical Methods in Engineering and Technology*, 12(1):102-105.

3. Khvostov, A.A., A.A. Zhuravlev, M.I. Slyusarev, and A.A. Vorobyev. 2018. “Calculation of the Relative Volatility of a Mixture of Nitrogen and Oxygen,” in *Proc. of the International Scientific Conf.: Engineering Technology of the Future of Food Technology*, pp. 251-255.
4. Ryazhskikh, V.I., A.A. Khvostov, A.A. Zhuravlev, and A.V. Ryazhskikh. 2018. “Calculation of the Vapor Pressure of Cryogenic Products from Experimental Data”, in *Proc. of the 3rd All Russian Scientific and Technical Conf.: Prospects for the Development of Processing Technology and Equipment in Engineering*, pp. 293-296.
5. Narinskiy, G.B. 1978. *Air Rectification*. Moscow: Mashinostroyeniye, 248 p.

2018 International Theoretical and Practical Conference on Alternative and Smart Energy (TPCASE 2018)
ISBN: 978-1-60595-617-6

Improving the Factor of Useful Action of Sliding Bearings for Workers in Dry Friction Sliding Modes

Alexander Bakumenko, Yuri Tkachenko and Marina Krasnova

ABSTRACT

This paper presents the technology to increase the efficiency of dry friction bearings, based on the impact on the working surface, highly concentrated energy flow, in order to reduce power consumption mechanisms and components of aviation equipment.

INTRODUCTION

Interest in bearings of dry sliding friction is relevant in some cases when special requirements are placed on the mechanism for size, weight and reliability, and also requires the use of linear bearings operating in aggressive environments: a sharp temperature difference of ± 60º, the presence of abrasive particles (sand), salt fog [1, 2]. Therefore, the task of reducing friction losses in dry friction bearings today is relevant in a number of modern industries.

THEORETICAL BACKGROUND

In this work, a pair of dry sliding friction was selected, where the aluminum alloy of the grade D16T acts as the base material. The basis of the friction layer of a friction pair is a coating based on silicon dioxide [3, 4]. In order to ensure the stability of the friction pair and the possibility of repair, the hardness of the friction shaft is 65 HRC, respectively, the hardness of the sleeve 60 HRC. For precision positioning and

Voronezh State Technical University, 14, Moskovsky Avenue, Voronezh, 394026, Russia

providing a gap of several microns, a final surface finish is required. As a rule, ceramic surfaces are subjected to diamond grinding (polishing is additionally performed for precision mechanisms), but during surface treatment, microcracks appear on the friction surface, which negatively affects the coefficient of friction, and also contributes to accelerated wear of the friction pair. As a result, the efficiency of the mechanism as a whole is reduced [5].

Modern technologies have made great strides with the emergence of highly concentrated energy flows. Namely, it is plasma and laser surface treatment of the friction pair under study with the purpose of quenching with and without melting. Highly concentrated energy fluxes allow the processing of refractory alloys and coatings [6, 7, 8].

In order to reduce the friction coefficient and increase the reliability of the dry friction bearings, as well as to avoid the formation of microcracks during the finishing treatment based on ceramic friction pairs, a method of "laser radiation finishing" was proposed [2, 9].

The manufacture of a friction pair has several stages:

1. Manufacture of the bearing housing (shaft and sleeve);
2. Application of friction coating;
3. Pretreatment of the obtained coating with diamond grinding, leaving a seam allowance;
4. Laser finishing.

RESULTS AND DISCUSSIONS

As a result, we get a better surface in which the concentration of stresses and microcracks is minimized, thereby reducing the time of running-in of a friction pair and increasing the resource by 1.5 times. In Figure 1, the relief (roughness) of the friction surface is conventionally represented before and after the finishing laser treatment.

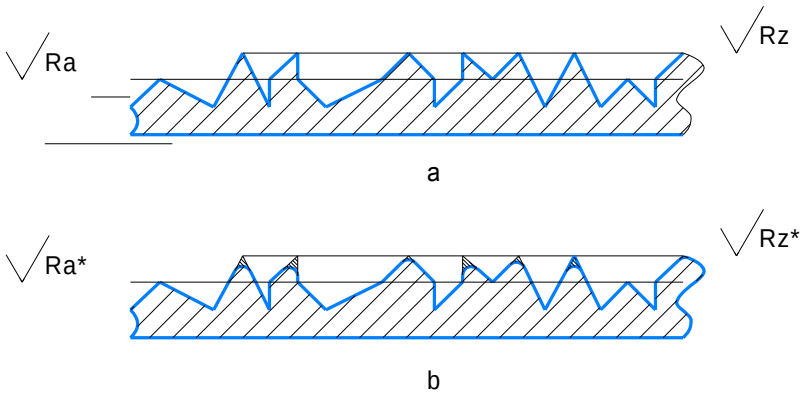

Figure 1. Friction surface relief
a) surface after diamond grinding; b) surface after laser finishing.

The proposed method is based on the equation proposed by N.N. Rykalin, describing the process of heat propagation of a point source of constant power q moving at a constant speed V, and having the form [10]:

$$T(R,z) = \frac{q}{2\pi\lambda R} exp\left(-\frac{V(R-x)}{2a}\right) + T_e, \quad (1)$$

where T (R, z) is the temperature at the point A under consideration;
λ is the thermal conductivity coefficient of the body, W/(m);
a is the coefficient of thermal diffusivity of the body, m^2/s;
$R\sqrt{x^2 + y^2 + z^2}$- the distance from the considered point A with the coordinates (x, y, z) to the beginning O of the moving coordinate system associated with the moving heat source;
T_e is the ambient temperature, i.e. the temperature of the object under study before exposure to a heat source [10].

The condition of heat balance [11]:

$$q = q_{el} + q_{ref} + q_{hc} + q_{rt} + q_c + q_d, \quad (2)$$

where q_{ph}– the power of the point heat source;
q_{el}– the loss of thermal capacity due to the absorption of the environment of the energy radiation heat source;
q_{ref} – the heat loss due to partial reflection of the radiation energy of the heat source surface of the investigated object due to the fact that the investigated material has a coefficient of reflection different from zero.
q_{hc} – the heat loss to the environment due to convective heat transfer;
q_{rt} – the heat loss to the environment due to radiant heat exchange;
q_c - the power distributed in the friction coating due to the conductive heat transfer;
q_d - the power distributed in the body processed detail account conductive heat transfer.

Let us consider the components of equation (2) in more detail.

The loss of thermal power due to absorption by the environment of the energy radiation of the heat source is determined by the following expression [12]:

$$q_{el} = q_{ph}[1 - exp(-\theta l)] = q_{ph}[1 - \beta], \quad (3)$$

where θ is the indicator of environmental degradation, 1/m;
l is the distance between the heat source and the object to be examined (distance from the part surface to the focal length), m;
β - the coefficient of environmental transparency.

Power loss due to incomplete absorption of laser energy by the surface of the opaque body being studied, taking into account losses q_{el} [13] is:

$$q_{ref} = r\beta q_{ph} = (1 - \alpha)\beta q_{ph}, \quad (4)$$

where r is the reflection coefficient;
α – the absorption coefficient.

It is known [13] that at the given temperature the emissivity of a body is equal to its absorption coefficient, i.e. $\varepsilon = \alpha$. With this in mind, expression (4) has the form:

$$q_{ref} = (1 - \varepsilon)\beta q_{ph}. \quad (5)$$

The loss of thermal capacity in the environment due to convective heat transfer, based on the theory of heat exchange [14], is determined by the following expression:

$$q_{hc} = \alpha_{hc}(T - T_e)S, \quad (6)$$

where α_{hc} – the coefficient of convective heat exchange, W/(m^2 K);
T is the surface temperature of the heated body, K;
T_e – the ambient temperature, K;
S – the heat-transfer surface area, m^2.

The loss of thermal power into the environment due to radiant heat transfer is determined by the following expression:

$$q_{rt} = \alpha_{rt}(T - T_e)S, \quad (7)$$

where $\alpha_{rt} = \varepsilon C_0 \left[(\frac{T}{100})^4 - (\frac{T_e}{100})^4\right]/(T - T_e)$ is the coefficient of radiative heat transfer, W/(m^2 K);
$C_0 = 5.67$ is the Stefan-Boltzmann constant, W/(m^2 K);
S – the heat-transfer surface area, m^2.

The power q distributed in a heated body due to conductive thermal conductivity with a non-contact thermal effect on it from a fixed point heat source, according to expression (1) is determined as follows [11]:

$$q = 2\pi\lambda R[T_m - T_e]\exp(\frac{V(R-x)}{2a}), \quad (8)$$

where T_m - the melting point of the processed material.

The power q_c; q_d is determined by expression (8)

The author of [11] found that the obtained expression describing the temperature field with $R \geq 20r_0$, (where r_0 is the radius of the point source) describes the temperature field acting on the body by a moving point heat source with an error of no more than 5%. But with $R<20r_0$ values, the error exceeds 40%.

In this case, it is necessary to introduce a numerically calculated correction factor γ(R) in order to obtain sufficiently accurate calculated data up to $R\sim1$. Then, with sufficient accuracy for practice, it is possible to calculate the effective absorbed power density [15]:

$$q_{ef} = \gamma q = \gamma(q_{el} + q_{ref} + q_{hc} + q_{rt} + q_c + q_d) \quad (9)$$

Using relations (3) - (8) for each of the terms of equation (9) after mathematical transformations, the expression describing the temperature thermal field in a semi-infinite thermal body under the action of its mobile point source of heat has the following form:

$$T(R,z) = \frac{\gamma q(1-\varepsilon\beta)(T_m - T_e)\left[2\pi\lambda_1\gamma R\exp\left(\frac{V(R-z)}{2a_1}\right) + 2\pi\lambda_2\gamma R\exp\left(\frac{V(R-z)}{2a_2}\right)\right]}{2\pi\lambda_1 R} \times \times\exp\left(-\frac{V(R-x)}{2a_1}\right) + T_e. \quad (10)$$

Thus, we determined the equation describing the working surface of the bearing, taking into account that the friction layer has distinctive characteristics of thermal conductivity and absorption of laser radiation, in comparison with the structural material. These mathematical calculations have become fundamental for the development of a mathematical model, laser micromelting, which is currently under active work.

The first experimental studies on steel surfaces showed an increase in the surface roughness class from 6 to 7 (it was Ra 1.6 microns and Ra 1.25 microns). Surface hardening was also observed on the steel surface.

Further studies are planned to be made with silica-based coatings. The result of the study should be the technology of finishing laser processing of refractory and ceramic coatings.

ACKNOWLEDGEMENTS

This work was supported by Company “Rusaviainter”.

REFERENCES

1. Panov, A.D., and I.M. Panova. 2015. “Tribological Features of Structural Ceramic Materials in Sliding Bearings,” *Internet-magazine "SCIENCE”*, 7(1)
2. Miyoshi, Kazuhisa. 2017. *Solid Lubricants and Coatings for Extreme Environments: State-of-the-Art Survey*, NASA
3. www.npo-oxide.ru
4. Zhang, L. 2014 “Manufacture of Selectively Commercially Pure Titanium,” *Materials Science and Engineering Journal* 06
5. Shamberov, V.N. 2004. “Influence of Dry Friction in the Actuators of Automatic Systems with a Driving Electric Motor on Their Stability,” *Scientific Instrument Making*, 14(4):39-45.

6. Bakumenko, A.V., G.I. Trifonov, and Yu.S. Tkachenko 2016. “Some Aspects of the Combined Methods of Processing Steel Parts,” in *Proc. of the All-Russian Scientific and Technical Internet Conference in High Technologies in Mechanical Engineering*: – Samara, pp. 9-12.
7. Kurlas, M. 2014. "German Selective Laser Melting Specialist Mulls IPO," *Journal Industrial Solutions*
8. Gärtner, F., H. Kreye, and H.J. Richter. 2007. *HVOF Spritzen mit Pulver und Draht, Tagungsband, 7. Kolloquium zum Hochgeschwindigkeits-Flammspritzen*. Erding, Germany, pp. 39-56
9. Adel, K.M., A.S. Dhia, and M.J. Ghazali. 2009. “The Effect of Laser Surface Hardening on the Wear and Friction Characteristics of Acicular Bainitic Ductile Iron,” *International Journal of Mechanical and Materials Engineering*, 4(2):167–171.
10. Rykalin, N.N. 1951. *Calculations of Thermal Processes during Welding*. Moscow: Mashgiz
11. Sysoev, E.V., and T.I. Chernyshov. 2002. “Simulation of Thermal Processes in Explored Objects at Non-Contact Thermal Effects in a Moving Point Source of Heat,” *Vestnik TSTU*, 8(1):70-78.
12. Kriksunov, L.Z. 1972. *Handbook of Basics of Infrared Technology*. Moscow: Sov.radio
13. Hudson, R. 1972. *Infrared Systems.* Moscow: Mir
14. Lykov, A.V., and Yu.A.Mikhailov 1963. *Theory of Heat and Mass Transfer*. Moscow: Gosenergo-izdat
15. Panchenko, V.Ya. 2009. *Laser technologies for processing materials: current problems of fundamental research and applied developments*. Moscow: FIZMATLIT.

2018 International Theoretical and Practical Conference on Alternative and Smart Energy (TPCASE 2018)
ISBN: 978-1-60595-617-6

Improving the Efficiency of the Supply-and-Exhaust Ventilation System

Alexandr Barakov, Dmitry Prutskikh, Nikolay Kozhukhov, Vladimir Dubanin and Anatoly Muravev

ABSTRACT

The article considers a schematic diagram of the supply-and-exhaust ventilation system. To increase its efficiency, a regenerative heat exchanger is proposed, which is a heat utilizer in a cold season and, in a warm season, it is a device for evaporative air cooling. The paper presents the results of theoretical studies of hydrodynamics, heat and mass transfer of the device. In addition, an experiment was performed to analyze these processes and experimental data were obtained. Analytical and empirical formulas are determined for the engineering methodology for calculating the heat exchanger on the basis of the two types of research.

INTRODUCTION

A significant amount of energy is currently being spent to create specific conditions for people in industrial and administrative premises. For these purposes, a supply-and-exhaust ventilation system is often used, a schematic diagram of which is shown in Figure 1 [1].

Voronezh State Technical University, 14, Moskovsky Avenue, Voronezh 394026, Russia

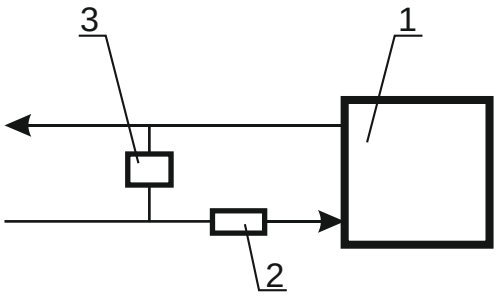

Figure 1. Diagram of a supply-and-exhaust ventilation system
1 - ventilated room; 2 - heater; 3 - heat exchanger.

We consider the main drawback of the presented system to be a large expenditure of energy (heat) for heating the supply air. This issue is particularly critical when the outside temperature decreases $t_{oa} < -16$ °C (the estimated temperature for the city of Voronezh is considered as an example). If $t_{oa} > 18$ °C, the indoor temperature becomes inconsistent with sanitary norms and rules. To reduce these drawbacks, we propose to include heat exchanger 3 in the circuit. In a cold season, it will act as an exhausted air heat utilizer and preheat the supply air by 5-7 °C, which will reduce the expenditure of energy consumed by the heater 2 by an amount from 20 to 25%. When $t_{oa} > 18$ °C due to the organization in this heat exchanger direct or indirect evaporation cooling of the air supplied to the room, this device will work as a cooler. The second version of cooling consists of two stages: 1) evaporation in the exhaust air flow; 2) cooling the supply air with a constant moisture content. Devices operating on such a principle, which essentially uses the thermodynamic irregularity of the surrounding air, are considered to be devices using a renewable energy source.

DESCRIPTION OF THE DESIGN OF THE HEAT EXCHANGER

Earlier theoretical and experimental studies [3-5] showed the high practical significance of the use of a regenerative heat exchanger with a "boiling" centrifugally circulating layer. Such an exchanger is applicable to the system of supply-and-exhaust ventilation. The movement of dispersed material here occurs under the action of two flows of air: main and auxiliary [6]. The design of the proposed device is shown in Figure 2.

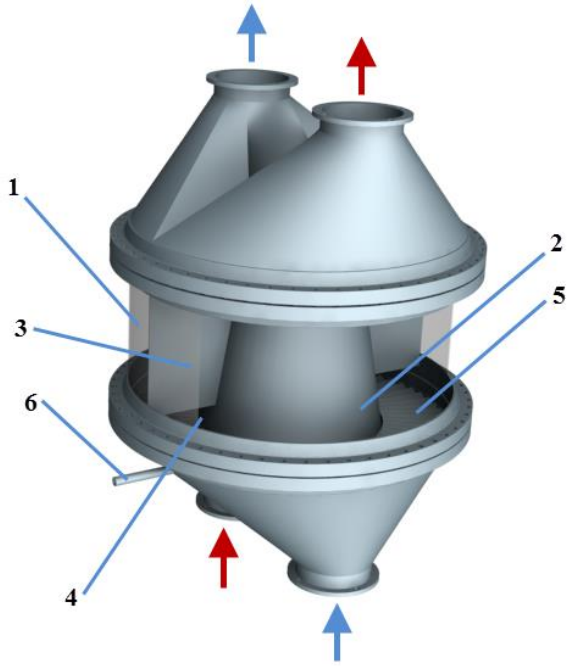

Figure 2. Design of the heat exchanger
1 – outer shell; 2 – inner shell; 3 – partition; 4 – overflow window;
5 – gas distribution grid; 6 – nozzle.

The heat exchanger consists of a body formed by two cylindrical shells having a common axis of symmetry. The material of the outer shell is transparent to visualize the processes happening inside. The two partitions 3 divide the inner space of the device into two chambers designed for different air flows: supply and exhaust air. Using the evaporation process in this heat exchanger allows us to call these chambers "wet" and "dry." The blades located at a certain angle to the air flow and the grid superimposed on them form the so-called gas distribution grid of this device. It allows us to orient the movement of the supply and exhaust air flows along with a layer of dispersed material located on the grid at the initial time. The nozzle 6 is located at the entrance to the "wet" chamber to moisten the attachment.

The temperature of the wetted particles of the dispersed material, which are in the "boiling" state, starts to decrease due to evaporation of moisture from their surface and becomes equal to the temperature of the wet thermometer. The dried particles are moved to the "dry" camera and reduce the temperature of the main air flow intended for supply to the consumer. The temperature of the particles of the dispersed material is increased to the temperature of the particles at the entrance to the “wet” chamber at the initial moment of time. Then the movement of the attachment is repeated, thus organizing a closed circular movement. In a cold

season, the water is not supplied to the nozzle and the heat exchanger works as a heat utilizer of the exhaust air.

Heat exchangers of this type are not yet widely used in the housing and utilities sector and in industrial enterprises due to the lack of engineering calculation methods based on a complete study of the heat and mass transfer process in the circulating "boiling" layer. We will model it in relation to the structure under consideration.

MODELING HEAT AND MASS TRANSFER IN A REGENERATIVE HEAT EXCHANGER

Using the heat balance equation (1) for a particle in a "wet" chamber, we find the time in which water is completely evaporated from one particle of the dispersed material. At the same time, it is assumed that a decrease in the volume of the water from a particle of the material by an amount dv happens at time $d\tau$.

$$qf_p d\tau = -\rho_f \left[c_f \left(t_{sat} - t_f \right) + r_v \right] dv, \tag{1}$$

where q - the heat flux density W/m^2; f_p - the surface area of a wetted particle, m^2; τ - the time, s; ρ_f - the water density, kg/m^3; c_f - the heat capacity of water, J/(kg·K); t_{sat} - the saturation temperature, K; t_f - the water temperature, K; r_v - the latent heat of vaporization, J/kg; v - the volume.

Taking into account that $dv = f_p dr$, we get from (1)

$$\tau = -\int_{r+\delta}^{r} \frac{\rho_f \left[c_f \left(t_{sat} - t_f \right) + r_v \right]}{q} dr, \tag{2}$$

where δ - the thickness of the water film on the surface of the particle, m; r - the particle radius, m;

To determine the heat flux density, it should be taken into account that thermal energy is supplied to the particle through the convection process and, therefore, the application of Newton-Richman law is possible. Therefore

$$q = \alpha \left(t_a - t_{sat} \right), \tag{3}$$

where α - the interphase heat transfer coefficient between the air flow and the particle of the dispersed material in the "wet" chamber, W/(m^2·K); t_a - the air temperature in the auxiliary flow.

The thickness of the water film on the surface of the particle of the dispersed material is very small. In this regard, its influence on the process of heat transfer is insignificant. Given this assumption, we can determine the heat transfer coefficient, using the following criterial equation [7]

$$Nu = 0.51\mathrm{Re}^{0.65}, \tag{4}$$

where $Nu = \frac{\alpha d_e}{\lambda_a}$ - Nusselt number; $\mathrm{Re} = \frac{w_в d_э}{\nu_в}$ - Reynolds number.

In the formulas to determine the criteria, the following notations are used: λ_a - the air thermal conductivity, W/(m·K); ν_a - the kinematic viscosity coefficient, m^2/s; d_e - the equivalent particle diameter, m; w_a - the air velocity, m/s.

From the joint solution (2), (3) and (4) and integration, we obtain

$$\tau = \frac{\rho_f \left[c_f \left(t_{sat} - t_f \right) + r_v \right]}{0.42 \lambda_a w_a^{0.65} \nu_a^{-0.65} \left(t_a - t_{sat} \right)} \cdot \left[\left(r + \delta \right)^{0.65} - r^{0.65} \right]. \tag{5}$$

To calculate the temperature fields in the “dry” chamber of the air cooler, a system of differential equations was solved, which included the heat balance equation and the Newton-Richman equation. This system was recorded for the elemental volume of the "boiling" circulating layer. For the air temperature at the height of the attachment layer, the following relationship is obtained

$$t_a = t_p + (t_a' + t_p') \exp\left(-\frac{\alpha (1-\varepsilon) f_p}{c_a w_a \rho_a} y \right), \tag{6}$$

where t_p – the temperature of particles of the dispersed material, K; t_a' , t_p' - the temperature of air flow and particles at the entrance to the “dry” chamber, K; ε - the porosity of the "boiling" layer; f_p - the specific surface of the attachment layer m^2/m^3; ρ_a - the air density, kg/m^3; c_a - the heat capacity of the air, J/(kg·K); y - the coordinate.

The independence of the temperature of particles from the y coordinate is due to their active mixing. With this in mind, the dependence for the temperature of the particles of the dispersed material is obtained as follows

$$t_p = t_p^{'} + \left(t_a^{'} - t_p^{'} \right) \exp\left\{ -\frac{c_a w_a \rho_a x}{c_p w_p (1-\varepsilon) \rho_p h} \left[1 - \exp\left(-\frac{\alpha f_p h (1-\varepsilon)}{c_a \rho_a} \right) \right] \right\}, \tag{7}$$

where ρ_p – the material checker density, kg/m^3; c_p - the heat capacity of the material checker, J/(kg·K); w_p - the material checker movement velocity, m/s; h - the height of the material checker layer, m; x – the coordinate, m.

EXPERIMENTAL STUDY OF A HEAT EXCHANGER

To examine the heat exchanger for compliance with the requirements of the specified technical parameters for the system of supply and exhaust ventilation, an empirical study of an experimental sample, the design of which is described above, was performed. Here we give only the specific geometric and thermal parameters and the method of organizing the physical process. Thus, the diameters of the outer and inner shells were 200 and 300 mm, respectively, and their height was 500 mm. The angle of installation of the blades could vary from 20 to 40°. The air supply to each of the chambers of the device was carried out by high-pressure fans VC 10-28 no. 3, and its consumption was measured by calculating and using anemometers TTM-2/4-06. Thermocouples TP-0188 were used to measure the air temperature at various points of the device. As a dispersed material of the attachment we used particles from various materials: zinc-aluminum alloy ($\rho_p = 2850\ kg/\text{m}^3$, $d_e = 2.6$; 2.9; 4.6 and 5.0 mm), sand ($\rho_p = 2650$ kg/m^3, $d_e = 2.7$ and 3.2 mm).To study the required number of operating modes of the heat exchanger, both types of attachments were used, and their mass was in the range from 0.5 to 3.5 kg. The flow rate of water through the mechanical nozzle ranged from $4\cdot10^{-4}$ to $24\cdot10^{-4}$ kg/s. The loss of air pressure in the chambers of the device was measured with high-precision micro manometers MMN-240.

The following experiment algorithm was used. The specified mass of particles of the dispersed material was poured into both chambers. Then VC 10-28 was activated. Using a frequency converter, the air consumption in the chambers was adjusted to the values corresponding to the steady displacement of the "boiling" layer along the grid. After that, the water mechanical nozzle was connected, which wetted the particles in the "wet" chamber of the device. After reaching the pseudo-stationary state of the entire system, various thermal and physical characteristics were measured: the temperatures, the air and water consumption, and the pressure. For this, the SCADA system was used along with the hardware and software of the OVEN firm. Thus, a study of more than fifty modes of operation of the heat exchanger was carried out.

According to the measurement results, the efficiency coefficient was calculated

$$\eta = \frac{t'_a - \overline{t}''_a}{t'_a - t_{wet}} \cdot 100, \qquad (8)$$

where $\bar{t}_a^{"}$ – the average integral temperature of the coolant at the outlet of the "dry" chamber, K; t_{wet} - the temperature of the "wet" thermometer, K.

Analyzing the results of the experiment, we determine the main parameters, the change of which leads to a change in the thermal efficiency of the heat exchanger. These parameters are w_a and M, present in (9). As a result of the approximation of the obtained data from the experiment by means of MathCad, the following equation was obtained

$$\eta = 4.55 w_a^{1.01} M^{0.94}, \tag{9}$$

where M – the dispersed material mass, kg.

The dependence of the efficiency coefficient on the mass of the attachment and the velocity of the main air flow is shown in Figure 3. The standard deviation is about 3%.

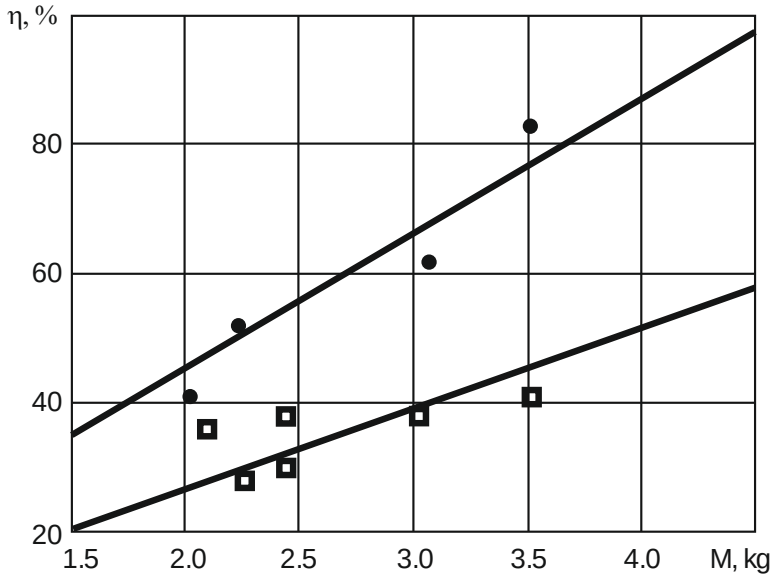

Figure 3. Dependence of the efficiency coefficient on the mass of the attachment and the velocity of the main air flow

• - $w_a = 5.13$ m/s, □ - $w_a = 3.06$ m/s; — - calculation by (9).

Experimental data on the pressure drop of the heat exchanger were also subjected to statistical processing, which resulted in the following relationship

$$\Delta P = 2.58 w_a^{2.15} M^{0.73}. \quad (10)$$

Figure 4 shows the dependence of the hydraulic resistance for some fixed values of the mass of the dispersed material, depending on the air velocity. Here, the error comparing to the calculated data was 4%. Also, the pressure difference between the "wet" chamber and the calculated value by (10) was determined. This value was 20%.

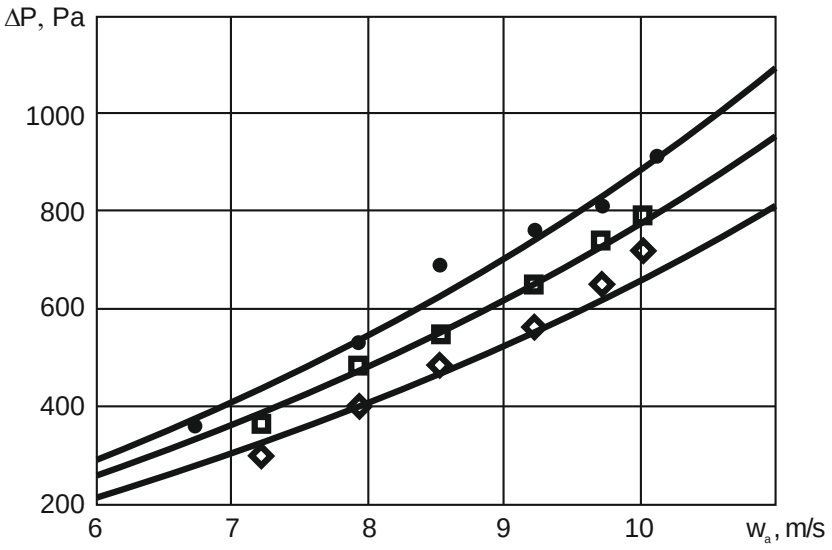

Figure 4. Dependence of the pressure drop of the air cooler chamber
• - $M = 3$ kg, □ - $M = 2.5$ kg, ◊ - $M = 2$ kg; — - calculation by (10).

CONCLUSIONS

As a result of the conducted research, it was shown that it is expedient to include the regenerative heat exchanger with the attachment in the form of a "boiling" centrifugally circulating layer of the dispersed material into the scheme of supply and exhaust ventilation of various premises. In a cold season, such a heat exchanger will act as an exhaust air heat utilizer, and in a warm season, it will cool the supply air due to the evaporation of water.

Theoretical and experimental studies have shown the efficiency of the device and also allowed us to obtain several analytical and empirical relationships that can create a scientific basis for its engineering calculation.

REFERENCES

1. Stefanovsky, E.V. 2005. *Ventilation and Air Conditioning*. St. Petersburg: Avok Severo-Zapad, 400 p.
2. Kokorin, O. Ya. 1965. *Evaporative Cooling for Air Conditioning Purposes*. Moscow: Stroiizdat, 160 p.
3. Barakov, A.V., V. Yu. Dubanin, and D.A. Prutskikh. 2007. "Study of Heat Transfer in the Regenerator with a Dispersed Nozzle," *Energy Saving and Water Treatment*, 4(48):45-46.
4. Barakov, A.V., V. Yu. Dubanin, D.A. Prutskikh, and A.M. Naumov. 2010. "Investigation of Indirectly Evaporative Air Cooler with Dispersed Nozzle," *Industrial Energy*, 11:37-40.
5. Barakov, A.V., V. Yu. Dubanin, D.A. Prutskikh, and S.A. Gerasimov. 2011. "Simulation of Heat and Mass Transfer in the Air Cooler of Indirect-Evaporation Type with a Circulating Dispersed Nozzle," *Industrial Energy*, 8:40-42.
6. Agapov, Yu. N., A.V. Barakov, and A.M. Naumov. 2006. "Air Cooler," patent of the Russian Federation #59786 RF IPC F28D15/00
7. Prutskih, D.A. 2009. "Hydrodynamics and Heat Transfer in the Regenerator with a Dispersed Nozzle," Cand. of Tech. Sciences Dissertation, Voronezh: VSTU, 108 p.

2018 International Theoretical and Practical Conference on Alternative and Smart Energy (TPCASE 2018)
ISBN: 978-1-60595-617-6

Heat Transfer of Newtonian Heat-Carrier Under Laminar Flow Through the Flat Porous Channel and Under Symmetric Border Conditions of the First Kind

Viktor Ryazhskikh, Dmitriy Konovalov, Igor Drozdov, Nikolay Kozhukhov and Dmitriy Shmatov

ABSTRACT

The precise analytical solution for the heat transfer problem in a porous flat channel with a laminar flow of a viscous incompressible coolant with boundary conditions of the first kind is obtained based on the assumption that the flow is unidirectional, phase transitions are absent, and the thermos-physical properties are constant. The model is based on the Schumann equations as an initial-boundary value task for the system of parabolic equations referring to the local temperature of the coolant and the porous matrix. The paper reveals the relation of the local Nusselt number and the conditions necessary to access the compactness of heat transfer systems with porous fillers.

INTRODUCTION

Porous fillers of the flow channels of various purpose heat transfer systems substantially intensify heat transfer [1], which causes their more compact design. However, the quantitative assessment of the possible degree of compactness is impossible without analyzing the phenomena of heat transfer in porous media on the basis of a fundamental approach that uses classical concepts of conjugated heat and mass transfer [2]. In this regard, heat exchange is studied in the plane parallel channel where a viscous incompressible coolant moves in the laminar mode with different temperature conditions of the first kind over through the "wetted" surfaces.

Voronezh State Technical University, 14, Moskovsky Avenue, Voronezh 394026, Russia

The physical model of a porous environment is accepted as the standard one [3]. It is a package of spherical particles, tightly compressed among each other. There are no closed pores. The free porous space is filled with coolant. Phase transitions are absent. The heat carrier flow is unidirectional and is carried out in a laminar mode [4]; inertial effects are also neglected. The validity of such assumptions is experimentally confirmed [5].

The efficiency of porous heat exchangers increases as its permeability decreases. It reaches its maximum when Darcy numbers are fixed at around 10^{-4}. This allows us to presume that the flow of coolant emanates in the mode of ideal displacement, i.e. the velocity profile inside the heat exchanger corresponds to the input profile [4]. This simplifies the solution of the thermal subtask and allows us to take the value of the dimensionless velocity equal to 1.

MATHEMATICAL MODEL

All the above considerations allowed us to use Schumann energy equations [6] for a plane layer under the assumption that the diffusion of heat in the transverse direction to the flow of the coolant is significantly higher than in the axial

$$\frac{\partial T_f(X,Y)}{\partial X} = \frac{1}{\varepsilon Pe}\frac{\partial^2 T_f(X,Y)}{\partial Y^2} + 6\left(\frac{1-\varepsilon}{\varepsilon}\right)\frac{Nu_p \,\mathrm{Re}}{\mathrm{Pr}\,\mathrm{Re}_p^2}\left[T_s(X,Y) - T_f(X,Y)\right]; \quad (1)$$

$$\frac{\partial^2 T_s(X,Y)}{\partial Y^2} = 6(1-\varepsilon)Bi_p\left(\frac{Re}{Re_p}\right)^2\left[T_s(X,Y) - T_f(X,Y)\right]; \quad (2)$$

$$T_f(0,Y) = 1; \quad (3)$$

$$T_f(X,0) = T_s(X,0) = 0; \quad (4)$$

$$T_f(X,1) = T_s(X,1) = 0, \quad (5)$$

where $X = x/h$; $Y = y/h$; $T_{f,s}(X,Y) = \left[t_{f,s}(x,y) - t_c\right]/(t_h - t_c)$; $Pr = \nu_f / a_f$ is Prandtl number; $Re = u_0 h/\nu_f$ is Reynolds number; $Pe = h(\rho c_p)_f u_0 / \lambda_e^{(f)}$ is Peclet number; $Re_p = u_0 d_p/\nu_f$ is local Reynolds number; $Nu_p = \alpha_{sf} d_p / \lambda_e^{(f)}$ – local Nusselt number; $Bi_p = \alpha_{sf} d_p / \lambda_e^{(s)}$ is local Bio number; x, y are the longitudinal and transverse Cartesian coordinates; h is the channel height, t_f, t_s is the local

temperature of the coolant and the porous matrix; t_h, t_c is the temperature of the coolant at the inlet to the porous channel and the temperatures of the lower and upper "wetted" surfaces; ν_f, a_f, ρ_f, c_{pf}, $\lambda_e^{(f)}$ are the kinematic viscosity, thermal diffusivity, density, mass heat capacity and "effective" thermal conductivity of the coolant; u_0 is the flow rate at the inlet to the channel; d_p is the number average of the spherical particle diameter in porous layer; α_{sf} is the heat transfer coefficient between the coolant and the porous matrix; $\lambda_e^{(s)}$ is the "effective" thermal conductivity of the porous matrix; ε is porosity.

SOLUTION

Precise solution presumes consistent application of the one-sided integral Laplace transform and the finite-integral sine Fourier transform, (1)-(5)

$$T_f(X,Y) = 2\sum_{n=1}^{\infty} exp\left[-\left(A\pi^2 n^2 + B - \frac{BC}{C+\pi^2 n^2}\right)X\right] sin(\pi nY); \qquad (6)$$

$$T_s(X,Y) = 2\sum_{n=1}^{\infty} \frac{C}{C+\pi^2 n^2} exp\left[-\left(A\pi^2 n^2 + B - \frac{BC}{C+\pi^2 n^2}\right)X\right] sin(\pi nY), \qquad (7)$$

where $A = \frac{1}{\varepsilon Pe}$; $B = 6\left(\frac{1-\varepsilon}{\varepsilon}\right)\frac{Nu_p\, Re}{Pr\, Re_p^2}$; $C = 6(1-\varepsilon)\, Bi_p \left(\frac{Re}{Re_p}\right)^2$.

By definition, the local Nusselt number is $Nu(X) = \left[\bar{T}_f(X) - T_f(X,0)\right]^{-1}$, where $\bar{T}_f(X) = \int_0^1 T_f(X,Y)\, dY$, thus, limited to the first member of the series (6) we will find the following solution (6)

$$Nu(X) \approx \frac{\pi}{4} \Big/ exp\left[-\left(A\pi^2 + \frac{B\pi^2}{C+\pi^2}\right)X\right]. \qquad (8)$$

If we consider that required cooling is $\bar{T}_f^{(0)}$, then, in case the channel does not contain porous filler ($\varepsilon = 1$), the channel length at which such cooling is achieved is

$$X_1^c = -\left[1/\left(\pi^2/Pe\right)\right] ln\left(\frac{\pi}{4}\bar{T}_f^{(0)}\right), \quad (9)$$

and, in case the filler is in place the solution is as following

$$X_2^c = -1/\left(\frac{\pi^2}{\varepsilon Pe} + \frac{B\pi^2}{C+\pi^2}\right) ln\left(\frac{\pi}{4}\bar{T}_f^c\right). \quad (10)$$

Since following the physical meaning $B > 0$ and $C > 0$, then, we presume that $X_2^c < X_1^c$ (9) and (10), i.e. the use of porous filler always leads to efficient heat transfer. At the same time in order to increase the compactness, it is necessary to increase the $B\pi^2/\left(C+\pi^2\right)$ complex, which determines the thermo-physical properties of the system, as well as the flow rate of the coolant.

REFERENCES

1. Delavar, M.A., and M.I. Azimi. 2013. "Using Porous for Heat Transfer Enhancement in Heat Exchangers: Review," *J. of Eng. Science and Technology Review*, 6(1):14-16.
2. Vafai, K. 2005. *Handbook of Porous Media*. NY: CRC Press Taylor & Francis Group, 742 p.
3. Bear, J., and Y. Bachmat. 1994. *Introduction to Modeling of Transport Phenomena in Porous Media*. Netherlands: Kluwer Academic Publishers, 553 p.
4. Ryazhskikh, V.I., D.A. Konovalov, M.I. Slusarev, and I.G. Drozdov. 2016. "Analysing Mathematical Model of Heat Removal from the plane Surface Using Laminar Moving Coolant through the Conjugated Porous Medium," *South Ural State University Newsletter*, 9(3):68-81.
5. Izadpanah, M.R., H. Muller-Steinhagen, and M. Vamilahmad. 1998. "Experimental and Theoretical Studies of Convective Heat Transfer in a Cylindrical Porous Medium," *Int. V. of Heat and Fluid Flow*, 19:629-635.
6. Gamal, A.A., and P. Furmanski. 1997. "Problems of Modeling Flow and Heat Transfer in Porous Media," *Biuletyn Instytutu Techniki Cieplnej Politechniki Warszawskiej*, 85:55-88.

2018 International Theoretical and Practical Conference on Alternative and Smart Energy (TPCASE 2018)
ISBN: 978-1-60595-617-6

Hydrogen Desorption Kinetics Derived from Electrochemical Ni-B Compositions

Alla Zvyagintseva

ABSTRACT

The paper studies how boron concentration exerts its influence on the structure of nickel-boron-hydrogen composites. An increase in the concentration of the alloying component of boron in nickel increases the dispersion and leads to the alignment of the micro-profile surface and the formation of the nano-sized structures. Boron is an impurity trap for hydrogen atoms in Ni–B electrochemical composites. The paper also presents the results of the studies of the kinetics of hydrogen desorption from Ni-B electrochemical composites. The hydrogen content in the Ni_x-B_y-H_z samples (9 at.% Boron), measured by the vacuum extraction method, was 600 cm^3/100 g, which significantly exceeds the corresponding value for electrochemical nickel ~ 100 cm^3 per 100 g. In this respect, deuterium thermal desorption spectrums from Ni–B composites pre-implanted with various doses of deuterium ions at T ~ 100 K were studied. It has been confirmed that the structure of the deuterium thermal desorption spectrum is the implantation dose function. The deuterium content for nickel corresponds to the following ratio: Ni: D = 1:1, whereas the ratio for the composite is $Ni_{95}B_5$ [Ni_{95}:B_5]:D = 1:1.25. Distinct peak with a maximum temperature of 325 K is formed for the nickel. Whereas for the Ni–B composite, the thermal desorption spectrum has a diffuse peak with a maximum temperature of 325 K and a deuterium desorption region where the temperature ranges from 250 to 500 K.

INTRODUCTION

The main requirements for the fuel cells materials were emphasized in [1]: materials for hydrogen storage should have high hydrogen content, low cost of

Voronezh State Technical University, 14, Moskovsky Avenue, Voronezh, 394026, Russia

thermal energy for dehydrogenation and fast kinetics of hydrogen desorption at the operating temperatures (80-120°C).

Solid metallic hydrides that reversibly desorb certain amounts of hydrogen are among the various options currently being considered by the researchers [2, 3]. They are attractive as base materials for hydrogen storage due to the simplicity of the process, low operating pressures, and relatively low cost. The complex boron-hydrides of $Me(BH_4)_n$ metals with their high hydrogen content also receive increased attention among researchers. Their synthesis and properties associated with hydrogen storage are discussed in [4, 5]. The increase in the kinetic rates of adsorption and desorption of hydrogen from complex metal hydrides plays an important role in the creation of materials for the storage of hydrogen. Experimental data [3, 6, 7] confirm that changes in the concentration of boron additives in nickel-based electrochemical composites affect the amount of hydrogen within them, which allows us to consider them as a potential hydrogen storage devices, especially for small size technical applications, which may require weight reduction.

The goal of our research is to find the susceptibility to hydrogen accumulation, which takes place during the structure transformation (during the generation of structural and impurity traps) and to study the kinetics of hydrogen desorption from Ni-B electrochemical composites.

EXPERIMENTAL TECHNIQUE

Nickel is chosen from a number of metals, as a material characterized by its tendency to accumulate hydrogen, characterized by catalytic activity.

Ni-B composites were synthesized by electro-crystallization in nickel plating sulfamic acid electrolyte with reversal of boron compounds of the class of higher polyhedral borates $Na_2B_{10}H_{10}$. Electrolysis conditions: current density (i_k) 0.5-4.0 A/dm^2; electrolyte temperature 30-50 °C; pH - 3.5-4.5. Anodes - Ni-00 nickel. Cathodes - M-1 copper grade. The boron concentration in the Ni-B composite was measured by the spectrophotometric method. The elemental composition of the synthesized materials was analyzed by the x-ray method on DRON–2.0 diffractometer. The structure was examined on UYMB-100AK electron microscope.

The amount of hydrogen incorporated was evaluated by vacuum extraction with a nitrogen trap. The Ni-B composite sample was heated to the temperature of 500 °C in a quartz chamber with a vacuum of 10^{-5} mm. The volume of water was calculated based on the pressure difference before and after heating. The introduction of hydrogen-deuterium isotopes and measurements of the spectra of thermal desorption were carried out using the “SKIF” facility, which is described in detail in [8]. The partial pressure of gases was evaluated in a dynamic mode of

the APDM-1 and MX-7304 analytical chamber of the monopole mass spectrometer.

EXPERIMENTAL PART

The paper studies the effect of boron concentration on the structure of nickel-boron-hydrogen composites (Figure 1). The histograms of the distribution of crystallites by size, depending on their amount for nickel and the nickel-boron-hydrogen composite are shown in Figure 2. From the photographs below it follows that: for nickel, the predominant amount of crystallites ~ 68 % is in the range of 0–400 A^0, and for nickel-boron the amount of crystallites is ~ 93 % and the resulting structure has an equiaxial shape. The structure of the nano-scale range is being formed. The increased concentration of the alloying component of boron in nickel enhances the dispersion and leads to the alignment of the surface micro-profile.

The correlation of structural transformations in the Ni-B composite and susceptibility to the accumulation of hydrogen is interpreted by the number of defects in the metal structure [7, 9]. In the monograph [9], it was recommended to evaluate the susceptibility of metals to hydrogen accumulation by structural transformations. Figure 3, curve 1 shows the principle of transformation of the susceptibility to hydrogen accumulation for a hypothetical metal in the transition from a pure single crystal to an amorphous structure. The experimental proof of the hypothesis of [9] is the dependence of the hydrogen content on the concentration of the nano-forming boron additive in the Ni-B-H composite obtained by the author (Figure 3, curve 2).

When doping nickel with boron concentration from 2 to 10 at. %, we could trace the meta-morphosis in its structure: crystalline (up to 5 at. %), implicitly pronounced crystalline (6-9 at. %), amorphous structure. The transformation in the structure is illustrated by the growth of extracted hydrogen from the composite sample with an increasing boron concentration in nickel. Synthesis of composites that form a combination of elements in the form of small crystallites, due to the appearance of structural and impurity traps in them creates conditions for the formation of internal structures with an increased number of defects per unit volume.

At a boron concentration up to 2-3 at. percent in nickel, the volumetric content of hydrogen in the metal decreases [3, 7], it segregates along the boundaries of crystallites and defects in the Granulated Nickel Superalloy (GNS), blocks them, which stops the incorporation of hydrogen. When the concentration of boron is more than 7 at., the transformation of the crystal structure into an amorphous structure is being fixed. As defects in the GNS are generated, they serve as the spots for hydrogen fixation.

In the vicinity of a substitution impurity of a small atomic radius - boron

embedded in the granulated nickel superalloy, tensile stresses arise and hydrogen segregates around boron with greater synergism than with nickel. Next, we observe the process of the formation of nickel hydride, which dissociates at a low temperature of 46 °C according to the following scheme: $3NiH_2 \rightarrow Ni + 2NiH + 2H_2$, based on [6, 7] of the undersigned authors and other researchers [5, 10].

The choice of boron concentration for subsequent thermal desorption studies is based on the feasibility and user-friendly samples in the form of a metal tape (foil) of Ni*x*-B*y*-H*z*. composites. The concentration of atomic boron in nickel varies from 5 to 10 at. %, whereas it maintains the monolithic state of the composite sample without modifying the powder consistency.

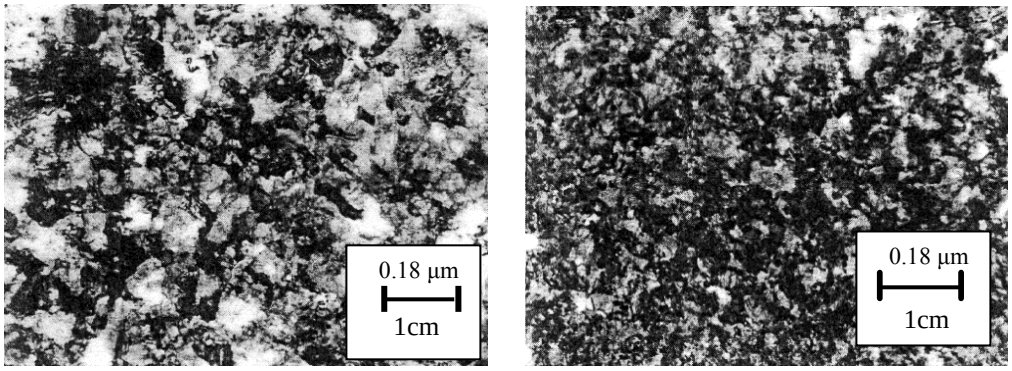

a) Nickel b) Nickel-boron

Figure 1. Effect of boron on the Ni-B composite microstructure. Microstructure of coating Ni (a) and composite Ni-B (b). Electrolysis mode: boron content in the composite Ni-B 5 atm. %; i_k = 3 A/dm^2; pH = 4,0; $t_{el\text{-}te}$ = 40 ^{0}C.

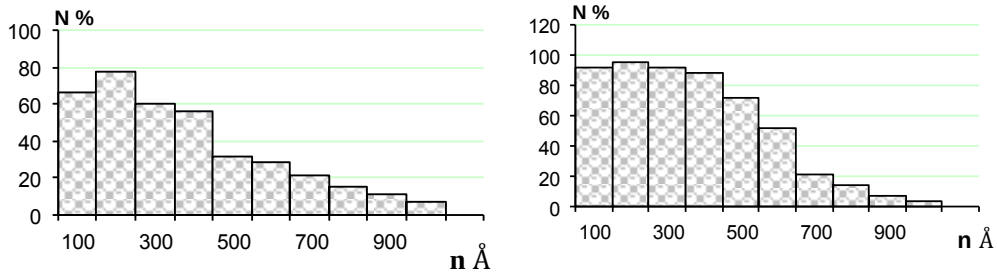

a) Nickel b) Nickel-boron

Figure 2. The histogram of the distribution of grains in the nickel coating (a) and composite Ni-B with a boron content of 5 atm. % (b) in size depending on their number (N – is the number of grains of the same size; n – is the grain size, A^o).

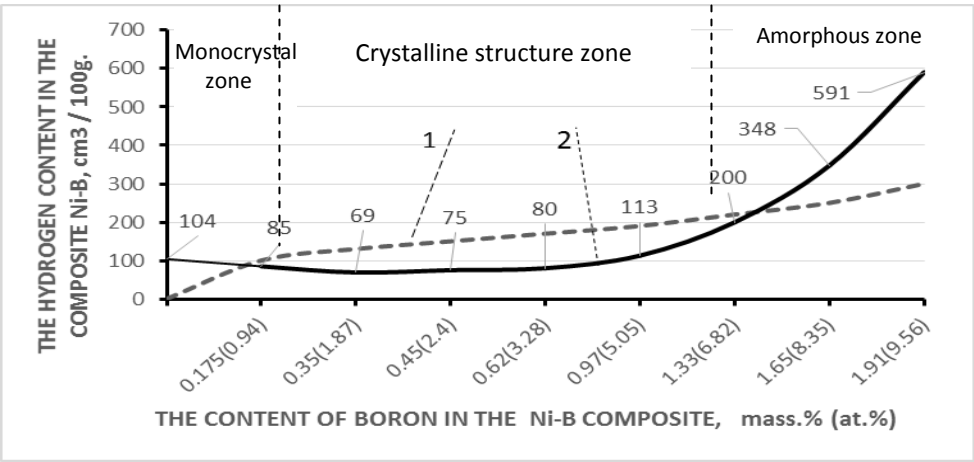

Figure 3. The principle of transformation susceptibility to hydrogen accumulation for metals and alloys: 1- hypothetical metal; 2 - Ni-B-H electrochemical composite. Modes electrolysis: i_k = 2 A/dm^2; $t_{el\text{-}ta}$ = 40 ºC; pH = 4.0; d = 4 μm; substrate - M-1 copper grade.

The kinetics of hydrogen desorption from nickel and Ni–B composite samples (1 wt. % - 5 atom. % boron) was evaluated by mass spectrometry. The preliminary implantation of the samples was carried out with deuterium ions with an energy of 12 keV (D_2 + energies of 24 keV) and a current density of 5 μA/cm^2 in the dose range of 10^{17}–10^{18} D/cm^2 at a sample temperature of ~ 100 K. The low temperature was chosen to limit the diffusion mobility of deuterium in samples.

The most characteristic thermal desorption spectra of deuterium from nickel and Ni–B composite samples for various doses of implanted deuterium are shown in Figures 4-6. As the dose of implanted deuterium increases, a distinct peak forms with a maximum temperature of 325 K. The kinetics of deuterium thermal desorption (TD) spectrum development from nickel and Ni–B composite samples is similar in structure. However, there is a significant difference (Figures 4, 5):

1. The spectrum of the TD of the Ni–B composite with a peak temperature of 325 K is strongly blurred.

2. A wide range of deuterium desorption is formed on a temperature scale in the temperature range of 250-500 K.

3. It is planned to shift the peak to low temperatures.

The presence of a deuterium desorption region that is long in the temperature scale and the smearing of the desorption peak with a maximum temperature of 325 K indicates the presence of an amorphous phase in Ni–B composites, which is shown in Figure 5.

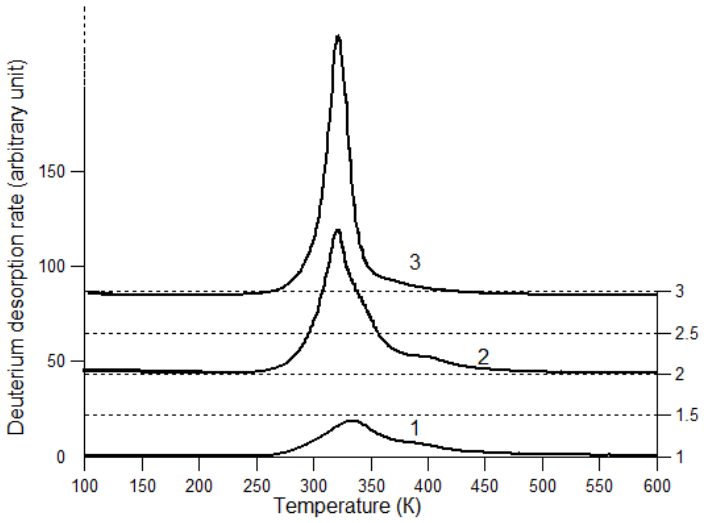

Figure 4. Thermal desorption spectra of deuterium implanted in nickel at a temperature of ~ 100 K, obtained for different doses of radiation: 1 – 2×10^{17}; 2 – 4×10^{17}; 3 – 1×10^{18} D/cm^2.

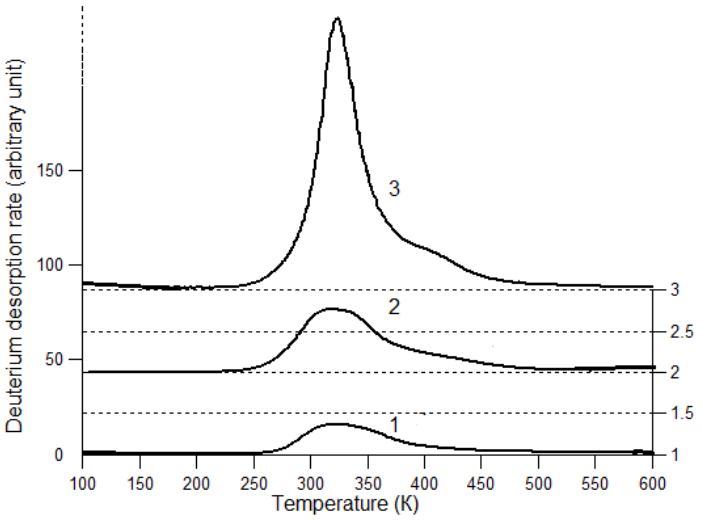

Figure 5. Thermal desorption spectra of deuterium implanted in a Ni-B composite (1 wt.% or 5 at.% B) at a temperature of ~ 100 K, obtained for different doses of radiation: 1 – 2×10^{17}; 2 – 4×10^{17}; 3 – 1×10^{18} D/cm^2.

For the nickel, the deuterium content corresponds to the following ratio: Ni: D = 1:1. For $Ni_{95}B_5$ composite, [Ni_{95}:B_5]: D = 1:1.25 correlation can be traced (Figures 4, 5, curve 3). Comparisons of the kinetics of desorption of deuterium from nickel and Ni-B composite indicates an increase in the concentration of hydrogen with the inclusion of boron in nickel and their further interdependence

[6, 7]. The potential of the interaction of a point defect with an impurity trap by a boron atom is determined by:

$$V = -\sigma_{rr}\delta\upsilon, \tag{1}$$

where σ_{rr} – is the radial component of the internal stress tensor in the vicinity of the first coordination sphere near the boron atom; $\delta\upsilon$ – is the variation of the crystal volume at the dislocation of the hydrogen atom.

For a boron atom $\sigma_{rr} > 0$ (tensile stress) and $\delta\upsilon > 0$ (hydrogen atom increases the volume of the crystal), the potential V takes a negative value. This indicates the attraction of a hydrogen atom with high diffusion mobility to a boron atom with the subsequent formation of a "boron-hydrogen" complex; it is discussed in more detail in the author's monograph [10].

The interaction potential of a hydrogen atom with an impurity trap by a boron atom was estimated by the following formula:

$$\sigma_{rr} \approx E_{Ni}\frac{r_{Ni} - r_B}{r_{Ni}}, \tag{2}$$

where E_{Ni} – Young's modulus of nickel is; r_{Ni} – is the atomic radius of nickel; r_B – is the atomic radius of boron. The potential of the interaction of a point defect with an impurity trap is $V = -0.67\times10^{-19}$ J (0.42 eV), which indicates a low value of the energy of the "boron-hydrogen" complex [10].

Therefore, the experimental result obtained by the authors verifies the principle of the transformation of susceptibility to hydrogen accumulation by metals depending on the number of defects and traps for hydrogen atoms in the structure [6, 7, 9, 10].

CONCLUSIONS

1. The chemical composition of Ni–B composites capable of accumulating hydrogen and retaining it due to structural, impurity traps in the metal structure has been established, and the modes of their synthesis have been compiled.

2. An increase in the concentration of the alloying component of boron in nickel increases the dispersion and leads to the alignment of the surface micro-profile and the formation of structures of the nano-scale range.

3. In the presence of boron, the hydrogen permeability of nickel is reduced, since in the vicinity of the impurity substitution of a small atomic radius - boron embedded in the Granulated Nickel Superalloy, tensile stresses occur and

hydrogen segregates around boron with greater synergism than with nickel. The potential of the interaction of a hydrogen atom with impurity trap by a boron atom $V = -0.67 \times 10^{-19}$ J (0.42 eV) is estimated, which indicates a low value of the energy of the boron-hydrogen complex.

4. The principle of transformation of susceptibility to hydrogen accumulation by metals was verified depending on the number of defects and traps for hydrogen atoms in the metal structure by correlating the hydrogen concentration in Ni – B composites from the time of "aging".

5. It has been proved that the structure of the thermal desorption spectrum of deuterium from nickel and nickel-boron samples previously implanted with various doses of deuterium ions at $T \sim 100$ K is a function of the implantation dose. As the dose of implanted deuterium increases for nickel, a distinct peak with a maximum temperature of 325 K is formed. For Ni – B composite, the thermal desorption spectrum has a diffuse peak with a maximum temperature of 325 K and a deuterium desorption region in the temperature range of 250–500 K.

6. The content of deuterium for nickel corresponds to the ratio Ni:D = 1:1, and for the composite of Ni-B, the content of deuterium for $Ni_{95}B_5$ corresponds to the ratio Ni_{95}:B_5:D = 1:1.25.

REFERENCES

1. Satyapal, S. 2015. "Fuel Cell Technologies Office in the Office of Energy Efficiency and Renewable Energy (EERE) at the Department of Energy DOE Hydrogen and Fuel Cells," *Program Annual Progress Report.*
2. Li, H.W., Y.G. Yan, S. Orimo, A. Zuttel, and C.M. Jensen. 2001. "Recent Progress in Metal Borohydrides for Hydrogen Storage," *Energies*, 4(1):185-214.
3. Zvyagintseva, A.V. 2008. "Interaction Peculiarities of Hydrogen and Ni-B Galvanic Alloys," *Carbon Nanomaterials in Clean Energy Hydrogen Systems*, Springer, pp. 437-442.
4. Fuka, Y. 2005. "The Metal-Hydrogen System," *Springer Series in Materials Science*, Berlin: Springer Verlag, 21:500 p.
5. Soloveichik, G.L. 2007. "Metal Borohydrides as Hydrogen Storage Materials," *Material Matters*, 2.2.:11.
6. Zvyagintseva, A.V. 2015. "The Ability of Materials Based on Nickel of the Nanoscale Range to the Accumulation of Hydrogen," *International Journal of Alternative Energy and Ecology (ISJAEE)*, Sarov: Publ. House "Scientific and Technical center "TATA", 21:150-155.
7. Zvyagintseva, A.V. 2017. "Hybrid Functional Materials that Form Metal Structures with Optimal Defectiveness for Storing Hydrogen in Hydride Form," *International Journal of Alternative Energy and Ecology (ISJAEE)*, Sarov: Publ. House "Scientific and Technical center "TATA", 16-18(228-230):89-103.
8. Ruzhitsky, V.V., Yu. A. Gribanov, V.F. Rybalka, S.M. Kazan, A.N. Morozov, and I.S. Martynov. 1989. "Multipurpose Experimental Setup "SKIF"," *Problems of Atomic Science and Technology. Series: Material Scientist*, 4(51):84.
9. Suzuki, K., H. Fujimori, and K. Hashimoto. 1987. *Amorphous Metals: Monograph*. Moscow: Metallurgiya, 328 p.
10. Vlasov, N.M., and A.V. Zvyagintseva. 2012. *Mathematical Modeling of the Hydrogen Permeability of Metals: Monograph.* Voronezh: VSTU, 248 p.

2018 International Theoretical and Practical Conference on Alternative and Smart Energy (TPCASE 2018)
ISBN: 978-1-60595-617-6

Microgrid Project: Research, Technologies and Training Courses

Anton Petrochenkov, Aleksandr Romodin,
Aleksandr Lyakhomskii and Thomas Frank

ABSTRACT

The main goal of the considered project is the concept development and creation of flexible and scalable smart University campus microgrid with a two-way data communication. In this case, the power system consists of two subsystems (heat supply subsystem and power supply subsystem). Also, a variant of the construction of the master's program of training specialists in energy management has been considered. The several scientific and educational trajectories are supported by the master's program. One of the key parts of the master's program is interuniversity collaboration due to workshops and joint research projects, both with Russian and foreign universities-partners.

INTRODUCTION

The main advantages of Smart Grid are the possibility of real-time data gathering and analysis so we can better forecasting and planning energy consumption [1].

Proceeding from different Smart Grid concepts reviews and analysis, one can define the following main areas covered today in the concept of Smart Grid [2-4]:

Anton Petrochenkov, Aleksandr Romodin, Perm National Research Polytechnic University, 29, Komsomolskiy Avenue, Perm, 614990, Russia
Aleksandr Lyakhomskii, National University of Science and Technology MISIS, 4, Leninskiy Avenue, 119049, Moscow, Russia
Thomas Frank, Envidatec GmbH, 2, Veritaskai, Hamburg, 21079, Germany

- Automation systems.
- Smart Metering and Home Energy Management.
- Communication systems for power facilities.
- Sensor and condition monitoring systems.
- Integration of small power sources and electricity storage devices.
- Integration of alternative and renewable energy sources.
- Data management systems.
- Microgrids.

The main goal of this project is concept development and creation of flexible and scalable smart campus microgrid with a two-way data communication. In this case, the power system consists of two subsystems (heat supply subsystem and power supply subsystem).

Increasing energy efficiency in this way is a complicated problem in terms of conceptual design and process engineering [5, 6].

RESEARCH WORK PACKAGE

The existing Perm National Research Polytechnic University (PNRPU) campus energy system can be described as a mini power system with a strong connection by electricity and gas, and the lack of connection by heat and water. It should be said that the existing energy system has only a heat generation source.

Figure 1 shows the general PNRPU campus plan, where we can see energy sources and consumers (academic buildings of PNRPU and Ural branch of Russian Academia of Sciences (UBRAS)).

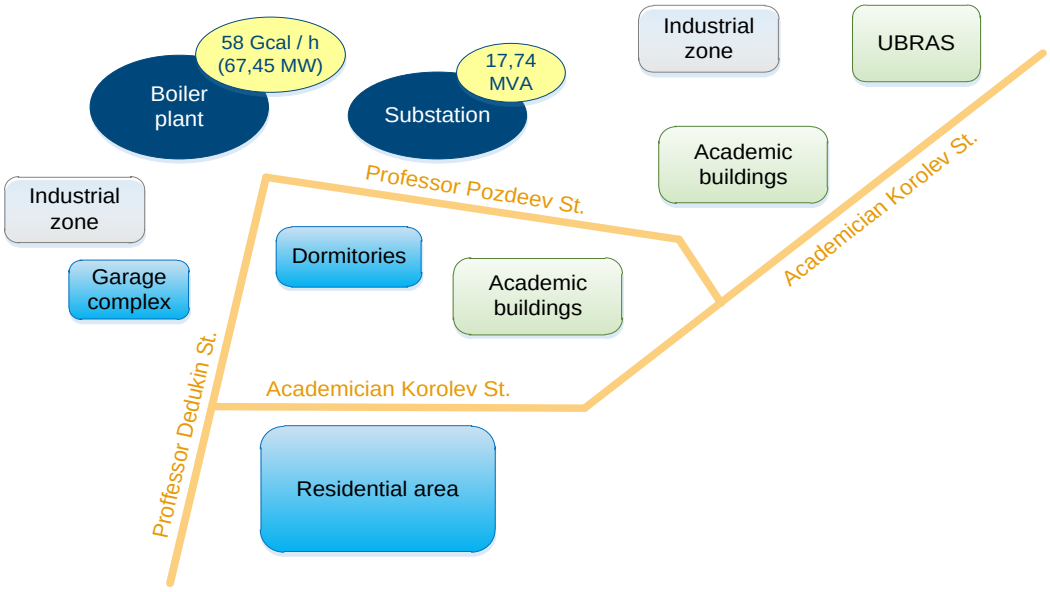

Figure 1. General PNRPU campus plan.

Electricity is produced by 110/10/6 kV substation and it is distributed to transformer substations by 6 and 10 kV. Transformer substations have from 250 to 1000 kVA transformers. The total connected load of all transformers is 17 740 kVA.

The heating is provided from the PNRPU boiler plant. The main consumers of the heat energy are the heating, ventilation, and hot water systems. The design capacity of the boiler plant is 58 Gcal/h (67.45 MW).

From the University side, one should start the creation of campus Smart Microgrid from the following steps:

- Development of the Smart Microgrid architecture.
- Creation of an automated smart system of accounting and control of the consumption of electricity and heat (Smart Metering).
- Light-emitting diode (LED) street and area lighting.
- Modernization of heating systems (modernization of heating main; boiler plant automation).
- Modernization of electric energy supply (h. e. 110/10/6 kV substation).
- Investigation of the possibility and efficiency of deployment of alternative energy sources (solar panels; gas turbines; heat pumps and etc.).

According to the given scheme, the basic task adds up to taking into account dataflow management, providing data system operation [7, 8].

AUTOMATED SMART SYSTEM OF ACCOUNTING AND CONTROL OF THE ENERGY CONSUMPTION

The existing campus electrical power system is equipped with the necessary number of accounting units, but it isn't automated. Some part of the installed meters has RS-485 interface, which allows the introduction of automation without the additional purchase of new meters [3, 4].

Commercial heat meters are set only on some outside organizations objects of campus.

At the project the following plan of action are proposed:

- Documentation request on the existing power supply system.
- Conducting energy audits.
- Creation of the Smart Microgrid vision.
- Selection of equipment based on analysis of energy audits data and technical documentation.

Also for heat supply subsystem ones should make such requirement as an automatic control of heat supply, which depends on various factors (inside and outside temperature, time of the day and etc.).

It is supposed to use the following solution: methods of genetic modeling [9, 10] and methods on the basis of the subjective estimate of risk factors [11].

EDUCATION WORK PACKAGE

The basis of cooperation between PNRPU and National University of Science and Technology "MISIS" is the joint participation in the development and implementation of a network form the master program "Conceptual design and engineering to improve energy efficiency" [12].

In the course of a regional industrial infrastructure reorganization and formation of essentially new lines of technology development, there was a necessity in preparation of new generation of experts and making of information-methodological support of innovative activity in power branch. The project is aimed at implementation into the universities-partners educational course for preparing of engineering skills, scientific brainpower and administrative bodies in power industry, network companies, and related sectors.

The Master program consists of three directions: engineering (support of devices and installations life cycle), innovative and social. Professional practice (4 months) is provided with industrial partner Envidatec GmbH.

CONCLUSION

At the moment the project is at its development phase. The system engineering is the work for the team not for a single specialist. The components which are realized within the student's master theses are the structural elements of the system and will be used for its assembly.

The project team has the successful experience of collaboration via developing the software and hardware of Smart Energy Monitoring and Analytic Systems based on SmardGrid and OpenJevis concept are presented.

DISCUSSIONS

The results of the research can be applied in different fields. E.g., knowing the amounts of energy consumption is of great importance for several reasons. First of all, for consumers of electrical energy knowledge about the electric load and the targeted is important for understanding their bills and better controlling their consumption [13]. For organizations, it is also useful to know periods of minimum and maximum of the consumption for planning the technological cycles, for planning budget costs.

Secondly analyzing the data of energy consumption is useful for in energy sales companies to predict probable future consumption and applying the costs for electrical units on the opt market of electrical energy [14].

Thirdly it is useful for power grid companies to regulate and determine the optimal loading of transformer substations [15].

ACKNOWLEDGMENT

Part of the research conducted was carried out with financial support from the Ministry of Education and Science of Russia within the framework of research projects carried out by the teams of research centers and research laboratories (project 8.4157.2017/Research Part).

Research is also supported by educational and research grant 573879-EPP-1-2016-1-FR-EPPKA2-CBHE-JP by European program Erasmus+ (Project INSPIRE).

REFERENCES

1. Armstrong, J.S. 2001. *Principles of Forecasting: A Handbook for Researchers and Practitioners*. Springer.
2. *IEC 61850-2. "*Communication Networks and Systems in Substations - Part 2: Glossary"
3. *IEC 61970-301. "*Energy Management System Application Program Interface (EMS-API) - Part 301: Common Information Model (CIM) Base"
4. *IEC/TR 61968-11. "*Application Integration at Electric Utilities - System interfaces for Distribution Management - Part 11: Common Information Model (CIM) Extensions for Distribution".
5. Lyakhomsky, A.V., A.B. Petrochenkov, and E.N. Perfil'eva. 2015. "Conceptual Design and Engineering Strategies to Increase Energy Efficiency at Enterprises," *Russian Electrical Engineering*, 86(6):305-308.
6. Guenter, B., N. Jain, and C. Williams. 2011. "Managing Cost, Performance, and Reliability Tradeoffs for Energy-Aware Server Provisioning", *Microsoft Research*, Redmond WA.
7. Petrochenkov, A.B. 2014. "An Energy-Information Model of Industrial Electrotechnical Complexes", *Russian Electrical Engineering*, 85(11):692–696.
8. Bagajewicz, M. 2002. "A Review of Techniques for Instrumentation Design and Upgrade in Process Plants," *Canadian Journal of Chemical Engineering*, 80(1):3-16.
9. Aytug, H., M. Khouja, and F.E. Vergara. 2003. "Use of Genetic Algorithms to Solve Production and Operations Management Problems: A Review," *International Journal of Production Research*, 47(17):3955-4009.
10. Petrochenkov, A. 2015. "Respecting Life Cycle Management of Electrotechnical Equipment Based on Genetic Modeling Methods", *Applied Mechanics and Materials*, 792:113-121.
11. Reinertsen, R. 1996. "Residual Life of Technical Systems; Diagnosis, Prediction and Life Extension," *Reliability Engineering and System Safety*, 54(1):23-34.
12. Lyakhomskii, A., E. Perfilieva, A. Petrochenkov, and S. Bochkarev. 2015. "Conceptual Design and Engineering Strategies to Increase Energy Efficiency at Enterprises: Research, Technologies and Personnel", in *2015 IV Forum Strategic Partnership of Universities and Enterprises of Hi-Tech Branches (Science. Education. Innovations)*, pp.44-47
13. Luzyanin, I.S., A.B. Petrochenkov, and B. Krause. 2016. "Problems of Tiny Changes Analysis in Complex Time Series Using Dynamic Time Warping Algorithm", in *2016 XIX IEEE International Conference on Soft Computing and Measurements (SCM)*, pp.419-422.
14. Kazantsev, V.P., A.B. Petrochenkov, A.V. Romodin, and N.I. Khoroshev. 2011. "Some Aspects of the Technology of Use of Electrical Objects on the Basis of Methods of Short Term Forecasting of Technical Condition," *Russian Electrical Engineering*, 82(11):600-606.
15. Petrochenkov, A.B., S.V. Bochkarev, A.V. Romodin, and D.K. Eltyshev. 2011. "The Planning Operation Process of Electrotechnical Equipment Using the Markov Process," *Russian Electrical Engineering*, 82(11):592-595.

2018 International Theoretical and Practical Conference on Alternative and Smart Energy (TPCASE 2018)
ISBN: 978-1-60595-617-6

Power Lines with Incomplete Phases

Evdokiia Maleeva, Nadezhda Buryanina and Yury Korolyuk

ABSTRACT

This paper describes new transmission lines for electrical power network of 6-35 kV. Four-phase overhead transmission lines have special advantages because of the good symmetry and the simple structure of the lines and poles. Under the same condition of parameters, four-phase transmission lines can increase the transmission capacity and reliability compared with three-phase lines.

POWER LINES WITH INCOMPLETE PHASES

Today, the issue of improving the quality of electricity is becoming a priority aim for not only power supply organizations, but also leading scientists in this field. Reducing power losses, improving the reliability of power supply, the use of new technology, are placed at the head of the tasks of energy. The solution to these problems can serve the proposed line.

A four-phase transmission line is obtained by converting from two three-phase lines (Figure 1).

M.K. Ammosov North-Eastern Federal University, 58 Belinsky Street, Yakutsk, 677027, Republic of Sakha (Yakutia), Russia

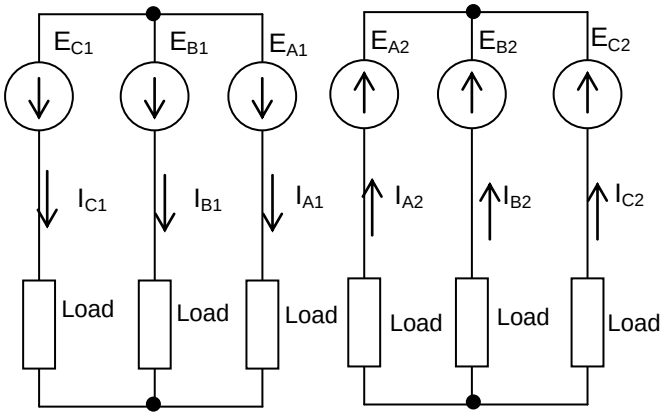

Figure 1. Two three-phase systems.

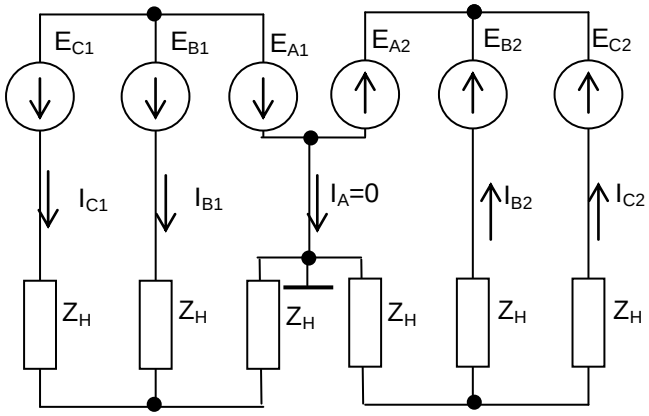

Figure 2. Three-phase system with grounded phase A.

Two three-phase systems have equal EMF modulus and equal load resistance. The EMF of one system is opposite in the direction of the EMF of the second system. Accordingly, the opposite currents:

$$\begin{aligned} I_{A1} &= -I_{A2}; \\ I_{B1} &= -I_{B2}; \\ I_{C1} &= -I_{C2}. \end{aligned} \qquad (1)$$

Currents and power flows in the circuit will not change if to insert a resistance between grounded points the EMF of phase A and load phase A (Figure 2). Then, exclude this branch (Figure 3).

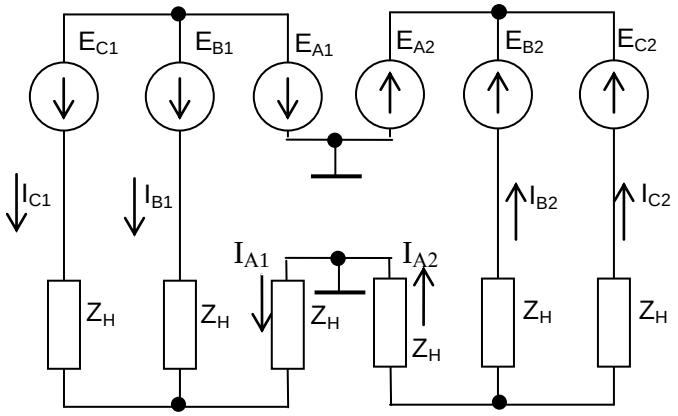

Figure 3. Three-phase system with excluded branch.

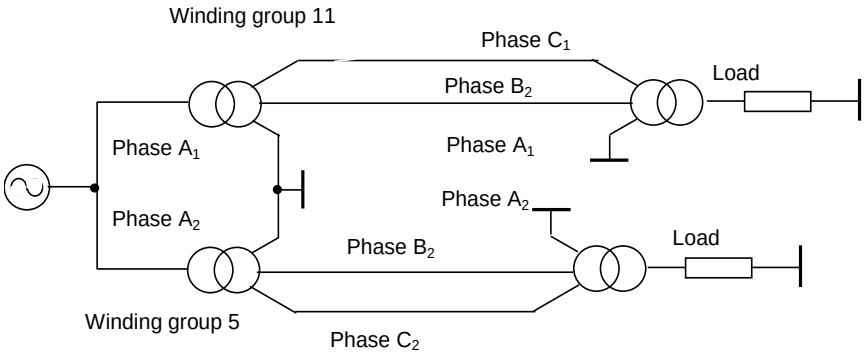

Figure 4. Four-phase power transmission scheme.

In the resulting system, the currents in the load resistances and in the EMF are symmetrical, and the line to ground voltage is equal line-to-line voltage. Therefore, the application area of the four-phase line is an Isolated neutral system (6 - 35 kV). These statements have been proven in the study of the mathematical model in MatLab.

Unlike the systems based on Scott's scheme [1-4], it does not require the development of new equipment [5]. The structure of transmission line is shown in Figure 4.

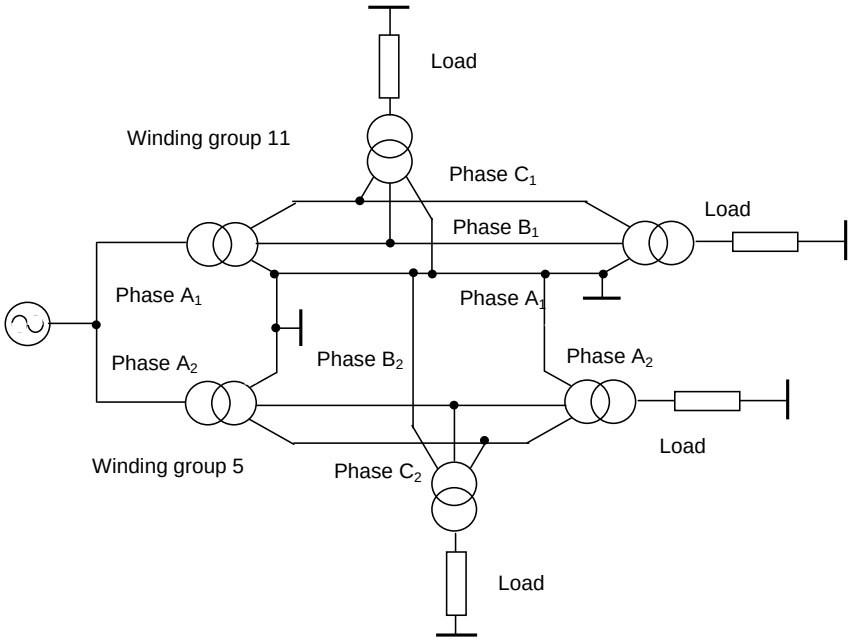

Figure 5. Scheme of a four-phase five-wire transmission line.

The voltages of similar phases of the different circuit have opposite signs. With the same loads of both circuits, there are no currents in the ground. Accordingly, there is no power loss in the earthed phases. Such a scheme can be applied in areas with the low resistance of the earthed phase [6]. In areas with permafrost in winter, the resistance of the earthed phase can have an active component of tens of Ohms. And the currents in the wires of each line will be phase opposition. That is, the coefficient of asymmetry of the currents will be equal to one. To eliminate this, it is proposed to add the fifth wire to the four-phase line, grounding it, and connecting to it the grounding windings of all load transformers [7].

CONCLUSION

The use of four-phase power lines is rational due to lower power losses in them compared to three-phase lines. The injection of an additional wire increases the reliability of the four-phase line to the reliability of the double-circuit three-phase line. By reducing the number of linear wires in the proposed electrical system, compared with a double-circuit three-phase line, the loss of electrical energy and voltage is reduced, as well as the cost associated with lower costs for the construction of the line.

ACKNOWLEDGENENTS

The research was carried out with the financial support of RFFI and constituent entity of the Russian Federation-the Republic of Sakha (Yakutia) #18-48-140 010.

REFERENCES

1. Srinivasa, R.R., K. Ravindra, and K. Satish. 2012. “Power Loss Minimization in Distribution System Using Network Reconfiguration in the Presence of Distributed Generation,” *IEEE Transactions on Power Systems*, 28(1):317-325.
2. Giovanni, M., and Q. Stefano. 2010. “Four-Phase AC Connections: An Alternative Possibility for the Expansion of Transmission Grids,” *IEEE Transactions on Power Delivery*, 25(2):1010-1018.
3. Liu, G.Y., and Y.H. Yang. 2002. “Study of Four-Phase Power Transmission Systems", *IEE Proceedings - Generation, Transmission and Distribution*, 149(4):397-401.
4. Della, T., S. Leva, and A.P. Morando. 2008. “Symmetrical Components and Space-Vector Transformations for Four-Phase Networks,” *Power Delivery IEEE Transactions*, 23:2191-2200.
5. Fillshtinsky, A.A. 1952. “Four-Wire Power Transmission as a Means of Increasing the Efficiency and Reliability of High-Voltage Networks,” *Electricity*, 1:17-22.
6. Buryanina, N.S., E.V. Buryanina, Yu.F. Korolyuk, V.L. Olesova, and L.A. Olesov. 2004. “Electrical System,” patent of the Russian Federation #2256273, IPC 7 H 02 J 3/00.
7. Buryanina, N.S., Yu.F. Korolyuk, and E.V. Lesnykh. 2006. “Four-Phase Five-Wire Power Line,” patent of the Russian Federation #2558697, IPC H2J 3/00.

2018 International Theoretical and Practical Conference on Alternative and Smart Energy (TPCASE 2018)
ISBN: 978-1-60595-617-6

Kinetics of Hydrogen Desorption From Ni—In Composites, Synthesized by Electrochemical Method

Alla Zvyagintseva

ABSTRACT

The results of the study of the kinetics of the thermal desorption spectrum of deuterium accumulated with $Ni_{64}In_{36}$-Dx composites synthesized by the method of electrochemistry are presented. The limits of desorption temperatures for ion-implanted deuterium were determined depending on the implanted dose. The measured content of deuterium alloy is 4 at. D/at. Met (~8.7 wt. % D; ~4.6 wt. % hydrogen). The formation of the deuterium thermal desorption spectrum depends on the implantation dose. An increase in the content of implanted deuterium contributes to the formation of a solid solution of hydrogen isotope in the electrochemical composite $Ni_{64}In_{36}$ with a destruction temperature in vacuum of ~520 K and nickel hydride with hydrogen with a decomposition temperature of ~330 K. The calculation of the activation energy of thermal desorption is produced for a hydrogen peak with a temperature of maximum 500 K. Arrhenius polyterms were obtained for two values of the reaction order index: $\gamma = 1$ and $\gamma = 2$. Arrhenius polyterms demonstrate the second order of reaction and the quadratic dependence of the desorption rate on the number of implant particles. The activation energy for a peak with a maximum temperature of 500 K is 2.9 eV, which indicates low energy extraction of the hydrogen isotope.

INTRODUCTION

Possessing enormous prospects, hydrogen energy is one of the important directions in the modern development of energy throughout the world. An

Voronezh State Technical University, 14, Moskovsky Avenue, Voronezh 394026, Russia

important component of the development progress in this area is the development of highly efficient and safe hydrogen storage systems.

The analysis of the methods studied shows that hydrogen storage in solid-state materials is superior to other methods, such as, for example, balloon or cryostat. The storage of hydrogen in the solid matrix is superior, in particular, in optimal characteristics of bulk and gravimetric density, in safe storage without complex cryostat systems, and also in hydrogen extraction under acceptable thermodynamic conditions, without high temperatures and pressures.

Works by foreign authors demonstrate various ways of storing hydrogen: in the form of combination hydrides [1, 2], metal hydrides [3], organometallic composites [4], carbon nanomaterials [5], however, not all of the proposed materials fully provide harmony production and consumption [6].

The strategy of the research is to form a material in which, for a specific technical application, accumulation processes with high density and hydrogen extraction of the required amount with minimal costs were fairly easily carried out.

To meet these requirements, it is most preferable to use nickel-based metals and alloys.

The purpose of this publication is to study the possibility of using nickel and materials based on it as energy storage devices.

The work clearly shows the fundamental possibility of changing the hydrogen permeability of the object of study due to the creation in the metal structure of various kinds of hydrogen traps (structural, impurity) in order to retain hydrogen in the metal structure. As an object of study, an electrochemical system was chosen - Ni-In alloy.

In the previously published work of the author, the properties of this alloy were already investigated and it was noted that when nickel was doped with indium [7] with indium content up to 10 % Ni-In alloy hydrogenation decreased.

However, new studies conducted by the author have shown that in materials synthesized by the electrochemical method, intermetallic metal compounds can serve as structural traps for hydrogen atoms. Therefore, this particular system, Ni-In, which is not prone to hydrogen accumulation and the formation of chemical compounds of hydrogen with metal in the form of hydrides, was the object of research in this article.

Physically, this can be interpreted as follows.

When the concentration of indium is 9 % wt. in solid solutions with nickel, the alloy does not constitute a trap for hydrogen atoms. The indium atom radius is larger than the nickel radius (rNi = 0.138 nm; rIn = 0.184 nm), and during the synthesis of the Ni-In composite, in the vicinity of indium, compressive stresses arise that displace hydrogen. Therefore, electrochemically synthesized Ni-In composites with an indium content of less than 9 % wt. are unable to occlude hydrogen. With increasing indium concentration of more than 10 % wt. intermetallic phases are formed and can act as structural traps for hydrogen

atoms, provided that the intermetallic phase is not coherent with the Ni matrix through a network of dislocations. Consequently, the accumulating properties of the composites will improve. Information on the possibility of formation of hydride phases in Ni-In composites was not found in publications, with the exception of the author's works [8–10].

EXPERIMENTAL TECHNIQUE

Ni-In composites were formed by electrochemical deposition on a copper substrate (0.05 mm thick) from the electrolyte composition: 140 g/l $NiSO_4 \cdot 7H_2O$; 20 g/l $Na_2SO_4 \cdot 10H_2O$; 1÷12 g/l $In_2(SO_4)_3$. Some components of the electrolyte cannot be disclosed [8]. The electrolysis was performed with a platinum anode and a copper cathode. The content of components in the composite Ni-In was measured by x-ray fluorescence method. X-ray diffraction studies were performed on HZG-4 diffractometer in CuKα radiation (β-filter).

To record the kinetics spectrum of deuterium desorption from Ni–In composites depending on the concentration of components and the dose of implanted deuterium, the method of thermal desorption mass spectrometry (TDS) was used. The introduction of deuterium and the recording of the spectra of thermal desorption were carried out on the SKIF facility, described in more detail in [8, 9]. In order to reduce the effect of background hydrogen contained in the composites and in the target chamber, the accuracy of the measurements was used as implant deuterium.

The implantation of deuterium ions into composites was carried out by bombardment with 12 keV ions and doses in the range of 3×10^{17}-3×10^{18} atD/cm^2. The amount of desorbed deuterium extracted from the composite when heated was calculated graphically from the area of the figure lying under the gas emission curve, according to the method described in [9, 10].

EXPERIMENTAL SECTION

Diffraction patterns of Ni-In composites with different concentrations of the components are shown in Figure 1. On diffractograms, one can observe intense narrow lines of the substrate (copper FCC structure), the line (220) is more intense than the other lines.

For composite no. 1 composition of 24 wt. % In, only the substrate lines (Cu) are visible on the diffractogram: a very intense line (220) and weak lines (111), (200) and (311) (Figures 1a and 1e). The increase in the concentration of indium in composites for samples no. 2 of 38 wt. % In and no. 3 composition of 45.6 wt. % In is accompanied by the appearance and increase in the intensity of new lines in diffraction patterns (Figures 1b and 1c).

The appearance of new lines can be explained by the formation of intermetallic compounds Ni_3In and In_2Ni, the possible formation of which is indicated by the phase diagram of the Ni–In system [11]. A further increase in the concentration of indium in sample no. 4 to 61.3 wt. % In (Figure 1d) indicates the formation of additional structural formations - intermetallic compounds: Ni_3In, In_2Ni, InNi, the existence of which was found on the phase diagram of the Ni-In system [11]. The presence of free indium is recorded on a diffraction pattern from pure indium (Figure 1g).

Experimental studies made it possible to select both the electrolyte composition and the electrolysis modes that synthesize the structure of the Ni-In composite with indium and nickel intermetallics. By the diffractometric method, it was found that with increasing indium concentration in the Ni–In composite phases of intermetallic compounds of the composition $InNi_2$, $InNi_3$, In_3Ni_2, η-$In_{27}Ni_{10}$are formed.

For the first time, the results on thermal desorption of deuterium from Ni–In electrochemical composites were obtained and published in [8–10]. In this paper, the results on the registration of thermally desorbed deuterium from the Ni-In composite were summarized and verified.

First, the amount of hydrogen embedded in the composites in the process of their production by electrolysis was recorded and taken into account, Figure 2. Thermal desorption of hydrogen for sample no. 2 of composition 38 wt. % In is observed at temperatures of 550 and 850 K. The amount of occluded hydrogen in composites of composition 38 % wt. In and 45.6 % wt. In corresponds to 2 at. H/at. Meth, 4 at.H/at.Met respectively. On the curves in Figure 2, two hydrogen peaks are observed at 550 K and 850 K. It is possible that hydrogen desorption at temperatures above 650 K is caused by both the desorption of hydrogen and hydrogen-containing gases from the measurement chamber designs during sample heating and the annealing of hydrogen traps at temperatures above 650 K. For the first time, the possibility of additional doping of hydrogen into an electrochemical system was demonstrated in [8–10]. The possibility of doping hydrogen into composites of the selected atomic composition $Ni_{70}In_{30}$ with an indium content of 38 wt. % and nickel 62 wt. %; composition $Ni_{64}In_{36}$ with an indium content of 45.6 mas. % and nickel 54.4 wt. %.

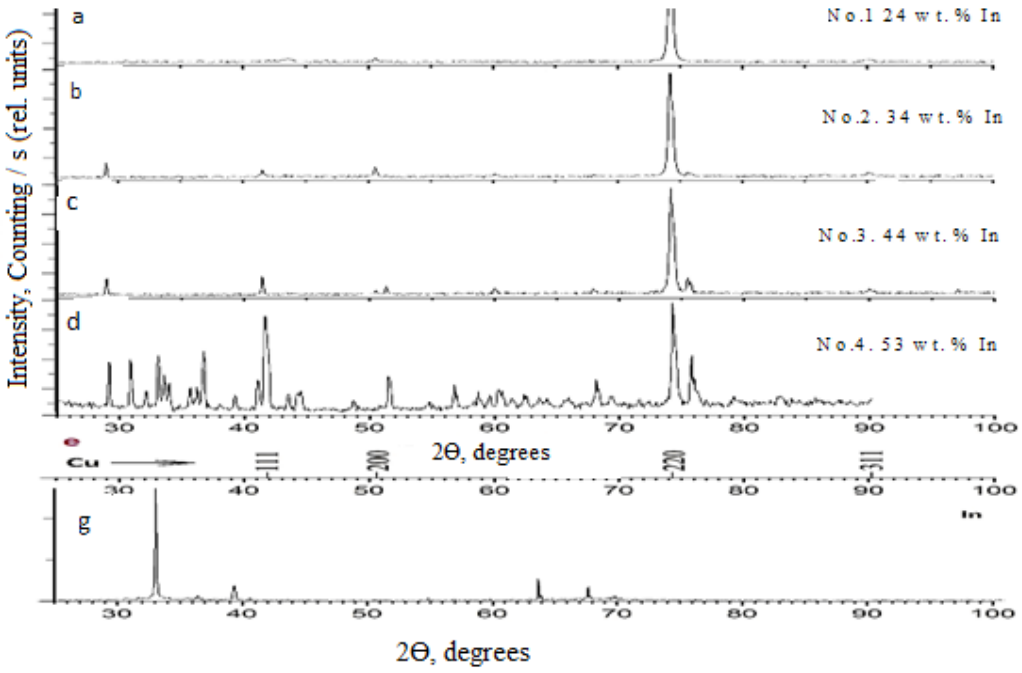

Figure 1. Diffraction patterns of Ni-In composites.

Figure 3 shows the characteristic thermal desorption spectrum of deuterium implanted in electrochemical $Ni_{64}In_{36}$ composite samples depending on the implanted deuterium dose and for one sample phase composition. The deuterium DTP spectra are a function of the implantation dose. The deuterium content of the composite with the $Ni_{64}In_{36}$ phase composition is 4 at. D/at. Met., which corresponds to (~8.7 wt. % D; ~4.6 wt. % hydrogen) at low doses of implanted deuterium, a single peak with a maximum temperature of ~ 550 K is present in the spectrum (Figure 3, curve 1). Increasing the dose leads to the appearance of a low-temperature peak with a maximum temperature of ~ 450 K (Figure 3, curve 2). With a further increase in the dose of implanted deuterium, the maximum temperature of the peak of gas evolution gradually shifts to lower temperatures (Figure 3, curves 3-5).

Using an example of a sample of composition 24 wt.% In and 76 wt.% Ni implanted with deuterium ions with a dose of 3×10^{17} D/cm^2, the activation energy of thermal desorption was calculated for a peak with a maximum temperature of 500 K (Figure 4a, curve 1) using the known equation desorption kinetics [12]:

$$dn_i/dt = -K_i n_i^{\gamma}(t) e^{-Ei/kT}, \quad (1)$$

where dn_i/dt - is the desorption rate, which at each moment of time corresponds to the ordinate of the envelope of the i-th peak of thermal desorption; $n_i(t)$ - the number of particles remaining in the sample to a given desorption point; K_i - desorption rate constant for the i-th peak; γ - reaction order; E_i - activation energy of desorption; k - is the Boltzmann constant; T - is the current temperature value.

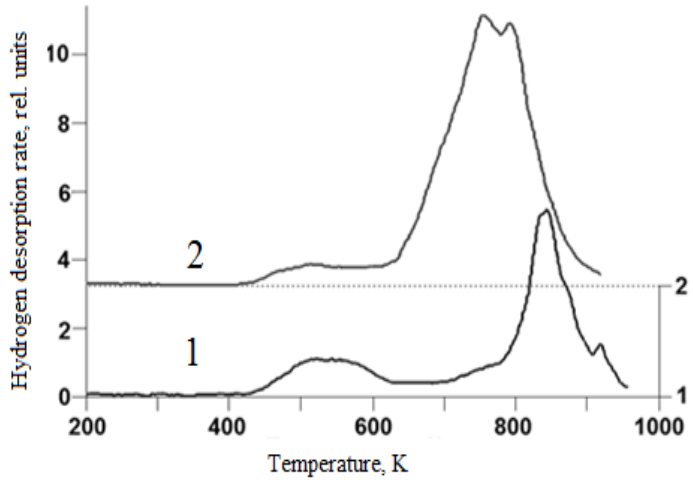

Figure 2. Spectra of thermal desorption of hydrogen released from Ni–In electrochemical composites: 1 - composition of 38 wt. % In; 2 - composition of 45.6 wt. % In.

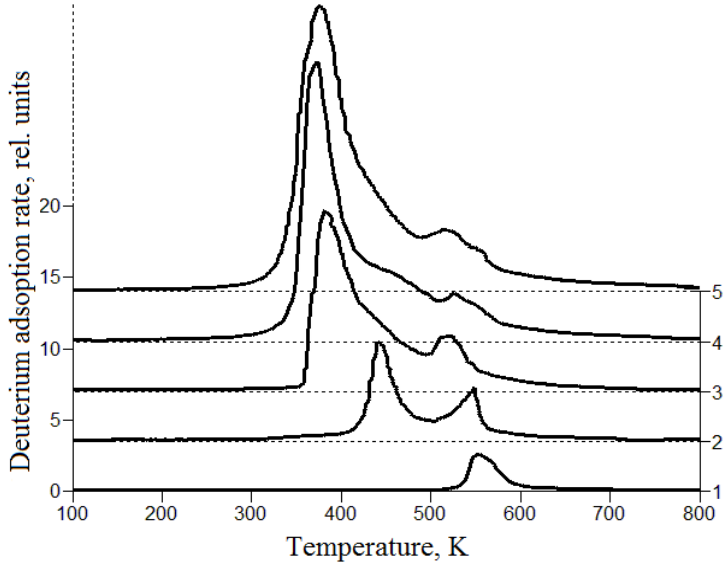

Figure 3. The thermal desorption spectra of deuterium implanted in electrochemical $Ni_{64}In_{36}$ composite samples: 1–3×10^{17} D/cm^2; 2 – 7.5×10^{17} D/ cm^2; 3–1.3×10^{18} D/cm^2; 4 –2×10^{18}.

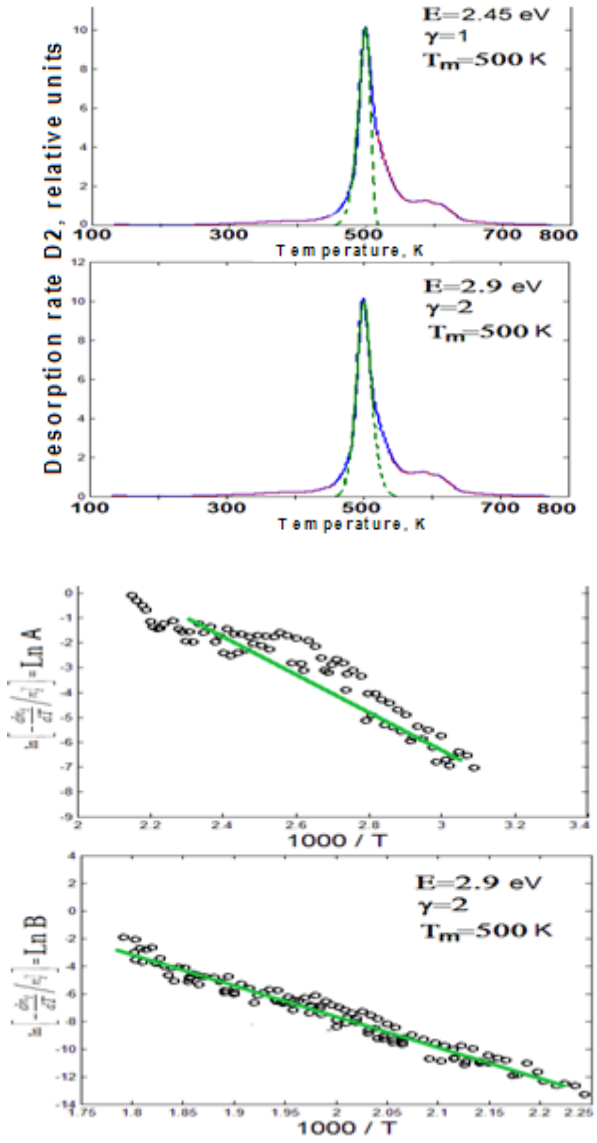

Figure 4. Arrhenius polyterms for the peak of the deuterium thermal desorption spectrum from sample composition of 24 wt.% In and, respectively, 76 wt.% Ni, implanted with deuterium ions with a dose of 3×10^{17} D/cm^2, calculated for two values of the reaction order $\gamma = 1$ and $\gamma = 2$.

The transformation of equation (1), taking into account $T = T_0 + \alpha t$ (where α is the heating rate of the sample) and the subsequent logarithm, leads to the relation:

$$\ln\left[-\frac{dn_i}{dT}\Big/ n_i^{\gamma}\right] = -\frac{E_i}{k}\frac{1}{T} + \ln K_i/\alpha. \qquad (2)$$

Substituting the values from the experimentally measured spectrum of thermal desorption, Arrhenius polyterms were constructed for two values of the reaction order index: $\gamma = 1$ and $\gamma = 2$.

Summarizing the above, we can conclude that the accumulating properties of nickel in the presence of indium intermetallics increase. In the vicinity of the indium intermetallide, tensile stresses can occur and hydrogen is segregated at the boundary of these compounds, which is confirmed by the thermal desorption data. Indium intermetallic compounds with nickel are traps for hydrogen atoms in the Ni-In composite. Mathematical modeling of the hydrogen permeability of metals in the presence of traps of different types was carried out by the author in the monograph [12].

CONCLUSION

During the work, the following main results were achieved:

1. The spectroscopies spectra of deuterium from electrochemical composites $Ni_{64}In_{36}$-Dx were studied by mass spectroscopy, from which the temperature ranges of, desorption of ion-implanted deuterium were determined depending on the implantation dose. The maximum achievable deuterium concentration of 4 at. D/at. Met, which corresponds to ~4.6 wt. % hydrogen.

2. The formation of the deuterium thermal desorption spectrum depends on the implantation dose. An increase in the content of implanted deuterium contributes to the formation of a solid solution of hydrogen isotope in the electrochemical composite $Ni_{64}In_{36}$ with a destruction temperature in the vacuum of ~ 520 K and nickel hydride with hydrogen with a decomposition temperature of ~ 330 K.

3. The activation energy of thermal desorption was calculated for a hydrogen peak with a maximum temperature of 500 K. The Arrhenius polyterms were obtained for two values of the reaction order index: γ =1 and γ = 2. The data of the Arrhenius polymer indicate the second order of reaction and the quadratic dependence of the desorption rate on the number of particles deuterium. The value of the activation energy for a peak with a maximum temperature of 500 K is 2.9 eV, which indicates low energy extraction of the hydrogen isotope.

REFERENCES

1. Orimo, S., Y. Nakamura, J.R. Eliseo, A. Züttela, and C.M. Jensen. 2007. "Complex Hydrides for Hydrogen Storage," *Chem Rev.*, 107(10):4111-32.

2. Jain, I.P., P. Jain, and A. Jain. 2010. “Novel Hydrogen Storage Materials: A Review of Lightweight Complex Hydrides,” *J Alloys Compd*., 503(2):303-39.
3. Graetz, J. 2009. “New Approaches to Hydrogen Storage,” *ChemSoc Rev.*, 38:73-82.
4. El-Kaderi, H.M., J.R. Hunt, J.L. Mendoza-Cortes, A.P. Cote, R.E. Taylor, M. O'Keeffe, et al. 2007. “Designed Synthesis of 3D Covalent Organic Frameworks,” *Science*, 316:268-72.
5. Berseth, P.A., A.G. Harter, R. Zidan, A. Blomquist, C.M. Araujo, R.H. Scheicher, et al. 2009. “Carbon Nanomaterials as Catalysts for Hydrogen Uptake and Release in $NaAlH_4$,” *Nano Lett.*, 9(4):1501-5.
6. Felderhoff, M., C. Weidenthaler, R. von Helmolt, and U. Eberle. 2007. “Hydrogen Storage: the Remaining Scientific and Technological Challenges,” *PhysChechenPhys.*, 9(21):2643-53.
7. Zvyagintseva, A.V. 2016. “Information about the Results of Research Work with the Report #216032140036.” Available at: https://esu.citis.ru/ikrbs/2T9zG00Kj3Yt15JGkc2cLb00.
8. Zvyagintseva, A.V., and A.O. Artemeva. 2017. “Modern hydrogen storage based on hybrid functional materials,” *The Bulletin of VSTU*, 13(5):133-138.
9. Zvyagintseva, A.V. 2017. “Hybrid Functional Materials that Form Metal Structures with Optimal Defectiveness for Storing Hydrogen in Hydride Form,” *International Journal of Alternative Energy and Ecology*, 16-18(228-230):89-103.
10. Ed. Lyakishev, N.P. 2001. *State Diagrams of Double Metallic Systems. Handbook.* Moscow: Mashinostroenie, 872 p.
11. Vlasov, N.M., and A.V. 2012. *Mathematical Modeling of Metal Hydrogen Permeability. Monograph.* Voronezh: VSTU Publ., 247 p.

2018 International Theoretical and Practical Conference on Alternative and Smart Energy (TPCASE 2018)
ISBN: 978-1-60595-617-6

Energy Savings in Buildings: A Global Approach

Sara Abd Alla, Vincenzo Bianco, Federico Scarpa
and Luca A. Tagliafico

ABSTRACT

The present paper reports a set of considerations and analysis of energy efficiency in buildings by approaching the problem from a full life-cycle perspective. In particular, the impact of the embodied energy, i.e. the energy necessary to produce a specific material, is analyzed, as it has a pivotal role in assessing the real energy saving obtained after a retrofitting.

Considerations related to the country of production of insulating materials are also provided, as the energy mix of a specific location has an impact on the embodied energy of the materials.

Finally, some numerical examples are provided in three Italian cities, namely Milan, Rome and Naples. A typical Italian building is considered in all of these three locations and a refurbishing intervention is hypothesized, namely the installation of an external insulation layer on the walls. Then, the global heating energy saving is assessed, i.e. also the embodied energy is considered in the calculation, to evaluate the energy effectiveness of the intervention.

It is found that in warmer locations, i.e. Naples and Rome, the installation of an insulation layer has a limited, or even negative impact, on the energy saving if embodied energy is considered. This means that the energy necessary to produce the insulating material is higher than the energy saved during its operating life.

INTRODUCTION

Buildings sector is responsible for 40% of carbon emissions worldwide [1], therefore it is mandatory to implement appropriate actions to reduce the number of emissions. On the basis of this, there are many initiatives which promote the energy

University of Genoa, 15/A, Via All'Opera Pia, Genoa, 16145, Italy

retrofitting of existing buildings and the adoption of the most modern approaches for the new ones [2].

Usually, when performing energy analysis on the effect of the installation of insulating panels on the envelope of buildings, only the operating energy, namely the one utilized to heat the internal environment, is taken into account [3]. Therefore, the energy saving is represented by the difference between energy used in the case without insulation and that used in the case with insulation.

Actually, this approach tends to overestimate the energy saving involved in the process, because the energy balance is based only on a partial portion of the lifecycle of the insulating material. If the perspective is enlarged the situation can radically change [4].

In particular, if a life cycle perspective is considered, then it is necessary to consider all the energy involved into all the phases of the life of the insulating material, namely extraction of basic substances, production process, logistics chain, installation, maintenance, removal, recycling and disposal treatment [5]. All these phases imply the utilization of energy, which must be accounted in the total balance, in order to assess the real energy saving of the insulation installation (or implementation of other energy efficiency measures). The energy associated with all the life-cycle of the insulating materials is called *embodied energy*, since it represents all the energy stored in the material, in other words, it can be seen as the *energy cost* of a specific material, therefore it is to be accounted in the energy balance.

To perform a full life-cycle analysis of insulating interventions, both embodied and operating energy should be taken into account and, according to the operating life of a specific material, it is possible to determine the global energy saving (or waste) of energy associated with a specific intervention.

Different studies on the impact of embodied energy are available in the literature. Koezjakov et al. [6] analyzed the impact of the embodied energy contribution in Dutch houses and determined that the impact of the embodied energy is 10%-12% in standard houses and 36%-46% in energy-efficient buildings. Furthermore, Rossellò-Batle et al. [7] performed different analysis in a Mediterranean climate to evaluate the impact of embodied energy on the feasibility of energy retrofitting of existing buildings. Similarly, Cellura et al. [8] developed a case study for Italy and detected that, if embodied energy is considered, the primary energy demand is nearly doubled.

The above mentioned literature highlights the relevant impact that the inclusion of embodied energy can have on buildings energy analysis, therefore its contribution must be considered if total energy savings are to be estimated.

On the basis of these considerations, the present paper aims at analyzing a set of typical Italian archetypes located in different cities, in order to evaluate the energy performances of standard energy retrofitting measures from the life-cycle perspective, therefore the embodied energy is estimated and taken into account.

In particular, the typical building blocks built in the period 1961-1975 are considered for the analysis, because they did not include any wall insulation, which was introduced by the Italian building code only starting from 1977. This class of buildings is a good candidate for energy retrofitting; therefore it is necessary to estimate the effective energy-saving potential.

For this purpose, an energy simulation model is set up and validated in order to perform all the energy calculations. The model is based on dynamic simulations with an hourly based resolution and historical average meteorological data are considered. The considered model allows a detailed representation of energy consumption in buildings and it is considered appropriate for the proposed analysis.

It is supposed that the present paper stimulates the debate on the issue of energy efficiency in buildings and it can serve to promote the utilization of more accurate energy savings estimation methodologies.

BUILDING MODELLING

A model of a building block built in the period 1961-1975 is considered. It consists of seven blocks and a basement. The building is divided into two thermal zones, a heated one, i.e. the inside of the apartments, and a cold one, i.e. the stairs.

The model is generated by using SketchUp Make and energy requirements were calculated through the Openstudio 2.4.0 – EnergyPlus program and then post-processed with IDF-editor 8.9.0.

The characteristics of the buildings were taken from the Tabula project [9] and comparison with the provided energy consumption data is performed by showing a high degree of correspondence. Once assessed the quality of the simulation results, different insulation typologies are considered in order to retrofit the building. In particular, three different types of insulation are taken into account, namely polyurethane foam, rock wool and resin-bonded fiberboard. The performance of a layer of 10 cm of the insulator is analyzed.

All interventions were simulated in EnergyPlus for the cities of Milan, Rome and Naples and the corresponding operational energy of the apartment block was compared with the reference operational energy based on the present envelope and system conditions.

The results of the dynamic simulations showed the real efficiency of the insulation interventions depending on the climate zones of the three cities. Polyurethane foam insulation leads to a significant site energy saving during the year, between 40% and 50%; the rock wool and resin-bonded fiberboard reached 40%. Also, the roof insulation was simulated but results showed less interesting savings as this intervention decreased the operational energy demand of only 2%.

Once estimated the operating energy through the simulation, the embodied energy is evaluated on the basis of cradle-to-gate values, which were taken from the Inventory of Carbon and Energy [10].

It has to be remarked that the embodied energy of the building materials has not been considered as this paper wants to propose an approach focused on the choice of the efficiency measures based on their embodied energy. The comparison between the embodied energy of the retrofit solutions and the corresponding energy savings in the use phase was finally carried out.

On the basis of the estimated parameters, it is possible to determine the energy pay-back of the energy efficiency interventions. The energy pay-back is given by the necessary time to recover the embodied energy of the energy saving interventions with the energy savings from operating energy.

It is intuitive that the higher is the operating energy saving and the shorter will be the energy payback period. Therefore, it can be said that if the savings in operating energy are limited, it could result to be not convenient to install an insulation layer on the buildings' walls. This conclusion can be reached only if the embodied energy is considered in the calculation.

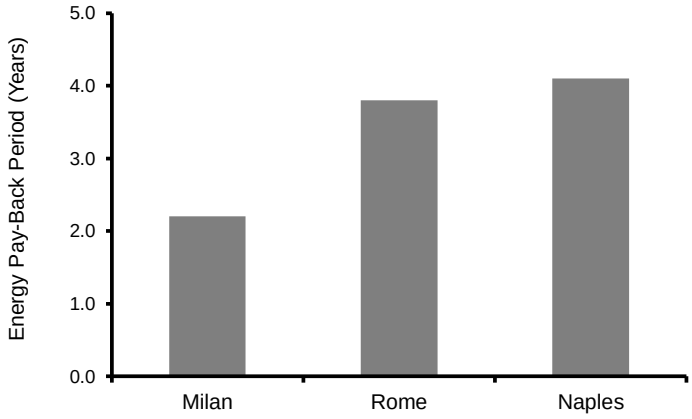

Figure 1. Energy pay-back period in the case of installation of polyurethane foam.

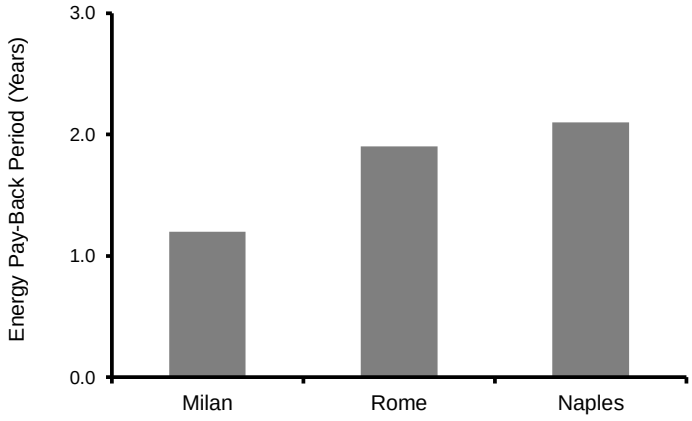

Figure 2. Energy pay-back period in the case of installation of rock wool.

RESULTS

The proposed pictures show the results for the building block under investigation in terms of the energy payback period. The results are referred to the three cities under investigation, namely Milan, Rome, and Naples. In particular, it is useful to specify that Milan is located in the Northern part of Italy, therefore it is characterized by colder climatic conditions, Rome is located in the central part of Italy and it has intermediate climatic conditions, whereas Naples is located in the Southern part of Italy and it has warmer climatic conditions.

From the analysis of Figures 1 and 2, it can be noticed how the location largely influences the energy pay-back. This is due to the fact that the warmer is the climate and the lower is the energy saving in operating energy. This causes the increase of the energy payback period which is longer as the climatic conditions become warmer. In the present analysis, the operating life of the insulating layer is fixed in 15 years.

For locations warmer than Naples, the energy pay-back period can be much longer and exceeds the operating life of the insulator. If this is the case, it is not convenient to use any insulation layer.

CONCLUSIONS

In conclusion, it can be said that specific attention is to be devoted to energy analysis of buildings and in order to assess the real impact of energy efficiency interventions, it is necessary to develop a life cycle analysis.

In order to develop a complete and significant energy assessment, it is mandatory to take into account the role of the embodied energy, which significantly the results of energy efficiency analysis. Embodied energy can be also seen as a design parameter for choosing an appropriate insulator according to the location of installation.

REFERENCES

1. Bianco, V., M. De Rosa, F. Scarpa, and L.A. Tagliafico. 2016. "Analysis of Energy Demand in Residential Buildings for Different Climates by Means of Dynamic Simulation," *International Journal of Ambient Energy*, 37(2):108-120.
2. Bianco, V., D. Righi, F. Scarpa, and L.A. Tagliafico. 2017. "Modeling Energy Consumption and Efficiency Measures in the Italian Hotel Sector," *Energy and Buildings*, 149:329-338.
3. De Rosa, M., V. Bianco, F. Scarpa, and L.A. Tagliafico. 2016. "Impact of Wall Discretization on the Modeling of Heating/Cooling Energy Consumption of Residential Buildings," *Energy Efficiency*, 9(1):95-108.
4. Lützkendorf, T., G. Foliente, M. Balouktsi, and A.H. Wiberg. 2015. "Net-zero Buildings: Incorporating Embodied Impacts," *Build. Res. Inf.*, 43(1):62-81.

5. Langston, Y. L., and C.A. Langston. 2008. "Reliability of Building Embodied Energy Modelling: an Analysis of 30 Melbourne Case Studies," *Construct. Manage. Econ.*, 26(2):147-160.
6. Koezjakov, A., D. Urge-Vorsatz, W. Crijns-Graus, and M. van den Broek. 2018. "The Relationship between Operational Energy Demand and Embodied Energy in Dutch Residential Buildings," *Energy and Buildings*, 165:233-245.
7. Rossellò-Batle, B., C. Ribas, A. Moià-Pol, and V. Martine Moll. 2015. "An Assessment of the Relationship between Embodied And Energy Demands in Dwellings in a Mediterranean Climate," *Energy and Buildings*, 109:230-244.
8. Cellura, M., F. Guarino, S. Longo, and M. Mistretta. 2014. "Energy Life-Cycle Approach in Net Zero Energy Balance: Operation and Embodied Energy of an Italian Case Study," *Energy and Buildings*, 72:371-381.
9. Corrado, V., I. Ballarini, and S. Corgnati. 2012. "Typology Approach for Building Stock Energy Assessment," IEE Project TABULA.
10. Hammond, G., and C. Jones. 2011. *Inventory of Carbon and Energy (ICE), Version 2.0.* Department of Mechanical Engineering, University of Bath, UK.

2018 International Theoretical and Practical Conference on Alternative and Smart Energy (TPCASE 2018)
ISBN: 978-1-60595-617-6

Carbon Cathode Catalyst for Fuel Cells with Alkaline Electrolyte

Elena Kiseleva, Boris Kleimenov, Victor Zakharov and Andrey Zhuk

ABSTRACT

This paper presents synthesized catalysts based on polyacrylonitrile pyropolymers for the oxygen reduction reaction. We developed gas diffusion cathodes using these catalysts, which provide a specific current density of about 0.35 A/cm^2 for cathodic polarization below 0.25 V. The specific power of the laboratory stack of fuel cells with an alkaline electrolyte is more than 350 mW/cm^2.

ELECTROCHEMICAL RESEARCH AND DISCUSSION OF THE RESULTS

The main advantage of alkaline electrochemical current generators is the possibility of using catalysts that do not contain precious metals. The discharge characteristics and service life of fuel cells are largely determined by the electrochemical parameters of the cathode due to the greatest polarization losses. Therefore, the development of cathode catalysts and the improvement of the cathode structure require special attention.

Among various types of metals (Mg, Al, Zn) for air batteries, if we compare them according to the main characteristics of work and the cost of raw materials, the most attractive are electrochemical generators based on aluminum [1].

As is known, with an increase in the concentration of alkali to 6M, on the one hand, the concentration of OH– - ions in the solution increases, which means that the conductivity of the solution increases; on the other hand, the solubility of oxygen and the diffusion coefficient decrease. In general, this can lead to a change in the rate of the oxygen reduction reaction in concentrated alkaline solutions, which can

Joint Institute for High Temperatures of the Russian Academy of Sciences, 13 Bd.2, Izhorskaya Street, Moscow, 125412, Russia

manifest itself in different ways in the kinetic and diffusion region of the electro-reduction of oxygen [2].

In addition, it is necessary to determine how the change in pH affects the value of the cathode potentials, which, depending on the nature of the catalyst, can be divided into several groups. The first group includes catalysts based on compound organic complexes that behave themselves like soot in different pH ranges. In acidic and neutral solutions, $\partial E/\partial$ pH = 0. In alkaline solutions, we can observe a shift of $\partial E/\partial$ pH by 30-60 mV. Activated carbon can be attributed to the second group, as well as those shown in [3] and, to some extent, catalysts with platinum group metals. In this case, we can observe a shift of $\partial E/\partial$ pH by 45-50 mV.

The equilibrium $HO_2\text{-}\leftrightarrow O_2$ establishes in the E_{st} region on cathode catalysts in the presence of oxygen in an alkaline electrolyte, which basically determines the value of the stationary potential.

The generally accepted mechanism of the reaction of oxygen reduction in an alkaline medium can be represented as follows:

$O_2 \rightarrow O_2$ (adsorption)
O_2 (adsorption)+ $e^- \rightarrow O_2^-$(adsorption) (slowly)
O_2^- (adsorption)+ $H_2O + e^- \rightarrow HO_2^- + OH^-$
$HO_2^- + H_2O + 2e^- \rightarrow 3OH^-$

One of the groups of cathode catalysts that significantly increase the activity and efficiency of an electrode in an oxygen reduction reaction include catalytic systems synthesized using various nitrogen-containing metal complexes on a carbon carrier [4, 5]. Phthalocyanines and porphyrins Fe, Co, Mn, Mo, and Cu can be used as precursors in the synthesis [6]. High-temperature pyrolysis is the most effective method for the synthesis of such catalysts. The widespread use of this method is due to the possibility of the synthesis of nitrogen-containing structures during the pyrolysis of complex organic precursors — polymers, heterocyclic compounds, as well as various N_x-complexes. It was shown in a number of works that non-pyrolyzed N_4-complexes - porphyrins and phthalocyanines Co, Fe, Ni, and Cr, deposited on a carbon carrier, show noticeable activity in the oxygen reduction reaction; however, after high-temperature treatment at 500-1000 °C in an inert atmosphere, the activity and stability of such catalysts increases several times [3]. The reasons for such a sharp increase in electrochemical activity have not been fully studied yet; however, there are a number of assumptions about the nature of the catalytic center.

The most common assumption among them states that the metal-N_4- center bound to the carbon of the carrier (substrate) is active, with the central metal atom of the macrocycle playing a key role in the oxygen reduction process [7-9]. Beck [10] suggested that oxygen reduction on N_4-transition metal complexes goes through a modified "reductive catalysis" mechanism, when the oxygen molecule, adsorbed on the metal of the catalytic center, forms a metal-oxygen complex with subsequent electron transfer through the central metal atom and regeneration of the reduced N_4-

chelate complexes. Dodelet et al. [11] discovered the formation of two different catalytic areas, FeN_4/C and FeN_2/C, present in the catalysts regardless of the type of Fe-containing precursor used, in which Fe is coordinated with N in the pyrrolitic and pyridine types, respectively.

The aim of this work is to create and study non-platinum cathode catalysts for alkaline electrolyte fuel cells based on N-doped carbon materials. To achieve it, we formulated the following tasks: 1) synthesis of catalysts; 2) the study of catalytic properties in the reaction of O_2 electro-reduction using the method of a rotating disk electrode; 3) study of the porous structure of catalysts, active layers, gas diffusion layers; 4) testing of gas diffusion cathodes in a half-cell and the studying impacts of various factors on the characteristics of the cathodes; 5) testing Al-air elements.

The three-layer gas diffusion cathode consists of a nickel grid, a barrier layer based on Vulcan XC72 soot, and an active layer based on a 15% TMPPCo /Vulcan XC72 catalyst. The catalyst was synthesized by pyrolysis of TMPPCo (tetra-(p-methoxyphenyl) -porphyrin cobalt), adsorbed on Vulcan XC72, at 850°C in the argon atmosphere for 1 hour. The active layer was obtained by calendering a mixture of catalyst/fluoroplastic (9:1 by weight), pressing with the nickel grid and the barrier layer, having 35% fluoroplastic in its composition.

The testing of the activity of the catalysts in the O_2 reduction reaction was carried out in a three-electrode electrochemical cell using the rotating disk electrode method in 1 M KOH at 60°C. The potential sweep rate was 5 mV/s, the electrode rotation speed was 1580 rpm, and the amount of catalyst on the electrode was 200 $\mu g/cm^2$.

The testing of the cathode was carried out in a three-electrode cell. A mercury oxide electrode (Hg|HgO) was used as a reference electrode, and 8 M NaOH was used as an electrolyte. Air cleaned from CO_2 was supplied to the cathode. Polarization measurements were performed by the potentiodynamic method, the potential sweep rate was 1 mV/s. The potential transient was measured by the galvanostatic method at a current density of 200 mA/cm^2. The values of the potentials are given in the scale of the normal hydrogen electrode with regard to pH and temperature. The testing of the laboratory layout of the Al-air element was carried out in a special cell. Al-In alloy (A99 + 0.45% In) was the material of the anode, which is more stable in alkaline electrolyte than Al. In order to reduce chemical corrosion of the alloy, sodium stannate Na_2SnO_3 (0.1 M) was added into the composition of 8 M NaOH. Heated to 60ºC, the electrolyte was continuously circulated through the working space of the cell, whose width was 3 mm. The geometric surface of the electrodes was 8 cm^2.

Preliminary tests of laboratory samples of alkaline aluminum-air elements (Figure 1) with polyacrylonitrile-based gas diffusion cathodes that we developed showed that the power density (260 mW/cm^2) is comparable to the previously obtained characteristics for cathodes based on porphyrin Co pyrolysis products (300-350 mW/cm^2), and exceeds the values 90 mW/cm^2 published in [12,13].

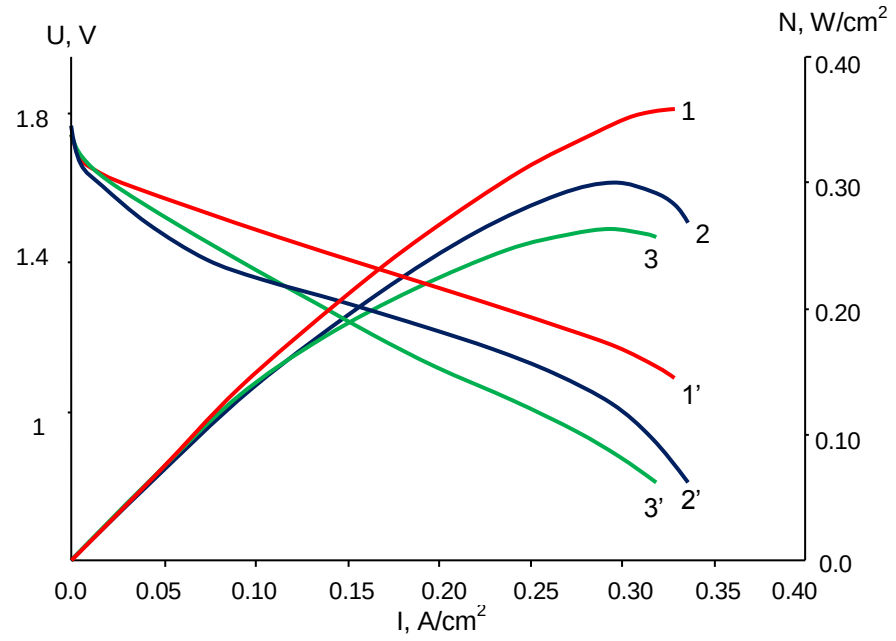

Figure 1. Volt-ampere (1'-3 ') and watt-ampere (1-3) characteristics of alkaline Al-air elements with non-platinum cathode catalysts based on PAN and TMPPCo.

CONCLUSIONS

When charging ~5-8 mg of catalyst per 1 cm^2, overall currents of 0.35 A/cm^2 were achieved with a cathode polarization not higher than 0.25 V and a steady-state potential of 0.09-0.14 V, which is comparable with the results obtained for Pt-containing cathodes or cathodes based on complex oxides. The power density of alkaline aluminum-air elements with polyacrylonitrile-based gas diffusion cathodes that we developed is 260 mW/cm^2, and that of the cathodes based on porphyrin Co pyrolysis products is 300-350 mW/cm^2, which exceeds the values published in the other works.

REFERENCES

1. Wang, X., P.J. Sebastian, M.A. Smit, et al. 2003. "Studies on the Oxygen Reduction Catalyst for Zinc–Air Battery Electrode," *J. Power Sources*, 124:278.
2. Kabanov, N.B., I.I. Astakhov, and I.G. Kiseleva. 1981. *Kinetics of Complex Electrochemical Reactions.* V.E. Kazarinov, ed. Moscow: Nauka, p. 200.
3. Tarasevich, M.R., K.A. Radyushkina, and V.A. Bogdanovskaya. 1991. *Electrochemistry of Porphyrins.* Moscow: Nauka, p.195.

4. Denga, X., X. Wanga, and Z.-F. Ma. 2004. “Influence of Preparation Process on Non-Noble Metal-Based Composite Electrocatalysts for Oxygen Reduction Reaction,” *J. Phys. Chem. B.*, (108):11375.
5. Maldonado, St., and K.J. Stevenson. 2004. “Direct Preparation of Carbon Nanofiber Electrodes via Pyrolysis of Iron(II) Phthalocyanine: Electrocatalytic Aspects for Oxygen Reduction,” *J. Phys. Chem. B.*, (108):11375.
6. Tributsch, H., U.I. Koslowski, and I. Dorbandt. 2008. “Experimental and Theoretical Modeling of Fe-, Co-, Cu-, Mn- based Electrocatalysts for Oxygen Reduction,” *Electrochim. Acta*., (53):2198.
7. Schulenburg, H., S. Stankov, V. Schunemann, et al. 2003. “Catalysts for the Oxygen Reduction from Heat-Treated Iron(III) Tetramethoxyphenylporphyrin Chloride: Structure and Stability of Active Sites,” *J. Phys. Chem. B.*, (107):9034.
8. Marcotte, S., D. Villers, N. Guillet, L. Roue, and J.P. Dodelet. 2004. “Electroreduction of Oxygen on Co-based Catalysts: Determination of the Parameters Affecting the Two-Electron Transfer Reaction in an Acid Medium,” *Electrochimica Acta.,* (50):179.
9. Sawai, K., and N. Suzuki. 2004. “Heat-Treated Transition Metal Hexacyanometallates as Electrocatalysts for Oxygen Reduction Insensitive to Methanol,” *J. Electrochem. Soc.*, (151):A682.
10. Beck, F. 1977. “The Redox Mechanism of the Chelate-Catalysed Oxygen Cathode,” *J. Appl. Electrochem*, (7):239.
11. Lefevre, M., J.P. Dodelet, and P. Bertrand. 2000. “O_2 Reduction in PEM Fuel Cells: Activity and Active Site Structural Information for Catalysts Obtained by the Pyrolysis at High Temperature of Fe Precursors,” *J. Phys. Chem. B.*, (104):11238.
12. Egan, D.R., C. Ponce de Leon, R.J.K. Wood, et al. 2013. “Developments in Electrode Materials and Electrolytes for Aluminium–Air Batteries,” *J. Power Sources*, (236):293-310.
13. Zein, El Abedin S., and A.O. Saleh. 2004. “Characterization of Some Aluminum Alloys for Application as Anodes in Alkaline Batteries,” *J. Appl. Electrochem*., (34):331-335.

2018 International Theoretical and Practical Conference on Alternative and Smart Energy (TPCASE 2018)
ISBN: 978-1-60595-617-6

Assessment of Ecological Risks Associated with the Impact of Energy Sources

Yakov Lvovich, Igor Lvovich, Aleksandr Ostapenko, Andrey Preobrazhenskiy and Oleg Choporov

ABSTRACT

This paper studies the problem associated with assessing environmental risks when using energy sources. Forming the methodological approach, the following was considered: a matrix of regional vulnerabilities, a matrix of dangerous energy sources, and a control matrix. Based on each of the matrices, an assessment of the corresponding risk was given.

INTRODUCTION

Currently, people actively use the natural environment. It is considered a rich source of various resources [1]. However, we can also see negative processes, which are caused by the influence of mankind on the environment [2]. In the course of its use, resources can be subjected to alteration; they are partly thrown back into the environment [3]. In some cases, after processing, they can become very dangerous and harmful. Then, in the first place, it is necessary to maintain the living conditions of people, ensuring their safe existence [4].

For their livelihoods, people use different energy sources. At the same time, on the one hand, they are involved in the redistribution and processing of resources, and on the other, they influence the environment [5, 6].

This paper discusses an approach that can be used when assessing the state of the environment under the influence of various energy sources.

Voronezh State Technical University, 14, Moskovsky Avenue, Voronezh, 394026, Russia

METHODOLOGICAL APPROACH OF RISK ASSESSMENT

The basis of this methodology is the matrix approach. It requires the use of several matrices: a matrix of vulnerabilities, a matrix of dangers of energy sources and a matrix of control. The risk assessment is performed by combining all the analyzed data. In the vulnerability matrix (Table I), links connect components of the living environment and vulnerabilities. The matrix of dander of energy sources (Table II) shows the connections comparing the vulnerabilities and hazards of energy sources. Finally, the control matrix (Table III) shows the connections between the hazards of energy sources and control. For each cell in the table, you can compare the numerical value, which demonstrates how strongly the elements of the rows and columns are connected (for example, the dangers of energy sources and vulnerability). Three levels of connections can be assigned: low, medium and high.

First, lists of hazards of energy sources, vulnerable components and control measures are generated. They are then added to the evaluation table. After this, a risk assessment can be carried out.

When assessing the significance of the analyzed components, the following scale was used: 0 - the contribution is absent, 1 - the contribution is weak, 3 - the contribution is average, 9 - the contribution is strong. Prioritization was conducted as follows: 1 and 2 - insignificant, 3 - is important, but not determinative, 4 - is determinative.

TABLE I. VULNERABILITY MATRIX FOR A SPECIFIC REGION.

Components		**Human**	**Fish**	**Animal kingdom**	**Plant kingdom**	**Insects**	**Degree of significance**	**Risk**
Vulnerable components of the region	Priority	5	4	3	2	1		
Water resources	4	9	9	3	3	1	97	0.385
Air	3	9	3	3	3	1	73	0.289
Soil resources	2	3	3	3	3	3	45	0.178
Forest resources	1	3	1	3	3	3	37	0.147

We will proceed from the fact that there are n components, and for the component a_j the relative value of the contribution is C_j *(j = 1,..., n).* In addition, we assume that c_{ij} is the contribution of the vulnerability v_i *(i = 1,..., m)* to the component a_j. As a result, for the total contribution of vulnerability v_i for the corresponding components, we have:

$$V_i = \sum_{j=1}^{n} v_{ij} * C_j \, . \tag{1}$$

We assume that there are p dangers that are connected to m vulnerabilities. At the same time, d_{ki} *(k = 1,..., p)* is regarded as the potential harm from the risk t_k when using vulnerability v_i. The total danger contribution to energy sources T_k is then determined:

$$T_k = \sum_{j=1}^{m} d_{ki} * V_i \, . \tag{2}$$

Let us proceed from the fact that there are q controls that are associated with p hazards to energy sources, and e_{lk} *(l = 1,..., q)* determines the influence of the control z_l on the danger t_k. As a result, for the total cumulative effect of control z_l we get:

$$z_l = \sum_{k=1}^{p} e_{lk} * T_k \, . \tag{3}$$

When studying risks it is important to bear in mind that various heterogeneous processes can take place within the environment, and there can be quite a lot of them.

The data was aggregated in the first matrix, after which they were sorted so that the relative significance of the vulnerabilities was determined. For example, in water resources there can be an accumulation of a large number of harmful factors, while water is required with the support of vital activity of organisms, therefore, the degree of significance for this resource will be maximum.

The aggregated matrix of vulnerabilities was added to the matrix of dangerous energy sources. The matrix of dangers of energy sources is presented in Table II. Table III shows how the control matrix is defined. It aggregates the data of the hazards of energy sources, and the corresponding control actions are added [7, 8].

The determination of the relative contribution for various control actions with respect to the hazards of energy sources can be made on the basis of the correspondent assessment [9, 10]. You can aggregate the data to define a list of

priority control actions. Such information, as well as ranged control actions, can be considered when planning activities related to improving the environmental situation within certain regions [11,12] when locating different energy sources.

TABLE II. ILLUSTRATION OF THE MATRIX OF HAZARDS OF ENERGY SOURCES.

Vulnerable components in the region		**Water resources**	**Air**	**Soil resources**	**Forest resources**	**Degree of significance**	**Risk**
Dangerous energy sources	Priority	4	3	2	1		
Wind sources	6	1	9	1	3	36	0.114
Hydro sources	5	9	3	9	1	64	0.208
Solar sources	4	3	9	1	1	42	0.133
Gas sources	3	3	9	3	3	48	0.152
Coal sources	2	3	9	9	3	60	0.189
Nuclear sources	1	9	3	9	3	66	0.209

TABLE III. ILLUSTRATION OF THE VULNERABILITY MATRIX FOR A CERTAIN REGION.

Dangerous energy sources		**Wind sources**	**Hydro sources**	**Solar sources**	**Gas sources**	**Coal sources**	**Nuclear sources**	**Degree of significance**	**Risk**
Control	Priority	6	5	4	3	2	1		
Implementation of special measures related to environmental cleanout	4	3	3	3	9	9	9	99	0.243
Conducting training	3	9	9	9	9	9	9	189	0.463
Monitoring policy	2	3	3	3	9	3	9	87	0.213
Possibilities for the implementation of resources recycling	1	1	1	3	3	3	3	33	0.081

CONCLUSIONS

In this paper, a methodical approach was developed within which the risks of using different energy sources in the regions can be assessed. Based on the fact that the dangers of energy sources, vulnerable components and other parameters are subjected to change depending on a region, the presented approach can be refined.

REFERENCES

1. Shchukina, N.A. 2017. "Economic-Mathematical Modeling of the Level of Public Health in the Regions of Russia," *Modeling, Optimization and Information Technology*, 4(19):1.
2. Volker, C., J. Kramm, H. Kerber, E. Schramm, M. Winker and M. Zimmermann. 2017. "More Than a Potential Hazard—Approaching Risks from a Social-Ecological Perspective," *Sustainability*, 9:1039.
3. Leung, K.M.Y., and D. Dudgeon. 2008. "Ecological Risk Assessment and Management of Exotic Organisms Associated with Aquaculture Activities," in *Understanding and Applying Risk Analysis in Aquaculture. FAO Fisheries and Aquaculture Technical Paper*. M.G. Bondad-Reantaso, J.R. Arthur, and R.P. Subasinghe, eds., pp. 67-100.
4. Fargašová, A. 2016. "Ecological Risk Assessment Framework," *Acta Environ. Univ. Comenianae (Bratislava),* 24(1):10-16.
5. Jambeck, J.R., R. Geyer, C. Wilcox, et al. 2015. "Plastic Waste Inputs from Land into the Ocean," *Science*, 347(6223):768–771.
6. Chernov, N.N., N.P. Zagray, M.V. Laguta, and A.Yu.Varenikova. 2018. "Numerical Simulation of the Field of Secondary Sources of an Acoustic Wave Passing through a Biological Environment," *Modeling, Optimization and Information Technology*, 6(3):40-49
7. Sorokin, S.O. 2018. "Optimization Modeling of the Functioning of a Homogeneous Objects System in a Multidimensional Digital Environment," *Modeling, Optimization and Information Technology*, 6(3):153-164.
8. Orlova, D.E. 2018. "Stability of Solutions in Ensuring the Functioning of Organizational and Technical Systems," *Modeling, Optimization and Information Technology*, 6(1):325-336.
9. Lvovich, I.Y., A.P. Preobrazhenskiy, and O.N. Choporov. 2018. "Simulation of Controlling Alternative Current Actuator on Neural Network Basis," in *17th International Ural Conference on Ac Electric Drives*. pp. 101-105.
10. Lvovich, I.Y., A.P. Preobrazhenskiy, and O.N. Choporov. 2017. "Simulation of Solar Energy Use in Livelihood of Buildings," in *IOP Conference Series: Materials Science and Engineering. Ser. "V International Workshop on Mathematical Models and their Applications."* 262:012202.
11. Kravets, O. Ya., A.P. Preobrazhensky, A.V. Kochegarov, O.N. Choporov, and V.E. Bolnokin. 2018. "Development of Algorithms for Complex Numerical Optimization of objects with a Modular Structure," *International Journal on Information Technologies and Security*, 10(4):45-56.
12. Artyukhov, V.G., E.A. Kalaeva, O.V. Putintseva, et al. 2007. "Mathematical Models of the Oxygen-Binding Function of Intact Human Hemoglobin and Hemoglobin Modified by UV-Radiation in the Presence of Carbon Oxide," *Biofizika*, 52(1):24-32.

2018 International Theoretical and Practical Conference on Alternative and Smart Energy (TPCASE 2018)
ISBN: 978-1-60595-617-6

Development of an Intrusion-Detection System in Distributed Energy Systems

Yakov Lvovich, Igor Lvovich, Aleksandr Ostapenko,
Andrey Preobrazhenskiy and Oleg Choporov

ABSTRACT

Actual problems associated with the detection of anomalies in distributed energy networks were considered. These anomalies can be correlated with intrusions. An analysis of promising algorithms that allow one to solve to a certain extent the problem of detecting anomalies is presented. The structure of the intrusion detection system in distributed energy systems is proposed.

INTRODUCTION

Distributed energy can be considered as one of the important components, showing the transition to modern technologies and their practical use [1, 2]. Modern energy systems are characterized by their digitalization, decentralization and intellectualization.

The distributed nature of such systems determines the appropriate security requirements. The objects of attacks can be a means of protecting information in the control computer networks, as well as various systems related to the prevention of intrusions. In this case, violations in the control system of intellectual energy facilities can be identified by analyzing the anomalies in the processed data.

FEATURES OF INTRUSION DETECTION IN DISTRIBUTED SYSTEMS

At the moment, it is impossible to talk about building a full-fledged theory that describes in a comprehensive way the process of detecting an intrusion in distributed

Voronezh State Technical University, 14, Moskovsky Avenue, Voronezh, 394026, Russia

energy networks. There are correspondent means and mechanisms, but not all of them can be correlated with the scientific description.

When detecting intrusions into distributed energy systems, several modules can be marked, which are combined to solve protection problems: a module designed for tracking; intrusion detection subsystem; subsystem related to the response to the recognized intrusion; control subsystem for all modules in the system data warehouse that is required for the functioning of the system; graphical interface module.

When detecting anomalies [3], it is assumed that any kind of abnormal behavior is associated with deviations from the profiles of normal behavior. A database should be created containing profiles for the activities to be monitored. In such cases, statistical methods are effective (associated with the apparatus of mathematical statistics). If the profile is described unambiguously, then any of the deviations can be considered as anomalous. But in practice, this is not always so.

You can talk about two extreme cases:

- the existence of false positives, when there is no possibility of an unambiguous correlation of anomalous and normal behaviors;

- the existence of omissions of intrusions into energy systems, when there is no possibility of unambiguous identification of anomalous behaviors.

In terms of practice, there are some problems:

- profiles showing normal behavior are not always easy to create;

- it is required that possible boundaries are determined according to the possible behavior of electricity consumers in order to avoid approaching the two extreme cases mentioned above.

Detection of abuse can be carried out on the basis of some action patterns that suggest anomalous activity.

Similar patterns can be built on the basis of different approaches:

- watching repetitions on some actions, when the attacker does not have sufficient information on access to some resources, but he will seek to do it again, and not once.

- control actions that do not correspond to current situations;

- demonstration of the use of vulnerabilities, both in software and hardware.

The main advantages associated with the statistical approach include the following: adaptation to how the object of research behaves; using key provisions of mathematical statistics as the basis.

Various sensors can be the objects of research, they read energy characteristics [4], as well as network devices [5, 6].

The approach is based on the fact that:

- for statistical evaluations of characteristics, one can speak of their permanent character [7];

- as an indication of the anomaly, one can consider a sharp character in the deviation of the expectation, as well as the variance.

PROPOSALS FOR THE STRUCTURE OF THE INTRUSION DETECTION SYSTEM IN THE DISTRIBUTED ENERGY SYSTEMS

In order to create a combined approach to detect anomalies in distributed energy systems, the use of the following algorithms is proposed: the one of Brodsky-Darkhovsky (method 1), the one based on the Kolmogorov-Smirnov fitting criterion (method 2), the one based on statistical criteria (method 3).

Basing on such approaches, it is possible to analyze energy flows from the point of view of the presence of anomalies and jointly through the use of weighted voting, to make decisions about the presence of anomalies. The use of this approach allows one to improve the accuracy and completeness of classification, by minimizing errors of the 1 and 2 kinds. The minimization of errors is achieved due to the fact that joint decisions are made on possible anomalies, taking into account the availability of information about the quality of the classification regarding the methods used.

The F-measure (1) can be considered an indicator of the quality of the classification of anomalies, which is a function of the accuracy *P1* (2) and completeness of *W* (3).

$$F = 2 \cdot \frac{P_1 \cdot W}{P_1 + W}, \tag{1}$$

$$P_1 = 2 \cdot \frac{N}{N + E_2}, \tag{2}$$

$$W = \frac{N}{N + E_1}, \tag{3}$$

where E_1– the first kind error, E_2 – the second kind error, N – the number of correctly identified anomalies.

The procedure for voting on the presence of an anomaly is based on the following formula:

$$V = \alpha F(A) + \beta F(B) + \gamma F(G), \tag{4}$$

where *F(A), F(B), F(G)* – the F-measures of the above methods – 1, 2, 3, correspondingly.

If, based on the results of classifications, according to method 1, an anomaly is present, then $\alpha=+1$, otherwise $\alpha=-1$. If in method 2, an anomaly is present, then $\beta=+1$, otherwise $\beta=-1$. If in method 3, an anomaly is present, then $\gamma=+1$, otherwise $\gamma=-1$.

If $S \geq 0$, then the result of applying the combined method means that a network anomaly is present, if $S < 0$, then an anomaly is absent.

Among the shortcomings of the statistical approach, we can point out the low sensitivity of statistical systems with respect to the order in which events follow.

The above algorithms are combined into one module of the system.

The second module is based on expert systems [8], while it becomes possible to describe the model of invasions into energy systems using natural language when a high level of abstractions is reached.

The expert system itself is formed on the basis of a set of rules and facts related to the knowledge of specialists who are experts in the field of energy security. The facts, in this case, are considered in the form of initial data on the operation of energy systems [9,10], and the rules - in the form of algorithms for logical decisions about the presence of an invasion, based on the existing set of facts [11].

The database of the expert system should contain information on the scenarios of most of the known intrusions into energy systems. The disadvantage of practical use of expert systems in solving this problem is in the fact that there is no possibility to identify an unknown intrusion for which there is no record in the information database. Due to a small change in the scenarios of a well-known intrusion, an attacker can introduce difficulties in the operation of protection systems.

Figure 1 shows a block diagram of the proposed intrusion detection system in distributed energy systems.

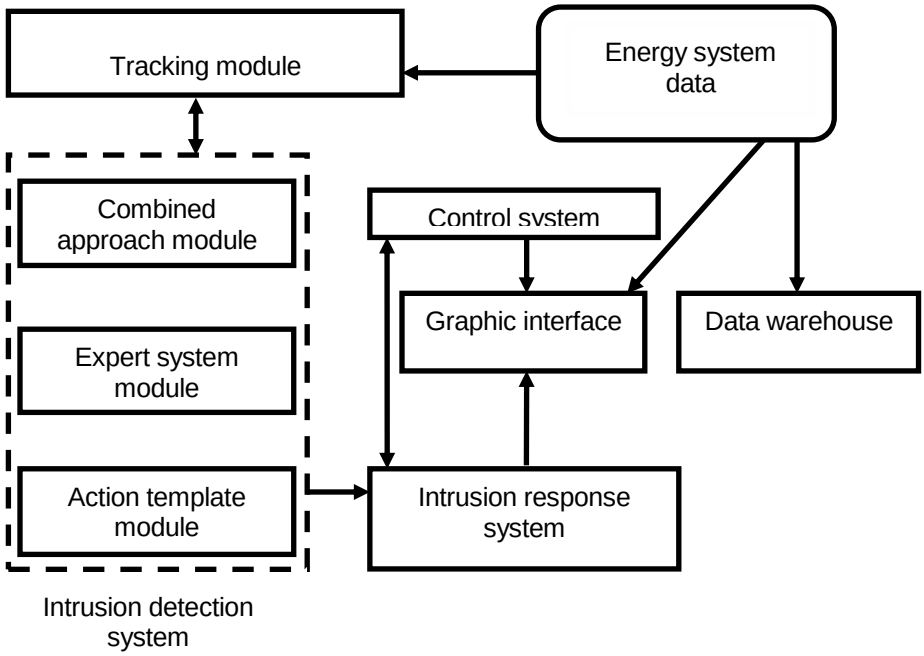

Figure 1. Block diagram of an intrusion detection system in distributed energy systems.

CONCLUSIONS

The features of algorithms for analyzing anomalies in distributed systems were considered. The article gives proposes for the formation of an intrusion detection system, due to which it is possible to significantly reduce the risks associated with interfering with the operation of distributed energy systems.

REFERENCES

1. Sipilä, K., M. Rämä, and E. Pursiheimo. 2015. *Distributed Energy Systems*. Julkaisija Utgivare Publisher. 190 p.
2. Acha, S. 2017. *Modelling Distributed Energy Resources in Energy Service Networks.* The Institution of Engineering and Technology, 207 p.
3. Jyothsna, V., Rama, and V.V. Prasad. 2011. "A Review of Anomaly based Intrusion Detection Systems," *International Journal of Computer Applications*, 28(7):28-34.
4. Lvovich, I.Y., A.P. Preobrazhenskiy, and O.N. Choporov. 2018. "Simulation of Controlling Alternative Current Actuator on Neural Network Basis," in *17th International Ural Conference on Ac Electric Drives*. pp. 101-105.
5. Kravets, O. Ya., A.P. Preobrazhensky, A.V. Kochegarov, O.N. Choporov, and V.E. Bolnokin. 2018. "Development of Algorithms for Complex Numerical Optimization of Objects with a Modular Structure." *International Journal on Information Technologies and Security*, 10(4):45-56.
6. Sorokin, S.O. 2018. "Optimization Modeling of the Functioning of a Homogeneous Objects System in a Multidimensional Digital Environment," *Modeling, Optimization and Information Technology*, 6(3):153-164.
7. Orlova, D.E. 2018. "Stability of Solutions in Ensuring the Functioning of Organizational and Technical Systems," *Modeling, Optimization and Information Technology*, 6(1):325-336.
8. Tishukov, B.N. 2018. "Improving the Efficiency of Functioning of Objects with a Structurally Variable Form of Management Based on Optimization Modeling," *Modeling, Optimization and Information Technology*, 6(1):288-298.
9. Lvovich, I.Y., A.P. Preobrazhenskiy, and O.N. Choporov. 2017. "Simulation of Solar Energy Use in Livelihood of Buildings," in *IOP Conference Series: Materials Science and Engineering. Ser. "V International workshop on mathematical models and their applications,"* 262:012202.
10. Lvovich, I.Y., Y.E. Lvovich, A.P. Preobrazhenskiy, D.V. Saleev, and O.N. Choporov. 2016. "Method for the Process Control of Integrated Circuits Production to Account the Influence of Uncontrolled Parameters," in *13th International Scientific-Technical Conference on Actual Problems of Electronic Instrument Engineering*, 1(1):71-74
11. Nedosekin, D.A. 2018. "Multivariate Choice in Managing Evolving Systems," *Modeling, Optimization and Information Technology*, 6(1):346-356.

2018 International Theoretical and Practical Conference on Alternative and Smart Energy (TPCASE 2018)
ISBN: 978-1-60595-617-6

Highly Efficient Mobile Electrical Power Generating Device with Direct Conversion of the Thermal Energy into the Electrical One

Yuri Shalimov, Vladlen Kudryash, Alla Zvyagintseva, Alexander Pomiguev and Alexander Russu

ABSTRACT

The paper reviews the possibility of using diesel generators and gas generators operating on solid fuel to power the remote facilities. The advantage of gas generators on solid fuel is proven in terms of cost, environmental safety and operating conditions. It has been also proved that the reinforcement of research work aimed at direct conversion of heat into electricity is determined by the need to provide energy for the remote areas detached from industrial power supply networks. The gas generator feedback system proposed by our research allows to optimize the gas generator operation and to vary the power consumption in a wide range of values. The proposed systems imply the minimum number of mechanically interacting elements to reduce the number of failures during the equipment operation.

INTRODUCTION

The increased interest in highly efficient mobile electrical power generating devices with direct conversion of thermal energy into electrical one prevailed in recent years due to the growing demand to develop the territories of the far north

Yuri Shalimov, Alla Zvyagintseva, Alexander Russu, Voronezh State Technical University, 14, Moskovsky Avenue, Voronezh, 394026, Russia
Vladlen Kudryash, Voronezh Institute of the Ministry of Internal Affairs of the Russian Federation, 53, Patriotov Avenue, Voronezh, 394065, Russia
Alexander Pomiguev, Military Scientific Educational Center of Military-Air Forces “N.E. Zhukovsky and Ju. A. Gagarin Military-Air Academy”, 54A Starikh Bolshevikov Street, Voronezh, 394064, Russia

of Russia. The main problems that arise in these areas are related both to the limitations of the fuel resource base and to the widespread use of the traditional type of fuel (diesel and kerosene) at the low ambient temperatures.

Storage of large reserves of hydrocarbon fuels is associated with certain difficulties in meeting safety requirements for safekeeping systems. In the meantime, the use of traditional mobile gasoline-diesel generator facilities confounds certain difficulties during their launch and operation, both in normal conditions and in low-temperature conditions.

Some solutions proposed on the basis of diesel generators are undoubtedly useful in terms of their further development:

– application of direct conversion of heat into electricity based on thermoelectric elements [1],

– application of biological fuels [2].

The most fully the above requirements are met by the previously known gas generation system, supplemented by new thermal control systems, which imply the feedback system, including the electrochemical converter as the main element. Briquettes with an improved solid fuel composition are used for loading the gas generator [3].

There is an urgent need to use unconventional fuels. Those are safe when storage conditions are changed, and, at the same time, they do not change their characteristics at low temperatures. Such systems allow the use the power plants in a wide range of low temperatures at the limit of values that could be reached in northern latitudes. The time period from the start-up mode of the gas generator to a full set of power normally varies from 10 to 15 minutes.

On the other hand, currently, the increased attention is focused on the direct generation of electrical energy from heat, which would exclude the use of complex multi-step transformations such as a water-vapor-mechanical drive-electric generator.

The main goal of this paper is to show additional capabilities and potential of the well-known energy systems in order to achieve higher levels of their operational quality and to satisfy basic consumer requirements.

EXPERIMENTAL PART

There is a specific list of the most significant typical characteristics (criteria) affecting the design of the generators and energy converters: increase in specific power—“power per unit weight”, “power per unit volume”; increase in lifetime and reliability; increased safety and “user-friendliness”; non-toxicity (harmlessness); the possibility of mobile performance; availability of production materials. This list must be supplemented with two more criteria important for studying the conversion of thermal energy into electrical energy: the working

temperature interval; the possibility of using processes associated with waste processing in the heat generator.

The use of a gas generator in conjunction with a feedback system creates a significant economic effect. Table I shows the corresponding comparison data (in prices relevant to the beginning of 2018).

Obviously, the costs of briquettes are an order of magnitude less than diesel fuel. Moreover, production waste can be used as a raw material for the production of fuel briquettes, that is, this solution implies additional "super effect" when the generation of energy is accompanied by the waste disposal. It is difficult to overestimate this benefit, since preserving the ecological balance and effective deep processing of waste are the most acute issues in the modern world.

Decomposition and thermal transformation of fuel in the generator of the reverse type is based on the following chemical circuit:

$$C + O_2 \rightarrow CO_2,\ CO_2 + C \rightarrow 2CO. \quad (1)$$

Carbon dioxide in the 'tuyere' belt area, when interacting with carbon, is reduced to CO according to the following circuit:

$$C + O_2 \rightarrow CO_2 + 284.3\ \text{kJ/mol} \quad (2)$$

$$C + ½\ O_2 \rightarrow CO + 109.4\ \text{kJ/mol} \quad (3)$$

$$C + CO_2 \rightarrow 2CO - 172.5\ \text{kJ/mol} \quad (4)$$

$$C + H_2O \rightarrow CO + H_2 - 131.4\ \text{kJ/mol} \quad (5)$$

$$CO + H_2O \rightarrow CO_2 + H_2 + 41.1\ \text{kJ/mol} \quad (6)$$

$$C + 2H_2 \rightarrow CH_4 - 74.8\ \text{kJ/mol} \quad (7)$$

$$CO + 3H_2 \rightarrow CH_4 + H_2O + 206.2\ \text{kJ mol} \quad (8)$$

$$CO + H_2 \rightarrow ½\ CH_4 + ½\ CO_2 + 123.8\ \text{kJ/mol} \quad (9)$$

TABLE I. COMPARISON OF FUELS.

	Calorific value, MJ/kg	**Cost (Thousands of RUBs)**
Diesel fuel	43.0	39.00-43.00
Solid fuel briquettes	20.5	1.20-1.50

Technical systems of direct conversion of thermal energy into electrical one alternate the one known as “classical systems of multistage energy conversion”. The multistage conversion circuit presumes the following main steps:

- transformation of the chemical (nuclear) composition of a substance in order to extract thermal energy;
- conversion of thermal energy into mechanical energy with a reciprocating or rotational type of motion;
- conversion of mechanical energy into electrical energy for subsequent transmission and distribution.

The most well-known multi-stage conversion circuits are the following ones: piston, steam turbine and gas turbine types of systems.

Direct conversion of thermal energy into electrical energy has its advantages in comparison with a multistage conversion. For example, noiseless operation. At the same time, according to such an important criterion as efficiency the technical systems of direct conversion of thermal energy into electrical energy (efficiency up to 25%) are still inferior to the multi-stage conversion circuit (with its efficiency of up to 40%) [4].

The direct conversion of thermal energy into electrical energy based on thermionic conversion is particularly interesting in this respect. Thermionic converter (TEC) is a heat engine, where the gas of free electrons in vacuum, plasma (Cs ions) or in inert gases (the Ramsauer – Townsend effect) are used as a working medium. The converter circuit is shown in Figure 1.

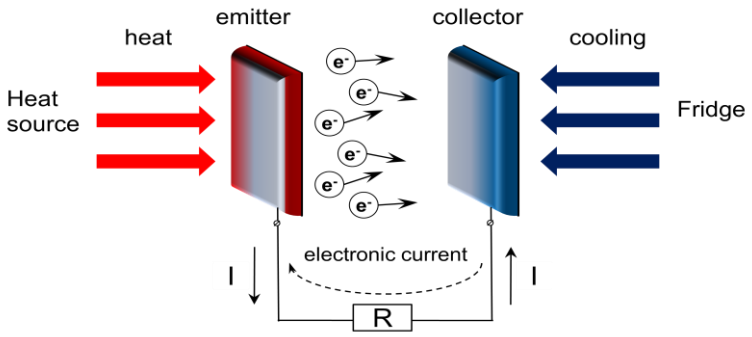

Figure 1. Thermionic energy converter.

An important advantage of this type of conversion is the fact that as long as the emission from the collector is lower compared to the emission from the emitter, the collector temperature can be high without a noticeable decrease in efficiency and power. For example, in the case when the operation efficiency of the emitter comprises 3 eV and 1.7 eV of the collector, the emitter temperature is 2000K, the current density of the emitter is $10A/cm^2$, the collector temperature can reach 1100K, while the efficiency factor will comprise ~ 21% [5].

DISCUSSION

We have proposed a solution for the modernization of the gas generator, taking into account the use of the physical principles of direct conversion of thermal energy into the electrical one. This solution is protected by a patent [6].

Thermal energy generated in the reactor of thermal decomposition of fuel is utilized with the help of two direct conversion systems: thermal emission and thermoelectric (Figure 1). The electrical energy obtained is converted using a switching device, taking into account the values of currents and voltages on each generating element, the total number of which depends on the type of gas generator.

The peculiarity of a reversed type gas generator is that in order to work effectively it is necessary to calculate in advance and manufacture the product for the corresponding heat load. If the heat load differs from the optimal value, that is, it is nonlinear, then, the efficiency of work decreases. Therefore, the gas generator must be equipped with a positive feedback system. Such a system is necessary to smooth the peaks of energy consumption. This is possible if the electrochemical converter based on hydrogen (and oxygen), equipped with automation elements, is applied as such a feedback system. Electrochemical converters are presented by the system of two electrodes immersed in an electrolyte solution of an indifferent type.

For coordination with the external load, the switch turns on (disconnects) the additional load. In this case, the following processes occur on the electrodes:

cathode – $2H_2O+2e \rightarrow 2H^0+2OH^-$ $H^0 + Me^0 \rightarrow MeH$ $2H^0 \rightarrow H_2$, (10)

anode – $2H_2O - 4e \rightarrow 4H^+ + O_2$. (11)

The cathode is made of a Ni-B composite for the possibility of formation of hydride fuel in its structure. The anode is an insoluble electrode obtained by fusing a compound of the lead with antimony.

The amount of the hydrogen is determined by the dependence $Q^{-1} = f(T)$ that is obtained by studying the behavior of the bending vibrations on a capacitive sensor, where the height of the internal friction peak is proportional to the amount of hydrogen absorbed by the sample, and the half width of the peak determines the binding energy of the hydrogen metal. For alumohydride, the extraction temperature is in the range of 142-145ºC. The functional diagram is shown in Figure 2

CONCLUSION

The use of direct energy conversion systems simplifies the operation of the energy complex since in this case, the processes associated with the conversion of energy into the mechanical form are completely unnecessary. This leads to a significant reduction in weight and size and increases the reliability and simplicity of the device, and simplifies its maintenance.

In general, the mobile power generating complex based on a reversed type gas generator in combination with thermoelectric, thermionic and electrochemical converters provides a solution to the power supply problem and at the same time surpasses the analogue systems based on its technical and economic indicators. Taking into account that the trend of developing of diesel generators indicates stagnation in this direction, the timely development of power engineering based on the new principles is an acute and natural step for the further improvement of defense and civil engineering equipment.

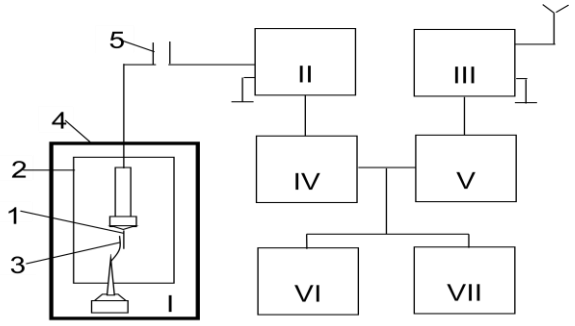

Figure 2. Installation of internal friction. Functional diagram:
1 - sample; 2 - heat chamber; 3 - fixed electrode; 4 - vacuum chamber;
5 - toggle switch; I - generator of high-frequency oscillations; II - low-frequency generator;
III - frequency modulation meter; IV - amplitude discriminator;
V-frequency meter (pulse counter); VI - electronic counter; VII – oscilloscope.

REFERENCES

1. Atalay, T., Y. Köysal, A.E. Özdemir, and E. Özbaş. 2018. “Evaluation of Energy Efficiency of Thermoelectric Generator with Two-Phase Thermo-Syphon Heat Pipes and Nano-Particle Fluids,” *International Journal of Precision Engineering and Manufacturing - Green Technology*, 5(1):5-12.
2. Algayyim, S.J.M., T. Yusaf, A.P. Wandel, and I. Hamawand. 2018. “Production and Application of ABE as a Biofuel,” *Renewable and Sustainable Energy Reviews*, 82:1195-1214.
3. Koido, K., Y. Watanabe, T. Ishiyama, K. Dowaki, and T. Nunoura. 2017. “Fate of Sulphur during Simultaneous Gasification of Lignin-Slurry and Removal of

Hydrogen Sulphide over Calcium Aluminate Supported Nickel Oxide Catalyst," *Journal of Cleaner Production*, 141:568-579.
4. Ghashami, M., K. Park, and S.K. Cho. 2017. "Near-field enhanced Thermionic Energy Conversion for Renewable Energy Recycling," *Journal of Quantitative Spectroscopy and Radiative Transfer*, 198:59-67.
5. Gryaznov, G.M. 2007. *Space Nuclear Power and New Technologies. Director's Notes*. Moscow: Publishing house FSUE "TSNIIA tominform", 136 p.
6. Pomiguev, A.V., I.K. Shuklin, Yu. N. Shalimov, and A.V. Russu. 2018. "Power Generating Complex," patent of the Russian Federation #2652241.

Author Index